

ERDC TR-03-3

Engineer Research and Development
Center



**US Army Corps
of Engineers®**
Engineer Research and
Development Center

Evaluation of Island and Nearshore Confined Disposal Facility Alternatives, Pascagoula River Harbor Dredged Material Management Plan

Barry W. Bunch, Mike Channell, William D. Corson,
Bruce A. Ebersole, Lihwa Lin, David J. Mark,
James P. McKinney, Steve A. Pranger,
Paul R. Schroeder, S. Jarrell Smith, Dorothy H. Tillman,
Barbara A. Tracy, Michael W. Tubman, and
Timothy L. Welp

September 2003

20031104 036

Evaluation of Island and Nearshore Confined Disposal Facility Alternatives, Pascagoula River Harbor Dredged Material Management Plan

William D. Corson, Bruce A. Ebersole, Lihwa Lin, David J. Mark, James P. McKinney, S. Jarrell Smith, Barbara A. Tracy, Michael W. Tubman, and Timothy L. Welp

*Coastal and Hydraulics Laboratory
U.S. Army Engineer Research and Development Center
3909 Halls Ferry Road
Vicksburg, MS 39180-6199*

Barry W. Bunch, Mike Channell, Steve A. Pranger, Paul R. Schroeder, and Dorothy H. Tillman

*Environmental Laboratory
U.S. Army Engineer Research and Development Center
3909 Halls Ferry Road
Vicksburg, MS 39180-6199*

Final report

Approved for public release; distribution is unlimited

**REPRODUCED FROM
BEST AVAILABLE COPY**

ABSTRACT: The U.S. Army Engineer Research and Development Center (ERDC) performed a number of engineering studies in support of U.S. Army Engineer District, Mobile (SAM) efforts to develop a Dredged Material Management Plan (DMMP) for the Federal navigation project at Pascagoula, MS. The studies focused on evaluating an option under consideration for the placement of dredged material in an island confined disposal facility (CDF). Numerical modeling of circulation, water quality, and wave climatology were performed to examine the potential impacts of an island CDF, and for engineering design considerations. Field measurements of currents and waves in the Mississippi Sound were made. A number of studies were performed to examine the sediment consolidation process in the CDF with the primary objective of assessing its dredged material volume capacity. Quantitative and qualitative studies results were produced for three alternative locations. The three locations are an island CDF just northeast of Round Island and southeast of the Singing River, between Round Island and the main navigation channel leading to Horn Island Pass and the Gulf of Mexico, and north of the point where the main navigation channel bifurcates to service the Pascagoula River and Bayou Casotte Harbors.

DISCLAIMER: The contents of this report are not to be used for advertising, publication, or promotional purposes. Citation of trade names does not constitute an official endorsement or approval of the use of such commercial products. All product names and trademarks cited are the property of their respective owners. The findings of this report are not to be construed as an official Department of the Army position unless so designated by other authorized documents.

Contents

Conversion Factors, Non-SI to SI Units of Measurement	xvii
Preface	xviii
1—Introduction.....	1-1
2—Field Data Collection and Analysis	2-1
Introduction	2-1
Wave Measurements	2-1
Gulf of Mexico Wave Gage (sta MS001).....	2-4
Mississippi Sound Wave Gages (sta MS00N and MS002)	2-6
Data Analysis	2-7
Gulf of Mexico wave gage (sta MS001).....	2-7
Mississippi Sound wave gages (sta MS00N and MS002)	2-8
Current measurements	2-9
Moored current measurements.....	2-9
Description of observed currents	2-12
3—Confined Disposal Facility Alternatives – Dike Elevation Requirements	3-1
Introduction	3-1
Background.....	3-1
Objective and scope	3-1
Surface areas of alternatives	3-4
Dredging and disposal scenario	3-4
Study Approach.....	3-6
Description of study	3-6
Processes affecting storage capacity	3-6
Method of analysis.....	3-8
Model Description and Assumptions	3-8
Theoretical basis	3-8
Modeling procedures	3-9
Assumptions and model input parameters	3-9
Dredged material properties.....	3-11
Dredged material disposal volumes and lifts	3-13
Site operation and management plan	3-15
Simulation Results.....	3-15

Conclusions	3-18
References	3-21
4—Circulation Studies of Mississippi Sound	4-1
Description of Tidal Circulation Model	4-1
Model Development	4-4
Model Calibration	4-7
Astronomical calibration	4-7
Meterological calibration	4-10
Adaptation of Calibrated Model	4-13
Analysis of Alternatives	4-15
Summary	4-18
References	4-20
5—3-D Circulation Model Studies (CH3D)	5-1
Model Background	5-1
Governing equations	5-2
Boundary conditions	5-3
Model Domain	5-5
Grid and Bathymetry	5-5
Boundary Conditions	5-7
Ocean boundary hydrodynamics	5-9
Freshwater input	5-11
Temperature	5-11
Surface heat exchange	5-12
Salinity	5-12
Wind	5-13
Friction	5-13
Mixing	5-13
Calibration and Verification	5-13
Astronomical	5-14
February-March 2001	5-16
April-September 1997	5-21
Design Alternatives	5-28
Geometry	5-28
Environmental conditions	5-28
Simulations	5-29
Summary and Conclusions	5-33
References	5-35
6—Water Quality Model Studies	6-1
Model Description	6-1
Conservation of mass equation	6-2
State variables	6-2
WQ Modeling Approach	6-3
CEQUAL-ICM grid	6-5
Meteorological data	6-7
Kinetic rates	6-8

Calibration and Alternative Results and Discussion	6-8
Calibration	6-8
Calibration results and discussion.....	6-9
Alternative results and discussion.....	6-11
Water Quality Summary and Conclusions	6-14
References	6-16
 7—Wave Modeling Studies.....	 7-1
Site Description and Objective.....	7-1
10-Year Wave Hindcast	7-2
Wind fields.....	7-3
Grid nesting	7-3
Hindcast products	7-5
Hindcast validation	7-6
Comparison with buoy data	7-6
Comparison with nearshore wave gage data, 2001.....	7-8
CDF Influences on Wave Conditions.....	7-17
Selection of representative wave conditions.....	7-17
Results for with-CFD simulations	7-23
Summary and Conclusions	7-29
References	7-30
 8—Hurricane Effects	 8-1
Description of Planetary Boundary Layer Model	8-1
Selection of Hurricanes	8-4
Implementation of PBL Model.....	8-5
Implementation of Storm-Surge Model.....	8-6
Implementation of Wave Model.....	8-9
Hurricane Model Results.....	8-11
Summary	8-20
References	8-20
 9—Summary and Conclusions	 9-1
CDF Capacity and Dike Elevation	9-2
Influence of CDF on Water Circulation and Quality	9-2
Results from 2-D hydrodynamic modeling.....	9-3
Results from 3-D hydrodynamic modeling.....	9-4
Results from water quality modeling.....	9-5
Influence of CDF on Local Wind Wave Conditions	9-6
 Appendix A—Gulf of Mexico Wave Gage Sta MS001 Data Plots	 A1
Appendix B—Mississippi Sound Wave Gage Sta MS00N Data Plots.....	B1
Appendix C—Mississippi Sound Wave Gage Sta MS002 Data Plots.....	C1
Appendix D—Current Data Plots	D1

Appendix E—Consolidation Characteristics of Foundation Material and Dredged Material	E1
Appendix F—Report of Field and Laboratory Data Subsurface Dredge Material Investigation	F1
Appendix G—Properties of Placed Sediments – Sample PH-05	G1
Background	G1
Column Settling Tests	G1
Physical characteristics of sediment	G1
Experimental Procedures.....	G3
Sample collection.....	G3
Settling test procedures	G4
Slurry preparation	G4
Zone settling test.....	G5
Compression settling test	G6
Flocculent settling test	G7
Data Analysis and Results	G7
Compression settling tests	G7
Zone settling tests	G8
Flocculent settling tests.....	G11
Turbidity	G13
Consolidation tests.....	G13
Conclusions	G17
References	G18
Appendix H—Additional Calibration and Verification Comparisons.....	H1
Appendix I—CH3D Grid Representation of Island Alternatives	I1
Appendix J—Hindcast Wave Information Products at CDF Sites	J1

List of Figures

Figure 1-1. Site map showing Pascagoula Navigation Project vicinity	1-2
Figure 2-1. Wave gage and current meter locations.....	2-2
Figure 2-2. Current-meter mooring locations.....	2-3
Figure 2-3. Deployment of Gulf of Mexico self-contained wage gage (sta MS001)	2-4
Figure 2-4. Remote Terminal Unit on Petit Bois Island.....	2-5
Figure 2-5. Redesigned RTU for minimizing lightning-strike induced damage	2-5
Figure 2-6. Deployment of Mississippi Sound wave gages	2-6
Figure 2-7. Station MS002 RTU installed on U.S. Coast Guard range marker	2-7
Figure 2-8. Example vessel wake time series for 14 March 2001	2-8
Figure 2-9. Example vessel wake time series for 16 April 2001.....	2-9
Figure 2-10. Acoustic Doppler Profiler (ADP)	2-10
Figure 2-11. Over-the-side Acoustic Doppler Current Profile.....	2-11
Figure 2-12. Average values of depth-averaged, horizontally-filtered current speed across Horn Island Pass on 27 February – 1 March 2001	2-11
Figure 2-13. Average values of depth-averaged, horizontally-filtered current speed across Horn Island Pass on 21 and 22 June 2001	2-12
Figure 2-14. Speed and direction from 26 April to 4 May 2001 for wind at Dauphin Island, AL, NDBC 42007, and for current at sta MS_CM02, 3.5 m above seafloor, and sta MS_CM02, and predicted tidal height at Horn Island Pass.....	2-13
Figure 2-15. Speed and direction from 18-20 May 2001 for wind at NDBC 42007 and for current at sta MS_CM01, 2.0 m above seafloor, sta MS_CM01, near-surface, sta MS_CM02 and MS_NGL17...	2-14
Figure 2-16. Speed and direction from 13-19 March 2001 for wind at Dauphin Island, AL, and for current at sta MS_CM01, near- surface, 3.5 m above seafloor, 2.0 m above seafloor, and approximately 0.5 m above seafloor.....	2-16
Figure 3-1. Dredged Material Placement Alternatives 1, 2, and 3	3-2
Figure 3-2. Alternative 1, dike configuration.....	3-3
Figure 3-3. Alternative 2, dike configuration.....	3-3

Figure 3-4. Alternative 3, dike configuration	3-3
Figure 3-5. Pascagoula Harbor sampling locations	3-12
Figure 3-6. Fill elevation predictions for Alternative 1	3-16
Figure 3-7. Fill elevation predictions for Alternative 2	3-16
Figure 3-8. Fill elevation predictions for Alternative 3	3-17
Figure 3-9. Fill elevation predictions for 900-acre Alternative 3	3-17
Figure 3-10. Fill elevation predictions for Alternative 3 for reduced dredging requirements	3-19
Figure 3-11. Fill elevation predictions for 900-acre Alternative 3 for reduced dredging requirements	3-19
Figure 3-12. Fill elevation predictions for Alternative 3 for various drainage efficiencies using Sediment P-04 consolidation characteristics ..	3-20
Figure 3-13. Fill elevation predictions for Alternative 3 for various drainage efficiencies using Sediment P-06 consolidation characteristics ..	3-20
Figure 4-1. Numerical grid	4-21
Figure 4-2. Numerical grid within Mississippi Sound	4-21
Figure 4-3. Numerical grid in vicinity of Pascagoula, MS	4-22
Figure 4-4. Location of tide gauges and current meters used in model calibration	4-22
Figure 4-5. Comparison of model- and constituent-synthesized water- surface elevations for Pascagoula, MS	4-23
Figure 4-6. Comparison of model- and constituent-synthesized water- surface elevations for Dauphin Island, AL	4-23
Figure 4-7. Comparison of water-surface amplitude constituents	4-24
Figure 4-8. Comparison of water-surface phase constituents	4-24
Figure 4-9. Comparison of model- and constituent-synthesized east-west current for sta 12	4-25
Figure 4-10. Comparison of model- and constituent-synthesized north-south current for sta 12	4-25
Figure 4-11. Comparison of model- and constituent-synthesized east-west current for sta 13	4-26
Figure 4-12. Comparison of model- and constituent-synthesized north-south current for sta 13	4-26
Figure 4-13. Comparison of model- and constituent-synthesized east-west current for sta 14	4-27
Figure 4-14. Comparison of model- and constituent-synthesized north-south current for sta 14	4-27
Figure 4-15. Time-series of wind speeds measured at NDBC C-Man sta DPIA1	4-28

Figure 4-16.	Time-series of wind directions measured at NDBC C-Man sta DPIA1	4-28
Figure 4-17.	Comparison of modeled and measured water-surface elevations measured at Pascagoula PI gauge	4-29
Figure 4-18.	Comparison of modeled and measured water-surface elevations measured at Gulfport gauge	4-29
Figure 4-19.	Comparison of modeled and measured current speed at Deployment Site 1	4-30
Figure 4-20.	Comparison of modeled and measured current direction at Deployment Site 1	4-30
Figure 4-21.	Time series of measured wind direction at NDBC C-Man sta DPIA1	4-31
Figure 4-22.	Numerical grid for Alternative 1 condition.....	4-31
Figure 4-23.	Numerical grid for Alternative 2 condition.....	4-32
Figure 4-24.	Numerical grid for Alternative 3 condition.....	4-32
Figure 4-25.	Current map of peak spring flood tide for existing configuration condition	4-33
Figure 4-26.	Current map of peak spring ebb tide for existing configuration condition	4-33
Figure 4-27.	Current map of peak spring flood tide for Alternative 1 condition	4-34
Figure 4-28.	Current map of peak spring ebb tide for Alternative 1 condition	4-34
Figure 4-29.	Location of stations used in comparing changes in current	4-35
Figure 4-30.	Comparison of computed currents at sta A; astronomical forcing	4-35
Figure 4-31.	Comparison of computed currents at sta A; February 1998 winter storm	4-36
Figure 4-32.	Comparison of computed currents at sta A; February 1998 winter storm	4-36
Figure 4-33.	Comparison of computed currents at sta A; February 1998 winter storm	4-37
Figure 4-34.	Current map of peak spring flood tide for Alternative 2 condition	4-37
Figure 4-35.	Current map of peak spring ebb tide for existing configuration condition	4-38
Figure 4-36.	Comparison of computed currents at sta C; astronomical forcing	4-38
Figure 4-37.	Comparison of computed currents at sta B; February 1998 winter storm	4-39

Figure 4-38.	Comparison of computed currents at sta C; February 1998 winter storm	4-39
Figure 4-39.	Comparison of computed currents at sta G; astronomical forcing	4-40
Figure 4-40.	Comparison of computed currents at sta H; astronomical forcing	4-40
Figure 4-41.	Current map of peak spring flood tide for Alternative 3 condition	4-41
Figure 4-42.	Current map of peak spring ebb tide for Alternative 3 condition	4-41
Figure 4-43.	Comparison of computed currents at sta I; astronomical forcing	4-42
Figure 4-44.	Comparison of computed currents at sta I; February 1998 winter storm	4-42
Figure 4-45.	Comparison of computed currents at sta D; astronomical forcing	4-43
Figure 4-46.	Comparison of computed currents at sta E; February 1998 winter storm	4-43
Figure 4-47.	Comparison of computed currents at sta F; February 1998 winter storm	4-44
Figure 4-48.	Comparison of current direction at sta E; February 1998 winter storm	4-44
Figure 4-49.	Comparison of current direction at sta F; February 1998 winter storm	4-45
Figure 5-1.	CH3D grid and model domain	5-6
Figure 5-2.	Grid resolution in study area	5-7
Figure 5-3.	CH3D bathymetry	5-8
Figure 5-4.	CH3D bathymetry in study area near Pascagoula, MS	5-8
Figure 5-5.	Illustration of boundary condition specifications for CH3D grid	5-9
Figure 5-6.	Location map of measurements included in calibration and verification exercises	5-14
Figure 5-7.	Comparisons of reconstructed tides and CH3D simulated tides	5-17
Figure 5-8.	Comparison of reconstructed tides and CH3D simulated tides at sta V12	5-18
Figure 5-9.	Comparison of reconstructed tides and CH3D simulated tides at sta V13	5-19
Figure 5-10.	Comparison of reconstructed tides and CH3D simulated tides at sta V14	5-20

Figure 5-11.	Comparison of CH3D to measured water-surface elevations at Pascagoula PI gauge for February-March 2001 verification	5-22
Figure 5-12.	Comparison of CH3D to measured current at Deployment 1 site for February-March 2001 verification	5-22
Figure 5-13.	Comparison of measured and modeled sea surface temperature at DPIAL	5-23
Figure 5-14.	Comparison of measured and modeled temperature and salinity at MSD03	5-25
Figure 5-15.	Comparison of measured and modeled temperature and salinity at MSD04	5-26
Figure 5-16.	Comparison of measured and modeled temperature and salinity at MSD03 during period of hourly data	5-27
Figure 5-17.	Location of dredged material disposal alternatives in relationship to existing land masses and CH3D grid	5-29
Figure 5-18.	Environmental conditions for August 1990 applied for design simulations	5-30
Figure 5-19.	CH3D bottom currents for Alternative 00 (13 August 1990 22:00). Filled contours indicate current magnitude, vectors indicate current direction	5-31
Figure 5-20.	CH3D bottom currents for Alternative 01 (13 August 1990 22:00). Filled contours indicate current magnitude, vectors indicate current direction	5-31
Figure 5-21.	CH3D bottom currents for Alternative 02 (13 August 1990 22:00). Filled contours indicate current magnitude, vectors indicate current direction	5-32
Figure 5-22.	CH3D bottom currents for Alternative 03 (13 August 1990 22:00). Filled contours indicate current magnitude, vectors indicate current direction	5-32
Figure 5-23.	CH3D bottom currents for Alternative 00 (14 August 1990 16:00). Filled contours indicate current magnitude, vectors indicate current direction	5-34
Figure 5-24.	CH3D bottom currents for Alternative 03 (14 August 1990 16:00). Filled contours indicate current magnitude, vectors indicate current direction	5-34
Figure 6-1.	Base alternative grid.....	6-17
Figure 6-2.	Option 1 grid	6-17
Figure 6-3.	Alternative 2 grid	6-18
Figure 6-4.	Alternative 3 grid	6-18
Figure 6-5.	MS DEQ observed station locations	6-19
Figure 6-6.	Calibration results for water quality constituents at sta 02480285 on West Pascagoula River	6-20

Figure 6-7.	Calibration results for water quality constituents at sta MS0 in Mississippi Sound	6-22
Figure 6-8.	Calibration results for water quality constituents at sta 640MSD03 in Mississippi Sound near Round Island.....	6-23
Figure 6-9.	Water quality calibration results at sta PR0248210 3 miles from mouth of East Pascagoula River.....	6-25
Figure 6-10.	Water quality calibration results at sta 2480215 located at mouth of East Pascagoula River	6-27
Figure 6-11.	Scatter plots.....	6-29
Figure 6-12.	Percent cumulative distribution curves of water quality constituents	6-31
Figure 6-13.	Comparison of CH3D results to CEQUAL-ICM results	6-33
Figure 6-14.	Comparison station locations and flow transect location for all options.....	6-38
Figure 6-15.	Comparison of Option 1 results to base results at six stations in study area	6-39
Figure 6-16.	Comparison of bottom DO results for base and Alternative 1 ...	6-45
Figure 6-17.	Comparison of bottom tracer results for base and Alternative 1 for West Pascagoula River release	6-45
Figure 6-18.	Comparison of bottom tracer results for base and Alternative 1 for East Pascagoula River release	6-46
Figure 6-19.	Comparison of Alternative 2 results to base results at six stations in study area	6-46
Figure 6-20.	Comparison of bottom DO results for base and Alternative 1 ...	6-52
Figure 6-21.	Comparison of bottom tracer results for base and Alternative 2 for West Pascagoula River release.....	6-53
Figure 6-22.	Comparison of bottom tracer results for base and Alternative 2 for East Pascagoula River release	6-53
Figure 6-23.	Comparison of Alternative 3 results to base results at six stations in study area	6-54
Figure 6-24.	Comparison of bottom DO results for base and Alternative 3 ...	6-60
Figure 6-25.	Comparison of bottom tracer results for base and Alternative 3 for West Pascagoula River release.....	6-60
Figure 6-26.	Comparison of bottom tracer results for base and Alternative 3 for East Pascagoula River release	6-61
Figure 7-1.	Mississippi Sound wave project area with bathymetry and nearshore measurement sites.....	7-2
Figure 7-2.	Nested grid system for Gulf of Mexico Wave hindcast.....	7-4
Figure 7-3.	Wave Rose for location southeast of Singing River Island in the Mississippi Sound for 1990-1999 wave hindcast.....	7-6

Figure 7-4.	Wave height comparison at a WIS Level 3 station and NDBC Buoy 42007 for January 1998.....	7-7
Figure 7-5.	Peak period comparison of WIS Level 3 with NDBC Buoy 42007 for January 1998	7-7
Figure 7-6.	Wave direction comparison of WIS Level 3 station with NDBC Buoy 42007 for January 1998.....	7-8
Figure 7-7.	Wave height and peak period comparison between sta 65 in Level 3 grid and NDBC Buoy 42015 for February of 1990	7-9
Figure 7-8.	Wind rose showing wind speeds and directions from 1987-2000 at Dauphin Island.....	7-11
Figure 7-9.	Comparison of WISWAVE and STWAVE wave heights with measurements at sta MS002 for April 2001	7-11
Figure 7-10.	Comparison of WISWAVE and STWAVE peak periods with sta MS002 measurements for April 2001	7-12
Figure 7-11.	Comparison of WISWAVE and STWAVE wave height with sta MS002 measurements for March 2001	7-13
Figure 7-12.	Comparison of simulated and measured peak periods for March 2001 at sta MS002, showing WISWAVE results using both Coamps and NCEP winds and STWAVE with Coamps winds.....	7-13
Figure 7-13.	Comparison of WISWAVE wave height with NDBC 42007 wave height for March 2001	7-14
Figure 7-14.	Comparison of WISWAVE peak period with buoy 42007 peak period for March 2001.....	7-14
Figure 7-15.	Comparison of WISWAVE wave direction with buoy 42007 wave direction for March 2001	7-15
Figure 7-16.	Comparison of WISWAVE wave height and measured wave height at sta MS001 for March 2001	7-15
Figure 7-17.	Comparison of WISWAVE peak period with measured peak period at sta MS001 for March 2001.....	7-16
Figure 7-18.	WISWAVE wave direction compared to measured wave direction at sta MS001 for March 2001	7-16
Figure 7-19.	Bar chart showing incident wave height and period characteristics, direction window from 135 to 144 deg	7-18
Figure 7-20.	Bar chart showing incident wave height and period characteristics, direction window from 145 to 154 deg	7-18
Figure 7-21.	Bar chart showing incident wave height and period characteristics, direction window from 155 to 164 deg	7-19
Figure 7-22.	Bar chart showing incident wave height and period characteristics, direction window from 165 to 174 deg	7-19
Figure 7-23.	Bar chart showing incident wave height and period characteristics, direction window from 175 to 184 deg	7-20

Figure 7-24.	Bar chart showing incident wave height and period characteristics, direction window from 185 to 194 deg	7-20
Figure 7-25.	Bar chart showing incident wave height and period characteristics, direction window from 195 to 204 deg	7-21
Figure 7-26.	Bar chart showing incident wave height and period characteristics, direction window from 205 to 214 deg	7-21
Figure 7-27.	Bar chart showing incident wave height and period characteristics, direction window from 215 to 224 deg	7-22
Figure 7-28.	Disposal alternatives	7-23
Figure 7-29.	Points along the 1-m contour	7-24
Figure 7-30.	Points near the Pascagoula navigation channels	7-24
Figure 7-31.	Wave height at alongshore points for incident wave 2.52 m at 9 sec.....	7-25
Figure 7-32.	Wave height at alongshore points for incident wave 0.61 m at 7 sec.....	7-25
Figure 7-33.	Wave height at alongshore points for incident wave 0.61 m at 6 sec.....	7-26
Figure 7-34.	Wave height at channel points for incident wave 2.52 m at 9 sec.....	7-26
Figure 7-35.	Wave height at channel points for incident wave 0.61 m at 7 sec.....	7-27
Figure 7-36.	Wave height at channel point for incident height 0.61 m at 6 sec.....	7-27
Figure 7-37.	Vector plots showing storm wave conditions 2.52 m, 9 sec, 180 deg	7-29
Figure 8-1.	Frequency of occurrence for Pascagoula, MS	8-5
Figure 8-2.	Storm surge hydrograph for station in close proximity to three disposal sites for Hurricane Carmen, September 1974.....	8-7
Figure 8-3.	Storm surge hydrograph for station in close proximity to three disposal sites for Hurricane Frederic, September 1979	8-7
Figure 8-4.	Storm surge hydrograph for station in close proximity to three disposal sites for Hurricane Georges, September 1998	8-8
Figure 8-5.	Storm surge hydrograph for station in close proximity to three disposal sites for Hurricane Juan, October 1985	8-8
Figure 8-6.	Tracks of the selected hindcast hurricanes in relation to Level 5 grid covering study area.....	8-10
Figure 8-7.	Interpolated hourly water level information from a site in close proximity to Singing River Island for each of selected hindcast hurricanes.....	8-12
Figure 8-8.	Wave height, period and direction and wind speed results for Hurricane Carmen at a location near Singing River	8-13

Figure 8-9. Wave height, period and direction and wind speed for Hurricane Frederic at a location near Singing River	8-14
Figure 8-10. Wave height period and direction for Elena at a location near Singing River.....	8-15
Figure 8-11. Wave height, period and direction and wind speed for Juan at a location near Singing River	8-16
Figure 8-12. Wave height, period and direction and wind speed for Hurricane Georges at a location near Singing River	8-17
Figure 8-13. Comparison of measured and computed wave height and peak period; NDBC 42007 and WIS Level 3 model.....	8-18
Figure 8-14. Track of Hurricane Carmen, September 1974	8-18
Figure 8-15. Wave height and period model results for Hurricane Carmen at a Level 3 grid point near its path	8-19
Figure 8-16. Wave height and period model results for Hurricane Carmen at a Level 5 grid point near Petit Bois Island.....	8-19
Figure 9-1. Locations of three alternative CDFs investigated in engineering studies	9-1
Figure D1. Current speed and direction at 2.0 m and 3.5 m above seafloor, and near-surface from 26 February to 15 March 2001 at sta MS_CM01	D2
Figure D2. Current speed and direction at 2.0 m and 3.5 m above seafloor, and near-surface from 15 to 22 March 2001 at sta MS_CM01.....	D3
Figure D3. Current speed and direction approximately 0.5 m above seafloor from 26 February to 18 April 2001 at sta MS_CM01.....	D4
Figure D4. Current speed and direction approximately 0.5 m above seafloor from 18-24 April 2001 at sta MS_CM01.....	D5
Figure D5. Current speed and direction at 2.0 m and 3.5 m above seafloor, and near-surface from 25 April to 12 May 2001 at sta MS_CM01	D6
Figure D6. Current speed and direction at 2.0 m and 3.5 m above seafloor, and near-surface from 12 May to 29 May 2001 at sta MS_CM01	D7
Figure D7. Current speed and direction at 2.0 m and 3.5 m above seafloor, and near-surface from 29 May to 15 June 2001 at sta MS_CM01	D8
Figure D8. Current speed and direction at 2.0 m and 3.5 m above seafloor, and near-surface from 15 June to 2 July 2001 at sta MS_CM01	D9
Figure D9. Current speed and direction at 2.0 m and 3.5 m above seafloor, and near-surface from 2 to 18 July 2001 at sta MS_CM01	D10
Figure D10. Current speed and direction approximately 0.8 m above seafloor from 25 April to 7 June 2001 at sta MS_CM02.....	D11
Figure D11. Current speed and direction 0.8 m above seafloor from 31 May to 19 July 2001 at sta MS_CM03	D12

Figure D12.	Horizontally-filtered, depth-averaged current profiles across Horn Island Pass on 27 February	D13
Figure D13.	Horizontally-filtered, depth-averaged current speed profiles across Horn Island Pass on 27 and 28 February	D14
Figure D14.	Horizontally-filtered, depth-averaged current speed profiles across Horn Island Pass on 28 February	D15
Figure D15.	Horizontally-filtered, depth-averaged current speed profiles across Horn Island Pass on 28 February	D16
Figure D16.	Horizontally-filtered, depth-averaged current speed profiles across Horn Island Pass on 28 February to 1 March.....	D17
Figure D17.	Horizontally-filtered, depth-averaged current speed profiles across Horn Island Pass on 1 March	D18
Figure D18.	Horizontally-filtered, depth-averaged current speed profiles across Horn Island Pass on 1 March	D19
Figure D19.	Horizontally-filtered, depth-averaged current profiles across Horn Island Pass on 20 June	D20
Figure D20.	Horizontally-filtered, depth-averaged current profiles across Horn Island Pass on 20 June	D21
Figure D21.	Horizontally-filtered, depth-averaged current profiles across Horn Island Pass on 20 June	D22
Figure D22.	Horizontally-filtered, depth-averaged current profiles across Horn Island Pass on 20 and 21 June	D23
Figure D23.	Horizontally-filtered, depth-averaged current profiles across Horn Island Pass on 21 June	D24
Figure D24.	Horizontally-filtered, depth-averaged current profiles across Horn Island Pass on 21 June	D24
Figure G1.	Grain-size distribution of Pascagoula sediment composite.....	G2
Figure G2.	Schematic of settling column	G5
Figure G3.	Pascagoula settling test	G6
Figure G4.	Compression settling curve	G9
Figure G5.	Pascagoula zone settling velocity curve.....	G9
Figure G6.	Flocculent settling test suspended solids relationship to time and depth below surface.....	G12
Figure G7.	Supernatant suspended solids curve.....	G12
Figure G8.	TSS versus turbidity curve	G15
Figure G9.	Self-weight consolidation test results for Pascagoula sediment	G15
Figure G10.	Time curves from standard oedometer consolidation test.....	G16
Figure G11.	Void ratio-effective stress relationship from standard oedometer consolidation test.....	G16

Figure G12. Combined void ratio-effective stress relationship.....	G17
Figure H1. Comparison of measured and modeled temperature and salinity at sta 0210.....	H2
Figure H2. Comparison of measured and modeled temperature and salinity at sta 0285.....	H3
Figure H3. Comparison of measured and modeled temperature and salinity at sta 0285 during April 1997.....	H4
Figure H4. Comparison of measured and modeled temperature and salinity at sta 0285 during July 1997	H5
Figure H5. Comparison of measured and modeled temperature and salinity at sta 0285 during September 1997	H6
Figure I1. Alternative 00, present conditions with island boundaries outlined in red.....	I2
Figure I2. Alternative 01, Singing River Extension.....	I2
Figure I3. Alternative 02, Island south of Singing River	I3
Figure I4. Alternative 03, Island in triangle between Pascagoula and Bayou Casotte Navigation Channels.....	I3

List of Tables

Table 2-1. Field Data Collection Durations	2-2
Table 2-2. Current Data Collection Locations	2-3
Table 3-1. Pascagoula Harbor Alternatives – Surface Areas	3-4
Table 3-2. Alternative 1 Filling Scenario.....	3-5
Table 3-3. Alternative 2 Filling Scenario.....	3-5
Table 3-4. Alternative 3 Filling Scenario.....	3-6
Table 3-5. PSDDF Parameters for Filling Simulations.....	3-10
Table 3-6. Pascagoula Harbor Sediment Characteristics	3-10
Table 3-7. Precipitation and Evaporation Rates at Pascagoula Harbor.....	3-11
Table 3-8. Consolidation Characteristics of Foundation Material and Dredged Material PH-2.....	3-14
Table 3-9. Pascagoula Harbor Alternatives – Dike Elevation Ranges.....	3-21
Table 3-10. Operating Efficiency Variable – Dike Elevation Ranges	3-21

Table 4-1.	Comparison of Peak Ebb Current at Station A During Winter Storm Events.....	4-16
Table 5-1.	Source(s) of Information for CH3D Boundary Conditions	5-10
Table 5-2.	CH3D Calibration/Verification Data	5-15
Table 6-1.	Water Quality Model State Variables.....	6-3
Table 6-2.	CEQUAL-ICM Grid Characteristics	6-5
Table 6-3.	Initial Conditions	6-5
Table 6-4.	Ocean Boundary Conditions.....	6-6
Table 6-5.	East Pascagoula Boundary Conditions	6-6
Table 6-6.	West Pascagoula Boundary Conditions.....	6-7
Table 6-7.	Net Flows Through Channel North of Singing River Island	6-12
Table 7-1.	Level 5 Output Save Stations	7-5
Table 7-2.	Wave Conditions Derived from 1990-1999 Wave Hindcast for Use in STWAVE Runs	7-22
Table 8-1.	Summary of Hurricanes	8-5
Table E1.	Consolidation Characteristics of Foundation Material and Dredged Material PH-2.....	E2
Table E2.	Consolidation Characteristics of Foundation Material and Dredged Material PH-4.....	E3
Table E3.	Consolidation Characteristics of Foundation Material and Dredged Material PH-5.....	E4
Table E4.	Consolidation Characteristics of Foundation Material and Dredged Material PH-6.....	E5
Table E5.	Consolidation Characteristics of Foundation Material and Dredged Material PH-10.....	E6
Table G1.	Sediment Physical Characteristics	G3
Table G2.	Total Solids Concentration of Column Slurry Sample	G5
Table G3.	Compression Settling Test Data	G8
Table G4.	Zone Settling Test Data	G10
Table G5.	Flocculent Settling Test Data.....	G11
Table G6.	Recommended Resuspension Factors For Various Ponding Areas and Depths.....	G13
Table G7.	TSS Concentrations and Turbidity Measurements	G14

Conversion Factors, Non-SI to SI Units of Measurement

Non-SI units of measurement used in this report can be converted to SI units as follows:

Multiply	By	To Obtain
acres	4,046.873	square meters
cubic yards	0.7645549	cubic meters
feet	0.3048	meters
inches	2.54	centimeters
pounds (force) per square foot	47.88026	pascals
miles (U.S. statute)	1.609347	kilometers
square miles	2,589,998	square meters

Preface

This report describes a multidisciplinary study conducted by the U.S. Army Engineer Research and Development Center (ERDC) to assist the U.S. Army Engineer District, Mobile in the evaluation of nearshore and island Confined Disposal Facility (CDF) placement options being considered for the Dredged Material Management Plan (DMMP), Pascagoula River Harbor, Pascagoula, MS. This effort involved circulation, wave, hurricane, and water quality studies supplemented by prototype data collection to assist in the design of the structures and evaluate their respective impacts in the study area.

The study was conducted for the Mobile District by the ERDC Coastal and Hydraulics Laboratory (CHL) and Environmental Laboratory (EL). Mr. John Crane was the project manager, Ms. Kimberly Otto (Mobile District) was the senior planner, and Ms. Linda Lillycrop (Mobile District) provided technical assistance and review of this report. Mr. Edmond Russo of the U.S. Army Engineer District, New Orleans, provided review of the report.

The ERDC study team project manager was Mr. Timothy Welp (CHL) with technical direction provided by Mr. Bruce Ebersole (CHL). Contributors to this report were Mr. Michael Tubman, Mr. Sam Corson, and Mr. Patrick McKinney (CHL) for prototype measurement; Dr. Paul Schroeder, Mr. Steve Pranger, and Mr. Michael Channell (EL) for dredged material consolidation and CDF sizing; Mr. David Mark and Mr. Jarrell Smith (CHL) for circulation and three-dimensional hydrodynamic studies; Dr. Barry Bunch and Ms. Dorothy Tillman (EL) for water quality studies; Ms. Barbara Tracy and Dr. Lihwa Lin (CHL) for wave and tropical storm studies, and Mr. Ebersole for study conclusions.

U.S. Coast Guard Station, Mobile, allowed wave gage telemetry systems to be installed on navigation channel range towers to collect the prototype wave and water level data.

Mr. Ebersole and Mr. Welp were the report technical editors. Ms. J. Holley Messing, Coastal Engineering Branch, CHL, completed final report word processing and formatting.

The study was conducted during the period January 2001 through March 2003 under the administrative supervision of Mr. Thomas W. Richardson, Director of CHL, and Dr. William D. Martin, Deputy Director, CHL.

COL James R. Rowan, EN, was Commander and Executive Director of ERDC. Dr. James R. Houston was Director.

1 Introduction

The U.S. Army Engineer District, Mobile, is in the process of developing a Dredged Material Management Plan (DMMP) for the Federal navigation project at Pascagoula, MS. The navigation project services two commercial harbors, the Pascagoula River Harbor and the Bayou Casotte Harbor, as well as the U.S. Navy/Naval Station, Pascagoula. The harbors are all situated on the northern coastline of the Mississippi Sound, near the entrance to the East Pascagoula River (Figure 1-1). Both the Pascagoula River Harbor and the U.S. naval facilities are located at the mouth of the East Pascagoula River; the Bayou Casotte Harbor is located approximately 4.83 km (3 miles)¹ east of the East Pascagoula River entrance. A single entrance channel extends from the Gulf of Mexico northward between Horn and Petit Bois Islands, passing just to the west of Petit Bois Island, to the center of Mississippi Sound just south of Bayou Casotte. At that point, the channel bifurcates. One branch, the Bayou Casotte Channel heads north to Bayou Casotte Harbor. The other branch, the Main or Upper Pascagoula Channel, veers to the northwest toward the entrance to Pascagoula River Harbor (Figure 1-1).

At the request of the Mobile District, the U.S. Army Engineer Research and Development Center (ERDC), was asked to perform a number of engineering studies in support of the District's efforts to develop a DMMP for Pascagoula. Formulation of the DMMP requires identification and evaluation of a range of options for disposing of sediment that will be dredged as a result of both continued maintenance of the authorized navigation channel and any future new dredging work. The future dredging requirement for the project is estimated to be 3 to 4 million cu yd every 3 years.

Among various disposal options, consideration is being given to construction of an island confined disposal facility (CDF) adjacent to the navigation channel where the majority of sediment is dredged. The channel section with the greatest dredging requirement is located between mile markers 2 and 5 of the Main Pascagoula Channel leading to the Pascagoula River Harbor and the naval facilities. A CDF is being considered at three possible locations near this section of channel (Figure 1-2): (a) an expansion of Singing River Island on its south and southwest sides (Alternative 1), (b) an island just to the northeast of Round Island and southeast of Singing River Island, between Round Island and the navigation channel (Alternative 2), and (c) north of the point where the

¹ Units of measurement in the text of this report are shown in SI units or SI units followed by non-SI units in parenthesis. A table of factors for converting non-SI units of measurement used in figures and tables is presented on page xvii.

navigation channel bifurcates, between the bifurcation point and the mainland (Alternative 3). Most of the engineering study tasks performed by ERDC pertained to the island CDF alternative.

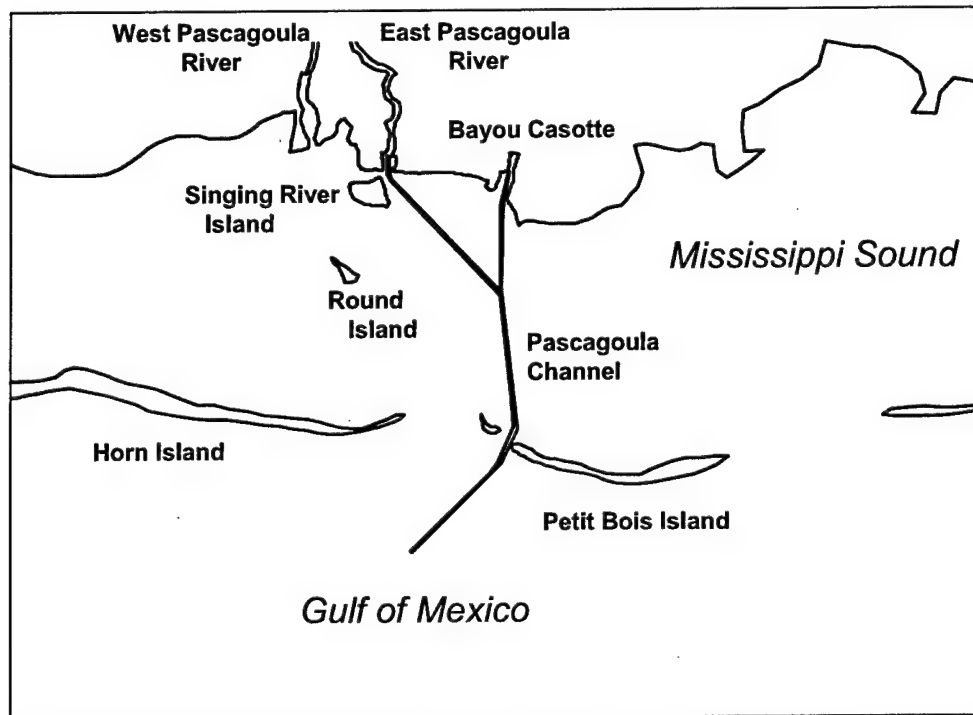


Figure 1-1. Site map showing the Pascagoula Navigation Project vicinity

Consideration of an island CDF has raised questions regarding the potential negative impacts of an island on water circulation and water quality. The influences of changes to circulation patterns on navigation and sediment transport processes are also of concern. Numerical modeling of circulation and water quality was performed to examine these potential impacts of an island. A two-dimensional (2-D) hydrodynamic modeling approach was adopted to simulate circulation in the northern Gulf of Mexico and the entire Mississippi Sound. This model provided boundary conditions to more detailed three-dimensional (3-D) modeling of circulation and water quality in the vicinity of the proposed CDF sites.

Construction of an island CDF will also influence the nearshore wind wave climate at the site, particularly in the sheltered lee of an island. Numerical wave modeling was performed both to assess the impact of an island on wave conditions along adjacent beaches and in the navigation channels, and to characterize the local wave climate for use in design of any shore protection measures that would be built around the periphery of an island to protect it from erosion.

Measurements of waves, currents, and water levels were made to aid in characterizing the hydrodynamic environment at and near the proposed CDF sites. Measured data were also used to assess the accuracy of the numerical models that were developed and applied in this study.

Sediments placed in an island CDF will consolidate with time, and consolidation is a key parameter in determining the capacity of an island CDF. A number of studies were performed to examine the sediment consolidation process and to assess the site capacity of the CDFs. Results of this study have implications concerning the degree of site management that is needed to increase storage capacity of the CDF.

Individual study tasks are presented in greater detail in subsequent chapters. Chapter 2 discusses the field data collection project that was undertaken to acquire wave, current, and water level data for model validation purposes and to characterize environmental conditions near the proposed island CDF sites. Chapter 3 presents the work done to investigate consolidation of dredged material and sizing of the CDF to accommodate the desired sediment volume. Results of the tidal circulation studies, using the 2-D depth-averaged modeling approach, are presented in Chapter 4; and more detailed 3-D modeling of water circulation and water quality are discussed in Chapters 5 and 6, respectively. Modeling of surface wind waves is discussed in Chapter 7. Chapter 8 documents work done to quantify the wave and circulation conditions at the island CDF sites under severe tropical storm conditions. A summary of the work and conclusions derived from it are discussed in Chapter 9.

2 Field Data Collection and Analysis

Introduction

The Pascagoula DMMP measurement program was conducted by ERDC in cooperation with Evans Hamilton, Inc. (EHI), under task order contract to ERDC. The program incorporated measurements of wind waves, water levels, and currents. Bottom-mounted wave and water level instruments, both internally recording and near-real-time, were deployed in the Gulf of Mexico and in the Mississippi Sound. Internal recording current meters were bottom-mounted for select periods of time at three locations in the Mississippi Sound, and over-the-side current profile transects were conducted across Horn Island Pass. Table 2-1 outlines the wave instrumentation deployment intervals and Figure 2-1 indicates the wave data collection stations. Table 2-2 outlines the current data collection locations and depths, and Figure 2-2 illustrates the current meter mooring locations.

Data collection was conducted both for project specific objectives, and for documenting and establishing the existing climatology as a baseline for future projects in the region. Project-specific objectives primarily concerned acquisition of data to assess the validity of numerical simulations and to provide measurements of non-modeled forces, i.e., vessel wakes. The data collection program was initially developed at ERDC with input from the Mobile District and EHI to meet the project objectives, including selection of types of instrument, sampling rates and bursts, and deployment lengths.

Wave Measurements

To provide ERDC modeling efforts with prototype wave data to meet the compressed milestones, a combination of directional and nondirectional wave measurements were made during the Pascagoula data collection effort. Two wave-gaging stations were established as shown by Figure 2-1.

Table 2-1**Wave Field Data Collection Durations**

Gage Type	Location	Collection Type	Parameters Collected	Deployment Dates
Civil Tec, Inc., 2-D Gage	Gulf of Mexico	Internal	Directional Wave Statistics	2/26/01 - 4/26/01
			Water Level	
Seapac 1-D Gage	Mississippi Sound	Internal	1-D Wave Statistics	2/27/01 - 7/15/01
			Water Level	
Seapac 1-D Gage	Mississippi Sound	Internal	1-D Wave Statistics	4/25/01 - 5/28/01
			Water Level	
Civil Tec, Inc., 2-D Gage	Mississippi Sound	Real-Time	Directional Wave Statistics	6/21/01 – lost
			Water Level	
Civil Tec, Inc., 2-D Gage	Gulf of Mexico	Real-Time	Directional Wave Statistics	10/24/01 – 12/11/03
			Water Level	

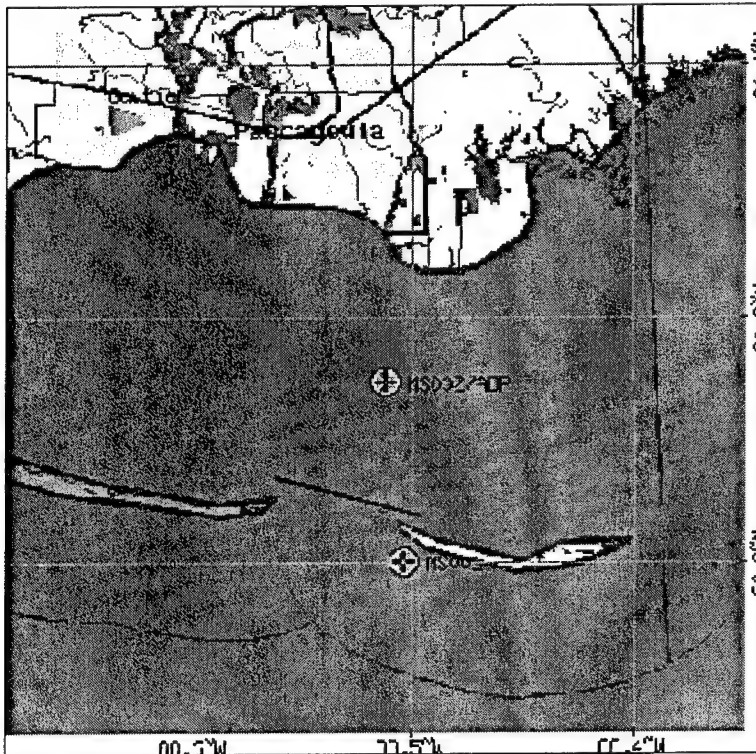
**Figure 2-1. Wave gage and current meter locations**

Table 2-2
Current Data Collection Locations

Name	Location	Depth
MS_CM01	30°16.42'N 88°30.77'W	6.1 m
MS_CM02	30°19.00'N 88°35.01'W	2.5 m
MS_CM03	30°18.40'N 88°30.88'W	2.5 m

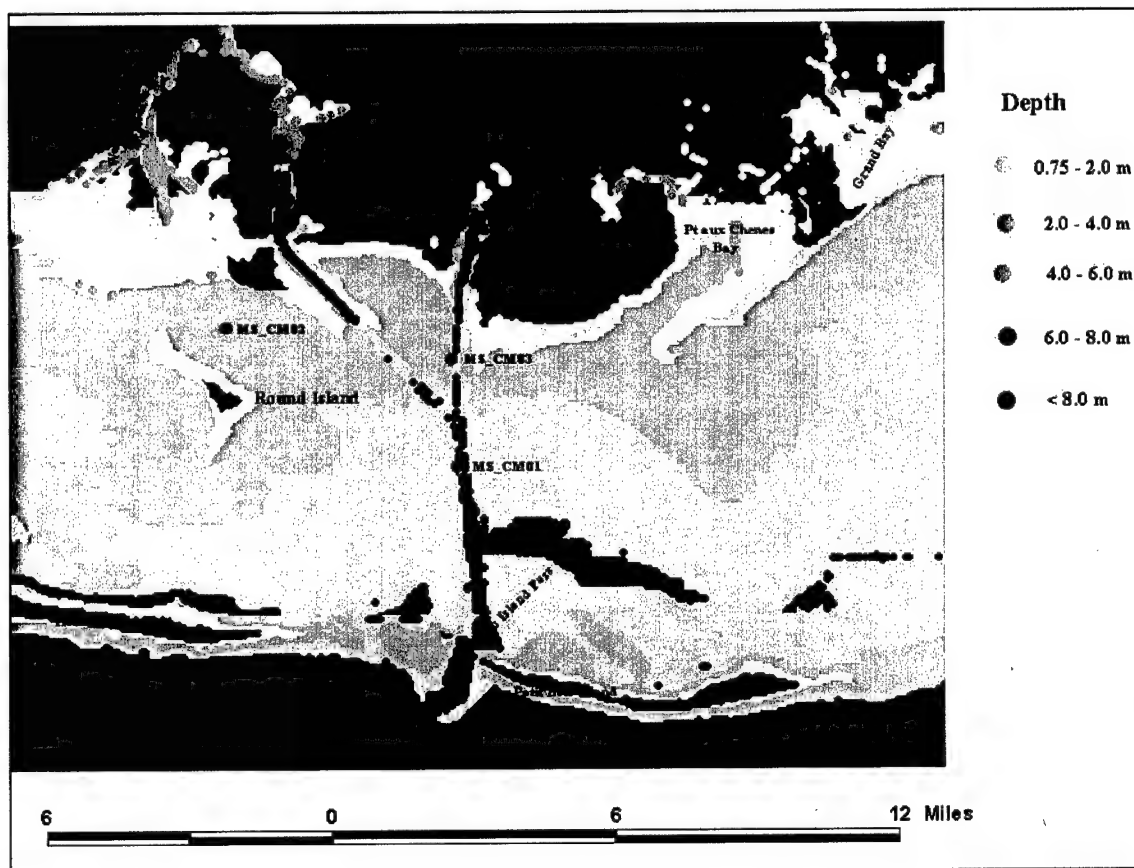


Figure 2-2. Current-meter mooring locations

Gulf of Mexico Wave Gage (sta MS001)

In order to have measured data available to begin validation of the numerical models, the Gulf of Mexico gage (sta MS001) was initially installed in early 26 February 2001 as a self-contained Civil Tec, Inc. wave gage (Figure 2-3). The Civil Tec, Inc. gage measured three channels of pressure data hourly at 1 Hz with a record length of 2,048 sec and stored analyzed data only. This gage was retrieved, downloaded, and another Civil Tec, Inc. gage was deployed as a near-real-time, water-level and directional wave gage on 26 April 2001. The near-real-time capability provides assurance of quality data collection and allows the user to receive wave conditions for operational or extreme event situations. This gage was deployed in the Gulf of Mexico approximately 2,000 ft offshore Petit Bois Island near Horn Island Pass at a depth of about 18 ft at 30.206°N 88.504°W. Station MS001 measured directional wave data hourly at 1 Hz with a record length of 2,048 sec. The gage was cabled to a Remote Terminal Unit (RTU) mounted on a U.S. Coast Guard range tower on Petit Bois Island. The RTU was a battery/solar panel-powered shore station (shown in Figure 2-4) that temporarily stored data, and transferred it via cell-telephone to ERDC for further processing. Shortly after installation, this RTU, along with all the navigational aids on the range tower, sustained damage from a lightning strike. It was replaced with a new RTU on an isolated mounting platform constructed and installed specifically for this study to reduce the probability of lightning strikes (Figure 2-5). Station MS001 was pulled in December 2003. Data are available through July 17, 2002.

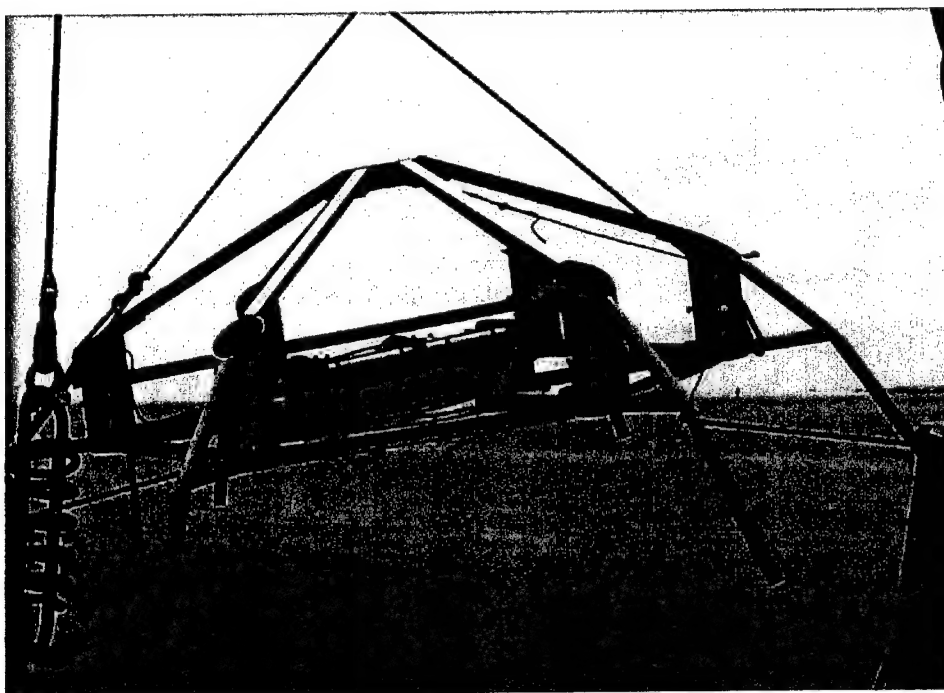


Figure 2-3. Deployment of Gulf of Mexico self-contained wave gage (sta MS001)

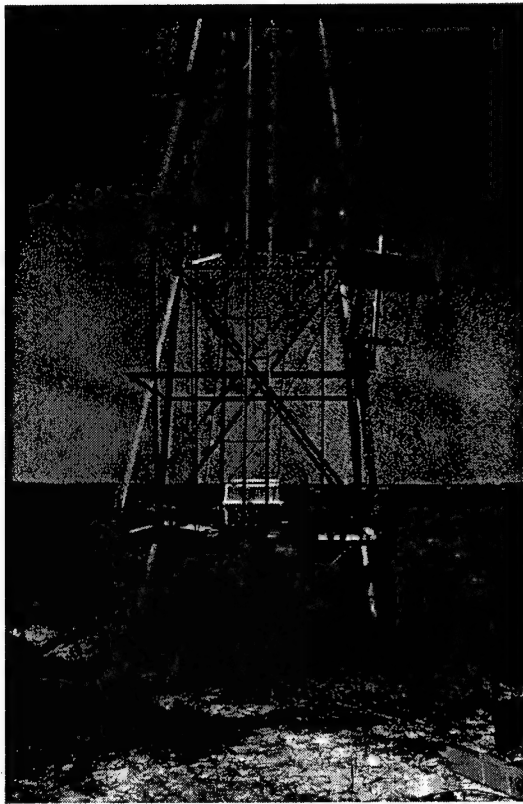


Figure 2-4. Remote Terminal Unit (RTU) on Petit Bois Island



Figure 2-5. Redesigned RTU for minimizing lightning-strike induced damage

Mississippi Sound Wave Gages (sta MS00N and MS002)

To meet time requirements to have measured data for numerical model validation in early 2001, two nondirectional internal-recording wave gages were deployed in 27 February 2001 (one for redundancy) in the Mississippi Sound (sta MS00N). They were mounted on a platform deployed by a support vessel and divers on the sound bottom (Figure 2-6). These gages were self-contained SeaPac systems, each with a Paroscientific, Inc. digi-quartz pressure sensor that measured one channel of pressure data hourly at 4 Hz with a record length of 1,024 sec. Sta MS00N was deployed at a depth of about 4.57 m (15 ft) adjacent to a Pascagoula Channel marker at 30.27°N 88.51°W. The deployment location was selected to balance the following objectives: placement of the gage in an optimal location in the Mississippi Sound for characterizing wave climatology, minimizing the chance of instrument damage or loss by shrimp trawlers, and minimizing wave-pressure fluctuation depth attenuation. Sta MS00N was retrieved 15 July 2001, and downloaded and analyzed at ERDC.

Sta MS00N was replaced by a near-real-time, water-level and directional Civil Tec, Inc. wave gage on 21 June 2001 and was redesignated as sta MS002. Sta MS002 was deployed in the Mississippi Sound approximately 4.57 m (15 ft) from the Pascagoula range marker "B" platform at 30.28°N 88.51°W. This location was selected for the same reasons previously mentioned, in addition to having a structure to mount the RTU on as shown in Figure 2-7. Sta MS002 measured/measures directional wave data hourly at 1 Hz with a record length of 2,048 sec. Communication problems were encountered with the RTU that, due to funding constraints, were not fixed. Although, the gage is designed to store analyzed data internally when this situation arises and the data gap was to be restored once the gage was retrieved, a tropical storm destroyed the range marker and the gage was lost.

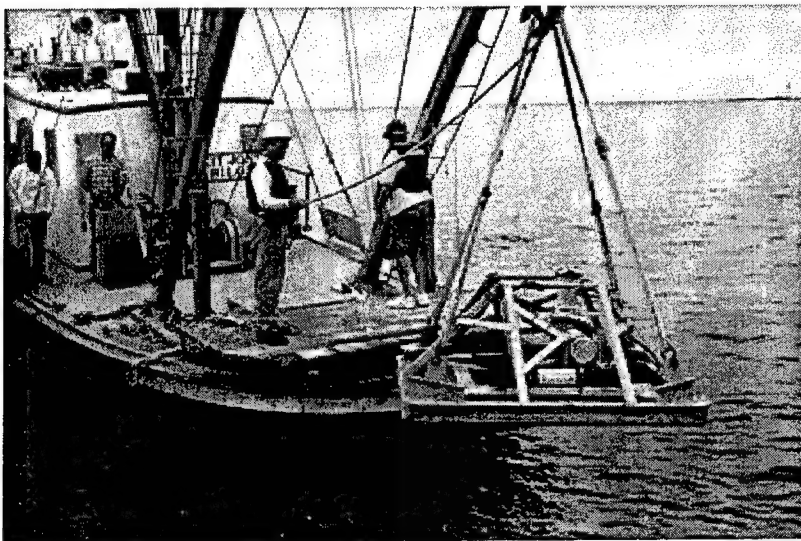


Figure 2-6. Deployment of Mississippi Sound wave gages

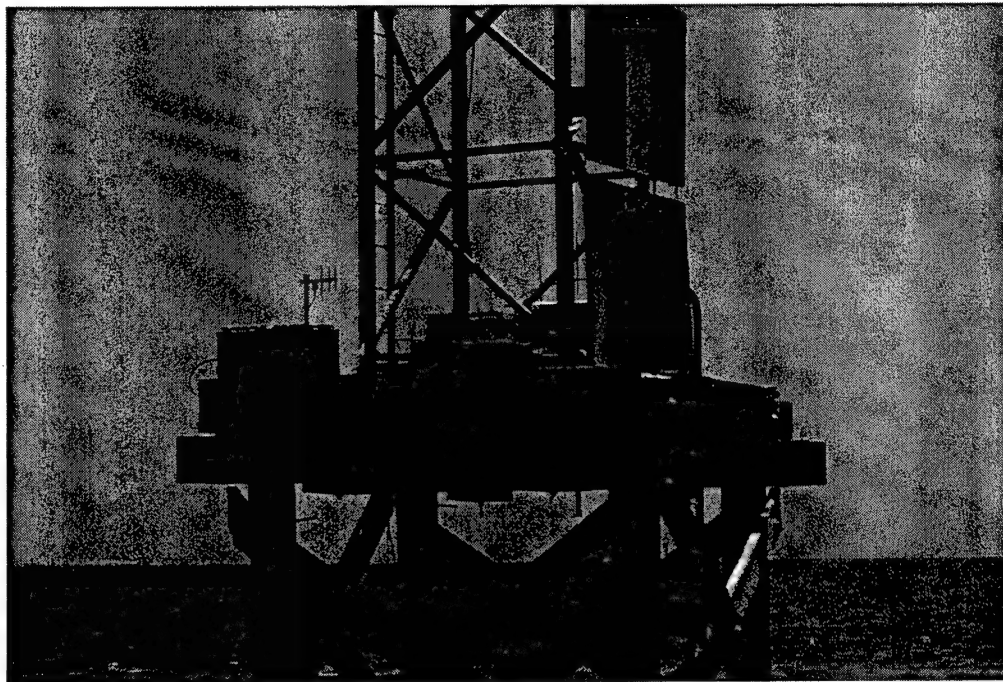


Figure 2-7. Station MS002 RTU installed on U.S. Coast Guard range marker

Data Analysis

Gulf of Mexico wave gage (sta MS001)

For February through April 2001, data for sta MS001 were collected and analyzed internally in the Civil Tec, Inc. gage using Civil Tec, Inc. analysis software. Results were reported for each hour. Data at sta MS001 were collected using the near-real-time RTU system after October 2001. These data were analyzed at ERDC. The analysis method uses the three raw pressure time series to determine time series of water slope between the sensors resulting from the passing waves. These three time series give an indication of the direction from which the waves at different frequencies are coming. This analysis also uses a Welch segmenting approach with 31-50 percent overlapping segments of 128 sec each, which results in a frequency resolution of 0.0078125 Hz. The standard pressure response criteria are applied. Data for sta MS001 are presented in Appendix B.

Mississippi Sound wave gages (sta MS00N and MS002)

Spectral analysis on the data for the SeaPac systems at sta MS00N utilized the Welch segmenting approach with 15-50 percent overlapping segments of 128 sec each, which resulted in a frequency resolution of 0.0078125 Hz. The results of analysis for each segment were averaged to obtain stability. Whenever subsurface pressure sensors are used to collect data, subsurface spectral results must be pressure compensated to obtain the surface spectral estimate. The standard analysis practice is to calculate a pressure compensation value for each frequency and mean water depth and terminate frequency analysis whenever this value becomes large. This pressure response cutoff practice helps prevent an overestimate of energy in very short period waves. For sta MS00N, the standard method calculated a high frequency cutoff of 0.3 Hz (3.3 sec). In an effort to obtain more of the small, short-period wave portion of the energy spectrums, the standard cutoff criteria were eliminated. Energy spectrums were calculated below 2 sec for all wave burst and were plotted for individual examination of their respective spectral tails. Through visual observation, it was determined that a cutoff of 0.45 Hz (2.2 sec) could be utilized for this analysis. With the selected sampling scheme, sta MS00N also recorded vessel wakes generated by large vessels and other boat traffic in the vicinity. Figures 2-8 and 2-9 show example plots of time series for records of vessel wakes. Plots for sta MS00N are presented in Appendix B.

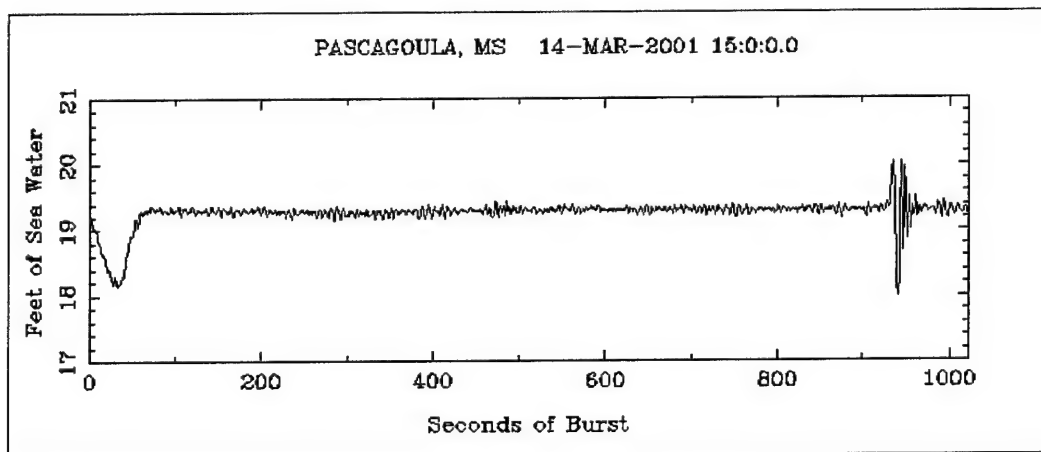


Figure 2-8. Example vessel wake time series for 14 March 2001

Station MS002 measured directional wave data hourly at 2.5 Hz with a record length of 2,048 samples or 819 sec. The analysis method is similar to sta MS001, except that the Welch segmenting approach was used 7-50 percent overlapping segments of 204.8 sec each, which results in a frequency resolution of 0.00488 Hz. The standard pressure response criteria were applied. Plots for sta MS002 are presented in Appendix C.

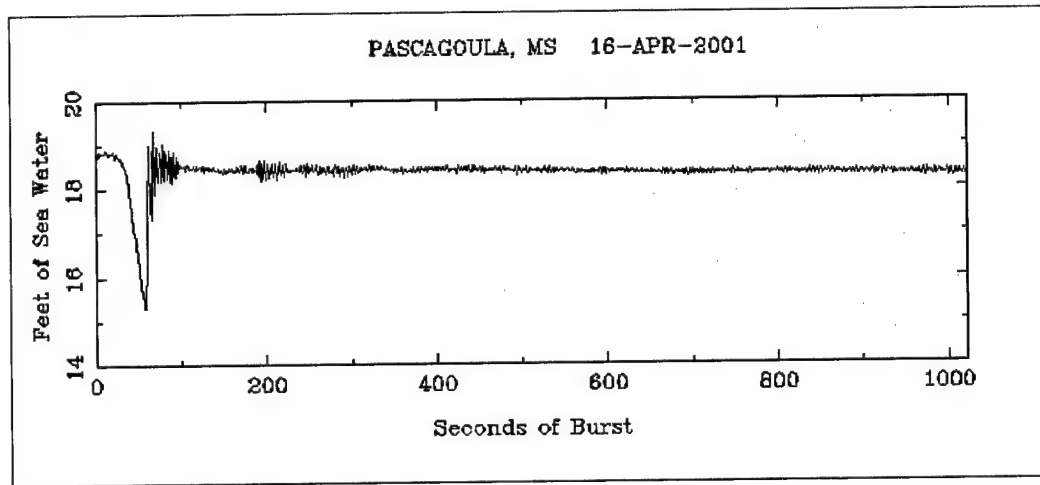


Figure 2-9. Example vessel wake time series for 16 April 2001

Current measurements

To define the current regime within the Mississippi Sound study area, two measurement strategies were used. Current meters were moored at three locations to collect current profiles and point measurements, and secondly, to define variations and define the net movement of water between Petit Bois Island and Horn Island (Horn Island Pass), transect data were collected with a profiling Acoustic Doppler Current Profiler (ADCP).

Moored current measurements

The three current-meter mooring locations are shown in Figure 2-2. Their names, location coordinates, and approximate depths are given in Table 2-2.

From 26 February to 24 April 2001, sta MS_CM01 (wave sta MS00N) was instrumented with two current meters. They were an upward-looking Sontek Acoustic Doppler Profiler (ADP), and a Nortek Aquadopp current meter. The mooring arrangement is shown in Figure 2-10. The ADP and its battery pack have yellow housings, and the Aquadopp is to the left in its black and gray housing. From 15 March to 25 April 2001, the ADP failed to collect data, and from 25 April to 18 July 2001, the Aquadopp was not part of the mooring at sta MS_CM01. The ADP collected data in 0.5-m bins from near the sensor head (4.6-m depth), to near the surface, thereby producing current profiles that were 5 min averages recorded every 12.5 min. The Aquadopp was angled downward to measure currents at a single location approximately 0.5 m above the seafloor (i.e., a depth of 5.6 m). It recorded a 5-min average every 13.33 min.

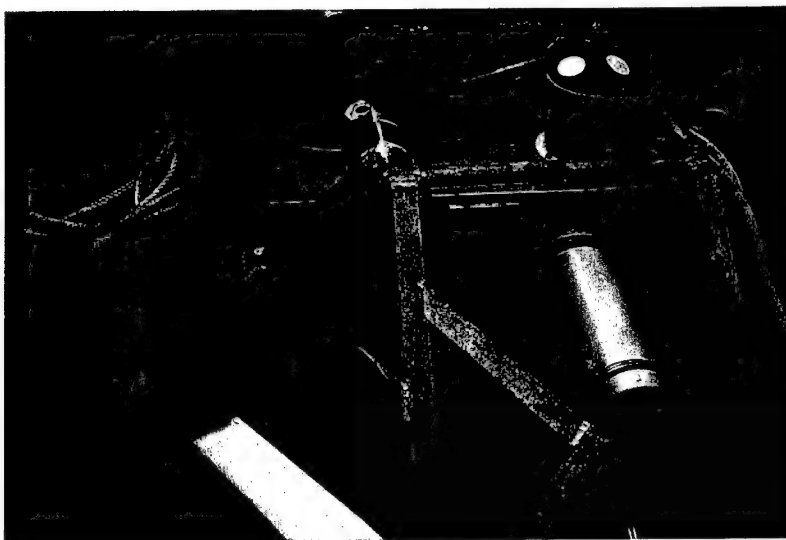


Figure 2-10. Acoustic Doppler Profiler (ADP)

In April, the Aquadopp used in sta MS_CM01 was moved to MS_CM02, and placed on a different mooring mount. At this location, the Aquadopp recorded 5-min averages every 20 min at a depth of approximately 1.7 m. Data were collected from 25 April to 7 June 2001.

From 31 May to 19 July 2001, a Sontek Acoustic Doppler Velocimeter (ADV) was deployed at sta MS_CM03. This current meter records current velocity at a single point, which in this mooring, was at a depth of 1.7 m. Data were recorded as 5.33 min averages every 45 min.

Plots of all these data are shown in Appendix D.

Transects of near-surface to near-bottom current profiles were collected approximately every hour for nearly 50 hr across Horn Island Pass (i.e., between Petit Bois and Horn islands) from 27 February to 1 March 2001, and again from 20-21 June 2001. The February-March cruise was during diurnal neap tides, and the June cruise was during diurnal spring tides. During the February-March cruise, current velocity was collected in 0.25-m bins, and in June in 0.5-m bins, using a 1,200-kHz RDI Broad Band Acoustic Doppler Current Profiler (BBADCP) mounted over-the-side of a survey vessel, as shown in Figure 2-11. Navigation information was obtained with a Trimble Global Positioning System (GPS) with differential correction. Profiles were recorded approximately every 2.7 sec, which corresponded roughly to every 7 m along the transect track. The RDI data acquisition software calculated the total ebb or flood transport through the pass. Horizontally-filtered, depth-averaged current speed profiles across Horn Island Pass, and the transports through the Pass are shown in Appendix D. Average values of depth-averaged, horizontally-filtered current speeds are shown in Figures 2-12 and 2-13.

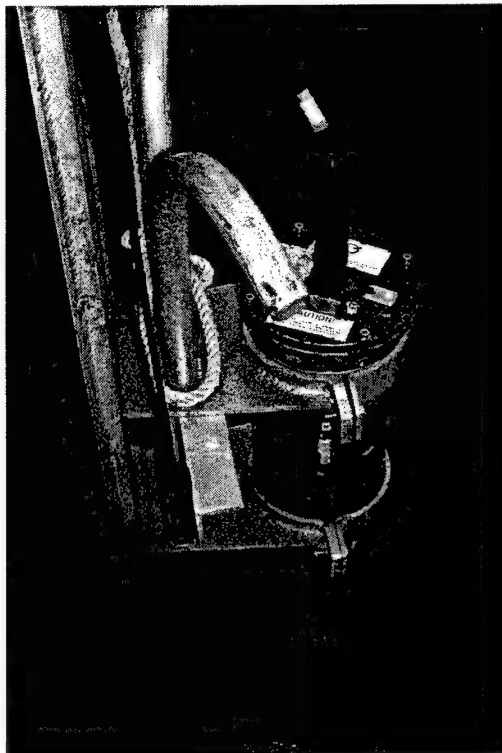


Figure 2-11. Over-the-side Acoustic Doppler Current Profiler (ADCP)

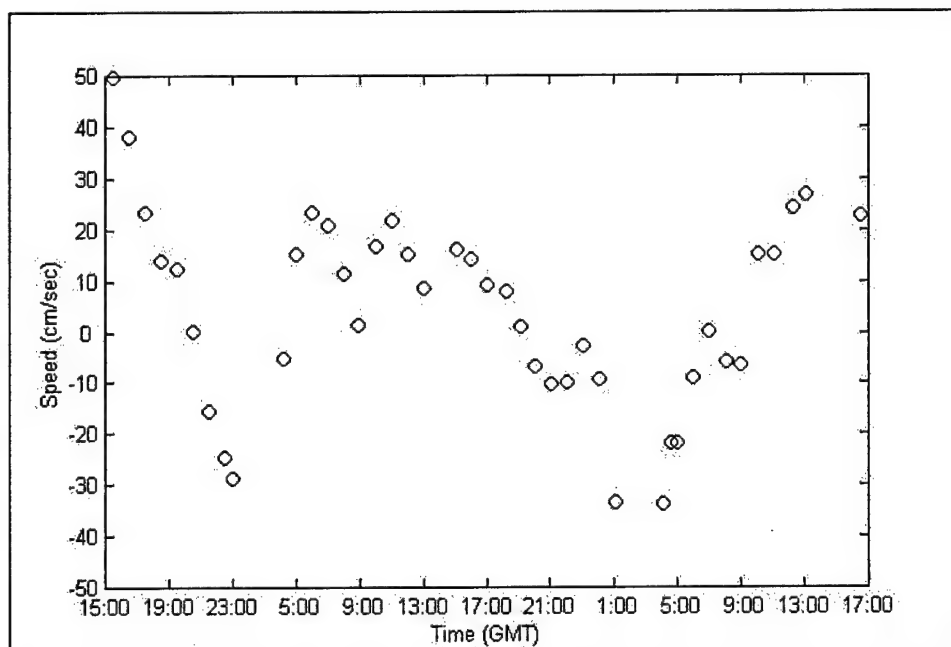


Figure 2-12. Average values of depth-averaged, horizontally-filtered current speeds across Horn Island Pass on 27 February – 1 March 2001. Negative speeds represent ebb currents, and positive values represent flood currents

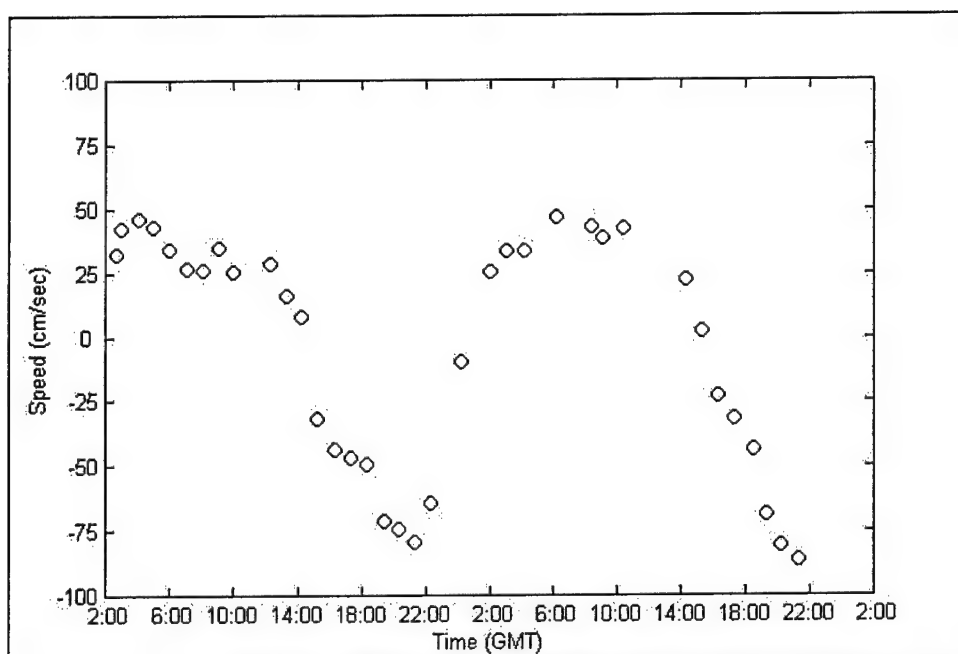


Figure 2-13. Average values of depth-averaged, horizontally-filtered current speeds across Horn Island Pass on 21 and 22 June 2001. Negative speeds represent ebb currents, and positive values represent flood currents

Description of observed currents

In this description of the observed currents, current directions were the directions currents were going toward, and wind directions are given as the directions winds were coming from. Figure 2-14 shows current speeds and directions at sta MS_CM01 and MS_CM02 from 26 April to 4 May 2001, and the wind speeds and directions for the same period at Dauphin Island, AL, and at the National Oceanographic and Atmospheric Administration (NOAA) data buoy NDBC 42007. This buoy is located approximately 22 n.m. south-southeast of Biloxi, MS. At the bottom of the plot shown in Figure 2-14, are the predicted tidal heights at Horn Island Pass. During this period, there was an obvious pattern of diurnal tidal currents. Current directions at sta MS_CM01 were rotary, while at sta MS_CM02, the tidal flow was east-west. During the period around 28 April diurnal spring tides were present, and from 27-30 April, the winds were light and variable. The onset of stronger steady winds from the east to southeast, and weaker tides on 30 April limited the tidal currents at sta MS_CM01 to southward to northwestward flow. The maximum current speeds observed when the currents were tidally dominated were on 29 April and were 29 cm/sec at sta MS_CM01, and 22 cm/sec at sta MS_CM02.

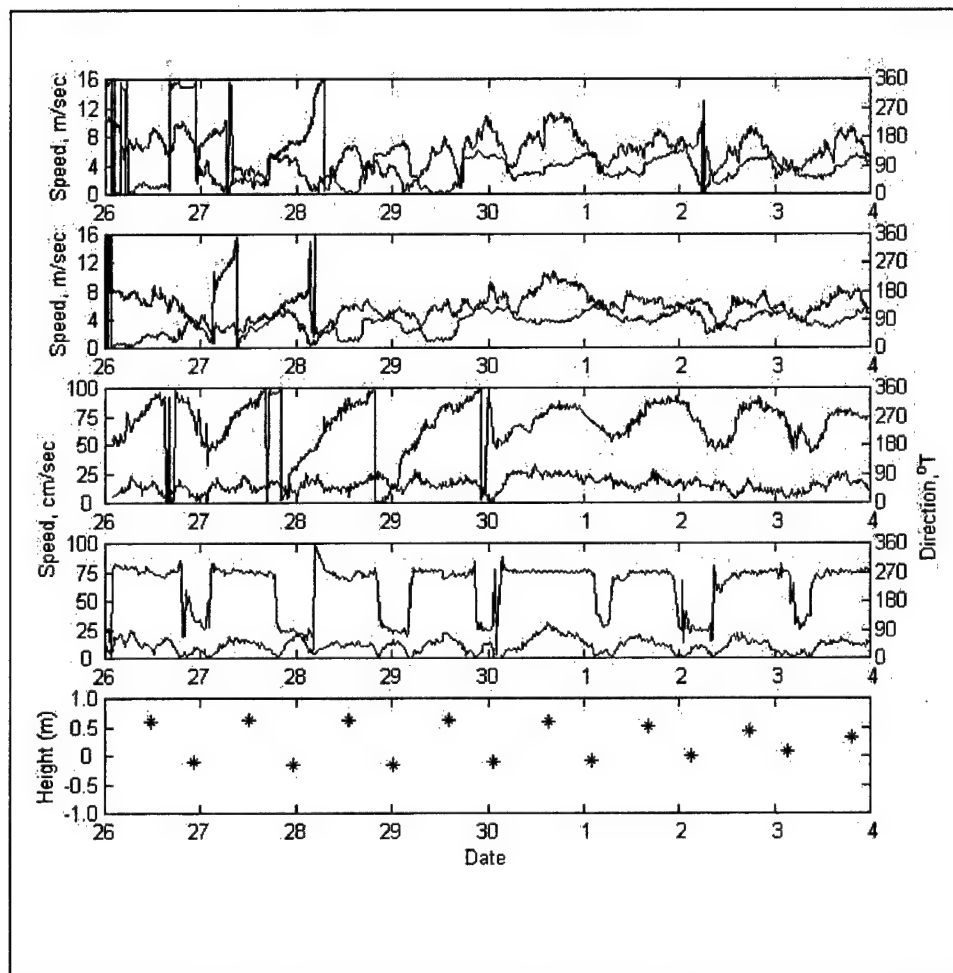


Figure 2-14. Speed (black) and direction (red) from 26 April to 4 May 2001 (from top to bottom) for wind at Dauphin Island, AL (30.25°N, 88.07°W), NDBC 42007 (30.09°N, 88.77°W), and for current at sta MS_CM01, 3.5 m above seafloor, and sta MS_CM02, and predicted tidal height at Horn Island Pass

Sustained southwest winds can make the tidal currents nearly unrecognizable on the basis of current directions. Figure 2-15 shows a period from 18-26 May where a pattern of steady southwest winds was broken by northwest winds from approximately midday on 22 May to midday on 23 May. At the top of Figure 2-15 are wind speed and direction at NDBC 42007, followed by current speed and direction at sta MS_CM01, 2.0 m above the seafloor and near-surface, current speed and direction at sta MS_CM02, and current speed and direction right at the surface from CODAR data taken approximately in the middle of the sound, 12 n.m. west of sta MS_CM01 (MS_NGLI 7). The southwest winds drove currents steadily to the east near-surface at sta MS_CM01, and also at MS_CM02 and MS_NGLI7. Current speeds showed some apparent tidal response, but not with a well-defined diurnal period. When the wind switched to

the northwest, nearly rotary current directions returned at sta MS_CM01 near-surface, and at MS_NGLI7. East-west flow was re-established at sta MS_CM02. When the southwest winds returned, steady eastward flow was again present at sta MS_CM01 and MS_CM02.

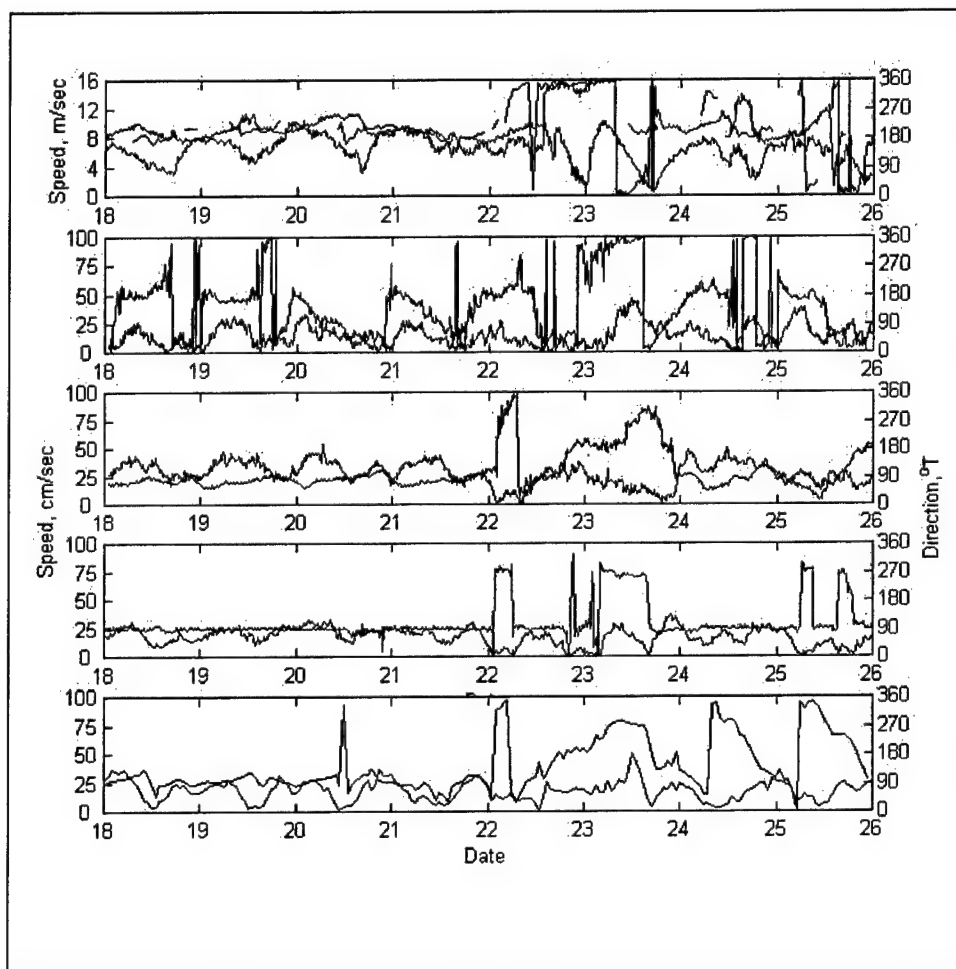


Figure 2-15. Speed (black) and direction (red) from 18-26 May 2001 (from top to bottom) for wind at NDBC 42007 (Gulfport wind direction in blue), and for current at sta MS_CM01, 2.0 m above seafloor, sta MS_CM01, near-surface, sta MS_CM02 and MS_NGLI7 (30.2939°N, 88.7495°W)

Figure 2-16 shows how complex the current response can become with changing winds. At the top of Figure 2-16 are wind speed and direction at Dauphin Island, followed by current speed and direction at sta MS_CM01 near-surface, 3.5 m above the seafloor, 2.0 m above the seafloor, and approximately 0.5 m above the seafloor. Particularly noteworthy was an occurrence of a strong, east-wind event which started late in the day on 14 May and continued until the early hours of 15 May. The current response in the form of a speed increase was seen in the near-surface record first, and was progressively observed in the records for the deeper layers. This increased flow appeared to be toward the south. West winds, which occurred on 16 May, drove sustained northeastward flow near-surface, with significant shear with depth. Currents near the bottom during this period were to the west. Figure 2-16 also shows the lack of response of currents at sta MS_CM01 to sustained north winds. These occurred from 17 May to the end of the record.

In general, the currents at sta MS_CM01 were wind-dominated. A tidal harmonic analysis of the data from this mooring accounted for only 7 percent of the variance. As a result, they were highly variable, and maximum speeds for the deployment period were recorded in March, which was the month with the highest wind speeds. During a period of strong west winds, the maximum observed current speeds at sta MS_CM01, 2.0 and 3.5 m above the seafloor were on 4 March. They were toward the northeast, and were 61 and 56 cm/sec, respectively. The near-surface current at this time was also to the northeast, with a speed of 71 cm/sec. The maximum near-surface current speed was 80 cm/sec (also toward the northeast) and occurred on 8 March. Why it occurred at this time was not clear, as the wind speeds were not large. The high speeds were only observed at the near-surface depth. At 2.0 and 3.5 m above the seafloor they were 9 and 12 cm/sec, respectively. It may be that vertical water-column stratification was a major factor at this time.

The presence of tidal currents at sta MS_CM02 was more obvious, but a harmonic tidal analysis of these currents still only accounted for about 7 percent of the variance. Each day of observed currents during the 25 April to 7 June deployment period was characterized by one maximum speed, typically between 20 and 30 cm/sec, and at least one near-zero speed. Current directions were typically a short period of eastward flow followed by a longer period of westward flow, as seen in Figure 2-14, but the pattern was regularly altered by wind, as seen in Figure 2-15. The maximum observed current speed at sta MS_CM02 was 39 cm/sec.

The situation at sta MS_CM03 was further complicated by the presence of oscillations with roughly a 5 cm/sec amplitude and a 3-hr period. Current directions were predominantly south-southeast and north-northwest. The maximum current speed was 40 cm/sec toward the southeast.

Current data for all these stations were presented in Appendix D.

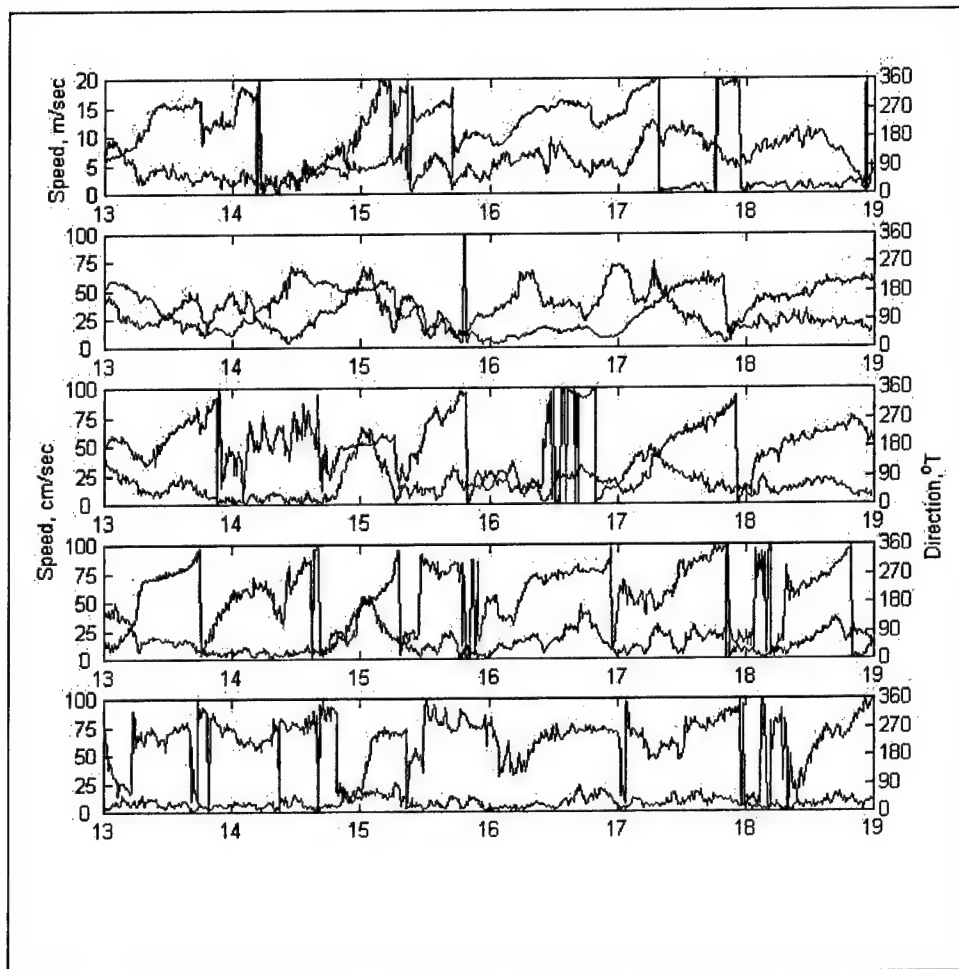


Figure 2-16. Speed (black) and direction (red) from 13-19 March 2001 (from top to bottom) for wind at Dauphin Island, AL, and for current at sta MS_CM01, near-surface, 3.5 m above seafloor, 2.0 m above seafloor, and approximately 0.5 m above seafloor

3 Confined Disposal Facility Alternatives – Diike Elevation Requirements

Introduction

Background

The Pascagoula Harbor (PH) and Pascagoula River channel has been dredged regularly over the past several decades. During that time, dredged material was placed in numerous CDFs located in or near Pascagoula Bay, MS. The Mobile District is investigating several alternative sites and configurations. 1,000-acre CDF alternatives of 4,046,825 sq m (1,000 acres) being investigated include: (a) an expansion of Singing River Island on its south and southwest sides (Alternative 1, see Figure 3-1), (b) an island just to the northeast of Round Island and southeast of Singing River Island, between Round Island and the navigation channel (Alternative 2), and (c) north of the point where the navigation channel bifurcates, between the bifurcation point and the mainland (Alternative 3).

Objective and scope

The overall objective of this work was to determine the required dike height of the proposed CDF sites. Each site has different dike configurations and some operations parameters were also changed as part of a sensitivity analysis.

The scope of the work consisted of two primary tasks.

- a. Determine the required dike height of the three sites based on specified operational parameters.
- b. Determine the required dike height by implementing various levels of site management (dewatering), reducing volumetric inflow and/or reducing the perimeter dike volumes.

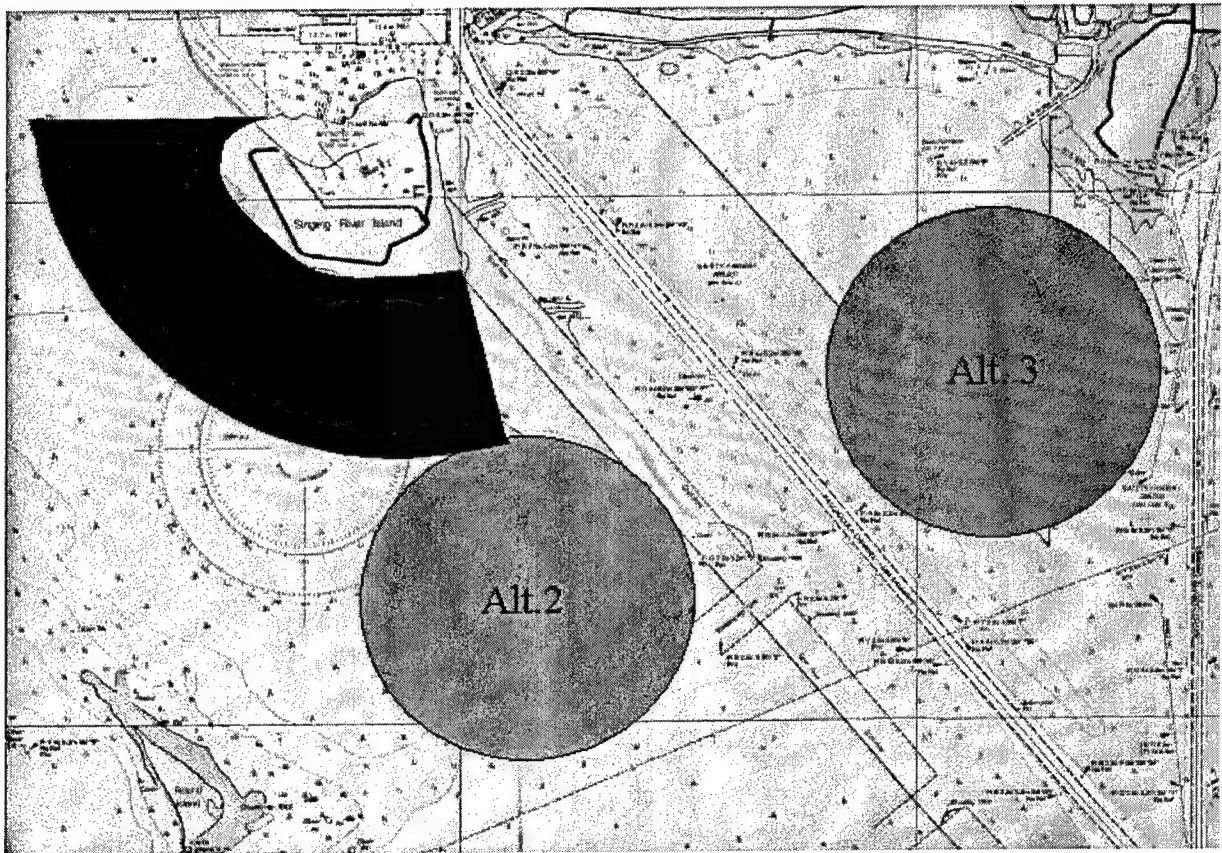


Figure 3-1. Dredged material placement Alternatives 1, 2, and 3

To accomplish Task a, several associated tasks were performed. The first subtask was to calculate the available capacity (surface area and depth) of the alternatives based on site selection and dike configurations. The next subtasks were to calculate sediment consolidation data for the Pascagoula Channel dredged material and to develop a projected filling scenario for each option. Footprints of each of the alternatives, geotechnical engineering analyses, dike construction data, and projected dredged material quantities plan were provided by Mobile District personnel.

Task a was then completed by simulating the three disposal alternatives using the U.S. Army Corps of Engineers (USACE) computer program, Primary Consolidation, Secondary Compression, and Desiccation of Dredged Fill (PSDDF) (Stark 1996)¹. Input requirements necessitated the compilation of the consolidation characteristics of dredged material as well as the appropriate values to simulate desiccation and site dewatering. The required dike heights of the

¹ Stark, T. D. (1996). "Program documentation and user's guide: PSDDF, primary consolidation, secondary compression, and desiccation of dredged fill," Draft, Instruction Report EL-96-XX, U.S. Army Engineer Waterways Experiment Station, Vicksburg, MS.
<http://www.wes.army.mil/el/elmodels/pdf/psddf/psddf.pdf>

three alternatives were determined from the filling simulations for 40 years. After an initial briefing to Mobile District personnel, additional runs were performed by changing several of the input parameters in order to perform a sensitivity analysis (Task b).

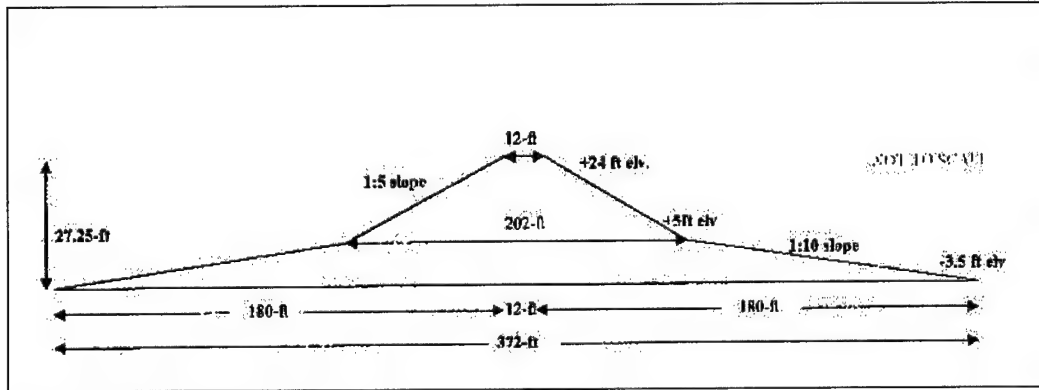


Figure 3-2. Alternative 1, dike configuration

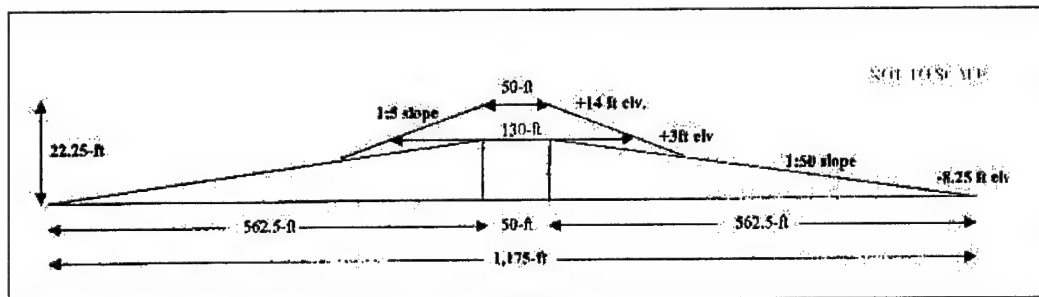


Figure 3-3. Alternative 2, dike configuration

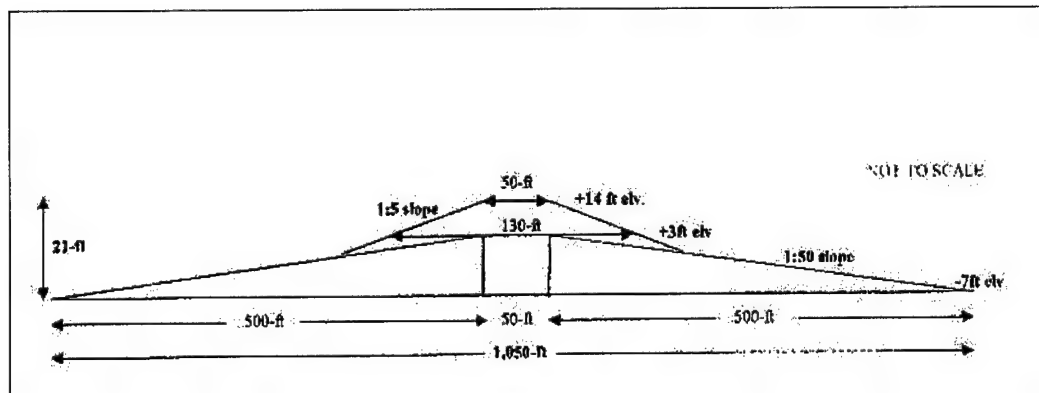


Figure 3-4. Alternative 3, dike configuration

Surface areas of alternatives

Dike configurations (Figures 3-4) were used to determine the available surface area of the CDF alternatives. The total dredged material storage capacity within each CDF was reduced by the volumetric requirements of the perimeter dikes and setbacks. Side slopes, crest dimensions and dike construction methods were used to calculate to a “dike straight wall equivalent” in order to reduce the surface area available for dredged material storage.

For the purpose of storage capacity evaluations, it was assumed that the initial perimeter dikes would be constructed to an elevation of +4.57 m (+15 ft) mean low water (mlw). Then, interior setback dikes will subsequently be raised in approximately 1.52-m (5-ft) increments. Based on field experience at other CDFs, the required setback from the perimeter dike center line for the interior dikes is approximately 152.4 m (500 ft) with inside slopes of approximately 1:3. However, for purposes of this study, the additional loss of surface area due to the 152.4-m (500-ft) setback was assumed to be offset by the removal of material for dike rising. In order to increase available surface area, a steel sheet-pile dike was also proposed, which resulted in a 3,642,143-sq m (900-acre) site. This alternate dike configuration was applied to the Triangle Island alternative and PSDDF simulations were performed.

The surface areas of the expansion alternatives and their dikes are listed in Table 3-1. The difference between initial and available surface area for each line of data in Table 3-1 reflects the reduction in storage capacity due to the dike volumes. The last two columns in Table 3-1 are the lift thickness for each alternative corresponding to an average annual disposal of 3.06 and 2.37 million cu m (4.0 and 3.1 million cu yd) of dredged material with the sediment characteristics of sample PH-04.

Dredging and disposal scenario

Based on past dredging history and anticipated channel maintenance, the Mobile District has estimated that 3.06 million cu m (4 million cu yd) of dredged material will need to be disposed every 3 years for the next 40 years. Using this amount and the available surface areas from Table 3-1, a filling scenario was developed for each alternative (Tables 3-2 through 3-4).

Table 3-1 Pascagoula Harbor Alternatives – Surface Areas¹				
CDF Site	Initial Footprint (acres)	Available for Disposal (acres)	Lift Thickness for 4.0 million cu yd (ft)	Lift Thickness for 3.1 million cu yd (ft)
Alternative 1	1,000	764	4.900	3.798
Alternative 2	1,000	565	6.626	5.135
Alternative 3	1,000	604	6.198	4.804
Alternative 3, Sheet Piles	1,000	900	4.160	3.224
¹ Characteristics for sediment PH-04 used in calculations.				

Table 3-2
Alternative 1 Filling Scenario¹

Month - Year Start of Disposal	Month - Year End of Disposal	Elapsed Time (days)	Volume In Channel (cu yd)	Volume In CDF (cu yd)	Surface Area (acres)	Lift Thickness (ft)
January 2000	September 2000	0	4,000,000	6,040,000	764	4.900
January 2003	September 2003	1095	4,000,000	6,040,000	764	4.900
January 2006	September 2006	2191	4,000,000	6,040,000	764	4.900
January 2009	September 2009	3287	4,000,000	6,040,000	764	4.900
January 2012	September 2012	4383	4,000,000	6,040,000	764	4.900
January 2015	September 2015	5478	4,000,000	6,040,000	764	4.900
January 2018	September 2018	6574	4,000,000	6,040,000	764	4.900
January 2021	September 2021	7670	4,000,000	6,040,000	764	4.900
January 2024	September 2024	8766	4,000,000	6,040,000	764	4.900
January 2027	September 2027	9861	4,000,000	6,040,000	764	4.900
January 2030	September 2030	10957	4,000,000	6,040,000	764	4.900
January 2033	September 2033	12053	4,000,000	6,040,000	764	4.900
January 2036	September 2036	13149	4,000,000	6,040,000	764	4.900
January 2039	September 2039	14244	4,000,000	6,040,000	764	4.900
Total						68.600

¹ Characteristics for sediment PH-04 used in calculations.

Table 3-3
Alternative 2 Filling Scenario¹

Month - Year Start of Disposal	Month - Year End of Disposal	Elapsed Time (days)	Volume In Channel (cu yd)	Volume In CDF (cu yd)	Surface Area (acres)	Lift Thickness (feet)
January 2000	September 2000	0	4,000,000	6,040,000	565	6.626
January 2003	September 2003	1095	4,000,000	6,040,000	565	6.626
January 2006	September 2006	2191	4,000,000	6,040,000	565	6.626
January 2009	September 2009	3287	4,000,000	6,040,000	565	6.626
January 2012	September 2012	4383	4,000,000	6,040,000	565	6.626
January 2015	September 2015	5478	4,000,000	6,040,000	565	6.626
January 2018	September 2018	6574	4,000,000	6,040,000	565	6.626
January 2021	September 2021	7670	4,000,000	6,040,000	565	6.626
January 2024	September 2024	8766	4,000,000	6,040,000	565	6.626
January 2027	September 2027	9861	4,000,000	6,040,000	565	6.626
January 2030	September 2030	10957	4,000,000	6,040,000	565	6.626
January 2033	September 2033	12053	4,000,000	6,040,000	565	6.626
January 2036	September 2036	13149	4,000,000	6,040,000	565	6.626
January 2039	September 2039	14244	4,000,000	6,040,000	565	6.626
Total						92.764

¹ Characteristics for sediment PH-04 used in calculations.

Table 3-4
Alternative 3 Filling Scenario¹

Month – Year Start of Disposal	Month - Year End of Disposal	Elapsed Time (days)	Volume In Channel (cu yd)	Volume in CDF (cu yd)	Surface Area (acres)	Lift Thickness (ft)
January 2000	September 2000	0	4,000,000	6,040,000	604	6.198
January 2003	September 2003	1095	4,000,000	6,040,000	604	6.198
January 2006	September 2006	2191	4,000,000	6,040,000	604	6.198
January 2009	September 2009	3287	4,000,000	6,040,000	604	6.198
January 2012	September 2012	4383	4,000,000	6,040,000	604	6.198
January 2015	September 2015	5478	4,000,000	6,040,000	604	6.198
January 2018	September 2018	6574	4,000,000	6,040,000	604	6.198
January 2021	September 2021	7670	4,000,000	6,040,000	604	6.198
January 2024	September 2024	8766	4,000,000	6,040,000	604	6.198
January 2027	September 2027	9861	4,000,000	6,040,000	604	6.198
January 2030	September 2030	10957	4,000,000	6,040,000	604	6.198
January 2033	September 2033	12053	4,000,000	6,040,000	604	6.198
January 2036	September 2036	13149	4,000,000	6,040,000	604	6.198
January 2039	September 2039	14244	4,000,000	6,040,000	604	6.198
Total						86.777
¹ Characteristics for sediment PH-04 used in calculations.						

Study Approach

Description of study

The storage capacity and dike elevation requirements for the PH alternatives were estimated by simulating future dredged material placement activities for the specified site configurations. The elevations of the dredged material were estimated using the PSDDF model (Stark 1996)¹, which considers both consolidation and desiccation of the dredged material and consolidation of the compressible foundation.

Processes affecting storage capacity

Processes affecting storage capacity of a CDF are described in Engineer Manual 1110-2-5027 (USACE 1987). Containment areas intended for use in conjunction with recurring disposal operations must be sized for long-term storage capacity over the service life (life-span) of the facility. Storage capacity is defined as the total volume available to hold additional dredged material and is equal to the total unoccupied volume minus the volume associated with ponding and freeboard requirements. A differential of approximately 1.22 m (4.0 ft)

¹ Stark, op. cit., p. 3-2

should be maintained between the top of the dredged material surface and the top of the dike crests; this allows for 0.61 m (2 ft) of ponding and 0.61 m (2 ft) of freeboard above the dredged material surface (Palermo, Montgomery, and Poindexter 1978).

The maximum available storage volume is dictated by the maximum dike height as determined by foundation conditions or other constraints and the containment surface area. Long-term storage capacity must consider not only the initial volume available for storage and the initial volume of dredged material, but also any long-term changes in the remaining storage volume available over time. The estimation of long-term storage capacity is an important consideration for long-term planning and design of new containment areas or evaluation of the remaining service life of existing sites.

After dredged material is placed within a confined disposal site, it immediately undergoes sedimentation, which is completed within a few days. The dredged material then enters the more time-consuming process of self-weight consolidation. Placement of the dredged material imposes a loading on previously placed lifts of dredged material and the containment area foundation, which may result in increased consolidation of the dredged material and compressible foundation. Settlement due to consolidation of both the dredged material and foundation soils is therefore a major factor in the estimation of long-term storage capacity. Since the consolidation process is slow, especially in the case of fine-grained materials, it is likely that total settlement will not have taken place before the containment area is required for additional placement of dredged material. For this reason, the time-rate of consolidation must be considered in estimating long-term containment area storage capacity.

An additional factor that may affect containment area storage capacity is settlement due to desiccation of the dredged material surface. If a site is well managed to eliminate surface water, the dredged material surface will be subjected to evaporative drying and may undergo significant settlement resulting from this drying. In cases where desiccation occurs, settlement as a function of time must be determined for dredged material subjected to the effects not only of self-weight consolidation but also of desiccation and the additional consolidation resulting from the surcharge created by formation of the desiccation crust. Procedures for prediction of dredged material settlement due to consolidation and desiccation have been developed.

Estimates of settlement caused by placement of subsequent lifts of dredged material should consider the continued consolidation of previously placed lifts and additional foundation consolidation. Because of the increasing complexity of calculations as additional lifts are placed, solution of all but the simplest problems is more easily accomplished through computer analysis.

The estimated time settlements due to dredged material and foundation consolidation may be combined to yield a time-surface settlement relationship resulting from placement of a single lift (USACE 1970). These data are sufficient for estimation of the remaining capacity in the short term. However, if the containment area is to be used for long-term placement of subsequent lifts, a projected plot of dredged material surface height versus time should be developed (Palermo, Montgomery, and Poindexter 1978). This plot can be developed using time-settlement relationships for sequential lifts combined with

surface height increases resulting from containment area filling operations. Such data may be used for preliminary estimates of the long-term service life of the containment area.

Method of analysis

The computer program PSDDF was used to perform the disposal site filling simulations. Use of a computer program was required because of the numerous complicated calculations necessary to account for both consolidation and desiccation of soft dredged materials.

For each disposal scenario, computer runs were made for each alternative with appropriate disposal site scenario. Later specific variables were changed and some of these scenarios were run again for comparison purposes. Results of the filling simulations for individual cells are shown graphically in the "Simulation Results" section along with summary tables.

Model Description and Assumptions

Management of confined dredged material disposal areas to provide maximum storage capacity is becoming more necessary as both the storage capacity of existing sites and the availability of land for creation of new sites decreases. Maximum site capacity is achieved through densification of the dredged material by removal of interstitial water. The volume reduction and the resulting increase in site capacity are obtained through both consolidation and desiccation of the dredged material.

Long-term management of dredged material containment areas has been facilitated by development of predictive techniques that allow accurate projection of the containment area surface elevation for repetitive disposal operations. Use of large strain consolidation test data in a finite strain mathematical model permits prediction of surface elevations to within the accuracy of measurement of the constituent variables. Techniques for predicting volume reduction resulting from evaporative drying have been developed and incorporated in the mathematical model PSDDF.

Theoretical basis

Finite strain consolidation. Because many soft, fine-grained dredged materials may eventually undergo 50 percent strain or more, Terzaghi's conventional small strain theory is not technically applicable to analyses of dredged material containment areas. A more appropriate approach involves use of a large, or finite, strain consolidation theory. The most general and least restrictive of the many 1-D primary consolidation formulations is the finite strain theory developed by Gibson, England, and Hussey (1967). This approach is well suited for the prediction of consolidation in thick deposits of soft dredged materials since it accounts for the large strains and nonlinear soil properties inherent in these materials.

Desiccation. The removal of water by desiccation from a normally consolidating dredged material layer will result in formation of a surface crust;

this in turn will cause additional consolidation due to the surcharge created by crust formation. Since surface drying may be significant between disposal operations, it is essential to incorporate predictions of desiccation settlement in evaluations of disposal site capacity. An empirical description of the desiccation process has been developed in terms of water balance in the upper portion of dredged material layers (Cargill 1985). Procedures for calculation of soil evaporation rates and depths of influence have been developed. Site-specific climatic conditions are incorporated in the analysis procedures. The model uses void ratios instead of water contents in order to be compatible with the consolidation model.

Modeling procedures

The mathematical model PSDDF was used for the storage capacity evaluations in this study. The model was initially developed by Cargill (1985) and subsequently modified by Stark (1991, 1996¹). The model considers consolidation and desiccation parameters for the dredged material, initial layer heights of dredged material applied as a function of time, consolidation of foundation soils, and precipitation and evaporation rates. Stark (1991) modified the model to account for 25 different dredged material and compressible foundation properties, thus allowing alternating layers of different dredged fill and foundation materials to be considered.

Assumptions and model input parameters

To simulate the filling of confined dredged material containment areas, numerous types of data are needed and assumptions must be made regarding initial site conditions, dredged material properties, dredging volumes, disposal lifts, and site operation and management. Additionally, assumptions for the construction of the dikes were made. In this section, the assumptions used in the study are summarized for reference.

The model parameters shown in Tables 3-5 and 3-6 were used to determine the dike elevations requirements for all simulation runs. The void ratio-effective stress and void ratio-permeability relations were obtained from the results of self-weight and large strain, controlled rate of strain (LSCRS) consolidation tests (Cargill 1986).

The desiccation parameters used in PSDDF, rate of precipitation, pan evaporation efficiency, maximum crust thickness, and drainage efficiency, represent an active dewatering condition. They are based on previous studies and modified after comparison with the field data. The precipitation and evaporation rates (Table 3-7) were based on historical climatic data obtained from the National Climatic Center.

¹ Stark, op. cit., p. 3-2

Table 3-5
PSDDF Parameters for Filling Simulations

Parameter	Value
Specific gravity of compressible foundation material	2.66
Void ratio of compressible foundation	0.65
Permeability of compressible foundation	0.4
Drainage length in compressible foundation, ft	15.15
Elevation at top of incompressible foundation, ft, mlw	-9.0
Elevation of fixed water table, ft, mlw	1.0
Surface drainage efficiency, percent	50.0
Maximum evaporation efficiency, percent	100.0
Length of dredging disposal period, days	240.0
Time to desiccation after filling, days	30.0

Table 3-6
Pascagoula Harbor Sediment Characteristics

Parameter	Sediment Sample Number				
	2	4	6	10	5
Specific gravity	2.67	2.66	2.69	2.67	2.74
Moisture content (percent)	111.00	79.10	95.20	58.40	186.50
Liquid Limit (LL)	77.0	105.0	67.0	38.0	136.0
Plastic Limit (PL)	24.0	34.0	23.0	16.0	37.0
Plasticity Index (PI)	53.0	71.0	44.0	22.0	99.0
Disposal void ratio	5.10	3.67	3.74	6.21	7.75
In situ void ratio	2.96	2.10	2.56	1.56	5.11
Bulking factor	1.54	1.50	1.33	2.82	1.43
Desiccation Limit (DL)	2.050	2.230	1.960	1.740	2.510
Shrinkage Limit (SL)	3.968	4.976	3.464	2.232	6.544
Maximum crust thickness (ft)	0.800	0.827	0.786	0.753	0.869
Moisture content at DL (percent)	28.80	40.80	27.60	19.20	44.40
Moisture content at SL (percent)	138.60	189.00	120.60	68.40	244.80
Degree of saturation	0.375	0.487	0.379	0.295	0.485

**Table 3-7
Precipitation and Evaporation Rates at Pascagoula Harbor**

Month	Precipitation (inches)	Pan Evaporation (inches)
January	3.94	2.39
February	4.83	2.54
March	6.18	3.22
April	5.00	2.72
May	5.00	2.59
June	5.93	3.38
July	7.66	4.19
August	6.67	3.58
September	7.26	3.34
October	2.50	1.97
November	3.16	1.73
December	6.56	2.02
Total	64.69	33.67

Dredged material properties

The most important parameters of PSDDF are the consolidation properties of the dredged material. Laboratory procedures for testing slurried sediments have been developed at ERDC. These procedures can provide compressibility and permeability data for soft materials and are useful in analyzing the finite strain consolidation of dredged materials. For soft soils, use of a series of consolidation tests is necessary to obtain the void ratio-effective stress and void ratio-permeability relationships over the entire range of potential field conditions.

To predict the consolidation of dredged material by finite strain theory, several pieces of data are required which can be determined through a geotechnical laboratory testing program. The necessary data include specific gravity of the solid particles, the Atterberg limits (liquid limit and plastic limit), the void ratio-effective stress relationship, and the void ratio-permeability relationship. The specific gravity and the Atterberg limits can be determined by routine laboratory testing, while the void stress and permeability relationships must be determined from one or more of a number of laboratory consolidation tests. The laboratory consolidation tests used by the U.S. Army Corps of Engineers for dredged material testing are the self-weight consolidation test, a large strain consolidation test, and the standard oedometer test.

The Mobile District contracted with Law Engineering & Environmental Services to conduct geotechnical testing of four sediments referred to as PH-2, PH-4, PH-6 and PH-10 in this report. These samples were collected from various locations in the PH Channel (Figure 3-5). Results of this investigation are contained in Appendix F, the report entitled, "Report of Field and Laboratory

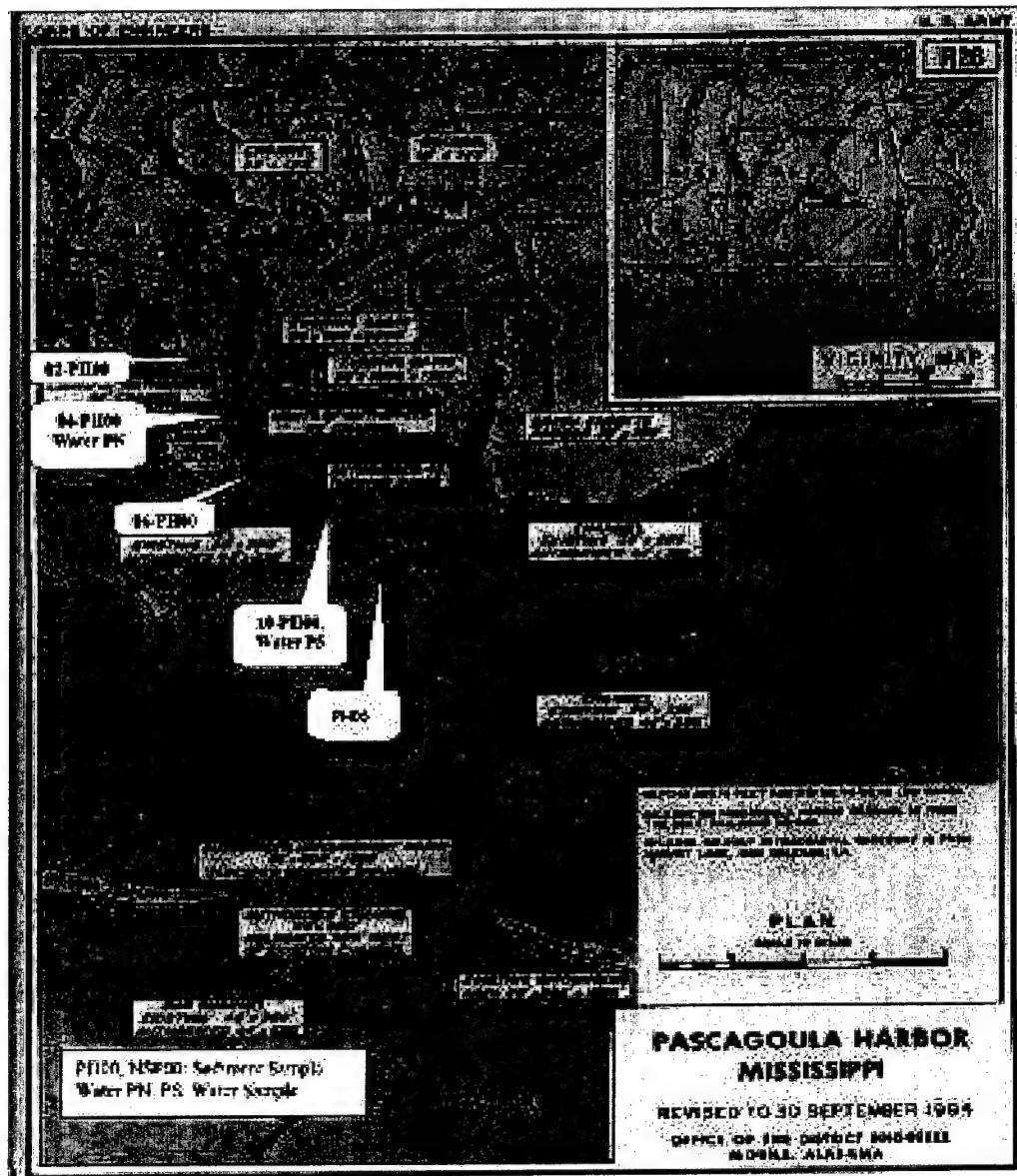


Figure 3-5. Pascagoula Harbor sampling locations

Subsurface Dredged Material Investigation," October 2001. The material properties are assumed to be representative of all maintenance material to be placed in the PH CDF in the future. Further, it is assumed that these properties (particularly compressibility and permeability) are also representative of the "new work" dredged material. In addition, a sediment sample (PH-5) was collected and analyzed by ERDC personnel. Results of the analysis are contained in Appendix G.

Test results from these studies were input into the REDUCE program of the PSDDF model. Output from the REDUCE program are the void ratio-effective stress relationships and void ratio-permeability relationships for the five sediment samples analyzed. These relationships were input for the PSDDF model simulations for the corresponding sediment consolidation analyses. Table 3-8 provides an example of the results of the REDUCE program. The data are presented in Appendix E.

Dredged material disposal volumes and lifts

Estimates were made by the Mobile District regarding the quantities of new work and maintenance material to be dredged. These quantities were based upon historical data, previous hydraulic modeling studies, and best estimates of future conditions. Lift heights of dredged material for each disposal operation were determined from the actual or projected future dredging volumes and the surface areas available for placement in the disposal area. Because PSDDF applies an entire lift instantaneously, the disposal history was subdivided into discrete time periods and lifts were applied at the end point of each subdivision. For the purpose of the simulations, it was assumed that the disposal volume was deposited once annually in August of the first year of the 3-year cycle. The average dredged material lift thickness was calculated for each alternative based on the available surface area and the specified disposal volume.

The disposal year and volume of in situ material applied for each option is shown in the filling scenario Tables 3-2 through 3-4. The height of each lift was obtained by dividing the CDF volume (in situ disposal volume multiplied by bulking factor) by the surface area of the cell being utilized. The PSDDF model initiates consolidation calculations for an initial material thickness corresponding to a void ratio at zero effective stress. The in situ disposal volumes shown in the tables correspond to dredged material at the in situ void ratio. For example, the average in situ void ratio of the PH-5 sediment is 5.11, and the void ratio at zero effective stress immediately following deposition is 10.1. However, since the lift is built over the course of a year of disposal, the material has on average of 4 months to settle and consolidate during the disposal. As such, the material throughout the lift is no longer at zero effective stress, and the height of the lift would be about one-third smaller. Using sedimentation data for compression settling, the void ratio following an average 6 months of compression settling or primary consolidation was estimated to be 7.75 as opposed to 10.1. Therefore, for a void ratio increase from 5.11 to 7.75 during dredging and disposal, the CDF volume of each lift is obtained by multiplying the in situ volume by 1.43. The use of 7.75 as the initial void ratio instead of 10.50 provides greater accuracy during disposal.

Table 3-8
Consolidation Characteristics of Foundation Material and Dredged
Material PH-2

Void Ratio	Effective Stress (psf)	Coefficient of Permeability (ft/day)	Void Ratio	Effective Stress (psf)	Coefficient of Permeability (ft/day)
Foundation Material			Dredged Material PH-2 (Concluded)		
2.50	0	2.00E-03	5.4	5.91	1.81E-03
2.45	1	1.89E-03	5.2	8.78	1.45E-03
2.42	2	1.75E-03	5	13.08	1.16E-03
2.25	16	1.21E-03	4.8	19.52	9.22E-04
2.15	32	9.49E-04	4.6	29.13	7.33E-04
2.05	64	7.33E-04	4.4	43.42	5.81E-04
1.76	256	2.60E-04	4.2	64.50	4.59E-04
1.58	512	1.20E-04	4	95.36	3.62E-04
1.39	1020	3.76E-05	3.8	140.06	2.85E-04
1.14	3000	8.00E-06	3.6	204.05	2.24E-04
			3.4	294.38	1.75E-04
Dredged Material PH-2			3.2	419.87	1.37E-04
8	0.10	2.65E-02	3	591.07	1.07E-04
7.8	0.12	2.19E-02	2.8	819.88	8.29E-05
7.6	0.15	1.80E-02	2.6	1118.79	6.43E-05
7.4	0.20	1.48E-02	2.4	1499.36	4.98E-05
7.2	0.26	1.21E-02	2.2	1970.21	3.84E-05
7	0.34	9.91E-03	2	2534.24	2.96E-05
6.8	0.47	8.08E-03	1.8	3185.65	2.27E-05
6.6	0.65	6.58E-03	1.6	3907.01	1.74E-05
6.4	0.91	5.34E-03	1.4	4667.36	1.33E-05
6.2	1.30	4.32E-03	1.2	5422.03	1.02E-05
6	1.87	3.49E-03	1	6115.04	7.70E-06
5.8	2.73	2.81E-03	0.8	6684.47	5.90E-06
5.6	4.00	2.26E-03	0.6	7070.48	4.40E-06

Site operation and management plan

It was assumed that the PH facility would be the only available disposal site. Therefore, it will receive all materials dredged during the 8-month dredging cycle. The need to actively manage the PH CDF as the site begins to fill is anticipated. The management of the PH should involve active dewatering measures allowing 8 months for active filling and over 2 years of drying. Other major aspects of a PH management plan may include removal of surface water through lowering of the weir's crest elevations and construction of surface trenches within the site to allow efficient drainage of the area. By placing trenches adjacent and parallel to the perimeter dikes as well as throughout the interior of the site, water is quickly moved from all parts of the site to the weirs and then offsite. As the dredged material dries and settles, the trenches may be progressively deepened; thus, the term "progressive trenching" is applied to this operation.

An active dewatering program was assumed to be implemented at the PH facility. The simulation of dredged material surface settlement allows flexibility in numerous input parameters describing the desiccation characteristics of a site. However, PSDDF cannot explicitly simulate specific dewatering management options, such as interior trenching. Rather, empirical coefficients are incorporated in PSDDF to provide a means to simulate the surface settlement due to desiccation of the dredged material. Thus, only one dewatering scenario was considered. An active management was assumed and a value of 0.5 for surface drainage efficiency was input into the PSDDF program. The desiccation input parameters are given in Tables 3-5 and 3-6. Since the relative values of evaporation and precipitation have a major effect upon desiccation, monthly climatic data are needed in the calculations. Climatic data for the PH are shown in Table 3-7.

It should be noted that all projections made in this study are based on the assumption that the Mobile District continues the same level of site management at the PH. If intense management of the site is not accomplished each year of its remaining life, the site will require higher dike elevations than projected in this study.

Simulation Results

This chapter presents the simulation results for the various PH scenarios. Results of the PSDDF simulations are presented in chart format and in summary tables.

The saw-toothed filling curves shown in Figures 3-6 through 3-9 are typical of the dredged material surface-elevation time series curves obtained for containment areas that are used periodically. Figures 3-6 through 3-8 shows the plotted fill elevation projections for the three PH alternative sites with all five sediments plotted on the same graph for comparison. In addition, Figure 3-9 presents the results for a 3,642,143 million cu m- (900-acre) site (modified Alternative 3). These figures show the range of expected dike elevations for the

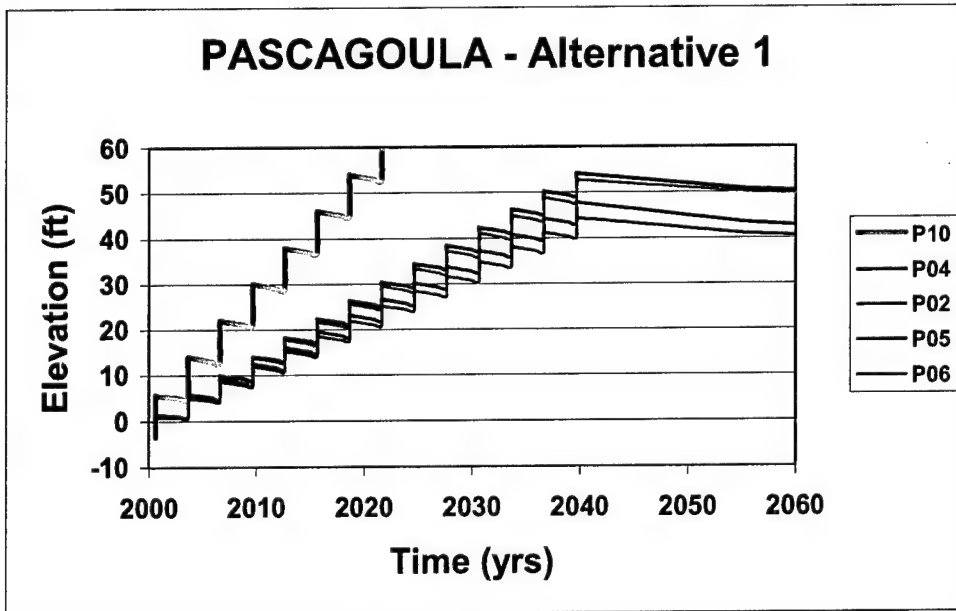


Figure 3-6. Fill elevation predictions for Alternative 1

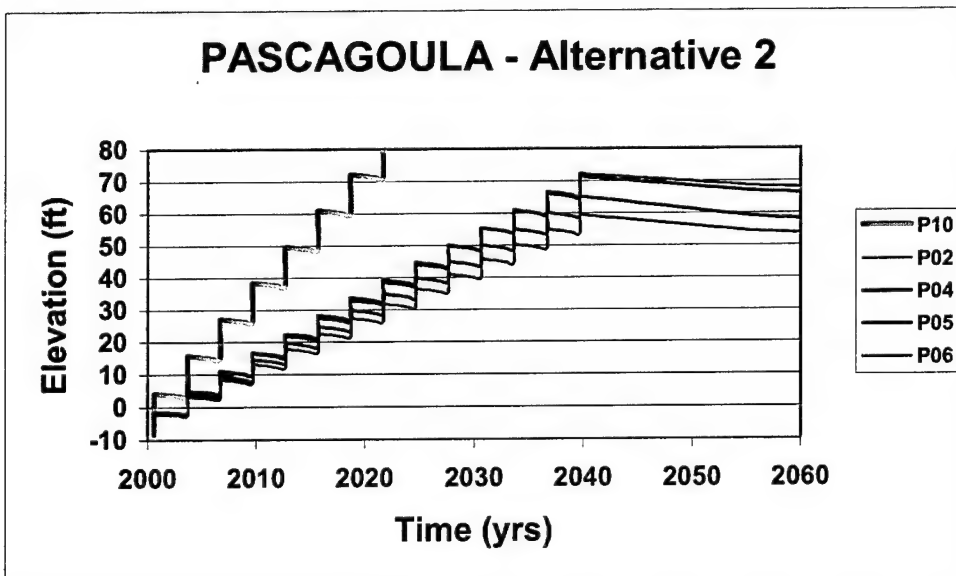


Figure 3-7. Fill elevation predictions for Alternative 2

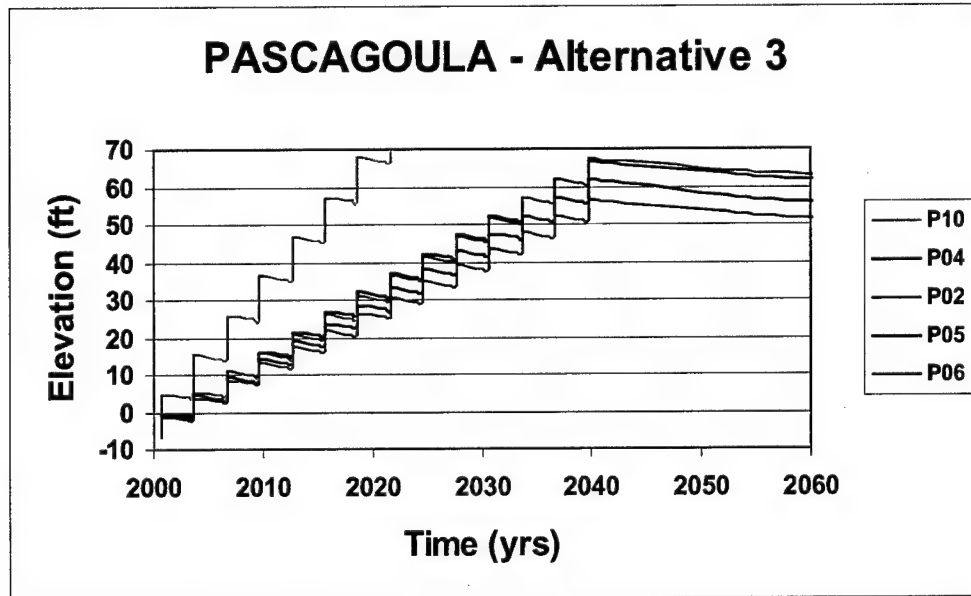


Figure 3-8. Fill elevation predictions for Alternative 3

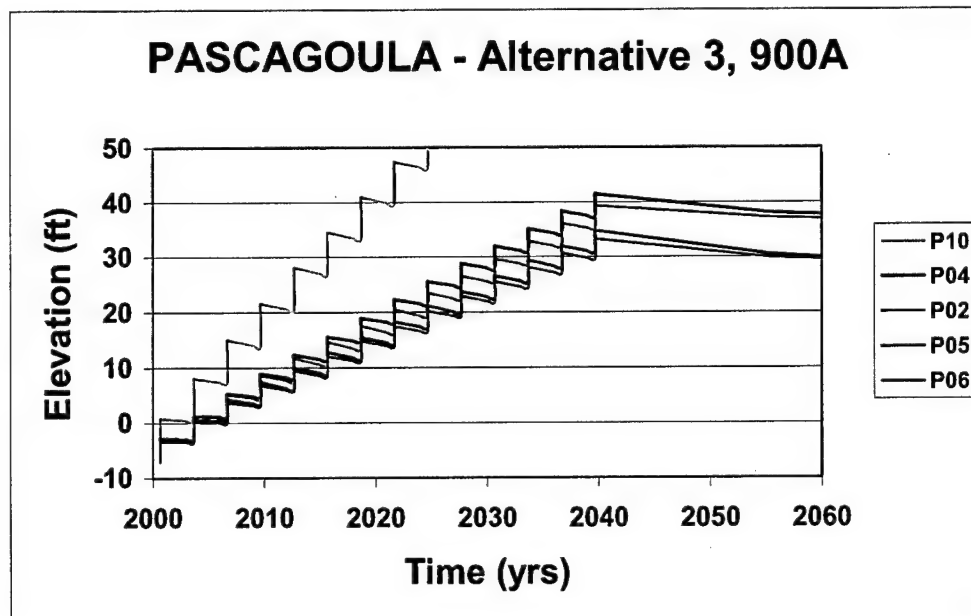


Figure 3-9. Fill elevation predictions for 3,642,143 cu m- (900-acres) Alternative 3

PH sediments for each of the alternatives, assuming that 3.06 million cu m- (4.0 million cu yd) of sediment are placed in the CDFs once every 3 years. These simulations incorporate the best estimates of drainage and desiccation properties based on good design and operation of the CDF with a low to moderate level of effort in site management as would be characteristic of management of island CDFs.

It is recommended that the results for the PH-10 sediment be ignored due to possible sediment analysis errors and the fact that this curve falls well outside the range of the other sediment curves.

The annual dredged material volume was reduced from 3.065 to 2.4 million cu m (3.06 to 4.0 to 3.1 million cu yd) for Alternative 3 and Alternative 3 modified with sheet pile with the results of the simulations presented in Figures 3-10 and 3-11. These simulations were run only for sediments PH-4 and PH-6 since these provide the minimum and maximum elevations. A sensitivity analysis of the operating efficiency was also conducted using sediments PH-4 and PH-6. The surface drainage efficiency values of 0.25 and 0.75 were compared to the original runs that used 0.50. These results are presented in Figures 3-12 and 3-13.

Dike elevations at the end of the simulations were compiled and are presented in Table 3-9 for the Pascagoula Harbor alternatives. Dike elevations for both 3.065 to 2.4 million cu m (4.0 and 3.1 million cu yd) for the annual dredging requirements for Alternative 3 and modified Alternative 3 (3,642,143-cu m (900-acre) sheet pile) are also included. Table 3-10 presents the data for the simulations runs where the operating (surface drainage) efficiency was changed in order to conduct a sensitivity analysis.

Conclusions

Based on the results of this study, the following conclusions are made:

- a. The Pascagoula Harbor Alternatives will require dike elevations in the range of 15.2-21.3 m (50-70 ft) for the original scenario (3.06 million cu m (4.0 million cu yd) annually, 50 percent efficiency) based upon four sediments tested. These results are for an 8-month disposal period once every 3 years for 40 years.
- b. If a reduced dike volume configuration (steel pilings) is used, then the required dike elevations would decrease to the 7.0-12.2 m- (23-40-ft) range.
- c. Simulations comparing dike elevations for varying levels of drainage efficiency indicate the following: if increased to 75 percent, the height decreased by an average of 4.0 m (13 ft) and, if the efficiency decreased to 25 percent, then the height required would increase by 2.7 m (9 ft).

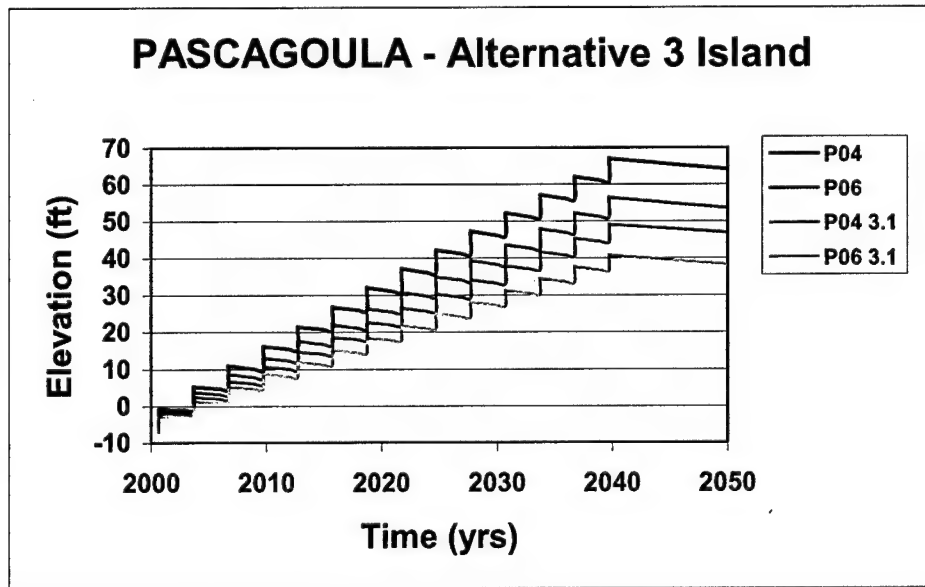


Figure 3-10. Fill elevation predictions for Alternative 3 for reduced dredging requirements

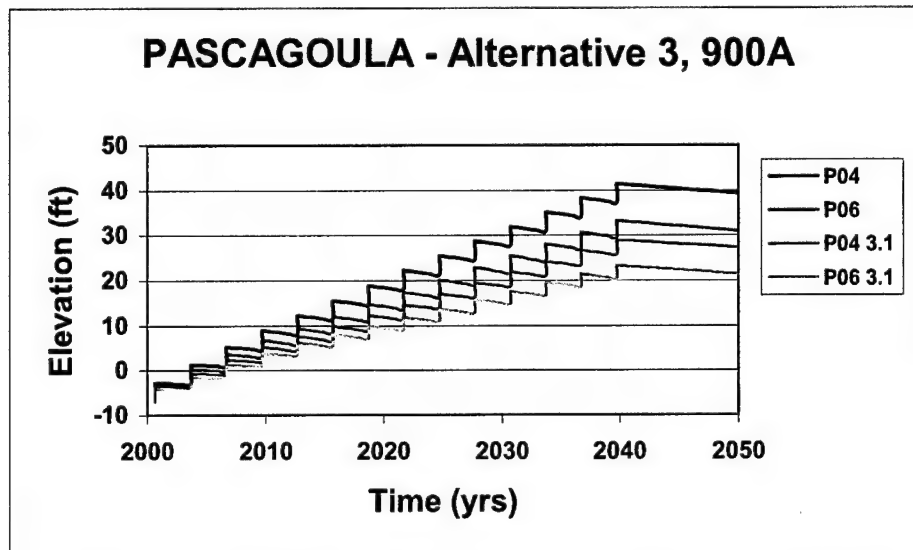


Figure 3-11. Fill elevation predictions for 3,642,143 cu m (900-acre) Alternative 3 for reduced dredging requirements

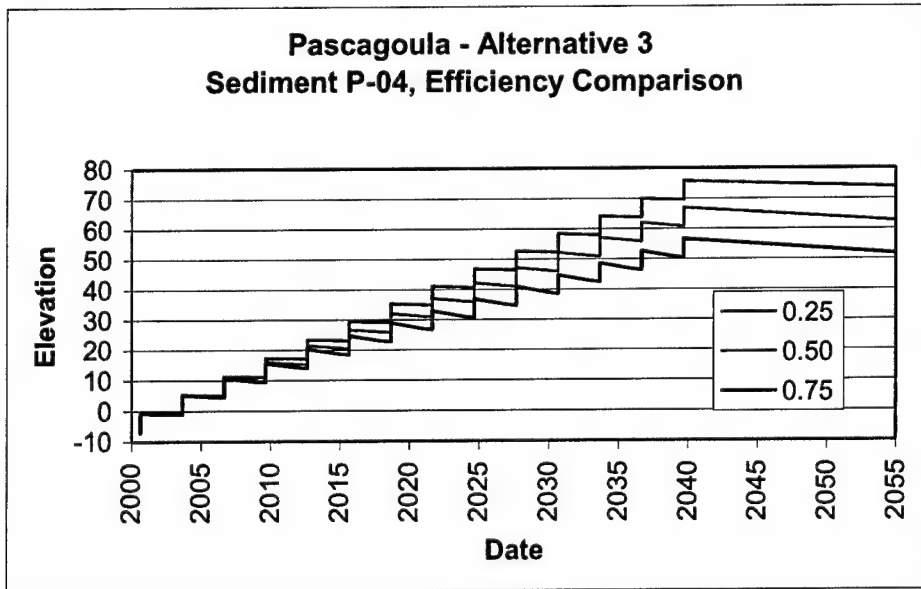


Figure 3-12. Fill elevation predictions for Alternative 3 for various drainage efficiencies using Sediment P-04 consolidation characteristics

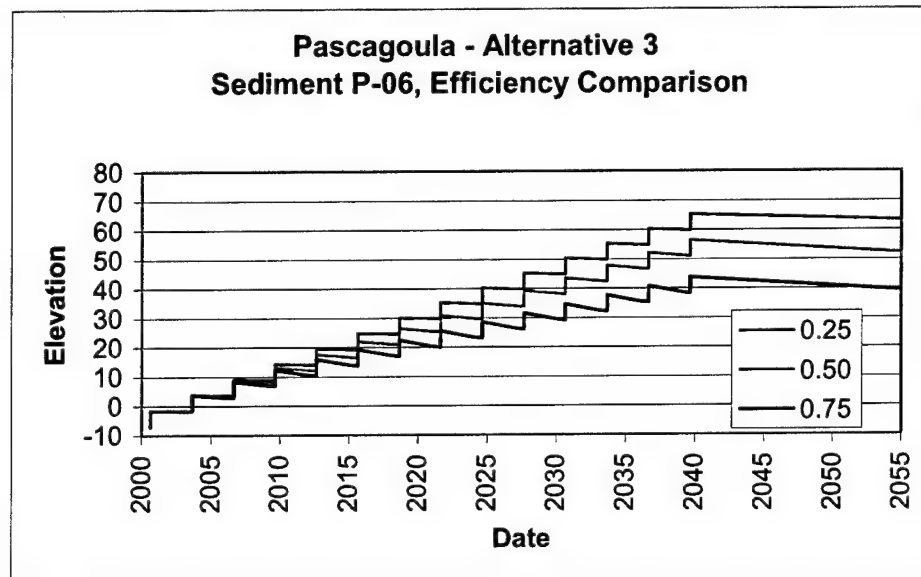


Figure 3-13. Fill elevation predictions for Alternative 3 for various drainage efficiencies using Sediment P-06 consolidation characteristics

Table 3-9
Pascagoula Harbor Alternatives – Dike Elevation Ranges

CDF Site	Available for Disposal (Acres)	DM Volume = 4.0 MCY ¹ (ft)	DM Volume = 3.1 MCY (ft)
Alternative 1	764	44 – 55	
Alternative 2	565	59 – 70	
Alternative 3	604	56 - 67	41 - 49
Alternative 3, Sheet Piles	900	33 - 41	23 - 29

¹ MCY is million cubic yards.

Table 3-10
Operating Efficiency Variable – Dike Elevation Ranges

Sediment Type	25 Percent	50 Percent	75 Percent
PH-2	51 ft	67 ft	75 ft
PH-4	56 ft	67 ft	76 ft
PH-5	36 ft	61 ft	70 ft
PH-6	44 ft	56 ft	65 ft

References

- Cargill, K. W. (1985). "Mathematical model of the consolidation/desiccation processes in dredged material," Technical Report D-85-4, U.S. Army Engineer Waterways Experiment Station, Vicksburg, MS.
- Cargill, K. W. (1986). "The large strain, controlled rate of strain (LSCRS) device for consolidation testing of soft fine-grained soils," Technical Report GL-86-13, U.S. Army Engineer Waterways Experiment Station, Vicksburg, MS.
- Gibson, R. E., England, G. L., and Hussey, M. J. L. (1967). "The theory of one-dimensional consolidation of saturated clays: I. Finite non-linear consolidation of thin homogenous layers," *Geotechnique* 17(3), 261-273.
- Headquarters, U.S. Army Corps of Engineers. (1970). "Laboratory soils testing," Engineer Manual 1110-2-1906, Washington, DC.
- Headquarters, U.S. Army Corps of Engineers. (1987). "Confined disposal of dredged material," Engineer Manual 1110-2-5027, Washington, DC.

- Palermo, M. R., Montgomery, R. L., and Poindexter, M. E. (1978). "Guidelines for designing, operating and managing dredged material containment areas," Technical Report DS-78-10, U.S. Army Engineer Waterways Experiment Station, Vicksburg, MS.
- Stark, T. D. (1991). "Program documentation and user's guide: PCDDF89, primary consolidation and desiccation of dredged fill," Instruction Report D-91-1, U.S. Army Engineer Waterways Experiment Station, Vicksburg, MS.

4 Circulation Studies of Mississippi Sound

This chapter summarizes the circulation studies conducted for the Mississippi Sound using the ADvanced CIRCulation (ADCIRC) long-wave hydrodynamic model. These studies aim to characterize water levels and currents throughout the sound as it exists today and to predict any potential impacts that may result from constructing a dredged-material disposal site. Comparing model-generated currents and water-surface elevations between pre- and post-construction conditions can provide insight, for example, whether a particular alternative will adversely impact navigation, or if one alternative is more susceptible to current-induced erosion than the others.

Furthermore, this component supplies model-generated currents and water-surface elevations to two other components comprising this study. First, ADCIRC-generated water-surface elevations and currents are used as boundary-forcing functions in the 3-D circulation model (CH3D) which, in turn, provides hydrodynamic information, required in the water quality simulations. Second, ADCIRC is used in developing time-series of hurricane-induced storm surge elevations that are subsequently input to the wave model for estimating wave heights and periods.

This chapter is composed of five sections, with the first describing the governing equations and algorithm contained in the ADCIRC model. Model development, which includes generating the numerical grid, was well as the forcing mechanisms used in driving the model, are discussed in the second section. The third section describes the calibration procedure for ensuring the model accurately depicts water-surface elevations and currents in the study area. The fourth section presents how the calibrated model was adapted for the three alternative CDF placement sites, whereas in the fifth section, comparisons of model-generated current fields, together with time-series of currents at selected locations in the vicinity of the proposed CDF alternatives, are presented.

Description of Tidal Circulation Model

The ADCIRC numerical model was chosen for simulating the long-wave hydrodynamic processes in the Mississippi Sound. Imposing wind fields extracted from the National Center for Environmental Prediction database, or wind and atmospheric pressure fields computed with the Planetary Boundary Layer (PBL) model, the ADCIRC model can accurately replicate tidally-driven

currents and hurricane-induced storm-surge levels. The ADCIRC model was developed in the USACE Dredging Research Program (DRP) as a family of two- and three-dimensional finite element-based models (Luettich et al. 1992; Westerink et al. 1992). Model attributes include the following capabilities:

- a. Simulating tidal circulation and storm-surge propagation over large computational domains while simultaneously providing high resolution in areas of complex shoreline configuration and bathymetry. The targeted areas of interest include continental shelves, nearshore areas, and estuaries.
- b. Representing properly all pertinent physics of the 3-D equations of motion. These include tidal potential, Coriolis, and all nonlinear terms of the governing equations.
- c. Providing accurate and efficient computations over time periods ranging from months to years.

In two dimensions, the model is formulated using the depth-averaged shallow water equations for conservation of mass and momentum. Furthermore, the formulation assumes that the water is incompressible, that hydrostatic pressure conditions exist, and that the Boussinesq approximation is valid. Using the standard quadratic parameterization for bottom stress and neglecting baroclinic terms and lateral diffusion/dispersion effects, the following set of conservation equations in primitive, nonconservative form, and expressed in a spherical coordinate system, are incorporated in the model (Flather 1988; Kolar et al. 1993):

$$\begin{aligned} \frac{\partial U}{\partial t} + \frac{1}{r \cos \phi} U \frac{\partial U}{\partial \lambda} + \frac{1}{R} V \frac{\partial U}{\partial \phi} - \left(\frac{\tan \phi}{R} U + f \right) V = \\ - \frac{1}{R \cos \phi} \frac{\partial}{\partial \lambda} \left(\frac{p_s}{\rho_0} + g(\zeta - \eta) \right) + \frac{\tau_{s\lambda}}{\rho_0 H} - \tau_* U \end{aligned} \quad (4-1)$$

$$\frac{\partial V}{\partial t} + \frac{1}{r \cos \phi} U \frac{\partial V}{\partial \lambda} + \frac{1}{R} V \frac{\partial V}{\partial \phi} - \left(\frac{\tan \phi}{R} U + f \right) U = \quad (4-2)$$

$$- \frac{1}{R} \frac{\partial}{\partial \phi} \left(\frac{p_s}{\rho_0} + g(\zeta - \eta) \right) + \frac{\tau_{s\phi}}{\rho_0 H} - \tau_* V \quad (4-3)$$

$$\frac{\partial \zeta}{\partial t} + \frac{1}{R \cos \phi} \left(\frac{\partial UH}{\partial \lambda} + \frac{\partial (UV \cos \phi)}{\partial \phi} \right)$$

where

t = ime

λ and ϕ = degrees longitude (east of Greenwich is taken positive) and degrees latitude (north of the equator is taken positive)

ζ = free surface elevation relative to the geoid

U and V = depth-averaged horizontal velocities in the longitudinal and latitudinal directions, respectively

R = the radius of the earth

$H = \zeta + h$ = total water column depth

h = bathymetric depth relative to the geoid

$f = 2\Omega \sin \phi$ = Coriolis parameter

Ω = angular speed of the earth

p_s = atmospheric pressure at free surface

g = acceleration due to gravity

η = effective Newtonian equilibrium tide-generating potential parameter

ρ_0 = reference density of water

$\tau_{s\lambda}$ and $\tau_{s\phi}$ = applied free surface stresses in the longitudinal and latitudinal directions, respectively

τ = bottom shear stress and is given by the expression $C_f(U^2 + V^2)^{1/2}/H$ where C_f = the bottom friction coefficient

The momentum equations (Equations 4-1 and 4-2) are differentiated with respect to λ and τ and substituted into the time-differentiated continuity equation (Equation 4-3) to develop the following Generalized Wave Continuity Equation (GWCE):

$$\begin{aligned}
& \frac{\partial^2 \zeta}{\partial t^2} + \tau_0 \frac{\partial \zeta}{\partial t} - \frac{1}{R \cos \phi} \frac{\partial}{\partial \lambda} \left[\frac{1}{R \cos \phi} \left(\frac{\partial HUU}{\partial \lambda} + \frac{\partial (HUV \cos \phi)}{\partial \phi} \right) - UVH \frac{\tan \phi}{R} \right] \\
& \left[-2\omega \sin \phi HV + \frac{H}{R \cos \phi} \frac{\partial}{\partial \lambda} \left(g(\zeta - \alpha \eta) + \frac{p_s}{\rho_0} \right) + \tau_* HU - \tau_0 HU - \tau_{s\lambda} \right] \\
& - \frac{1}{R} \frac{\partial}{\partial \phi} \left[\frac{1}{R \cos \phi} \left(\frac{\partial HVV}{\partial \lambda} + \frac{\partial (HVV \cos \phi)}{\partial \phi} \right) + UUH \frac{\tan \phi}{R} + 2\omega \sin \phi HU \right] \\
& + \frac{H}{R} \frac{\partial}{\partial \phi} \left(g(\zeta - \alpha \eta) + \frac{p_s}{\rho_0} \right) + \tau_* - \tau_0 HV - \frac{\tau_{s\lambda}}{\rho_0} \Bigg] \\
& - \frac{\partial}{\partial t} \left(\frac{VH}{R} \tan \phi \right) - \tau_0 \left(\frac{VH}{R} \tan \phi \right) = 0
\end{aligned}
\tag{4-4}$$

The ADCIRC-2DDI model solves the GWCE in conjunction with the primitive momentum equations given in Equations 4-1 and 4-2. The GWCE-based solution scheme eliminates several problems associated with finite-element programs that solve the primitive forms of the continuity and momentum equations, including spurious modes of oscillation and artificial damping of the tidal signal. Forcing functions include time-varying water-surface elevations, wind shear stresses, atmospheric pressure gradients, and the Coriolis effect. Also, the study area can be described in ADCIRC using either a Cartesian (i.e., flat earth) or spherical coordinate system.

The ADCIRC model uses a finite-element algorithm in solving the defined governing equations over complicated bathymetry encompassed by irregular sea/shore boundaries. This algorithm allows for extremely flexible spatial discretizations over the entire computational domain and has demonstrated excellent stability characteristics. The advantage of this flexibility in developing a computational grid is that larger elements can be used in open-ocean regions where less resolution is needed, whereas smaller elements can be applied in the nearshore and estuary areas where finer resolution is required to resolve hydrodynamic details.

Model Development

The grid used for this study was adapted from one developed in the Regional Sediment Management (RSM) Pilot Study, where various models were developed for studying sediment transport in the coastal area serviced by the Mobile District. This grid, in turn, was adapted from one generated in the study conducted by Hagen et al. (2001), and was generated using a Linear Truncation Error Analysis (LTEA) algorithm.

Analogous with finite difference models, where each differential term in the governing equations has associated with it an infinite series of differential terms that have been truncated, each integral evaluated with a finite element model has an infinite series of terms that have been truncated as well. Their significance in model solutions is a function, in part, of the nodal spacing and representation of bathymetric and current gradients in a grid. Poorly constructed grids can exacerbate the influence of these terms, and depending on the formulation of the governing equations in a model, leading to spurious modes of oscillations or dampened solutions. The LTEA algorithm seeks to determine the optimal placement of nodes in order to minimize the errors induced by the truncated terms, thus increasing model accuracy.

In using the LTEA algorithm, a high-resolution, uniform grid composed of equilateral triangles is developed, encompassing the study domain. (Nodal spacing for the high-resolution grid produced by Hagen et al. (2001) was 3 km (1.86 miles). A simulation is made, allowing the model to reach a dynamic steady-state solution. Model output is harmonically analyzed yielding elevation, x- and y-component amplitudes and phases. With this information, the truncation terms are evaluated; with the modeler defining the minimum acceptable truncation error, x- and y-coordinates are computed for nodes comprising the new grid so that the truncation error associated with each node equals the selected minimum acceptable truncation error; increasing nodal resolution computed with the LTEA algorithm can further reduce the error.

The high-resolution grid created by Hagen et al. (2001), and the resulting model grid, used a coastline database developed by the U.S. Central Intelligence Agency and bathymetry extracted from the National Center for Atmospheric Research's ETOPO5 database. Both databases have been found to contain discrepancies with coastlines and bathymetry displayed on charts published by the Department of Defense National Imagery and Mapping Agency (NIMA) and NOAA National Ocean Service (NOS). Consequently, this grid was used as a guide in defining the minimum resolution required while developing the grid in the RSM pilot study.

Figure 4-1 displays the grid developed for this study. As shown in the figure, the model domain encompasses the entire Gulf of Mexico and the western extent of the Caribbean Sea. Figure 4-2 displays the grid in the Mississippi Sound, whereas Figure 4-3 shows the grid in the vicinity of Pascagoula, MS. The grid encloses the Gulf of Mexico entirely and includes the lower 40.23-km (25-mile) reaches of the east and west branches of the Pascagoula River, together with the Escatawpa River, which are approximately the distances to the head-of-tides. (These rivers have been idealized with each being represented as a straight channel.) Open-ocean boundaries are specified through the Straits of Florida and within the Caribbean Sea. This grid consists of 40,844 nodes and 76,034 elements. The largest elements reside in the Caribbean Sea, having nodal spacing of about 49.25 km (30.6 miles), whereas the smallest elements resolve the Escatawpa River, where its idealized width is 45.72 m (150 ft). The Pascagoula Channel is represented in the grid as a trapezoid (in cross section) with a line of nodes, running its entire length, positioned along its center line together with a line of nodes along both sides of its 106.68 m (350-ft) base (i.e., the channel bottom is represented in the model with three "streamlines").

Additional lines of nodes are placed parallel to its base for resolving its banks. Nodal spacing along the channel bottom is approximately 60.96 m (200 ft).

For areas outside of the United States, the grid boundary is aligned with the shoreline depicted on nautical charts produced by NIMA. These charts are referenced to the World Geodetic System (WGS) 1984 horizontal datum, which is equivalent to the North American Datum (NAD) 1983 coordinate system used by United States governmental agencies. For areas within the United States, shoreline positions are based on nautical charts produced by NOS. Except for the chart of Mobile Bay, which is referenced to the NAD 1927 datum, all charts are referenced to the NAD 1983 datum.

Bathymetry specified in the grid were obtained from three sources. For regions outside of the Mississippi Sound, depths are based on digitized contour lines displayed on NIMA and NOS nautical charts. Contours were digitized for the entire Gulf of Mexico as well as for portions of the Caribbean Sea and Straits of Florida that lie within and immediately outside of the modeling domain. Depths were converted from fathoms or feet, depending on the chart, to meters, and their vertical datums were adjusted to mean-tide-level (mtl). Contour data were augmented with soundings extracted from the NIMA Digital Nautical Chart database; these soundings coincide, with respect to location and depth, to those printed on NOS and NIMA charts. As with the contours, soundings were converted to mean-tide-level, using the conversion factors printed on the nautical charts.

The second source of data is a database generated in the Northern Gulf of Mexico Littoral Initiative (NGLI), a consortium of Federal and state agencies, universities and private contractors. The U.S. Navy serves as lead agency in the consortium. The NGLI is a pilot program for developing regional-scale forecasting systems in the littoral zone for military training and coastal resource management. One task performed by the NGLI included bathymetric surveys over portions of the Mississippi Sound. These data were augmented with depths taken from NOS-published charts, and then interpolated on to a uniform mesh having 3 arc-sec resolutions, in latitude and longitude, to form its bathymetric database.

In the vicinity of Horn Island Pass and along the Pascagoula Channel, depths obtained from the Mobile District were extracted from pre- and post-dredging bathymetric surveys. These soundings, exceeding 260,000 in number, are referenced to the Mississippi east state plane NAD 1927 coordinate system and their vertical datum is mean-lower-low-water (mllw). These data were converted from state plane coordinates to latitude and longitude coordinates referenced to NAD 1983 using the USACE coordinate transformation program, Corpscon. Furthermore, the vertical datum were converted from mllw to mean-tide-level (mtl), where mtl is defined as 2.78 m (0.85 ft) above mllw.

Assigning depths to the grid nodes were performed by first assembling data from each source into a single database. Nodal depths were computed using a distance-weighted algorithm that weights each sounding or data point inversely proportional to its distance from that node. After completing the interpolation task, coastline nodes were assigned depths equal to 1 m (0.3 ft) over the majority of the grid. Along the Island of Cuba and the eastern shore of the Yucatan Peninsula, shoreline nodes were assigned depths of 10 m (30.5 ft).

One significant error exists in the NGLI bathymetric database. In the region between Singing River Island and the mainland is a turning basin and port servicing a U.S. naval base that is dredged to a depth of about 12.19 m (40 ft). However, the NGLI database contains depths of about 0.91 m (3 ft) for this area. Consequently, nodal depths were corrected to reflect the actual depth of the port.

Model Calibration

During the process of establishing a numerical model to represent a given study area, calibration is performed to ensure it adequately predicts hydrodynamic conditions. Accuracy of a model is influenced by the accuracy of the forcing functions specified at open-water boundaries, representation of the geometry of the study area (i.e., bathymetry and shoreline), errors induced by the truncated terms associated with the governing equations, and to values of certain model parameters, principally the bottom friction coefficient. A satisfactory comparison between calculations and measurements in the calibration procedure provides confidence that the model adequately replicates hydrodynamic processes.

Calibration exercises for this study were conducted in two phases: In the first phase, the model was simulated under solely astronomical forcing, whereas both astronomical and meteorological forcing was imposed in the second phase. Performing the calibration in this fashion permits evaluating model accuracy with respect to each forcing mechanism, identifying sources of error. Because constituents are synthesized from long-term time-series of measured tides and currents, they implicitly contain the attenuation of the tide and current induced by bottom friction.

Forcing mechanisms specified in the model included tide, tide-generating potential, river discharge, and the Coriolis force. Time-varying tidal elevations specified at nodes along the open ocean boundaries were synthesized using the following eight tidal constituents: M_2 , S_2 , N_2 , K_1 , O_1 , Q_1 , P_1 , and K_2 . Constituent information was extracted from a database developed by LeProvost and Poncet (1987). Because the model domain is of sufficient size that celestial attraction induces tide within the grid proper, tide-generating potential functions were included in the simulation calculations, and these functions incorporated the eight tidal constituents.

Astronomical calibration

The hydrodynamic model was calibrated by adjusting the bottom friction and the lateral eddy diffusivity coefficients so that model-generated water-surface elevation and current time-series compared favorably to those reconstructed from tidal constituents. Water-surface elevation constituents were downloaded from the World Wide Web site maintained by NOS. Additional constituent information was obtained from Outlaw (1983) that documents a tidal data analysis for Mississippi Sound. Data collected includes time-series of water-surface elevations and currents. Under contract to the Mobile District, the NOS deployed 24 gages in and around the sound and collected water-surface elevations for a 182-day period, and subsequently processed these measurements.

Raytheon Oceans Systems Company conducted a current measurement program in the sound where 20 m (65.62 ft) of data were collected over a 60-day period. Information stemming from the field measurement programs was analyzed by Outlaw (1983) and subsequently used by Schmalz (1985) in a hydrodynamic investigation of the sound for the Mobile District. (Although NOS collected the water levels synthesized by Outlaw, this report refers to those extracted from Outlaw as prototype so as to avoid confusion between these constituents and those obtained from the NOS Web site.) Station locations are shown in Figure 4-4.

Calibration simulations were conducted for equilibrium tidal conditions (i.e., all eight constituents mentioned previously begin the simulation in phase.), which depicts spring tide. A 5-sec time-step was used in each simulation, and the bottom friction and eddy diffusivity coefficients were specified globally throughout the model domain.

The optimum values of the global bottom friction and eddy diffusivity coefficients were found to be 0.002 and 1.0 sq m/sec (0.021 and 10.7 sq ft/sec), respectively. Comparisons of model- and constituent-generated water-surface elevations for the Pascagoula and Dauphin Island gages are presented in Figures 4-5 and 4-6. Spring tidal range for the Pascagoula and Dauphin Island gages is approximately 0.61 m (2.0 ft) at both locations (for simulation day 15). Furthermore, for both stations, model-generated peak tidal elevations are generally within 0.03 m (0.1 ft) of those elevations synthesized from the prototype constituents, with the model overestimating the peak water-surface elevations at peak flood tide. Model-generated tides led the constituent-generated tides by approximately 2 min at peak spring flood tide.

A harmonic analysis was conducted of the model-generated time-series of water-surface elevations for determining the amplitudes and phases of the eight tidal constituents. Comparison of model-generated and NOS-published constituent amplitudes and phases for the Pascagoula station are presented in Figures 4-7 and 4-8, respectively. A line is drawn diagonally across these plots to aid in interpreting comparisons; a symbol lying on this line signifies perfect agreement between the model-generated and prototype-published constituents. A symbol falling to the right or below the line indicates that the model over-predicted the published amplitude (in Figure 4-7) or phase (in Figure 4-8). Conversely, a symbol falling to the left or above the line indicates that the model underpredicted the amplitude or the phase.

For the study area, the K_1 and O_1 constituents are the most dominant constituents, accounting for nearly 74 percent of the spring tide signal. Model- and prototype-generated O_1 amplitudes are nearly identical, with the ADCIRC-generated constituent equal to 0.152 m (0.50 ft) versus 0.149 m (0.49 ft) for the prototype value. For the K_1 constituent, the second largest constituent, the model overpredicted the amplitude by approximately 10 percent, 0.158 m (0.52 ft) as opposed to 0.143 m (0.47 ft). In general, model-generated diurnal constituents compared more favorably with the NOS constituents than did the semidiurnal constituents. For example, model-generated M_2 and S_2 constituents exceeded the prototype-synthesized constituents by 14 and 43 percent, respectively. This difference in accuracy may be due to the duration of the simulation (i.e., 60 days) used in the harmonic analysis; amplitudes of the semidiurnal constituents were generally smaller than for the diurnal constituents, suggesting that a greater

number of tidal cycles may be necessary for extracting these constituents from the harmonic analysis.

The greatest differences in phase between the model- and prototype-generated constituents occurred with the Q_1 and P_1 constituents, where ADCIRC computed a phase of 12.5 deg for the Q_1 constituent versus 283.7 for the prototype-generated phase; for the P_1 constituent, the ADCIRC- and prototype-generated phases were 16.9 and 309.4 deg, respectively. NOS-generated constituents derived from long-term gage records recorded at Dauphin Island, AL, and Gulfport, MS, define the phases for the Q_1 constituent as 26.6 and 28.2 deg, respectively, and 49.9 and 58.1 deg, respectively, for the P_1 constituent. Because the constituents were synthesized from longer-term records, they are probably more accurate than those published in Outlaw (1983). ADCIRC-generated phases agree more closely with the long-term phases computed by NOS than with the phases computed in the shorter-term prototype analysis (i.e., 180 days).

Comparisons of constituent-synthesized current time-series are presented in Figures 4-9 through 4-14, and station numbering is consistent with those presented in Outlaw (1983). Sta 12 (shown in Figure 4-4) is centrally located in the Sound, approximately midway between Biloxi and Pascagoula, MS; currents can be characterized as weak, with peak spring current approaching 0.06 m/sec (0.2 ft/sec) in the east-west direction and 0.03 m (0.1 ft) in the north-south direction. For both the north-south and east-west directions, currents computed with the ADCIRC-generated constituents were within 0.015 m/sec (0.05 ft/sec) with the prototype-synthesized constituents at peak spring tide. Current at this station was predominately in the east-west direction. Figure 4-9 shows, for both the model and prototype water levels, spring tide occurring at about day 14. In Figure 4-10, however, water levels synthesized with the prototype-computed constituents show peak spring tide occurring at about simulation day 18. This discrepancy is attributed to phase errors in the semidiurnal constituents; synthesized using currents measured over a 60-day period, this length of time may be too short for extracting weaker constituents in the harmonic analysis. For example, two current meters were deployed at this site, one towards the bottom and a second towards the surface; for the M_2 constituent, the north-south phases for the bottom and surface current meters were 233.0 and 281.9 deg, respectively, or a difference of almost 49 deg. Given the shallow waters in the sound, precluding the likelihood of a stratified flow regime, this discrepancy was most likely due to a combination of the short measurement period together with the sound being a wind-dominated system.

Sta 13 resides on the western bank of the Pascagoula Channel in close proximity to the Gulf Intercoastal Waterway (GIWW). Comparisons of current for this station are presented in Figures 4-11 and 4-12. These figures show the north-south current is approximately 0.12 m/sec (0.4 ft/sec), whereas the east-west current is about 0.030 m/sec (0.1 ft/sec) at peak spring tide. For the north-south current, model-synthesized current is generally within 0.015 m/sec (0.05 ft/sec) of the prototype current at peak spring tide, whereas ADCIRC overestimates the east-west current by about 0.030 m/sec (0.1 ft/sec). Small discrepancies can be seen between the two time-series at neap tide in both figures. As with sta 12, these errors are attributed to the weak semidiurnal constituents.

Sta 14 is located in Horn Island Pass to the west of the Pascagoula Channel, and comparisons of constituent-generated current are presented in Figures 4-13 and 4-14. Model- and prototype-synthesized current, for the east-west current, show peak spring tide occurring on day 14. The model-synthesized north-south shows peak spring tide occurring on this day, as well. However, the prototype-synthesized current shows peak spring tide occurring 1 day earlier, possibly due to the weaker semidiurnal constituents.

Model- and prototype-synthesized current speeds are generally within 0.030 m/sec (0.1 ft/sec) in the east-west direction; however, model-synthesized currents are 0.152 m/sec (0.5 ft/sec) during peak spring ebb tide than the prototype speed. These differences may be due to the geomorphologic changes in Horn Island Pass over the past 2 decades. This pass contains several shoal areas with relatively deep channels passing between them. Given the pass is directly exposed to severe weather, and resulting extreme wave action and current, it is likely that shoal areas have migrated over the years. Because current is a function, in part, of the bathymetry, changes in bathymetry may have induced greater currents at this site.

Meteorological calibration

Model testing under meteorological conditions was made via a hindcast simulation beginning on Year Date 32 (i.e., 1 February 2001) at 0000 Greenwich Mean Time (GMT) and concluded at 0000 GMT on Year Date 76 (i.e., 15 March 2001). The bottom friction and eddy diffusivity coefficients remained unchanged from the astronomical calibration simulation. A 5-sec time-step was used in the simulation and a 5-day ramping function was applied to the tidal signal and the wind fields in order to prevent generating spurious modes of oscillation by starting the model under full forcing.

Wind fields supplied to the model were extracted from the NOAA National Centers for Environmental Prediction (NCEP) database. This database contains wind speeds and directions, at 6-hr intervals, having a spatial resolution of about 1.9 deg in latitude and longitude. Subsequent processing interpolated these winds onto a Gaussian grid having a spatial resolution of 0.25 deg. Winds were also interpolated in time, yielding hourly wind fields. Thereafter, measured wind speeds and directions, recorded at eight buoys and Coastal-Marine Automated Network (C-MAN) stations operated by the NOAA National Data Buoy Center (NDBC) in the gulf, were blended with the NCEP wind fields, making the wind fields more representative of the wind conditions experienced in the study area during the calibration period. Figures 4-15 and 4-16 display the wind speeds and directions, respectively, measured at the NDBC C-MAN sta DPIA1 during the calibration period. This station is located at lat. 30°15'N., long. 88°4'W., or along the eastern shore of Dauphin Island.

Time series of measured water-surface elevations were obtained from the Mobile District, which maintains 14 gages in the sound and archives these data. Gages for which data are available include the Pascagoula PI gage, located in the triangle between the Pascagoula and Bayou Casotte Channels, and Gulfport, residing about 48.28 km (30 miles) west of the study site. These data were augmented with current measurements collected at a station in close proximity to

the intersection of the Pascagoula Channel and the GIWW. This station was deployed as part of this study (see Chapter 2).

In the initial calibration simulation, the model underpredicted measured current. This finding is consistent with previous model applications in coastal areas where wind is the dominant forcing mechanism. Furthermore, these areas are located in colder regions, including Oregon and Alaska, where the air temperature can be lower than the ambient water temperature. Shear stress imparted on the water surface is a function of the wind speed as well as the air density. In situations when the air is colder than the water, shear stresses can be twice as great than if the water is cooler than the air.

ADCIRC uses Garratt's (1977) wind drag formula for computing wind shear stresses in the model. The formula is based on an empirical relationship between wind speed and resulting shear stress, and was developed using in-situ wind and current measurements, principally collected during strong wind events. This formulation does not directly account for temperature differences between the air and water. Because currents were measured during February and March, it is likely that air temperatures were as cool, or colder than the water temperature. Consequently, wind speeds were adjusted to account for the increased shear stresses.

Several tests were conducted where wind speeds were increased prior to their processing by the model. The most accurate test occurred when wind speeds were increased by 50 percent at all nodes lying outside of the sound. Within the Sound, winds were increased by 50 percent if the wind was blowing from the southeast or southwest quadrants, or roughly from the sea. No adjustments were made to winds if they were blowing from the northeast or northwest quadrants. (Increasing speeds for these winds led to excessive drying of low-lying areas and/or model instabilities.)

Figure 4-17 displays a comparison of modeled and measured time-series of water-surface elevation for the Pascagoula PI gage. The time-series of measured water levels shows that wind has a significant influence on water levels in the study area. Astronomical tides for this site approach 0.73 m (2.4 ft) during spring tide, whereas with wind, water levels varied over 1.37 m (4.5 ft) during the calibration period. Furthermore, wind can suppress, such as on Year Date 58, the sinusoidal oscillations of the astronomical tide.

From Year Date 36 through 49, the predominant wind direction was from the southeast, and wind speed averaged about 6 m/sec (13 mph). Within this time frame, shorter periods, such as Year Date 42, winds were from the north. Over this 14-day period, the model tends to overpredict peak high water levels while underpredicting low water. This overprediction varies from less than 0.030 m (0.1 ft) on Year Date 38, to about 0.182 m (0.6 ft) on Year Date 45. The greatest discrepancy in low water occurs on Year Date 39, where the model overestimates the water level by about 0.243 m (0.8 ft).

Model accuracy improved from Year Date 50 through 68, where the simulated water levels more closely matched the measured data. During this period, modeled peak water-surface elevations are generally within 0.1 ft of the measured data, and at low water, model-predicted water levels are within 0.3 ft. From Year Date 69 through 76, wind dominates the astronomical forcing, suppressing the sinusoidal oscillations in the water level. Water levels computed

by the model displays this suppression, although it underestimates the drawdown in water level on Year Date 70, and overestimates the drawdown on Year Date 72 and 73.

As shown in Figure 4-18, model results show the same characteristics at the Gulfport gage as it had at Pascagoula gage. Over the 14-day period from Year Date 36 through 49, the model tended to overpredict peak water levels while underpredicting low water. However, discrepancies between modeled and measured data are less at the Gulfport gage than at Pascagoula. For example, on Year Date 48 and 49, the model underpredicted the drawdown in water levels by 0.121 m (0.4 ft) and 0.182 m (0.6 ft) on these dates, respectively at Gulfport, versus 0.182 m (0.6 ft) and 0.243 m (0.8 ft) at Pascagoula.

From Year Date 50 through 62, the model closely matched the measured water levels recorded at Gulfport, where the model-generated peak water levels were within 0.030 m (0.1 ft) of those measured. From Year Date 63 through 69, the model overpredicts the drawdown in water levels with the greatest discrepancy occurring on Year Date 64, where the model overpredicted the water level by 0.243 m (0.8 ft).

Figures 4-19 and 4-20 display current speed and direction measured at deployment site 1 for the period Year Date 69 through 75. (This site is located at lat. 30°25.6', long. 88°46.5', or in close proximity to the GIWW at the Pascagoula Channel.) In general, the model captures the trends in both the current speed and direction, such as from Year Date 70 at 1200 GMT through Year Date 72 at 0600 GMT, where the model matches the 0.304 m/sec (1 ft/sec) southerly current measured at the deployment site. Model accuracy does, however, diminish over certain periods of the simulation, such as Year Date 69 at 1200 GMT, Year Date 70 at 1200 GMT, and Year Date 74 at 0000 GMT. On each occasion when model accuracy diminishes, it is immediately preceded by rapid shifts in wind direction.

Figure 4-21 presents wind directions measured at the NDBC C-MAN sta DPIA1. Prior to Year Date 69 at 1200 GMT, winds were blowing from the north-northeast, then, shifting over about a 1-hr period, began blowing from the south-southeast. On Year Date 72, winds blew from the east-southeast, then shifted over a 6-hr period, and began blowing from the west-northwest. For Year Date 74, winds blew from the east-northeast, shifting to the west-northwest over a 6-hr period. After about a 6- to 12-hr period from when the winds began shifting, the model then produced currents that matched the measured currents in speed and direction.

Decreasing model accuracy during periods of rapidly changing wind directions is attributed to the coarse temporal and spatial resolution of the NCEP winds. Fast moving storm fronts can pass through a region with forward speeds exceeding 64.37 km/hr (40 mph). Over a 6-hr period, which is the temporal resolution of the NCEP wind fields, a front can travel 386.24 km (240 miles), or about twice the spatial resolution (i.e., 1.93 deg) of the grid used in generating winds; the edge of the front will traverse three grid nodes. The edge of a slower moving front having a forward speed of 32.18 km/hr (20 mph), e.g., will traverse two grid nodes. As a consequence, should the edge of the storm not coincide with a particular node, peak storm-induced wind speeds will be underestimated,

and the passage or phasing of the leading edge of the storm will be smeared across the 6-hr period between wind field "snapshots."

Adaptation of Calibrated Model

The grid constructed for the existing sound condition was adapted to represent each of the three proposed confined disposal facility (CDF) configurations. These grids are shown in Figures 4-22 through 4-24. The surface area of each CDF is 4,046,825 sq m (1,000 acres). Alternative 1 was constructed by expanding Singing River Island along its southern and western shore. Aligned with the northern shore, the expansion extends 1,310.64 m (4,300 ft) towards the west, and aligned with the eastern shore, the expansion extends about 1,188.72 m (3,900 ft) to the south. The southern shoreline of the expansion roughly parallels the existing arc-shaped southern shoreline of the island, and is displaced about 1,188.72 m (3,900 ft) from the present shoreline.

Alternative 2 is circular in shape, having a diameter of about 2,286 m (7,500 ft). Its northern shoreline is approximately 1,056 m (3,450 ft) south of Singing River Island, and its southwestern edge is located about 1,188.72 m (3,900 ft) from Round Island. Pascagoula Channel resides about 813.81 m (2,670 ft) (at its closest approach) to the east-northeast from this alternative. As with Alternative 2, Alternative 3 is circular in shape with a diameter of 2,286 m (7,500 ft). Its southern extent resides about 2,682.24 m (8,800 ft) north from the intersection of the Pascagoula and Bayou Casotte Channels, and the minimum distance between this island and the mainland is about 609.6 m (2,000 ft). Furthermore, it is positioned such that its southwestern boundary resides 259.08 m (850 ft) from the Pascagoula Channel (north of the intersection), and its eastern boundary lies 850 ft from the Bayou Casotte Channel.

The existing-condition grid was developed with the nodes lying along the outer extents/limits of each CDF. Furthermore, elements were aligned such that they outlined each CDF. Consequently, a CDF is incorporated into the grid by deleting those elements and nodes lying within the lateral extent of a particular CDF. Designed in this fashion, the existing-condition mesh was readily adapted for an alternative CDF, and comparisons between alternatives can be made more accurately because the nodal positions and their connectivity (i.e., elements) were not changed. One exception to this is at the southeastern extent of Alternative 1, where it extends into the footprint of Alternative 2; at this location the connectivity between three nodes was changed because no one design could be developed to incorporate both alternatives without changing the connectivity. Other than for those nodes along the CDF boundaries, depths in the alternative-configuration grids were unchanged from the existing-configuration grid. Along the CDF boundaries, nodes were assigned depths of 1 m (3 ft) to minimize wetting and drying of adjacent elements during a tidal cycle.

Two series of simulations were conducted for evaluating the hydrodynamic changes induced by constructing a CDF. The first series represents peak spring tidal conditions during fair weather. Two sets of simulations were conducted for the first series, and each set consisted of four simulations: one simulated existing-sound conditions and one simulation for each alternative CDF configuration. In the first set, the annual-average daily river discharge was specified at the upstream boundaries of the Pascagoula and Escatawpa Rivers,

whereas in the second set, specified river discharges were 50 percent greater than the annual-average daily flow rates.

Annual daily-averaged river discharges for the Pascagoula and Escatawpa Rivers were extracted from a database maintained by the U.S. Geological Survey. Discharges assigned to the Pascagoula River are based on measurements recorded at the Merrill, MS, gage, whereas Escatawpa River discharges are based on records collected at the Agricola, MS, station.

River inflows that were increased by 50 percent are likely more representative of the average river inflows experienced at the confluence of the East and West Pascagoula Rivers and the gulf than the averaged flows measured at the Merrill gage; the average river inflows are more representative of low river flow conditions. The total area of the Pascagoula River watershed is approximately 2.4 billion sq m (9,500 square miles), with the drainage area upstream of the Merrill gage accounting for 1.7 billion sq m (6,600 square miles), or 56 percent of the total area (Schmalz 1985). Given that the downstream portion of the watershed represents about 44 percent of the total drainage area, flows increased by 50 percent account for drainage from the lower area (with 6 percentage points added to account for uncertainty).

Downstream of Merrill, the Pascagoula River divides into two branches, each meandering through expansive marshland before their confluence with the sound. Further complicating the riverine/coastal hydraulics, are the many small channels connecting these branches. Rather than attempting to model this system, the east and west branches of the Pascagoula River were defined in the grid as two separate rivers, with no interconnecting channels, and no storage areas (for representing marshlands) adjacent to the branches. In a study sponsored by the State of Mississippi Department of Environmental Quality, the Hazan Company determined that the West Pascagoula River transported approximately 65 percent of the flow measured at the Merrill gaging station, whereas the eastern branch carried the remaining 35 percent. Discharges specified in the model reflect these percentages.

The second series of tests simulated winter storm conditions within the sound. Six winter storms were selected from the 10-year period of 1990 through 1999, and hindcast simulations were conducted for each storm. As with the calibration hindcast, tidal conditions were imposed in the model to correspond with the dates of the storms, and bottom friction and eddy diffusivity coefficients remained unchanged from the calibration simulation. The duration of each simulation was 8 days, with the storm arriving at about day 7 of the simulation. A 2-day ramping function was applied to the tidal signal and the wind field for minimizing spurious oscillation modes. A 2-sec time-step was used in each simulation.

As with the calibration simulation, applicable wind fields were extracted from the NCEP database and blended with measured winds. Wind speeds were increased by 50 percent for all nodes lying outside of the sound. Within the sound, winds blowing in a clockwise direction from the east (i.e., 90 deg) to those blowing from the west (i.e., 270 deg) were increased by 50 percent. Winds blowing in a clockwise direction from the west to those coming from the east were unchanged.

Analysis of Alternatives

Figures 4-25 and 4-26 display peak spring flood and ebb current, respectively, under solely astronomical forcing for the existing-configuration condition. At peak flood, currents in the study area are generally slow, with speeds of about 0.15 m/sec (0.5 ft/sec), and have trajectories towards the west-northwest. In the vicinity of the West Pascagoula River, river inflows empty into the sound along its western bank and flow westward. For the East Pascagoula River, river inflow is directed southward along the Pascagoula Channel, subsequently bending towards the west as it flows along the southern shore of Singing River Island; a portion of the discharge emanating from the eastern channel empties into the naval turning basin located north of Singing River Island.

During peak spring ebb, the greatest currents occur at the mouth of the West Pascagoula River where speeds are approximately 0.27 m/sec (0.9 ft/sec). Discharge emanating from the river spreads in a semicircular fashion, with the bulk of the discharge directed towards the south, where it changes trajectory towards the southeast as it passes Singing River Island to the north of Round Island. Currents between these islands have speeds reaching about 0.17 m/sec (0.6 ft/sec). A portion of the river discharge is directed towards the southeast at the river mouth, and flows into the turning basin.

Figures 4-27 and 4-28 display peak spring flood and ebb current, respectively, for the Alternative 1 condition. For both peak flood and ebb tide, expanding Singing River Island by approximately 1,158.24 m (3,800 ft) towards the southwest induces faster current speeds between this island and Round Island. Maximum flood current increased from 0.18 to 0.21 m/sec (0.6 to 0.7 ft/sec), whereas the ebb current increased from 0.21 to 0.27 m/sec (0.7 to 0.9 ft/sec). These increases are attributed to reducing the conveyance, or cross-sectional area, between the islands. For both flood and ebb, the increased current is below the incipient speed (i.e., 0.3048 m/sec (1 ft/sec)) for sediment transport of noncohesive sediment.

By extending Singing River Island approximately 1,310.64 m (4,300 ft) to the west, Alternative 1 blocks a greater portion of the southerly current flowing from the West Pascagoula River and diverts it towards the naval basin. Time-series of currents for the existing-configuration and Alternative 1 conditions at the sta A location are displayed in Figure 4-29 and compared in Figure 4-30. (Comparisons are made with currents computed in shallower water because these currents would be more representative of those a pilot would encounter while navigating a ship.) Peak ebb current increased from 0.27 to 0.36 m/sec (0.9 to 1.2 ft/sec), or by 33 percent; a negligible change in peak flood current was noted at this station.

Storm conditions increase the disparity in current between the existing-configuration and Alternative 1 conditions computed at sta A. As shown in Figure 4-31, the February 1998 winter storm increased the current from 0.85 m/sec (2.8 ft/sec) for the existing-configuration condition to 1.005 m/sec (3.3 ft/sec) with Alternative 1 in place. These currents reflect flood tide during the storm's passage. During the subsequent ebb tide, the peak current computed at sta A for the existing and Alternative 1 configurations were 0.57 and 0.79 m/sec (1.9 and 2.6 ft/sec), respectively, an increase of 37 percent. Table 4-1

compares peak ebb current under storm conditions at sta A. As shown, Alternative 1 increases the storm-induced ebb current entering the turning basin with increases ranging from 19 to 43 percent.

Table 4-1
Comparison of Peak Ebb Current at Station A During Winter Storm Events

Storm Date	Peak Ebb Current Alternative 1 (ft/sec)	Peak Ebb Current Existing Configuration (ft/sec)	Increase in Peak Ebb Current (percent)
March 1993	2.7	2.0	35
January 1996	2.6	1.9	37
March 1996	4.3	3.6	19
February 1998	3.3	2.8	43

For sta G, Figure 4-32, which resides between Singing River and Round Islands, peak flood current was 0.67 and 0.79 m/sec (2.2 and 2.6 ft/sec) for the existing and Alternative 1 conditions, respectively. Similarly, for sta H, Figure 4-33, peak flood current was 0.60 and 0.79 m/sec (2.0 and 2.6 ft/sec) for the existing and Alternative 1 conditions, respectively. With the increased current, a possibility exists that Round Island may become more susceptible to erosion with the construction of Alternative 1.

For determining a more "typical" or average ebb-wind condition, computed ebb currents at sta A were compared for the three peak ebb events occurring prior to the arrival of the January 1996 winter storm. For each peak ebb tide, currents increased by 18 percent to 33 percent with the Alternative 1 configuration compared to those computed with the existing-configuration condition. Currents increased from 0.27 to 0.36 m/sec (0.9 to 1.2 ft/sec), 0.36 to 0.48 m/sec (1.2 to 1.6 ft/sec), and 0.67 to 0.79 m/sec (2.2 to 2.6 ft/sec) for the three ebb events.

Figures 4-34 and 4-35 display peak spring flood and ebb currents under solely astronomical forcing for the Alternative 2 condition. For both spring and ebb conditions, the CDF modifies the present-day current patterns as waters flow around this obstruction, increasing the current along its southwestern and northern extent. For example, during spring flood, currents along its southwestern and northern edges are about 0.2 m/sec (0.7 ft/sec), although the spatial area exhibiting higher current is greater along the southwestern edge than its northern edge. In addition, Alternative 2 induces greater currents, during peak ebb tide, to the north and south of Round Island, although differences are small.

Furthermore, during ebb tide, Alternative 2 diverts currents between this CDF and Singing River Island towards the east, as opposed to the southeast for the present-day condition. At sta C, presented in Figures 4-36, peak current increases from 0.22 to 0.27 m/sec (0.75 to 0.90 ft/sec). At hour 316, peak currents are 0.20 and 0.14 m/sec (0.66 and 0.46 ft/sec) for the Alternative 2 and existing-configuration conditions, respectively. Their easterly velocity components, which are roughly perpendicular to the channel, are 0.19 and 0.11 m/sec (0.65 and 0.38 ft/sec). However, model tests conducted with wind forcing show no significant change in current direction between the existing condition and Alternative 2 configurations. It is a possibility that, under a

westerly wind and ebb tide event, Alternative 2 could induce greater crosscurrents at the channel in the vicinity of sta C.

Prior to the arrival of the January 1996 winter storm, the magnitude of the ebb current computed at sta C was 0.48 and 0.36 m/sec (1.6 and 1.2 ft/sec) for the Alternative 2 and existing-condition configurations, respectively. During the passage of this storm, which induces a setdown in the water level, the computed current was 0.73 m/sec (2.4 ft/sec) for both configurations.

For the February 1998 winter storm, Alternative 2 induces greater current speeds at sta B and sta C, which are displayed in Figures 4-37 and 4-38. For sta B, the flood current increased from 0.43 to 0.55 m/sec (1.4 to 1.8 ft/sec), whereas for sta C, the flood current increased from 0.46 to 0.61 m/sec (1.5 to 2.0 ft/sec). At both stations, current direction is to the northwest, roughly parallel to the channel. At sta E and F, the CDF diverts the current towards the north, as opposed to a northwesterly heading for the existing-configuration condition.

Comparing the three tide cycles occurring prior to the arrival of the January 1996 winter storm, current directions at sta E during flood tide are 350 deg for the Alternative 2 condition versus 300 deg for the existing-configuration condition. For sta F, current directions are 345 and 300 deg for the Alternative 2 and existing-configurations conditions, respectively. Current speeds during these tide cycles are relatively small at 0.12 m/sec (0.4 ft/sec).

At sta G and H, currents under solely astronomical forcing for the Alternative 2 condition are slower for both flood and ebb tide than those computed with the existing-configuration condition. Figures 4-39 and 4-40 display these comparisons for sta G and sta H, respectively. For peak spring flood tide under solely astronomical forcing, currents at sta G are 0.12 and 0.17 m/sec (0.40 and 0.55 ft/sec) for the Alternative 2 and existing-configuration conditions, respectively. Similarly, for sta H, currents are 0.12 and 0.16 m/sec (0.38 and 0.52 ft/sec) for the Alternative 2 and existing-configuration conditions, respectively. For peak spring ebb tide, currents at sta G are 0.17 and 0.22 m/sec (0.55 and 0.72 ft/sec) for the Alternative 2 and existing-configuration conditions, respectively. For sta H, peak spring ebb currents are 0.14 and 0.21 m/sec (0.47 and 0.70 ft/sec) for the Alternative 2 and existing-configuration conditions, respectively.

Similar reductions in current are also noted for the winter storms. For example, prior to the passage of the February 1998 winter storm, the model predicted a 0.64 m/sec (2.1 ft/sec) flood current at sta G (Figure 4-32) for the existing-configuration condition, and a flood current of 0.49 m/sec (1.6 ft/sec) for Alternative 2 condition. Immediately after the storm passage, the model-predicted ebb currents for the existing-configuration and Alternative 2 conditions are 0.43 and 0.30 m/sec (1.4 and 1.0 ft/sec), respectively. Reduction in currents immediately west of Alternative 2 suggests that a greater percentage of West Pascagoula River discharge will be transported south of Round Island than presently occurs.

Figures 4-41 and 4-42 display peak spring flood and ebb currents under solely astronomical forcing for the Alternative 3 condition. For both spring and ebb conditions, the CDF modifies the present-day current patterns as waters flow around this obstruction, increasing the current along its southwestern and

northeastern extent. For example, during spring ebb tide, the current along its northeastern edge is about 0.12 m/sec (0.4 ft/sec).

For Alternative 3, minimal changes in current are noted at sta I, which is located between the CDF and the mainland, under solely astronomical forcing. As shown in Figure 4-43, currents for the Alternative 3 and existing-condition configurations at this station are 0.05 and 0.07 m/sec (0.18 and 0.23 ft/sec) for peak spring flood and ebb tide, respectively. Prior to the arrival of the January 1996 winter storm, the magnitude of the flood and ebb current computed at sta I for both the Alternative 3 and existing-configuration conditions were 0.34 and 0.24 m/sec (1.1 and 0.8 ft/sec), respectively. Minimal changes in current are also noted at this station for the February 1998 winter storm. As shown in Figure 4-44, the greatest differences between the existing-configuration Alternative 3 condition occur at hour 125, and are due to a phase shift.

This alternative does impact, however the magnitude and direction of currents along the Pascagoula Channel. As shown in Figure 4-45, peak spring current magnitude at sta D with Alternative 3 in place is 0.27 m/sec (0.9 ft/sec) versus 0.21 m/sec (0.7 ft/sec) with the existing-configuration condition. Prior to the arrival of the January 1996 winter storm, the magnitude of the flood and ebb current computed at sta F for Alternative 3 are 0.52 and 0.42 m/sec (1.7 and 1.4 ft/sec), respectively; for the existing-condition configuration, flood and ebb currents are 0.40 and 0.34 m/sec (1.3 and 1.1 ft/sec), respectively. Comparing the three tide cycles occurring prior to the arrival of the January 1996 winter storm, current directions at sta D during flood tide are 340 deg for the Alternative 3 configuration versus 300 deg for the existing-condition configuration.

Summary

A numerical model for simulating tidal circulation in the Mississippi Sound was developed and calibrated via comparisons to constituent-synthesized and measured water-surface elevations and currents. Tidal harmonic constituent information was obtained from a field measurement program conducted in the early 1980s, and this information was available for 24 sites throughout the sound for water-surface elevation and 20 sites for current. Measured water levels were provided by the Mobile District at 14 gages, including gages located at Pascagoula PI and Dauphin Island. Measured currents were recorded in the vicinity of the intersection of the GIWW with the Pascagoula Channel. The model calibration was conducted in two phases. In the first phase, the model was driven under solely astronomical forcing, whereas in the second phase, hindcast simulations were conducted with the model being run with both astronomical and meteorological forcing. Hindcast simulations were conducted for the period beginning 1 February 2001 and concluding 15 March 2001.

The model reproduced the constituent-synthesized water-surface levels to within 0.03 m (0.1 ft) in amplitude and 2 min in phase at peak spring tide, whereas differences between modeled and constituent-generated currents were generally within 0.03 m/sec (0.1 ft/sec) and 2 min. For meteorological testing, the calibration period began on 1 February 2001 and concluded on 15 March 2001. The model generally matched measured water-surface elevations at the Pascagoula PI gage within 0.06 m (0.2 ft). Model-generated currents agreed well with those measured at the intersection of the GIWW with the Pascagoula

Channel. However, model accuracy diminishes when winds rapidly shift direction, and is attributed to using wind fields having a temporal resolution of 6 hr. This resolution is too coarse to depict rapidly changing wind directions.

Changes to the current fields that can result from construction of each alternative are summarized in the following sections:

Alternative 1. This alternative is constructed by expanding Singing River Island along its southern and western shore. Aligned with the northern shore, the expansion extends 1,310.64 m (4,300 ft) towards the west, and aligned with the eastern shore, the expansion extends about 1,188.72 m (3,900) ft to the south. The southern shoreline of the expansion roughly parallels the existing arc-shaped southern shoreline of the island, and is displaced about 1,188.72 m (3,900 ft) from the present shoreline. The westward expansion blocks a greater portion of the inflow emanating from the West Pascagoula River and diverts it into the naval turning basin, located between Singing River Island and the mainland. Under solely astronomical forcing, model simulations show currents increasing by about 29 percent, whereas under winter storm conditions, model simulations show currents increased in the range of 19 to 43 percent. For more "typical" or average conditions, currents at the naval basin will increase from 18 to 33 percent. This expansion also increases currents flowing between Singing River and Round Islands, possibly leading to erosion of Round Island.

Alternative 2. This alternative is circular in shape, having a diameter of about 2,286 m (7,500 ft), and a surface area of 4,046,835 sq m (1,000 acres). Its northern boundary is approximately 1,051.56 m (3,450 ft) south of Singing River Island, whereas its southwestern edge is located about 1,188.72 m (3,900 ft) from Round Island. Pascagoula Channel resides about 813.81 m (2,670 ft) (at its closest approach) to the east-northeast from this alternative. Under solely astronomical forcing, the model predicts that ebb-current direction north of this CDF is directed towards Pascagoula Channel. However, model tests conducted with wind forcing show no significant change in current direction between the existing-condition and Alternative 2 configurations; it is possible that, under a westerly wind and ebb tide condition, Alternative 2 could induce greater crosscurrents at the channel. Also, a reduction in currents immediately west of Alternative 2 suggests that a greater percentage of West Pascagoula River discharge will be transported south of Round Island than presently occurs.

Alternative 3. As with Alternative 2, this alternative is circular in shape with a diameter of 2,286 m (7,500 ft). Its southern extent resides about 2,682.24 m (8,800 ft) north from the intersection of the Pascagoula and Bayou Casotte Channels, and the minimum distance between this island and the mainland is about 609.6 m (2,000 ft). Furthermore, it is positioned so that its southwestern boundary resides 259.08 m (850 ft) from the Pascagoula Channel (north of the intersection), and its eastern boundary lies 259.08 m (850 ft) from the Bayou Casotte Channel. This alternative does not appear to modify currents between this CDF and the mainland. This alternative does impact, however, the speed and direction of currents along the Pascagoula Channel. Increases in speed are small (about 0.12 m/sec (0.4 ft/sec)) and currents have a northerly, as opposed to a northwesterly, heading in the vicinity of Singing River Island and the channel.

References

- Flather, R. A. (1988). "A numerical model investigation of tides and diurnal-period continental shelf waves along Vancouver Island," *Journal of Physical Oceanography* 18, 115-139.
- Garratt, J. R. (1977). "Review of drag coefficients over oceans and continents," *Monthly Weather Review* 105, 915-929.
- Hagen, S. C., Westerink, J. J., Kolar, R. L., and Horstmann, O. (2001). "Two-dimensional, unstructured mesh generation for tidal models," *International Journal for Numerical Methods in Fluids* 35, 669-686.
- Kolar, R. L., Gray, W. G., Westerink, J. J., and Luetlich, R. A. (1993). "Shallow water modeling in spherical coordinates: Equation formulation, numerical implementation, and application," *Journal of Hydraulic Research* 32(1), 3-24.
- Luetlich, R. A., Jr., Westerink, J. J., and Scheffner, N. W. (1992). "ADCIRC: An advanced three-dimensional circulation model for shelves, coasts, and estuaries," Technical Report DRP-92-6, U.S. Army Engineer Waterways Experiment Station, Vicksburg, MS.
- LeProvost, C., and Poncet, A. (1987). "Finite element method for spectral modelling of tides," *International Journal of Numerical Methods Engineering* 12, 853-871.
- Outlaw, D. G. (1983). "Prototype tidal data analysis for Mississippi Sound and adjacent areas," Miscellaneous Paper CERC-83-1, U.S. Army Engineer Waterways Experiment Station, Vicksburg, MS.
- Schmalz, R. A., Jr. (1985). "Numerical model investigation of Mississippi Sound and adjacent areas," Miscellaneous Paper CERC-85-2, U.S. Army Engineer Waterways Experiment Station, Vicksburg, MS.
- Westerink, J. J., Luetlich, R. A., Jr., Baptista, A. M., Scheffner, N. W., and Farrar, P. (1992). "Tide and storm surge predictions using finite element model," *Journal of Hydraulic Engineering* 118(10), American Society of Civil Engineers, 1,373-1,390.

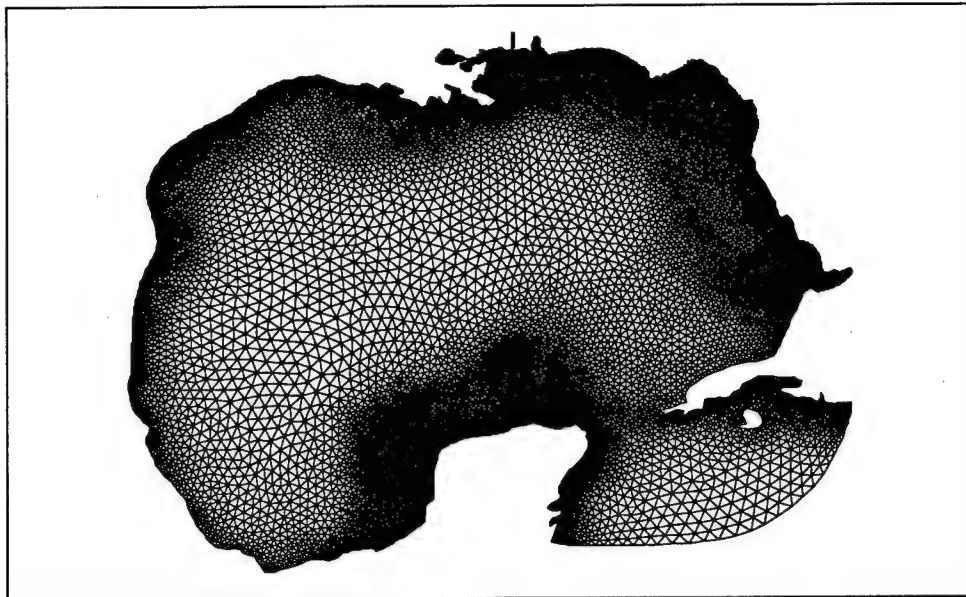


Figure 4-1. Numerical grid

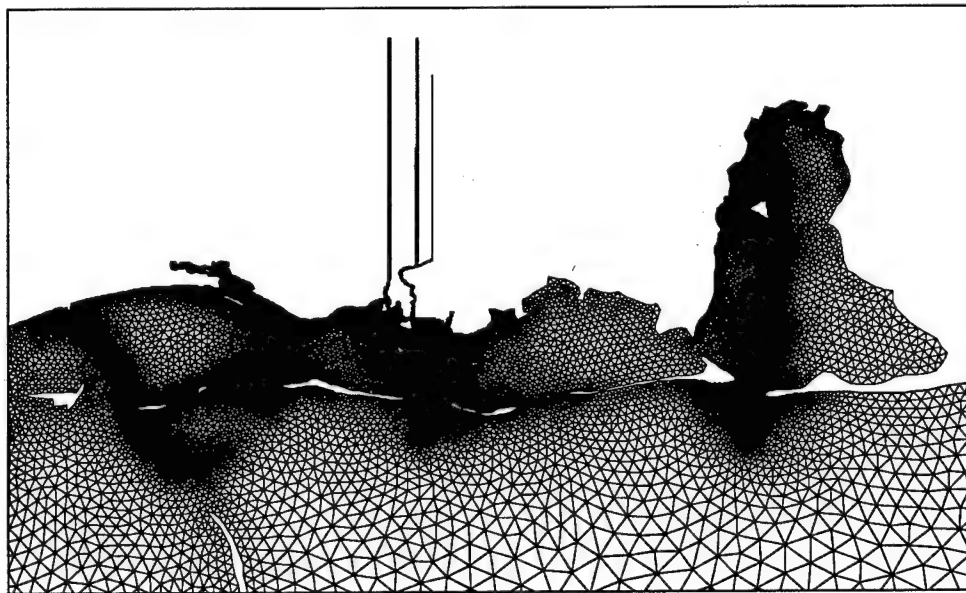


Figure 4-2. Numerical grid within Mississippi Sound

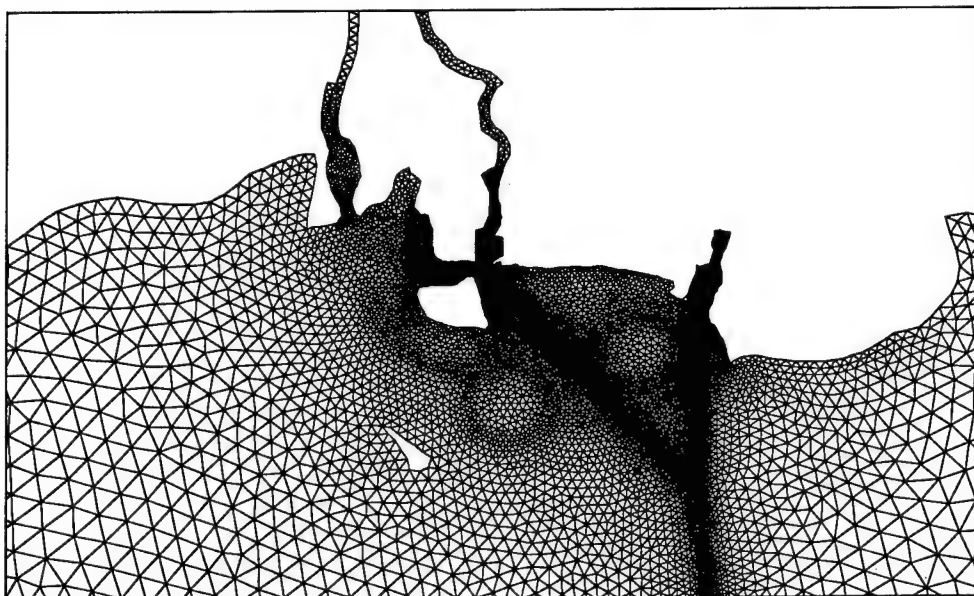


Figure 4-3. Numerical grid in vicinity of Pascagoula, MS

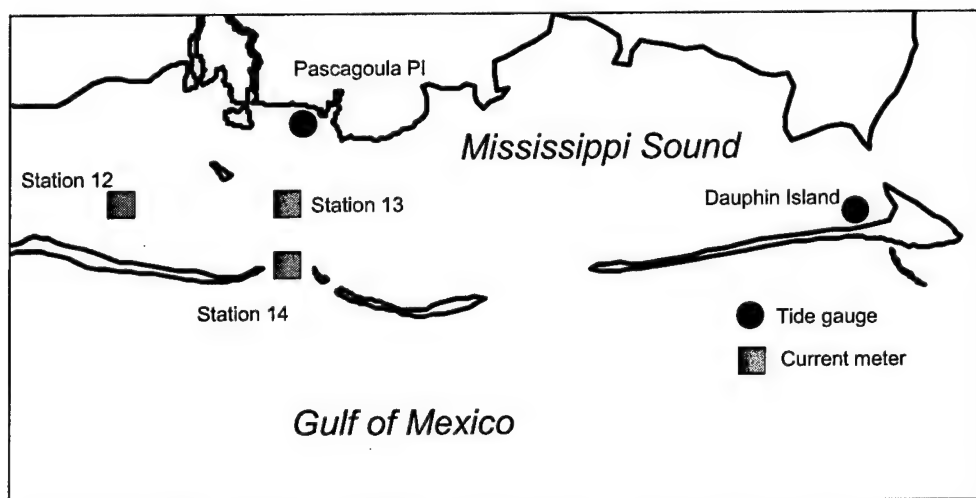


Figure 4-4. Location of tide gages and current meters used in model calibration

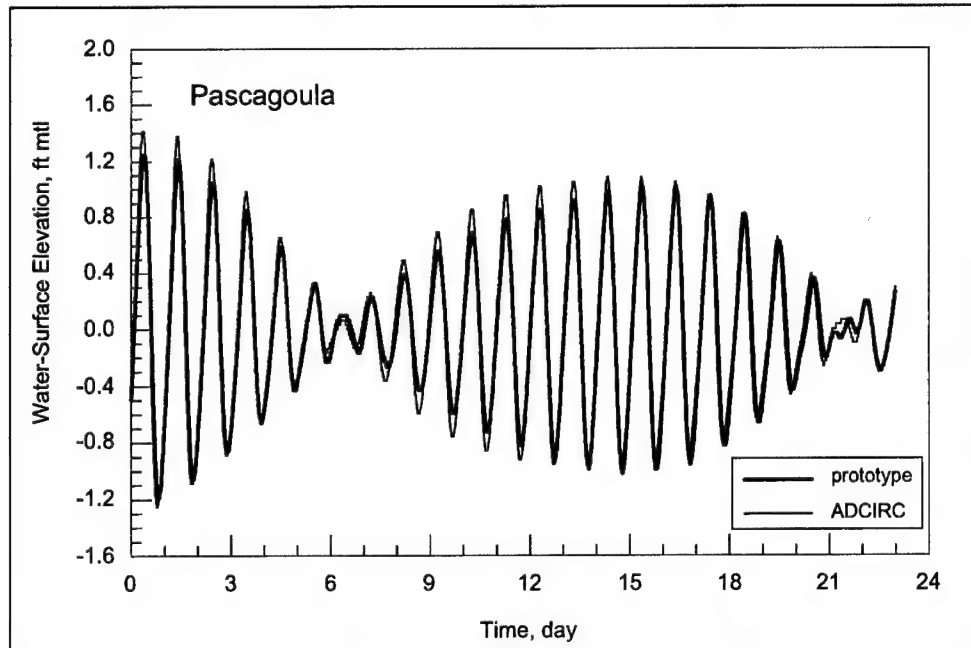


Figure 4-5. Comparison of model- and constituent-synthesized water-surface elevations for Pascagoula, MS

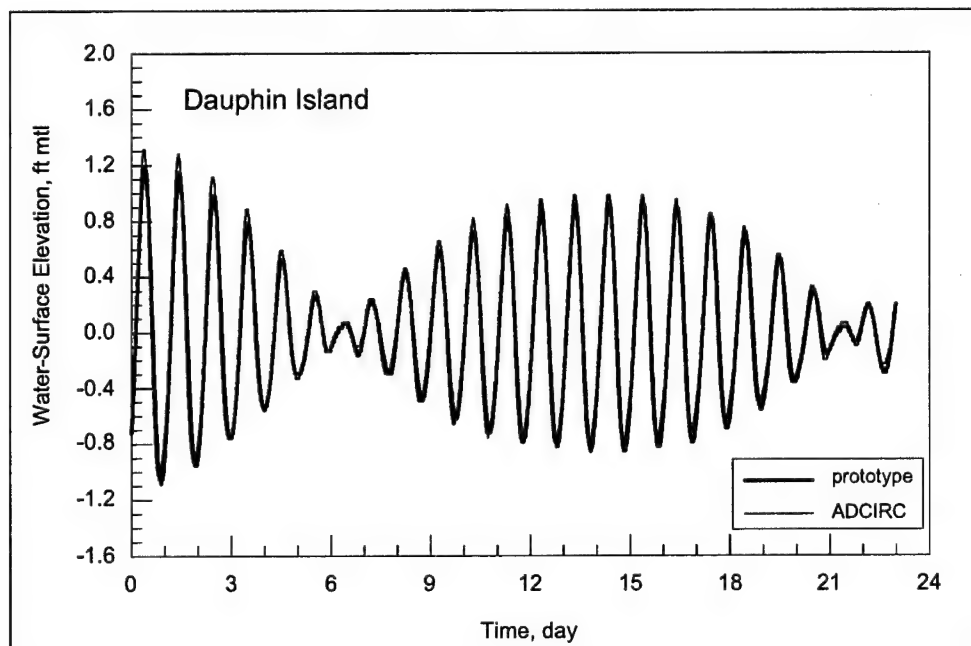


Figure 4-6. Comparison of model- and constituent-synthesized water-surface elevations for Dauphin Island, AL

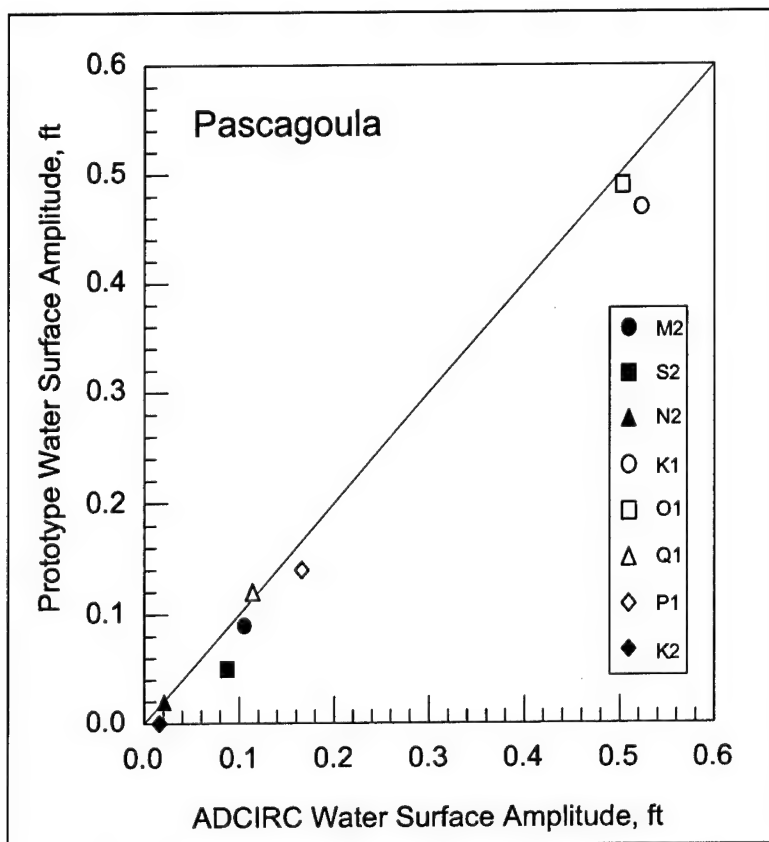


Figure 4-7. Comparison of water-surface amplitude constituents

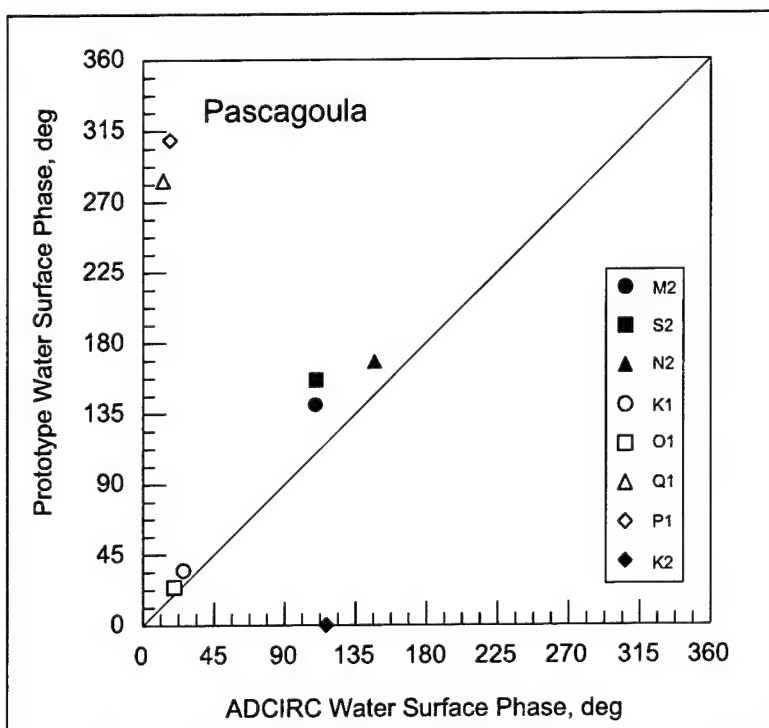


Figure 4-8. Comparison of water-surface phase constituents

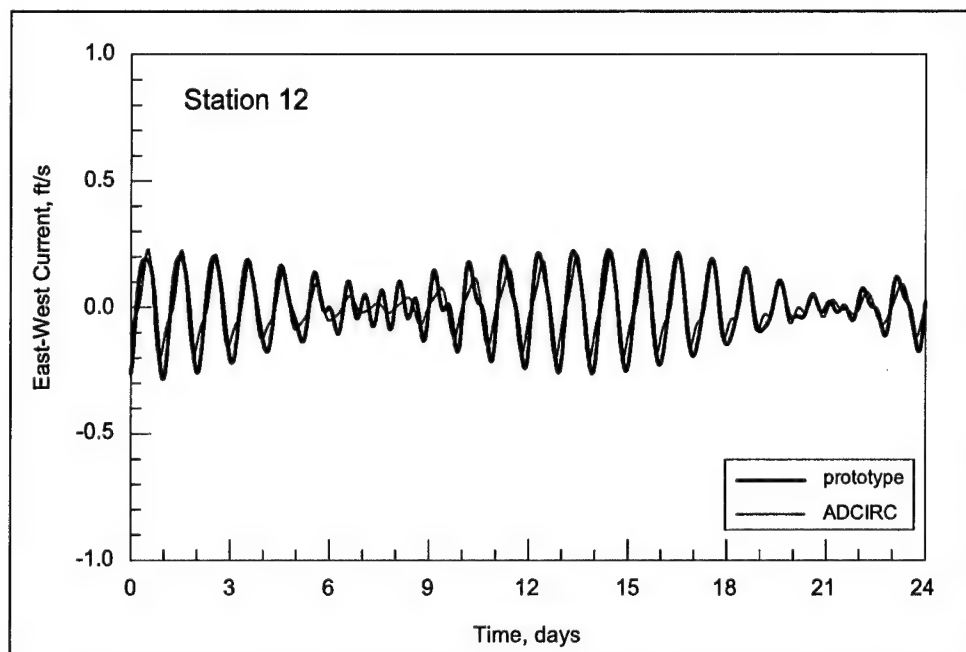


Figure 4-9. Comparison of model- and constituent-synthesized east-west current for sta 12

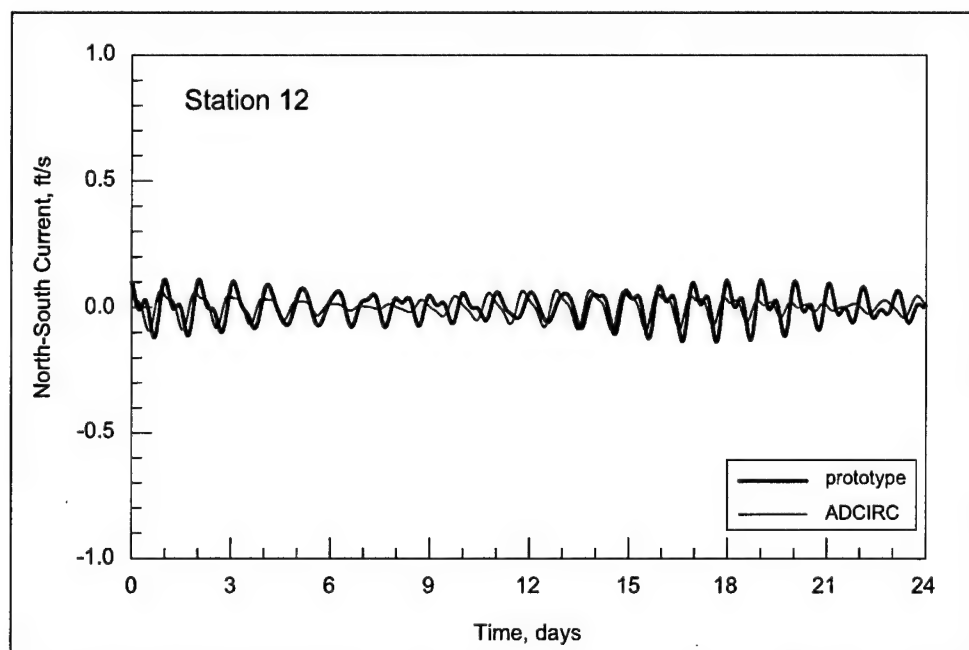


Figure 4-10. Comparison of model- and constituent-synthesized north-south current for sta 12

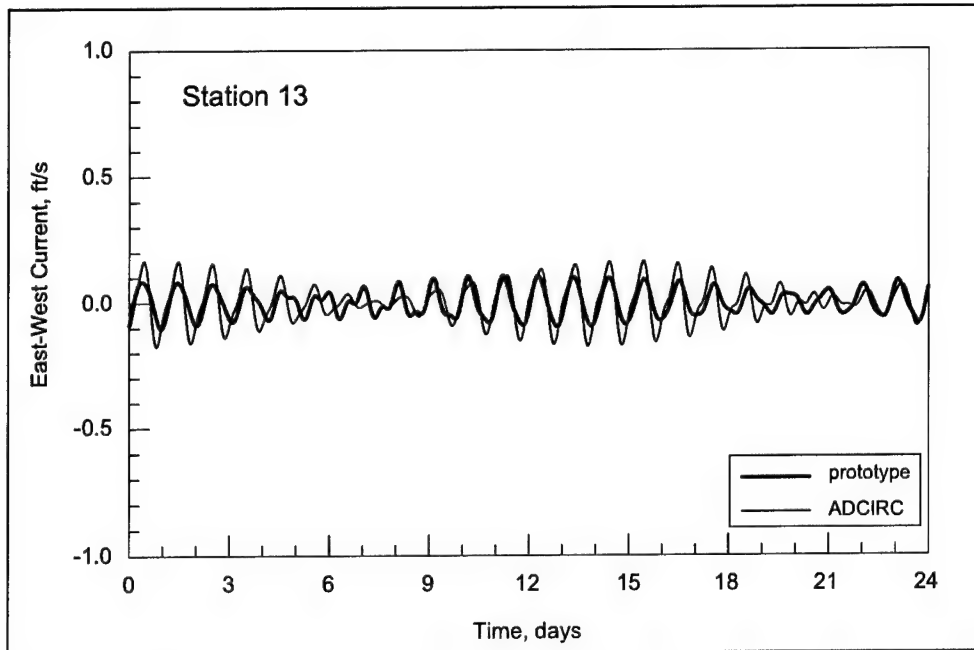


Figure 4-11. Comparison of model- and constituent-synthesized east-west current for sta 13

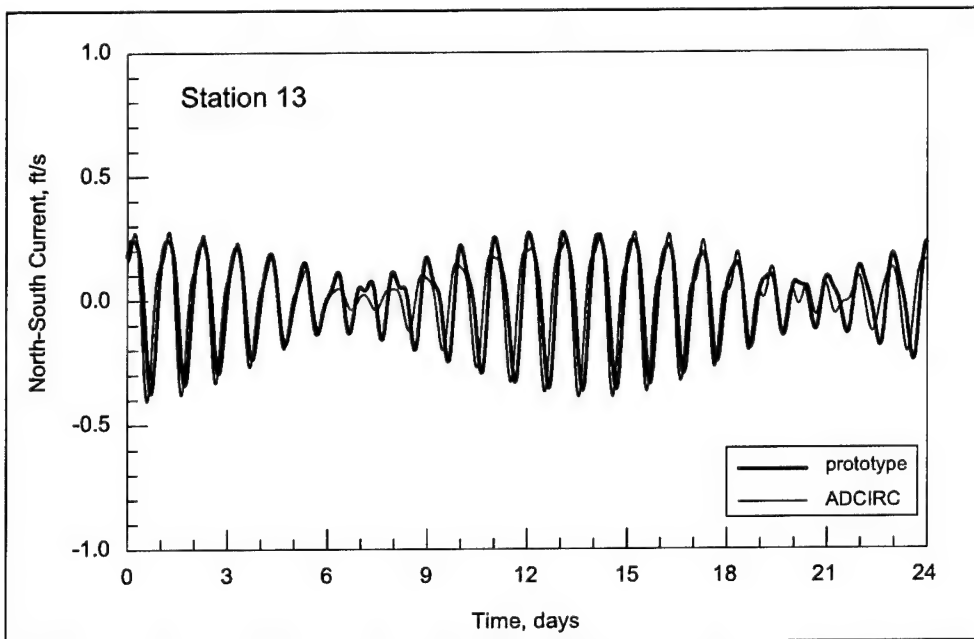


Figure 4-12. Comparison of model- and constituent-synthesized north-south current for sta 13

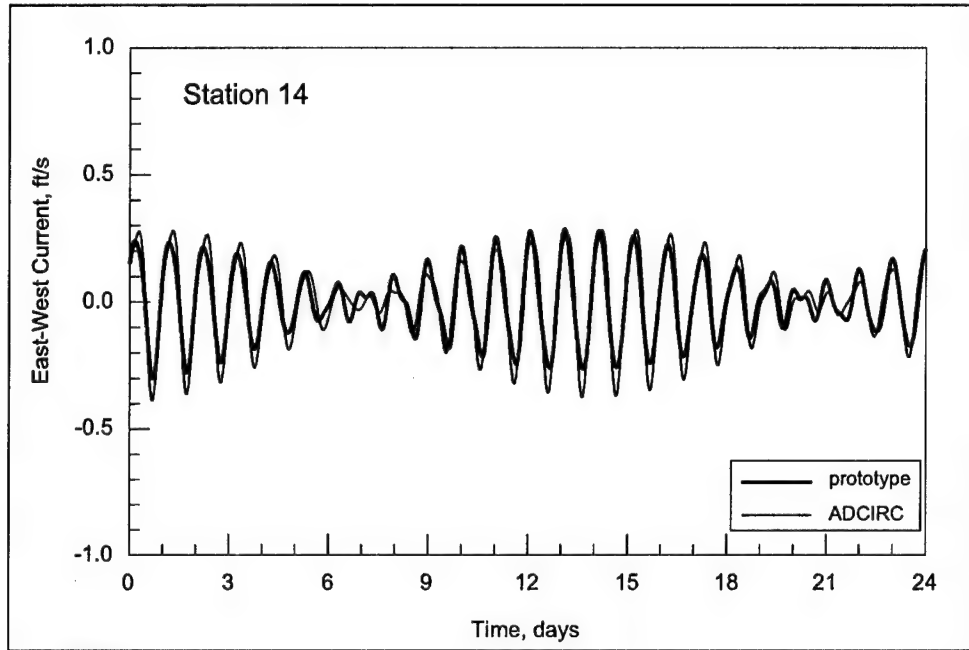


Figure 4-13. Comparison of model- and constituent-synthesized east-west current for sta 14

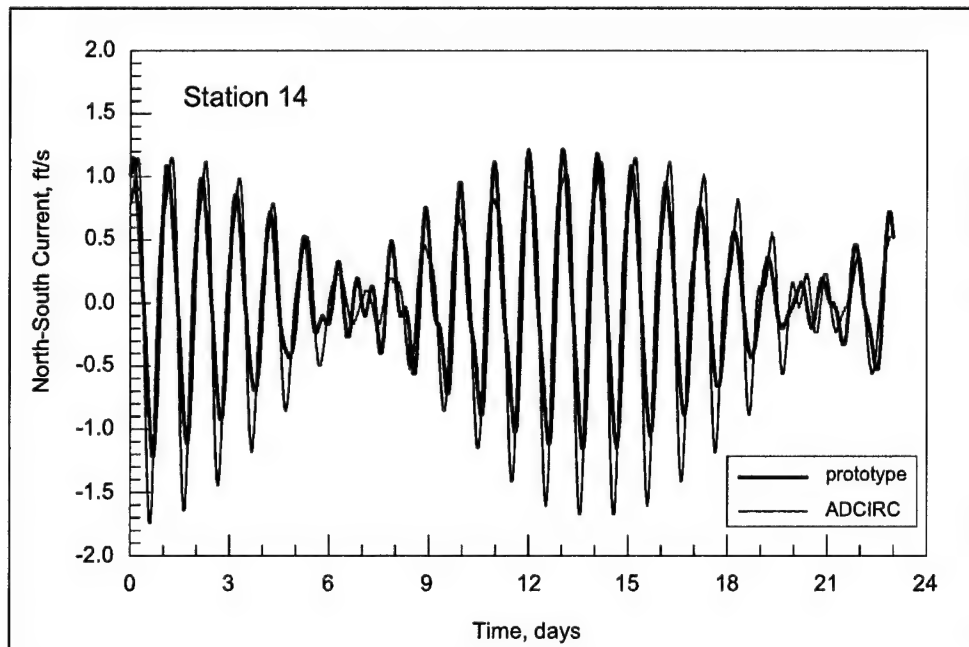


Figure 4-14. Comparison of model- and constituent-synthesized north-south current for sta 14

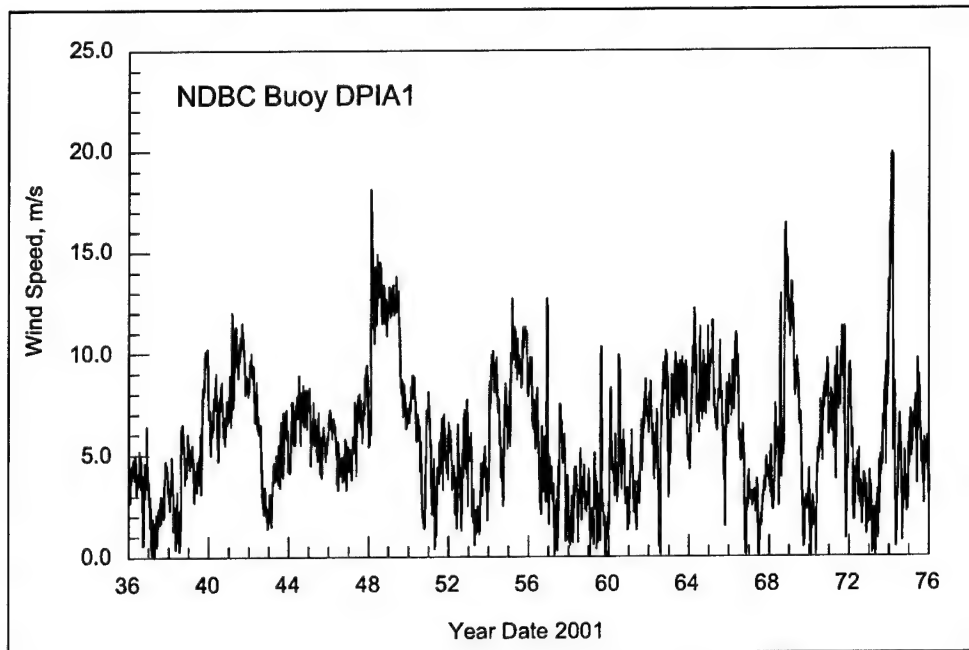


Figure 4-15. Time-series of wind speeds measured at NDBC C-MAN sta DPIA1

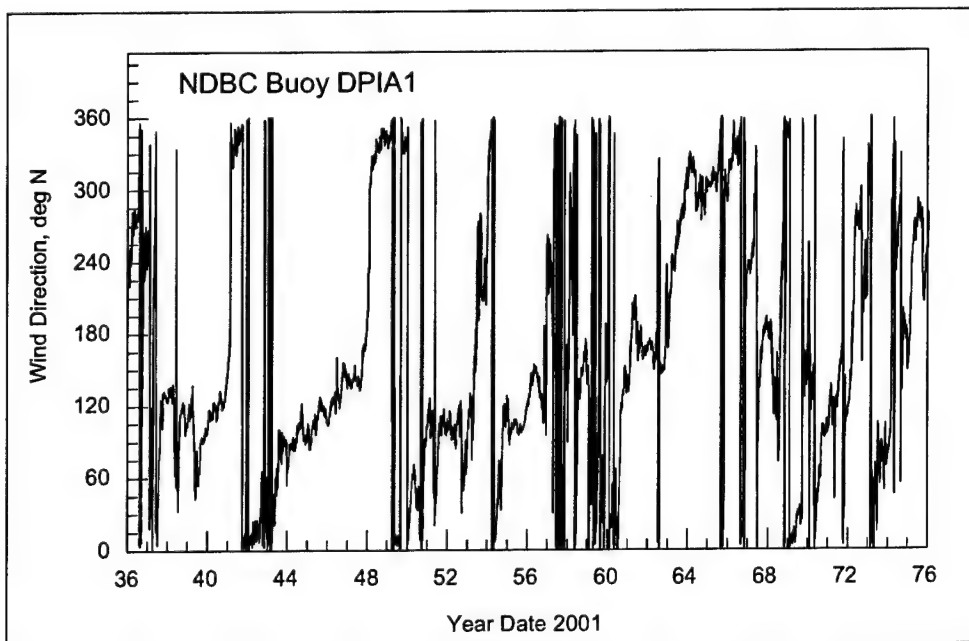


Figure 4-16. Time-series of wind directions measured at NDBC C-MAN sta DPIA1

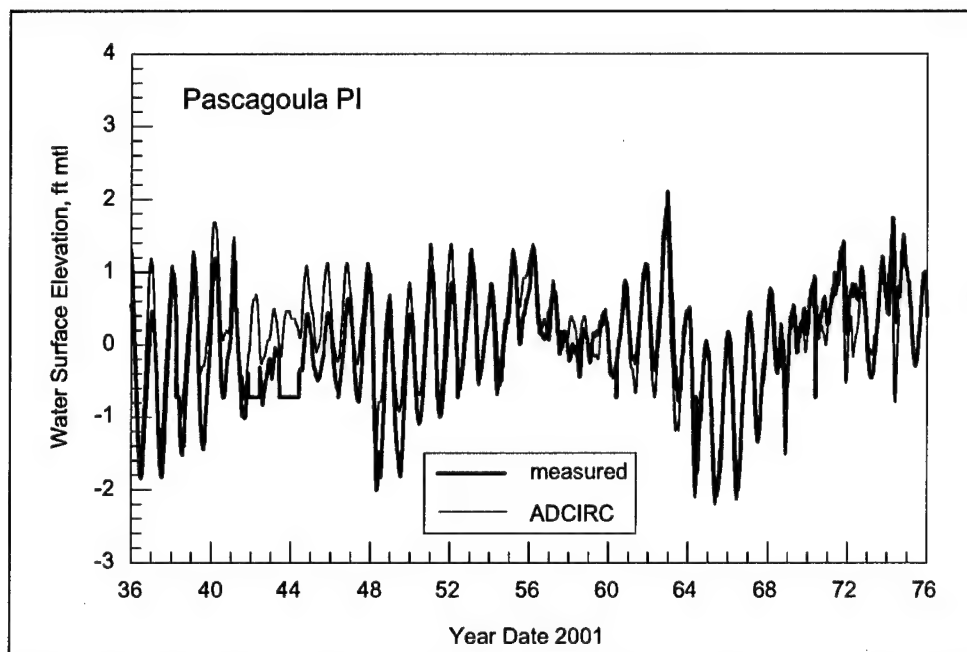


Figure 4-17. Comparison of modeled and measured water-surface elevations measured at the Pascagoula PI gage

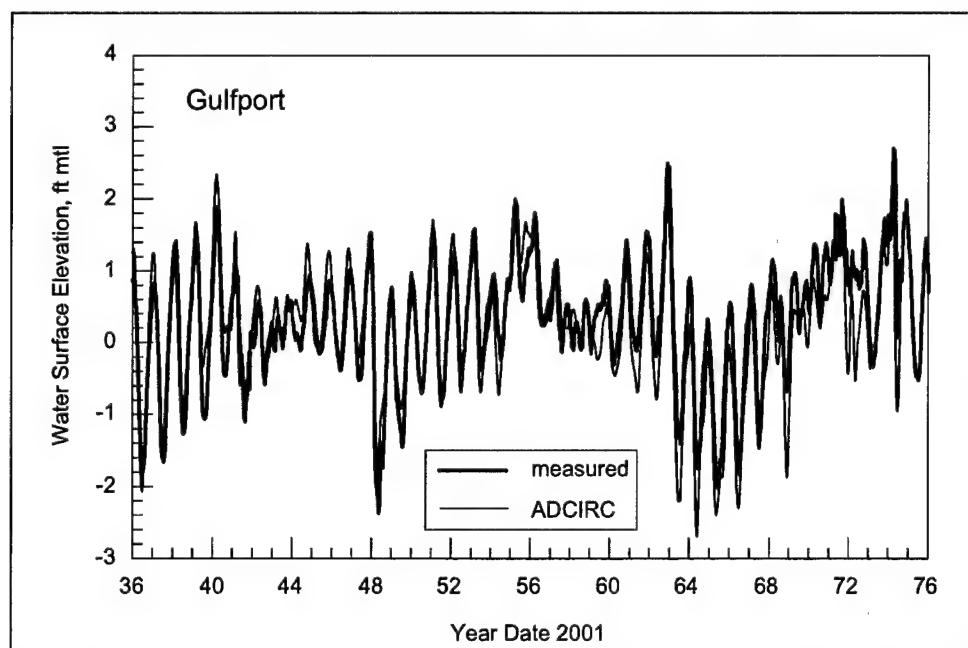


Figure 4-18. Comparison of modeled and measured water-surface elevations measured at the Gulfport gage

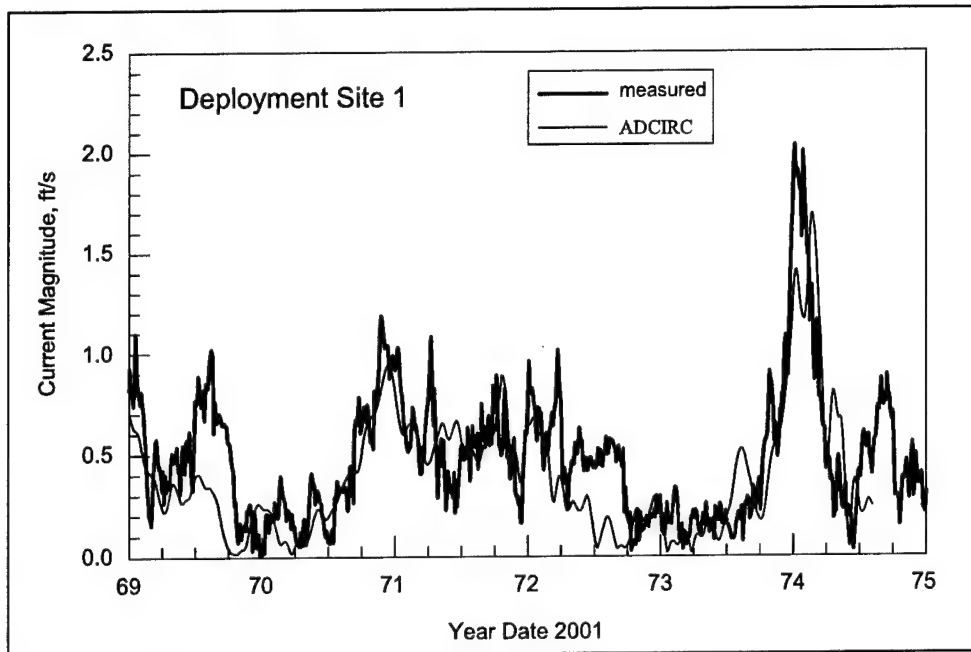


Figure 4-19. Comparison of modeled and measured current speed at Deployment Site 1

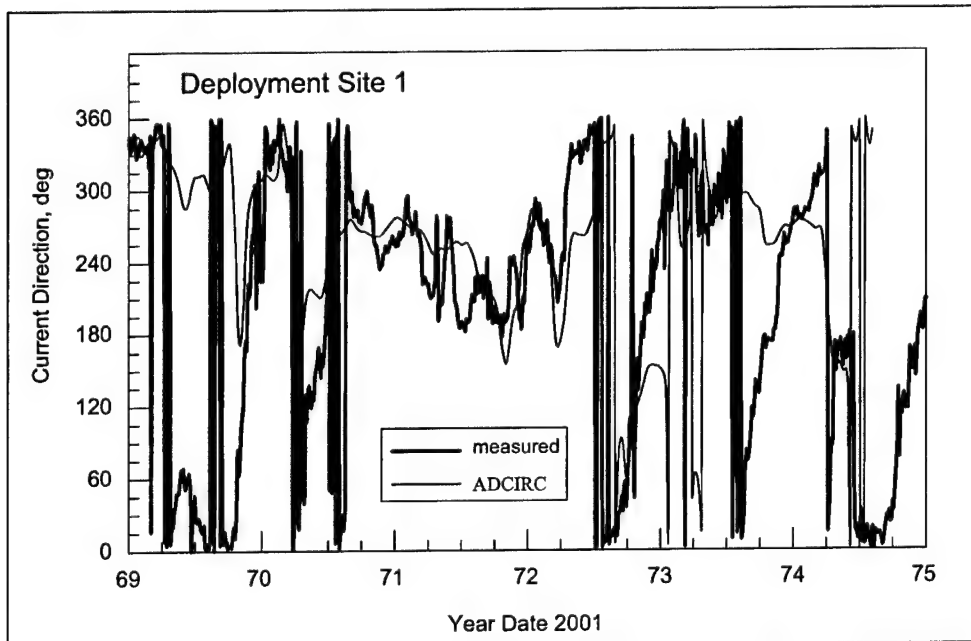


Figure 4-20. Comparison of modeled and measured current direction at Deployment Site 1

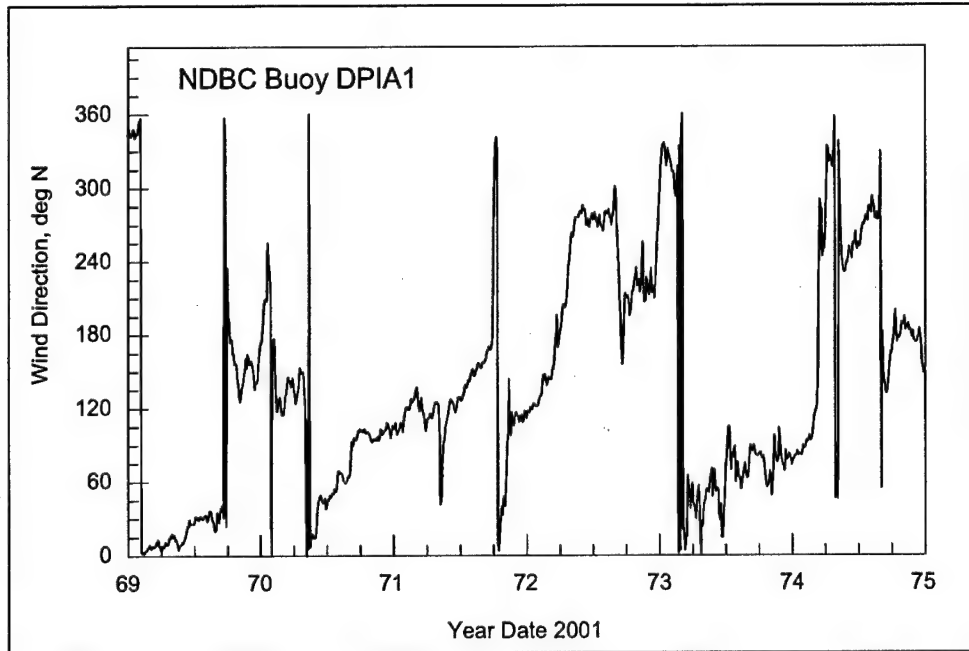


Figure 4-21. Time-series of measured wind direction at NDBC C-MAN sta DPIA1

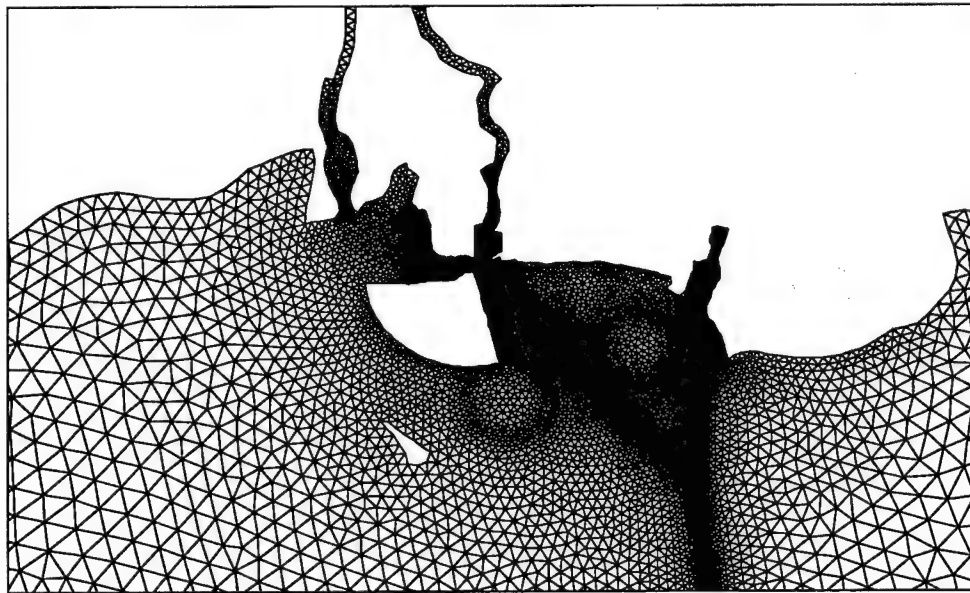


Figure 4-22. Numerical grid for Alternative 1 condition

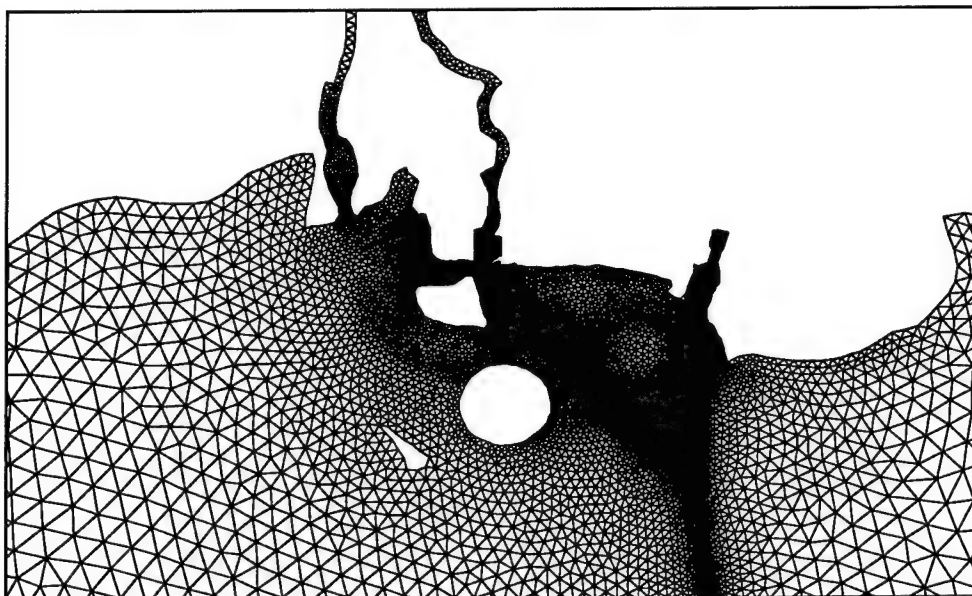


Figure 4-23. Numerical grid for Alternative 2 condition

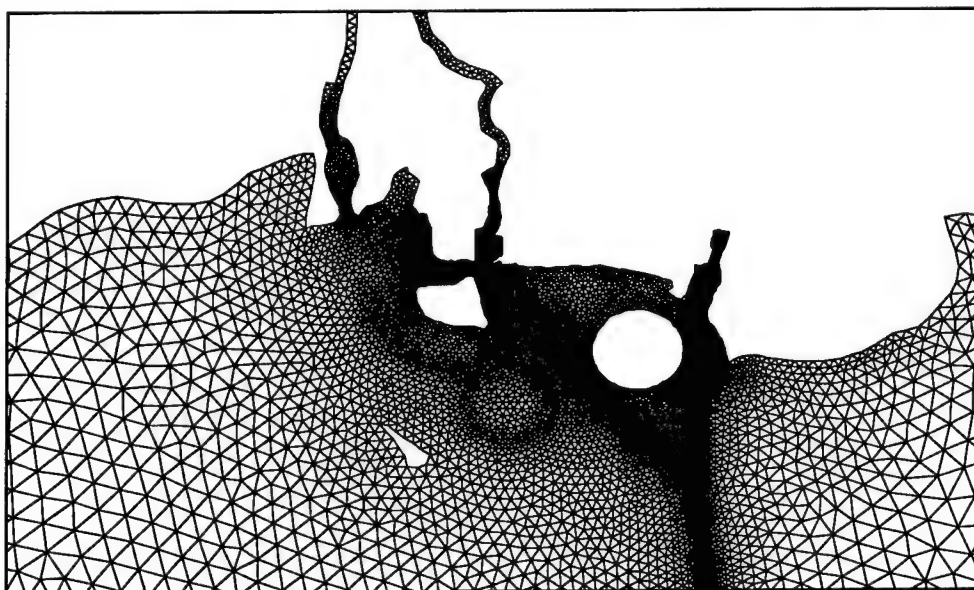


Figure 4-24. Numerical grid for Alternative 3 condition

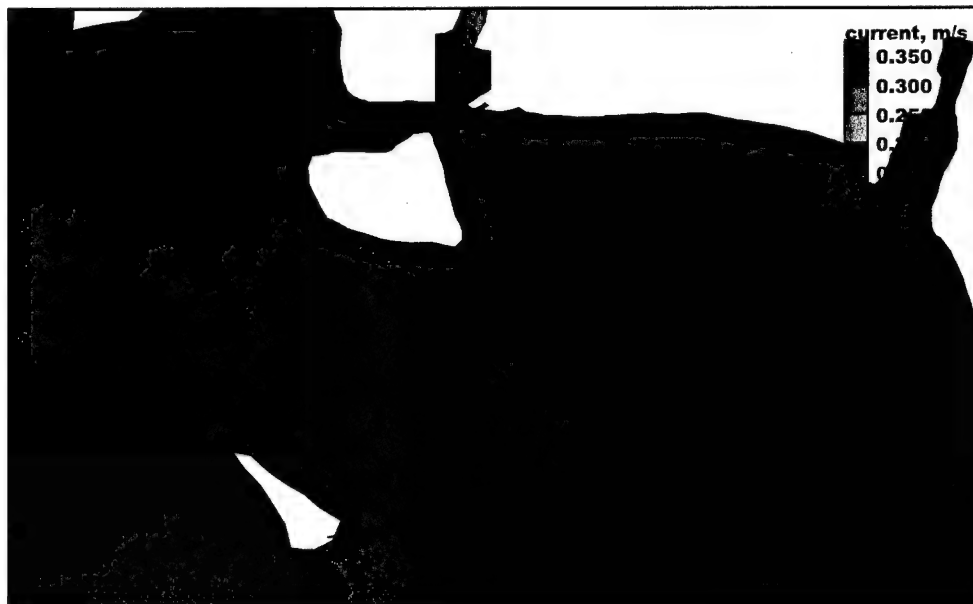


Figure 4-25. Current map of peak spring flood tide for existing-configuration condition



Figure 4-26. Current map of peak spring ebb tide for existing-configuration condition



Figure 4-27. Current map of peak spring flood tide for Alternative 1 condition

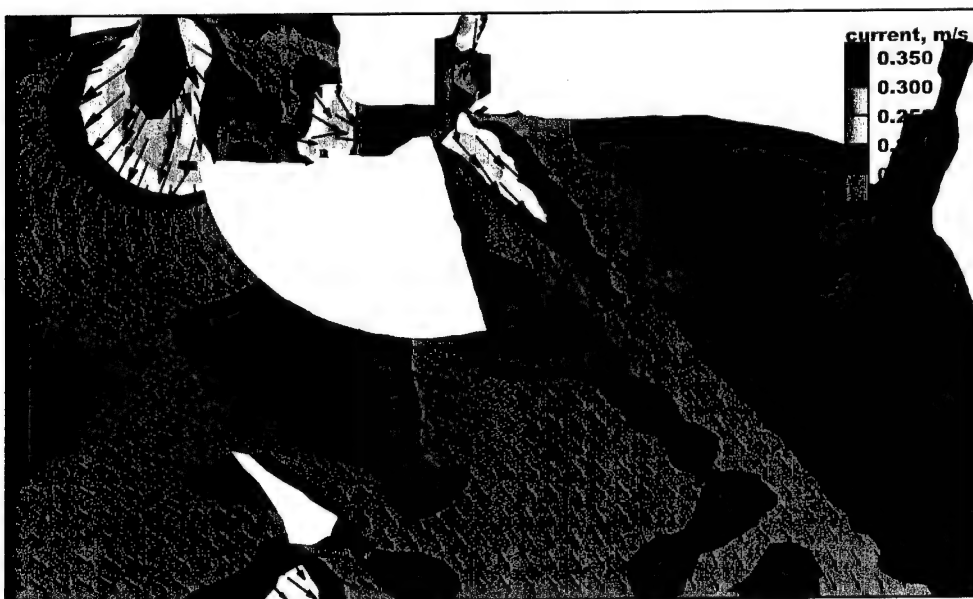


Figure 4-28. Current map of peak spring ebb tide for Alternative 1 condition

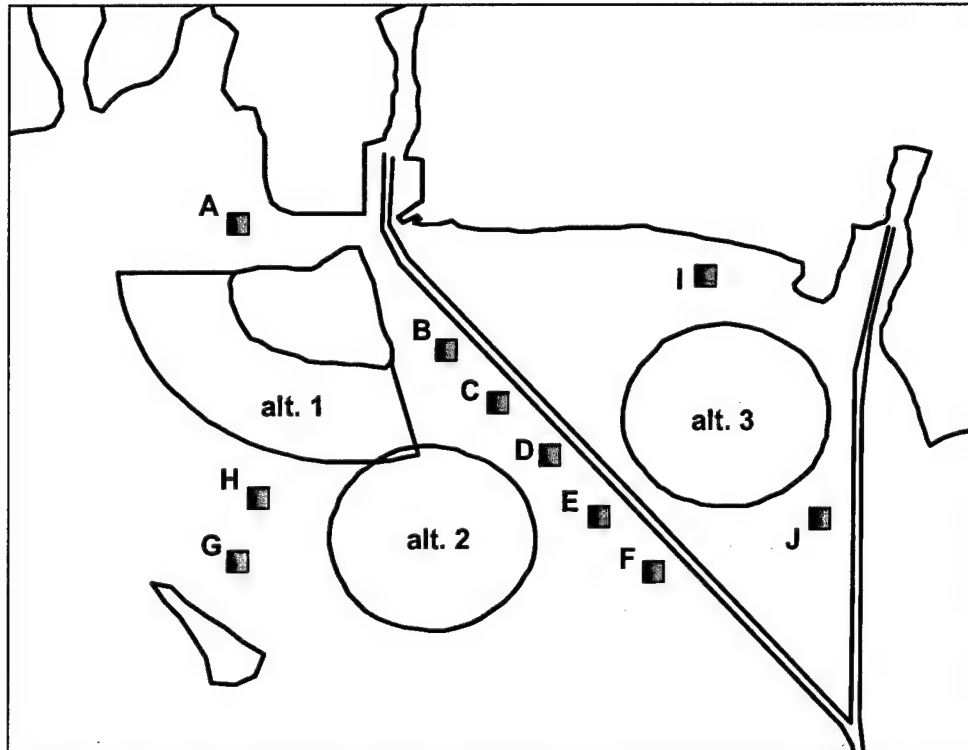


Figure 4-29. Location of stations used in comparing changes in current

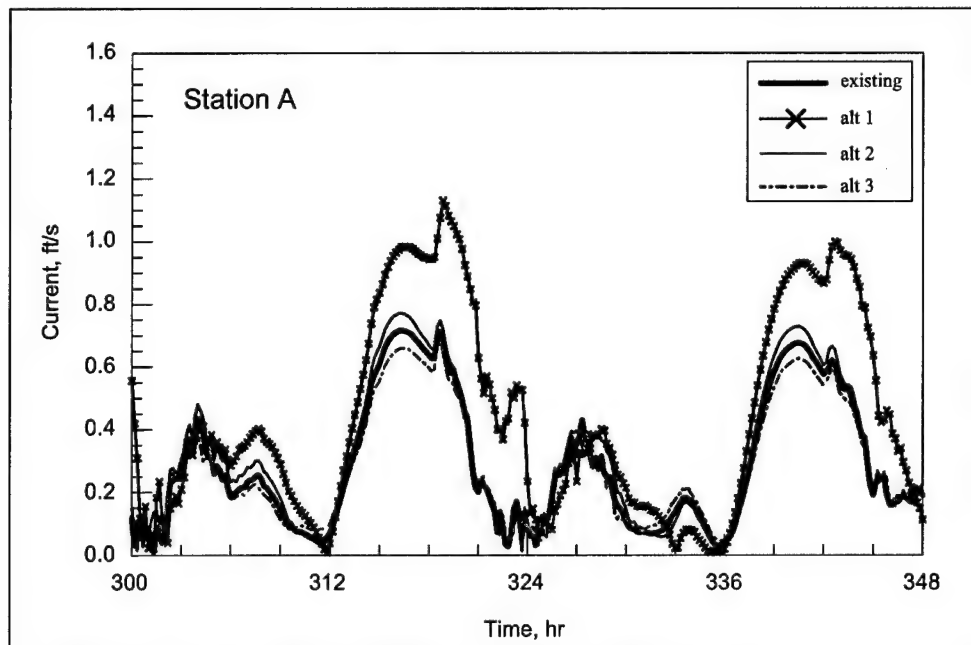


Figure 4-30. Comparison of computed currents at sta A; astronomical forcing

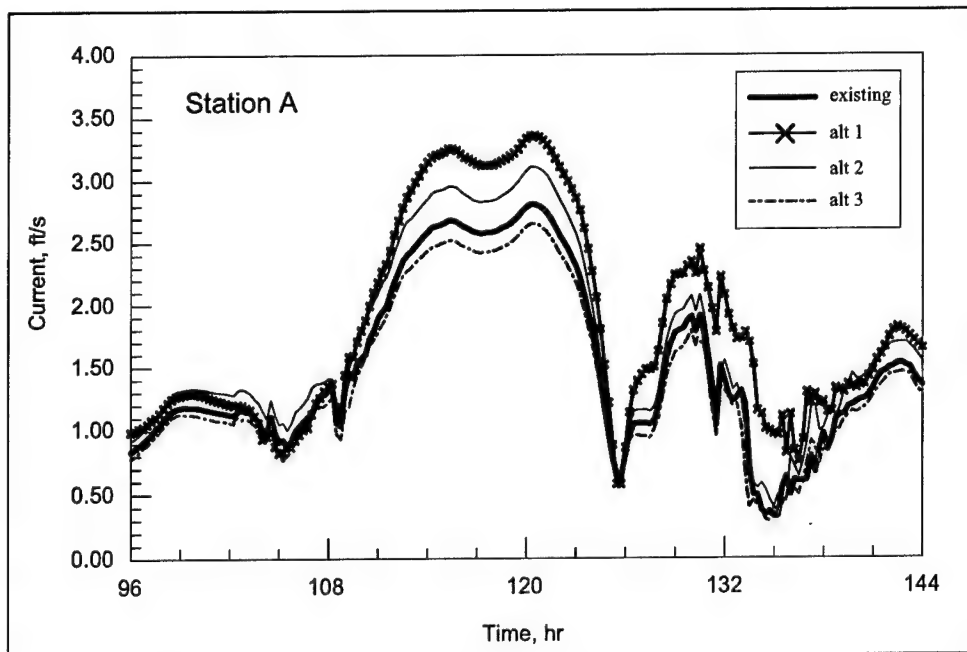


Figure 4-31. Comparison of computed currents at sta A; February 1998 winter storm

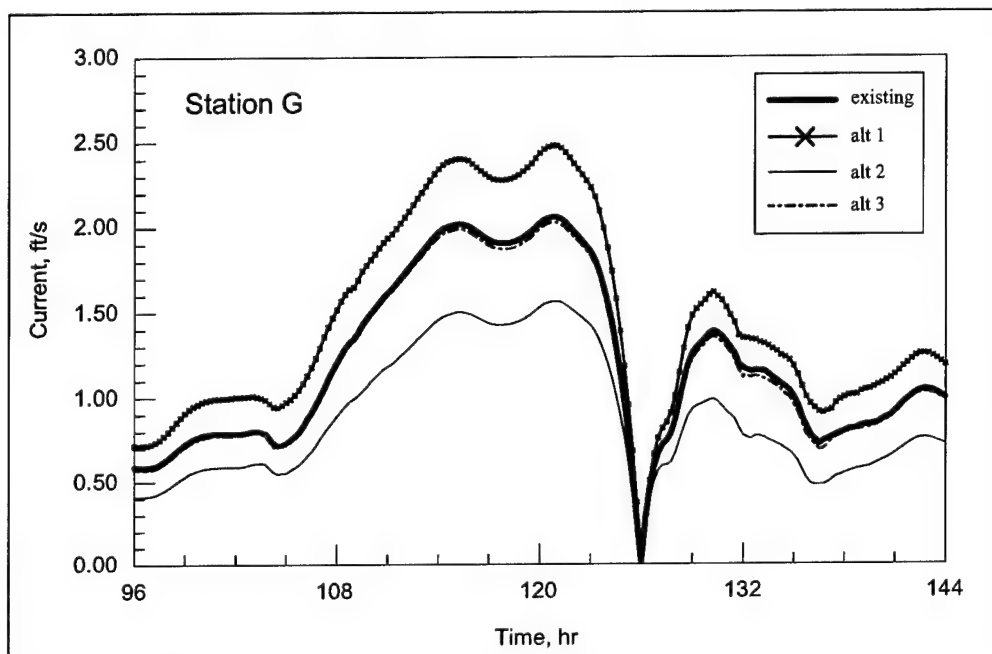


Figure 4-32. Comparison of computed currents at sta A; February 1998 winter storm

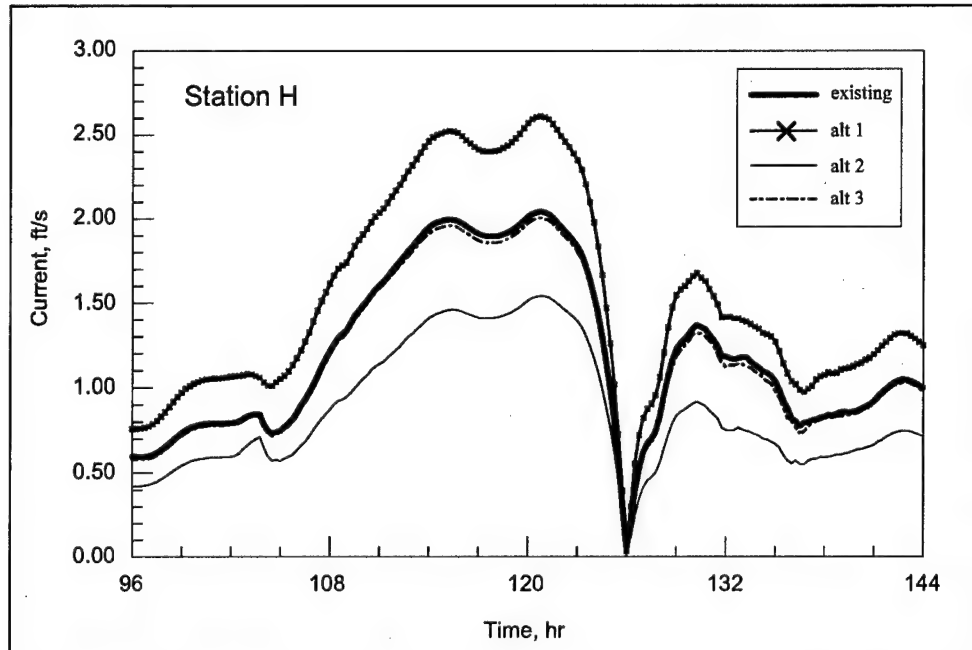


Figure 4-33. Comparison of computed currents at sta A; February 1998 winter storm



Figure 4-34. Current map of peak spring flood tide for the Alternative 2 condition

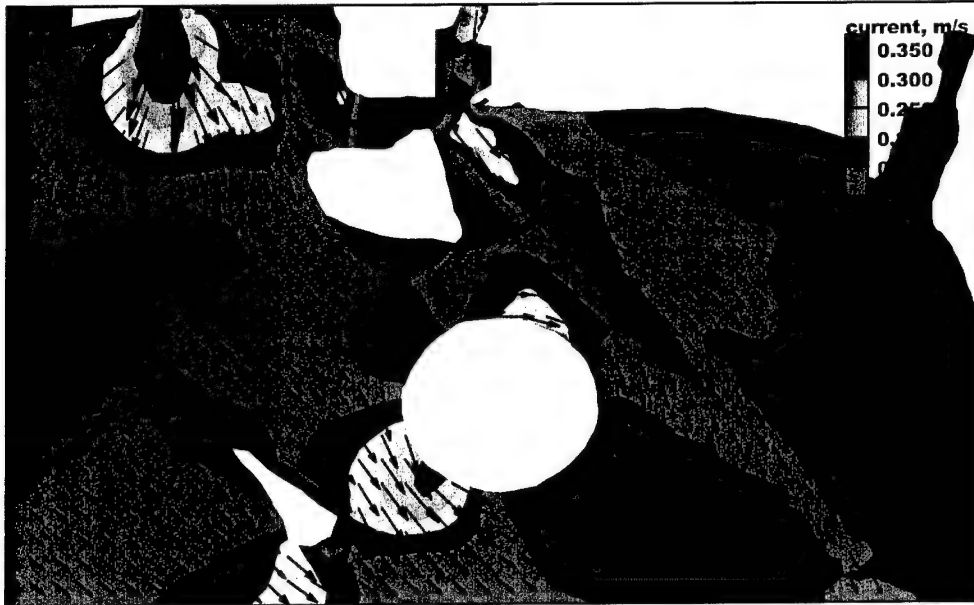


Figure 4-35. Current map of peak spring ebb tide for existing-configuration condition

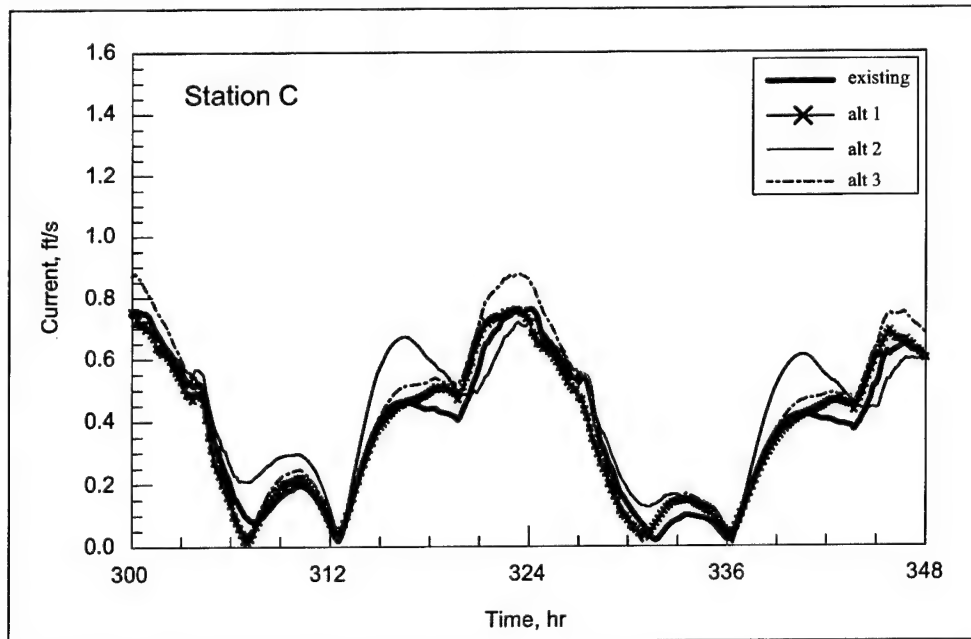


Figure 4-36. Comparison of computed currents at sta C; astronomical forcing

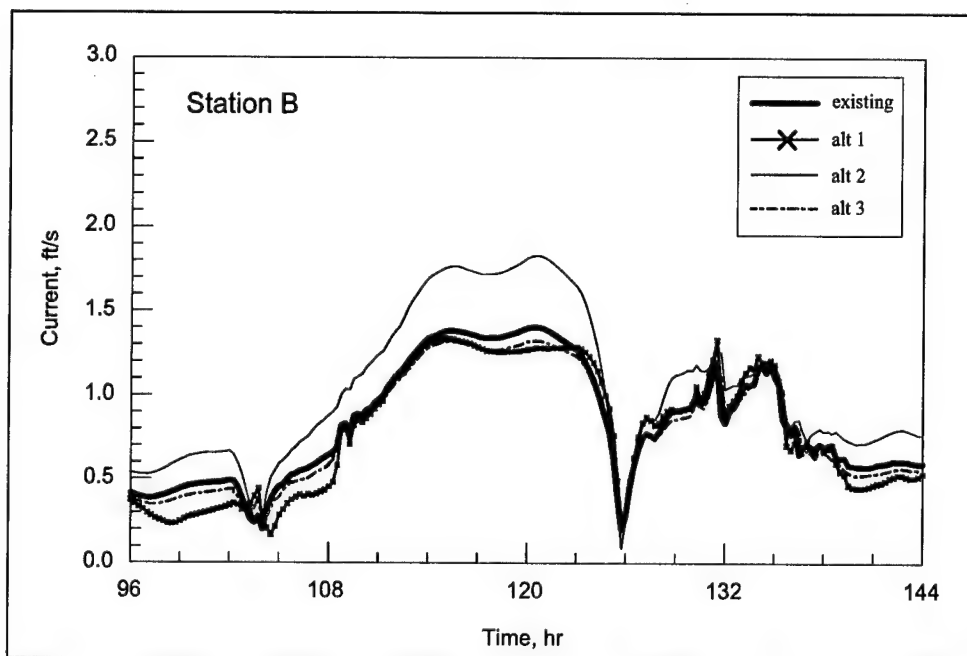


Figure 4-37. Comparison of computed currents at sta B; February 1998 winter storm

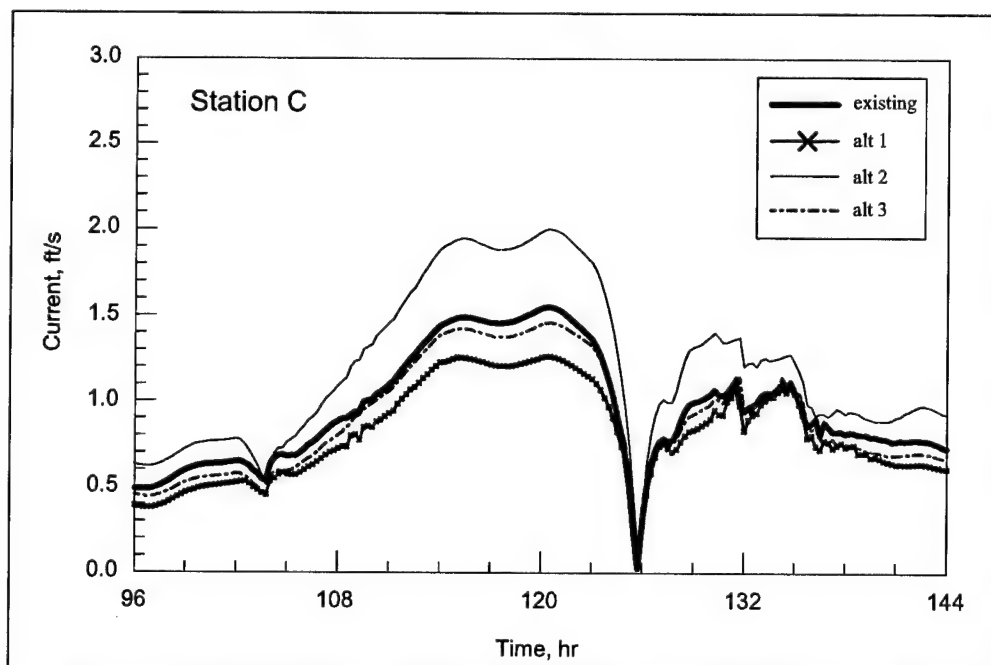


Figure 4-38. Comparison of computed currents at sta C; February 1998 winter storm

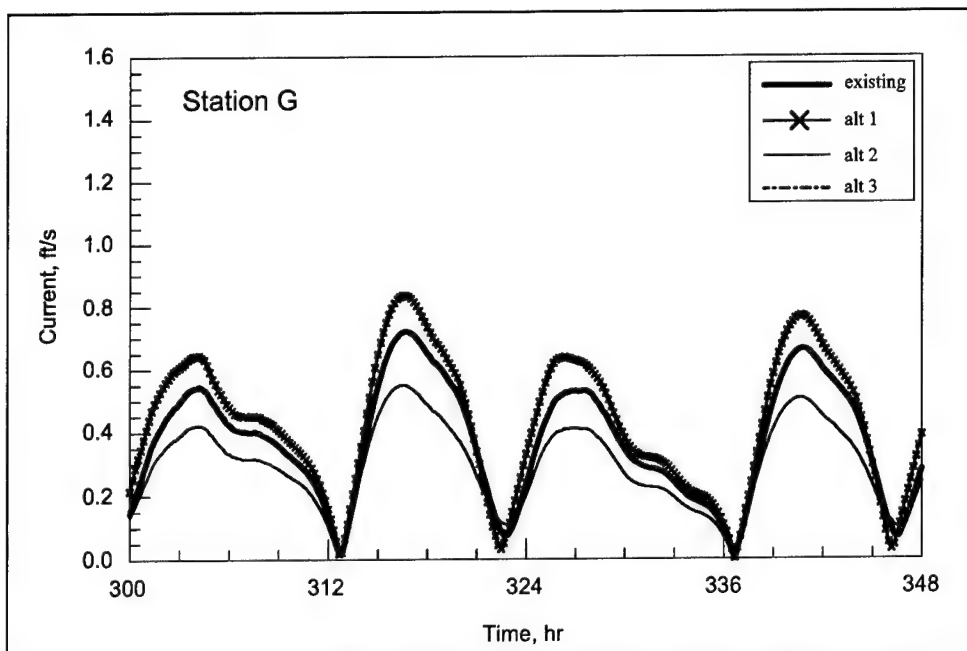


Figure 4-39. Comparison of computed currents at sta G; astronomical forcing

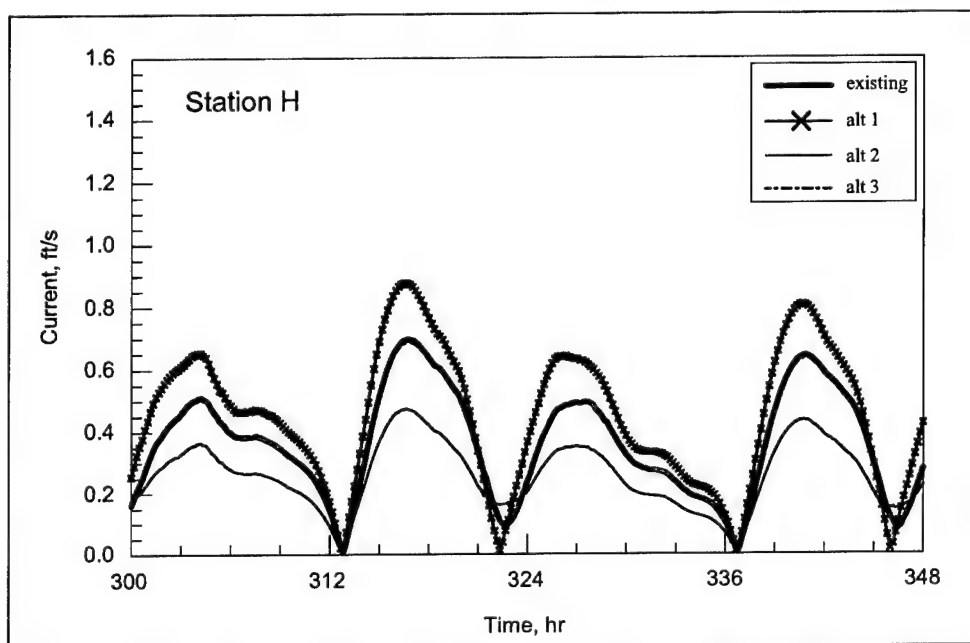


Figure 4-40. Comparison of computed currents at sta H; astronomical forcing



Figure 4-41. Current map of peak spring flood tide for Alternative 3 condition



Figure 4-42. Current map of peak spring ebb tide for Alternative 3 condition

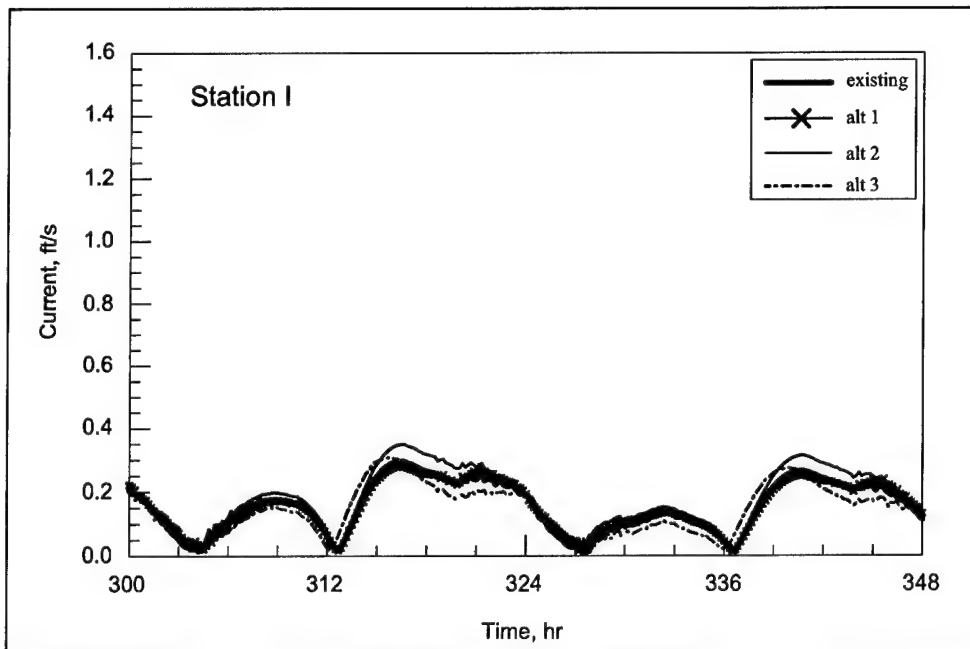


Figure 4-43. Comparison of computed currents at sta I; astronomical forcing

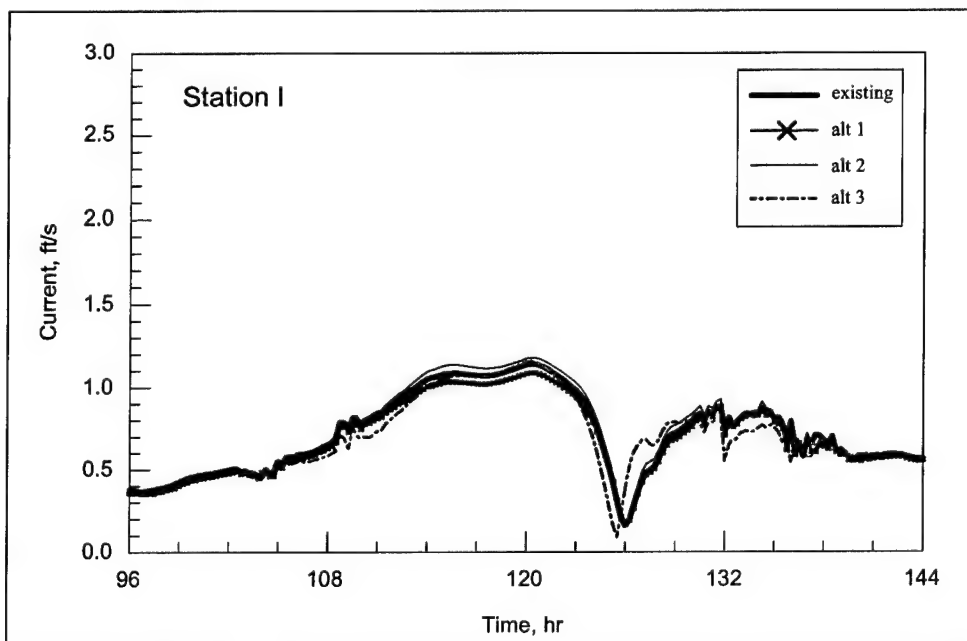


Figure 4-44. Comparison of computed currents at sta I; February 1998 winter storm

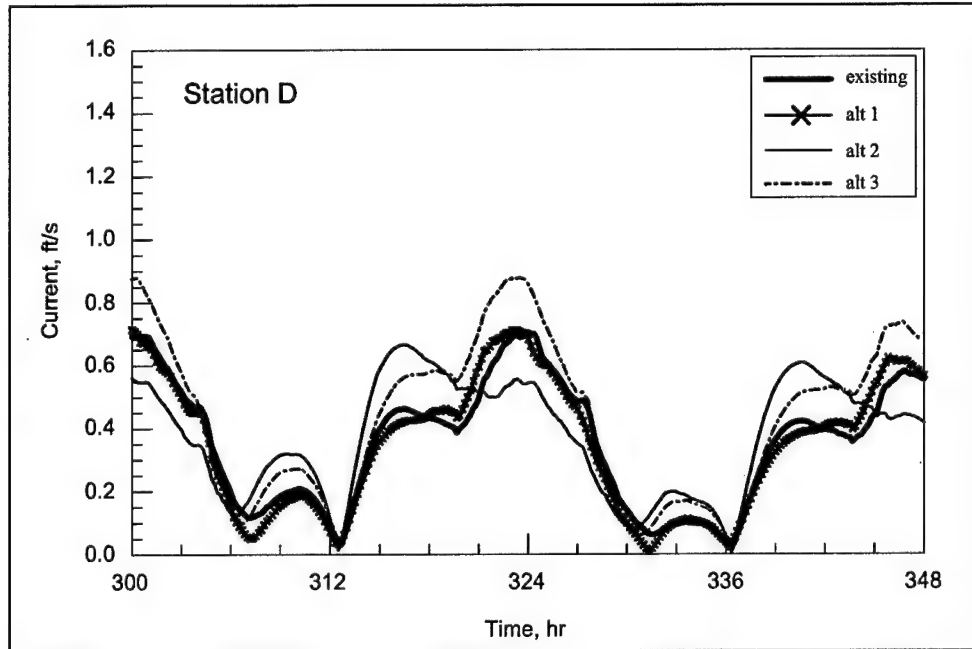


Figure 4-45. Comparison of computed currents at sta D; astronomical forcing

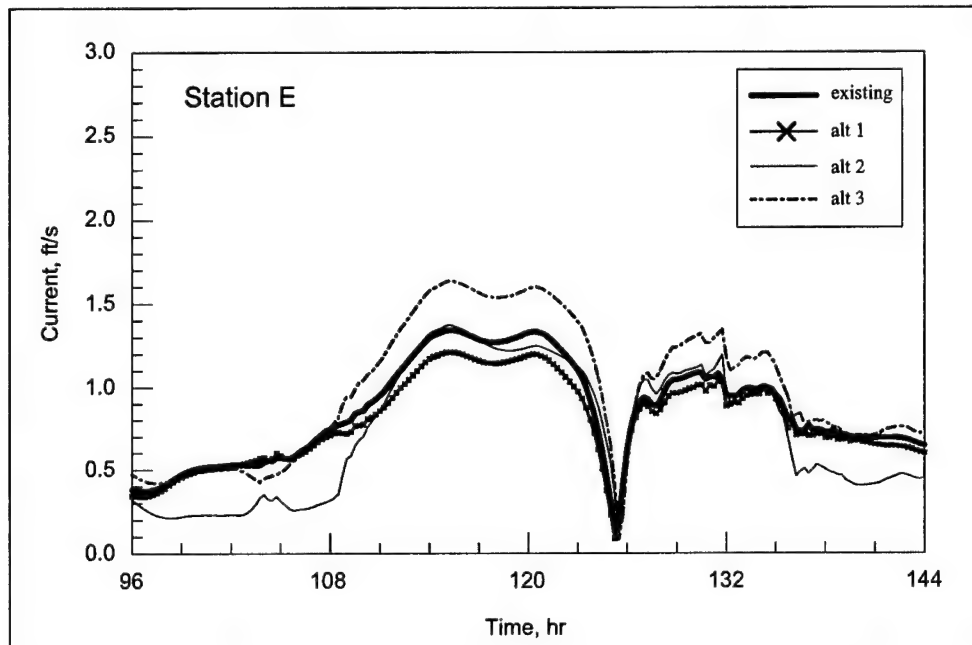


Figure 4-46. Comparison of computed currents at sta E; February 1998 winter storm

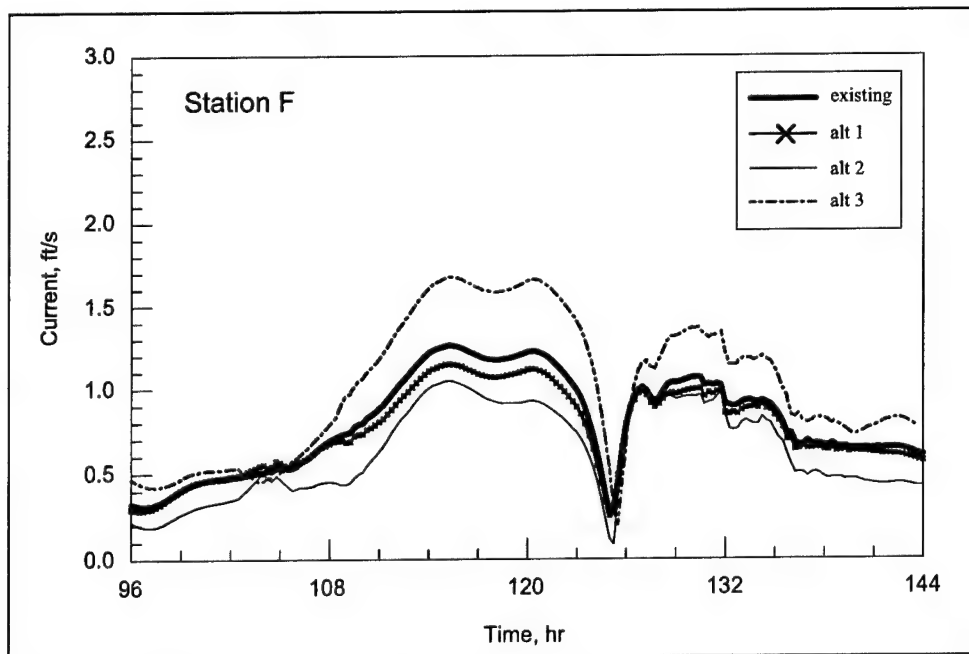


Figure 4-47. Comparison of computed currents at sta F; February 1998 winter storm

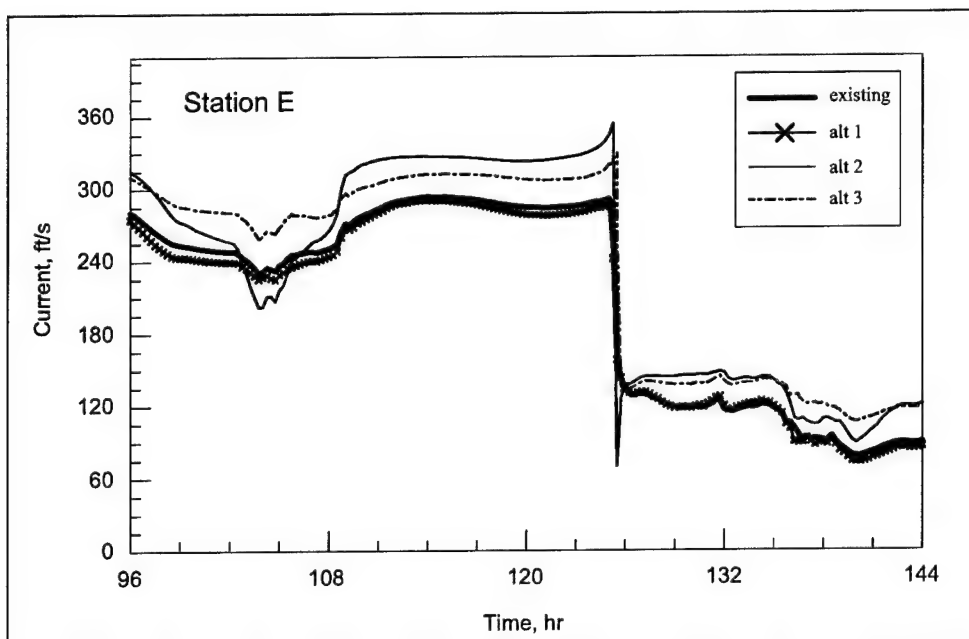


Figure 4-48. Comparison of current direction at sta E; February 1998 winter storm

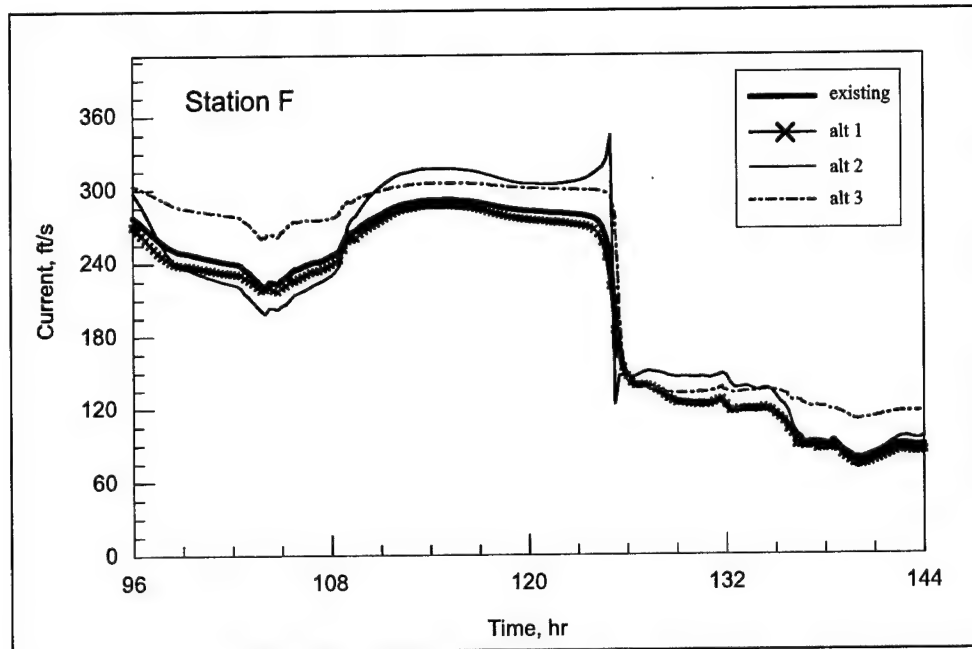


Figure 4-49. Comparison of current direction at sta F; February 1998 winter storm

5 3-D Circulation Model Studies (CH3D)

Dredged material islands are proposed as one solution for future management of dredged material in the vicinity of the Pascagoula River navigation channel, near Pascagoula, MS. As part of a study to address the potential environmental impacts of creation of dredged material islands in the Mississippi Sound, island scenarios were represented in 3-D circulation and water quality models. To provide the hydrodynamic forcing for the CEQUAL-ICM water quality model, the sigma-stretched version of Curvilinear Hydrodynamics in 3-D model (CH3D) was applied. The goal of the modeling work was to represent 3-D hydrodynamics, temperature, and salinity during a period of poor water quality for evaluating the effects of three alternatives for placement of dredged material islands.

This chapter presents the approach taken for modeling of 3-D hydrodynamics with demonstrations of model agreement with available measurements. (Description of the water quality model application is found in Chapter 6.) Chapter 5 presents model background, model domain and grid development, application of boundary conditions, model calibration, and results from the modeling of the island alternatives.

Model Background

A general overview of the sigma-stretched CH3D model background is provided with emphasis on the pertinent details for application of the model for this study. Much of the model background is extracted from the model user's guide (Chapman, Johnson, and Vemulakonda 1996).

CH3D was developed by Sheng (1986), but has been modified to implement different basic numerical formulations of the governing equations and to provide more efficient computing. A description of modifications to the model is provided in Chapman, Johnson, and Vemulakonda (1996). Physical processes impacting circulation and vertical mixing that are modeled include tides, wind, density effects (salinity and temperature), freshwater inflows, turbulence, and the effect of the earth's rotation.

The boundary-fitted coordinate feature of the model provides grid resolution enhancement necessary to adequately represent deep navigation channels and irregular shoreline configurations of the flow system, important factors for the present study. The curvilinear grid also permits adoption of accurate and

economical grid schematization software. The solution algorithm employs an external mode, consisting of vertically averaged equations, which provides a solution for the free surface displacement for input to the internal mode, which contains the full 3-D equations.

Governing equations

The governing partial differential equations are based on the following assumptions: (a) the hydrostatic pressure distribution adequately describes the vertical distribution of fluid pressure, (b) the Boussinesq approximation is appropriate, and (c) the eddy viscosity approach adequately describes turbulent mixing in the flow.

The basic equations for an incompressible fluid in a right-handed Cartesian coordinate system (x, y, z) are (Johnson et al. 1991):

$$\frac{\partial u}{\partial x} + \frac{\partial v}{\partial y} + \frac{\partial w}{\partial z} = 0 \quad (5-1)$$

$$\begin{aligned} \frac{\partial u}{\partial t} + \frac{\partial u^2}{\partial x} + \frac{\partial uv}{\partial y} + \frac{\partial uw}{\partial z} = & f_v - \frac{1}{\rho_o} \frac{\partial p}{\partial x} + \frac{\partial}{\partial x} \left(A_h \frac{\partial u}{\partial x} \right) \\ & + \frac{\partial}{\partial y} \left(A_h \frac{\partial u}{\partial y} \right) + \frac{\partial}{\partial z} \left(A_v \frac{\partial u}{\partial z} \right) \end{aligned} \quad (5-2)$$

$$\begin{aligned} \frac{\partial u}{\partial t} + \frac{\partial uv}{\partial x} + \frac{\partial v^2}{\partial y} + \frac{\partial vw}{\partial z} = & -fu - \frac{1}{\rho_o} \frac{\partial p}{\partial y} + \frac{\partial}{\partial x} \left(A_h \frac{\partial v}{\partial x} \right) \\ & + \frac{\partial}{\partial y} \left(A_h \frac{\partial v}{\partial y} \right) + \frac{\partial}{\partial z} \left(A_v \frac{\partial v}{\partial z} \right) \end{aligned} \quad (5-3)$$

$$\frac{\partial p}{\partial z} = -\rho g \quad (5-4)$$

$$\frac{\partial T}{\partial t} + \frac{\partial uT}{\partial x} + \frac{\partial vT}{\partial y} + \frac{\partial wT}{\partial z} = \frac{\partial}{\partial x} \left(K_h \frac{\partial T}{\partial x} \right) + \frac{\partial}{\partial y} \left(K_h \frac{\partial T}{\partial y} \right) + \frac{\partial}{\partial z} \left(K_v \frac{\partial T}{\partial z} \right) \quad (5-5)$$

$$\frac{\partial S}{\partial t} + \frac{\partial uS}{\partial x} + \frac{\partial vS}{\partial y} + \frac{\partial wS}{\partial z} = \frac{\partial}{\partial x} \left(K_h \frac{\partial S}{\partial x} \right) + \frac{\partial}{\partial y} \left(K_h \frac{\partial S}{\partial y} \right) + \frac{\partial}{\partial z} \left(K_v \frac{\partial S}{\partial z} \right) \quad (5-6)$$

$$\rho = \rho(T, S) \quad (5-7)$$

where

- (u, v, w) = velocities in (x, y, z) directions
- t = time
- f = Coriolis parameter defined as $2\Omega \sin \phi$
- Ω = rotational speed of the earth
- ϕ = latitude
- ρ = density
- p = pressure
- A_h, K_h = horizontal turbulent eddy coefficients
- A_v, K_v = vertical turbulent eddy coefficients
- g = gravitational acceleration
- T = temperature
- S = salinity

Equation 5-4 implies that vertical accelerations are negligible and thus the pressure is hydrostatic. Various forms of the equation of state can be specified for Equation 5-7. In the present model, the following formulation is used:

$$\rho = P/(\alpha + 0.698P) \quad (5-8)$$

where

- ρ = density in grams per cubic centimeter
- $P = 5890 + 38T - 0.375T^2 + 3S$
- $\alpha = 1779.5 + 11.25T - 0.745T^2 - (3.8 + 0.1T)S$
- T = temperature in degrees Celsius
- S = salinity in parts per thousand (ppt)

Within the model, these basic equations are normalized, boundary-fitted, and sigma-stretched as presented in Chapman, Johnson, and Vemulakonda (1996).

Boundary conditions

The governing equations are subject to boundary conditions at the surface, bottom, and lateral boundaries. Refer to Chapman, Johnson, and Vemulakonda (1996) for additional details.

The free-surface boundary condition is affected primarily by wind stresses and heat exchange. Wind stresses enter as source terms into the momentum equations (Equations 5-2 and 5-3) for the top layer in the following form:

$$A_v \left(\frac{\partial \bar{u}}{\partial z}, \frac{\partial \bar{v}}{\partial z} \right) = (\tau_{s_x}, \tau_{s_y}) / \rho = (C W_x^2, C W_y^2) \quad (5-9)$$

where

τ_s = wind shear stress

C = surface drag coefficient

W = wind speed (m/sec)

The surface drag coefficient is calculated by the method of Garratt (1977) as follows:

$$C = (0.75 + 0.067 W) \times 10^{-3} \quad (5-10)$$

Heat exchange at the surface is represented through a surface heat exchange coefficient and the daily equilibrium temperature and enters as a source term in Equation 5-5. The surface heat exchange coefficient and equilibrium temperature are calculated from geographical and meteorological conditions (latitude, wind speed, cloud cover, and wet and dry bulb temperatures). Zero salinity flux is imposed in the surface layer.

The bottom boundary condition is primarily influenced by bottom friction, expressed in the governing equations for the bottom layer as:

$$A_v \left(\frac{\partial \bar{u}}{\partial z}, \frac{\partial \bar{v}}{\partial z} \right) = (\tau_{b_x}, \tau_{b_y}) / \rho = \frac{U_r}{A_{vr}} Z_r C_d (\bar{u}_1^2 + \bar{v}_1^2)^{1/2} (\bar{u}_1, \bar{v}_1) \quad (5-11)$$

where

τ_b = bottom shear stress

U_r = reference velocity

Z_r = reference height

C_d = bottom drag coefficient

u_1, v_1 = near-bottom horizontal velocity

Bottom friction can be specified by a variety of methods. The bottom friction for the present study was specified as a spatially constant bottom friction coefficient, and values applied are discussed with model calibration. Other

bottom boundary conditions imposed by the model include zero temperature and salinity fluxes.

Lateral boundary conditions are specified at open-water boundaries and can consist of water level, flow, temperature, and salinity. Ocean boundaries include specification of water-surface elevation along with time-variant vertical distributions of temperature and salinity. During flood flow or flux into the model domain, the specified values of temperature and salinity advect into the domain whereas during ebb flow, the interior values of temperature and salinity advect out of the grid. River boundaries are prescribed where freshwater flow enters the grid and time-variant flow and temperature are defined along with an assumption of zero salinity. For the present application, one ocean boundary was treated as a river boundary by specifying flow and temperature at the boundary along with a zero-spatial-gradient assumption for salinity. This boundary condition will be described in greater detail later.

Model Domain

Selection of the model domain is a crucial first step in any application. Without adequate representation of the environmental factors influencing the study area, little can be done to accurately represent the system. In the case of Mississippi Sound near Pascagoula, the key influences of the system are tides from the Gulf of Mexico, wind stresses, and freshwater influx from the Pascagoula River system. Another potentially significant influence is freshwater influence from the Alabama and Tombigbee Rivers (two large watersheds) through Mobile Bay.

To accommodate the primary influences of the system near Pascagoula, the model domain (Figure 5-1) was selected as a roughly 120- by 75-km (74.56 by 46.60-miles) region extending from just east of Mobile Bay to the western tip of Ship Island and from approximately 20 km (12.43 miles) south of the barrier islands to the head of Mobile Bay. The Pascagoula, West Pascagoula, and Escatawpa Rivers were represented as straight channels with representative cross sections, and the Alabama and Tombigbee Rivers were represented as a simple freshwater source into Mobile Bay.

Grid and Bathymetry

Bathymetry within the model domain was obtained primarily from the NGLI as 3-arc-sec (approximately 90 m (295.27 ft)) resolution gridded bathymetry over the model domain. This data were supplemented by river cross sections and navigational charts in localized areas near the study site.

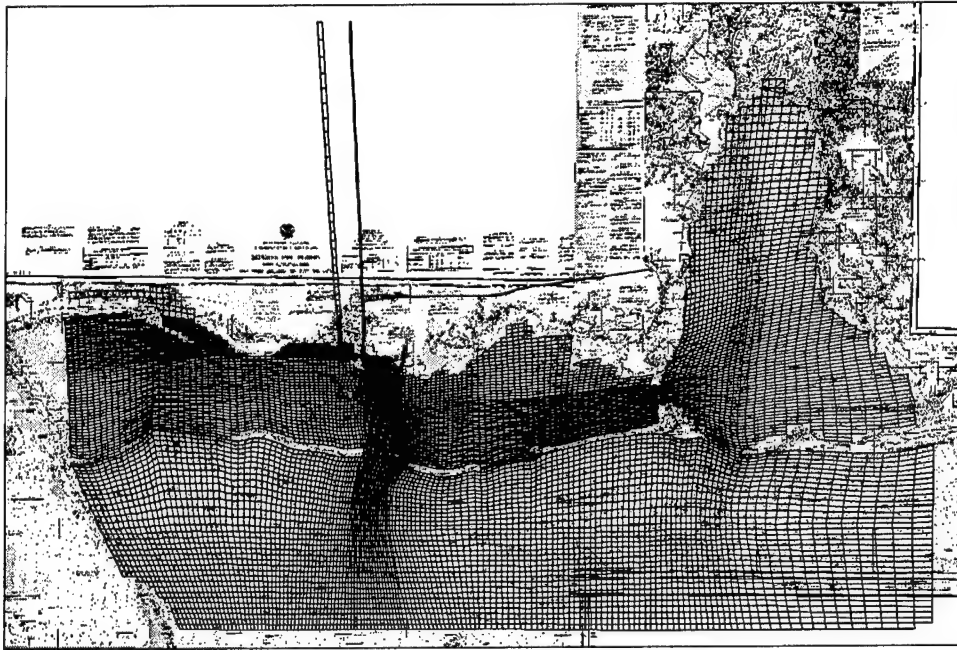


Figure 5-1. CH3D grid and model domain

Local corrections to the navigation channel depths for the Pascagoula River and Mobile Bay navigation channels were obtained from authorized depths published on NOS navigation charts. The Pascagoula River navigation channel was assumed to have a uniform depth of 12 m (39.37 ft) and the Mobile Bay navigation channel was assumed to have a uniform depth of 9 m. Bathymetry in the naval turning basin north of Singing River Island was modified according to information published in NOS 1:40000 nautical charts that indicate an approximate depth of the turning basin of 12 m. The NOS 1:40000 nautical charts were also utilized in the specification of channel depths near the mouths of the Pascagoula and West Pascagoula Rivers.

Escatawpa, Pascagoula, and West Pascagoula River cross sections were estimated from a modeling study of the river system performed for the State of Mississippi Department of Environmental Quality (Harza Engineering Company 1995). River cross sections from the DYNHYD5 model used in that study (provided by Dr. David Huddleston, Mississippi State University¹) were approximated in the CH3D grid by representing the river channels as straight channels with one-cell-wide, rectangular cross sections. The Pascagoula and West Pascagoula Rivers were represented within the grid to a distance approximately 45 km (27.96 miles) north of the Mississippi Sound, a distance far enough upstream to avoid salinity intrusion at the river boundary condition.

A boundary-fitted grid (Figure 5-1) was constructed to define the numerical domain of the model. The grid cells were boundary fitted to the seaward side of the barrier islands, to the Pascagoula River navigation channel, to the Mobile Bay navigation channel, and (when practical) to islands and other land

¹ Personal Communication, October-November 2001, Dr. David H. Huddleston, Associate Professor of Civil Engineering, Mississippi State University, e-mail and phone conversations.

boundaries. The final grid dimensions were 151 cells (east-west) \times 115 cells (north-south) \times five vertical layers. Grid resolution ranged from 300 to 2,500 m (984.25 to 8,202.08 ft), with the finer resolution provided primarily in the study area as shown in Figure 5-2. The bathymetry from combined sources was interpolated to the constructed mesh, resulting in model bathymetry as shown in Figures 5-3 and 5-4. The maximum grid depth was 27.0 m (88.58 ft) at the offshore boundary and the minimum depth was restricted to 1.5 m (4.92 ft) in shallow flats. The depth restriction in shallow water was implemented to prevent wetting/drying of cells, which is not supported by the model.

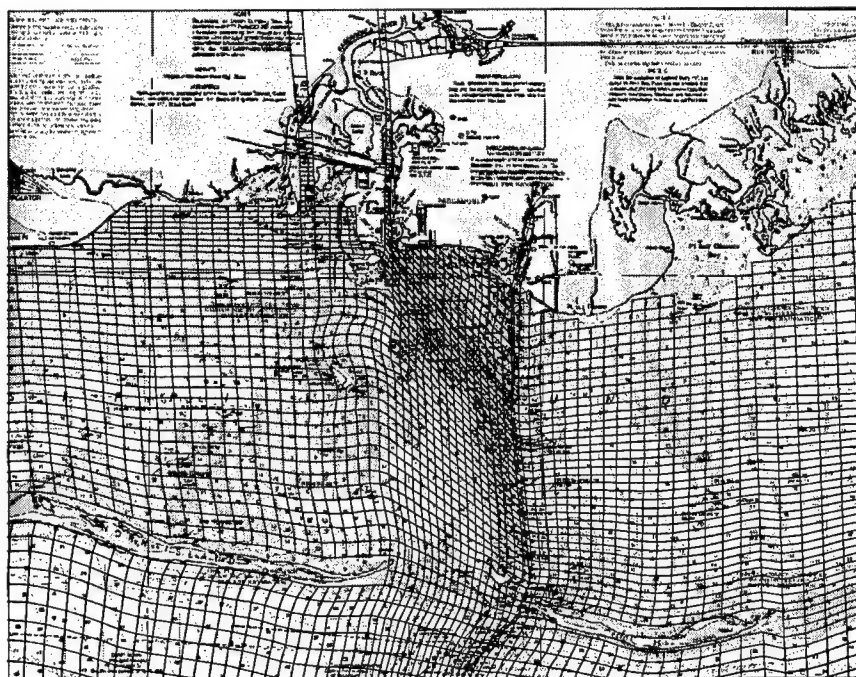


Figure 5-2. Grid resolution in study area (notice boundary fitting of grid to islands and Pascagoula River navigation channel)

Five layers of vertical resolution were specified in the model with uniform weighting so that each vertical layer represented one fifth of the water column at each cell. With this vertical resolution, layer thickness ranged from 5.4 m (17.72 ft) at the offshore boundary to 0.3 m (0.98 ft) in shallow areas near the Pascagoula River.

Boundary Conditions

As mentioned in the model background, boundary conditions are required at the surface, bottom, and lateral boundaries of the model. Conditions applied to the model boundaries were developed from numerical models, measured data, engineering judgment, or a combination of these sources. Application of boundary conditions to the CH3D grid is indicated in Figure 5-5 with additional information regarding the sources of boundary conditions in Table 5-1.

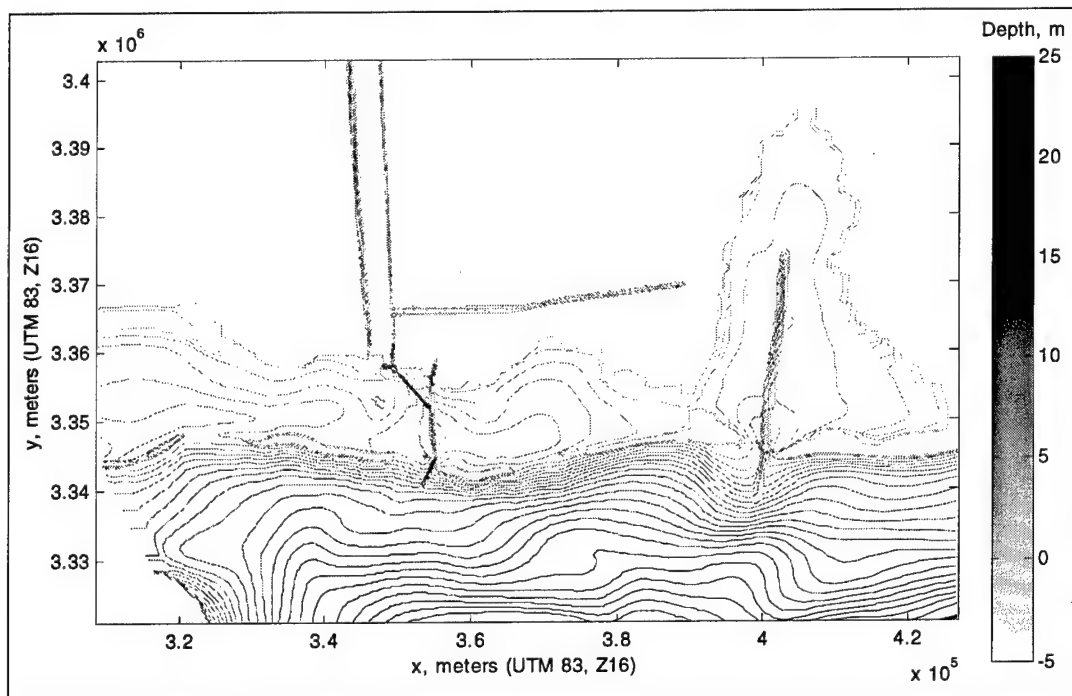


Figure 5-3. CH3D bathymetry

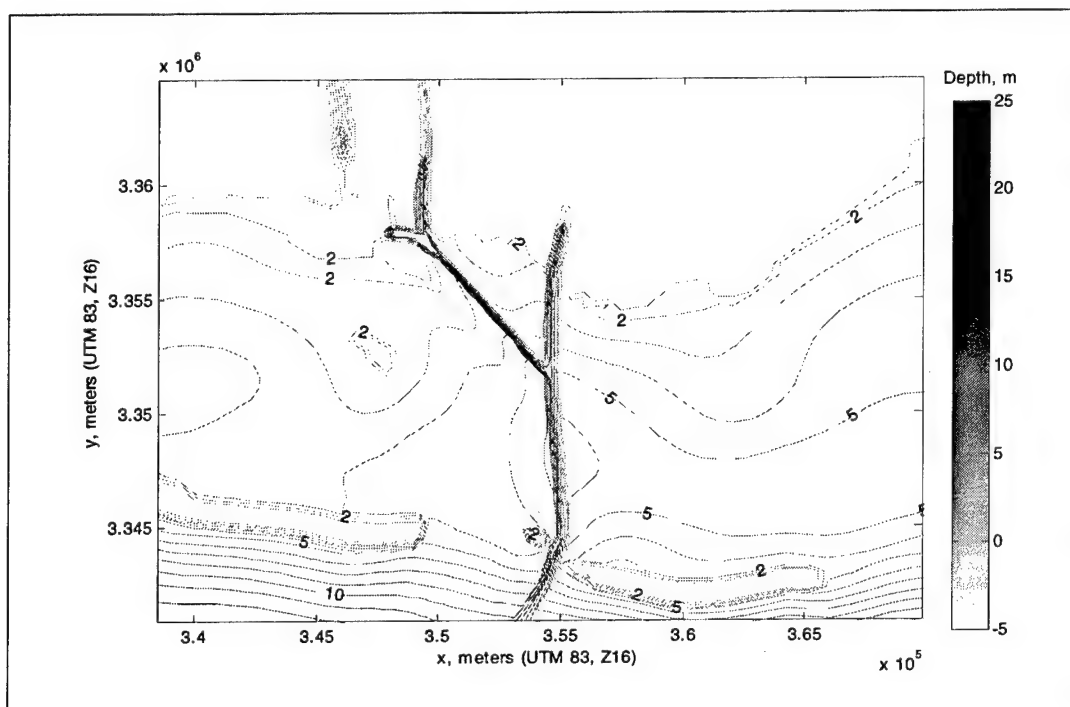


Figure 5-4. CH3D bathymetry in study area near Pascagoula, MS

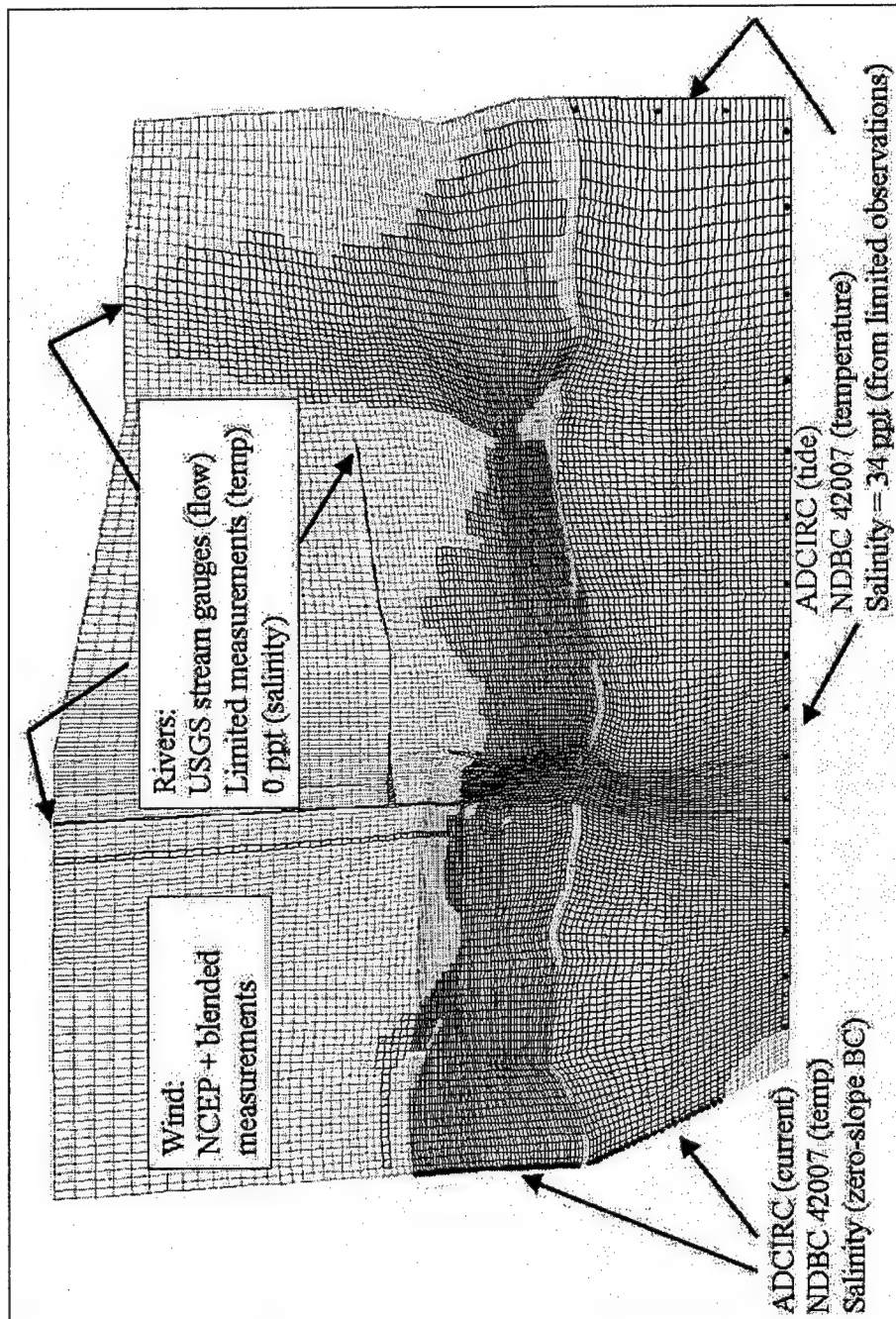


Figure 5-5. Illustration of boundary condition specifications for CH3D grid

Ocean boundary hydrodynamics

The boundary conditions for ocean hydrodynamics (water surface and velocity) were developed from ADCIRC simulations (see Chapter 4). Water surface and current information were saved from ADCIRC at 12.5-min temporal resolution along the lateral boundaries of the CH3D grid as indicated in Figure 5-5. ADCIRC water levels were applied to the southern and eastern CH3D ocean boundaries and ADCIRC velocities were applied to the western CH3D ocean boundary as a “river” boundary condition.

Table 5-1 Source(s) of Information for CH3D Boundary Conditions		
Parameter	Source(s)	Reference
Wind	NCEP and blended measurements	Chapter 2 Chapter 4
Ocean Hydrodynamics	ADCIRC	Chapter 4
Salinity	Engineering judgment based on information from: SEAWIFs satellite imagery and NGLI surveys	SEAWIFs www.lvanova.gsfc.nasa.gov/outreach/EOSDIS-CD-03 NGLI www.navo.navy.mil/NGLI
Water Temperature	Ocean: NDBC Buoy 42007 River: USGS station data at Claiborne Lock and Dam (02428400)	www.usgs.gov/ www.ndbc.noaa.gov
River Discharge	USGS Stations: Pascagoula River at Merrill, Mississippi (02479000) Escatawpa River at Agricola, Mississippi (02479560) Alabama River at Claiborne Lock and Dam (02428400) Tombigbee River at Coffeville Lock and Dam (02469761)	www.usgs.gov

The tidal boundary condition was specified by providing a time-series of tidal elevation (from ADCIRC) at 19 points along the southern and eastern boundaries of the CH3D grid. During simulation, CH3D interpolated (in space and time) the water-surface elevations from this discrete number of points to provide boundary conditions for all cells along the boundary.

The western boundary of the CH3D grid was treated as a flux boundary, where the exchange of fluid was specified from ADCIRC simulations of similar conditions. Depth-averaged velocities were saved from ADCIRC at each open-water CH3D cell on the western boundary of the grid. The fluid flux into the CH3D grid was determined from the ADCIRC velocities and the CH3D cell face orientation, and a time-series of flow rate into each cell on the western boundary was specified on a 12.5-min interval. CH3D applied this boundary condition by interpolating the specified values in time to produce smoothly varying flow.

Freshwater input

Freshwater inflows from the Pascagoula and Escatawpa Rivers enter Mississippi Sound in close proximity to the proposed dredged material disposal islands, and are important factors in the stratification of the sound in the study area. Additionally, large freshwater input from the combined Alabama River and Tombigbee River watersheds into Mobile Bay and the consequent tidal exchange between Mobile Bay and Mississippi Sound through Pass aux Herons influences the stratification of the Mississippi Sound. Other, smaller watersheds were neglected for this study.

The freshwater conveyance of the Pascagoula River is distributed to the lower Pascagoula River and West Pascagoula River approximately 18 km (11.18 miles) north of the river mouths, but hydraulic communication between the two main channels is maintained to some degree through marsh and smaller connecting channels. The representation of the complex network of interconnecting channels and tidal marsh within CH3D was not appropriate within the scope of work for this study, and the two branches of the Pascagoula River were represented as straight, one-cell-wide rectangular channels. This representation of the rivers allowed development and advancement of a salt-wedge up the channels and mixing of the fresh and salt water prior to discharge into Mississippi Sound.

Freshwater flow boundary conditions for the Pascagoula River were developed from data collected at the U. S. Geological Survey (USGS) gaging station at Merrill, MS (sta 02479000). To correctly distribute the freshwater discharge to the east and west channels of the Pascagoula River, 65 percent of the freshwater discharge was directed to the West Pascagoula River and 35 percent directed to the lower Pascagoula River channel (Harza Engineering Company 1995). Freshwater flow boundary conditions for the Escatawpa River were developed from data collected at the USGS gauging station near Agricola, MS (USGS sta 02479560).

The Alabama River and Tombigbee River discharge into the head of Mobile Bay through a series of channels. The input of fresh water into Mobile Bay is a considerable distance from the study area. For the purpose of evaluating the effects of dredged material islands on water quality, the details of fresh and salt water mixing at the head of Mobile Bay are not required to be represented. However, to accurately represent the exchanges of salinity between Mobile Bay and the Mississippi Sound, the mass influx of fresh water into the system from the Alabama and Tombigbee Rivers must be represented. The freshwater input into Mobile Bay was represented in the model by summing the freshwater discharges of the Alabama River (from USGS sta 02428400 at Claiborne Lock and Dam) and the Tombigbee River (from USGS sta 02469761 at Coffeetown Lock and Dam) and distributing the combined flow across the three model cells at the head of Mobile Bay (Figure 5-5).

Temperature

Temperature is a required boundary condition at lateral flow boundaries. As seen in Figure 5-5, temperature was specified at all ocean and river boundaries. Twenty-one years (1981-present) of sea-surface temperature data were measured at an offshore NOAA buoy (42007) located 41 km (25.48 miles) south-southeast

of Biloxi, MS, near the western portion of the southern grid boundary. Hourly sea surface temperature measurements from buoy 42007 were applied to all ocean boundaries of the model for all simulations. Only sparse records of ocean temperature profiles near the model boundaries were found, and therefore a uniform temperature distribution was applied for boundary conditions.

Temperature at the freshwater river boundaries was applied to the model from a limited dataset of temperatures collected on the Pascagoula, Escatawpa, Alabama, and Tombigbee Rivers. The dataset at Claiborne Lock and Dam on the Alabama River was found to have the most frequent measurements (weekly) and water temperature comparisons of available data were quite similar. To develop a continuous temperature boundary condition at the rivers, linearly interpolated (in time) water temperature from the Alabama River was applied to each of the modeled freshwater flows.

Surface heat exchange

The daily surface heat exchange coefficient and equilibrium temperature were computed from meteorological data obtained from the EarthInfo CD-ROM database by the method of Edinger, Brady, and Geyer (1974). Factors included in the analysis are wind speed, cloud cover, and wet and dry bulb air temperatures, and latitude. Surface heat exchange coefficients from the Edinger, Brady, and Geyer model are computed in units of $W/m^2/^\circ C$ and must be converted to units of cm/sec to be dimensionally consistent with CH3D. The CH3D surface heat exchange coefficient is given by:

$$k = \frac{K_T}{\rho C_p} \quad (5-12)$$

where

K_T = Edinger, Brady, and Geyer surface heat exchange coefficient
($W/m^2/^\circ C$)

ρ = water density (taken as 1,025 kg/cu m)

C_p = specific heat of water (taken as 4,000 J/kg/ $^\circ C$)

Salinity

Little directly measured salinity data were available near the offshore boundaries. Remote sensing through satellite imagery and surface-sampled data from the NGLI program suggest that outside of major flood events from the Mississippi River, the surface salinity near the model boundaries is approximately 34-35 ppt. Salinity of 34 ppt was applied to the southern and eastern ocean boundaries for all scenarios. The western open-water boundary was treated with a zero-slope salinity boundary condition when fluid advected into the model. Salinity was allowed to freely advect out of this boundary.

Wind

Because tidal forcing is of such a small magnitude in the study area, surface shear stresses produced by wind often play an important factor in the hydrodynamics of the Mississippi Sound and Mobile Bay. Wind fields were developed for the circulation and wave modeling presented in Chapters 4 and 7, respectively. For calibration simulations of conditions during February/March 2001 and April/September 1997, the wind fields developed for ADCIRC were used to apply wind forcing to the CH3D grid. Wind from a point in the wind field near the Pascagoula navigation channel was selected and was applied uniformly over the CH3D grid, as variable wind fields are not supported in the model.

Friction

The bottom friction coefficient was specified as a uniform value over the model domain and was used as a calibration coefficient for velocity and water surface.

Mixing

Water column mixing is of primary interest in this study because it is through vertical mixing that higher levels of dissolved oxygen are brought to the lower portions of the water column. Physical processes that influence vertical mixing are flow-generated turbulence, wind, density stratification, and waves. With the exception of waves, these processes are represented in the model. For the evaluation of the design alternatives, assume that mixing due to wave action is negligible. The remaining physical processes are represented in the model through a vertical k - ϵ turbulent eddy viscosity model, which includes the effects of wind shear, bottom shear, velocity gradient turbulence production, dissipation, diffusion, and stratification. A general overview of the k - ϵ model is given by Chapman, Johnson, and Vemulakonda (1996).

The vertical eddy viscosity and diffusivities estimated by the k - ϵ model are limited by user-specified bounds. For the present study, the minimum and maximum vertical eddy viscosities were set to 0.005 and 100 cm^2/sec and the minimum and maximum vertical eddy diffusivities were set to 0.001 and 50 cm^2/sec , respectively. Mixing through horizontal velocity gradients is represented through the horizontal eddy viscosity coefficient, which was set to a value of 15,000 cm^2/sec for the present study.

Calibration and Verification

CH3D was calibrated to available water surface, current, temperature, and salinity data within the study area. The primary goal of the calibration exercise was to achieve reasonable agreement with the hydrodynamic, temperature and salinity measurements through adjustment of friction coefficients within justifiable limits. Measurements of hydrodynamics, temperature, and salinity were not available at concurrent times, so separate calibration efforts were

conducted to compare model simulations to: (a) water surface and current and (b) temperature and salinity.

Complexities in the wind forcing of the period February-March 2001 (see discussion in Chapter 4) resulted in periods of uncertainties in the ADCIRC forcing during this period. Recall that this application of CH3D relies on ADCIRC forcing for boundary conditions. To avoid the influence of uncertainties in the estimated wind fields, initial model calibration for hydrodynamics was performed to a simulation of the model domain to tide only. Following this initial calibration, the model underwent meteorological calibration similar to that of ADCIRC (Chapter 4) for the period February-March 2001. Finally, CH3D was calibrated/verified for temperature and salinity to available data during the period April-September 1997. Positions of measurements included in the calibration/verification exercise are presented in Figure 5-6 and position, sources, and measured quantities are presented in Table 5-2.

Astronomical

Calibration of CH3D to astronomical tides began with calibration to astronomical forcing only. The interest in CH3D modeling for this study was to provide hydrodynamics to the CEQUAL-ICM model under worst-case environmental conditions (in this case low wind forcing). This consideration makes the tide-only calibration most suitable for the 3-D hydrodynamic modeling objectives.

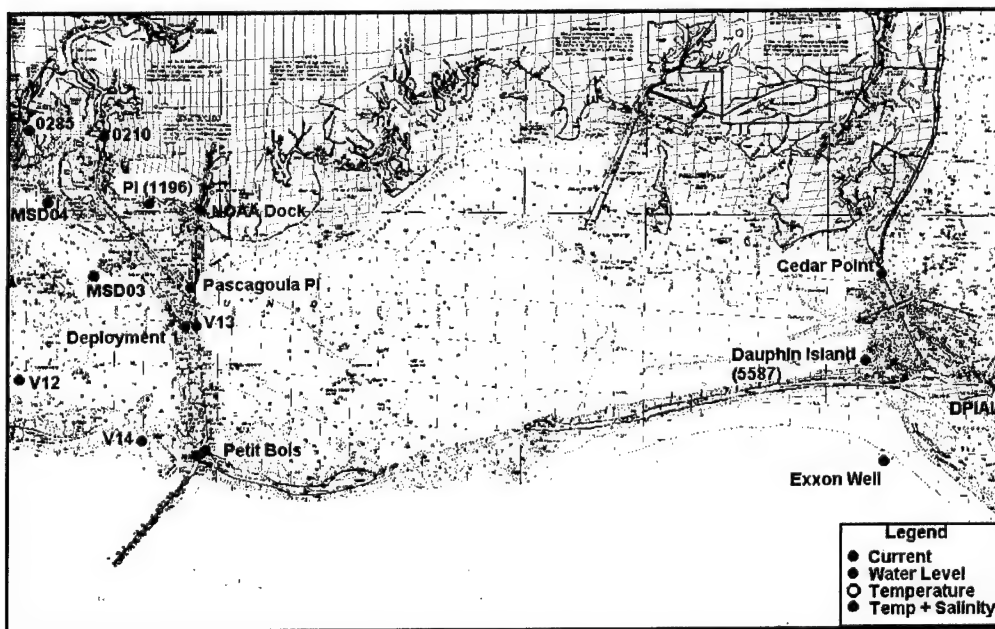


Figure 5-6. Location map of measurements included in calibration and verification exercises

**Table 5-2
CH3D Calibration/Verification Data**

Station	Type	Date(s)	Position	Source(s)	Reference
PI (1196)	Water level	Astronomical constituents	30°20.4'N 88°32.0'W	USACE	Outlaw (1983)
Dauphin Island (5587)	Water level	Astronomical constituents	30°15.5'N 88°06.8'W	USACE	Outlaw (1983)
V12	Current	Astronomical constituents	30°16.14'N 88°40.82'W	USACE	Outlaw (1983)
V13	Current	Astronomical constituents	30°15.96'N 88°30.61'W	USACE	Outlaw (1983)
V14	Current	Astronomical constituents	30°13.32'N 88°32.40'W	USACE	Outlaw (1983)
NOAA Dock	Water level	February - March 2001	30°20.09'N 88°30.68'W	USACE	Web
Pascagoula PI	Water level	February - March 2001	30°17.75'N 88°30.95'W	USACE	Web
Deployment 1	Current water level	February - March 2001	30°16.62'N 88°31.07'W	USACE	www.sandbar.wes.army.mil
Petit Bois	Current water level	February - March 2001	30°13.12'N 88°30.39'W	USACE	www.sandbar.wes.army.mil
Cedar Point	Water level	February - March 2001	30°18.32'N 88°08.23'W	USACE	Web
Exxon Well	Water level	February - March 2001	30°12.92'N 88°08.10'W	USACE	Web
0210	Temperature salinity	4/17/1997 7/22/1997	--	MSDEQ	--
0285	Temperature salinity	4/17/1997 7/22/1997 9/10-12/1997	--	MSDEQ	--
MSD03	Temperature salinity	4/17/1997 7/22/1997	--	MSDEQ	--
MSD04	Temperature salinity	9/10-12/1997	--	MSDEQ	--
DPIAL	Temperature	April - September 1997	30°14.9'N 04.4'W	NOAA /NDBC	www.ndbc.noaa.gov

The CH3D ocean boundaries for astronomical calibration were forced by hydrodynamics of the ADCIRC astronomical calibration. Outlaw (1983) performed a harmonic analysis of measured water surface and current data from Mississippi Sound. Outlaw computed astronomical tidal constituents for water surface (sta 1196 and 5587) and current (sta V12, V13, and V14). These stations are represented in Figure 5-6. The harmonic analysis of tides and currents were performed on a limited-length data set (40-60 days for currents and 180 days for water surface) and a degree of uncertainty is associated with the derived constituents. A tidal signal for the months of April and May 1997 was reconstructed from the astronomical tidal constituents, and calibration of the model to astronomical tides was performed to the reconstructed data. Bottom roughness was varied between 0.003 and 0.010 and the best fit to the data was found with a roughness value of 0.004.

Figure 5-7 presents water-surface comparisons between the reconstructed (Outlaw 1983) and the CH3D modeled astronomical tides at tide sta 1196 and 5587. Notice that as the harmonics of the Gulf of Mexico develop (after 21 April) from the initial quiescent conditions, that the agreement with the reconstructed tides are good at sta 1196 and 5587. Root mean square (RMS) errors reported by Outlaw (1983) in comparing reconstructed tides to filtered measurements were 0.03 m (0.10 ft) at sta 1196 and 5587. The differences between CH3D and Outlaw after model spin-up are of similar magnitude and calibration of the model to water level is considered satisfactory.

Figures 5-8 through 5-10 present comparisons between reconstructed tidal currents and currents estimated by CH3D at sta V12, V13, and V14 during the period of April-May 1997. Notice that the tidal currents at sta V12 and V13 are fairly weak, not greater than 0.1 m/sec (0.33 ft/sec), while the currents at sta V14 between the barrier islands are larger (but still relatively weak) at 0.2 – 0.3 m/sec (0.66 – 0.98 ft/sec). Wind-generated currents in the study area will later be shown to have equal or greater magnitude than the spring tidal currents, and Mississippi Sound is frequently a wind-dominated system.

Good agreement between the reconstructed currents from Outlaw's (1983) harmonic analysis and CH3D modeled currents is shown in Figures 5-8 through 5-10. In some instances an unexplained phase lag exists between the modeled and reconstructed currents, however the frequency and amplitude of the tidal currents are in agreement. The RMS error from Outlaw's analysis is approximately 0.03 m/sec (0.10 ft/sec) at sta V12 and V13, and 0.05 m/sec (0.16 ft/sec) at sta V14. The model differences in astronomically forced currents are within the range of differences of the harmonic analysis. Recall that the objective of 3-D hydrodynamic modeling for this study is to provide hydrodynamics to a water quality model for evaluation of the effects of proposed dredged material islands on water quality under a worst-case scenario. For water quality in the study area, the worst-case scenario is mild hydrodynamic forcing (or near-zero wind) and the hydrodynamics are dominated by astronomical forcing. The calibration of the model to astronomical forcing has been demonstrated in this section to be successful. Issues of model representation of meteorological forcing and temperature and salinity effects remain and will be addressed in following sections.

February-March 2001

Verification of current and water level was performed for the period February-March 2001, during which current and water level data were collected for this study (Chapter 2) and the same period of ADCIRC meteorological calibration (Chapter 4). Station locations (Deployment 1, Pascagoula PI, NOAA Dock, Petit Bois, Exxon Well, and Cedar Point) and data sources are provided in Table 5-2 and Figure 5-6. Bottom roughness and horizontal dispersion coefficients determined in the astronomical calibration were not modified for comparison to the collected data set.

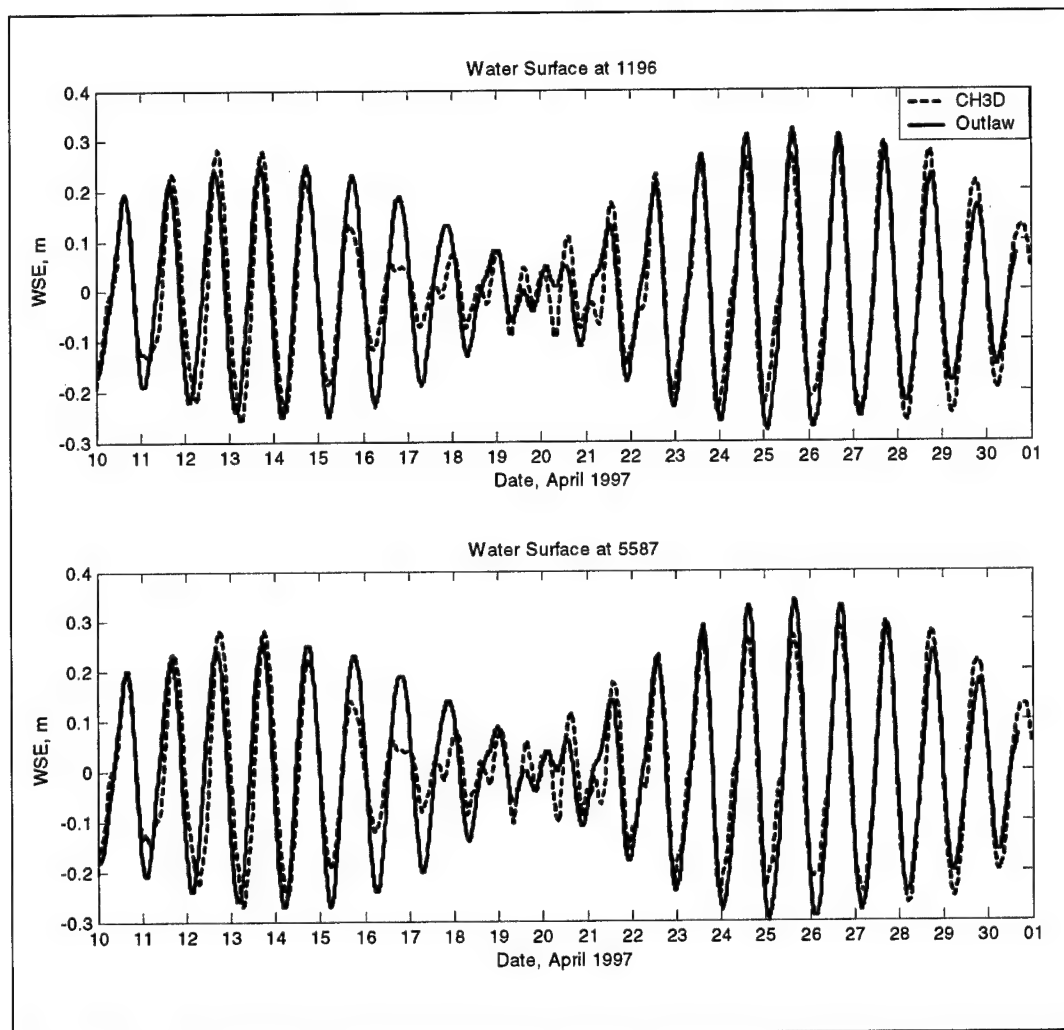


Figure 5-7. Comparisons of reconstructed tides from Outlaw (1983) and CH3D simulated tides

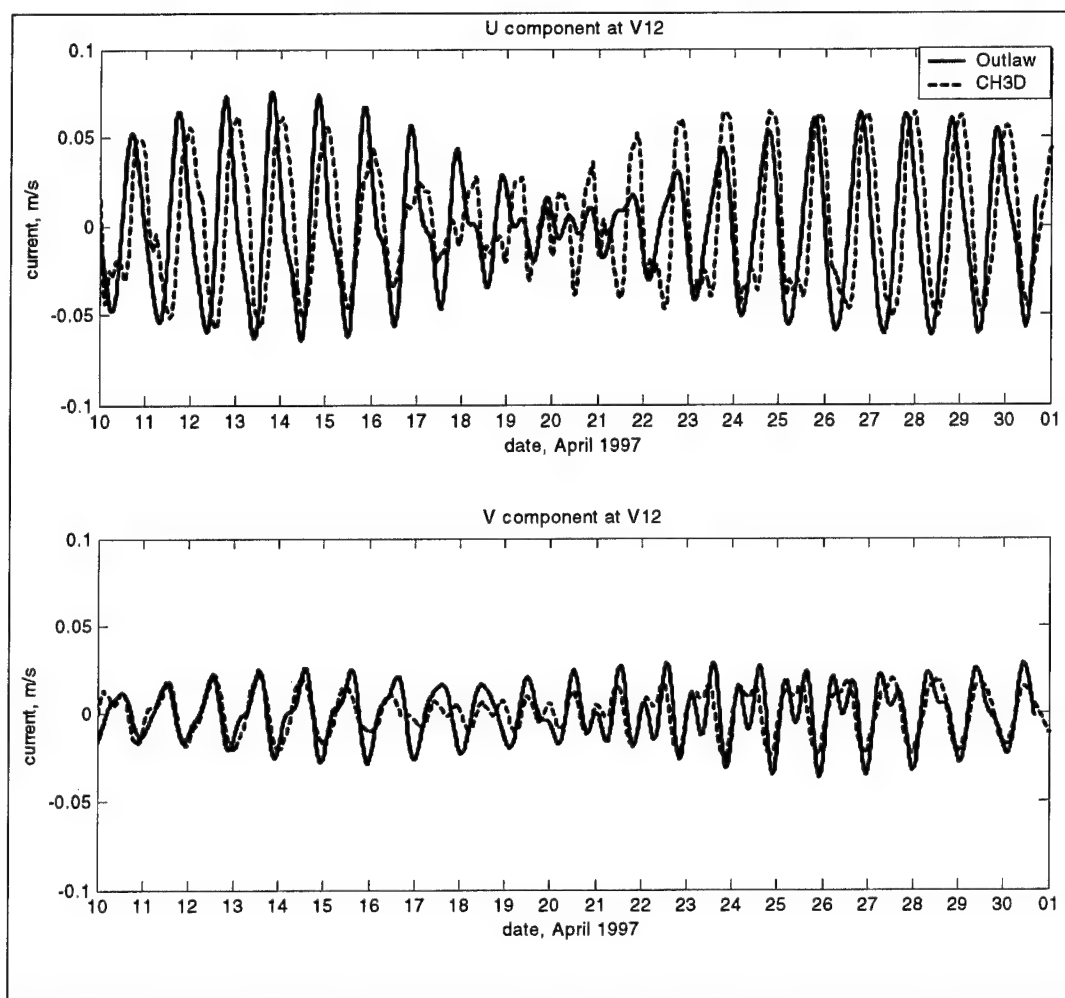


Figure 5-8. Comparison of reconstructed tides (from Outlaw 1983) and CH3D simulated tides at sta V12

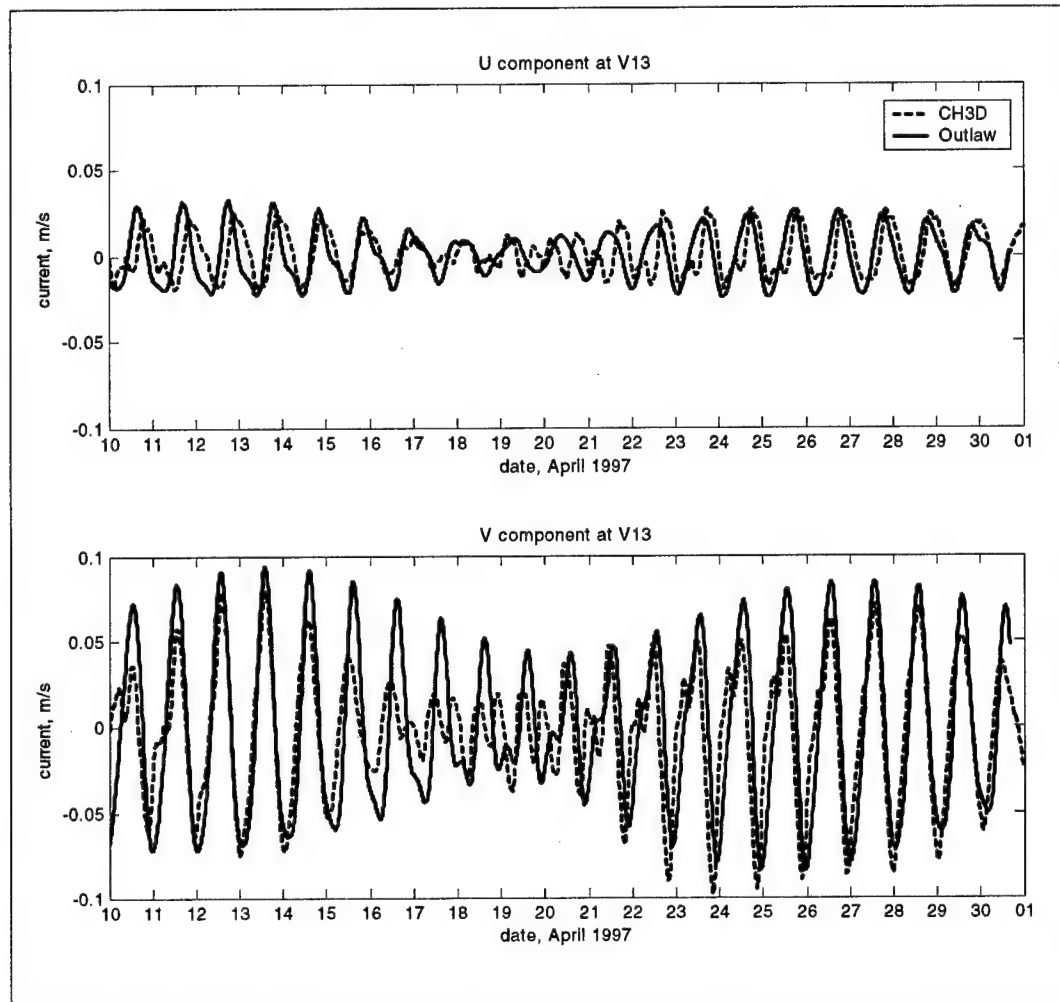


Figure 5-9. Comparison of reconstructed tides (from Outlaw 1983) and CH3D simulated tides at sta V13

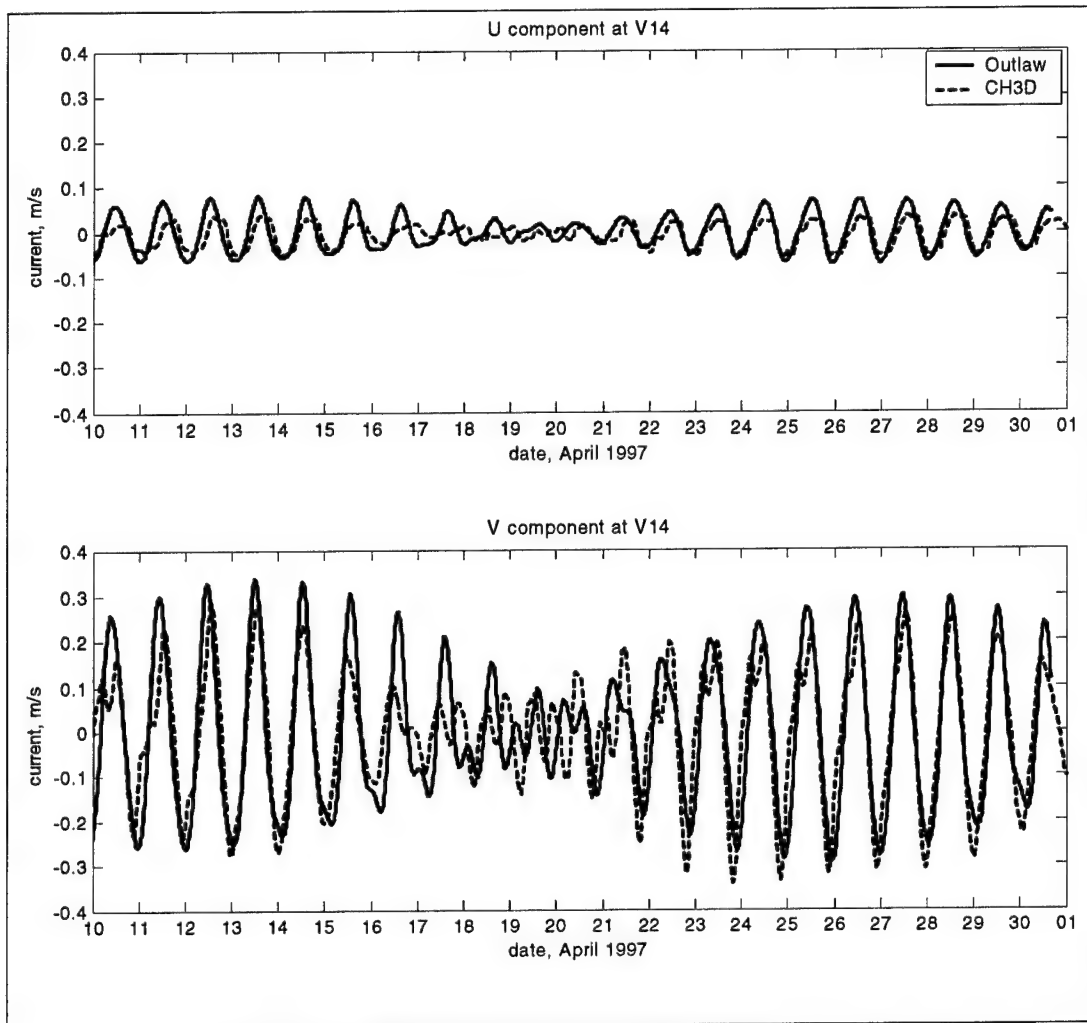


Figure 5-10. Comparison of reconstructed tides (from Outlaw 1983) and CH3D simulated tides at sta V14

For this simulation, ocean boundary hydrodynamics from ADCIRC were applied as indicated in Figure 5-5, and a time-variant but spatially uniform wind was applied from the NCEP wind field near the Pascagoula navigation channel in the Mississippi Sound. Comparisons of modeled and measured water surface elevation at the Pascagoula PI gage are presented in Figure 5-11 and are comparable to the results produced by ADCIRC (see Figure 4-17). The comparisons to water surface are generally good, but some noticeable differences exist for days at a time, suggestive of inaccuracies in the surface shear stresses generated by the blended NCEP wind fields (as noted in Chapter 4).

Modeled current magnitude and direction are compared to measurements at the Deployment 1 location in Figure 5-12. Note that the 16-day period of measured currents is shorter than the period of measured water level and corresponds to the end of the record presented in Figure 5-11. CH3D represents currents well for larger-scale events occurring on 12 and 15 March but poorly represents peak current magnitudes for an event occurring 1 March. Short-term and local-scale wind-related events occurring during the period of measurements are poorly represented by the 6-hr temporal resolution and spatially uniform application of the wind. To better represent these conditions in the model requires higher temporal resolution of winds and development of spatial wind resolution in the model. Note that modeled current direction agrees fairly well with current direction during the longer duration events (1, 12, and 15 March), but shows less agreement for the milder currents (less than 0.2 m/sec (0.66 ft/sec)).

Presentation of model/data comparisons at other stations in the study area are presented in Appendix H.

April-September 1997

To assess the representation of temperature and salinity within the system, a comparison of model results to available data was performed. Conditions were modeled for April-September 1997 because of the availability of temperature and salinity data collected by the Mississippi Department of Environmental Quality (MSDEQ) during this period. Locations of temperature and salinity data collection are represented in Figure 5-6. Temperature and salinity data were collected quarterly at sta MSD03, 0210, and 0285 near the study site. In addition, hourly data collection of temperature and salinity were conducted 10-12 September at sta MSD04 and 0285. Data collected quarterly was obtained from a range of depths typically through the water column, however the short-term continuous data were collected at 1 m (3.28 ft) below the free surface. The National Ocean Service (NOS) maintains a data collection platform, DPIAL, on the eastern tip of Dauphin Island. A continuous hourly record of sea surface temperature was available at this station for the duration of the simulation.

DPIAL The longest continuous record of temperature data is at stat DPIAL off the eastern tip of Dauphin Island. Hourly sea surface temperature data are compared to model estimates for the duration of the simulation in Figure 5-13. After the first few days of the simulation (when the initial conditions influence the

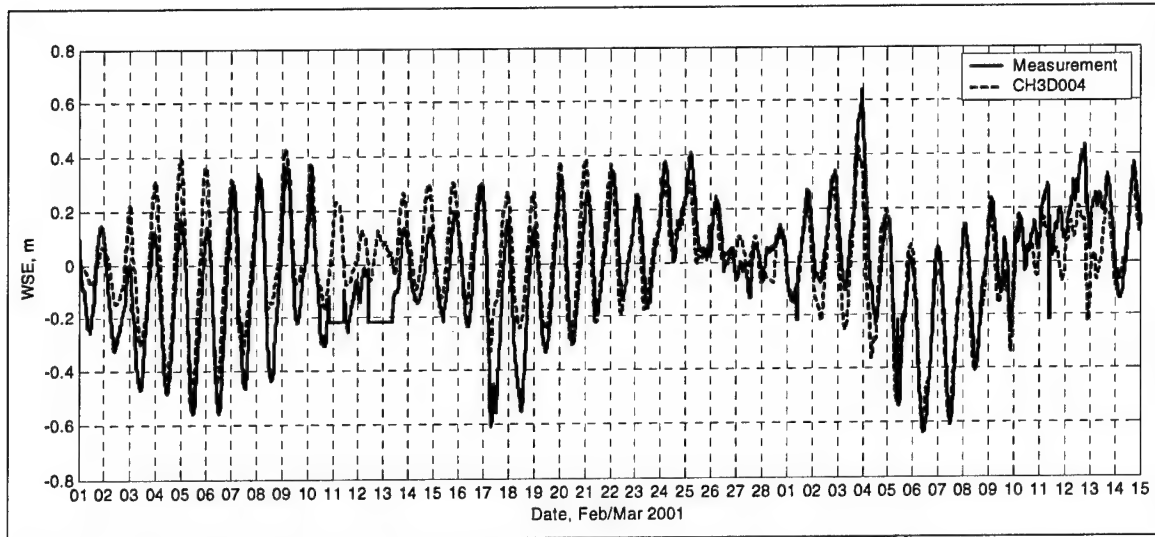


Figure 5-11. Comparison of CH3D to measured water-surface elevations at Pascagoula PI gage for February-March 2001 verification

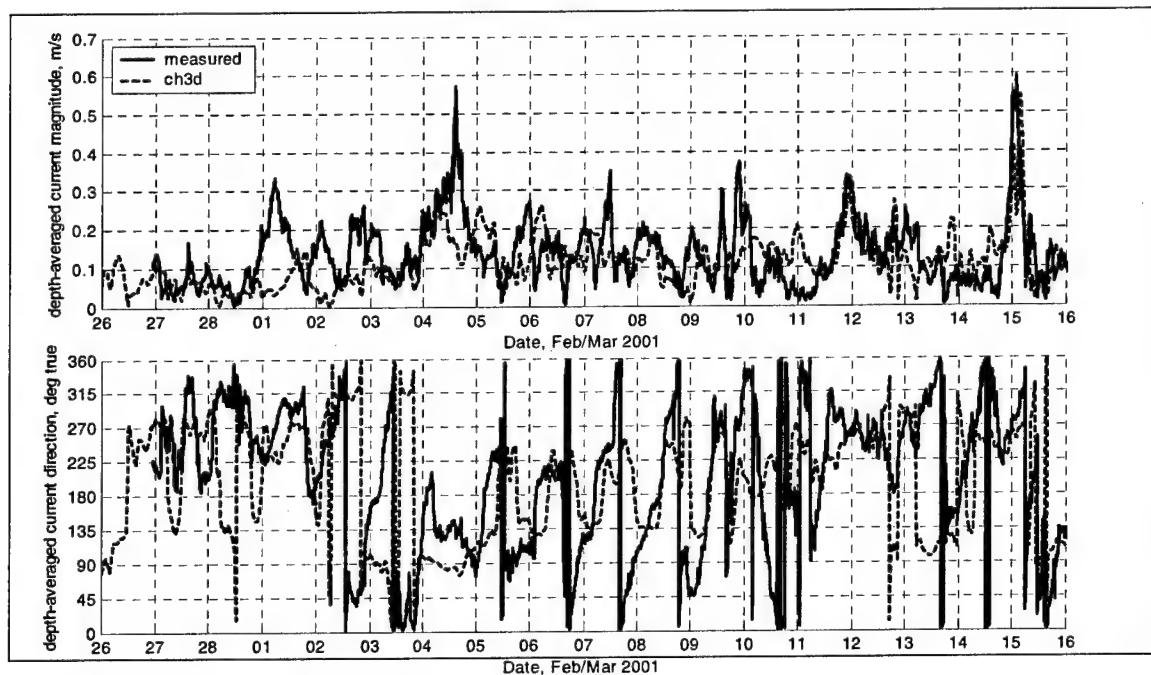


Figure 5-12. Comparison of CH3D to measured currents at Deployment 1 site for February-March 2001 verification

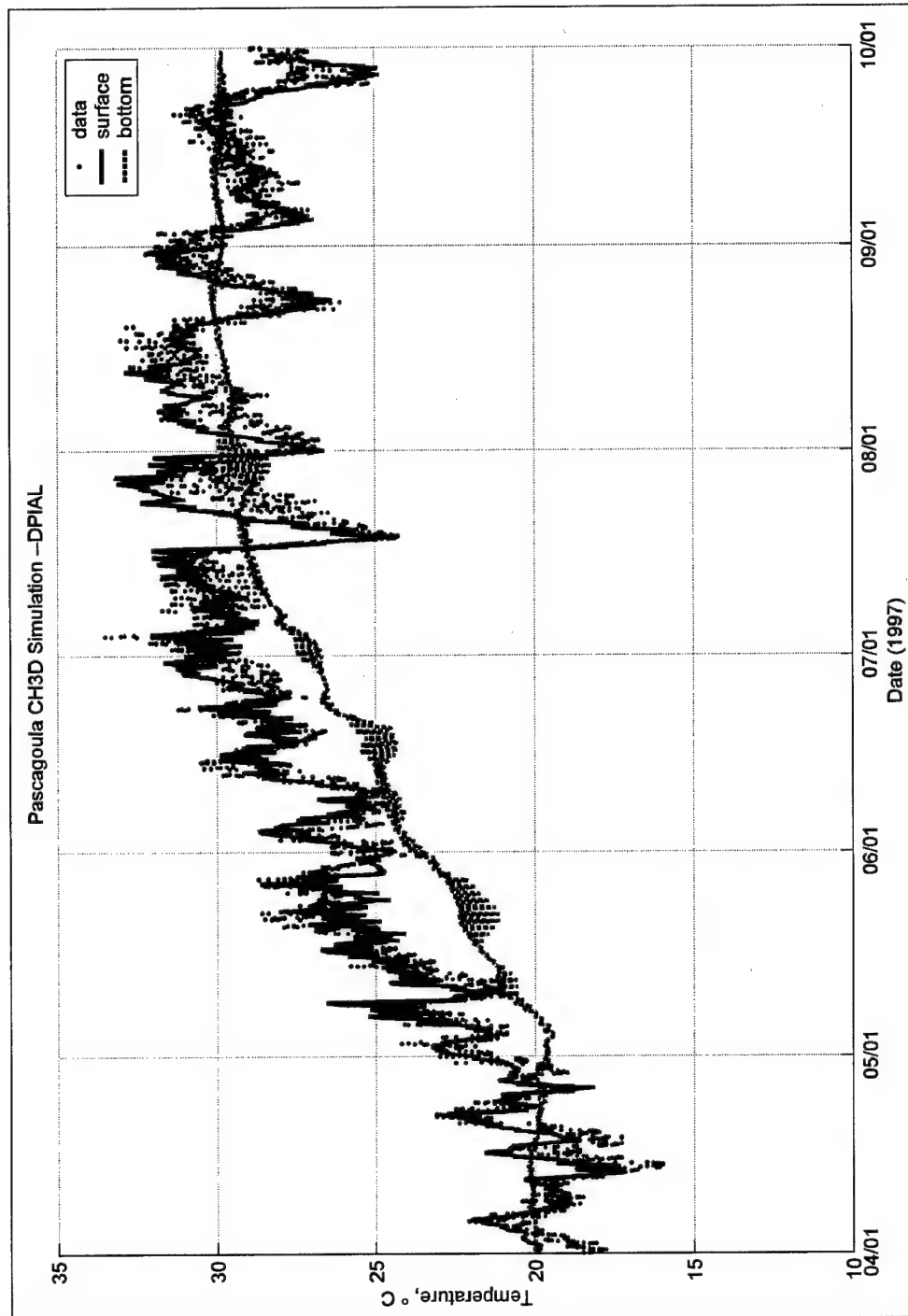


Figure 5-13. Comparison of measured and modeled sea surface temperature at DPIAL (see Figure 5-6). Points are measured data, solid line represents surface layer of model, and dashed line represents bottom layer of model

model estimates), the model results agree with the measured data. Notice that there is significantly more high-frequency variation in the measured data than evidenced in the model results. On closer inspection, strong diurnal variability is contained in the measured data. The equilibrium-temperature surface heat exchange method performs remarkably well in representing the seasonal and daily heat exchange at the water surface, but does not resolve the diurnal variation.

MSD03. Station MSD03, located south of Pascagoula Harbor and east of Round Island (Figure 5-6), is near the proposed dredged material islands and is of interest in validation of modeled temperature and salinity. Profiles of temperature and salinity data were collected 17 April and 22 July 1997 at the station and data from these events are presented in Figure 5-14. The values associated with each depth in the figure indicate the normalized position of the measurement in the water column (for instance, a surface measurement would have a normalized depth of 0.0 and a near-bottom measurement may have a value of 0.9).

Modeled temperatures at MSD03 compare well to the measured data with maximum differences between the model and measurements generally less than 1°C. Modeled salinity is also in good agreement with the limited number of measured values. The measured surface salinity in July agrees closely with the modeled surface salinity, and the near-middepth salinity measured in April is close to the modeled value at middepth. The measured salinity at a normalized depth of 0.2 suggests a weaker salinity gradient between the surface and middepth. Although the data at this station are sparse, the available data are consistent with the trends evident in the modeled quantities.

MSD04. Sta MSD04 is south of the terminus of the West Pascagoula River and just west of Singing River Island. Like MSD03, this station is located near proposed locations for dredged material island creation and expansion, and therefore significant for model validation of temperature and salinity. Two days of continuous temperature and salinity measurements were made at sta MSD04 during 10-12 September 1997. These data are presented with the 6 months of simulated temperature and salinity from CH3D in Figure 5-15. The hourly measurements were taken at 1 m (3.28 ft) below the water surface, which translates to approximately half the total water depth at this shallow location.

The quality of the model-to-data comparisons is not apparent in Figure 5-15, but becomes clearer when presented over a shorter duration as in Figure 5-16. In this figure, the diurnal variation of water temperature is clearly seen in the measurements, but is absent from the model predictions because of the time-scale of the surface heat transfer method in the model. However, the middepth model temperature does not vary by much more than 1°C from the time-averaged value of measured temperature. The proximity of sta MSD04 to the freshwater flow of the West Pascagoula River is evidenced in significantly larger vertical salinity gradients. Although measurements of vertical salinity gradients at the site are unavailable, it is encouraging to note the close agreement of the temporal variation in salinity at middepth over the 2 days of measurements.

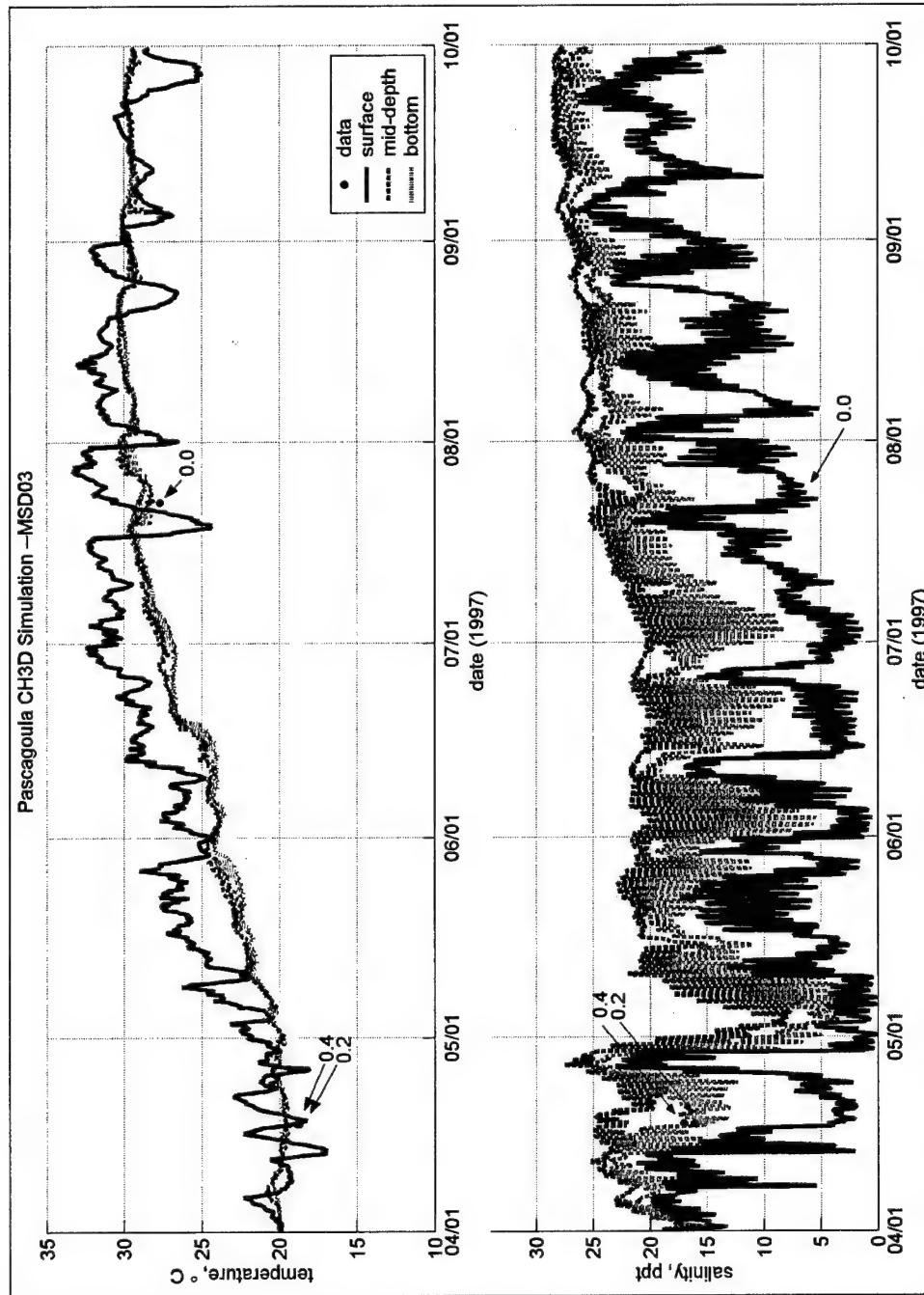


Figure 5-14. Comparison of measured and modeled temperature and salinity at MSD03 (see Figure 5-6). Points are measured data, solid line represents surface layer of model, and dashed line represents bottom layer of model. Values assigned to data points indicate normalized position in water column. 0 = surface, 1 = bottom

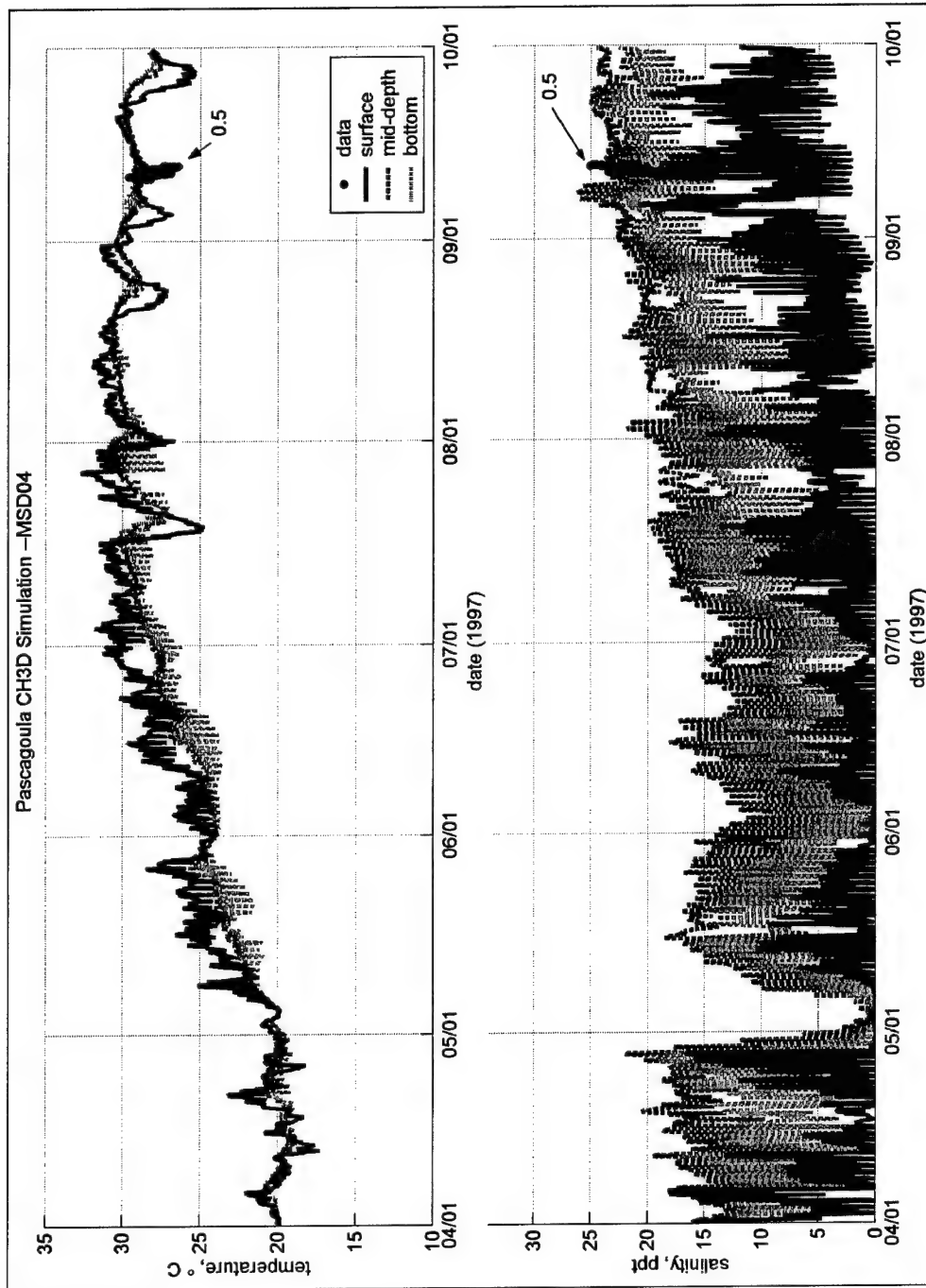


Figure 5-15. Comparison of measured and modeled temperature and salinity at MSD04 (see Figure 5-6). Points are measured data, solid line represents surface layer of model, and dashed line represents bottom layer of model. Values assigned to data points indicate normalized position in water column. 0= surface, 1= bottom

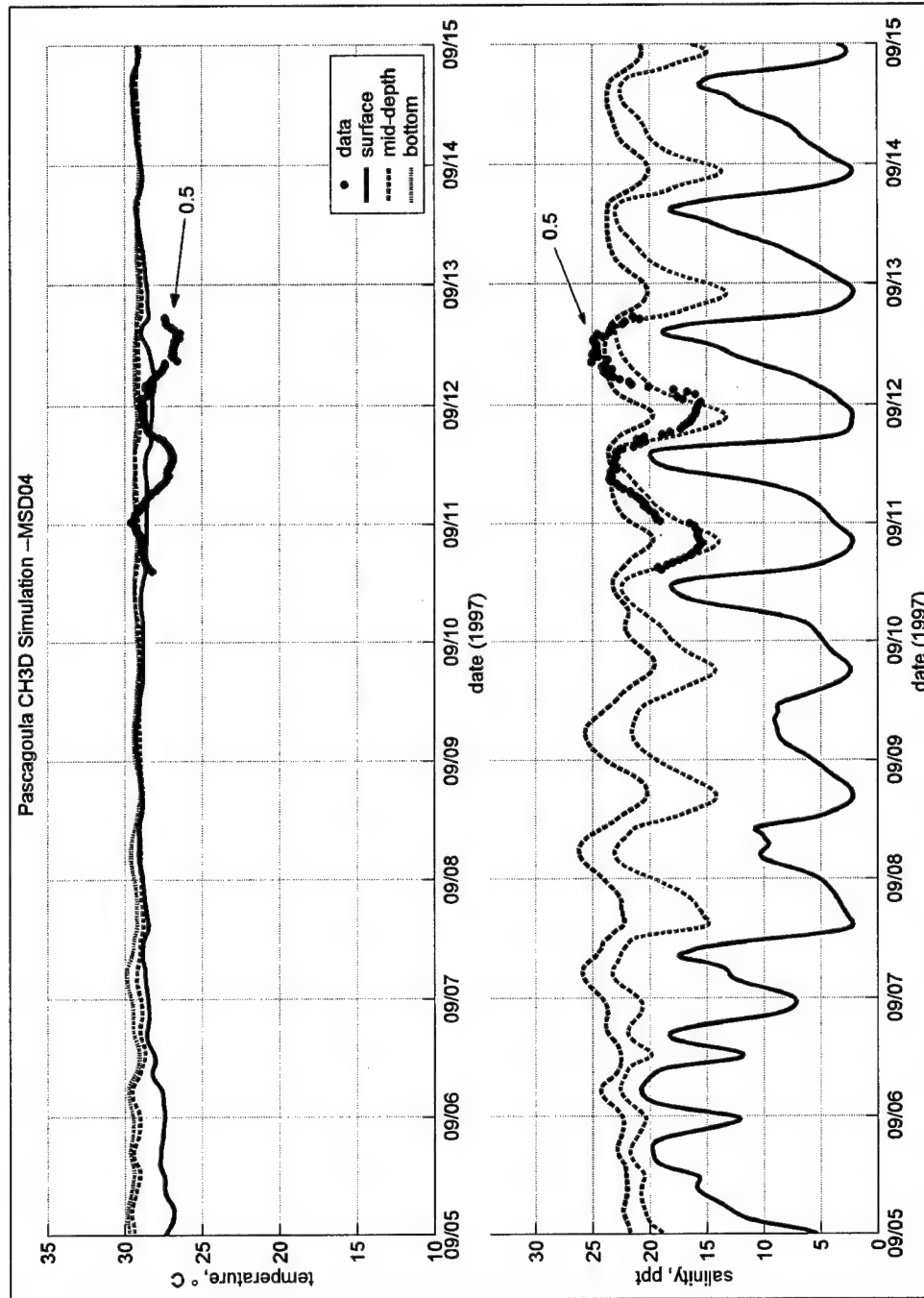


Figure 5-16. Comparison of measured and modeled temperature and salinity at MSD03 during period of hourly data collection (see Figure 5-6). Points are measured data, solid line represent surface layer of model, and dashed line represents bottom layer of model. Values assigned to data points indicate normalized position in water column. 0 = surface, 1 = bottom

Stations 0210 and 0285. Model comparisons of temperature and salinity to available data at sta 0210 and 0285 are presented in Appendix H. Although these stations were within the idealized Pascagoula and West Pascagoula River Channels, comparisons to vertical temperature and salinity gradients were favorable.

Design Alternatives

Three design alternatives were evaluated for this study, with each alternative consisting of a single dredged material disposal island covering an area of approximately 4,046,825 sq m (1,000 acres). Each design alternative was simulated under a condition with weak wind forcing and high and water temperature as a worst-case scenario for dissolved oxygen. Changes in hydrodynamics and water quality were compared between each alternative and the base alternative (the existing geometry and bathymetry).

Geometry

The proposed location and configuration of the three studied alternatives is shown in Figure 5-17. Notice that the grid is boundary-fitted where practical to the margins of the proposed islands. Alternative 01 is represented as a quarter-circular arc, expanding Singing River Island to the southwest. Alternative 02 is a circular island located south-southeast of Singing River Island. Alternative 03 is a circular island located in the "Y" of the Bayou Casotte and Pascagoula River navigation channels. The grid representation of each modeled scenario is presented in Appendix I.

Environmental conditions

The environmental conditions applied to CH3D for evaluation of the design alternatives were developed with interest in representing a worst-case scenario for dissolved oxygen. Statistical analysis of a 48-year record of dry-bulb temperature at the Mobile airport resulted in the selection of August 1990 to represent the month with the worst-case conditions (see discussion of the selection process in Chapter 6). River flow, sea surface temperature, wind, and astronomical forcing were assembled for August 1990 using the methods and databases discussed previously in development of the CH3D initial and boundary conditions. Because salinity requires a substantial spin-up period before reaching an equilibrium state, several 1-month simulations were performed and the resulting salinity and temperature fields were passed from the end of the previous run to the initial conditions of the following run until equilibrium was achieved. The resulting fields of temperature and salinity were then applied as initial condition for the simulations of design alternatives. A summary of meteorological conditions for the month of August 1990 is provided in Figure 5-18. Equilibrium temperature (calculated by method of Edinger, Brady, and Geyer (1974)) and sea surface temperatures (at buoy 42007) are high. Wind speed is generally low (with peak

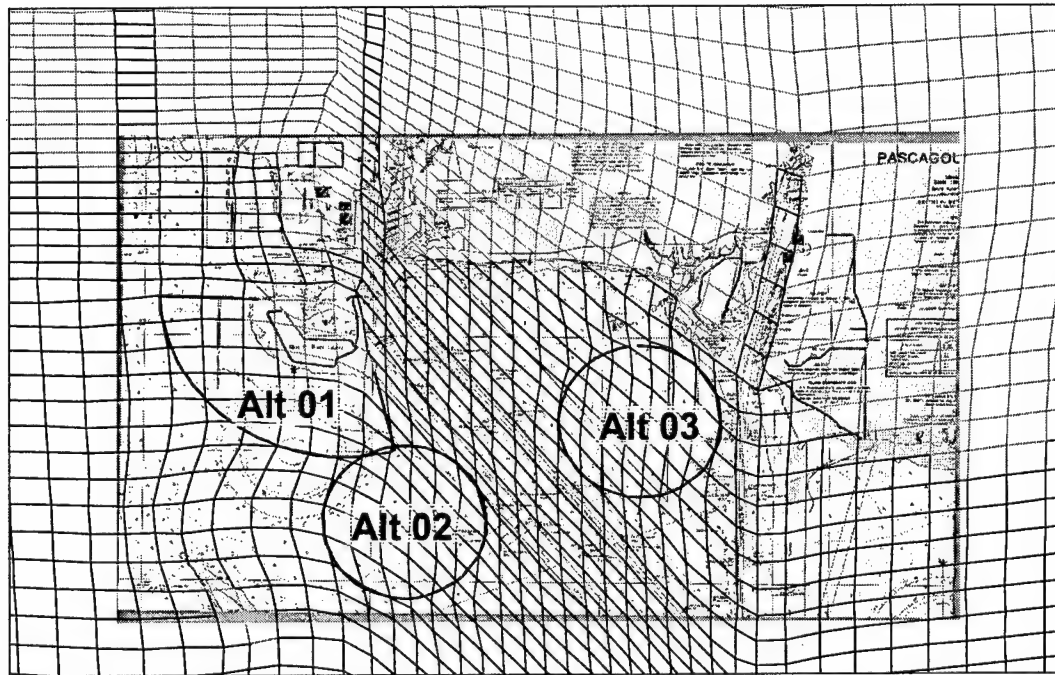


Figure 5-17. Location of dredged material disposal alternatives in relationship to existing land masses and CH3D grid

in diurnal variation approximately 6 m/sec 19.68 ft/sec)) and primarily from the south. Also, river discharges into Mobile Bay and through the Pascagoula River are low, approximately 5-10 percent of the flow of the spring of 1997 (from the April-September 1997 simulation).

Simulations

Model simulation of the base condition and three island alternatives provided hydrodynamics for the ICM water quality model. Effects of the island alternatives on water quality are discussed in Chapter 6. General discussion of the effects of each island alternative on circulation patterns is presented in the following paragraphs. Many of the observations concerning changes to the circulation patterns are evident in model output from 13 August 1990, 2200 GMT (310 hr into the simulation) and snapshots of currents from the bottom layer are presented for each alternative in Figures 5-19 through 5-22.

Alternative 01. Alternative 01 (westward expansion of Singing River Island) constricts the area between Singing River Island and Round Island and results in increased velocities between the two islands during both ebb and flood currents. Another change in circulation is located northwest of the expanded Singing River Island, where currents are decreased during flood tide. Comparison of Figures 5-19 and 5-20 presents one example of the described behavior.

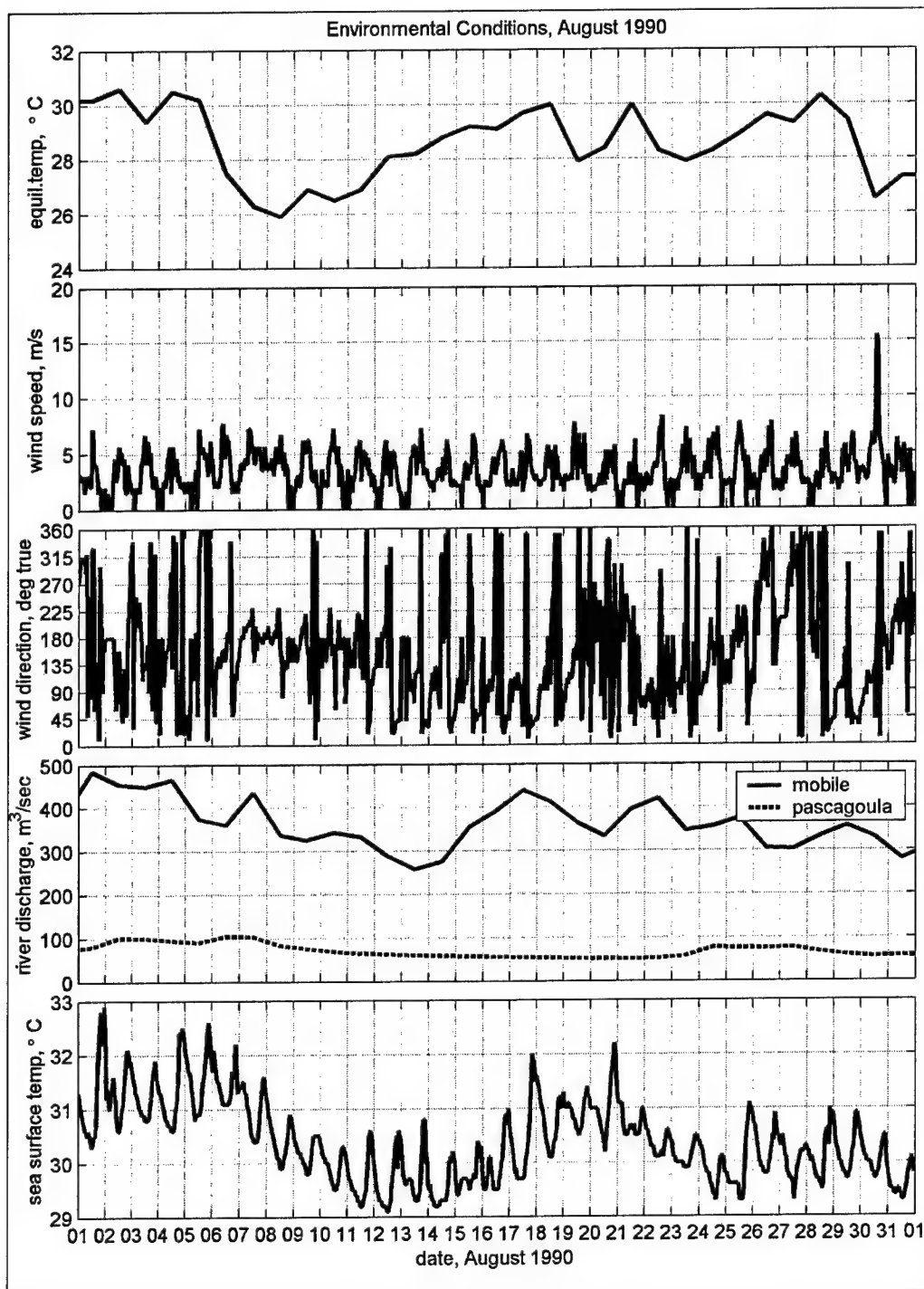


Figure 5-18. Environmental conditions for August 1990 applied for design simulations

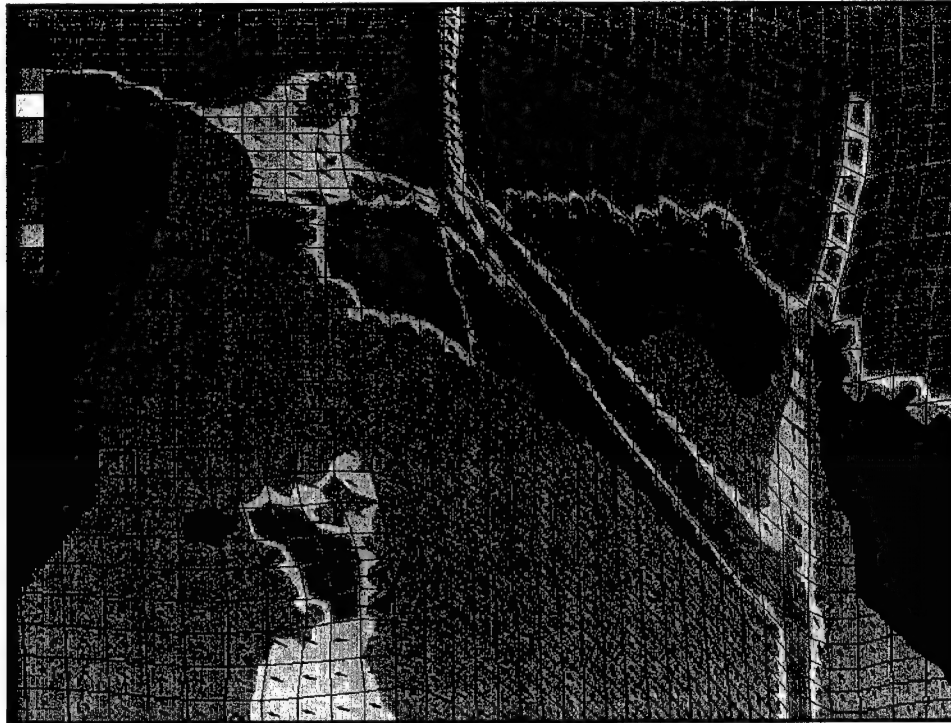


Figure 5-19. CH3D bottom currents for Alternative 00 (13 August 1990, 2200 GMT). Filled contours indicate current magnitude, vectors indicate current direction

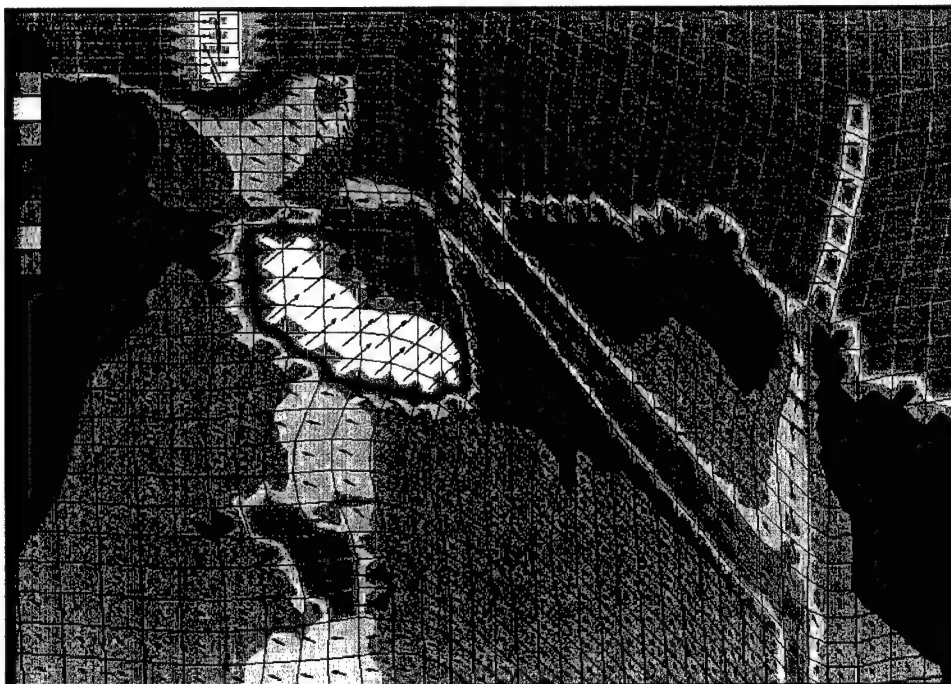


Figure 5-20. CH3D bottom currents for Alternative 01 (13 August 1990, 2200 GMT). Filled contours indicate current magnitude, vectors indicate current direction

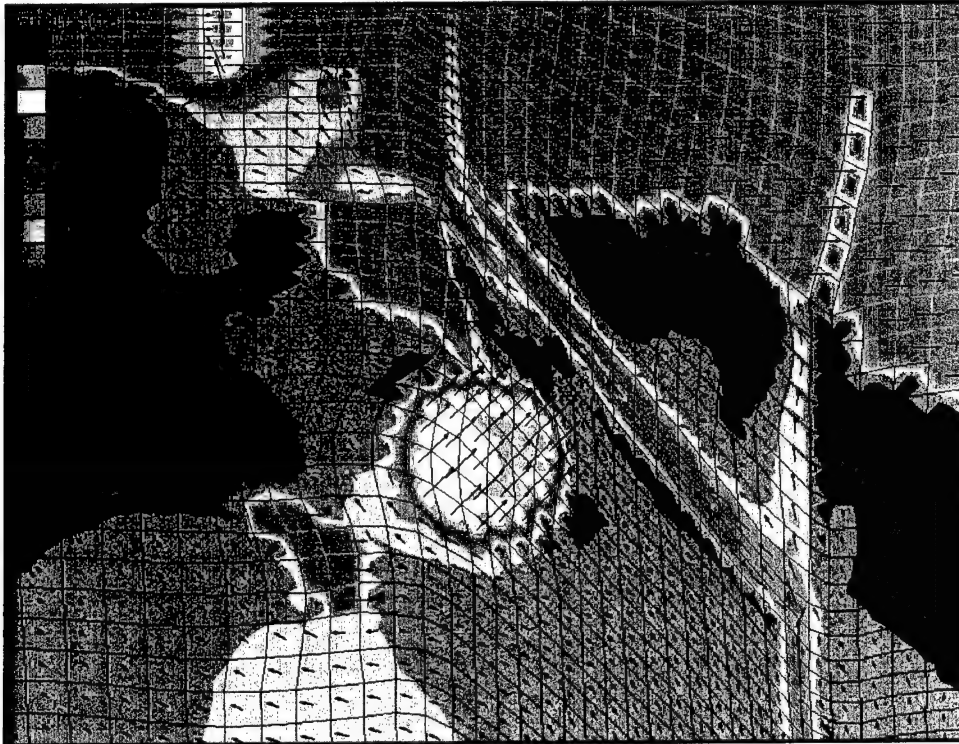


Figure 5-21. CH3D bottom currents for Alternative 02 (13 August 1990, 2200 GMT). Filled contours indicate current magnitude; vectors indicate current direction

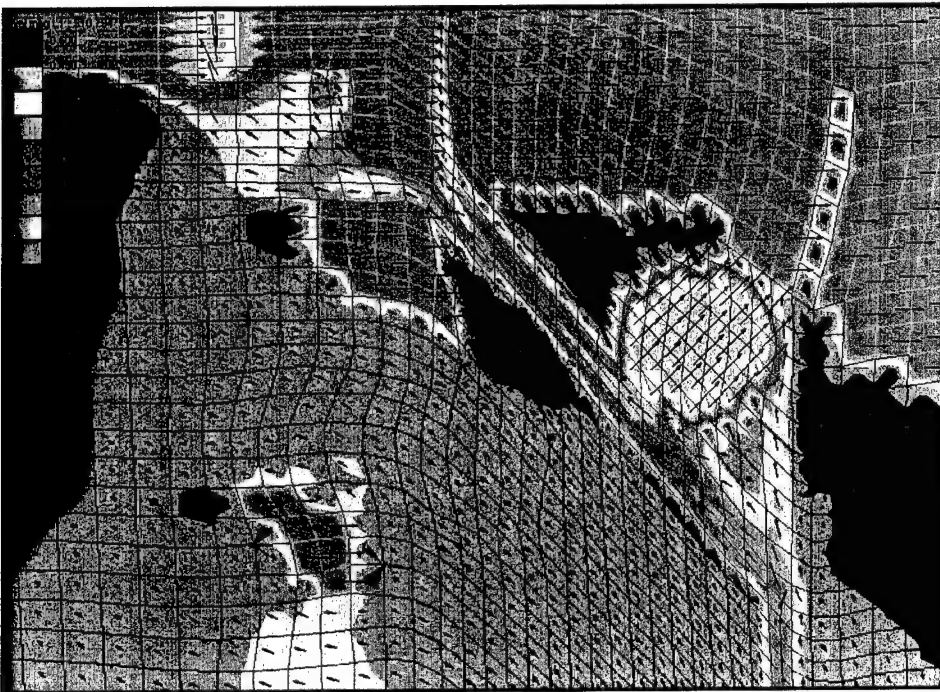


Figure 5-22. CH3D bottom currents for Alternative 03 (13 August 1990, 2200 GMT). Filled contours indicate current magnitude; vectors indicate current direction

Alternative 02. Alternative 02 (creation of island south of Singing River Island) also constricts the flow between Singing River Island and Round Island, and noticeably more than Alternative 01. The constriction tends to increase velocities between the islands during both ebb and flood flows. In addition, stronger flood flows are estimated in the near-bottom currents through the turning basin north of Singing River Island, but weaker currents are observed between the western tips of Singing River and Round Islands. Comparison of Figures 5-19 and 5-21 indicates the change in circulation patterns between Alternatives 00 (existing conditions) and 02. The changes in currents for this alternative are modest (approximately 0.05 m/sec) from the perspective of tidal circulation.

Alternative 03. Alternative 03 (creation of an island in the triangle) does not appear to have great influence on tidal circulation. Comparison of Figures 5-19 and 5-22 indicates that differences in circulation patterns between Singing River Island and Round Island and near the Pascagoula River mouth are hardly noticeable. A slight increase in bottom currents between the West Pascagoula River mouth and the turning basin north of Singing River Island is one of the few noticeable differences. However, for the flood tide presented in Figures 5-23 and 5-24, a zone of weaker currents develops in the lee of the proposed island. This calm zone does not persist for long and was seen to last for only a few hours during a portion of the flood cycle.

While differences in the tidal circulation were observed for each of the alternatives, the changes in velocities in the low-energy tidal environment were not remarkable from a tidal circulation perspective. However, decreases in the already weak currents may prove to be very significant from the perspective of water quality. Analysis and discussion of the impacts of the three island alternatives will be presented in Chapter 6.

Summary and Conclusions

The focus of modeling presented in this chapter is to develop a 3-D hydrodynamic model of Mississippi Sound to represent currents for three alternatives of dredged material disposal islands near the Pascagoula Navigation Channel. The hydrodynamics represented by this model will be included in the integrated compartment method (ICM) water quality model discussed in Chapter 6.

CH3D was calibrated to a reconstructed tide produced from astronomical tidal constituents developed from a limited dataset of water surface and current (Outlaw 1983). The model reproduced currents with a comparable degree of accuracy as Outlaw's constituents. CH3D hydrodynamics were further validated by comparison of prototype data collected in February/March 2001. The modeled water surface and currents compared well with measurements for larger-scale weather events, but limitations in the temporal and spatial scales of the wind fields and the model's representation of wind fields limited the representation of small-scale weather phenomenon. Validation of the modeling of temperature and salinity was performed to available data from April-September 1997. Comparisons of model simulations to measured data indicate that the model is accurately representing temperature and salinity within the study area.

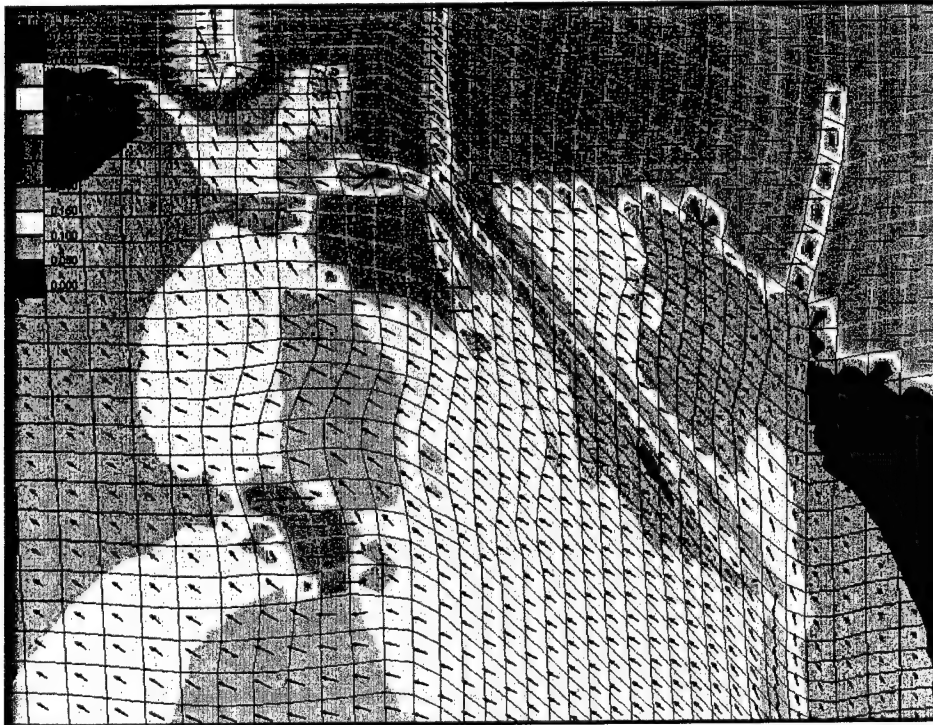


Figure 5-23. CH3D bottom currents for Alternative 00 (14 August 1990, 1600 GMT). Filled contours indicate current magnitude; vectors indicate current direction

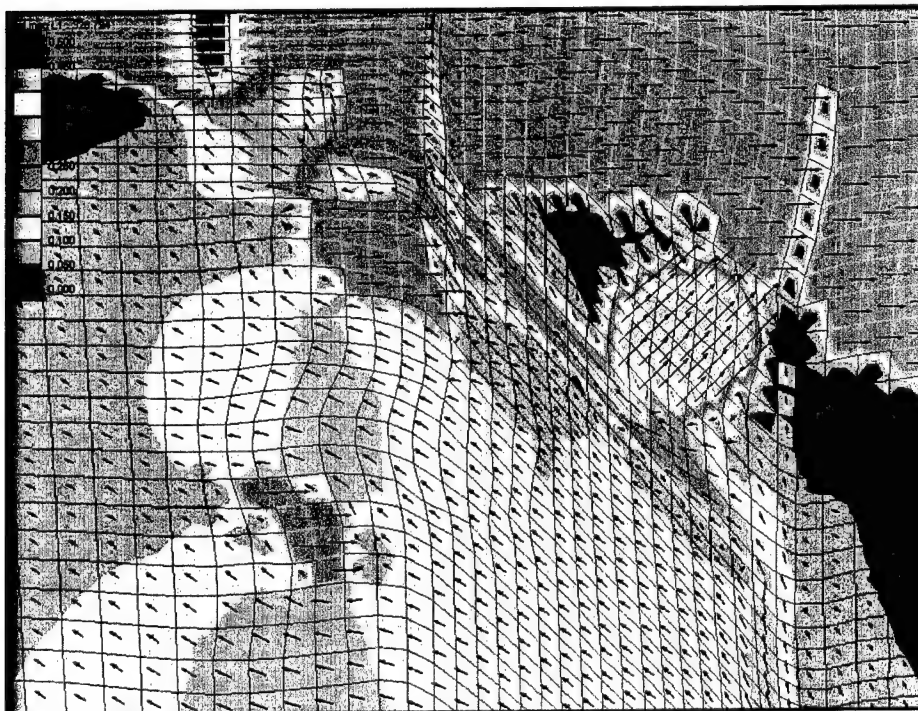


Figure 5-24. CH3D bottom currents for Alternative 03 (14 August 1990, 1600 GMT). Filled contours indicate current magnitude; vectors indicate current direction

August 1990 was selected from statistical analysis as one of the hottest months on record at Mobile, AL. Environmental conditions for the model were developed from measurements in the area and a 1-month simulation was performed for the base condition and the three island alternatives. Hydrodynamics from these four simulations were provided to the ICM model for evaluation of water quality effects from the island scenarios.

References

- Chapman, R. S., Johnson, B. H., and Vemulakonda, S. R. (1996). "User's guide for the sigma stretched version of CH3D-WES," Technical Report HL-96-21, U.S. Army Engineer Waterways Experiment Station, Vicksburg, MS.
- Edinger, J. E., Brady, D. K., and Geyer, J. C. (1974). "Heat exchange and transport in the environment," Report 14, EPRI Publication No. 74-049-00-3, prepared for Electric Power Research Institute, Palo Alto, CA.
- Garratt, J. R. (1977). "Review of drag coefficients over oceans and continents," *Monthly Weather Review* 105, 915-29.
- Harza Engineering Company (1995). "Pascagoula River low flow management study: Phase 4 report," prepared for State of Mississippi Department of Environmental Quality.
- Johnson, B. H., Kim, K. W., Heath, R. E., and Butler, H. L. (1991). "Verification of a three-dimensional numerical hydrodynamic model of Chesapeake Bay," Technical Report HL-91-7, U.S. Army Engineer Waterways Experiment Station, Vicksburg, MS.
- Outlaw, D. G. (1983). "Prototype tidal data analysis for Mississippi Sound and adjacent areas," Miscellaneous Paper CERC-83-1, U.S. Army Engineer Waterways Experiment Station, Vicksburg, MS.
- Sheng, Y. P. (1986). "A three-dimensional mathematical model of coastal, estuarine and lake currents using boundary fitted grid," Report No. 585, A.R.A.P Group of Titan Systems, Princeton, NJ.

6 Water Quality Model Studies

Model Description

CE-QUAL-ICM (ICM) was designed to be a flexible, widely applicable, state-of-the-art eutrophication model. Initial application was to Chesapeake Bay (Cерco and Cole 1994). Since the initial Chesapeake Bay study, the ICM model code has been generalized with minor corrections and model improvements. Subsequent additional applications of ICM included the Delaware Inland Bays (Cерco et al. 1994), Newark Bay (Cерco and Bunch 1997), the San Juan Estuary (Bunch et al. 2000), Florida Bay (Cерco et al. 2000), St. Johns River (Bunch, Tillman, and Mark in preparation) and Port of Los Angeles (in preparation). Each model application employed a different combination of model features and required addition of system-specific capabilities.

General features of the model include:

- a. Operational in 1-, 2-, or 3-D configurations.
- b. Twenty-two state variables including physical properties.
- c. Sediment-water oxygen and nutrient fluxes may be computed in a predictive submodel or specified with observed sediment-oxygen demand rates (SOD).
- d. State variable may be individually activated or deactivated.
- e. Internal averaging of model output over arbitrary intervals.
- f. Computation and reporting of concentrations, mass transport, kinetics transformations, and mass balances.
- g. Debugging aids include ability to activate and deactivate model features, diagnostic output, volumetric and mass balances.
- h. Operates on a variety of computer platforms. Coded in ANSI Standard FORTRAN F77.

ICM is limited by not computing the hydrodynamics of the modeled system. Hydrodynamic variables (i.e., flows, diffusion coefficients, and volumes) must be specified externally and read into the model. Hydrodynamics may be specified in binary or ASCII format and are usually obtained from a hydrodynamic model such as the CH3D_WES model (Johnson et al. 1991).

Conservation of mass equation

The foundation of CE-QUAL-ICM is the solution to the 3-D mass-conservation equation for a control volume. Control volumes correspond to cells on the model grid. CE-QUAL-ICM solves, for each volume and for each state variable, the equation:

$$\frac{\delta V_j C_j}{\delta t} = \sum_{k=1}^n Q_k C_k + \sum_{k=1}^n A_k D_k \frac{\delta C}{\delta x_l} + \sum S_j \quad (6-1)$$

which

V_j = volume of j^{th} control volume (m^3)

C_j = concentration in j^{th} control volume (g m^{-3})

t, x = temporal and spatial coordinates

n = number of flow faces attached to j^{th} control volume

Q_k = volumetric flow across flow face k of j^{th} control volume ($\text{m}^3 \text{s}^{-1}$)

C_k = concentration in flow across face k (g m^{-3})

A_k = area of flow face k (m^2)

D_k = diffusion coefficient at flow face k ($\text{m}^2 \text{s}^{-1}$)

S_j = external loads and kinetic sources and sinks in j^{th} control volume (g s^{-1})

Solution of “**Error! Reference source not found.**” On a digital computer discretization of the continuous derivatives and specification of parameter values are required. The equation is solved explicitly using upwind differencing or the QUICKEST algorithm (Leonard 1979) to represent C_k . The time-step, determined by stability requirements, is usually 5 to 15 min. For notational simplicity, the transport terms are dropped in the reporting of kinetics formulations.

State variables

CE-QUAL-ICM incorporates 22 state variables in the water column including physical variables, multiple algal groups, and multiple forms of carbon, nitrogen, phosphorus and silica (Table 6-1). Two zooplankton groups, microzooplankton and mesozooplankton, are available and can be activated when desired.

Table 6-1
Water Quality Model State Variables

Temperature	Salinity
Fixed Solids	Cyanobacteria
Diatoms	Other Phytoplankton
Dissolved Organic Carbon	Refractory Particulate Organic Carbon
Labile Particulate Organic Carbon	Nitrate + Nitrite Nitrogen
Ammonium	Dissolved Organic Nitrogen
Refractory Particulate Organic Nitrogen	Labile Particulate Organic Nitrogen
Total Phosphate	Dissolved Organic Phosphorus
Refractory Particulate Organic Phosphorus	Labile Particulate Organic Phosphorus
Chemical Oxygen Demand	Dissolved Oxygen
Dissolved Silica	Particulate Biogenic Silica

WQ Modeling Approach

The creation of offshore CDFs and the expansion of existing CDF islands in the Mississippi Sound off of Pascagoula, MS, has the potential to impact water quality. Circulation would be altered in the vicinity of the new/expanded CDFs, which could result in redistribution of oxygen demand and increases in residence time. Together, these processes could act to decrease dissolved oxygen (DO) concentrations from current levels.

Water quality modeling techniques can be used to determine the DO impact of CDF island creation/expansion. Various levels of modeling effort are available and were presented to the Mobile District to address these issues. The various levels of modeling are:

- a. *Eutrophication*. Involves the modeling of dissolved oxygen, algae, nutrients, and carbon. Realistic loads (observed or estimated) are required for all major discharges in the system. In addition, information on constituent concentrations is required for development of boundary conditions and for calibration. Sediment processes could either be specified or simulated with a sediment diagenesis model. This is the most involved approach in time and money and would provide the most defensible results provided there is an adequate database for model development.
- b. *DO/BOD/SOD*. This approach is similar to *eutrophication* except that all oxygen demand is specified as a Biochemical Oxygen Demand (BOD). SOD is specified as a constant rate and together with BOD are the only sinks for DO. Information is required on DO and BOD levels throughout the system for cursory model calibration. Information (observed or estimated) is required for all significant discharges. While less involved than Level 1, this approach still requires some calibration. The results from this study are less defensible as algae are left out and the impact of algal photosynthesis and respiration is omitted.

- c. *DO/OD/SOD No calibration.* This approach is similar to the second approach but with more simplified processes. Rather than BOD, a zero-order, background oxygen demand (OD) in units of mg/L/day is used. No loads are input. Boundary concentrations are held constant. OD and SOD are sinks for DO. No reaeration is allowed. The value for background OD is assumed. No model calibration is required. Dissolved oxygen is essentially modeled as a nonconservative tracer. Relative changes in DO can be determined by comparing results from a base condition simulation (present conditions) to a simulation made with a proposed island. The driving mechanism in this approach is that localized circulation changes result in differences in residence time which impact DO. The results from this approach are defensible in that the relative impact of island creation/expansion is clearly demonstrated. The results are easily criticized for the oversimplification of a complex system.
- d. *Residence time.* This approach does not provide a measure of DO but a measure of the impact that circulation changes have on the time that water stays in a certain area. Assuming that oxygen demands are the same throughout the system, an increase in residence time would indicate a decrease in flushing and a decrease in DO. This is a very simplified approach relying heavily on inferences.

For this study the Mobile District chose Level 2 because of limited observed data and study time constraints.

Hydrodynamic and water quality modeling were used to define the degree of impact that island creation/expansion in the Mississippi Sound will have on the waters in the areas of island expansion/creation. Models chosen for this study were the hydrodynamic model, CH3D, and the water quality model, CEQUAL-ICM. CH3D was used to investigate currents, water-surface elevations, and flows in the Mississippi Sound. Output from CH3D was then used to drive CEQUAL-ICM (see Chapter 5 for boundary conditions driving the hydrodynamic model during calibration). CEQUAL-ICM simulated the water quality constituents necessary for Level 2 approach previously discussed (e.g., DO, temperature, BOD/dissolved organic carbon, and salinity) plus the movement of a conservative tracer released in cells of the West Pascagoula and East Pascagoula Rivers. The calibration period was chosen based on availability of observed data and began 1 April 1997 and ended 30 September 1997.

In addition to the base/calibration grid (present conditions), there were a total of three DMMP alternatives modeled. The base run and each DMMP alternative were modeled with hydrodynamic and water quality input conditions, which are expected to have the most impact to DO (see Chapter 5 for boundary conditions used during alternative runs). Each alternative was simulated for 31 days. The DMMP alternatives modeled were: (a) an expansion of Singing River Island on its south and southwest sides (Alternative 1), (b) an island just to the northeast of Round Island and southeast of Singing River Island, between Round Island and the navigation channel (Alternative 2), and (c) north of the point where the navigation channel bifurcates, between the bifurcation point and the mainland (Alternative 3). Results from each alternative were compared to base run results.

CEQUAL-ICM grid

The computational grids used for the Pascagoula DMMP study are shown in Figures 6-1 through 6-4. The grids are identical to the hydrodynamic grid except that one row of cells is deleted along the southern and eastern boundary. These cells are removed from the water quality grid due to differences between how ICM handles flows at ocean boundaries. CH3D specifies a water-surface elevation or head condition at the ocean boundary while CEQUAL-ICM requires a flow for the face along the boundary. Removing cells along the ocean boundary have no impact upon water quality computations on the interior of the grid. Grid information is contained in Table 6-2 for calibration and alternatives modeled.

Alternative runs. Values used for water quality initial and boundary conditions for the four alternative runs were a subset of the calibration data (August 1997 data) provided by the MS DEQ and data found in the USGS Water Resource Data Report for 1997 (Plunkett et al. 1998). Initial conditions for the water column were specified as uniform for all layers based on the closest observed data to the 1 August start date and are listed in Table 6-3. Boundary water quality conditions were from the same period and were specified as uniform for each layer along the ocean boundary (see Table 6-4) but were varied by depth on the rivers (listed in Tables 6-5 and 6-6). Boundary flow discharges for worst-case conditions to be simulated in the production runs are discussed in Chapter 5. The same uniform SOD of $0.25 \text{ grams O}_2 \text{ m}^{-2} \text{ day}^{-1}$ used for calibration was specified over the entire study area except on the West and East Pascagoula Rivers which was set to $1.5 \text{ grams O}_2 \text{ m}^{-2} \text{ day}^{-1}$ based on values collected during the 1997 Escatawpa River Study.

Table 6-2
CEQUAL-ICM Grid Characteristics

Number of Grid Cells and Flow Faces	Base and Calibration	Alternative 1	Alternative 2	Alternative 3
Total Cells	56130	56010	55975	55950
Surface Cells	11226	11202	11195	11190
Total Flow Faces	154969	154608	154465	154390
Total Horizontal Flow Faces	110065	109800	109685	109630
Surface Horizontal Flow Faces	22013	21960	21937	21926

Table 6-3
Initial Conditions

Constituent	Calibration Value	Alternative Value
Temperature (°C)	18.4	28.4
Salinity (ppt)	34.0	34.0
BOD/Dissolved Organic Carbon (g/m^3)	4.0	4.0
Dissolved Oxygen (g/m^3)	9.1	7.5

Table 6-4
Ocean Boundary Conditions

Date	Constituent	Calibration Value	Alternative Value
4/17/97	Temperature (°C)	18.8	-
4/17/97	Salinity (ppt)	34.0	-
4/17/97	BOD/DOC (g/m ³)	4.0	-
4/17/97	Dissolved Oxygen (g/m ³)	9.1	-
7/22/97	Temperature (°C)	27.7	27.7
7/22/97	Salinity (ppt)	34.0	34.0
7/22/97	BOD/DOC (g/m ³)	4.0	4.0
7/22/97	Dissolved Oxygen (g/m ³)	8.7	8.7
8/27/97	Temperature (°C)	28.2	28.2
8/27/97	Salinity (ppt)	34.0	34.0
8/27/97	BOD/DOC (g/m ³)	4.0	4.0
8/27/97	Dissolved Oxygen (g/m ³)	6.9	6.9

Table 6-5
East Pascagoula Boundary Conditions

Date	Constituent	Layer 1		Layer 2		Layer 3		Layer 4		Layer 5	
		Cal	Alt	Cal	Alt	Cal	Alt	Cal	Alt	Cal	Alt
4/17/97	Temperature (°C)	17.6	-	17.6	-	18.6	-	18.9	-	18.9	-
4/17/97	Salinity (ppt)	0.1	-	0.1	-	0.1	-	0.1	-	0.1	-
4/17/97	BOD/DOC (g/m ³)	4.0	-	9.0	-	4.0	-	4.0	-	4.0	-
4/17/97	Dissolved Oxygen (g/m ³)	8.1	-	8.1	-	6.5	-	6.2	-	6.2	-
7/22/97	Temperature (°C)	17.6	26.4	17.6	26.4	18.6	26.4	18.9	26.0	18.9	26.0
7/22/97	Salinity (ppt)	0.1	0.1	0.1	0.1	0.1	0.1	0.1	0.9	0.1	0.9
7/22/97	BOD/DOC (g/m ³)	4.0	4.0	9.0	4.0	4.0	9.0	4.0	9.0	4.0	9.0
7/22/97	Dissolved Oxygen (g/m ³)	8.1	8.1	8.1	9.3	6.5	9.6	6.2	9.6	6.2	9.6
7/22/97	Dissolved Oxygen (g/m ³)	8.1	8.1	8.1	9.3	6.5	9.6	6.2	9.6	6.2	9.6
8/27/97	Temperature (°C)	17.6	26.4	17.6	26.4	18.6	26.4	18.9	26.0	18.9	26.0
8/27/97	Salinity (ppt)	0.1	0.1	0.1	0.1	0.1	0.1	0.1	0.9	0.1	0.9
8/27/97	BOD/DOC (g/m ³)	4.0	4.0	9.0	4.0	4.0	9.0	4.0	9.0	4.0	9.0
8/27/97	Dissolved Oxygen (g/m ³)	8.1	8.1	8.1	9.3	6.5	9.6	6.2	9.6	6.2	9.6

Table 6-6
West Pascagoula Boundary Conditions

Date	Constituent	Layer 1		Layer 2		Layer 3		Layer 4		Layer 5	
		Cal	Alt	Cal	Alt	Cal	Alt	Cal	Alt	Cal	Alt
4/17/97	Temperature (°C)	17.6	-	17.6	-	17.6	-	17.6	-	17.6	-
4/17/97	Salinity (ppt)	0.5	-	0.5	-	0.5	-	0.9	-	0.9	-
4/17/97	BOD/DOC (g/m ³)	4.0	-	4.0	-	4.0	-	4.0	-	4.0	-
4/17/97	Dissolved Oxygen (g/m ³)	7.7	-	7.7	-	7.7	-	7.9	-	7.9	-
7/22/97	Temperature (°C)	29.7	26.0	29.7	26.0	29.7	26.0	28.2	29.70	28.2	29.70
7/22/97	Salinity (ppt)	0.5	0.9	0.5	0.9	0.5	0.9	0.9	0.5	0.9	0.5
7/22/97	BOD/DOC (g/m ³)	4.0	9.0	4.0	9.0	4.0	9.0	5.0	4.0	5.0	4.0
7/22/97	Dissolved Oxygen (g/m ³)	9.4	9.6	9.4	9.6	9.4	9.6	6.3	9.4	6.3	9.4
8/27/97	Temperature (°C)	28.5	28.5	28.5	28.5	28.5	28.5	28.5	28.5	28.5	28.5
8/27/97	Salinity (ppt)	0.5	0.5	0.5	0.5	0.5	0.5	0.9	0.5	0.9	0.5
8/27/97	BOD/DOC (g/m ³)	3.6	3.6	3.6	3.6	3.6	3.6	3.6	3.6	3.6	3.6
8/27/97	Dissolved Oxygen (g/m ³)	9.1	9.6	9.1	9.6	9.1	9.6	3.1	9.1	3.1	9.1

Tracer runs. A tracer was simulated as a point source load and injected into a bottom cell at a rate of 100 kg/day on the East and West Pascagoula Rivers. The tracer initial and boundary conditions for these runs were set to zero. Boundary flow conditions were set the same as for the alternative runs (refer to Chapter 5).

Meteorological data

Calibration runs. Meteorological data measured at the Mobile airport and Keesler Air Force base for the calibration period were obtained from the Air Force Combat Climatological Center. Daily average values for cloud cover, dry bulb temperature, dew point temperature, and wind speeds are used in the heat exchange program (Eiker 1977) to compute heat exchange coefficients, solar illumination, fractional day length, and equilibrium temperature. Comparisons were made between meteorological data at both stations to see if major differences occurred. Differences were minimal; thus data from the Mobile airport were used in the calibration runs.

Alternative and tracer runs. Meteorological conditions were established for worst-case conditions to be simulated in the alternative and tracer runs. Statistical results (monthly average, maximums, and minimums) were examined to determine the warmest August dry bulb temperature in a 48-year period of meteorological data for the Mobile airport station. Meteorological data from August 1990 were chosen because it was one of the warmest August periods where meteorological and river flow data were available. Observed data from the Mobile airport were obtained from Earthinfo CD-ROM database.

Kinetic rates

Complete listings of kinetic rates used in this study are available upon request. Complete descriptions of the kinetic processes in CEQUAL-ICM can be found in Appendix A of Bunch, Tillman, and Mark (in preparation).

Calibration, Alternative Results and Discussion

Calibration

Calibration was accomplished through an iterative process that included:

- a. Running ICM and comparing model output to observed data.
- b. Modifying kinetic rates and parameters based upon comparison of results to observed data.
- c. Then running the model again until model performance was satisfactory.

ICM calibration performance was evaluated by comparing model output with observed data. Three forms of graphical comparison were used, time-series plots, scatter plots, and percent cumulative frequency plots. In addition, two statistics, mean error (ME) and root mean square error (RMS), were calculated to further evaluate model performance.

The RMS is an indicator of the deviation between predicted water quality values and observed values. A value of zero would indicate no variation between the observed and predicted. The ME indicates on average how the model is performing. For example, a positive ME indicates predictions are less than observed and a negative ME indicates predictions exceed observed. A value of zero for ME would also indicate complete agreement between predicted and observed. Each statistic was calculated for all data where observed data were available; data were not distinguished by layer, thus in essence getting the overall model performance. The equations for ME and RMS are:

$$ME = \frac{\sum(O - P)}{n} \quad (6-2)$$

where

ME = mean error

O = observation

P = model prediction

n = number of observations

and

$$RMS = \sqrt{\frac{\sum (O - P)^2}{n}} \quad (6-3)$$

where

RMS = root mean square error

The value for each statistic is presented on the scatter plot for a particular water quality constituent.

Time-series plots of daily-averaged model output and observed data demonstrate model performance over time and provide indications of interactions between modeled parameters. Time-series plots were generated for stations sampled by the MS DEQ shown in Figure 6-5. Scatter plots provide a synopsis of overall model performance, such as over/underpredicting or missing high/low values while percent cumulative distribution plots present how distribution of the predicted values compare with observed. Data for all layers where observed data were available were used in creating the scatter and cumulative distribution plots.

ICM model output consisted of daily-averaged concentrations for all constituents modeled, computed in all cells. From the model output, constituent concentrations were selected that corresponded to the day and location at which the observed data were collected. Points to consider when viewing the plots are: (a) model output represents daily-averaged concentrations, whereas the observed data are instantaneous measurements, and (b) parameters such as dissolved oxygen exhibit strong diurnal patterns which are not captured in daily-averaged outputs and give the appearance that the model is over- or underpredicting observed data.

Calibration results and discussion

Time-series calibration results are shown in Figures 6-6 through 6-10. Results are presented for all stations for which observed data were available (Figure 6-5). Circles represent observed surface data, triangles represent observed mid-layer data, and squares represent observed bottom data. A solid line for the surface layer, a dashed line for the mid-layer, and a dotted line for the bottom layer denote model output.

Temperature. The model reproduced the observed temperature time series profiles quite accurately with an RMS of approximately 1°C and a ME of 0.17°C (Figure 6-11). The scatter plot (Figure 6-11) and cumulative distribution plot (Figure 6-12) also denoted model accuracy with predicted values slightly on the low side of the observed on the average (ME of 0.17 °C). Most of the discrepancies between predicted and observed temperatures that occurred were probably due to comparing a daily averaged value to observed data collected at a specific time. Temperatures are influenced by the time of day the data were taken and can change several degrees over the course of a day.

Salinity. ICM captured the trends in salinity over the simulation period (higher salinity values in the spring to lower summer values and back to higher

values in September). At the low and high ends of the salinity cumulative distribution plot and the scatter plots (Figures 6-11 and 6-12), ICM accurately predicted salinity. However, in the midrange for salinity, ICM underpredicted salinity values as indicated by the ME of 5.11 and RMS of 7.5. The RMS and ME were highly influenced by the wide disparity of salinity values during the simulation days around 161 through 164. Salinity values collected during this period were collected diurnally with values ranging from approximately 12 ppt through 28 ppt. On other simulation days where observed data were available, salinity comparisons were good. Averaging the diurnally collected observed data over the day to get an equivalent value to compare to model output only improved the comparison slightly. More frequent salinity boundary conditions would probably improve model results for salinity.

ICM does not model salinity; it only transports it based on the hydrodynamic information. Initial and boundary conditions are important in accurately predicting salinity. However, it is extremely important that the hydrodynamics accurately predict transport. Comparisons of ICM salinity results to CH3D results (Figure 6-13) show similar trends. Some differences are noted during the first 2 weeks of the calibration simulation because of how initial conditions were set in ICM as compared to CH3D calibration. This only affected results at the beginning of the calibration. Differences between ICM and CH3D results also occur from comparison of daily averaged values (ICM) to more frequent output intervals (CH3D).

Dissolved oxygen. In general, ICM captured the trend of the slow decline in DO concentrations from the spring to end of the summer with the bottom layer showing a steeper decline (Figures 6-6 through 6-10). At some stations, the decline leveled off toward the end of the summer (e.g., sta WPR1 and PR0). Model performance showed a tendency to be more accurate in the mid DO concentration range while in the higher and lower concentration ranges, there was a tendency to under or overpredict, respectively (Figures 6-11 and 6-12). The RMS appeared to be influenced by several points in the upper and lower DO concentration range. All in all a RMS of 1.63 g/m^3 and an ME of -0.15 g/m^3 were very acceptable given the limited observed data available for boundary conditions to drive the model and for comparison purposes. Additionally, the inability of ICM to accurately predict the DO concentrations above saturation was because algal dynamics were not modeled. As discussed previously, algal dynamics can increase or decrease DO through photosynthesis or respiration. Diurnal effects were also missing in the predicted data but not in the observed. Observed data collected diurnally around simulation days 161 through 164 were averaged to get an equivalent value for comparison to model output during this time period.

BOD/DOC. Observed BOD measurements were limited, however for most stations there were observed total organic carbon (TOC) measurements. TOC is the combination of dissolved organic carbon (DOC) and particulate organic carbon (POC). Since ICM does not actually model BOD but is estimated from the state variables, DOC and POC, most of the TOC was assumed to be DOC and modeled as such. When observed BOD measurements were not available but TOC measurements were, comparisons were made between 90 percent of the observed TOC and DOC model output. Overall this assumption was not a bad assumption. The time series showed that ICM was predicting the increase in

BOD/DOC during the summer months of the simulation occurring at most stations. The scatter plot showed good agreement except for two outlying points which greatly influenced the RMS value. The ME indicated that on average the model was overpredicting BOD/DOC concentrations by 0.32 g/m^3 .

Alternative results and discussion

Numerous means were used to present and analyze alternative results. Time series plots and color shading plots were the main visual means to analyze water quality and tracer results. Since DO was the constituent of concern, time series plots of surface and bottom DO were generated for six locations (Figure 6-14) within the study area. Locations of stations were selected to determine impacts of the island CDF expansion/creations upon the water quality of the Mississippi Sound. Color shading plots of DO in bottom waters were used to assess the extent of changes in water quality. Since surface DO did not vary much, only the bottom DO color shading plots were examined. Color shading plots were also used to assess the extent of tracer movement and the degree that tracer distribution changed as a result of bathymetry modifications. The shading plots are only a snapshot in time, so if there are minimal concentration changes on a particular day between alternatives they will appear the same on the plot. In viewing the color shading plots, be aware that the color shading technique used in preparing these plots is a step function in which there is no blending or smoothing of colors going from one concentration level to the next in the legend. For example, a small change in DO concentration (3.95 g/m^3 to 4.05 g/m^3) can be misleading since it may result in the next color level on the legend.

Shading plots for bottom DO and tracer are presented in this chapter for simulation day 30. However, they were generated at daily intervals starting at day 1 and are available upon request.

Comparisons of results for time series plots and color shading plots are presented for pairs of the different alternatives (e.g., base and Alternative 1, base and Alternative 2, base and Alternative 3). By making comparisons in this manner, changes to water quality resulting from the creation/expansion of the islands (e.g., creation of the island between Singing River Island and Round Island, Alternative 2) in the Mississippi Sound could be assessed. Note in figures alternatives are referred to options.

Base vs. Alternative 1. For these runs, the base grid is the same as the calibration grid while the Alternative 1 grid includes the expansion of Singing River Island (Figure 6-2). Figure 6-15 presents the time series of surface and bottom DO along with the difference between the two runs calculated as Alternative 1 results minus base results for six stations (Figure 6-14). Base results are identified as Alternative 0 on the time series plots. Any negative difference would indicate reduced DO concentrations for Alternative 1. There are minor or insignificant differences seen at most stations. Station 2 shows the greatest differences (an average difference of approximately -0.5 g/m^3) for the bottom layer. Sta 2 is located at the same location as the calibration station, MSO, which is behind and slightly west of Singing River Island (Figure 6-14). This station is also closest to the expanded island. Total averaged flow passing through a transect (identified on Figure 6-14) behind Singing River Island was calculated for both runs to see if changes in circulation had occurred. Water

flows through the transect flows in an east to west direction as indicated by the negative sign in Table 6-7. Decreased flow is indicated for Alternative 1 for all layers and total averaged flow through the transect as compared to base flow results (Table 6-7) This is especially true in the bottom layers, indicating changes in circulation in this area possibly resulting in reduced bottom DO concentrations at sta 2.

Table 6-7 Net Flows (m³/sec) Through Channel North of Singing River Island				
Layer	Base	Alternative 1	Alternative 2	Alternative 3
1	-11.43	-7.84	-8.59	-8.00
2	-14.00	-12.29	-12.89	-13.25
3	-20.86	-17.90	-20.83	-21.99
4	-29.42	-23.08	-29.76	-31.64
5	-35.37	-24.48	-35.37	-37.13

Shading plots comparing bottom DO for the base alternative and Alternative 1 (indicated as scenario 1 on plot) for day 30 of the 30-day simulation (Figure 6-16) show similar results. Differences are usually less than 0.5 g/m³; otherwise a greater change than 0.5 would cause the shading color to go to the next color level, which has not occurred. This is also verified by the time series plots since at day 30, bottom DO concentrations do not show much difference. As mentioned previously, shading plots are only a snapshot of the concentrations occurring on a specific day so if shading plots for around day 10 of each simulation were compared, one would probably see more color shading changes in the area of sta 2 where the maximum difference in concentration is noted on the time series plot. This is a one-time occurrence probably due to wind or flow effects.

Changes in transport were examined by releasing a continuous tracer in the bottom layer on the West and East Pascagoula Rivers at a rate 100 g/d for each alternative. Shading plots comparing bottom concentration of a continuous tracer release on the West and East Pascagoula Rivers are shown in Figures 6-17 and 6-18, respectively, for the base alternative and Alternative 1 for day 30 of the 30-day simulation. Tracer concentrations for releases coming from the East Pascagoula River are similar indicating that transport has not changed much. However, for the West Pascagoula River tracer release, Figure 6-16 shows tracer concentration decrease west of Singing River Island and increase south of Round Island and east of the East Pascagoula River mouth for Alternative 1 as compared to base results. Lower and higher concentrations in these areas indicate changes in circulation from increasing Singing River Island.

Base vs. Alternative 2. For these runs, again the base grid is the same as the calibration grid while the Alternative 2 grid includes creation of an island between Singing River Island and Round Island. Figure 6-19 presents the time series of surface and bottom DO along with the difference between the two runs

calculated as Alternative 2 results minus base results for six stations (Figure 6-14). Any negative difference would indicate reduced DO concentrations for Alternative 2. Minor differences (approximately $\pm 0.5 \text{ g/m}^3$) in bottom DO are seen at most stations. Sta 3 shows the greatest differences (greatest maximum difference of approximately -1.0 g/m^3) for the bottom layer. This was expected since this station is closest to the island created between Singing River Island and Round Island (Figure 6-14). This island has changed circulation by either increased residence time or transport of lower DO water from nearby areas. In looking at velocity vector plots, the island has decreased velocities to the southeast during ebb tide thereby increasing residence time. This results in lower DO being advected from this area to sta 3. During flood tides, the velocities between the base and Alternative 2 are similar. Increased bottom DO concentrations at sta 1 appear to be advected from the area southeast of sta 1 or from the area of sta 3. If water were being advected from the area of sta 2, bottom DO concentrations at sta 1 would be similar to what is occurring at sta 2 (probably around 4 g/m^3 instead of 2 g/m^3).

Shading plots comparing bottom DO for the base alternative and Alternative 2 (indicated as scenario 2 on plot) for day 30 of the 30-day simulation (Figure 6-20) show very similar results. Like comparison of Alternative 1 to base results, differences on day 30 of both simulations are minimal showing very little color variations in the two plots.

Changes in transport were examined using the same conditions as discussed previously for the base and Alternative 1 run. Shading plots comparing the bottom tracer of a continuous tracer release on the West and East Pascagoula Rivers are shown in Figures 6-21 and 6-22, respectively, for the base alternative and Alternative 2 for day 30 of the 30-day simulation. Tracer concentrations for releases coming from the East Pascagoula River show minor differences between concentration levels of 0.001 and 0.01 g/m^3 east of Singing River and Round Islands indicating that transport changed slightly. The West Pascagoula River tracer release plots (Figure 6-21) show tracer concentrations decreased around Singing River Island and increased south of Round Island and east of the East Pascagoula River mouth for Alternative 2. Lower and higher tracer concentrations in these areas indicate changes in circulation from the creation of the island between Singing River Island and Round Island.

Base vs. Alternative 3. For these runs, again the base grid is the same as the calibration grid while the Alternative 3 grid includes creation of an island in the triangle, off Mobile Beach. Figure 6-23 presents the time series of surface and bottom DO concentrations along with the difference between the two runs calculated as Alternative 3 results minus base results for six stations (Figure 6-14). Any negative difference would indicate reduced DO concentrations for Alternative 3. Comparison of Alternative 3 results to the base results produced similar results to that of the comparison on Alternative 1 results to the base results. Minor or insignificant differences are observed at all stations. Sta 5 shows the greatest differences (an average difference of -0.3 g/m^3) for bottom DO concentrations. This is to be expected since sta 5 is located in the channel formed from the creation of the island off Mobile Beach (Figure 6-4). Total average flow (Table 6-7) calculated for the transect entering the channel behind the Singing River Island had slightly increased for Alternative 3 compared to base flows for the bottom three layers modeled and decreased for

the top two layers; this indicates some change in circulation. Bottom DO concentrations at sta 2, however, do not change very much compared to base results (less than 0.2 g/m^3). Circulation changes are also noted at sta 1 since bottom DO concentrations were increased possibly by higher DO concentrations being advected to this area from southwest around Round Island (Figure 6-23). It does not appear to be advected from the area close to sta 2 based on the DO concentrations at both stations. Bottom DO concentrations at sta 2 were slightly reduced instead of being increased. Advection of water from this area would have produced a decrease not an increase in bottom DO concentrations at sta 1.

Shading plots comparing bottom DO for the base alternative and Alternative 3 (indicated as Scenario 3 on plot) for day 30 of the 30-day simulation (Figure 6-24) show similar results between the alternative runs. Differences are usually less than 0.5 g/m^3 , thus will not show up on the shading plots. In examining time series plots of surface and bottom DO, differences are less than 0.5 g/m^3 during the entire simulation period so snapshot color shading plots plotted for any day will be similar for both runs.

As was the case for alternatives previously discussed, changes in transport were examined by releasing a continuous tracer in the bottom layer on the West and East Pascagoula River at a rate 100 g/d for each alternative. Shading plots comparing bottom tracer of a continuous tracer release on the West and East Pascagoula Rivers are shown in Figures 6-25 and 6-26, respectively, for the base alternative and Alternative 3 for day 30 of the 30-day simulation. Tracer concentrations for releases coming from the East Pascagoula River are similar indicating that transport has not changed much. Same as Alternative 1 and 2, the West Pascagoula River tracer release for Alternative 3, Figure 6-25, shows tracer concentrations decrease west of Singing River Island and increase south and east of Round Island and east of Singing River Island in comparison to base results. Lower and higher tracer concentrations in these areas again indicate changes in circulation from the creation of the island off of Mobile Beach.

Water Quality Summary and Conclusions

ERDC conducted a water quality model study of the Mississippi Sound to determine potential impacts from expansion or creation of offshore CDFs. Two numerical models, one hydrodynamic (CH3D) and one water quality model (CEQUAL-ICM), were applied to the study area to simulate hydrodynamics and water quality in the Mississippi Sound.

In addition to the base/calibration grid (present conditions), there were a total of three DMMP alternatives modeled. The base run and each DMMP alternative were modeled with worst-case conditions of hydrodynamic and water quality input. Each alternative was simulated for 31 days. The DMMP alternatives modeled were:

- a. *Alternative 1.* Expand Singing River 100 percent of total dredging requirement.
- b. *Alternative 2.* Create Island/CDF 100 percent close to South Singing River.
- c. *Alternative 3.* Create Island/CDF 100 percent in triangle.

The water quality model, CEQUAL-ICM was calibrated for the period of 1 April 1997 through 30 September 1997 using observed data provided by the MS DEQ and USGS Water Resource Data and appropriate kinetic rates determined in calibration. The modeling approach for this study was referred to as Level 2, Level 1 being a full eutrophication calibration. This approach is similar to full calibration except that all oxygen demand is specified as a Biochemical Oxygen Demand (BOD). Sediment Oxygen Demand (SOD) is specified as a constant rate and together with BOD are the only sinks for DO. Final calibration results compared favorably to observed data given the limited amount of comparison and boundary data available to evaluate and drive the model, respectively.

Changes in bottom DO were an indicator of changes to water quality. Results for each alternative as compared to base results are presented as follows:

- a. Comparison of Alternative 1 results to base results showed minimal difference in water quality at all stations. Sta 2 showed the greatest differences in bottom DO concentrations, but that was to be expected since it was the closest station to the expanded Singing River Island. Total averaged flows for Alternative 1 calculated for a transect entering the channel behind the island had decreased for all layers modeled in comparison to base total averaged flows; thus indicating that circulation had changed (especially in the lower layers) causing decreased DO concentrations.
- b. Comparison of Alternative 2 results to base results showed decreases in bottom DO concentrations ranging approximately 0.2 g/m^3 to 1.0 g/m^3 at most stations except at sta 1 where a maximum increase of approximately 0.4 g/m^3 was noted. Sta 3 showed the greatest differences, but again that was expected since it was the closest station to the island created between Singing River Island and Round Island. There does not appear to be much vertical advection in the system; consequently, concentrations are being affected through horizontal advection, diffusion, or increased residence time in an area. Once residence time is increased/decreased bottom DO concentrations are affected, and higher/lower DO concentrated water is moved to different areas through horizontal advection. This was seen at sta 1 and 3 for Alternative 2.
- c. Comparison of Alternative 3 results to base results showed minimal differences at all stations. Similar to the other two alternatives, the station closest to the island created off Mobile Beach (sta 5) showed the greatest differences with the maximum difference being around 0.6 g/m^3 . Total average flow calculated for the transect entering the channel behind the Singing River Island had increased for the bottom three layers modeled; this indicated a change in circulation. In addition, higher concentrations of bottom DO in the area of sta 1 also indicate circulation changes with water being advected from southwest of Round Island and not from behind Singing River Island.

Overall, comparison of results from all alternatives to base results showed slight changes in circulation resulting in minor effects to surface and bottom DO concentrations in the area of the expanded/created islands. Creation of the island

for Alternative 2 seemed to create the greatest effects to bottom DO concentrations at sta 3 (maximum decrease of approximately 1.0 g/m³); surface DO was only minimally affected.

References

- Bunch, B. W., Tillman D. H., and Mark, D. J. (in preparation). "Port of Los Angeles (POLA) main channel deepening water quality and hydrodynamic modeling study," Technical Report EL-00-XXX, U.S. Army Engineer Research and Development Center, Vicksburg, MS.
- Bunch, B., Cerco, C., Dortch, M., Johnson, B., and Kim, K. (2000). "Hydrodynamic and water quality model study of San Juan Bay and Estuary," Technical Report ERDC TR-00-1, U.S. Army Engineer Research and Development Center, Vicksburg MS.
- Cerco, C. F., Bunch, B. W., Teeter, A. M., and Dortch, M. S. (2000). "Water quality model of Florida Bay," ERDC/EL TR-00-10, U.S. Army Engineer Research and Development Center, Vicksburg, MS.
- Cerco, C. and Bunch, B. (1997). "Passaic River tunnel diversion model study, Report 5, water quality modeling," Technical Report HL-96-2, U.S. Army Engineer Waterways Experiment Station, Vicksburg, MS.
- Cerco, C., Bunch, B., Cialone, M., and Wang, H. (1994). "Hydrodynamic and eutrophication model," Technical Report EL-94-4, U.S. Army Engineer Waterways Experiment Station, Vicksburg, MS.
- Cerco, C., and Cole, T. (1994). "Three-dimensional eutrophication model of Chesapeake Bay," Technical Report EL-94-4, U.S. Army Engineer Waterways Experiment Station, Vicksburg, MS.
- Eiker, E. E. (1977). "Heat exchange programs, thermal simulation of lakes, user's manual," U. S. Army Engineer District, Baltimore, Baltimore, MD.
- Johnson, B. H., Heath, R. E., Hsieh, B. B., Kim, K. W., and Butler, H. L. (1991). "Development and verification of a three-dimensional numerical hydrodynamic, salinity, and temperature model of Chesapeake Bay," Technical Report HL-91-7, U.S. Army Engineer Waterways Experiment Station, Vicksburg, MS.
- Leonard, B. (1979). "A stable and accurate convection modeling procedure based on quadratic upstream interpolation," *Computer Methods in Applied Mechanics and Engineering* 19, 59-98.
- Plunkett, M. L., Morris III, F., Oakley, W. T., Turnipseed, D. P. (1998). "Water resources data, Mississippi, water year 1997," U.S. Geological Survey, Pearl, MS.

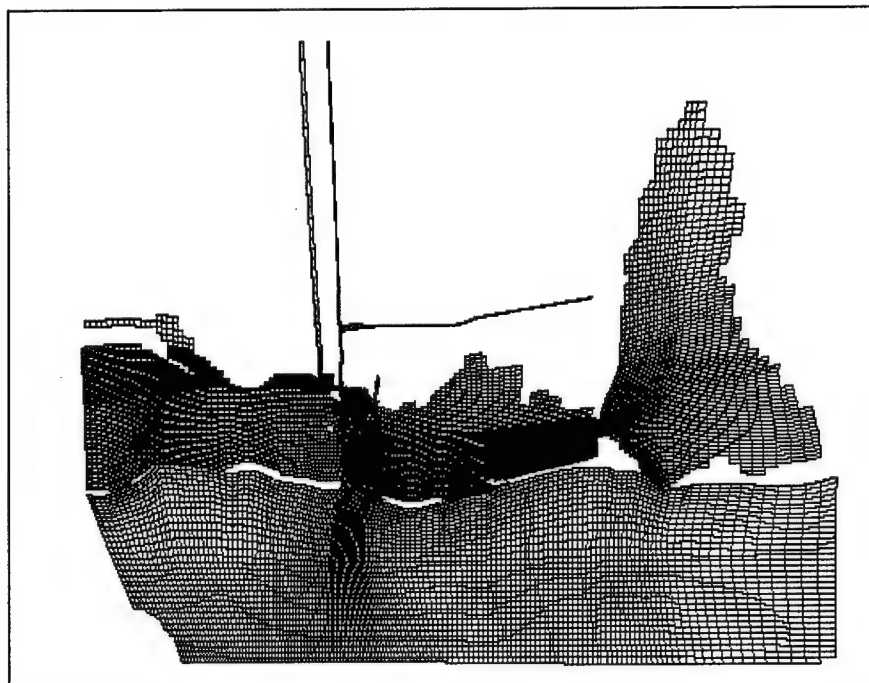


Figure 6-1. Base alternative grid

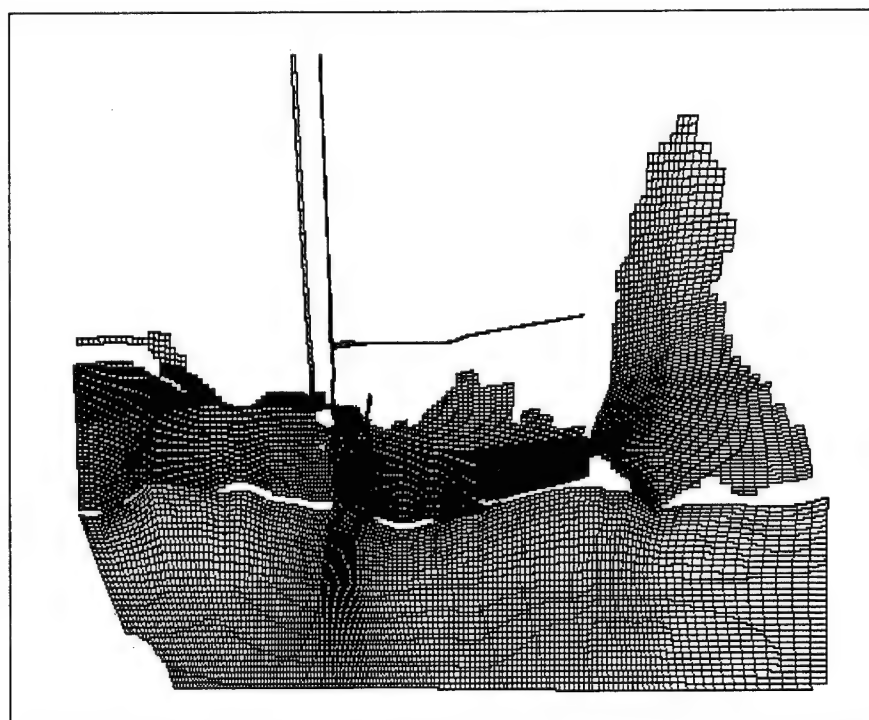


Figure 6-2. Option 1 grid

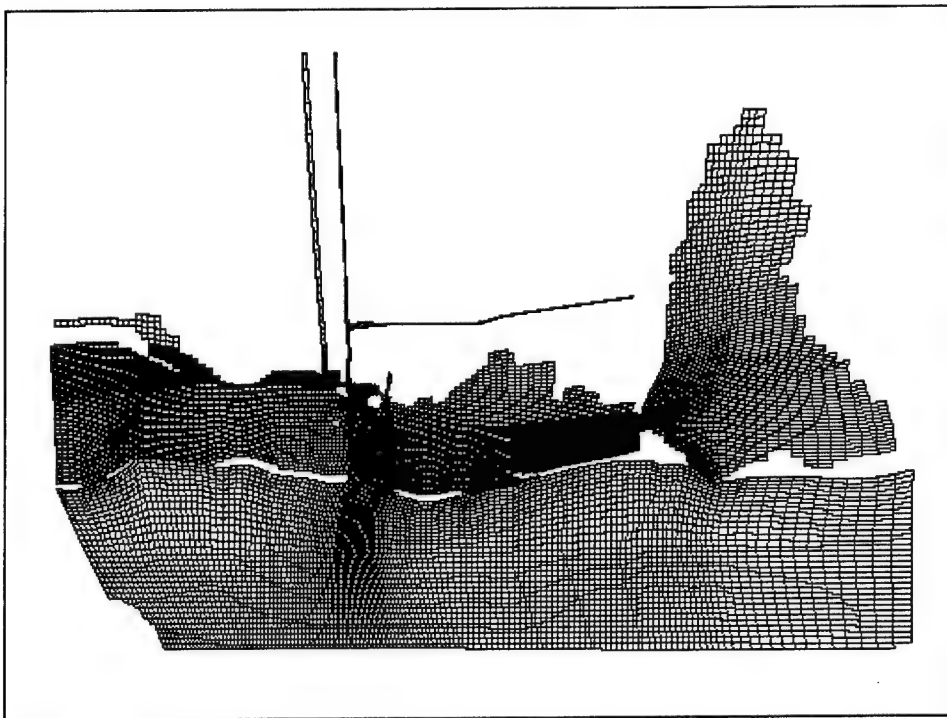


Figure 6-3. Alternative 2 grid

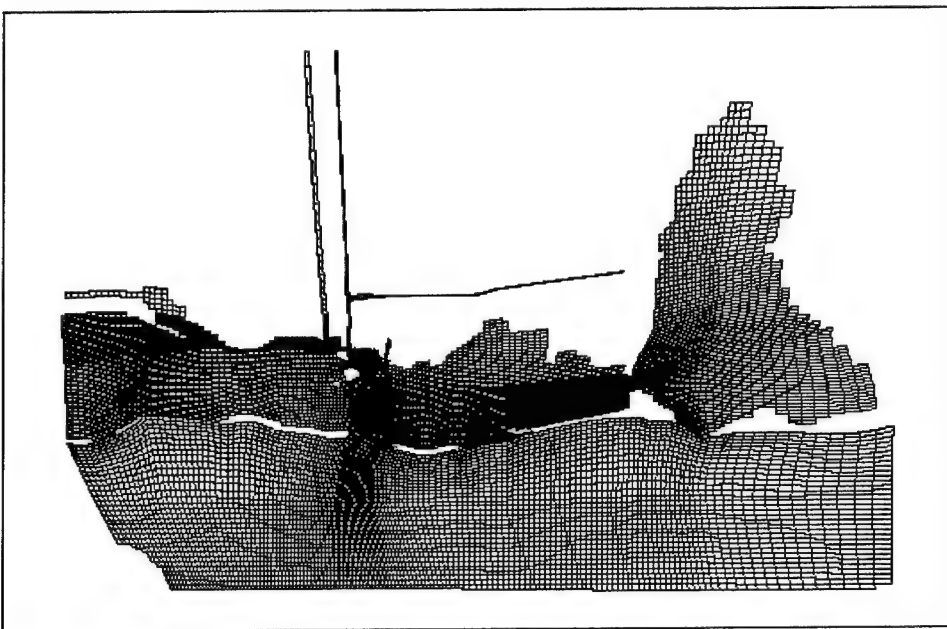


Figure 6-4. Alternative 3 grid

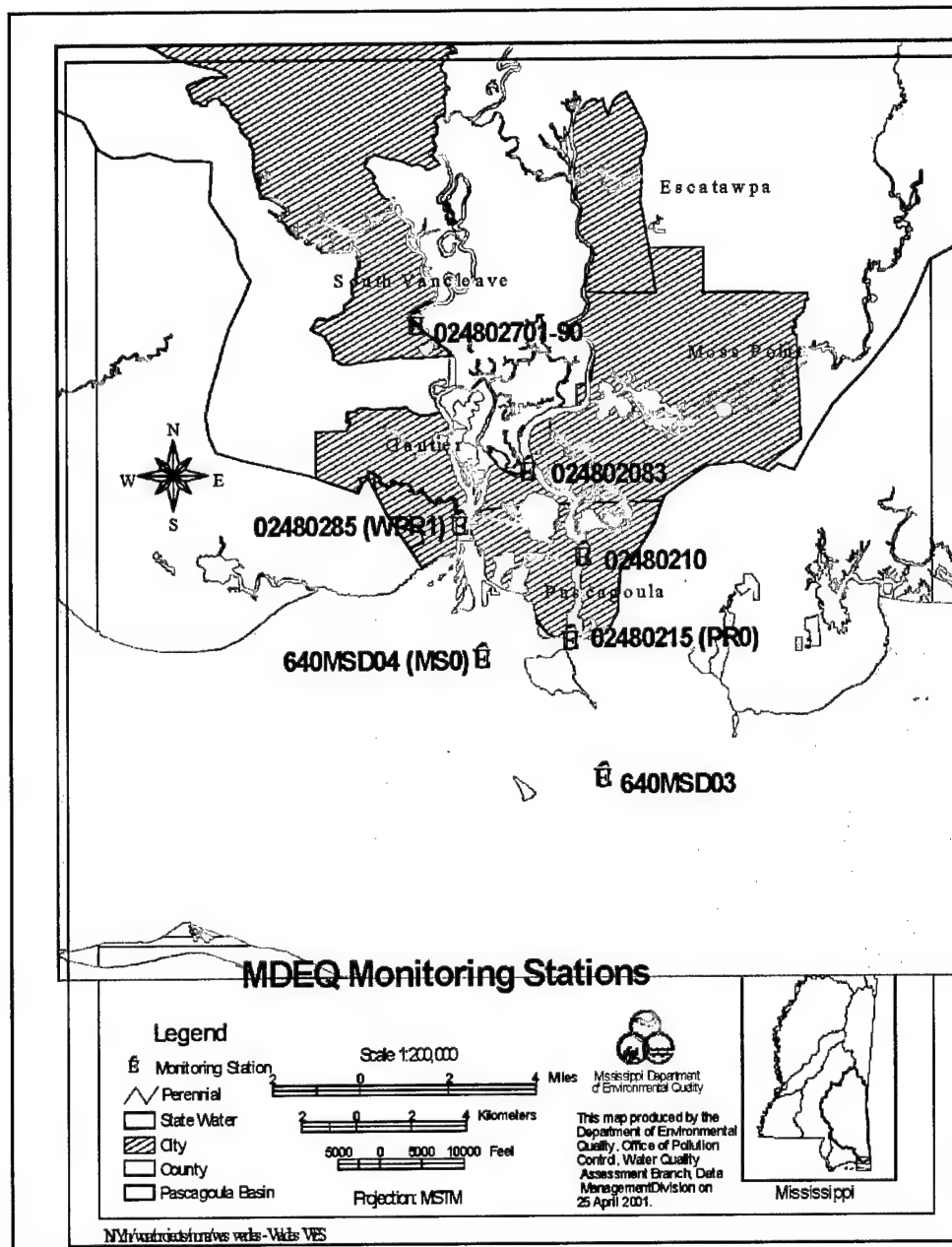


Figure 6-5. MS DEQ observed station locations

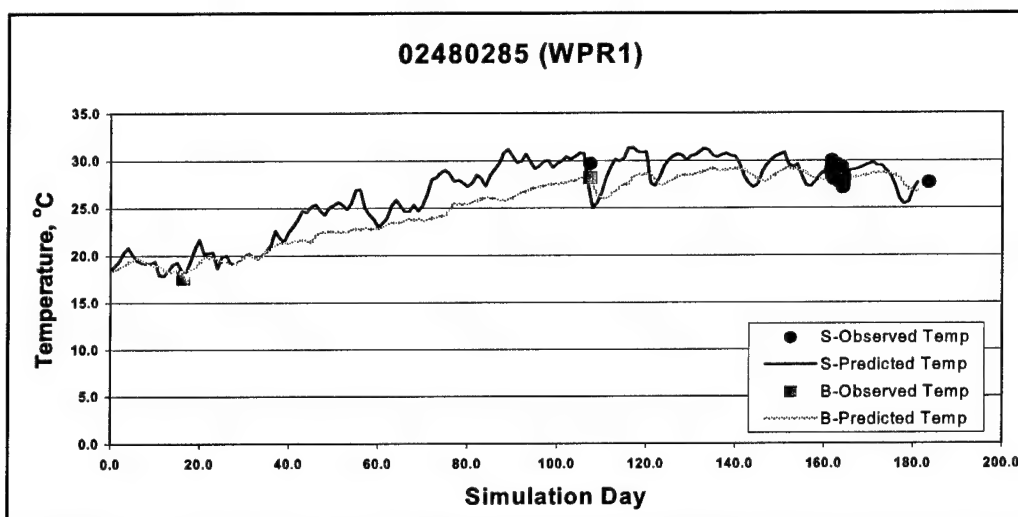


Figure 6-6. Calibration results for water quality constituents at sta 02480285 on West Pascagoula River (Sheet 1 of 4)

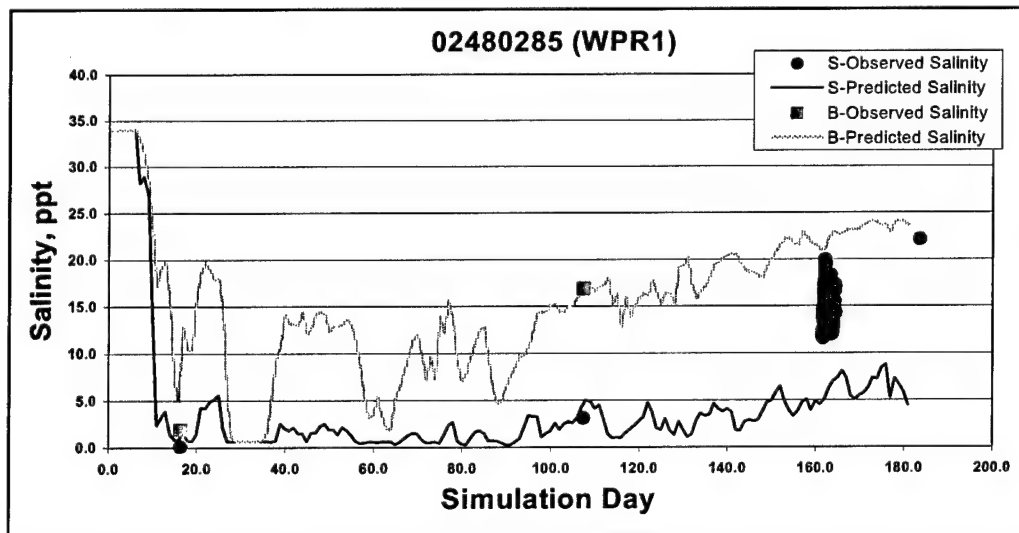


Figure 6-6. (Sheet 2 of 4)

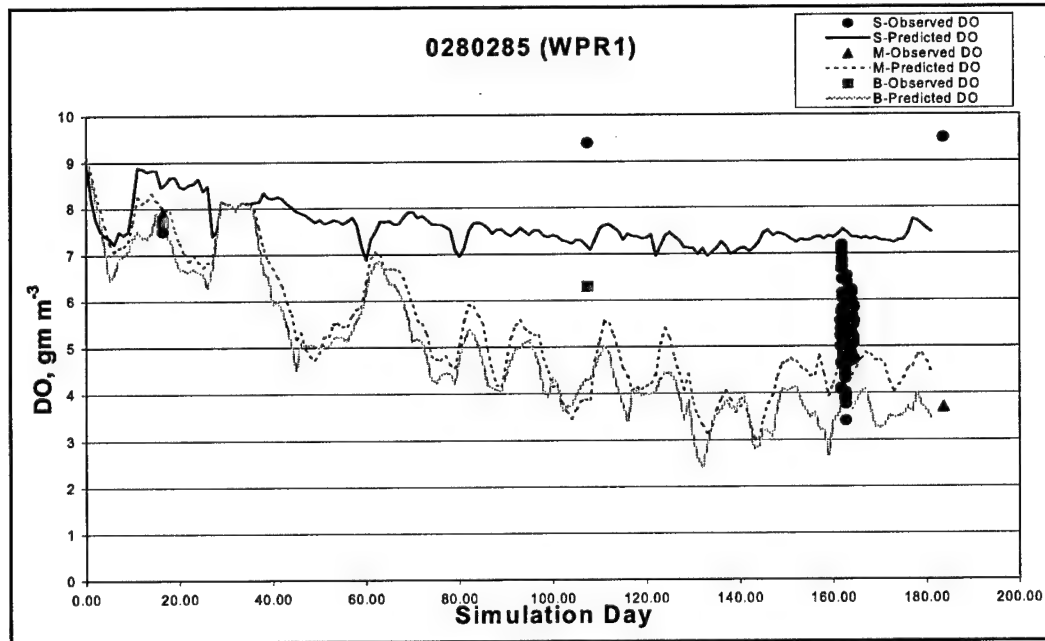


Figure 6-6. (Sheet 3 of 4)

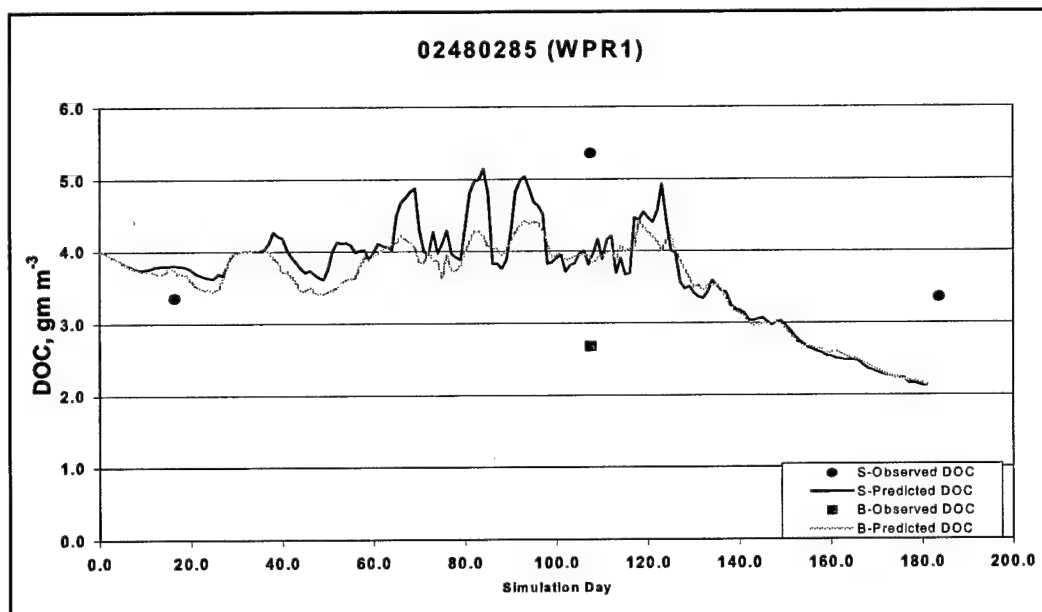


Figure 6-6. (Sheet 4 of 4)

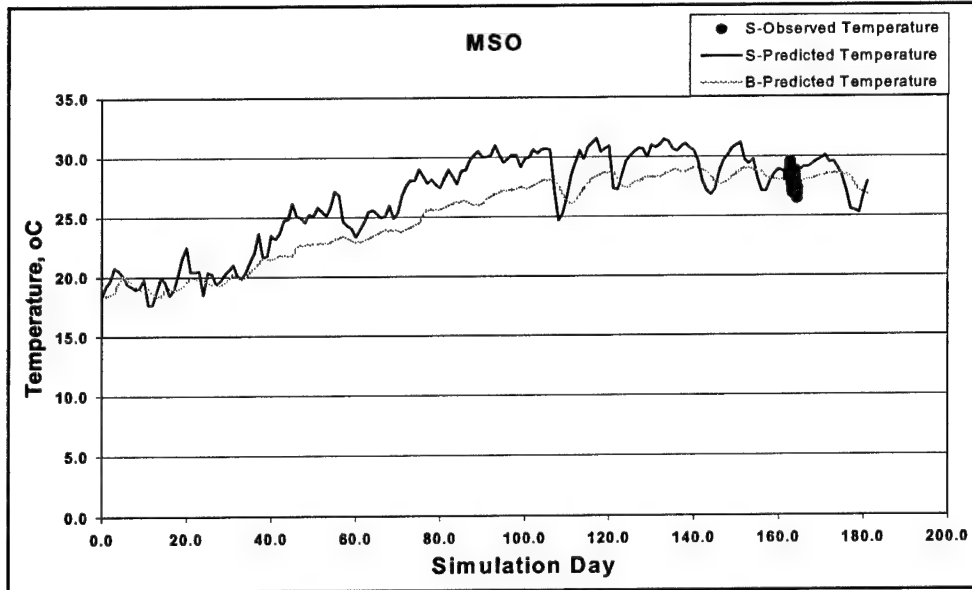


Figure 6-7. Calibration results for water quality constituents at sta MS0 in Mississippi Sound (Sheet 1 of 3)

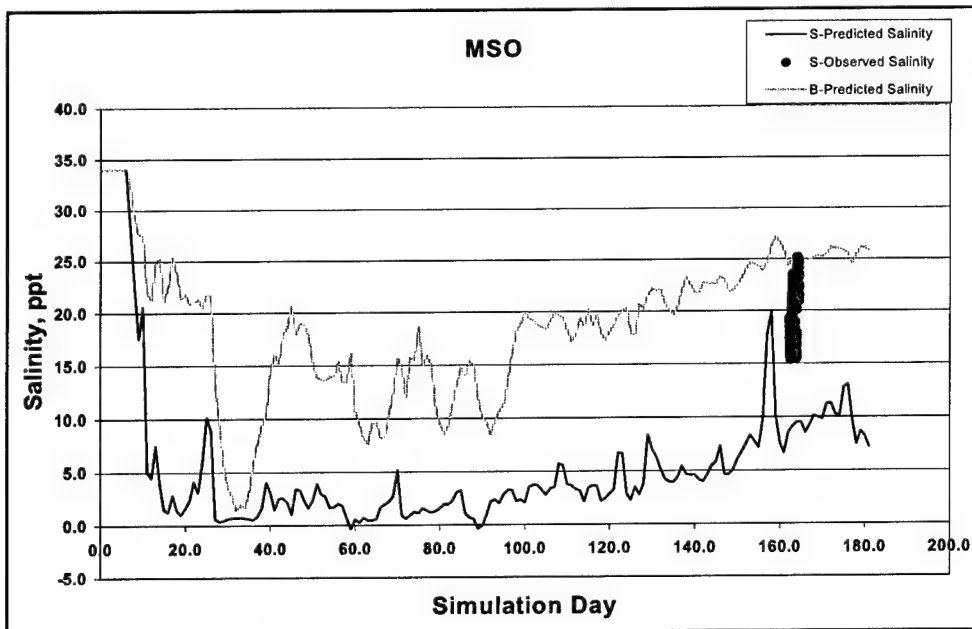


Figure 6-7. (Sheet 2 of 3)

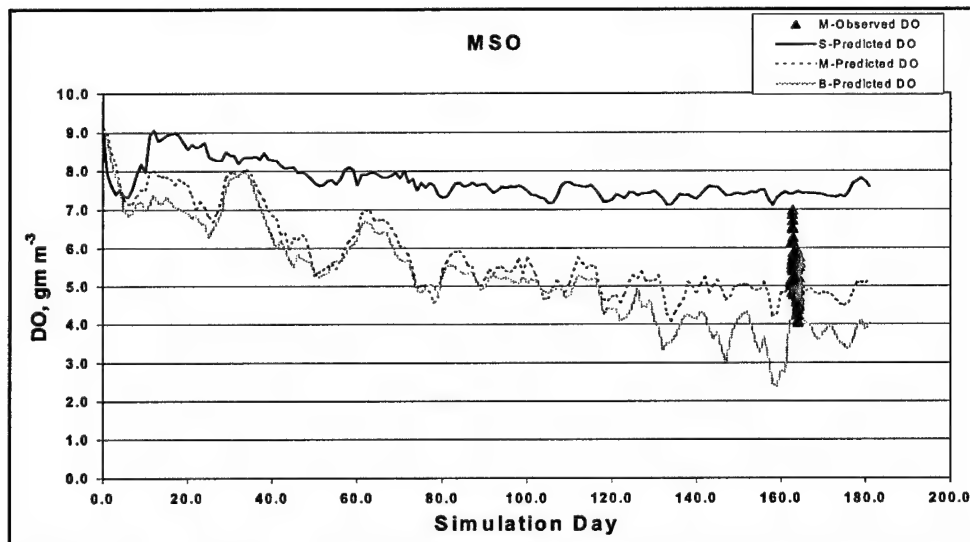


Figure 6-7. (Sheet 3 of 3)

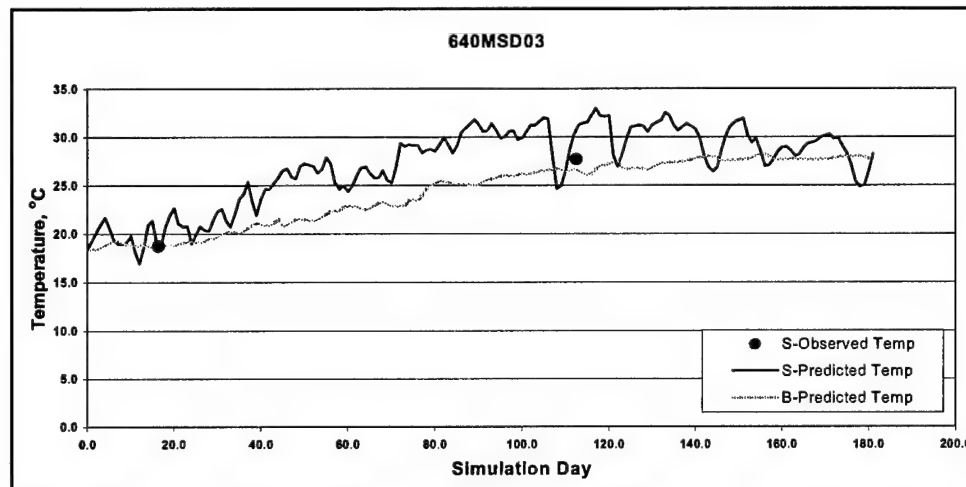


Figure 6-8. Calibration results for water quality constituents at sta 640MSD03 in Mississippi Sound near Round Island (Sheet 1 of 4)

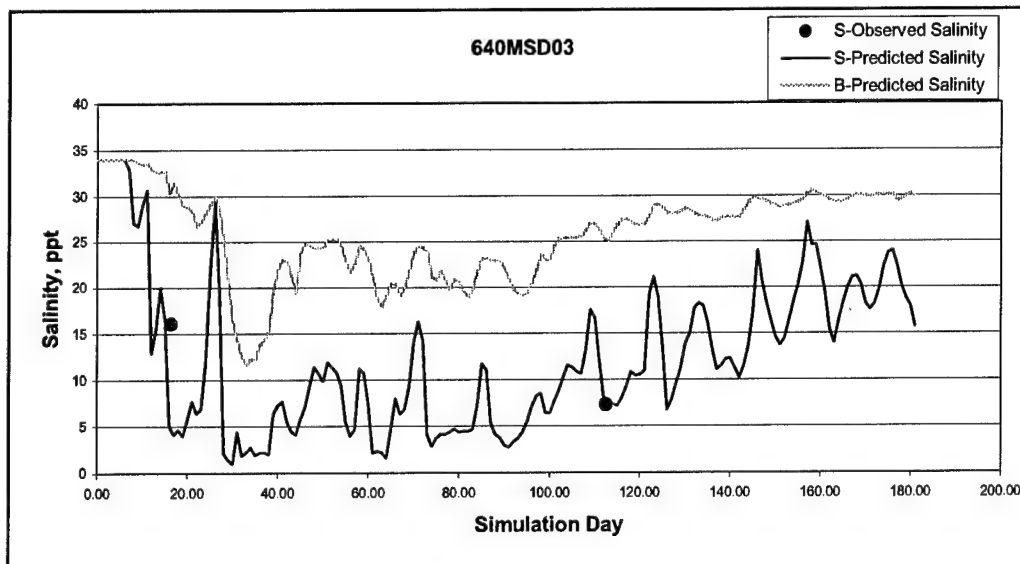


Figure 6-8. (Sheet 2 of 4)

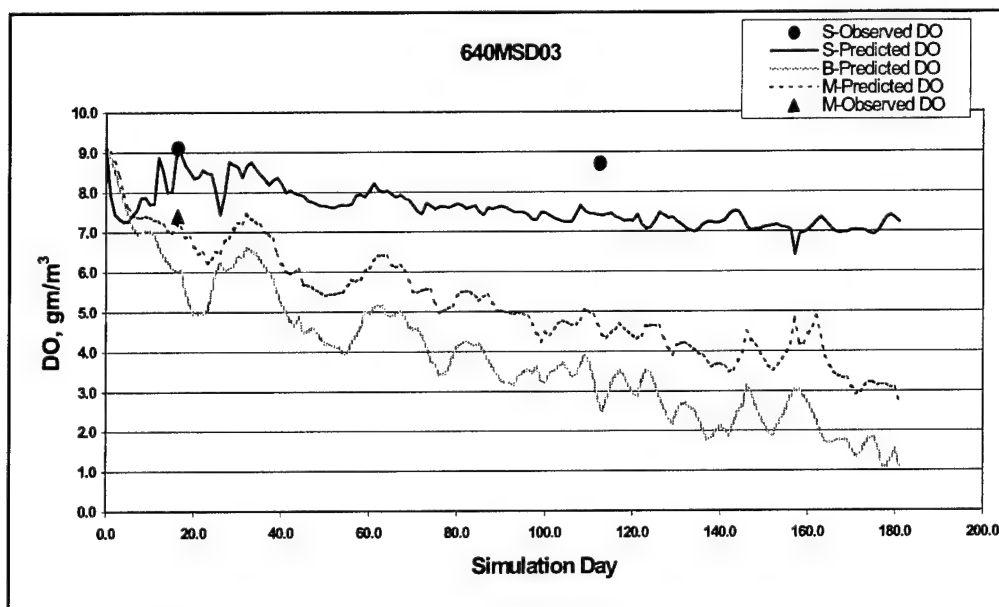


Figure 6-8. (Sheet 3 of 4)

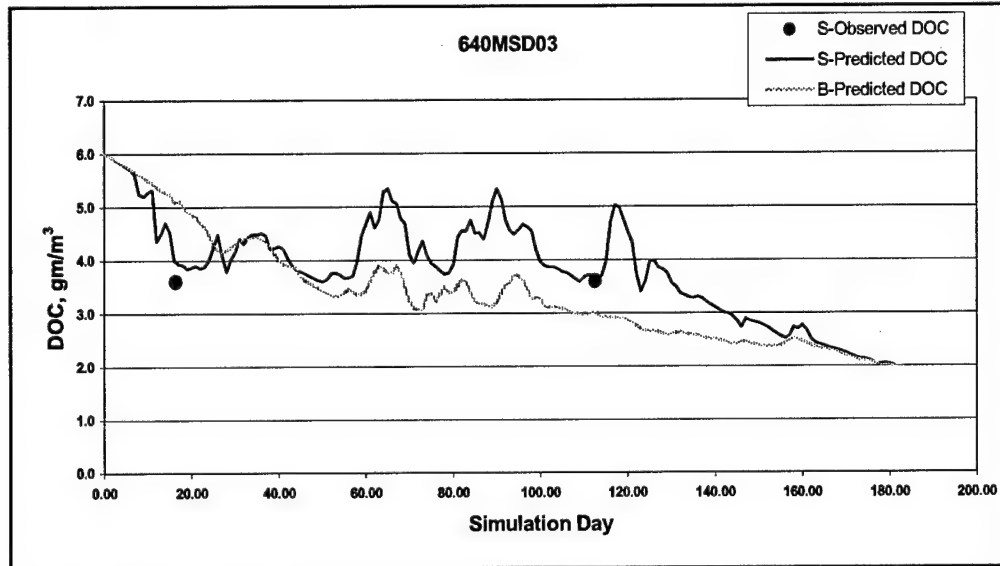


Figure 6-8. (Sheet 4 of 4)

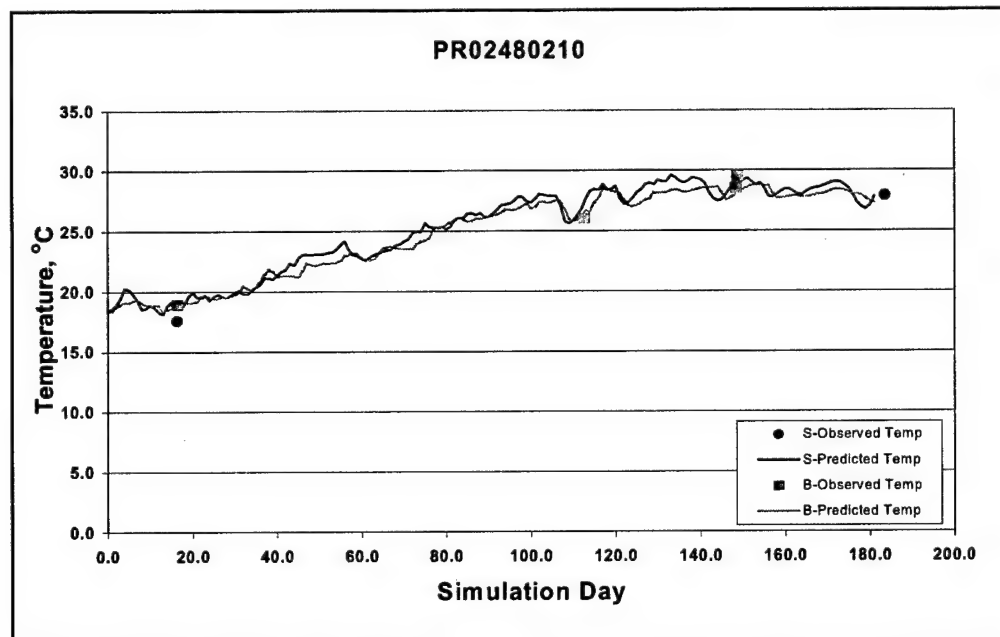


Figure 6-9. Water quality calibration results at sta PR0248210 3 miles from mouth of East Pascagoula River (Sheet 1 of 4)

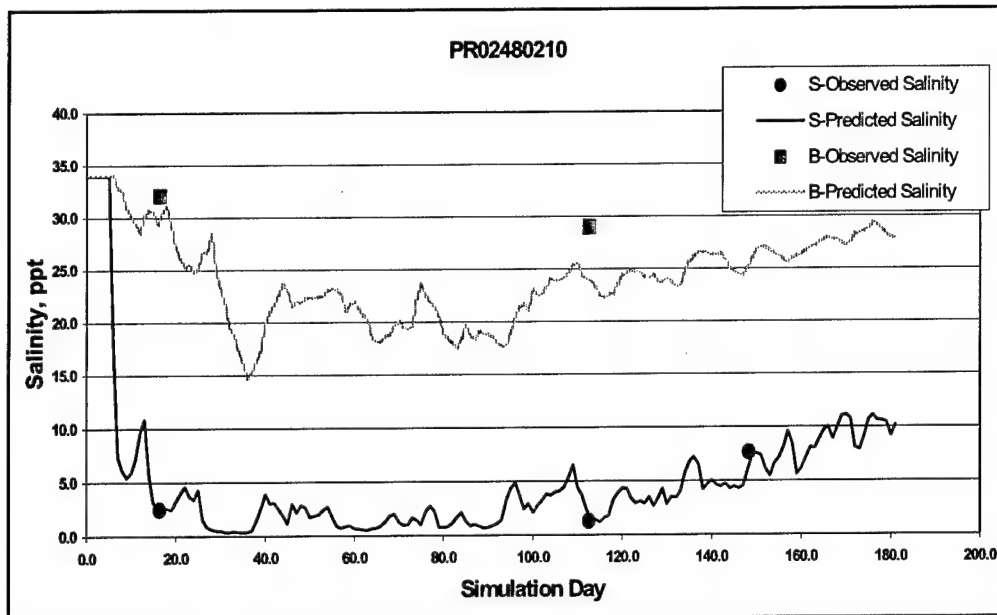


Figure 6-9. (Sheet 2 of 4)

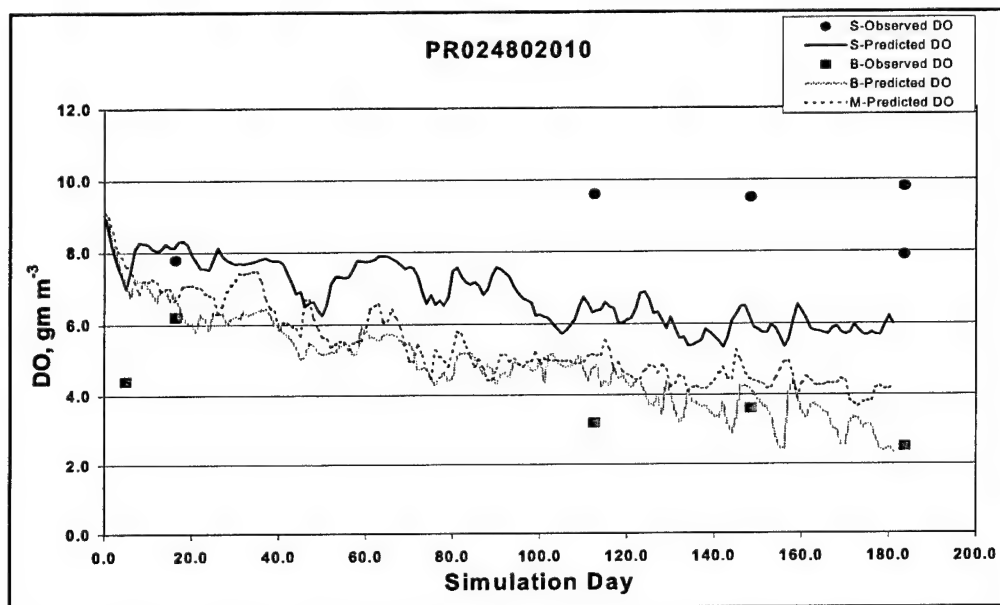


Figure 6-9. (Sheet 3 of 4)

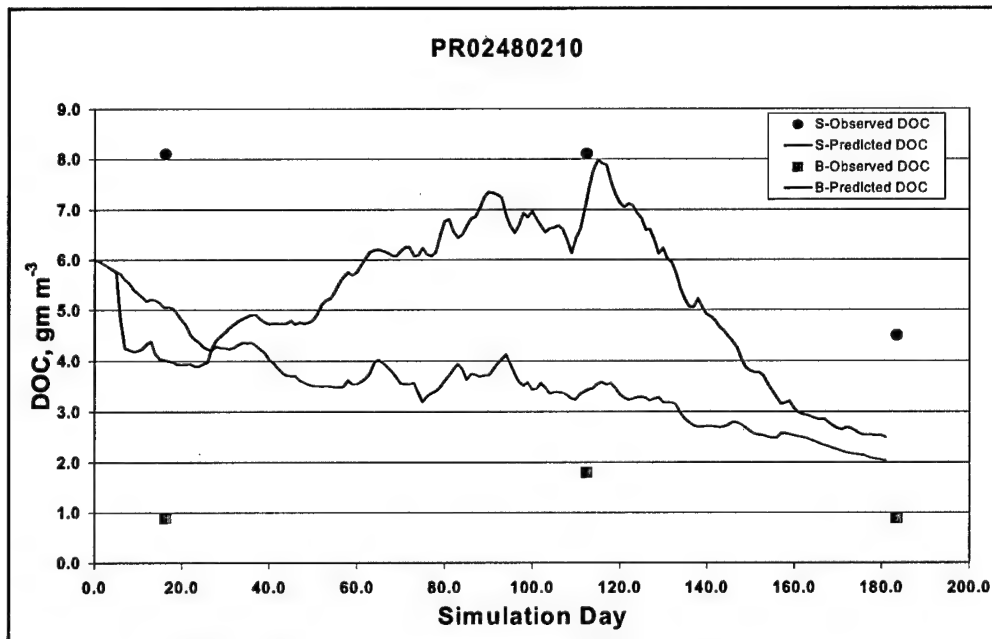


Figure 6-9. (Sheet 4 of 4)

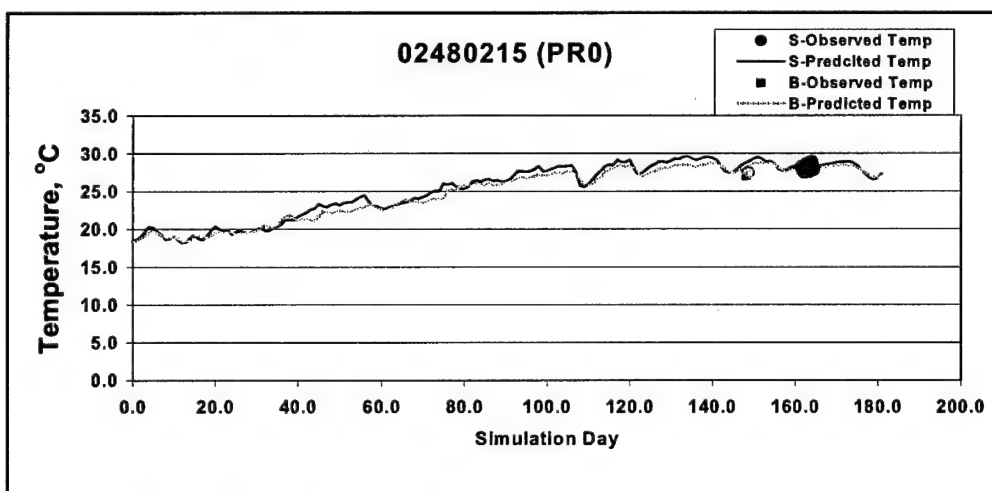


Figure 6-10. Water quality calibration results at sta 2480215 located at mouth of East Pascagoula River (Sheet 1 of 4)

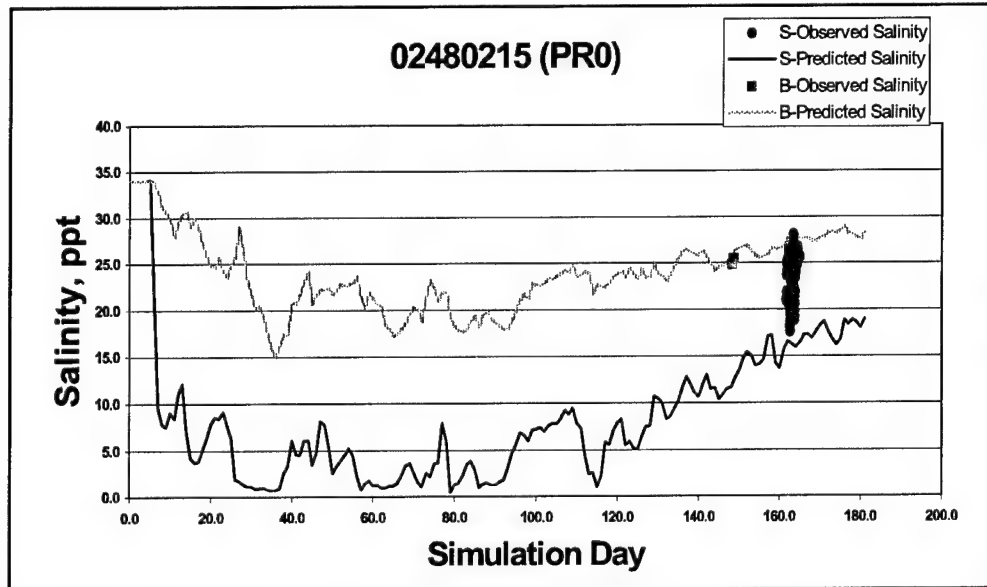


Figure 6-10. (Sheet 2 of 4)

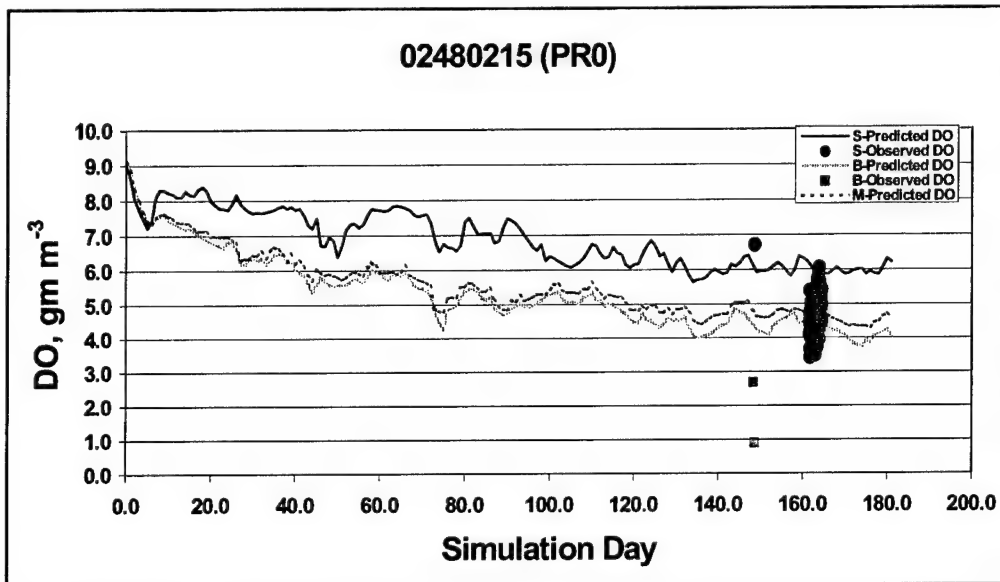


Figure 6-10. (Sheet 3 of 4)

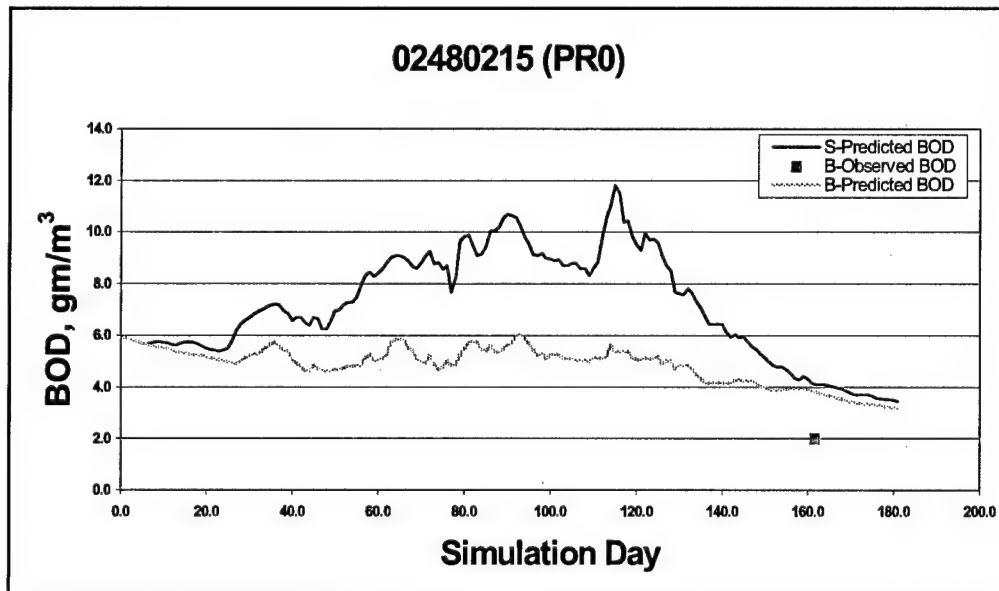


Figure 6-10. (Sheet 4 of 4)

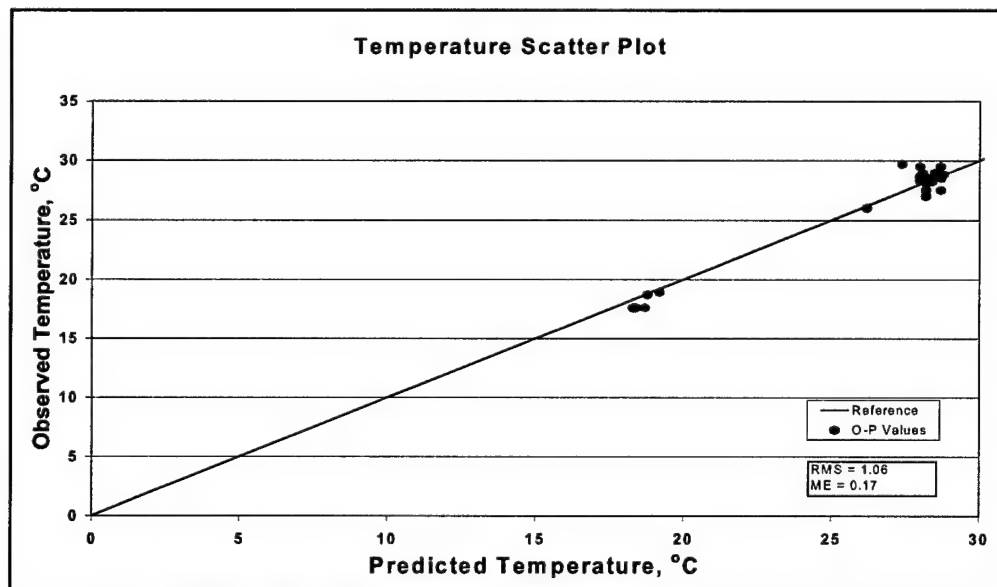


Figure 6-11. Scatter plots (Sheet 1 of 4)

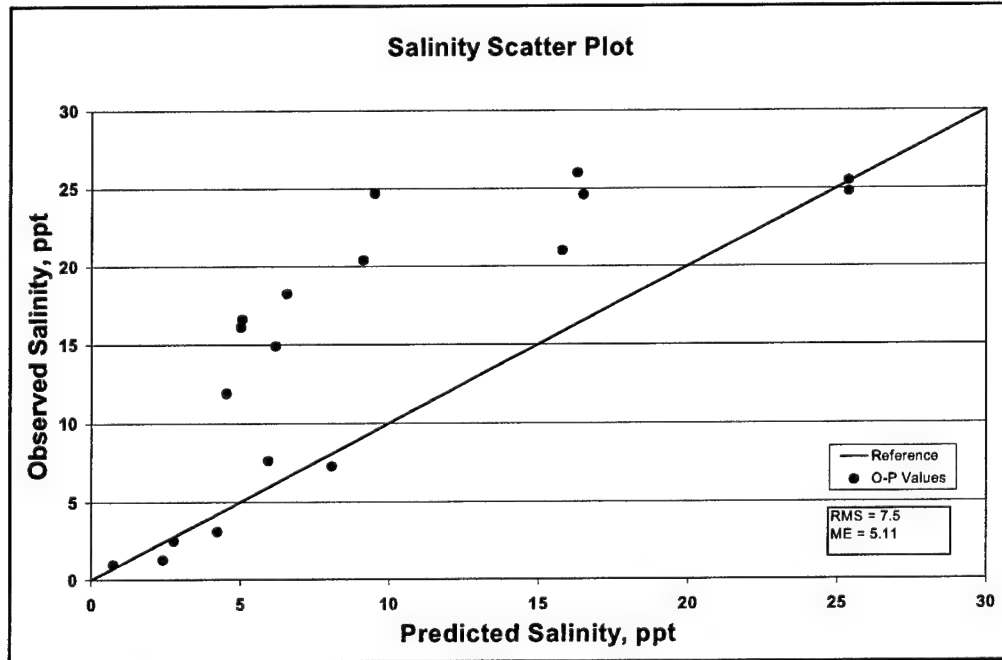


Figure 6-11. (Sheet 2 of 4)

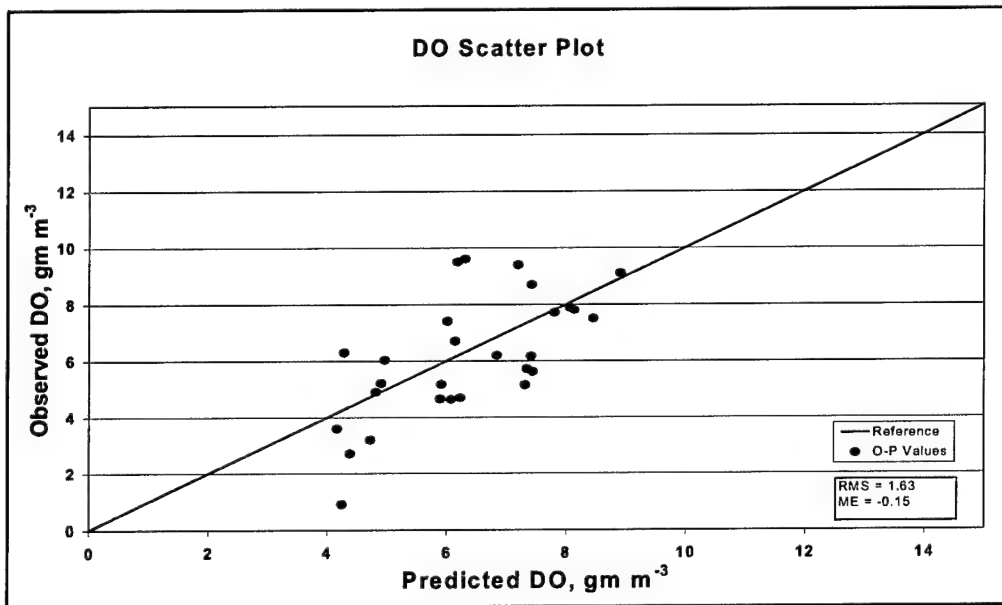


Figure 6-11. (Sheet 3 of 4)

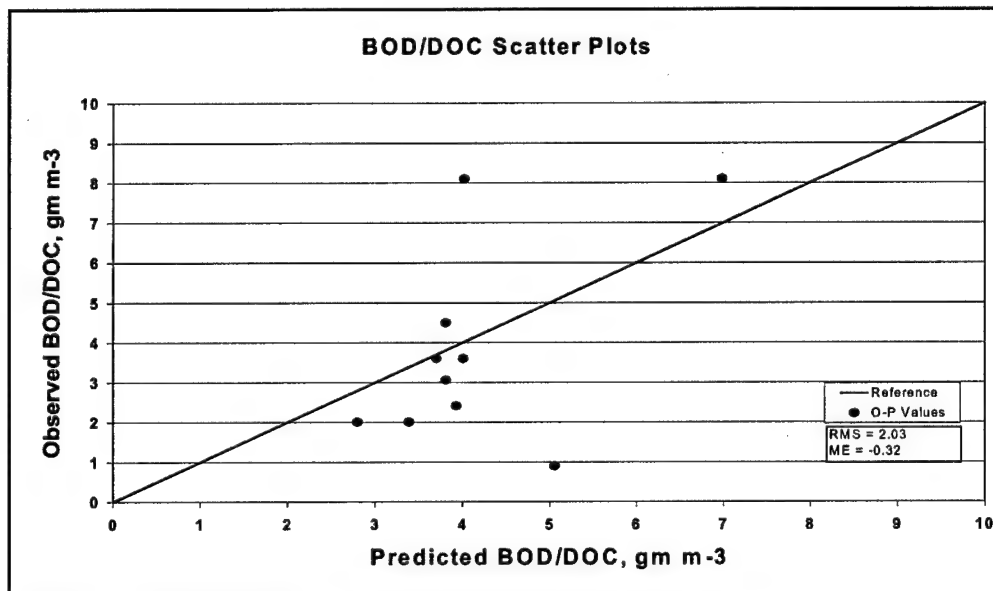


Figure 6-11. (Sheet 4 of 4)

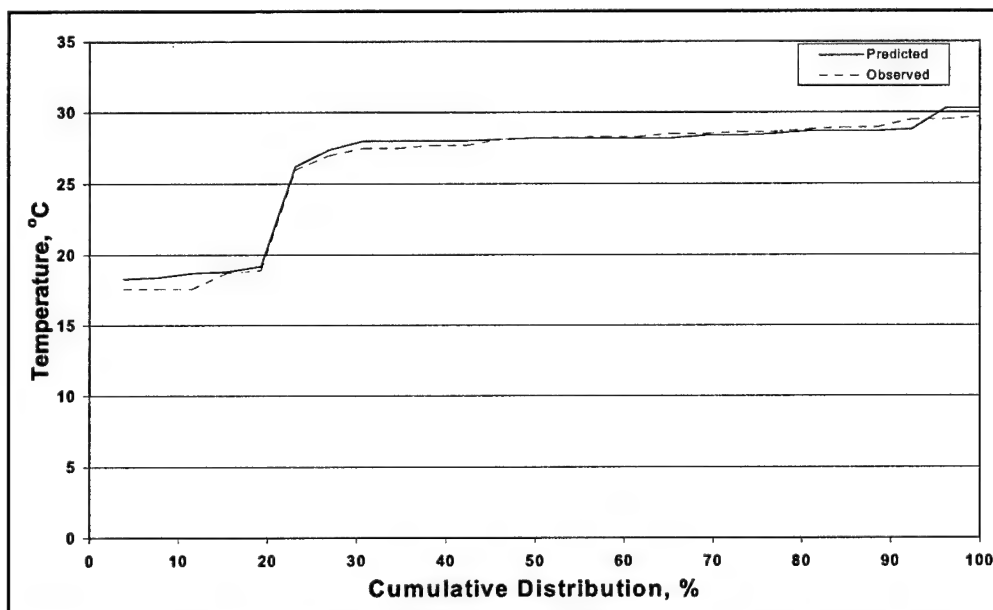


Figure 6-12. Percent cumulative distribution curves of water quality constituents (Sheet 1 of 4)

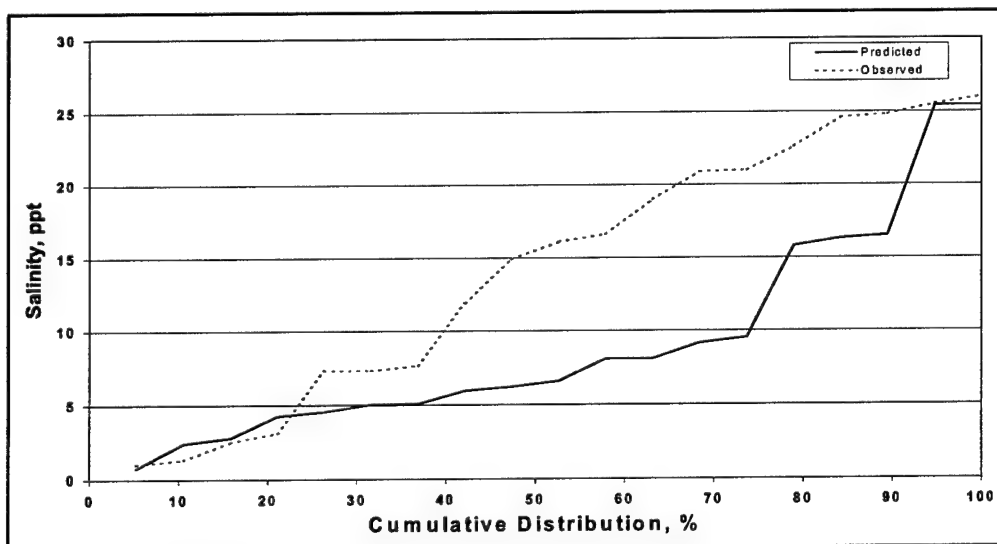


Figure 6-12. (Sheet 2 of 4)

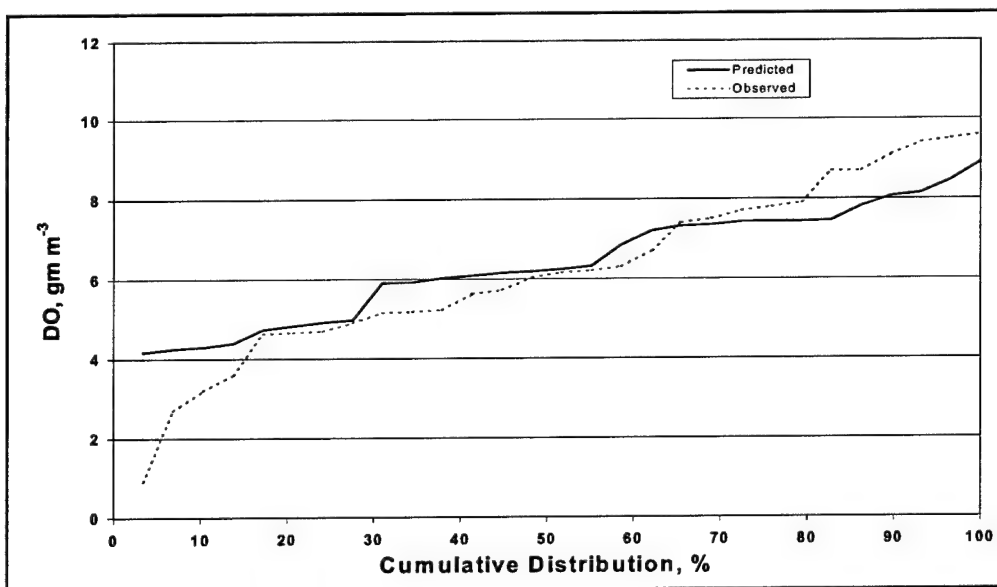


Figure 6-12. (Sheet 3 of 4)

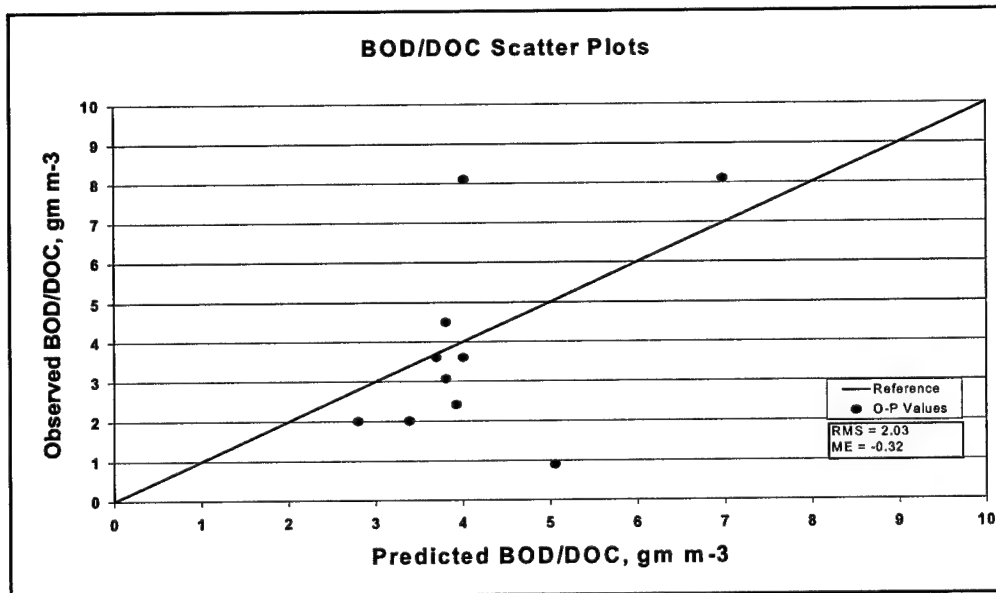


Figure 6-11. (Sheet 4 of 4)

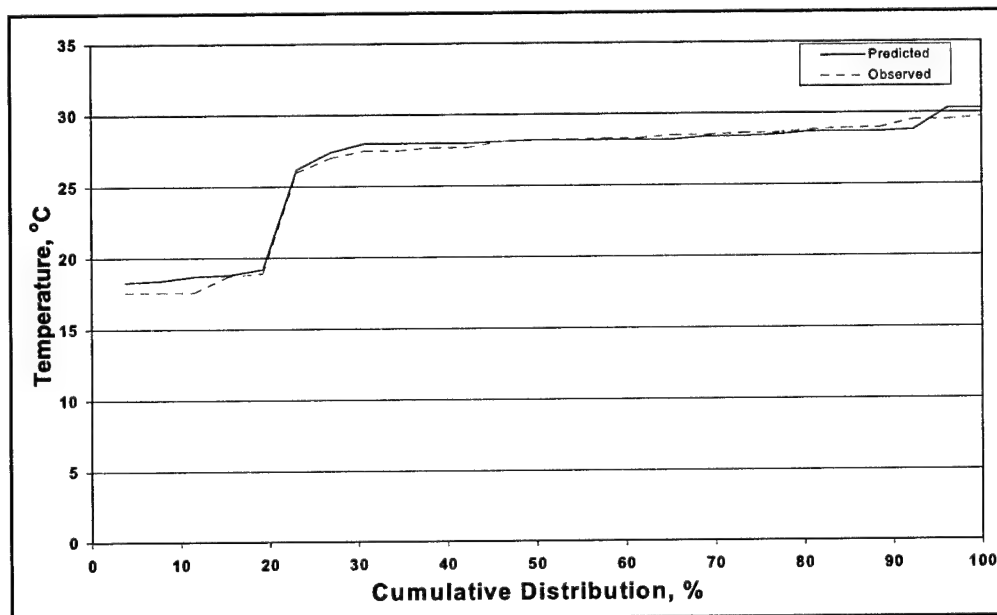


Figure 6-12. Percent cumulative distribution curves of water quality constituents (Sheet 1 of 4)

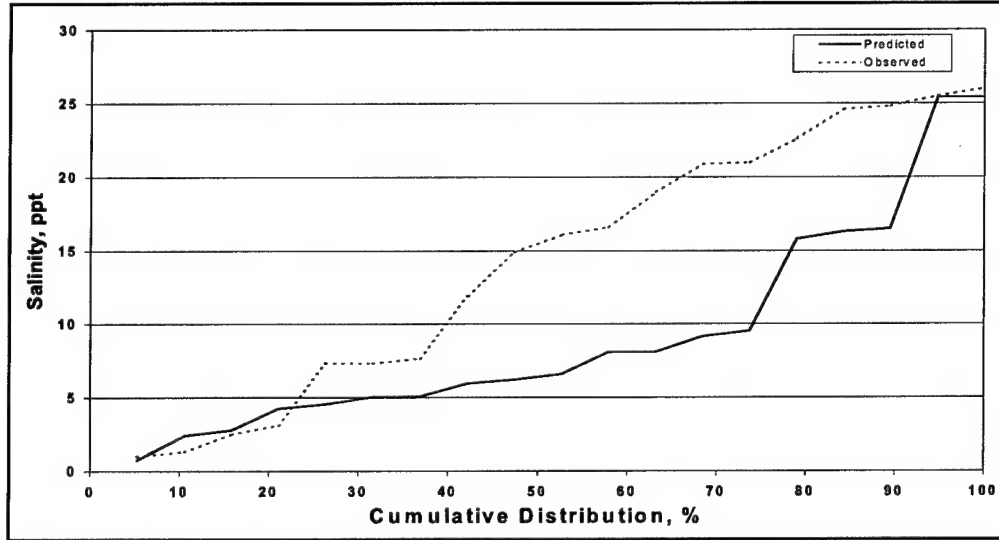


Figure 6-12. (Sheet 2 of 4)

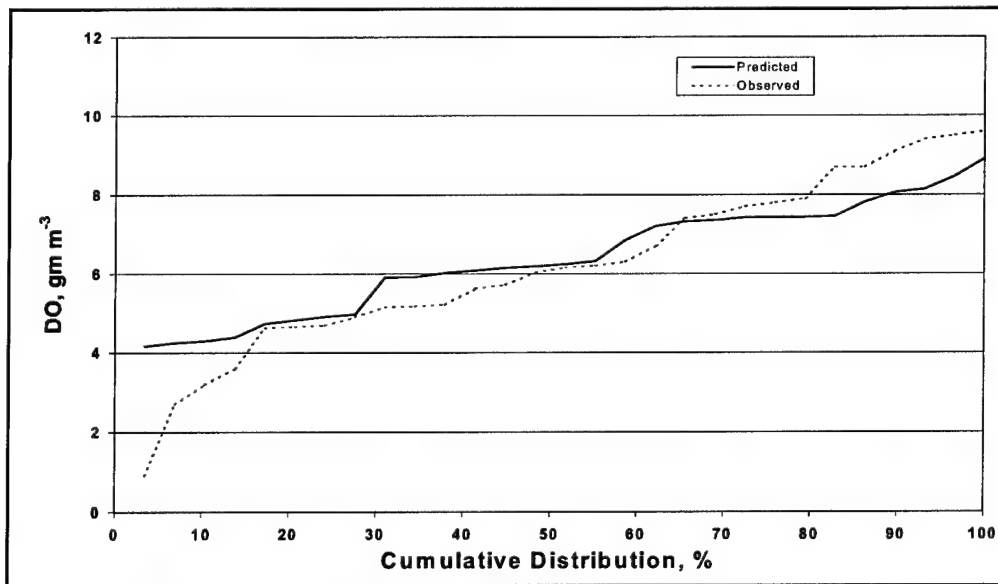


Figure 6-12. (Sheet 3 of 4)

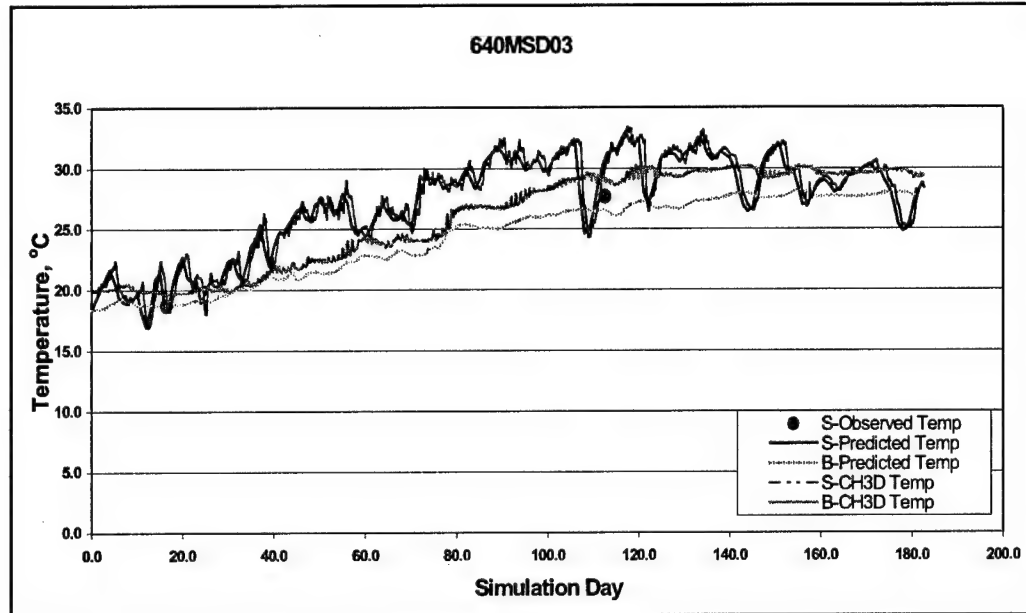


Figure 6-13. (Sheet 4 of 10)

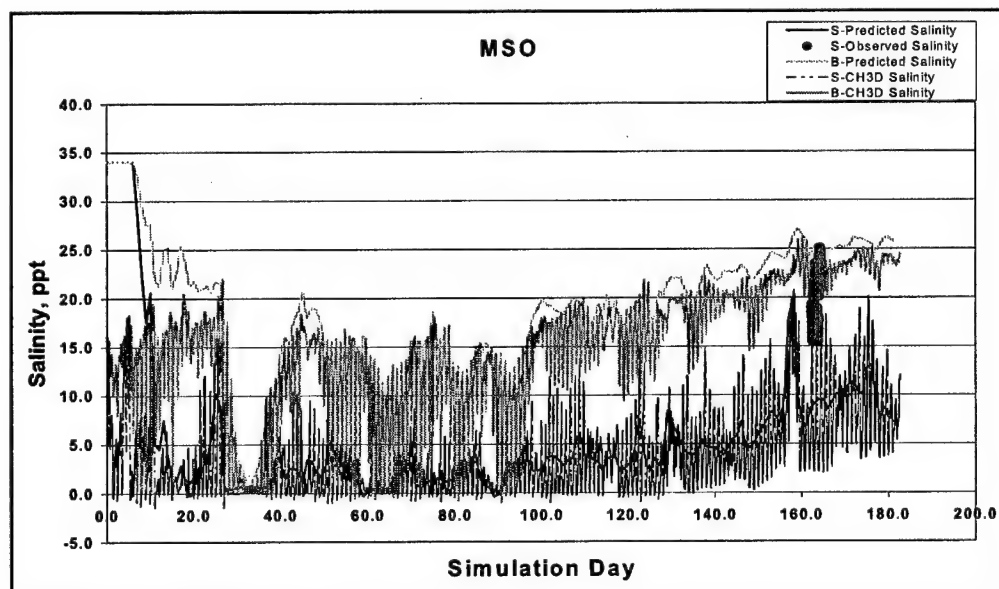


Figure 6-13. (Sheet 5 of 10)

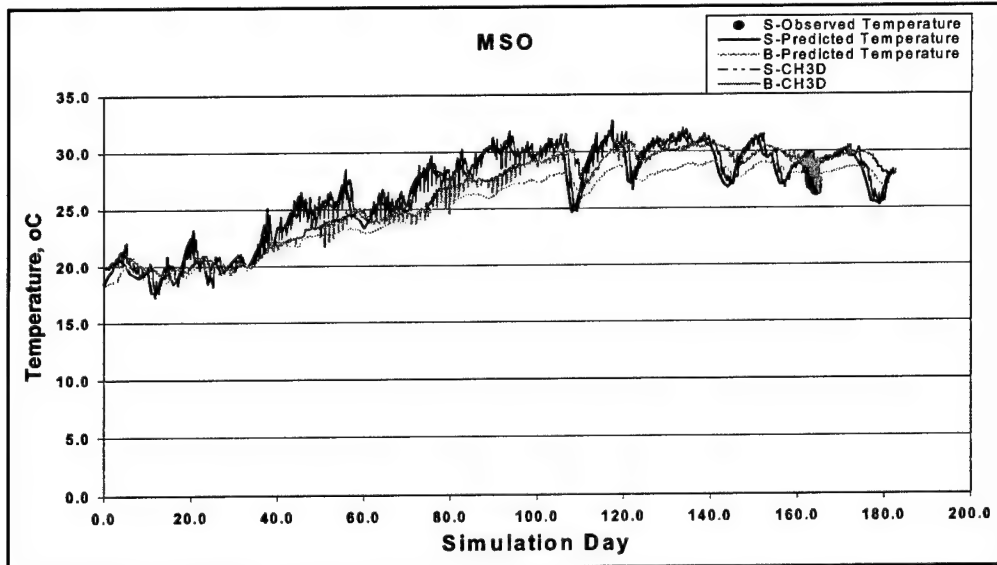


Figure 6-13. (Sheet 6 of 10)

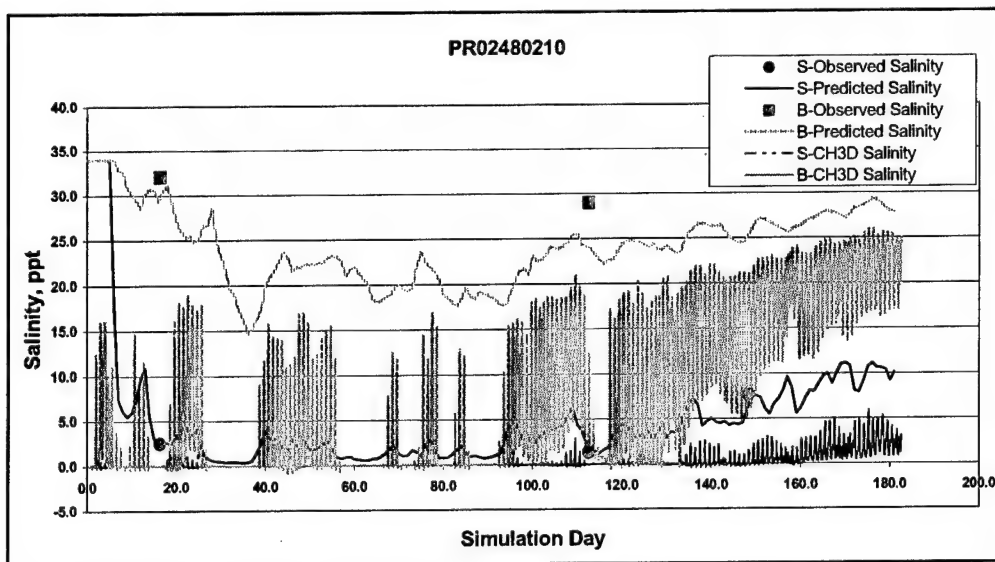


Figure 6-13. (Sheet 7 of 10)

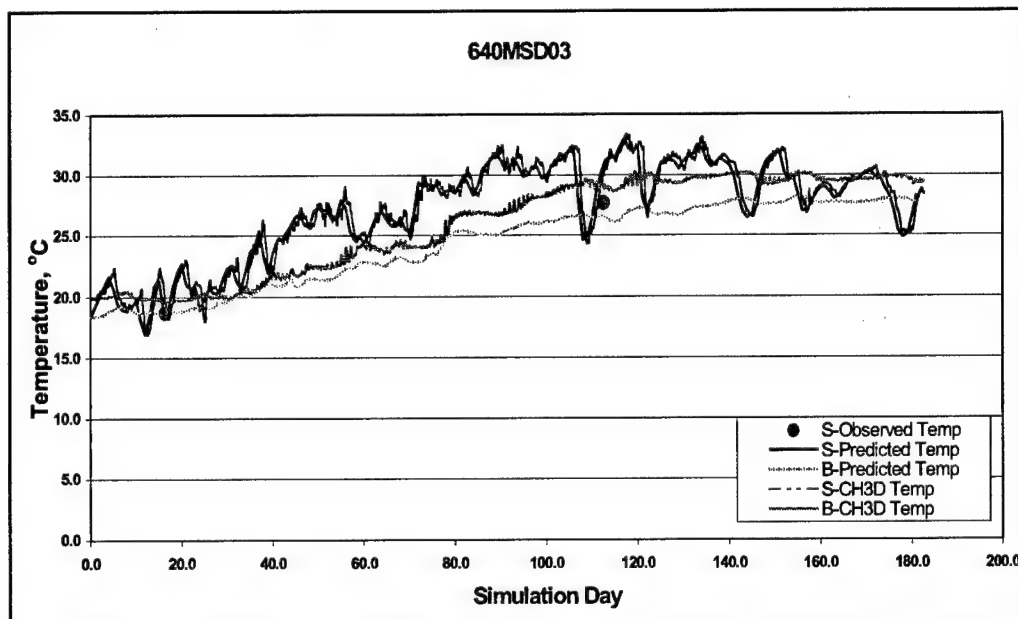


Figure 6-13. (Sheet 4 of 10)

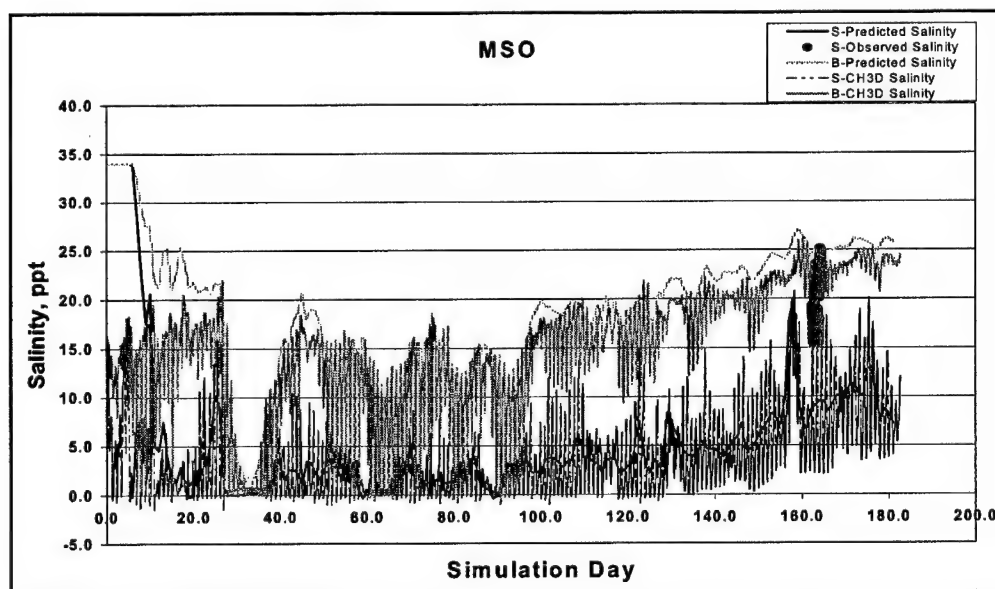


Figure 6-13. (Sheet 5 of 10)

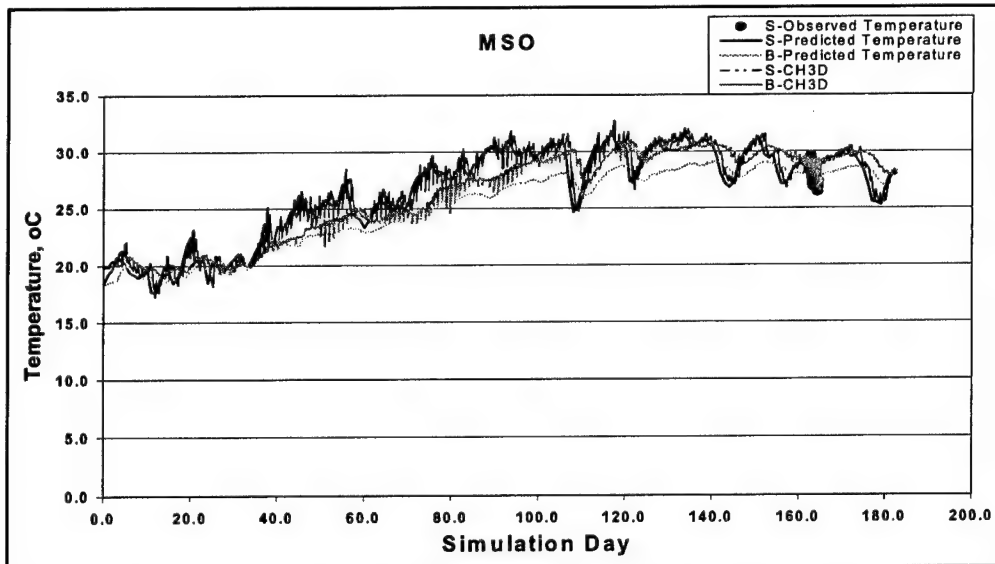


Figure 6-13. (Sheet 6 of 10)

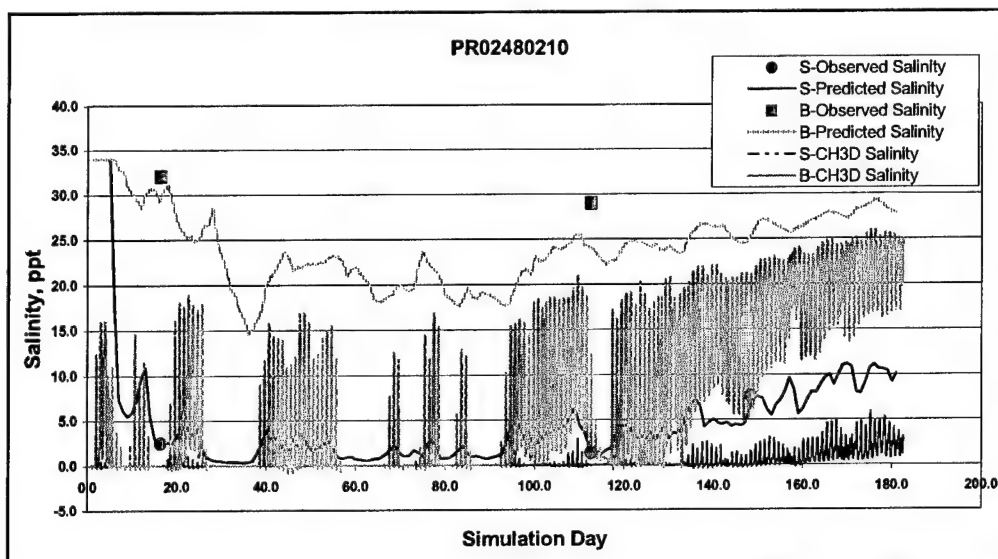


Figure 6-13. (Sheet 7 of 10)

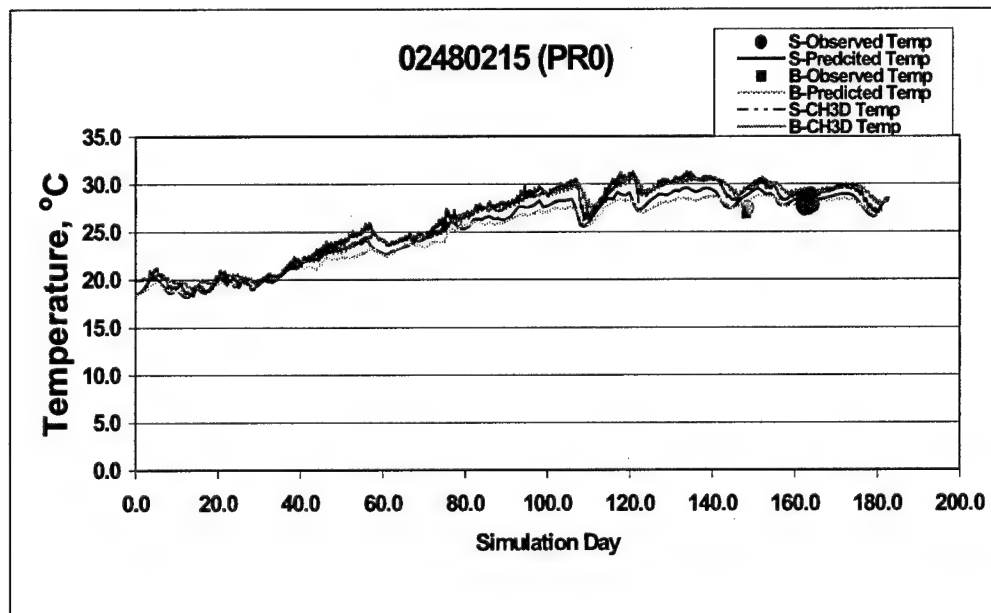


Figure 6-13 (Sheet 8 of 10)

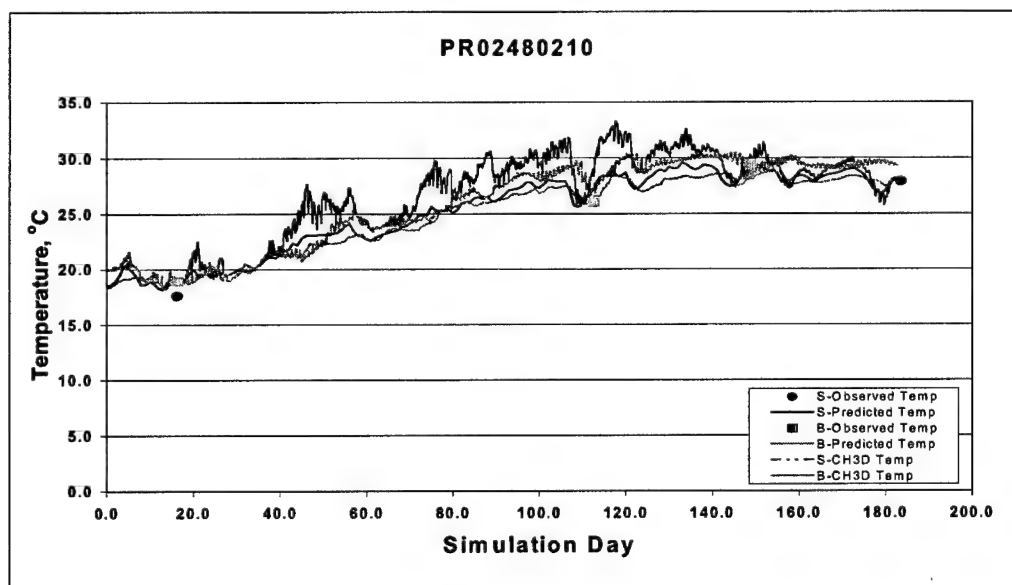


Figure 6-13. (Sheet 9 of 10)

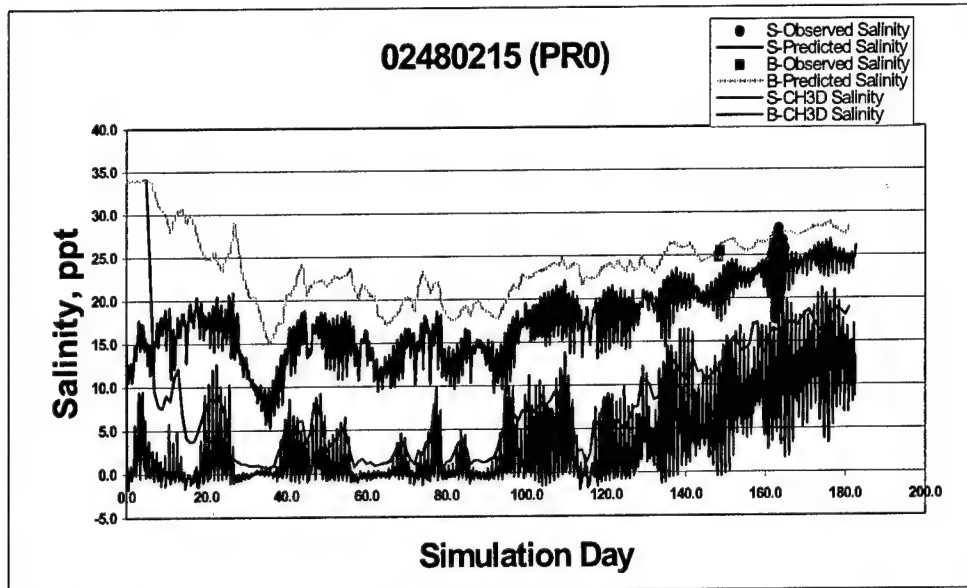


Figure 6-13. (Sheet 10 of 10)

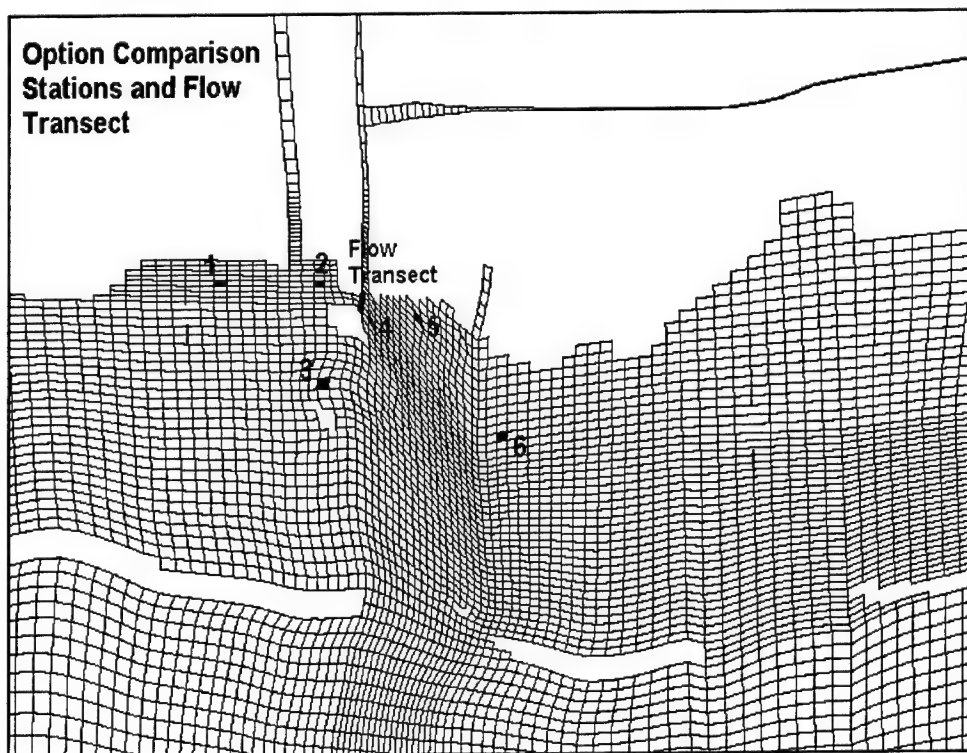


Figure 6-14. Comparison station locations and flow transect location for all options

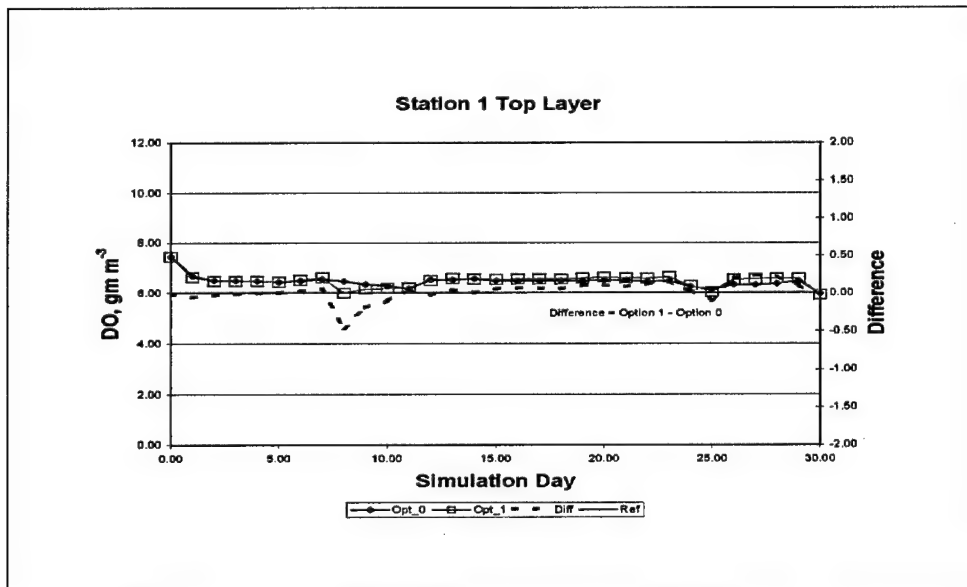


Figure 6-15. Comparison of option 1 results to base results at six stations in study area (Sheet 1 of 12)

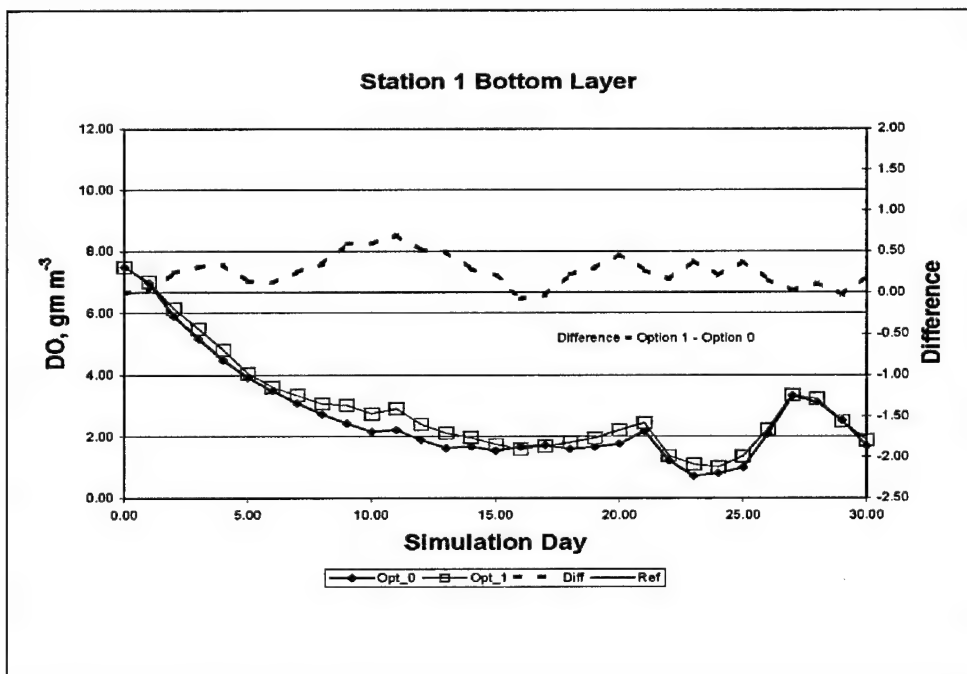


Figure 6-15. (Sheet 2 of 12)

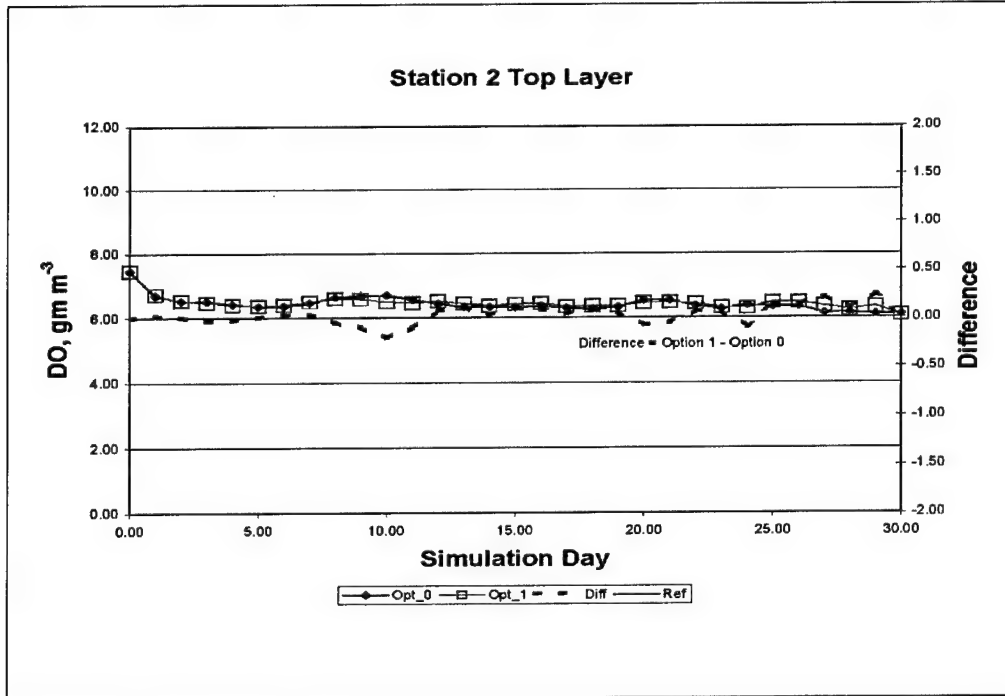


Figure 6-15. (Sheet 3 of 12)

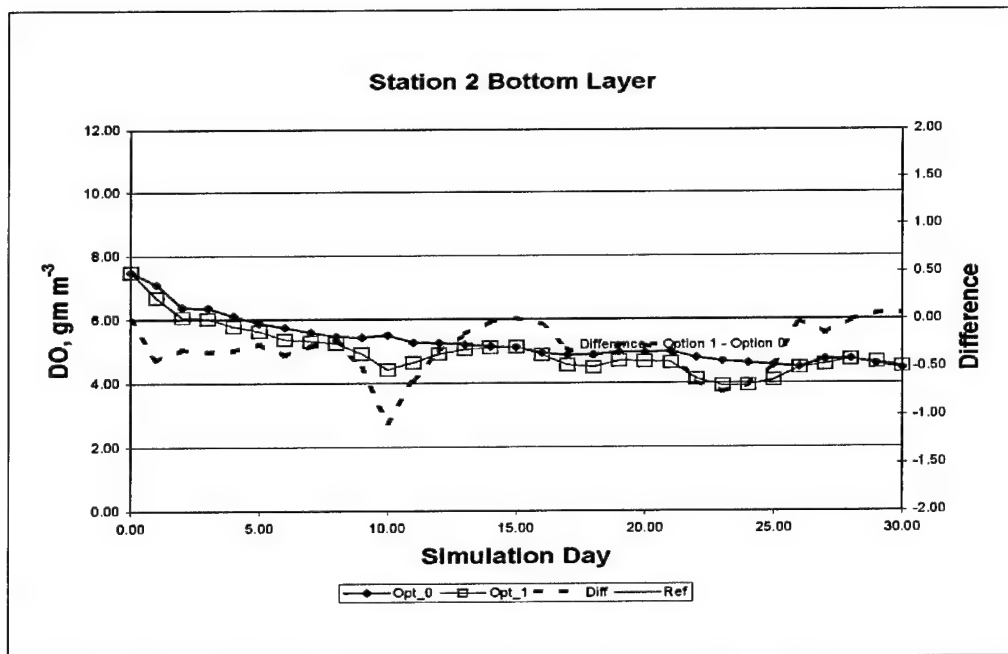


Figure 6-15. (Sheet 4 of 12)

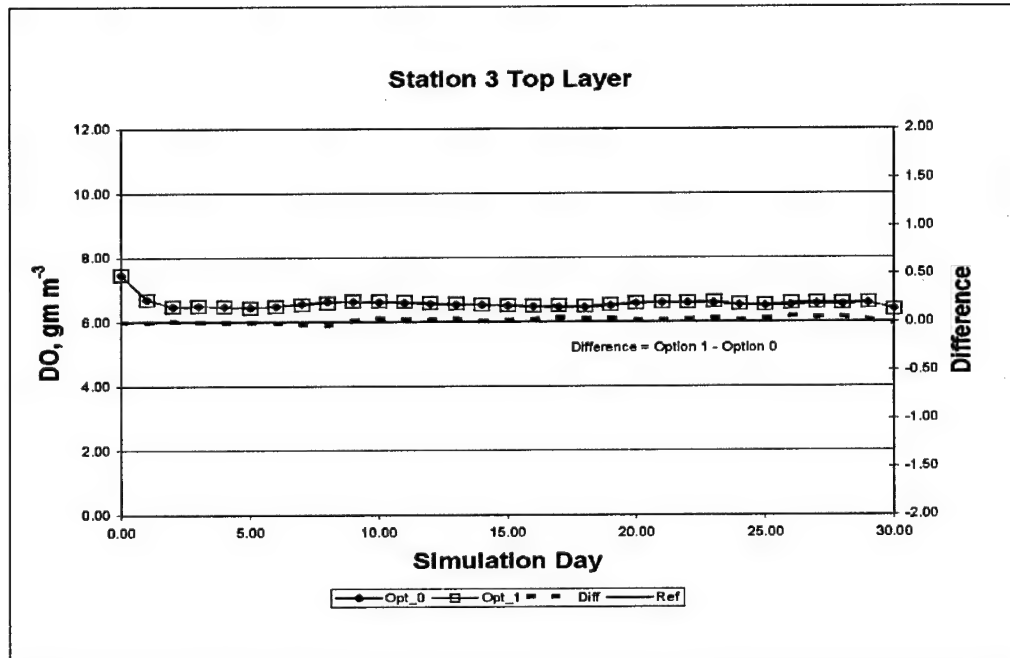


Figure 6-15. (Sheet 5 of 12)

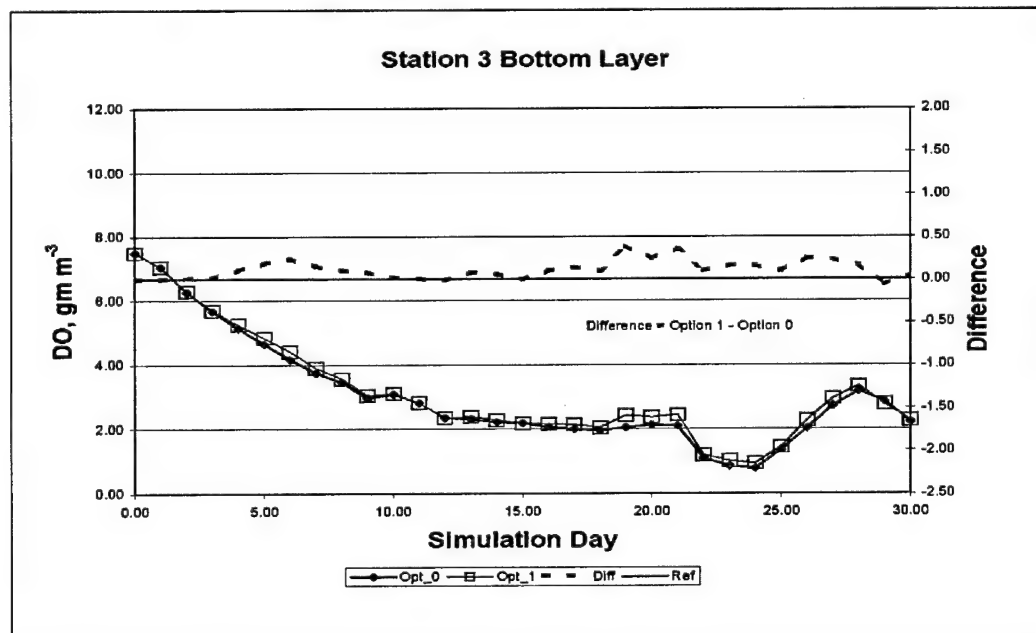


Figure 6-15. (Sheet 6 of 12)

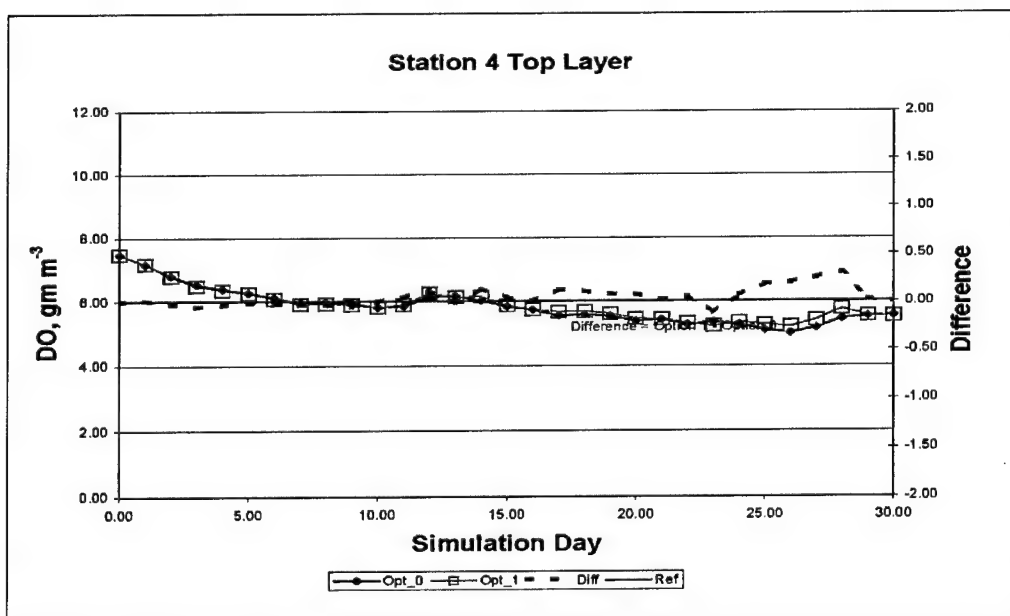


Figure 6-15. (Sheet 7 of 12)

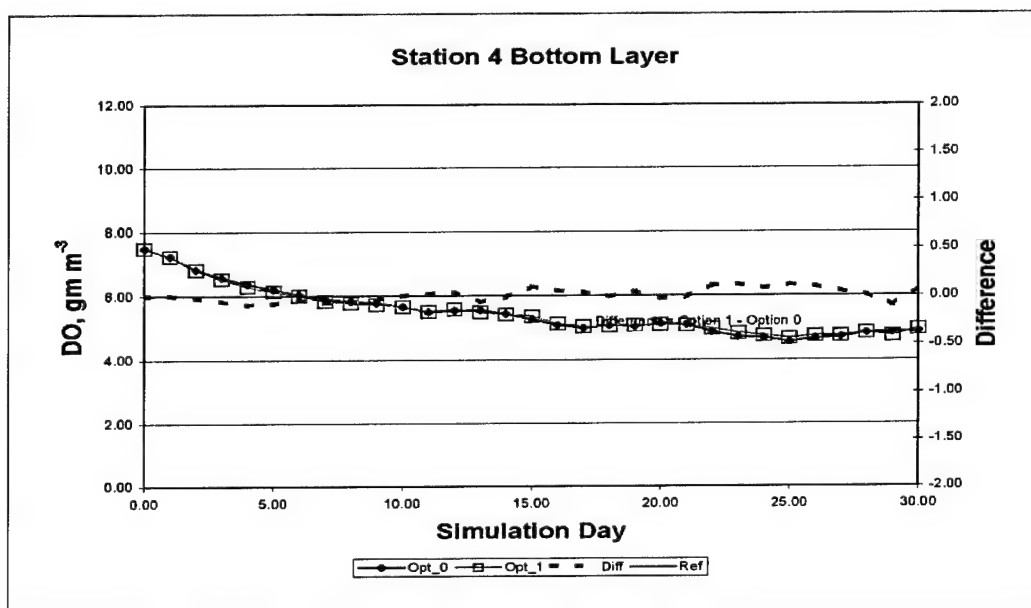


Figure 6-15. (Sheet 8 of 12)

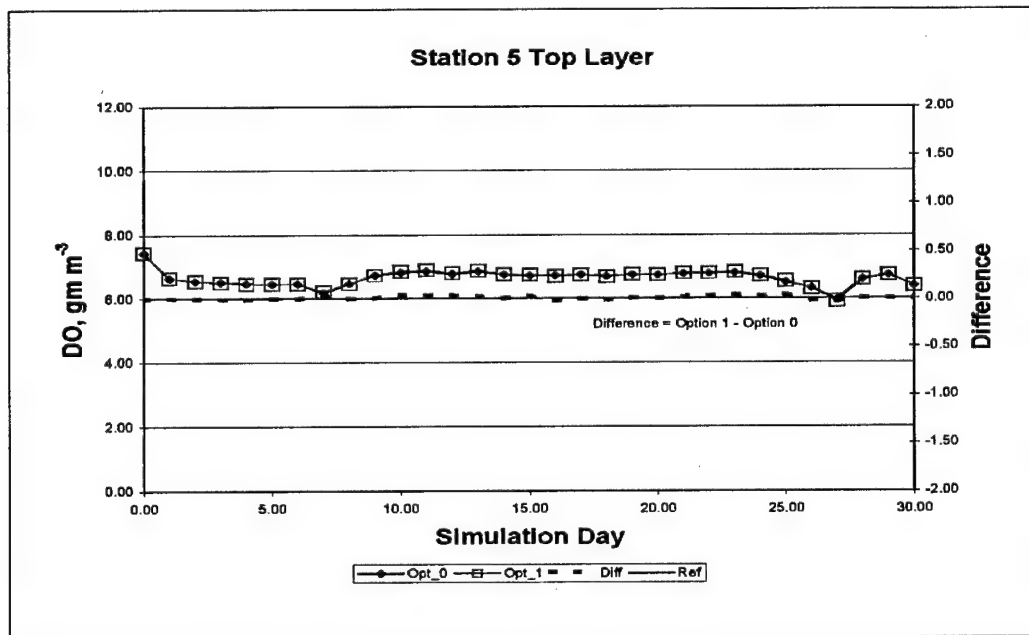


Figure 6-15. (Sheet 9 of 12)

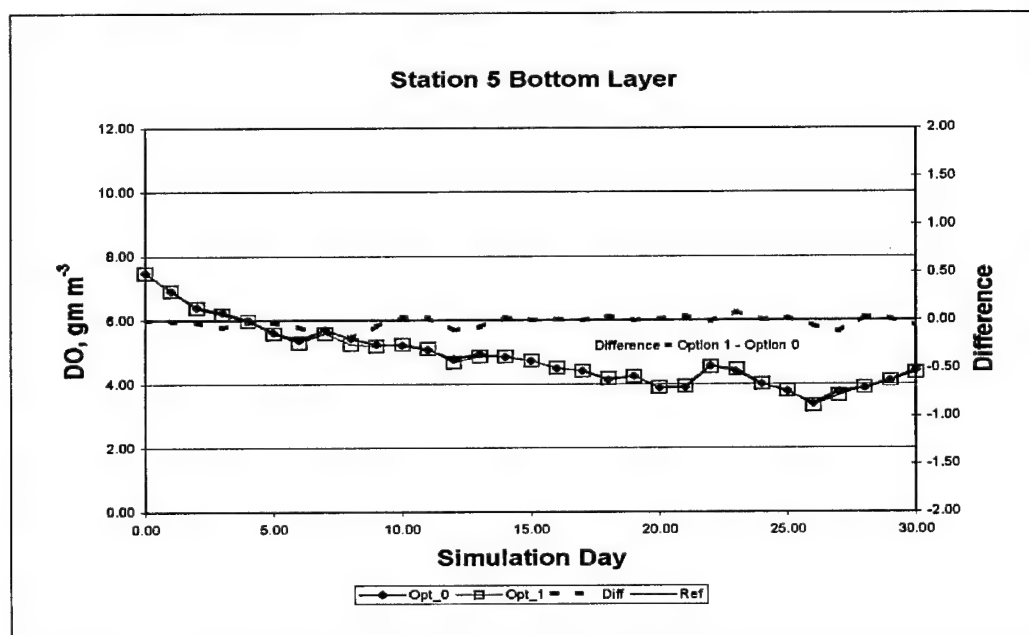


Figure 6-15. (Sheet 10 of 12)

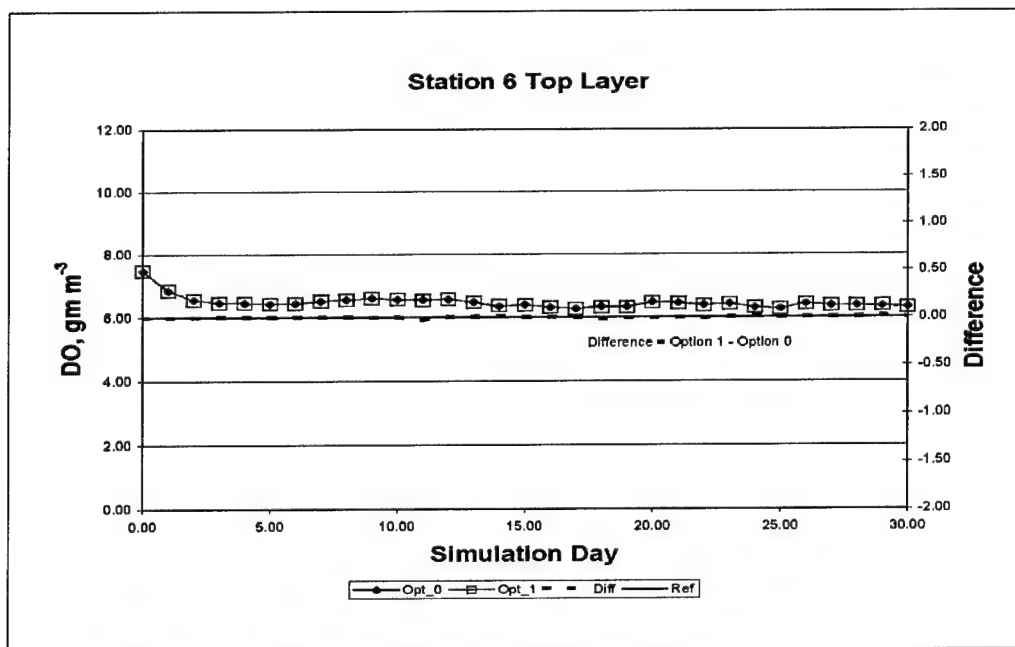


Figure 6-15. (Sheet 11 of 12)

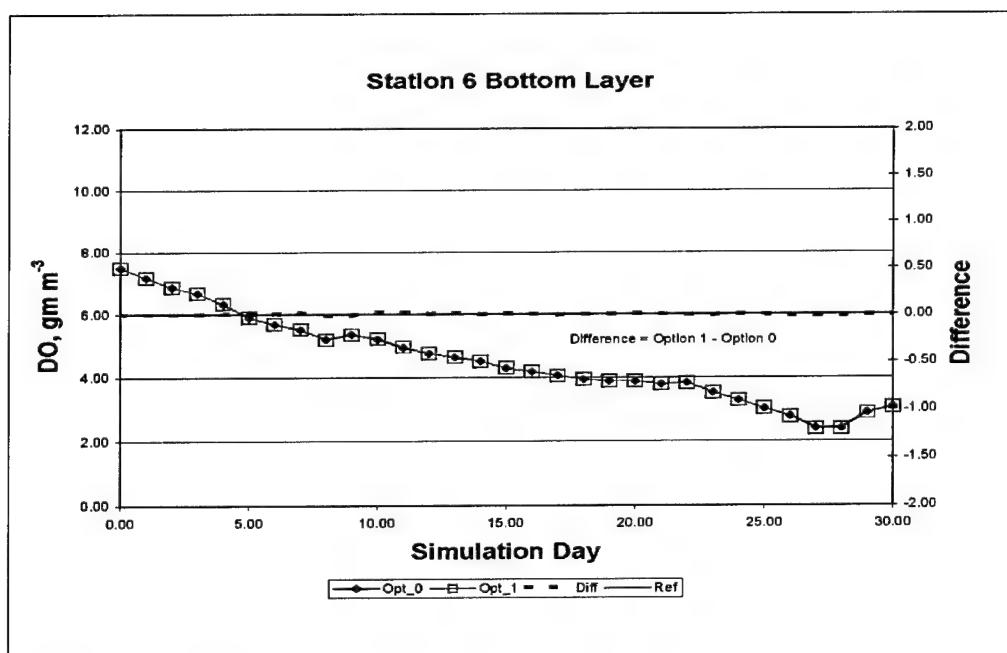


Figure 6-15. (Sheet 12 of 12)

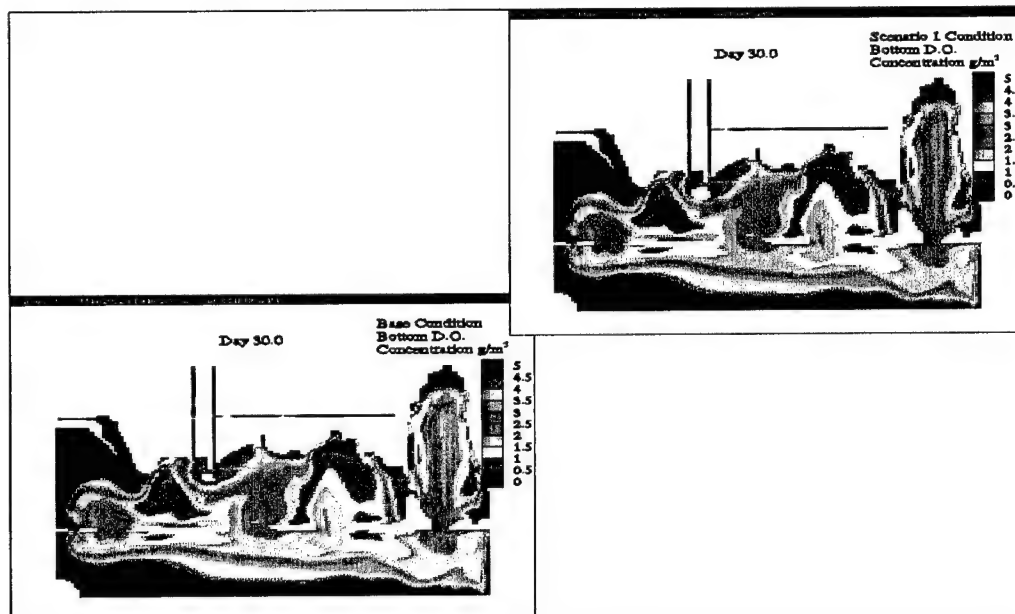


Figure 6-16. Comparison of bottom DO results for base and Alternative 1

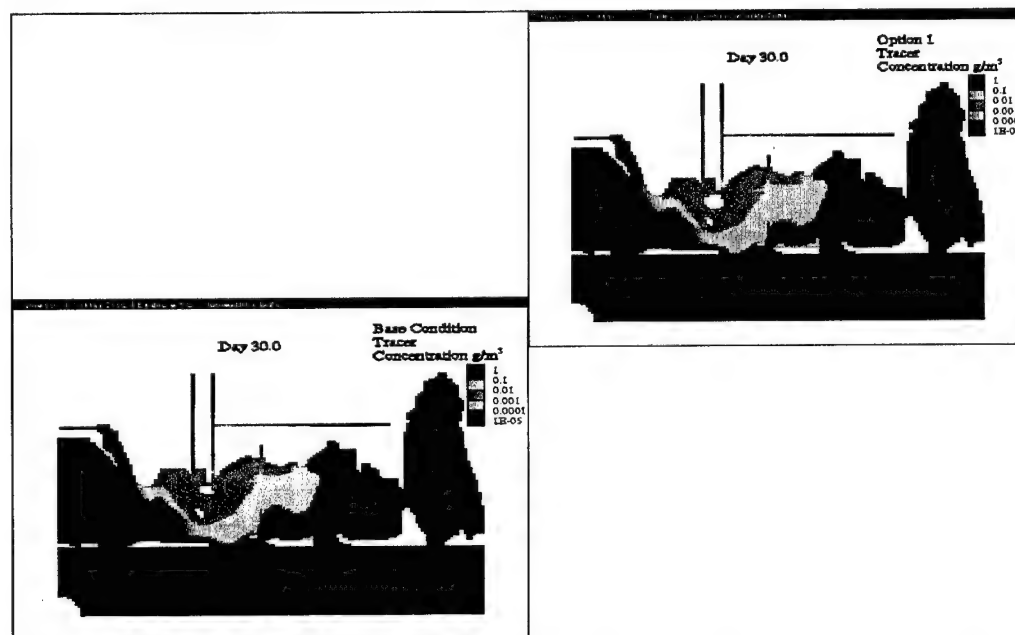


Figure 6-17. Comparison of bottom tracer results for base and Alternative 1 for West Pascagoula River release

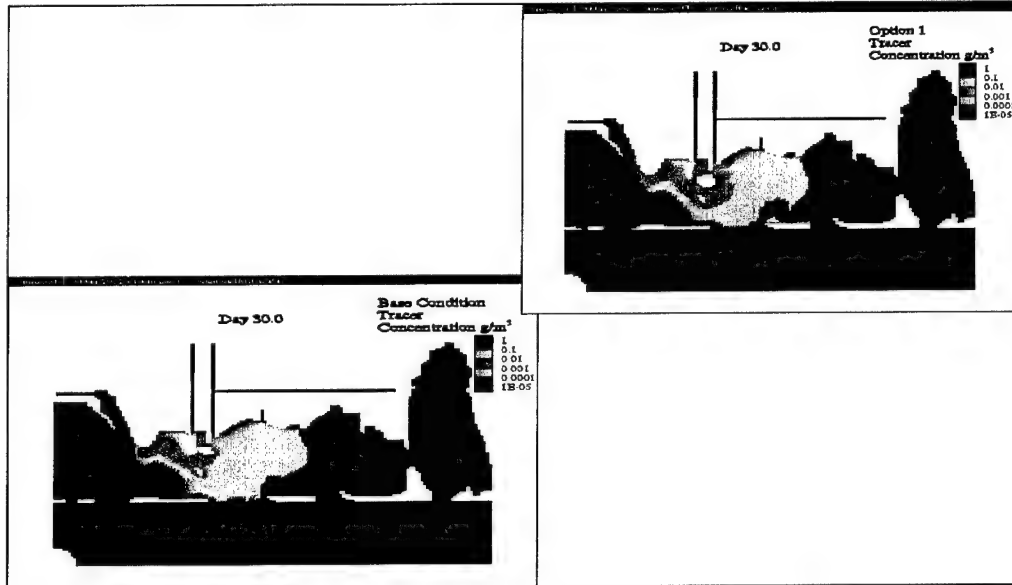


Figure 6-18. Comparison of bottom tracer results for base and Alternative 1 for East Pascagoula River release

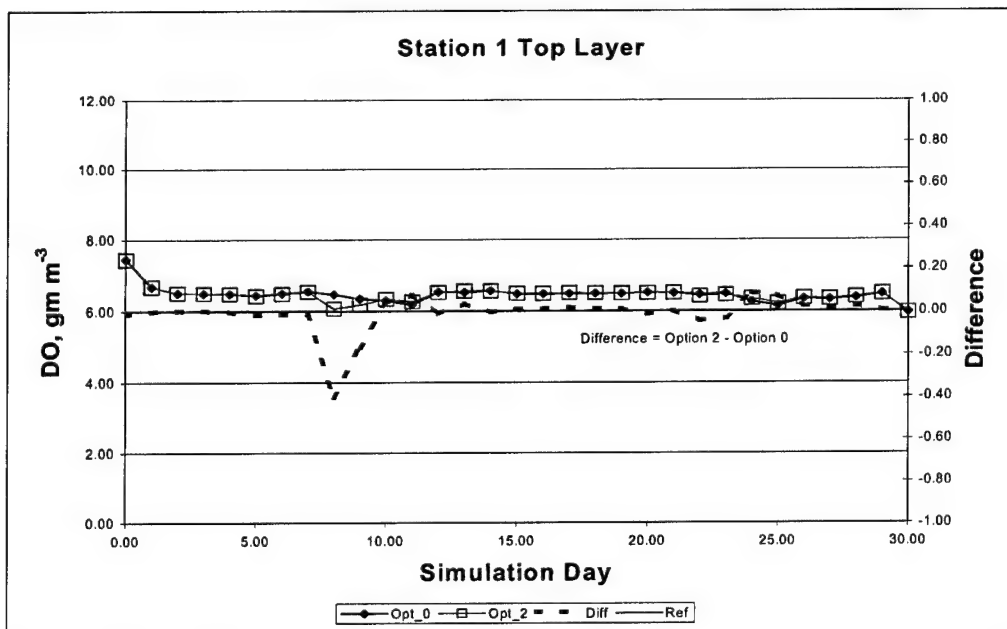


Figure 6-19. Comparison of Alternative 2 results to base results at six stations in study area (Sheet 1 of 12)

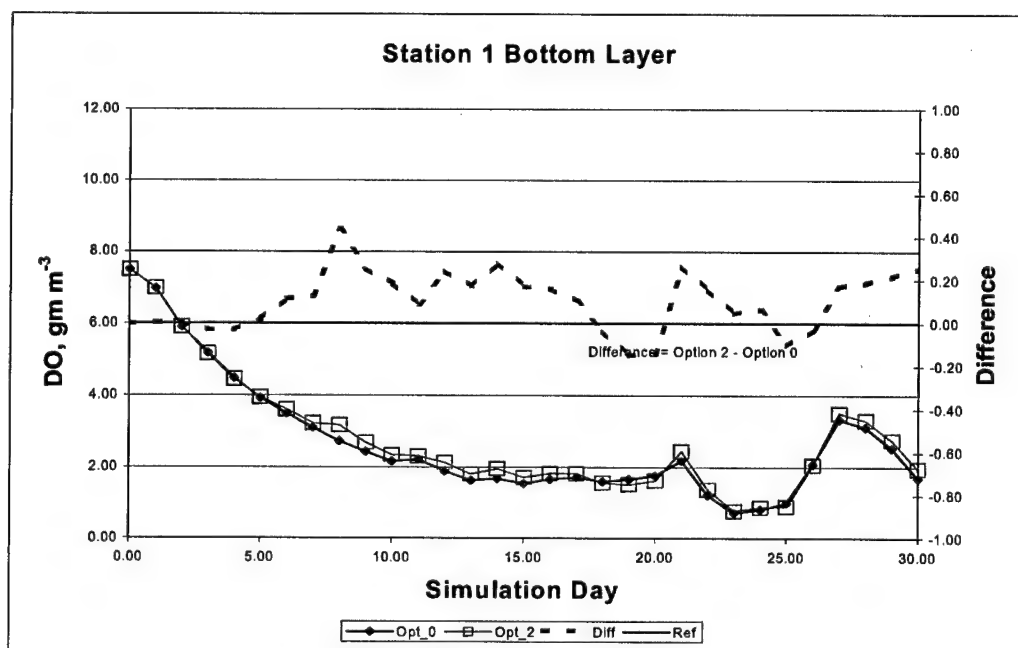


Figure 6-19. (Sheet 2 of 12)

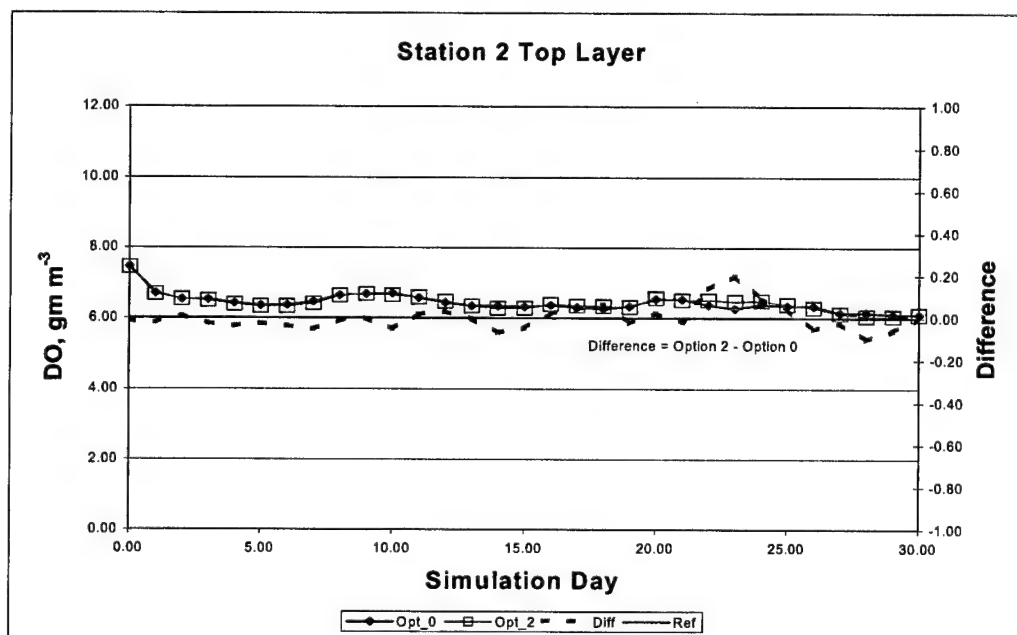


Figure 6-19. (Sheet 3 of 12)

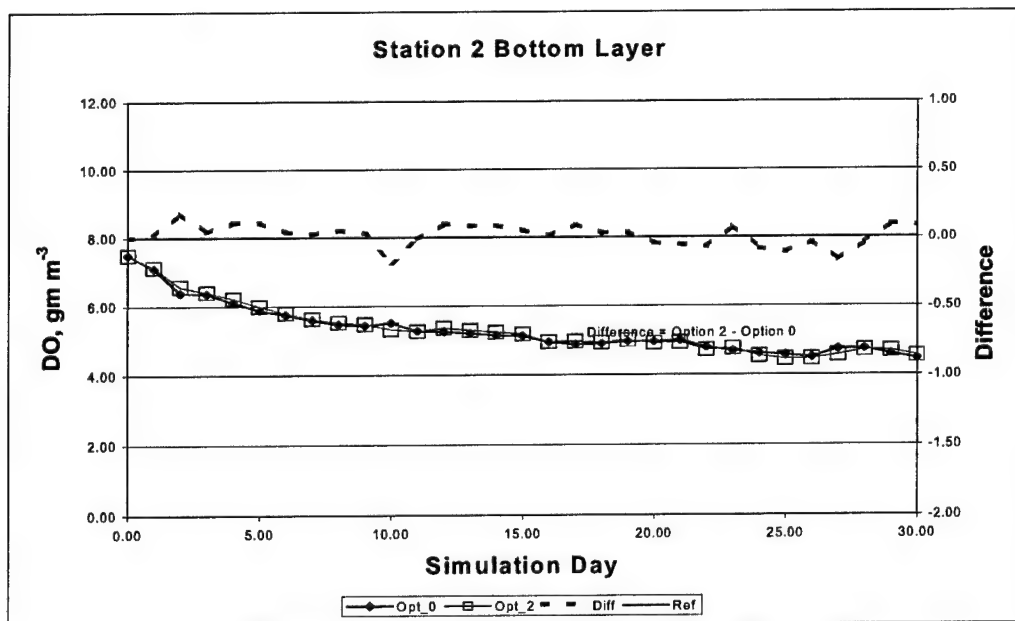


Figure 6-19. (Sheet 4 of 12)

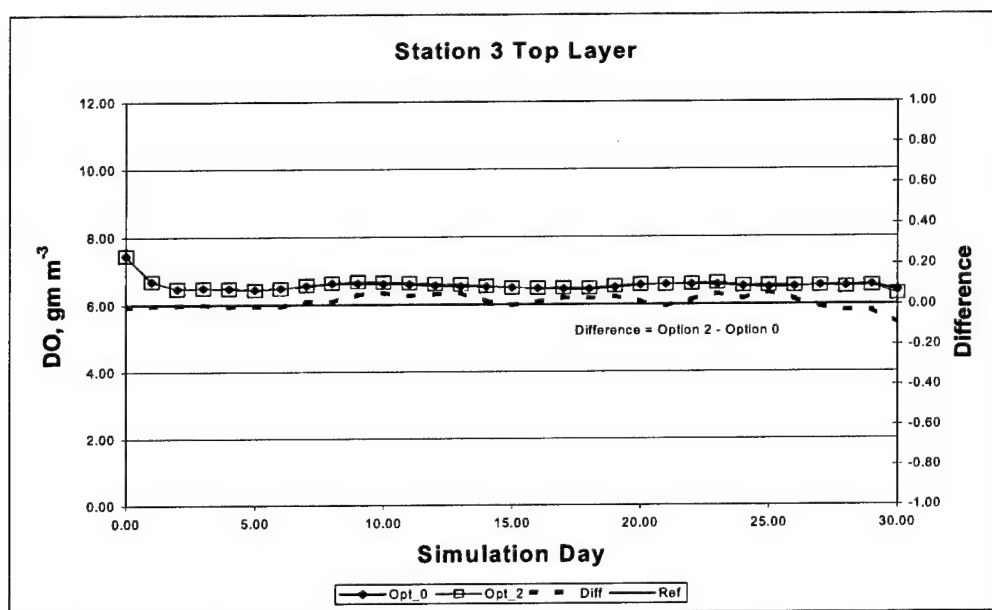


Figure 6-19. (Sheet 5 of 12)

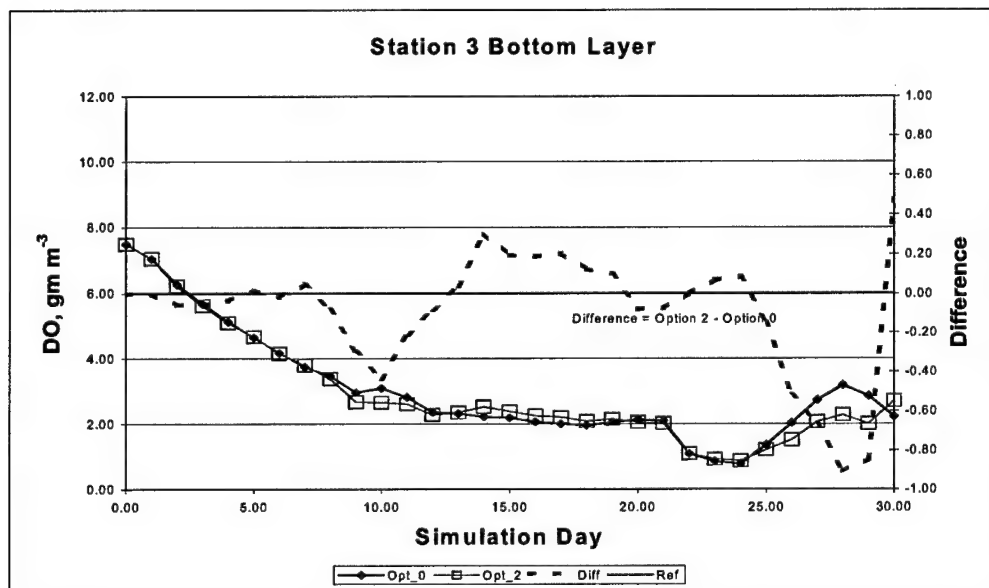


Figure 6-19. (Sheet 6 of 12)

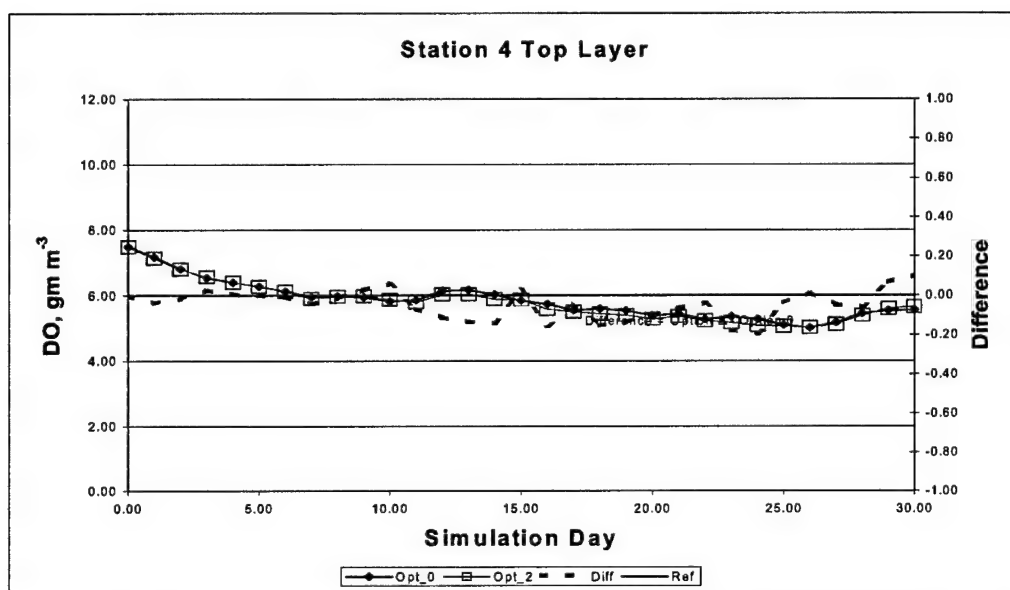


Figure 6-19. (Sheet 7 of 12)

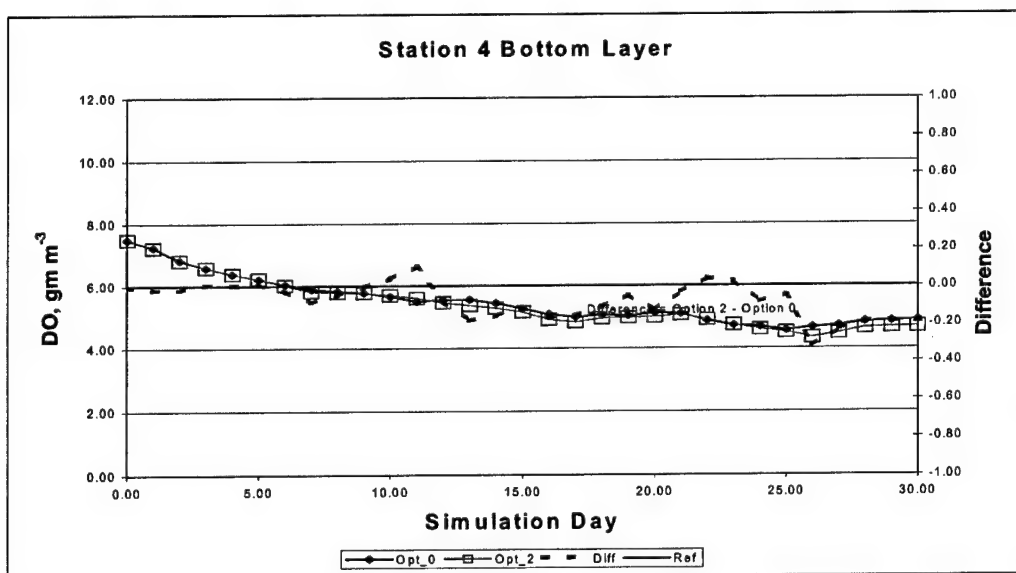


Figure 6-19. (Sheet 8 of 12)

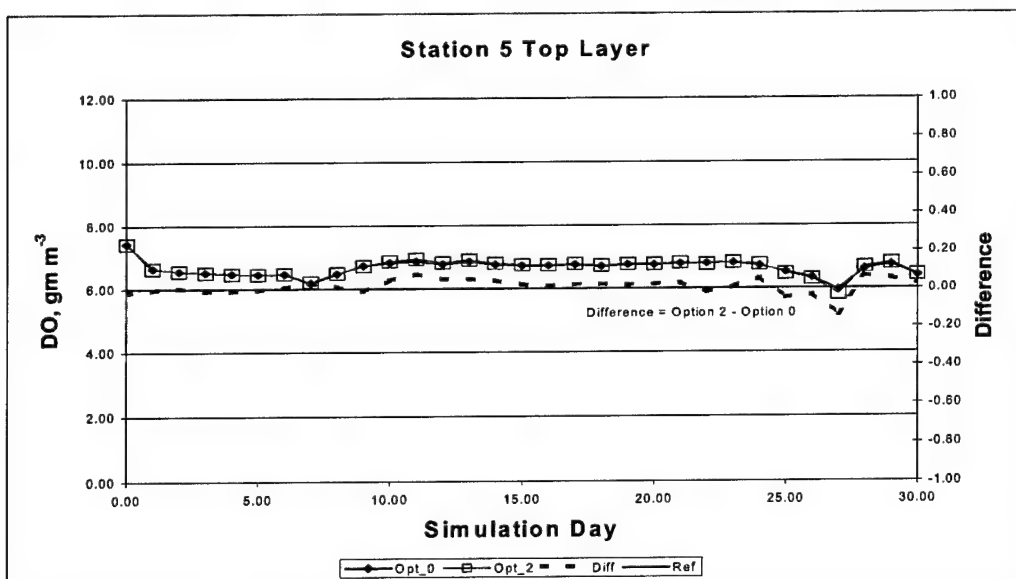


Figure 6-19. (Sheet 9 of 12)

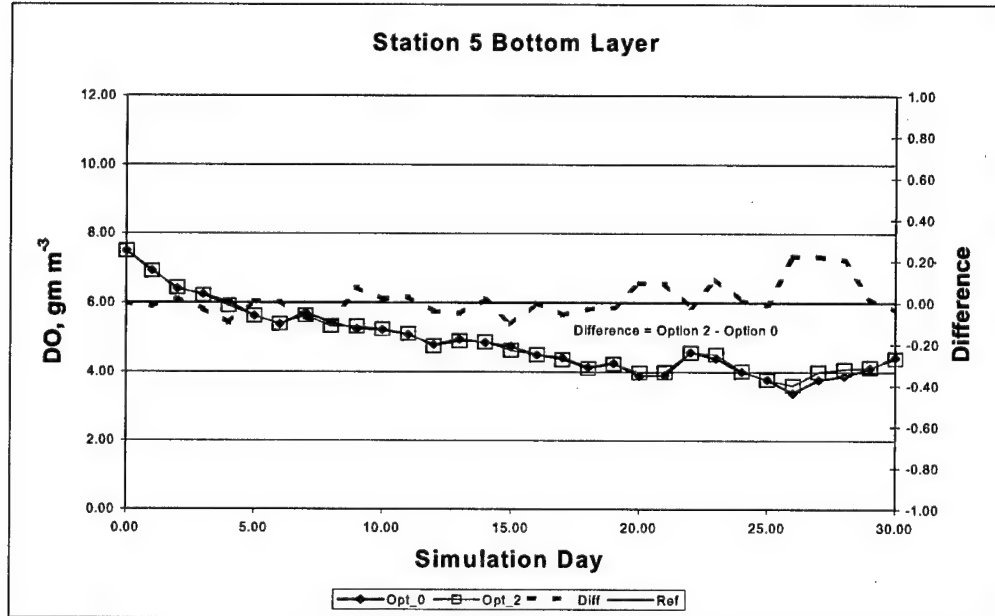


Figure 6-19. (Sheet 10 of 12)

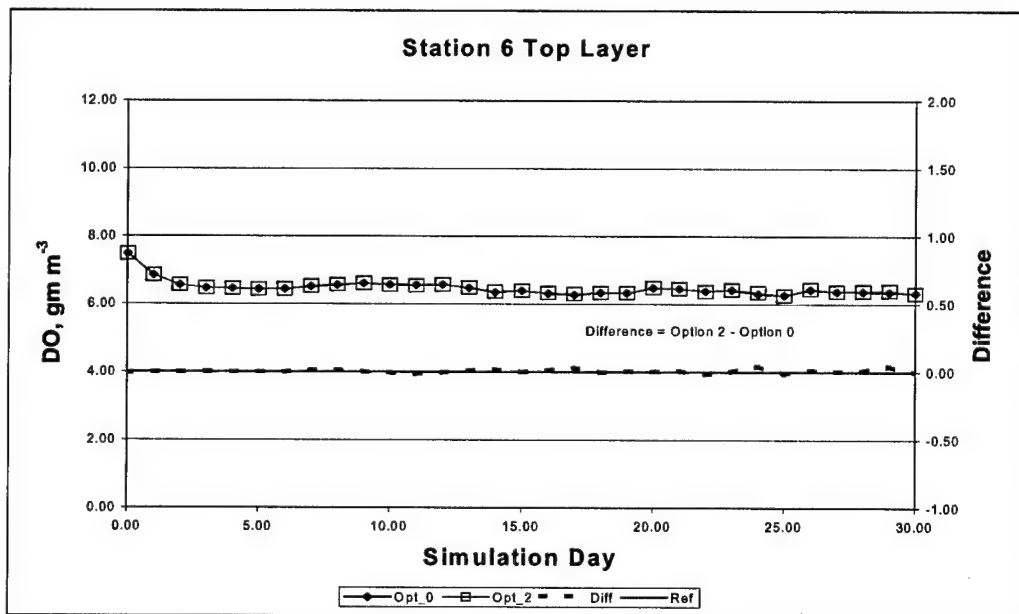


Figure 6-19. (Sheet 11 of 12)

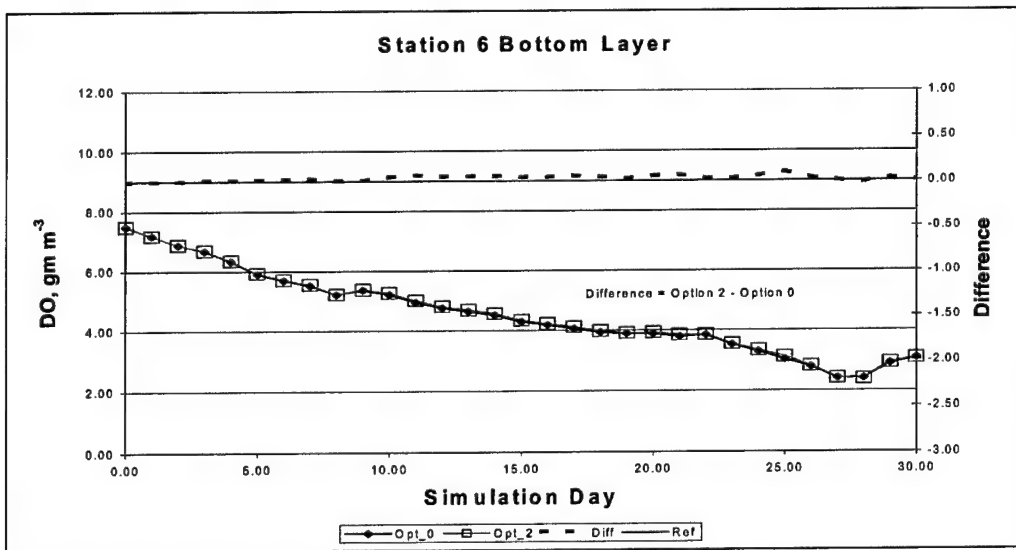


Figure 6-19. (Sheet 12 of 12)

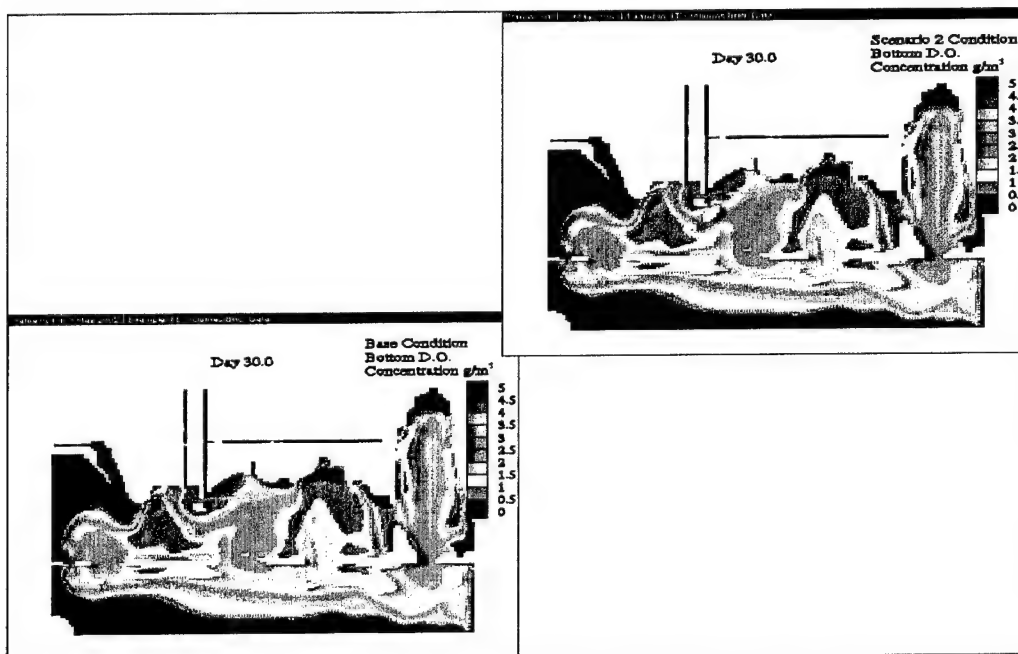


Figure 6-20. Comparison of bottom DO results for base and Alternative 1

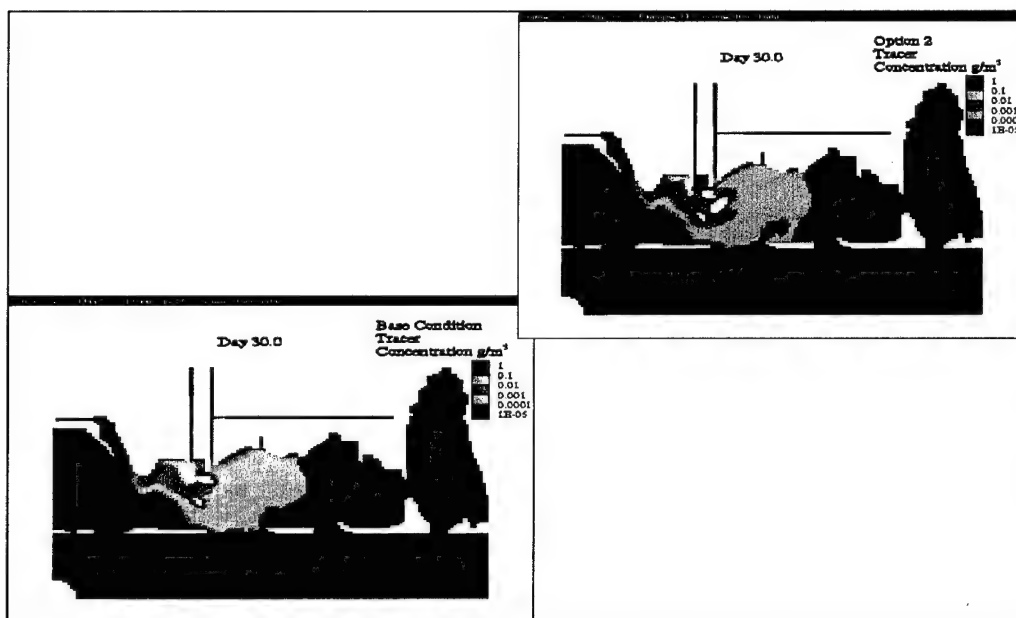


Figure 6-21. Comparison of bottom tracer results for base and Alternative 2 for West Pascagoula River release

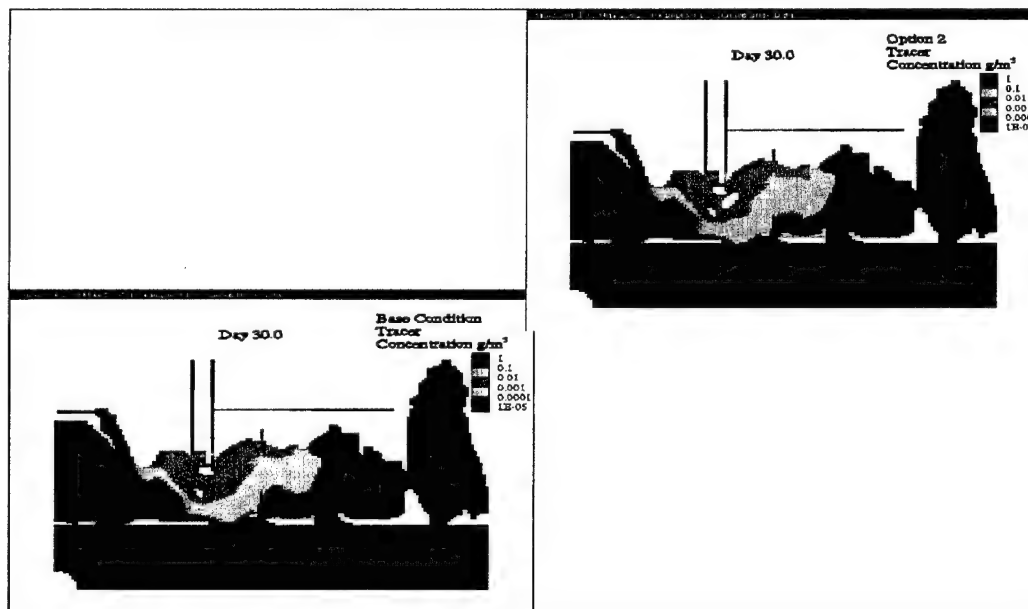


Figure 6-22. Comparison of bottom tracer results for base and Alternative 2 for East Pascagoula River release

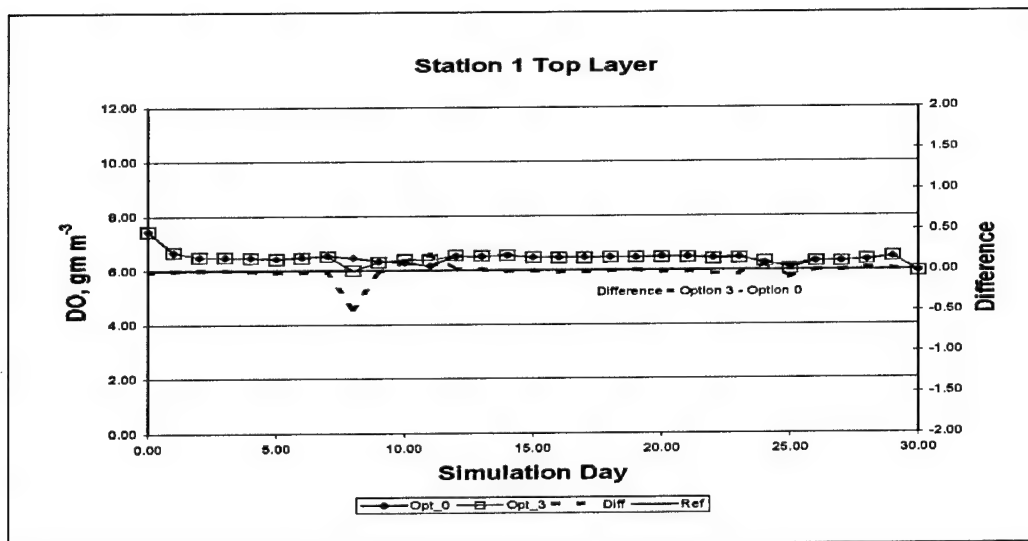


Figure 6-23. Comparison of Alternative 3 results to base results (option 0) at six stations in study area (Sheet 1 of 12)

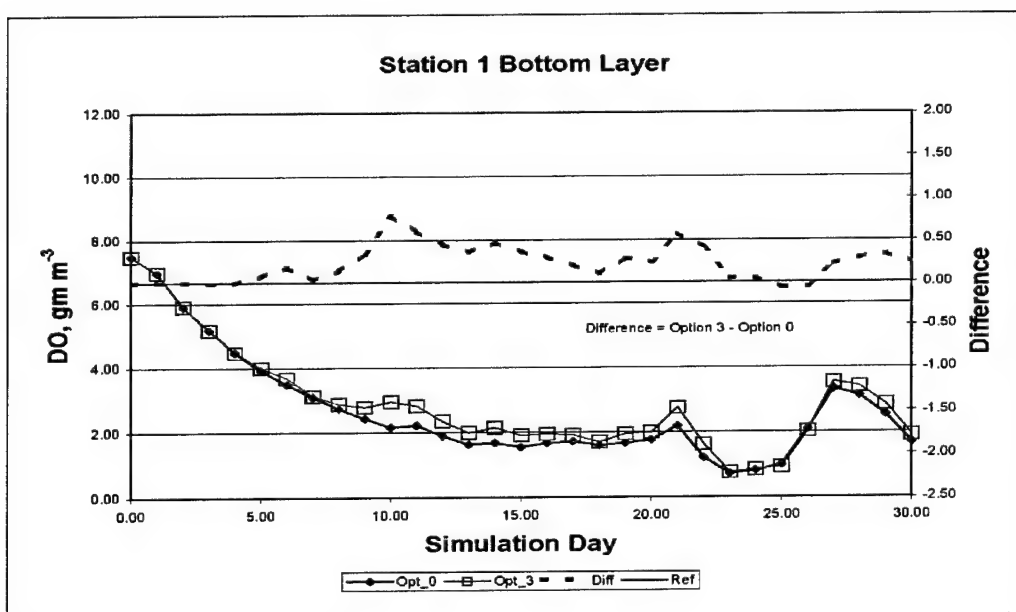


Figure 6-23. (Sheet 2 of 12)

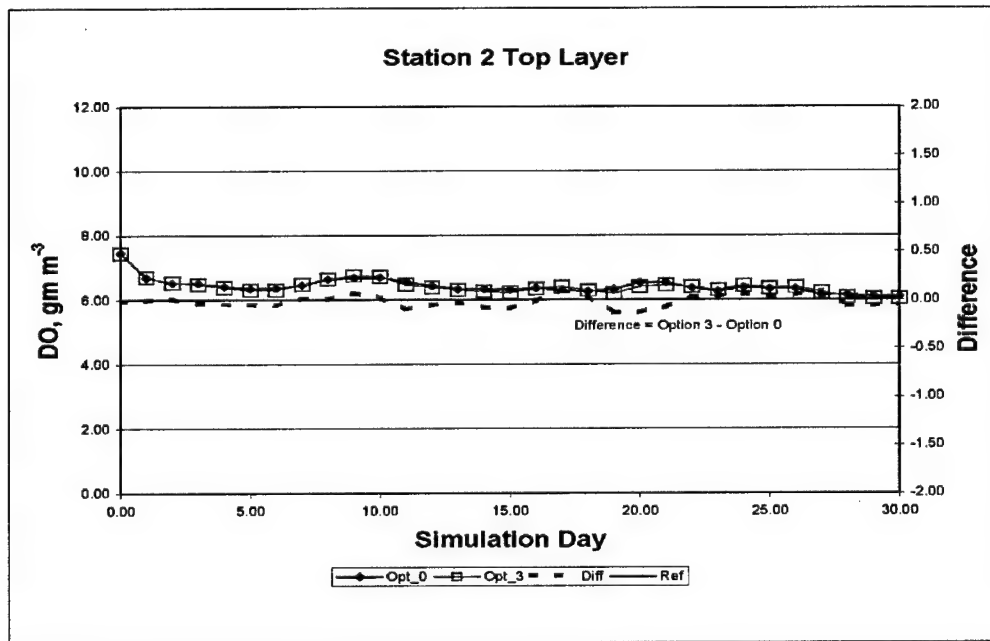


Figure 6-23. (Sheet 3 of 12)

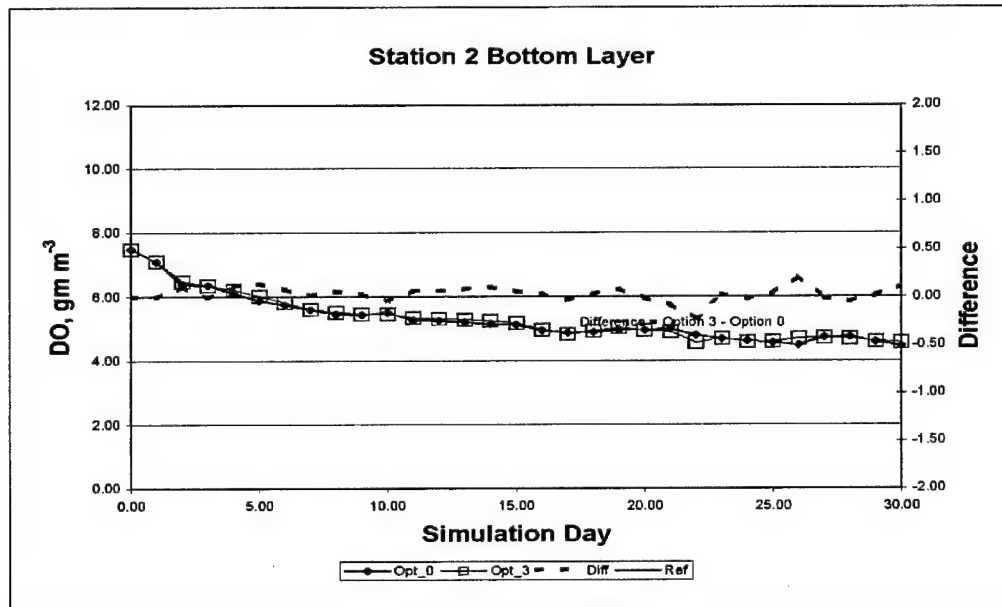


Figure 6-23. (Sheet 4 of 12)

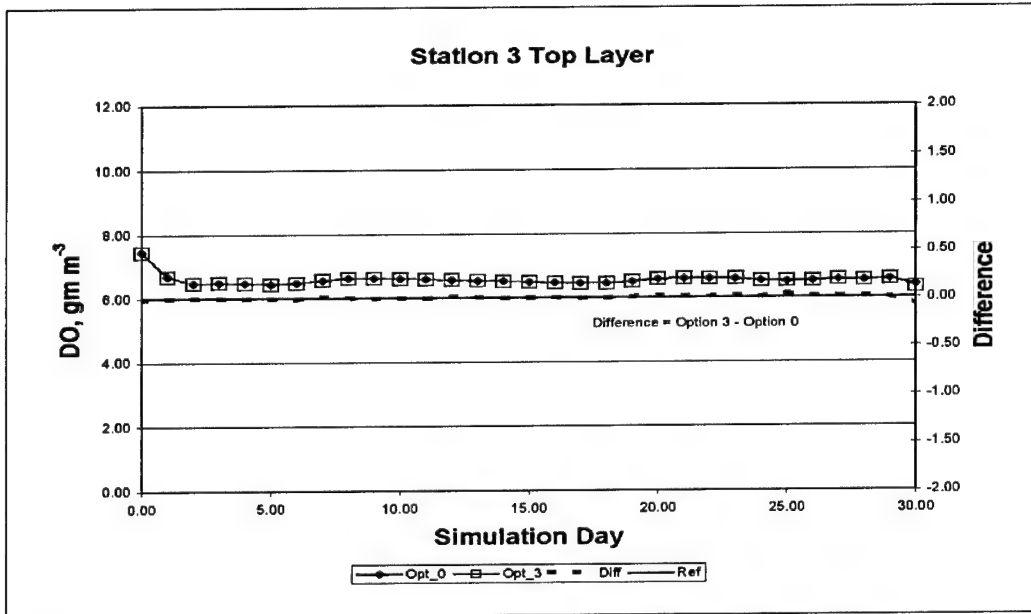


Figure 6-23. (Sheet 5 of 12)

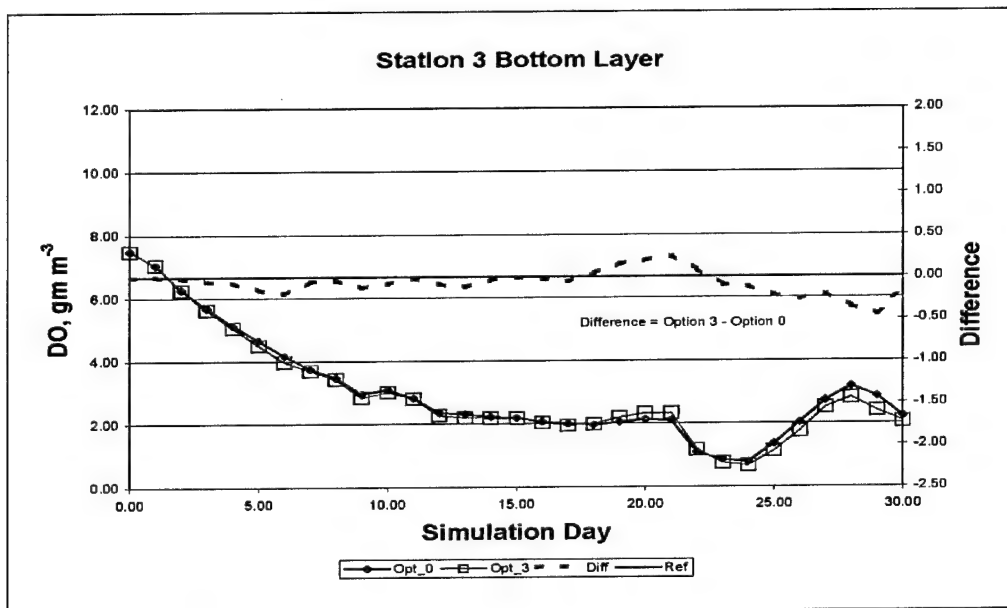


Figure 6-23. (Sheet 6 of 12)

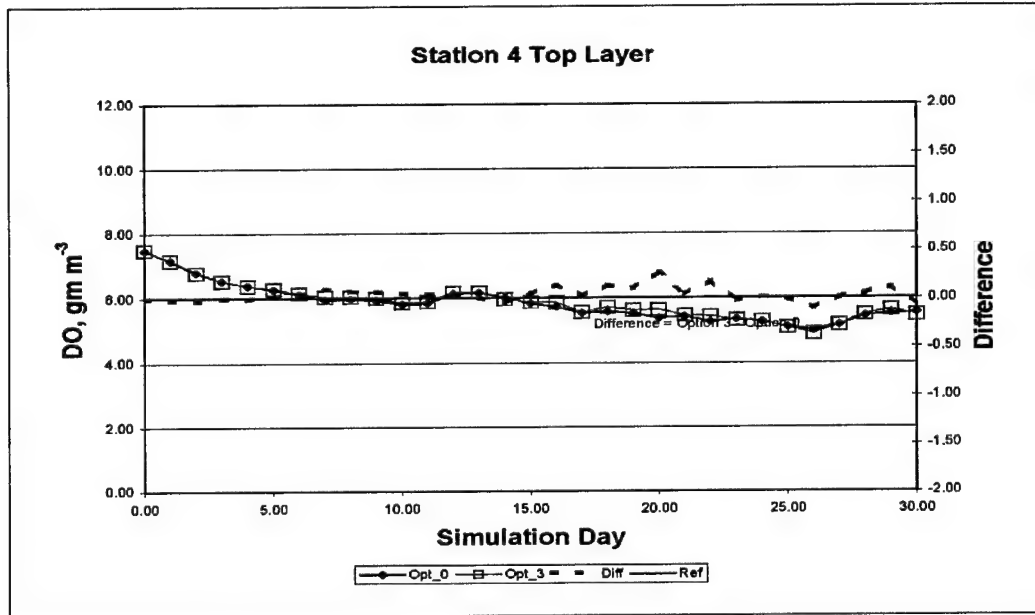


Figure 6-23. (Sheet 7 of 12)

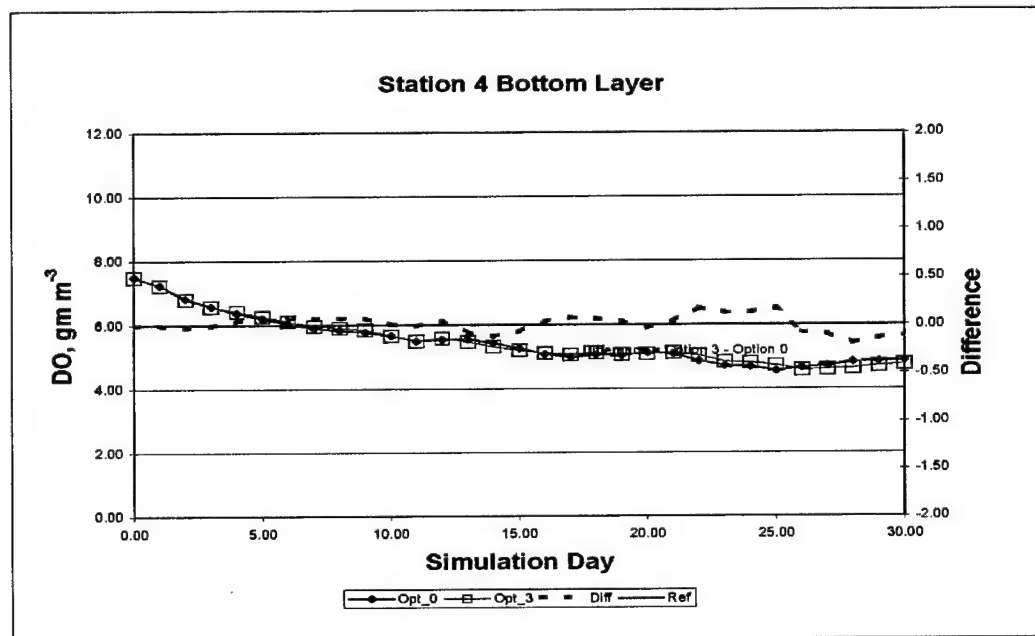


Figure 6-23. (Sheet 8 of 12)

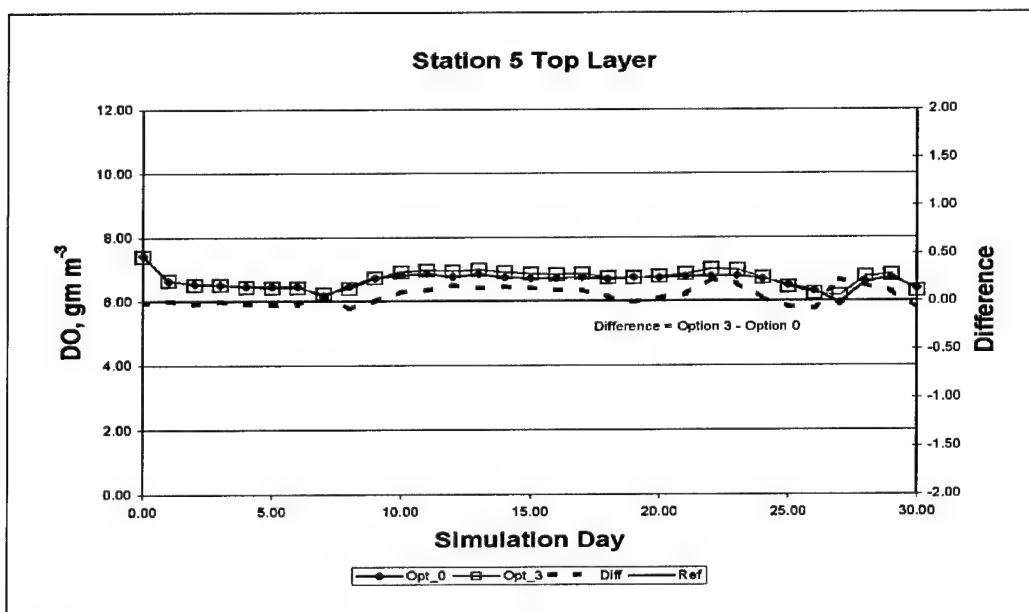


Figure 6-23. (Sheet 9 of 12)

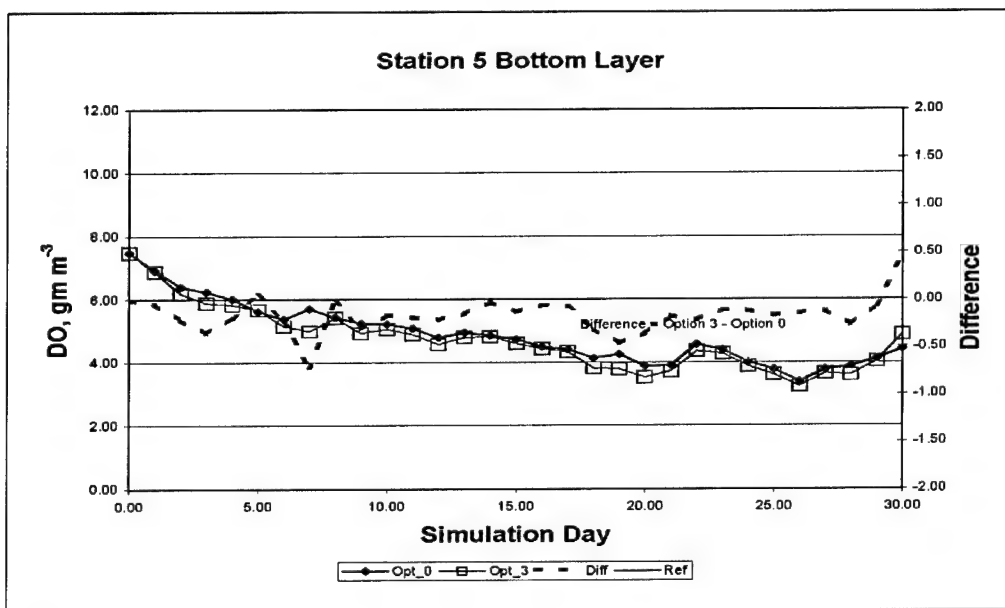


Figure 6-23. (Sheet 10 of 12)

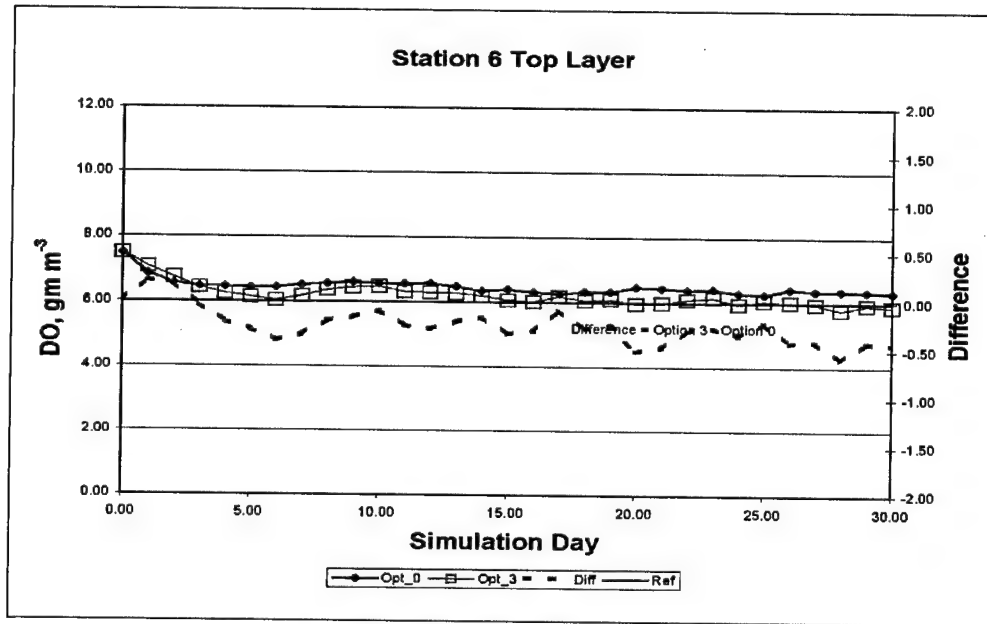


Figure 6-23. (Sheet 11 of 12)

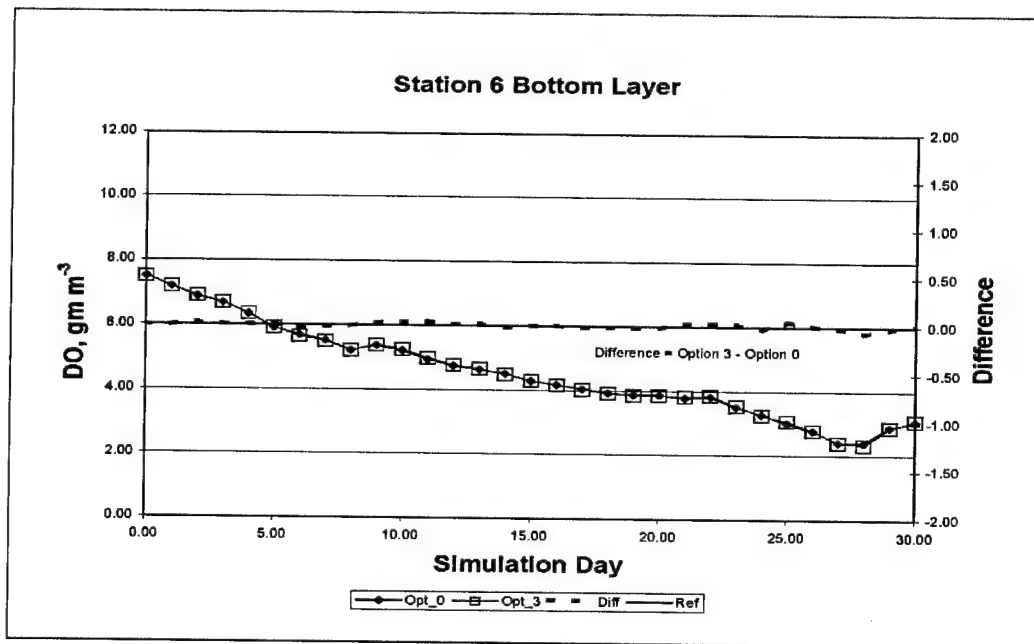


Figure 6-23. (Sheet 12 of 12)

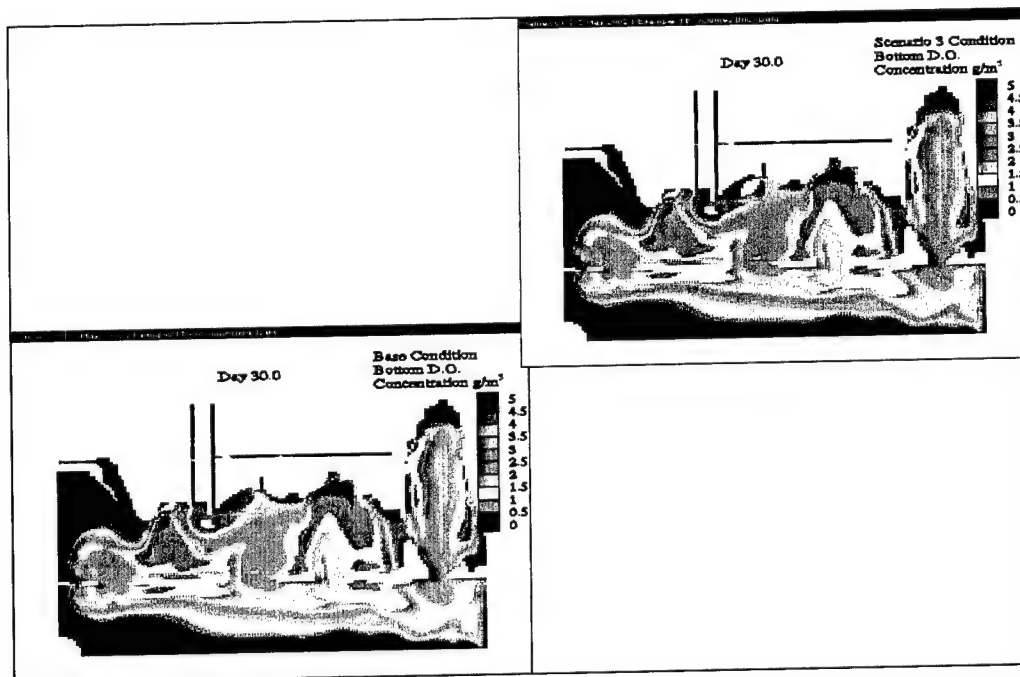


Figure 6-24. Comparison of bottom DO results for base and Alternative 3

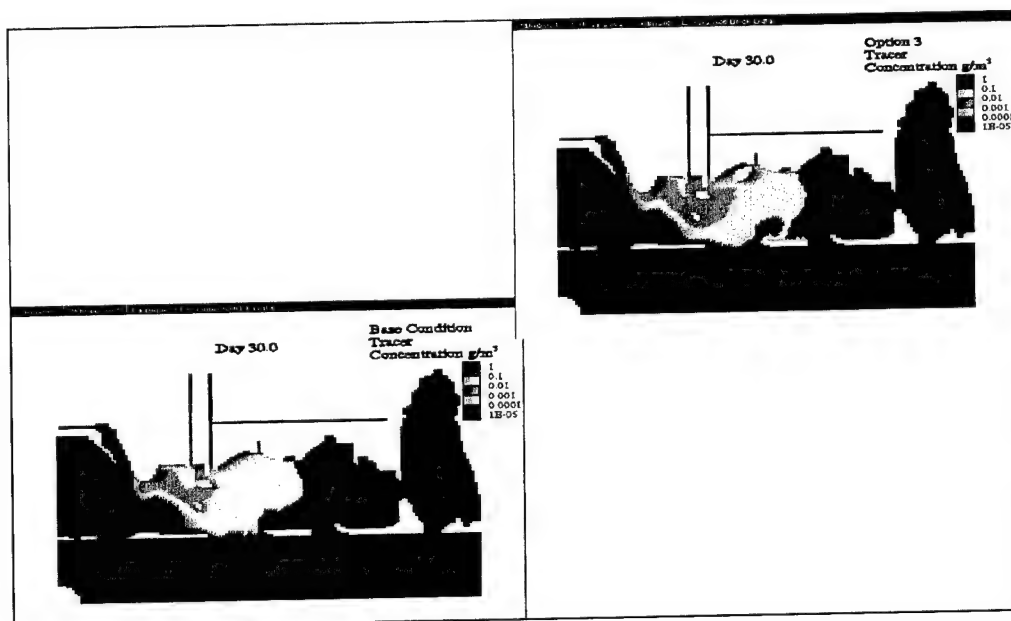


Figure 6-25. Comparison of bottom tracer results for base and Alternative 3 for West Pascagoula River release

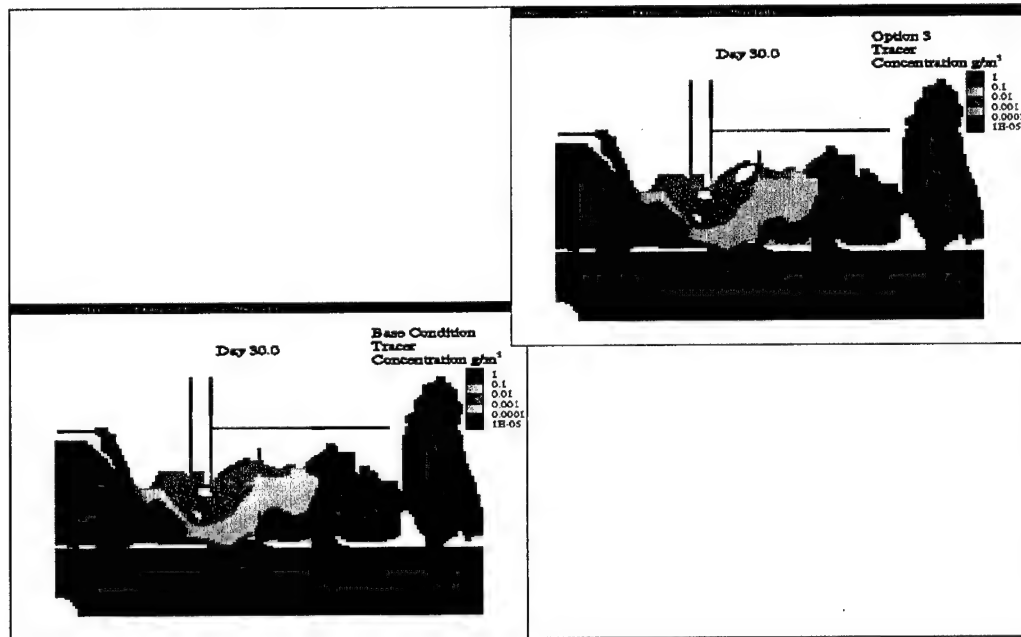


Figure 6-26. Comparison of bottom tracer results for base and Alternative 3 for East Pascagoula River release

7 Wave Modeling Studies

Site Description and Objective

A 10-year wave hindcast (1990-1999) was performed to determine existing wave conditions in the Mississippi Sound near Pascagoula, MS, as part of the study to find a suitable CDF site for disposing of dredged material. The study area is located in the northern Gulf of Mexico in the Mississippi Sound, adjacent to Pascagoula. Figure 7-1 shows a map of the study area with bathymetry contours. The area shown extends from lat. 30.17 to 30.37°N and from long. 88.48 to 88.63°W. The Mississippi Coast with the Port of Pascagoula is at the top of Figure 7-1.

To assess wave hindcast accuracy, a verification hindcast for March and April of 2001 was run to coincide with a period of field data collection at two measurement sites: one near the channel (sta MS002 in Figure 7-1) with a depth of 5.6 m and a second site on the gulf side of Petit Bois Island (sta MS001 in Figure 7-1) with a depth 6.2 m (20.34 ft). Sta MS002 is interior to the islands and adjacent to the navigation channel; MS001 captures waves that propagate from the deeper areas of the Gulf of Mexico into the project site. Details on the measurement sites can be found in Chapter 2, "Field Data Collection and Analysis." Figure 7-1 shows that project depths interior to the islands range from very shallow to about 7.5 m (24.61 ft). Figure 7-1 does not have enough resolution to show fine details of depths in the navigation channels. The quality of wind fields used in the verification hindcast are not as good as those used in the 10-year hindcast, for reasons discussed later, but they were the best available at the time.

The 10-year hindcast provides information that can be used to design an island CDF in the sound at Pascagoula, particularly a design of any shore protection constructed around the periphery of the CDF. It is expected that the degree of protection required around the periphery of a CDF would vary due to differing degrees of exposure to incident waves. A few selected wave conditions from the 10-year hindcast were used to determine if the island CDF alternatives would alter wave conditions in the adjacent navigation channels and along adjacent beaches. Alterations to wave conditions by the CDF have implications on navigability and shoreline erosion/accretion processes. The numerical wave model, WISWAVE, was used for the 10-year wave hindcast and the 2001 verification hindcast; the numerical model, STWAVE, was used to evaluate the proposed disposal options using selected wave conditions from the 10-year hindcast. This chapter discusses the wave hindcast, comparisons between hindcast wave conditions and measured data, and analysis of the various disposal

alternatives in terms of their influence on wave conditions. Wave hindcasting also included four hurricane events with stage-frequency return periods less than 20 years (maximum surge of 1.5 m (4.92 ft) and below). These hurricanes were selected to evaluate conditions at the site associated with moderate hurricanes. Hurricanes with higher waves and surge and paths directly through the area would cause significant damage. It is unlikely that a CDF would be designed to withstand the effects of a major hurricane. Hurricane wave effects are discussed in Chapter 8.

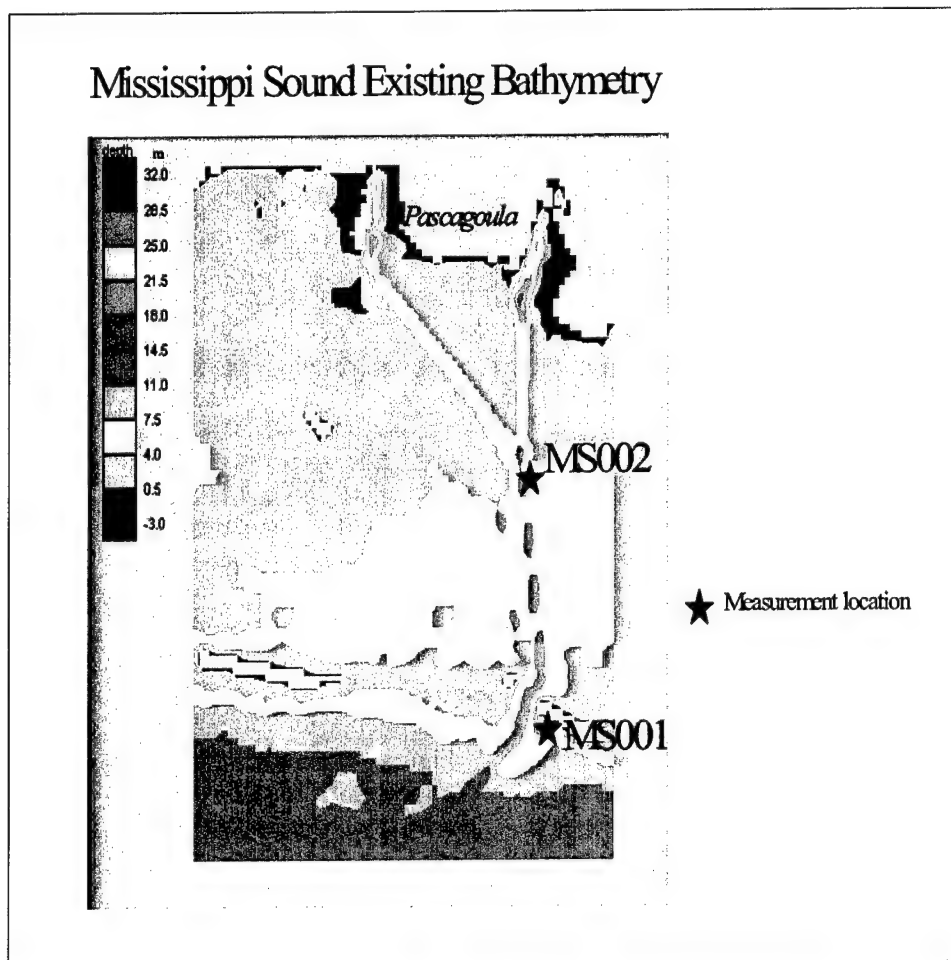


Figure 7-1. Mississippi Sound wave project area with bathymetry and nearshore measurement sites

10-Year Wave Hindcast

The Wave Information Study (WIS) has produced wave climate information for all the coastlines of the United States. The first Gulf of Mexico hindcast produced wave conditions for 1956-1975. Hurricanes during 1956-1975 were also hindcast, but in a separate study. A Gulf of Mexico hindcast including hurricanes was produced for 1976-1995. Details of these hindcasts can be found

in WIS Reports 18 and 19 (Abel et al. 1989; Hubertz and Brooks 1989). A new hindcast for 1990-1999 was done to take advantage of more wave/wind measurement locations in the Gulf of Mexico, improved wind fields, and improvements in the numerical wave hindcast model. The WIS hindcasting procedure builds upon the numerical model WISWAVE (Resio and Tracy 1983; Hubertz 1992), a second generation spectral finite depth wave model which models the physics of wave generation from a wind source function and uses a finite difference propagation scheme to propagate the wave energy on a set of rectangular grid points based on latitude and longitude. Accurate wind fields are necessary to produce an accurate wave climate.

Wind fields

The 1990-1999 wind fields were purchased from Oceanweather, Inc., in connection with the WIS mission to develop hindcasts for all the U.S. coastlines. These wind fields (0.25-deg spacing) were developed using satellite information assimilated into the NCEP wind fields (at 6-hr intervals) available from NOAA. Available measured wind data is also assimilated and blended into the final wind product. Oceanweather, Inc. also added additional information on tropical storm winds to the product. The final product for input into the wave hindcast is an hourly representation of the gulf wind fields utilizing all available information and expert meteorological analysis. The value added by Oceanweather, Inc. results in wind field products of higher quality than the wind products used in the verification hindcast.

Grid nesting

A system of five nested grids was set up to run the 10-year wave hindcast. Figure 7-2 shows the grid system. The Level 1 grid covers the Atlantic Ocean and has a spacing of 1.0 deg. Boundary information from Level 1 Atlantic is fed into the Level 2 gulf grid at the location where the gulf meets the Atlantic. The Level 1 grid is not shown in this figure. The grid that covers the entire Gulf of Mexico (Level 2 defined by blue box in Figure 7-2) has a spacing of 0.25 deg. The Level 3 grid (red box in Figure 7-2) has a spacing of 0.05 deg and covers the northern gulf area from New Orleans to Alabama. Level 4 (green box in Figure 7-2) has a spacing of 0.01 deg and extends from lat. 30.1 to 30.4°N and long. 88.1 to 88.8°W inside the Level 3 domain. The finest interior grid, Level 5 defined by the magenta box in Figure 7-2, encompasses the Mississippi Sound near Pascagoula and has a spacing of 0.002 deg. The Level 5 grid area is shown in Figure 7-1 and encompasses lat. 30.17 to 30.37°N and long. 88.48 to 88.63°W. Each grid receives boundary spectral wave information on all the water boundaries from the grid one level up. This nesting process allows high bathymetric resolution to define shallow-water wave conditions in the project site area with minimal computational effort. Wind fields are interpolated to each of these grids from the 0.25-deg wind fields from Oceanweather, Inc., described in the previous paragraph.

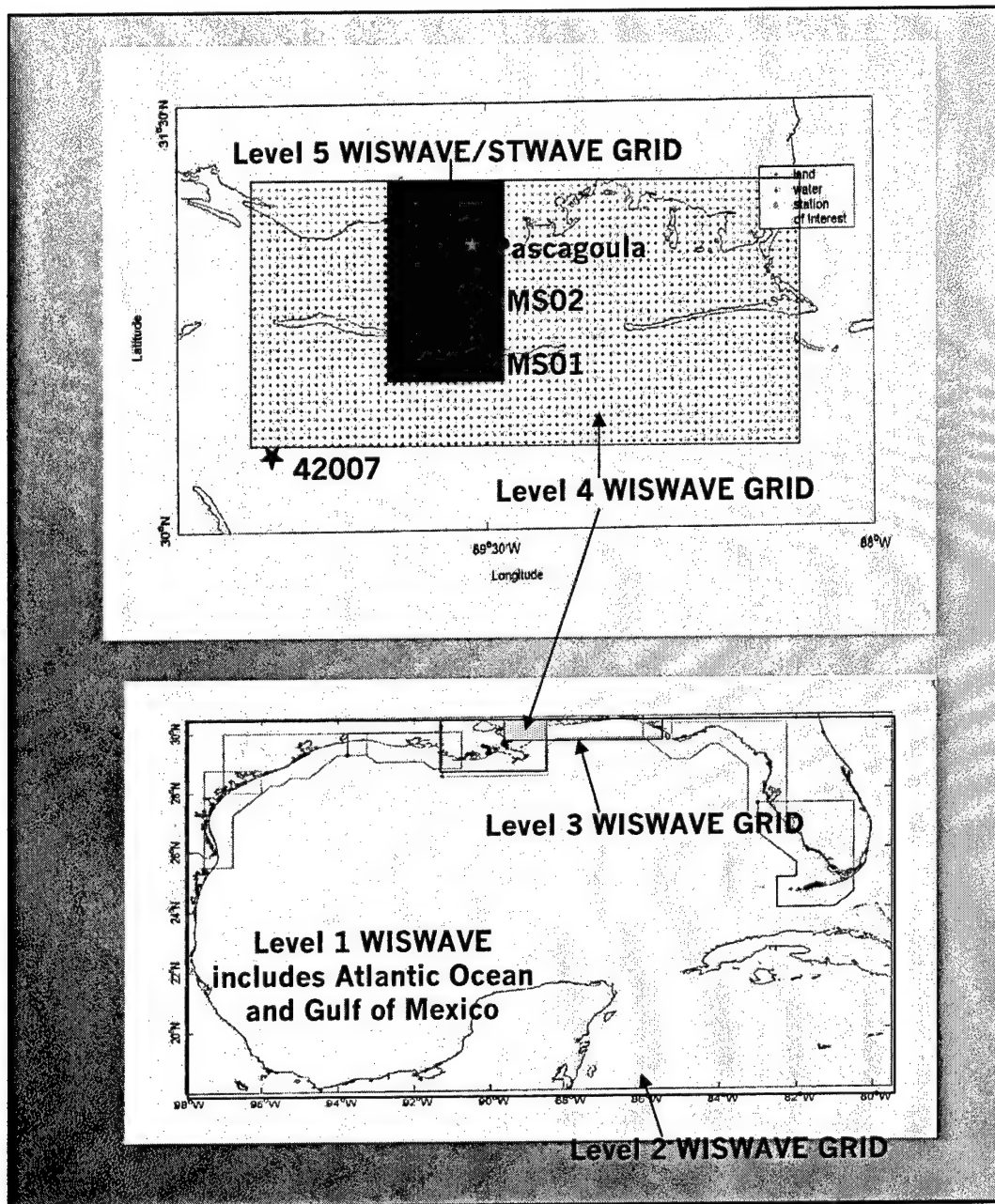


Figure 7-2. Nested grid system for Gulf of Mexico wave hindcast

Hindcast products

Several save stations with wave parameter and spectral information were located in the Level 5 grid area. Table 7-1 gives the location of the save stations for the Level 5 grid. Figure 7-3 shows a wave rose for a save location near Singing River Island in Mississippi Sound (sta 10). The hindcast wave information suggests that all the larger waves and most of the waves below 1.5 m (4.92 ft) approach from due south, through the gap between the barrier islands. The WISWAVE Level 5 hindcast procedure allows boundary energy to enter the grid from east, south, and west.

Table 7-1
Level 5 Output Save Stations

Station Number	Latitude (deg N)	Longitude (deg W)	Depth (m)
1	30.280	88.510	4
2	30.206	88.504	4
3	30.300	88.510	3
4	30.260	88.510	12
5	30.240	88.510	5
6	30.240	88.540	3
7	30.240	88.570	4
8	30.260	88.570	4
9	30.280	88.570	3
10	30.300	88.570	3
11	30.300	88.540	3
12	30.280	88.540	4
13	30.260	88.540	4
14	30.274	88.514	5

Appendix J presents tables that summarize the 1990-1999 wave information at sta 10 in the Level 5 grid. Frequency-of-occurrence tables listing information by month are available for wave height, peak period, and direction. Frequency-of-occurrence in terms of specific wave height and period bands are given for each of the direction bins and for all directions. Wind speed and wind direction occurrence tables listing information by month are also shown. Mean wave height by month including the 10-year monthly mean and the yearly mean are also included. The last table in the appendix lists the maximum wave height and associated period and direction for each of the months in the hindcast. Maximum wave and maximum wind information and overall mean wave height and peak period along with the standard deviations are listed after the last table. This information is useful for designing the CDF. Most of the significant wave activity penetrates through the gap between the barrier islands. Significant wave height exceeds 1 m (3.28 ft) only about 9 percent of the time. For the 10-year hindcast, the maximum significant wave height was approximately 1.8 m. For 60 percent of the time, significant wave height is less than 0.5 m (1.64 ft).

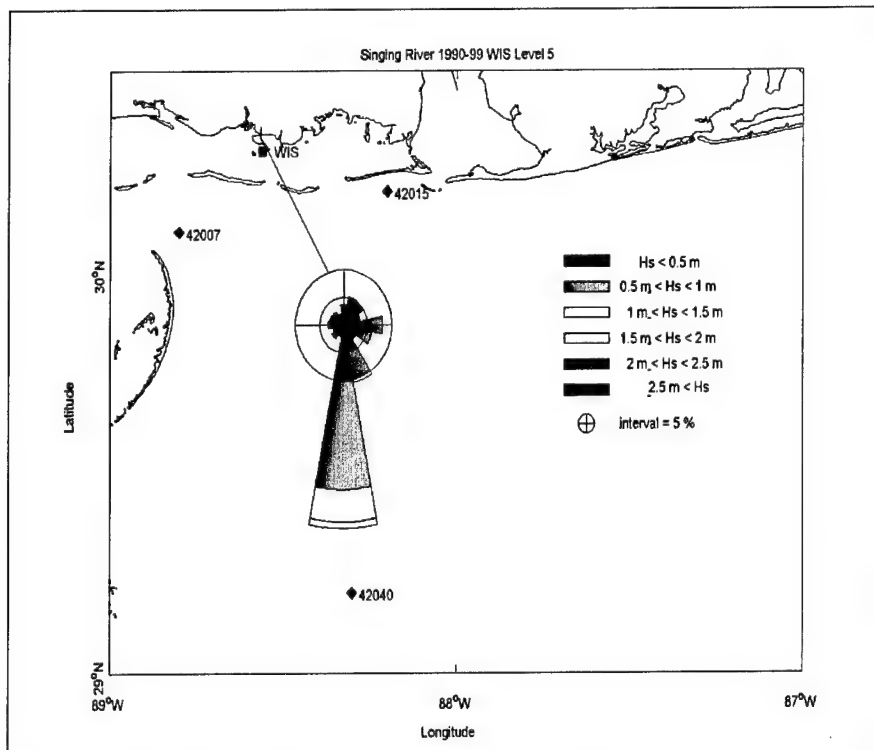


Figure 7-3. Wave rose for location southeast of Singing River Island in Mississippi Sound for 1990-1999 wave hindcast

Hindcast validation

Considerable effort was expended to assess the accuracy of the hindcast, through comparisons with measured wave data, including data acquired using shallow-water gages deployed as part of this study (see Chapter 2) and deepwater National Data Buoy Center (NDBC) buoys. Validation was assessed for arbitrarily selected months during the hindcast period, 1990-1999, when measured data were available, and for 2 months in 2001. In light of study schedules, validation using the 2001 data was restricted to the first 2 months of the data collection period.

Comparison with buoy data

No buoy information was available inside the Level 4 and Level 5 grids for the 1990-1999 hindcast period. NDBC buoy 42007 is located 22 n.m. south-southeast of Biloxi, MS, at lat. 30.09°N, long. 88.77°W, within the Level 3 domain; and data from it was used in the hindcast verification. This buoy was operational during the 1990-1999 hindcast and has directional information available. Figure 7-4 shows a wave height comparison of a coincident location from the Level 3 wave hindcast grid and buoy 42007 for January 1998. Figure 7-5 shows the peak period comparison for a Level 3 WISWAVE location and NDBC buoy 42007. Figure 7-6 shows the wave directions for the same site

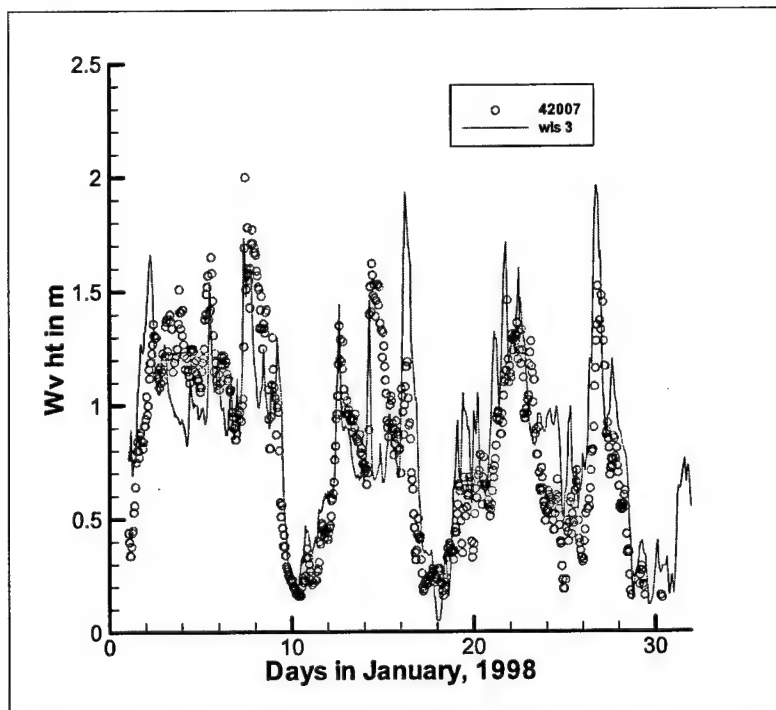


Figure 7-4. Wave height comparison at a WIS Level 3 station and NDBC buoy 42007 for January 1998

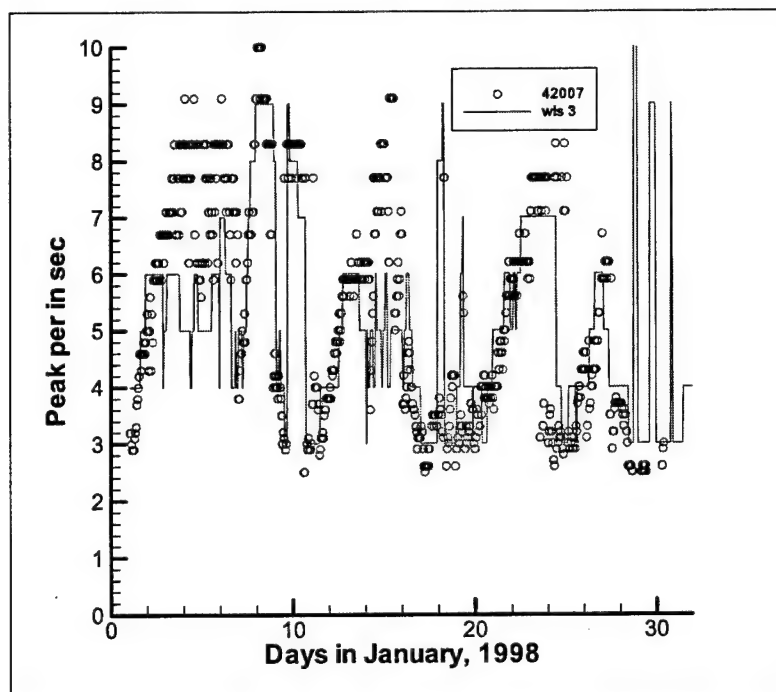


Figure 7-5. Peak period comparison of WIS Level 3 with NDBC buoy 42007 for January 1998

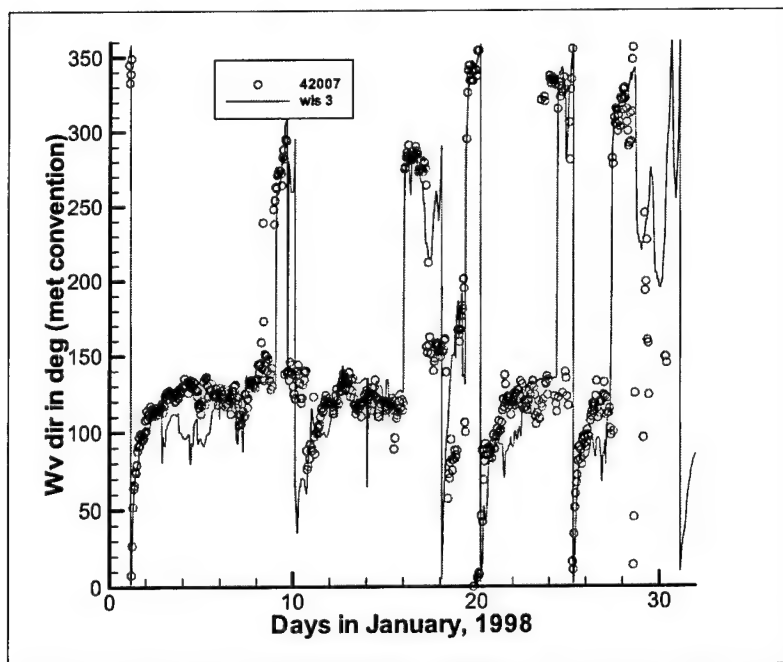


Figure 7-6. Wave direction comparison of WIS Level 3 station with NDBC buoy 42007 for January 1998

shown in Figures 7-4 and 7-5. Wave height agreement is good; modeled peak periods are generally slightly low; wave direction shows good agreement. Events are captured reasonably well in the hindcast.

NDBC buoy 42015 was operational for January-September 1990, and was also used in the verification work. Figure 7-7 shows a wave height and period comparison for February 1990 between WIS sta 65 and the buoy. WIS sta 65 is located at coordinates lat. 30.1°N, long. 88.1°W; buoy 42015 is located at coordinates lat. 30.1°N, long. 88.2°W. Significant wave height is plotted on the left-hand y-axis, and peak period is plotted on the right-hand y-axis. Wave height agreement is excellent; wave period agreement is excellent for events over 1.5 m (4.92 ft).

Comparison with nearshore wave gage data, 2001

Results from a 2001 verification hindcast were also compared with wave measurements at locations sta MS001 and MS002, shown in Figure 7-1. These two measurement sites reside inside the Level 5 grid area. See Chapter 2 for a description of the data collection effort. Both gages provide directional spectral information in addition to wave parameters. Measurements at both sta MS001 and MS002 were available for both March and April 2001 so wind field products for March and April 2001 were found to produce waves using a hindcasting procedure similar to the 10-year wave hindcast.

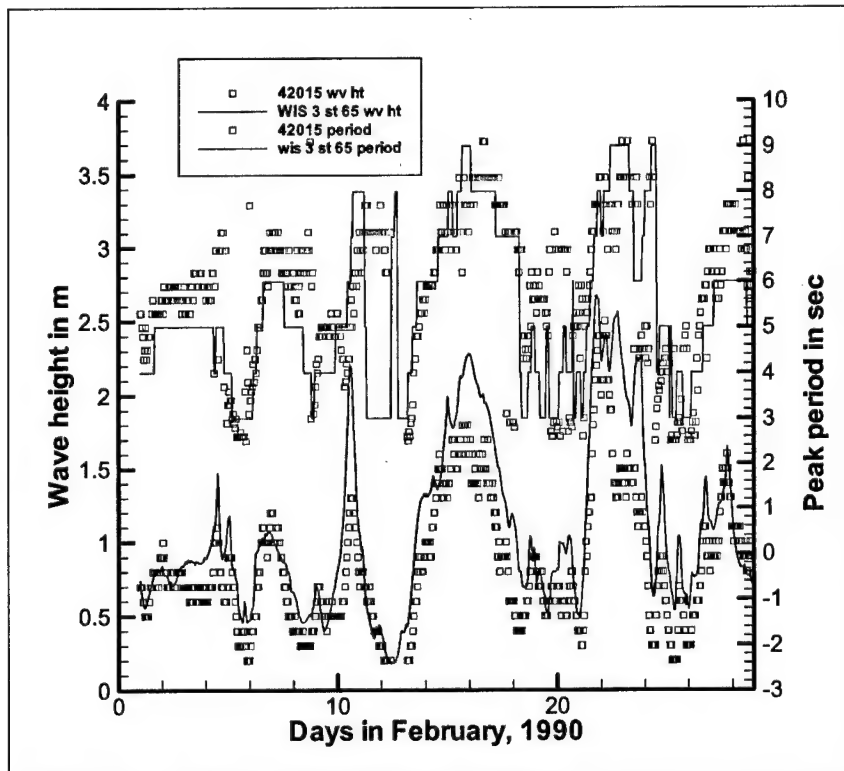


Figure 7-7. Wave height and peak period comparison between sta 65 in Level 3 grid and NDBC buoy 42015 for February of 1990

Generation of wind fields. Wind fields of high quality similar to the Oceanweather, Inc. product used for the 1990-1999 hindcast were not available for the 2001 verification hindcast. March 2001 wind fields were obtained from NCEP (6-hr intervals at 0.25-deg spacing). Buoy wind measurements using all the NOAA buoys and C-MAN stations in the gulf (sta MS001 and MS002 were not included) were blended into these NCEP wind fields. At the time of the validation hindcast, NCEP winds were not available for April 2001. Coupled Ocean/Atmosphere Mesoscale Prediction System (COAMPS) wind fields available from the Navy Research Laboratory Monterey Marine Meteorology Division with 0.2-deg spacing in 12-hr time increments were available for both March and April 2001. Buoy wind measurements were not blended into the COAMPS wind fields. This verification hindcast did not use the Level 1 Atlantic grid to produce boundary input into the gulf from the Atlantic; all other levels and procedures remained the same as the 1990-1999 hindcast. The hindcast was run using the WIS gulf hindcasting procedure with the Level 2 through Level 5 grids using the NCEP input wind field for March 2001 and a separate hindcast was run using the COAMPS wind fields for both March and April 2001.

STWAVE and WISWAVE applications to Level 5. The Level 5 grid encompasses a shallow area so the shallow-water, steady-state numerical model STWAVE (Smith, Sherlock, and Resio 2001) was also run for the Level 5 grid area using spectral boundary energy conditions from the Level 4 WISWAVE run. STWAVE uses boundary input on the south boundary, so a spectral boundary

input point directly between the islands on the southern edge of the Level 5 WISWAVE grid was selected for input into STWAVE. The STWAVE model does not include energy input from the east and west boundaries. The Level 5 WISWAVE hindcast includes boundary input from all water boundaries. A wind rose from Dauphin Island (see Figure 7-8) and the wave rose in Figure 7-3 indicate most significant wave energy is coming from the south and south-southeast so boundary input only along the southern grid boundary of STWAVE is a reasonable choice.

STWAVE is a numerical phase-averaged spectral wave model used to estimate nearshore wind-wave growth and transformation. It is a steady-state finite difference model that solves the wave action balance equation. This model is capable of using input water level information and currents but this application only used the option for boundary spectral energy input and wind input. This application used STWAVE's depth-induced wave refraction and shoaling, depth- and steepness-induced wave breaking, diffraction, wind-wave growth, wave-wave interactions, and whitecapping. STWAVE is able to simulate shallow-water processes in complex shallow-water situations.

WISWAVE contains many of these same source functions but does not include diffraction. WISWAVE is a general depth wave model and its source functions generally work best in cases where the depths are 10 m (32.81) or greater; STWAVE is better able to define situations in very shallow depths. The STWAVE wave hindcast verification runs for this study used a time series of spectra for both March and April 2001. These input spectra came from the set of boundary spectra output by the Level 4 WISWAVE grid. The STWAVE runs used the same Level 5 grid and bathymetry as the WISWAVE run.

Verification results for 2001. Figures 7-9 and 7-10 show a comparison between significant wave height and peak period from STWAVE and WISWAVE (Coamps winds) and the measurements at sta MS002 for April 2001. WISWAVE results are shown in red and STWAVE results are shown in green. Measurements are indicated by blue triangles. All comparison spectra at sta MS001 and MS002 were plotted to verify that spectral analysis techniques produced reasonable spectra. Some of the measured spectra showed high frequency tails with rapidly increasing energy with increasing frequency. This is most likely due to limitations in resolving high-frequency wave energy, and this situation produces artificially high wave heights and gives a false estimation of the peak wave period. These suspect measured spectra were eliminated from the comparison plot and not used in the comparisons and statistics. WISWAVE wave height results tend to follow the measurements except for an event around 18 April. This event must have been a locally generated wind event not well represented in the wind fields, and it is not evident in sta MS001 measurements. The wind fields may not have the temporal resolution required to capture short-duration locally-generated wave events. Period results for WISWAVE and STWAVE are consistent but the measurements show much lower peak period conditions. It is possible that multiple wave trains are captured in the measurements, but the high frequency seems to dominate in the measurements. In general, peak wave heights for the various events are simulated fairly well, some are slightly overpredicted and some are slightly underpredicted.

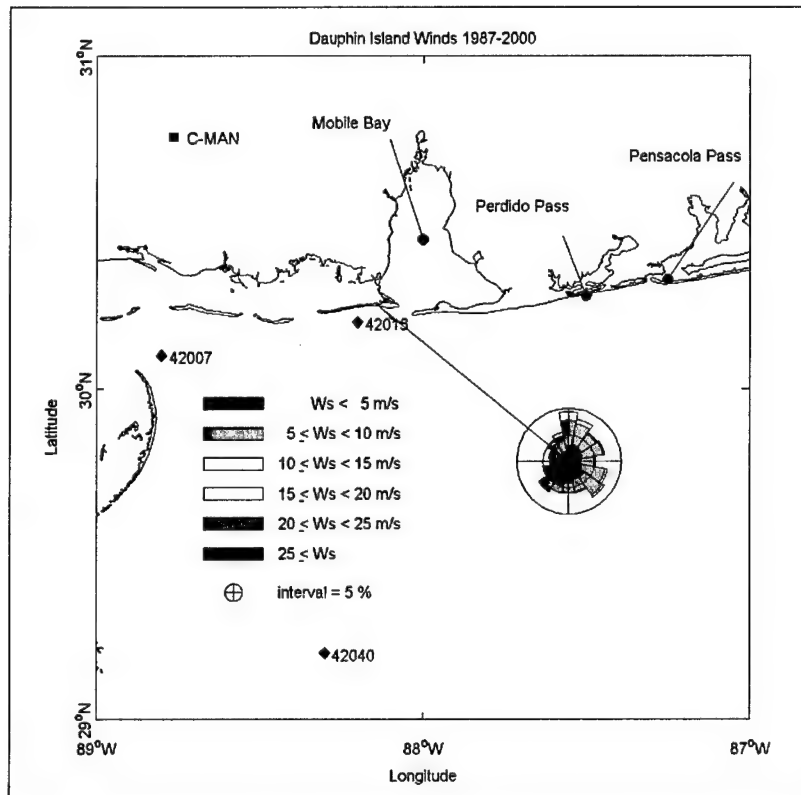


Figure 7-8. Wind rose showing wind speeds and directions from 1987-2000 at Dauphin Island

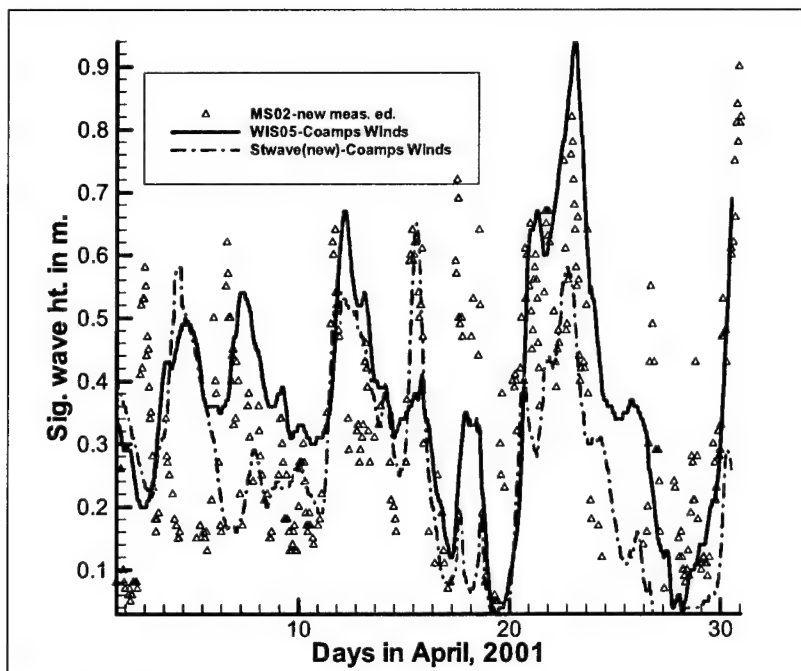


Figure 7-9. Comparison of WISWAVE and STWAVE wave heights with measurements at sta MS002 for April 2001

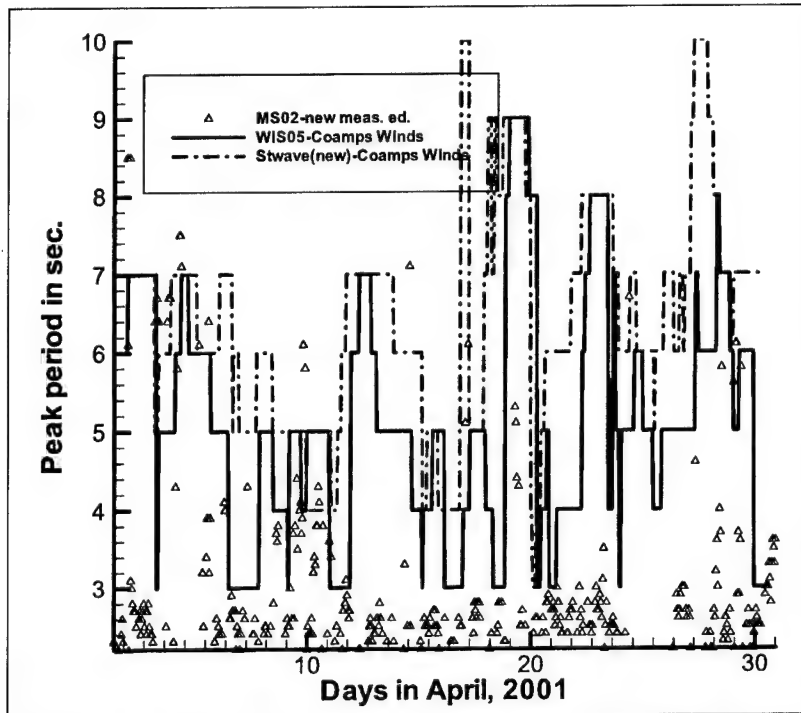


Figure 7-10. Comparison of WISWAVE and STWAVE peak periods with sta MS002 measurements for April 2001

Figures 7-11 and 7-12 show March wave height and peak period comparisons at sta MS002 (includes WISWAVE and STWAVE results). For March, in the sound, the hindcast produces peaks in wave height that are generally less than the measurements. Measured periods are also mostly less than 3 sec; modeled peak periods are often higher, in the range of 6 to 9 sec. Figures 7-13 through 7-15 show comparisons between Level 3 WISWAVE and NDBC buoy 42007 for the same period of time, March 2001. Heights, periods, and direction are reasonably well predicted by the hindcast model at buoy 42007, which is in the Gulf of Mexico. The model does miss the peak wave height around 13 March. Other peaks are simulated well. The largest wave events, those characterized by peak wave heights that exceed 1.5 m (4.92 ft), are associated with waves from the southeast. These waves would be expected to penetrate through the gap in the barrier islands. At buoy 42007 these event peaks are characterized by peak wave periods of 5 to 10 sec. Simulated peak wave periods at buoy 42007 and at sta MS002 are often between 5 and 10 sec. It is unclear why the sta MS002 measurements show peak periods of less than 3 sec much of the time. Figures 7-16 through 7-18 show Level 5 WISWAVE height, peak period, and direction comparisons with data from sta MS001. Comparisons look good except for what looks like a local wind event on 15 March that was missed in the hindcast. Simulated wave heights inside the sound may also be sensitive to the accuracy of wave direction simulated outside the barrier islands. Use of WISWAVE for Level 5 appeared to produce more accurate wave height information inside the sound. It also treats wave energy input from the east and west inside the sound, unlike STWAVE. Therefore, WISWAVE was used in the 10-year Level 5 hindcast.

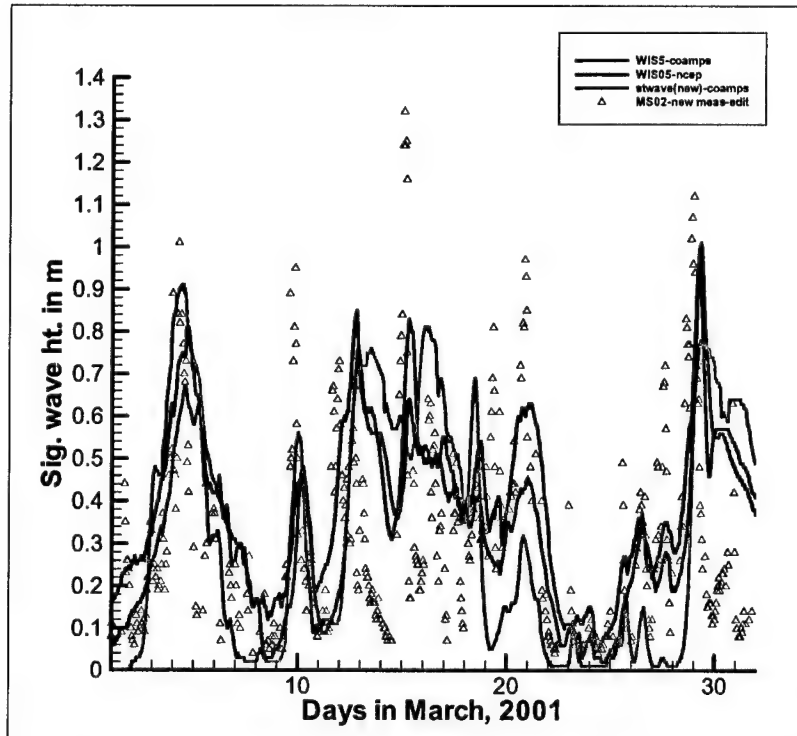


Figure 7-11. Comparison of WISWAVE and STWAVE wave height with sta MS002 measurements for March 2001

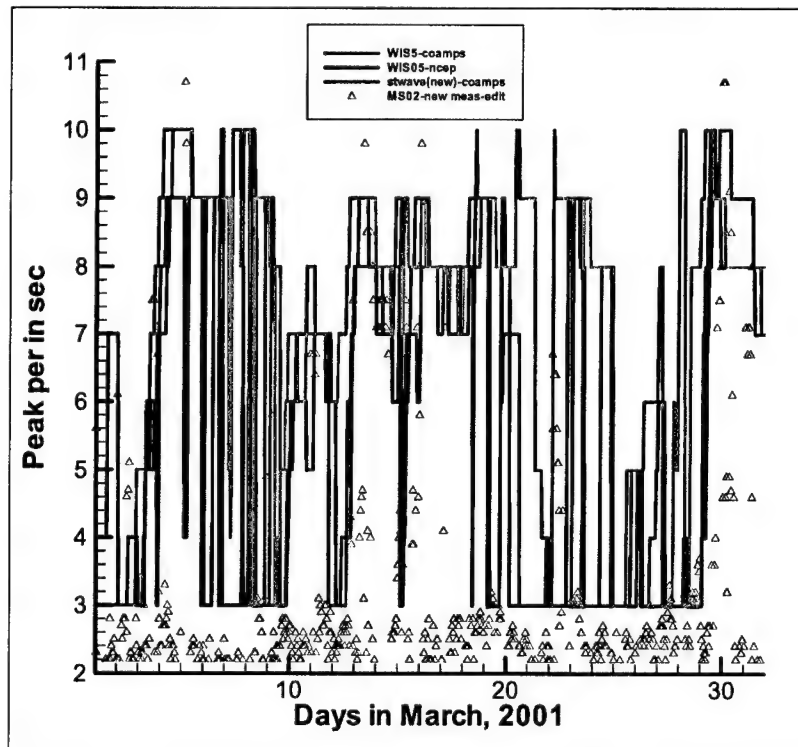


Figure 7-12. Comparison of simulated and measured peak periods for March 2001 at sta MS002, showing WISWAVE results using both Coamps and NCEP winds and STWAVE with Coamps winds

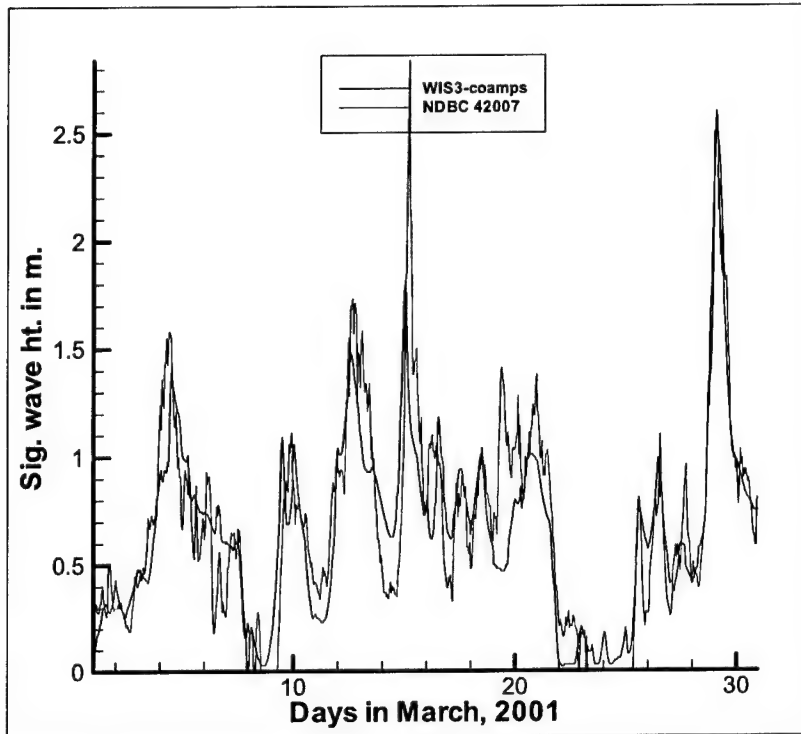


Figure 7-13. Comparison of WISWAVE wave height with NDBC buoy 42007 wave height for March 2001

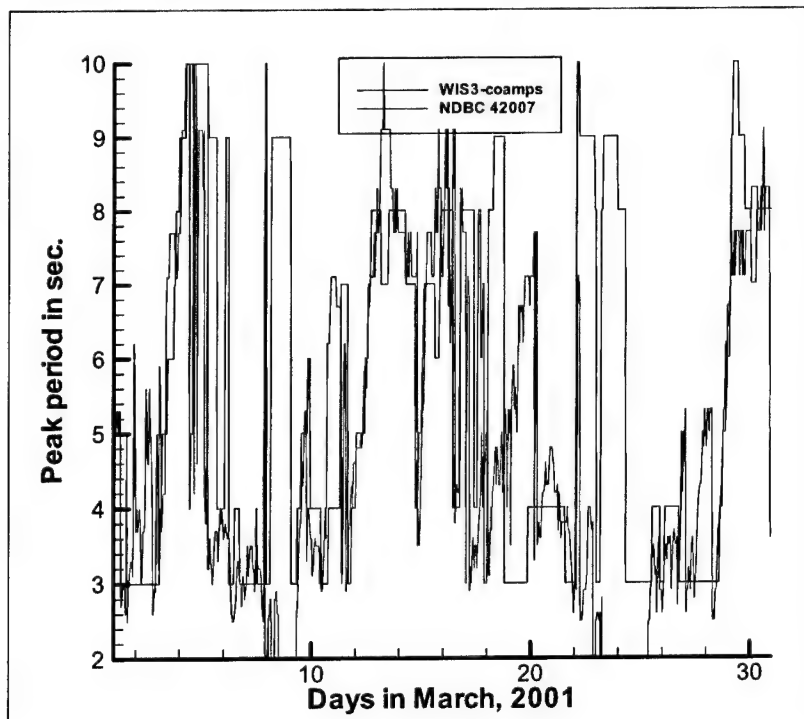


Figure 7-14. Comparison of WISWAVE peak period with NDBC buoy 42007 peak period for March 2001

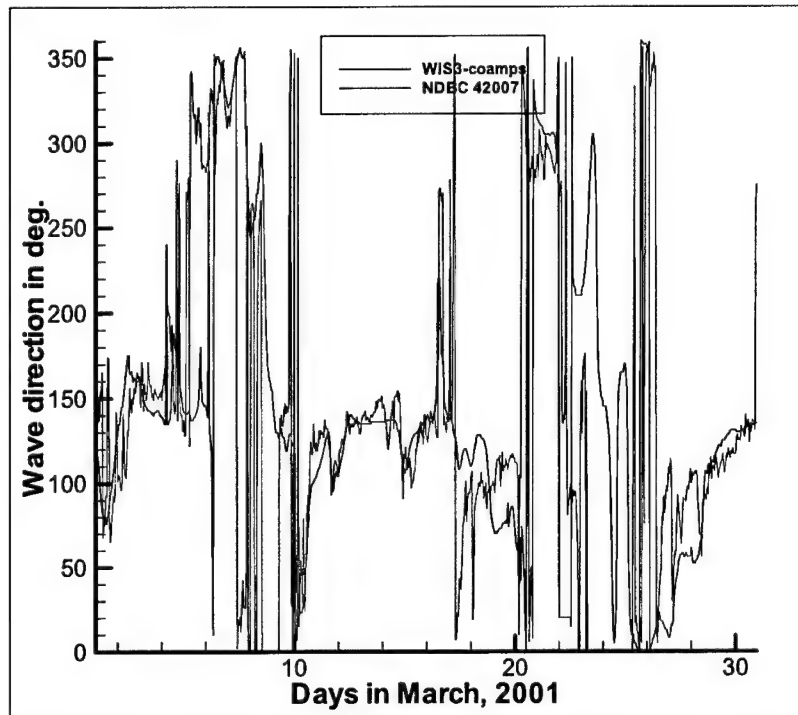


Figure 7-15. Comparison of WISWAVE wave direction with NDBC buoy 42007 wave direction for March 2001

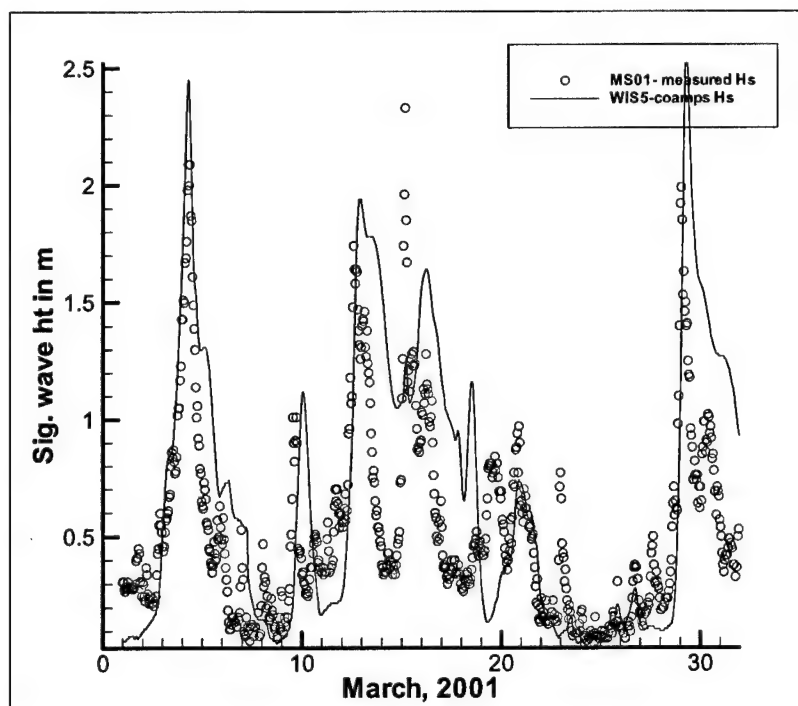


Figure 7-16. Comparison of WISWAVE wave height and measured wave height at sta MS001 for March 2001

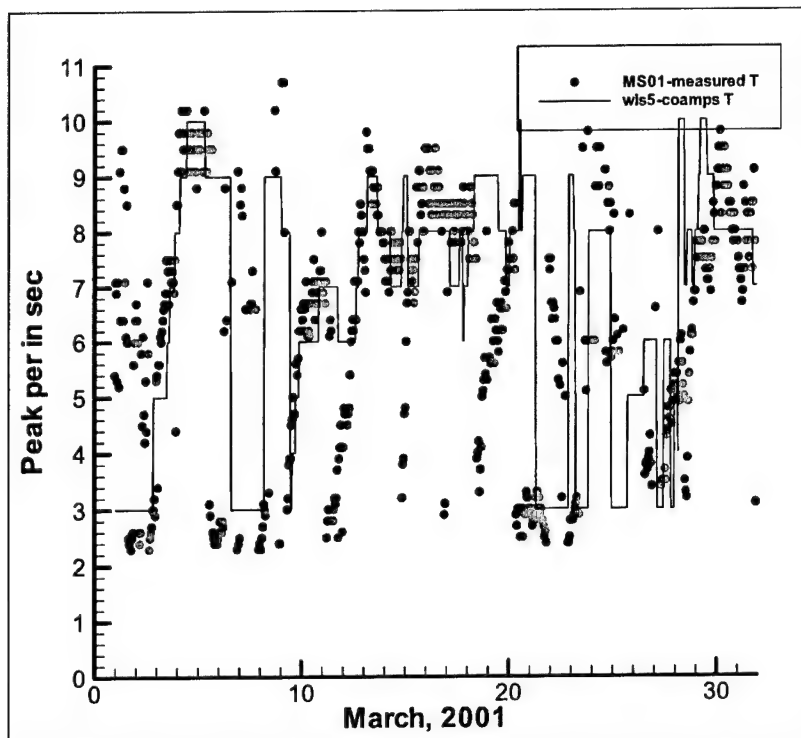


Figure 7-17. Comparison of WISWAVE peak period with measured peak period at sta MS001 for March 2001

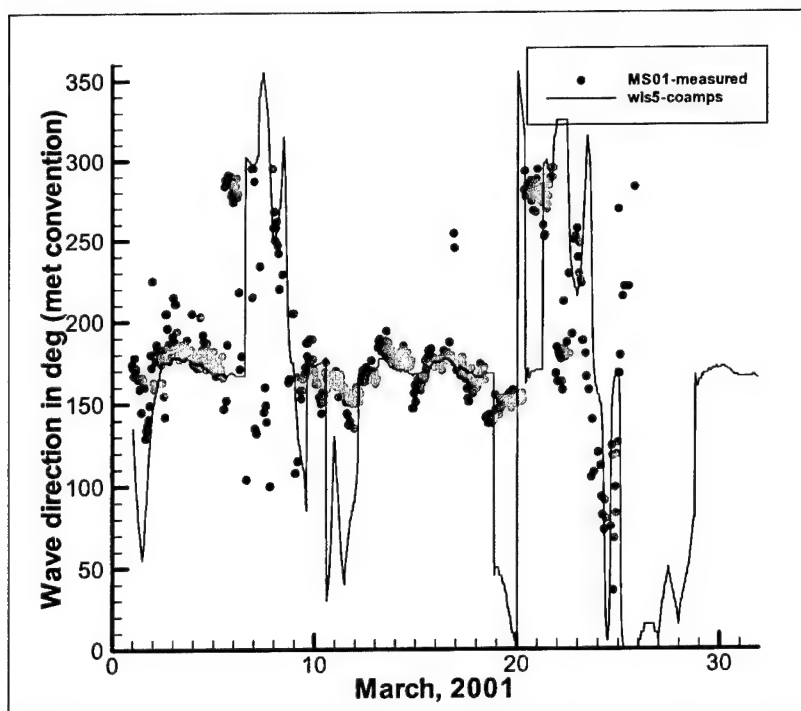


Figure 7-18. WISWAVE wave direction compared to measured wave direction at sta MS001 for March 2001

CDF Influences on Wave Conditions

Ten years of wave parameter data at the same location near sta MS001 (see Figure 7-1) outside the barrier islands on the gulf side of the Level 5 WISWAVE grid were used to select a set of representative and storm wave conditions. Most significant wave energy at the CDF sites appears to originate in the Gulf of Mexico and propagate into the sound through the gap in the barrier islands. Since propagation, and the impact of the CDF on wave propagation was a concern, STWAVE was selected for the analysis. Wave energy from the east and west was not considered. The set of representative wave conditions were simulated with STWAVE for the Level 5 grid area for the existing situation and three island CDFs.

Selection of representative wave conditions

Figures 7-19 through 7-27 show a series of plots showing all wave events from the 1990-1999 WISWAVE hindcast coming from within ± 45 deg of due south (due south comes from a wave direction of 180 deg). Wave direction is measured in meteorological convention with zero degrees corresponding to waves coming from the north and 90 deg corresponding to waves coming from due east. Each plot represents frequency of wave height and period conditions for a 10-deg direction window. The x-axes identify wave period bands and the y-axis is number of wave events. Different colored bars indicate the wave height categories. The direction band from 165 to 174 deg (waves approaching from just east of south) is the most prevalent, with direction windows 155-164 deg and 175-184 deg also being significant.

Representative wave conditions used in the STWAVE simulations with the existing-condition case and the various CDF alternatives are shown in Table 7-2. These conditions were selected from information in Figures 7-19 – 7-27 and an analysis of the most prevalent and storm conditions at each of these direction bands. Table 7-2 presents the frequency of each representative wave condition as a percentage of the total waves at this location, as a percentage of waves within ± 45 deg of due south, and as a percentage of waves in the 10-deg band. The date column gives the month and year of the condition; the last column in Table 7-2 describes the condition as either a storm situation or a most-prevalent condition. Boundary spectra at a location between the two islands on the south edge of the Level 5 area shown in Figure 7-1 were archived for each of these conditions and used as input to STWAVE along with the wind speed and direction at that point and time.

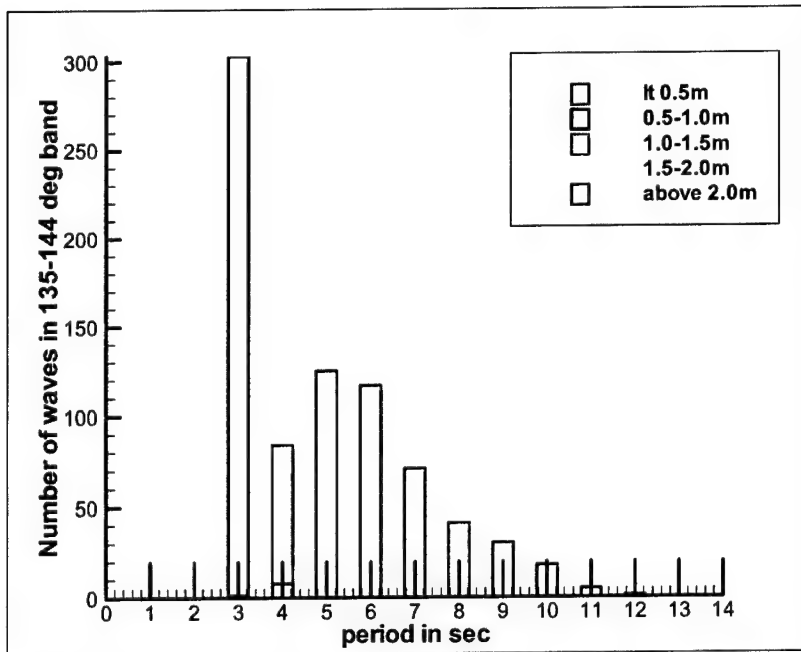


Figure 7-19. Bar chart showing incident wave height and period characteristics, direction window from 135 to 144 deg

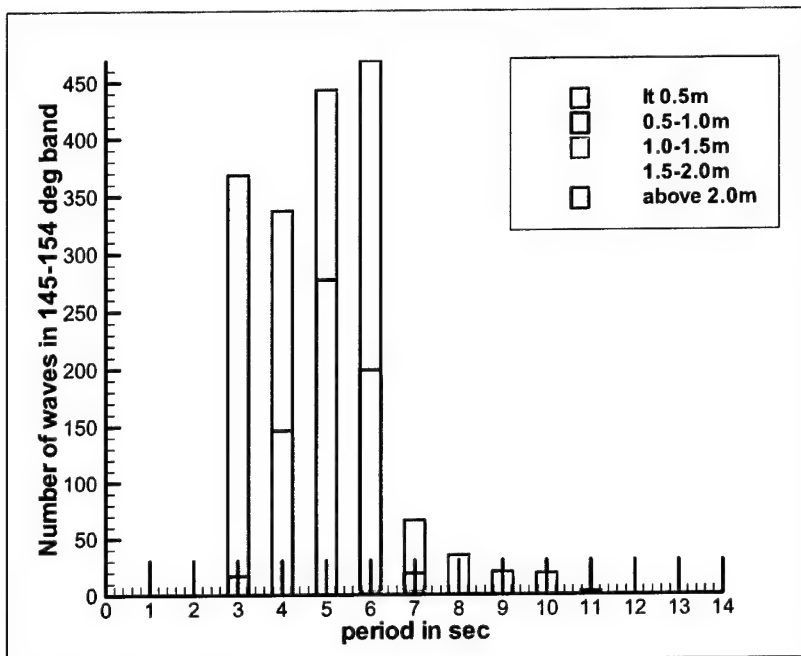


Figure 7-20. Bar chart showing incident wave height and period characteristics, direction window from 145 to 154 deg

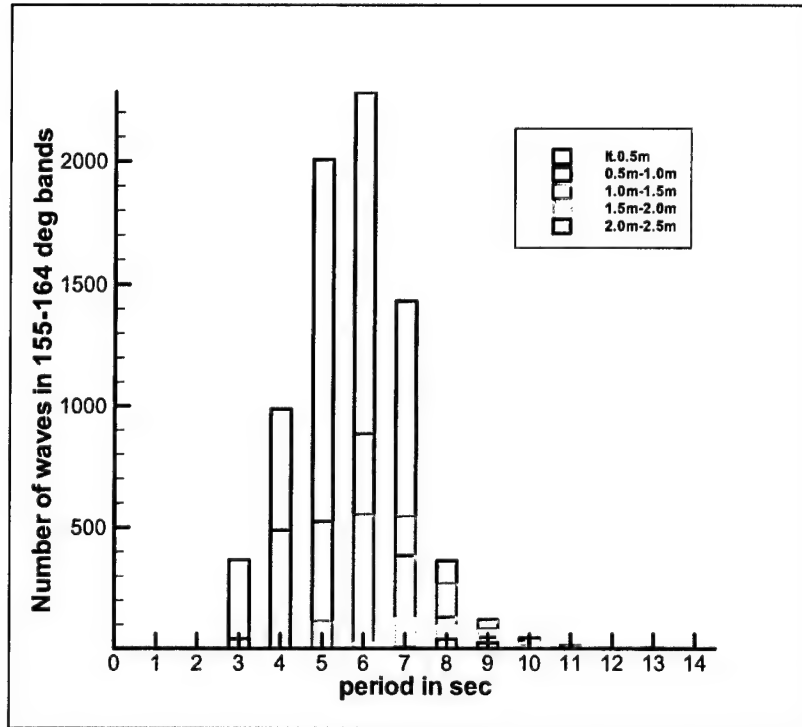


Figure 7-21. Bar chart showing incident wave height and period characteristics, direction window from 155 to 164 deg

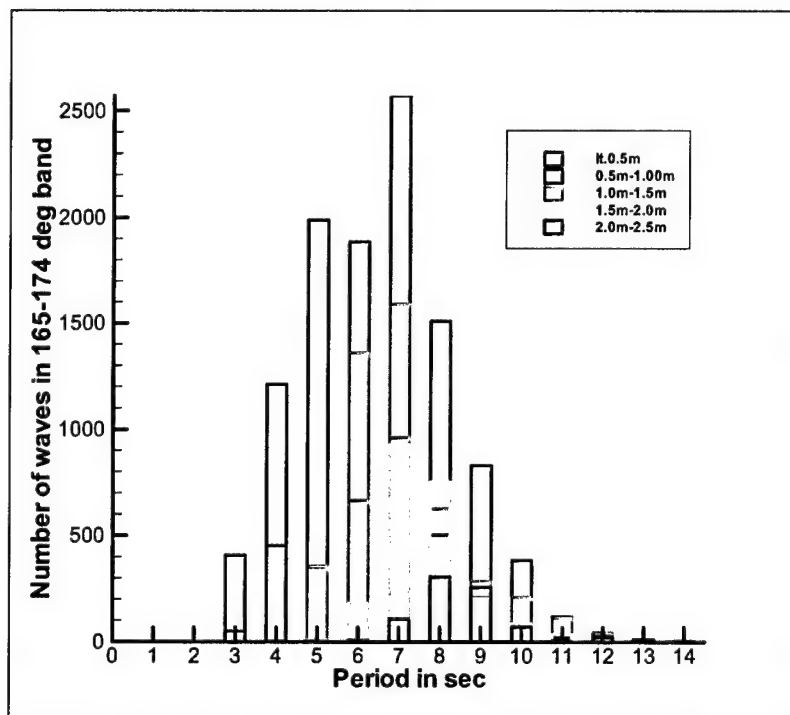


Figure 7-22. Bar chart showing incident wave height and period characteristics, direction window from 165 to 174 deg

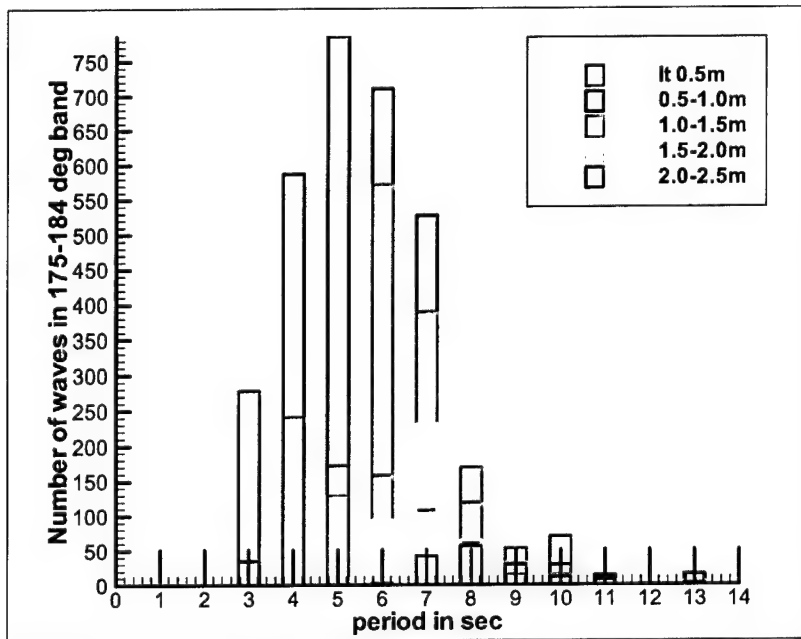


Figure 7-23. Bar chart showing incident wave height and period characteristics, direction window from 175 to 184 deg

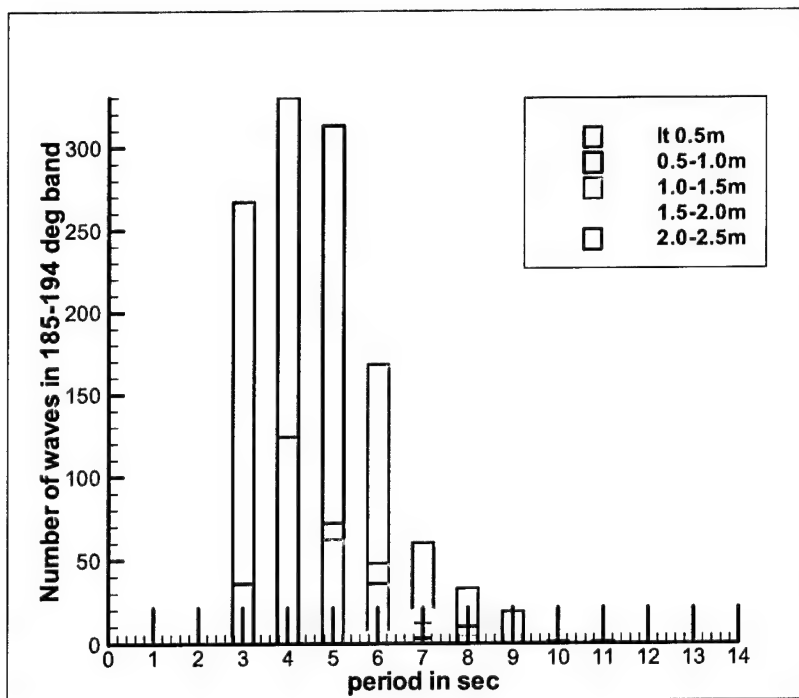


Figure 7-24. Bar chart showing incident wave height and period characteristics, direction window from 185 to 194 deg

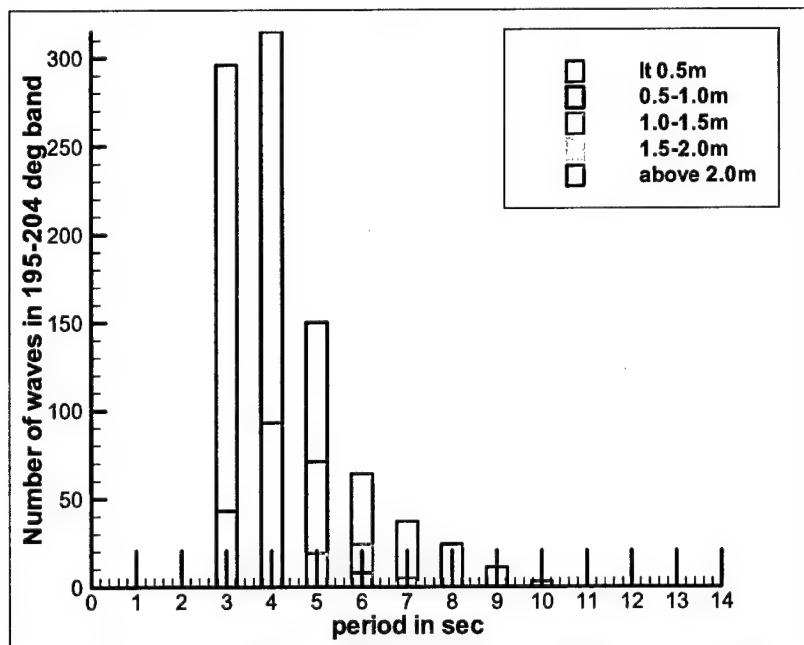


Figure 7-25. Bar chart showing incident wave height and period characteristics, direction window from 195 to 204 deg

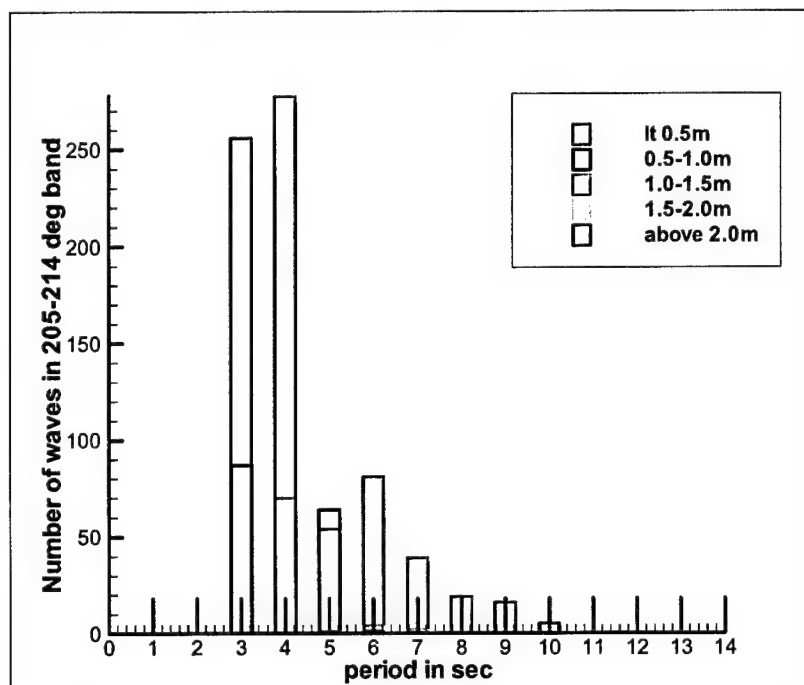


Figure 7-26. Bar chart showing incident wave height and period characteristics, direction window from 205 to 214 deg

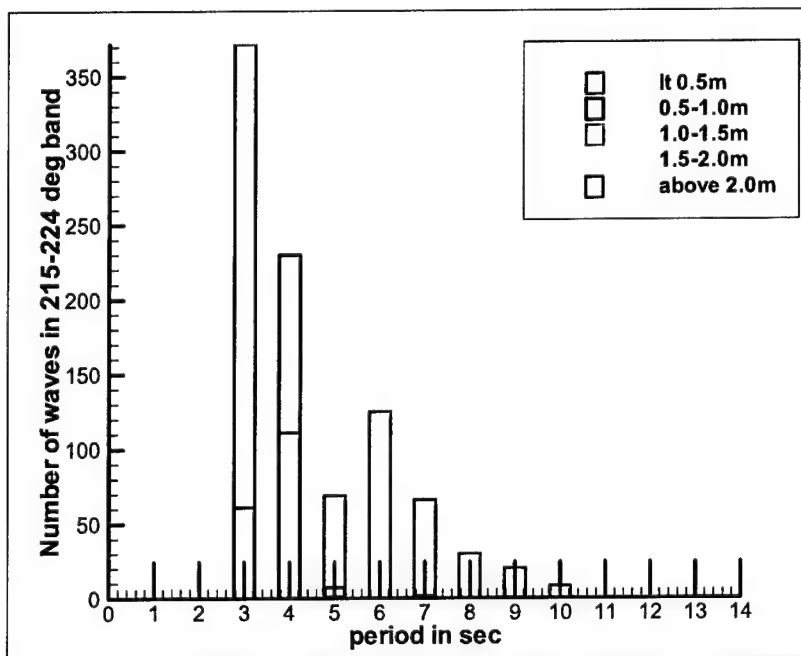


Figure 7-27. Bar chart showing incident wave height and period characteristics, direction window from 215 to 224 deg

Table 7-2 Wave Conditions Derived from 1990-1999 Wave Hindcast for Use in STWAVE Runs							
Height (m)	Period (sec)	Direction (deg)	Percent of all Waves	Percent ± 45 deg of 180 deg	Percent in 10-deg band	Date	Description
0.64	5	180	0.8	1.6	13.0	9708	Most prevalent
1.77	7	180				9603	Storm
2.52	9	180				9502	Storm
1.89	7	170	1.0	1.8	4.0	9201	Most prevalent
0.61	7	170	3.0	5.0	11.0	9302	Most prevalent
0.61	6	160	2.0	4.0	18.0	9005	Most prevalent

Results for with-CFD simulations

Figure 7-28 shows the three alternative island disposal configurations. Alternative 1 is an expansion to Singing River Island, on its southern and eastern sides. Alternative 2 is an island southeast of Singing River Island, between Round Island and the navigation channel. Alternative 3 is an island in the triangle, north of the junction of the Pascagoula and Bayou Casotte navigation channels. The existing condition is shown in Figure 7-1.

Wave heights were saved at a series of points for both with- and without-project conditions. A line of numbered points along the 1-m (3.28-ft) depth contour (shown in Figure 7-29) and a series of numbered points in the channels (shown in Figure 7-30) were saved to determine if there were significant wave height changes for any of the alternatives. Figure 7-31 through 7-33 shows the STWAVE wave height results from a storm situation and two of the most prevalent conditions for the points along the shore defined by Figure 7-29. The three island CDF alternatives are labeled the same as in Figure 7-28. Figures 7-34 through 7-36 show wave height results for the same three wave conditions, at the channel points labeled in Figure 7-30. Patterns of change in the wave height field are similar for each of the three wave conditions. Each of the islands reduces wave conditions in its lee.

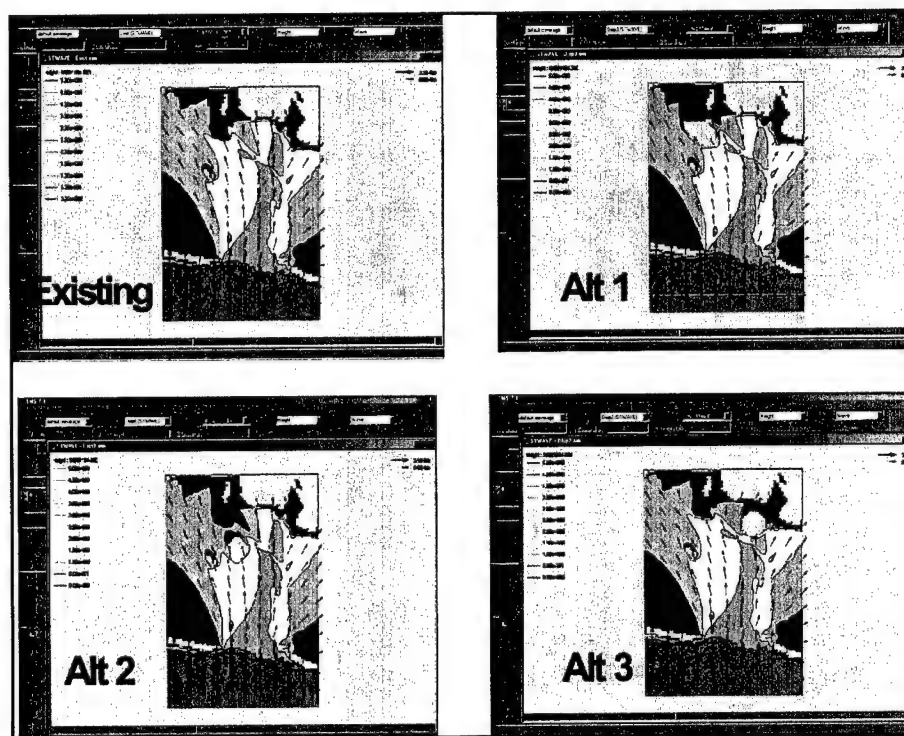


Figure 7-28. Disposal alternatives

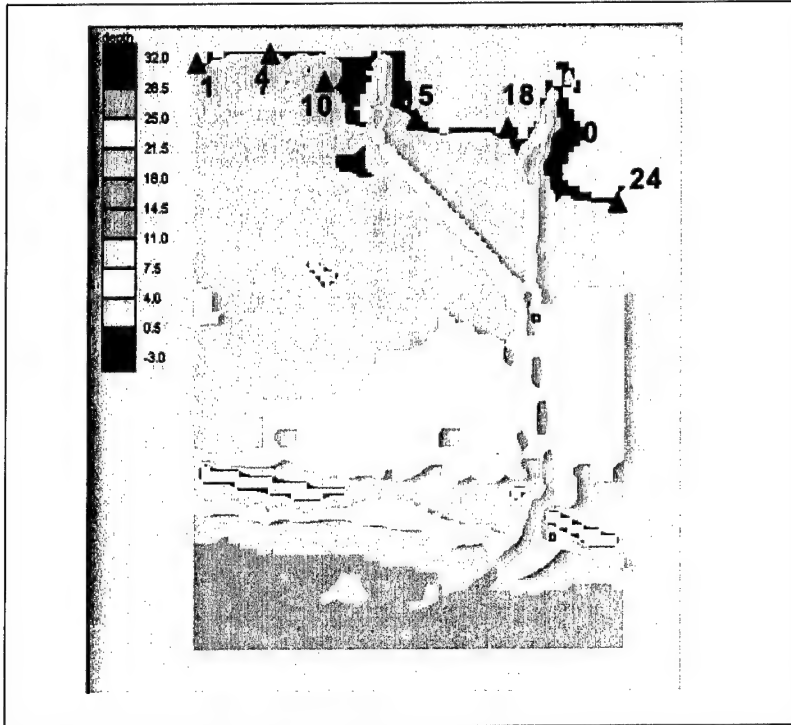


Figure 7-29. Points along 1-m contour

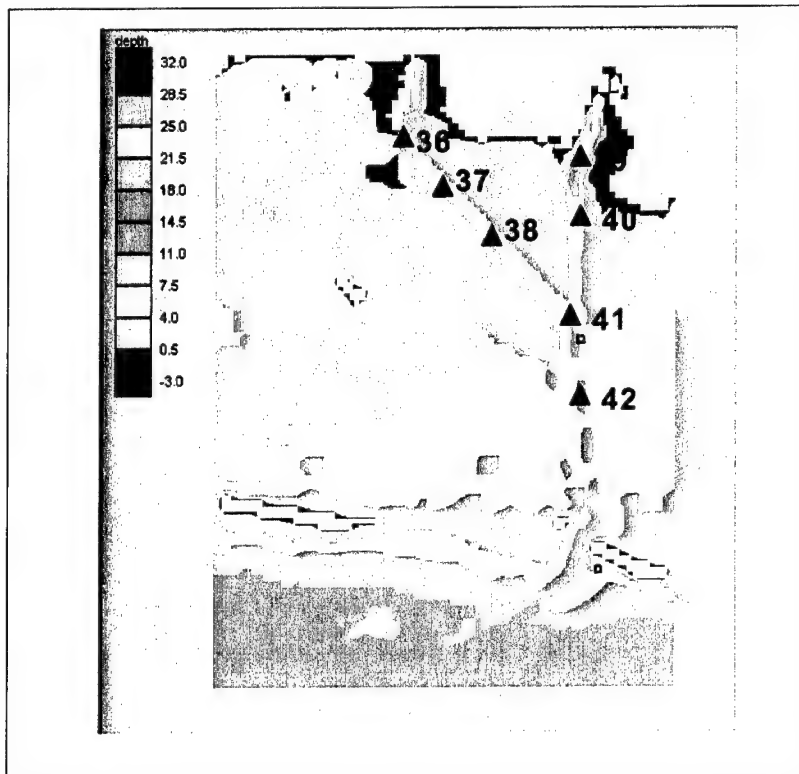


Figure 7-30. Points near Pascagoula navigation channels

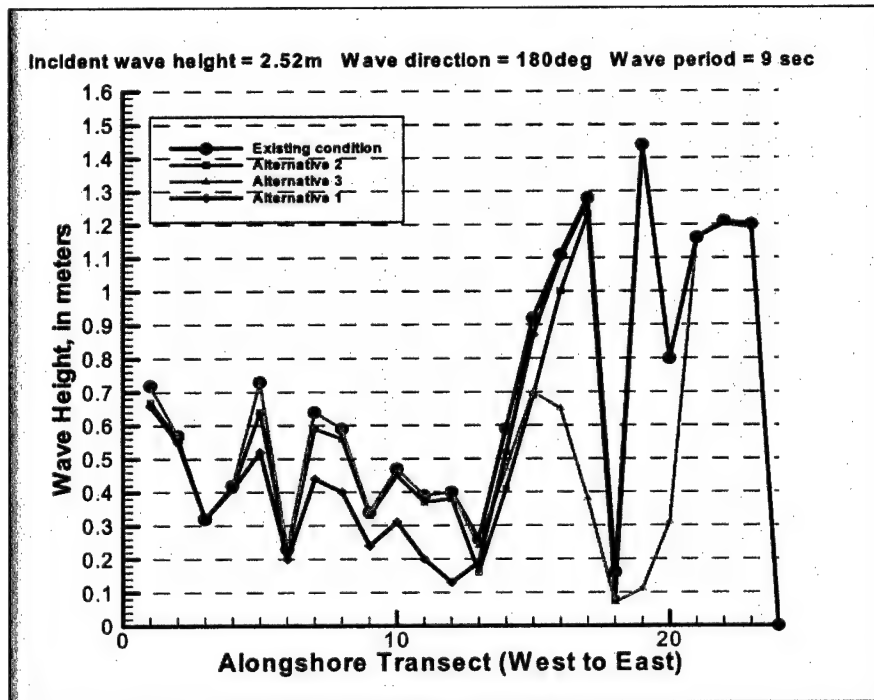


Figure 7-31. Wave height at alongshore points for incident wave 2.52 m at 9 sec

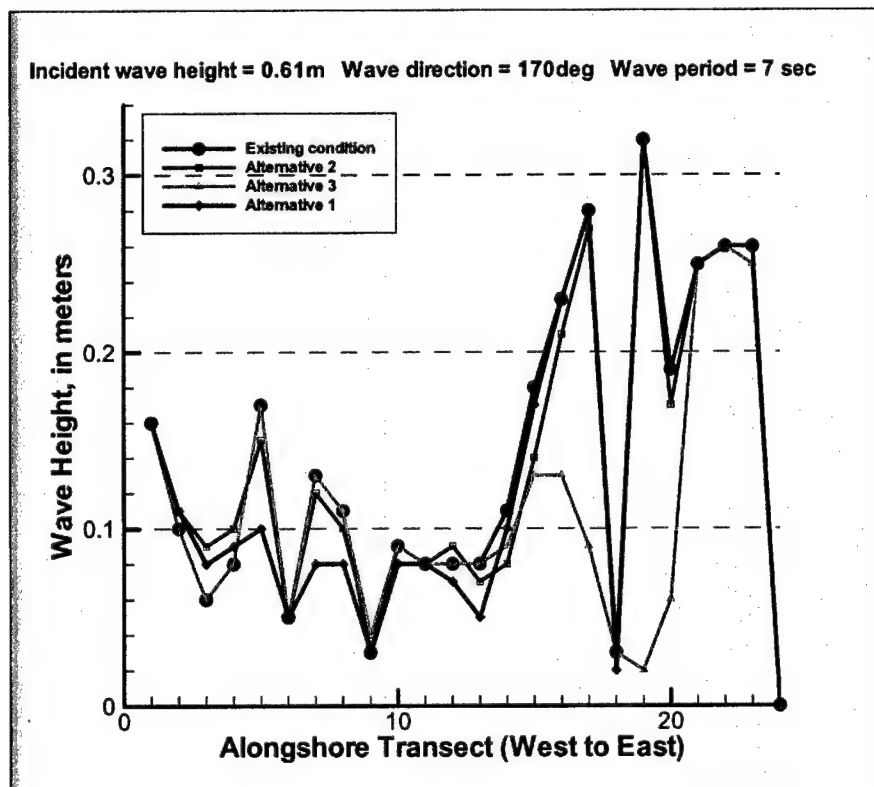


Figure 7-32. Wave height at alongshore points for incident wave 0.61 m at 7 sec

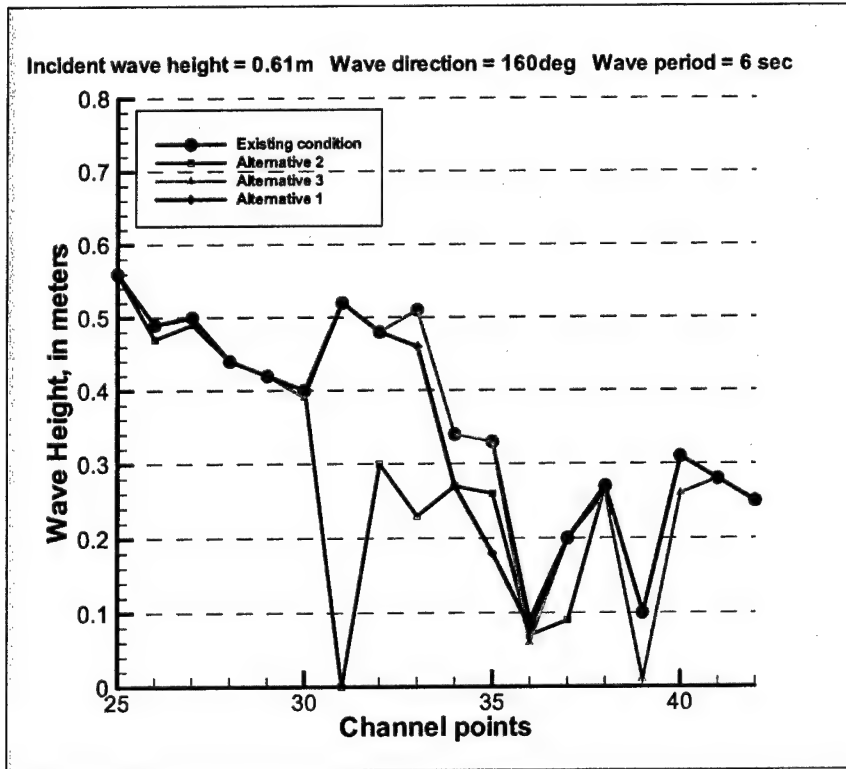


Figure 7-33. Wave height at alongshore points for incident wave 0.61 m at 6 sec

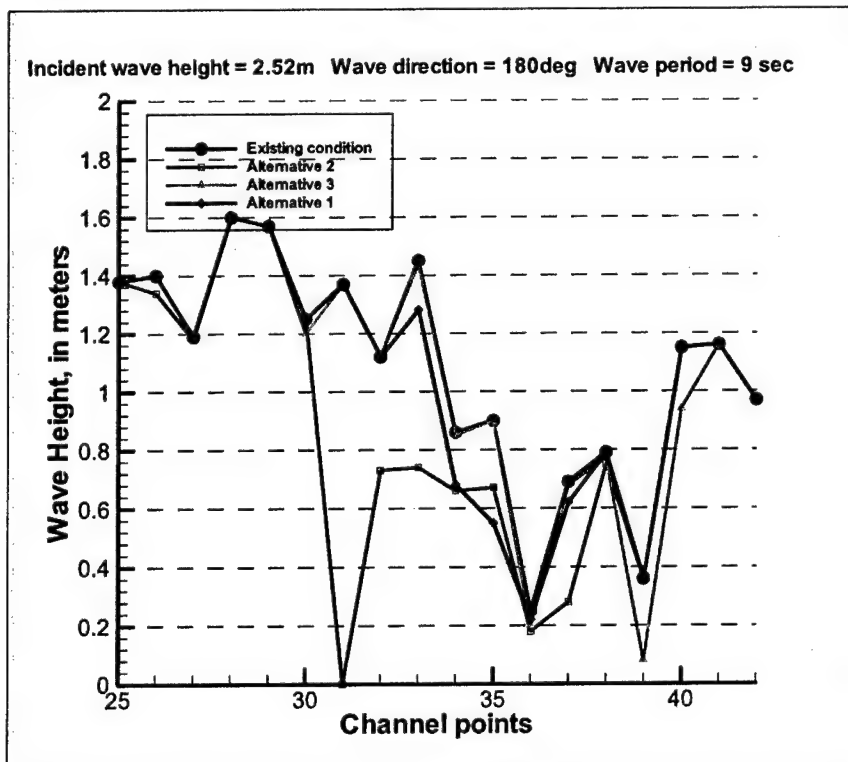


Figure 7-34. Wave height at channel points for incident wave 2.52 m at 9 sec

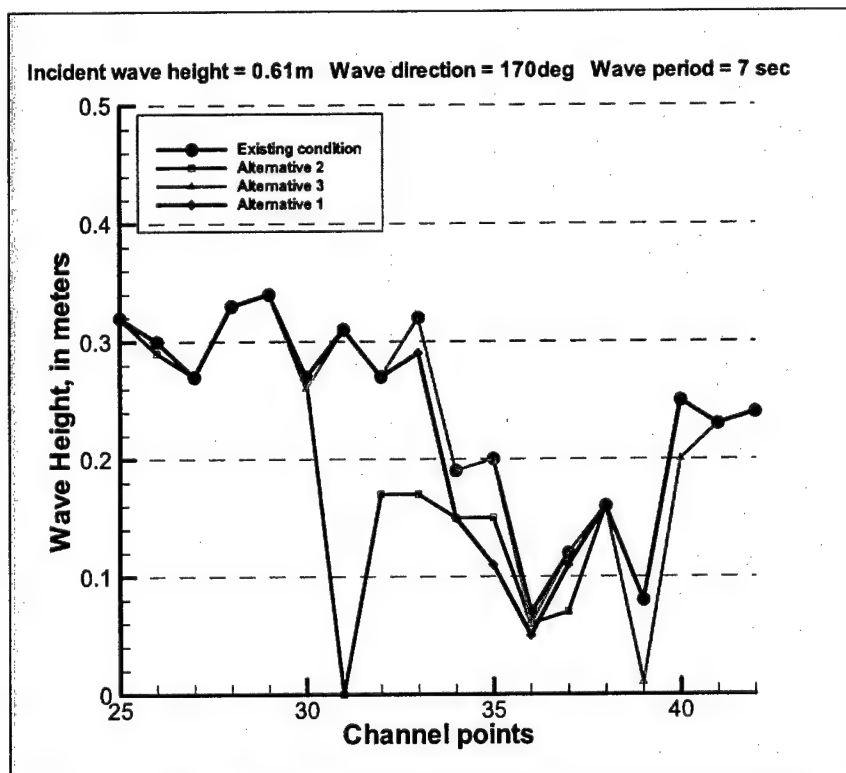


Figure 7-35. Wave height at channel points for incident wave 0.61 m at 7 sec

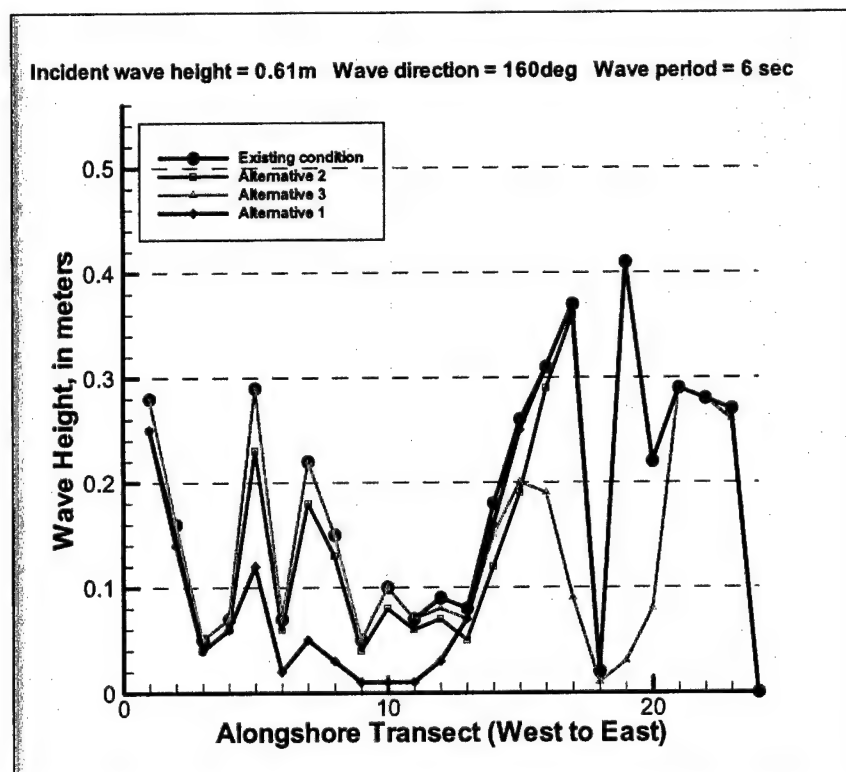


Figure 7-36. Wave height at channel point for incident height 0.61 m at 6 sec

Alternative 1. Alternative 1 is an expansion of Singing River Island and would provide the best protection to the existing Singing River Island. For these three wave conditions, this island expansion would cause a 40-60 percent reduction in wave heights along the adjacent shoreline behind the expansion and could provide protection to wetlands located west of Singing River Island. This alternative would cause no changes in wave heights in the main navigation channels. Overall, Alternative 1 will have the least impact on the local wave climate.

Alternative 2. Alternative 2, an island CDF near Round and Singing River Islands, has the least impact on wave energy along the adjacent mainland shoreline. This is due to the fact that the island is located the greatest distance from the mainland shoreline. With Alternative 2 in place, adjacent shorelines could experience a 0.1-0.2-m (0.33-0.66-ft) reduction in wave heights when waves arrive from the south. The existing Singing River Island would be sheltered from most significant wave energy propagating in from the south. The channel section immediately behind CDF 2 would experience a 40-60 percent reduction in wave height due to wave sheltering. Wave conditions immediately adjacent to an island would be affected by the composition of material used to construct the periphery of the island. A sloping rock or rubble structure would dissipate wave energy, as would sand beach. A sheet-pile structure would be highly reflective. The reflection of waves from an island CDF was not considered in this study, only sheltering.

Alternative 3. Alternative 3 would have the greatest impact on wave energy along the adjacent shoreline because it is located so close to the shoreline. This island CDF lies immediately above the channel junction. The area directly behind the island would be protected from storm waves and experience up to a 95 percent local reduction in wave height. For example, Figure 7-31 shows that waves of more than 1 m (3.28 ft) in height without the island in place are reduced to 0.1 to 0.6 m (0.33 to 1.97 ft) in height in the lee of the island. The wave sheltering and resulting longshore sediment transport pattern in the island's lee would probably lead to local sediment accumulation behind the island. The CDF is expected to act like a detached breakwater. Any accumulation would likely come at the expense of erosion of adjacent beach areas. The channel to the east of the CDF would experience a small reduction in wave energy for this alternative.

Figure 7-37 displays a set of vector wave plots of a storm wave condition for the existing and three alternatives. Color contours depict wave height. The vectors indicate wave direction. The patterns show how wave energy that propagates through the gap between the barrier islands spreads as it passes into the sound. The shallow shoals in the gap also act to limit wave energy through wave breaking that can enter the sound.

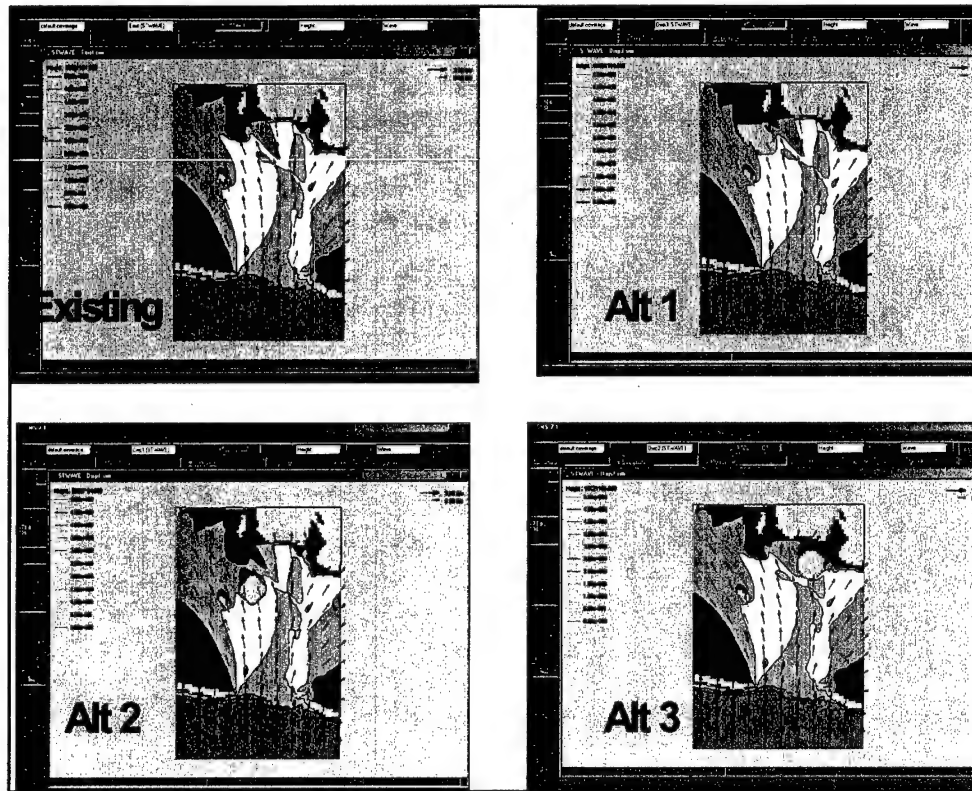


Figure 7-37. Vector plots showing storm wave conditions 2.52 m, 9 sec, 180 deg (existing condition and three CDF alternatives)

Summary and Conclusions

The 1990-1999 wave hindcast provided information to characterize the local wind and wave climate at the sites of the island CDFs. The successful verification of the hindcast with deepwater buoy and nearshore gage measurements gives credence to the hindcast results. Most significant wave energy at the three CDF sites appears to originate in the Gulf of Mexico, and propagates into the sound through the gap between Horn and Petit Bois Islands. The maximum significant wave height simulated during the 10- year hindcast period, at a location near the proposed CDF locations, was about 1.8 m (5.91 ft). For 60 percent of the time, significant wave heights are less than 0.5 m (1.64 ft). The wave climate information is useful in designing any peripheral protection integrated into construction of a CDF. The wave climate data were used to identify a set of most prevalent and storm wave conditions, which were then used to analyze the impact of the three alternative CDFs on adjacent beaches and channels. Patterns of wave height change induced by the CDFs were similar because of the dominance of southerly incident wave directions. The results of the STWAVE application, using prevalent and storm waves with the existing and three alternative conditions, aided evaluation of the impact of the proposed CDFs. Alternative 3, an island CDF in the triangle, had the most dramatic effect on waves in its lee, due to its proximity to shore. The sheltering of wave energy would likely produce local sediment accumulation behind the island, and of the three alternatives would have the greatest impact on the adjacent shoreline.

Alternative 2, an island CDF near Round and Singing River Islands, has the least impact on the adjacent mainland shoreline. This alternative provides a reduction in wave energy within the navigation channel behind it. Alternative 1, an expansion to Singing River Island, would provide protection to the existing Singing River Island and could also serve to protect wetlands west of Singing River Island from incident wave energy. Alternative 1 would have little or no impact on wave conditions in existing navigation channels.

References

- Abel, C. E., Tracy, B. A., Vincent, C. L., Jensen, R. E. (1989). "Hurricane hindcast methodology and wave statistics for Atlantic and Gulf Hurricanes from 1956 - 1975," WIS Report 19 (AD A207 849), U.S. Army Engineer Waterways Experiment Station, Vicksburg, MS.
- Hubertz, J. M. (1992). "User's guide to the Wave Information Studies (WIS) wave model, Version 2.0," WIS Report 27 (AD A254 313), U.S. Army Engineer Waterways Experiment Station, Vicksburg, MS.
- Hubertz, J. M., and Brooks, R. M. (1989). "Gulf of Mexico hindcast wave information," WIS Report 18 (AD A208 899), U.S. Army Engineer Waterways Experiment Station, Vicksburg, MS.
- Resio, D. T., and Tracy, B. A. (1983). "A numerical model for wind-wave prediction in deepwater," WIS Report 12 (AD A125 985), U.S. Army Engineer Waterways Experiment Station, Vicksburg, MS.
- Smith, J. M., Sherlock, A. R., and Resio, D. T. (2001). "STWAVE: Steady-state spectral wave model user's manual for STWAVE, Version 3.0," ERDC/CHL SR-01-01, U.S. Army Engineer Research and Development Center, Vicksburg, MS.

8 Hurricane Effects

This chapter presents an analysis for characterizing hurricane-induced wave climates and water levels. This analysis was performed to aid in designing the confining dike of the CDF so that it withstands local wave forces. This analysis is limited to weaker hurricanes with return periods of less than 25 years, the approximate design life of the CDF. Wave height in the immediate study area is limited by shallow water but storm surge associated with a hurricane increases the water surface level permitting greater wave heights so both waves and storm surge were modeled in this analysis. Storm surge was modeled with the 2-D circulation model, ADCIRC, presented in Chapter 4; waves were modeled with WISWAVE, discussed in Chapter 7. Both ADCIRC and WISWAVE models used a time-series of wind fields produced by the PBL model.

This chapter is organized into five sections. The first section describes the governing equations and computation scheme of the PBL model together with required storm parameters. The second section describes the procedure used in selecting the hurricanes that were modeled for this task. Section three describes the implementation of the storm-surge model, and wave model implementation is presented in section four. The fifth section presents modeling results and their analysis.

Description of the Planetary Boundary Layer Model

The PBL wind field model was selected for simulating hurricane-generated wind and atmospheric pressure fields. The model employs the vertically averaged primitive equations of motion for predicting wind velocities experienced within a hurricane. Through hindcast applications, Cardone, Greenwood, and Greenwood (1992) found that their model yields accurate surface wind speeds and directions when compared with measured data collected while the hurricane is in the open water. It is, therefore, the Coastal and Hydraulics Laboratory (CHL)-preferred model for generating tropical wind and atmospheric pressure fields.

Additionally, a moving coordinate system is defined so that its origin always coincides with the moving low-pressure center of the eye of the storm. Therefore, the standard equations of motion are transformed into the following relationships in Cartesian coordinates:

$$\frac{\partial u}{\partial t} + u \frac{\partial u}{\partial x} + v \frac{\partial u}{\partial y} - fv = \frac{1}{\rho} \frac{\partial p_c}{\partial x} + \frac{\partial}{\partial x} \left(K_H \frac{\partial u}{\partial x} \right) + \frac{\partial}{\partial y} \left(K_H \frac{\partial u}{\partial y} \right) + \frac{C_D}{h} |V| u \quad (5)$$

$$\frac{\partial v}{\partial t} + u \frac{\partial v}{\partial x} + v \frac{\partial v}{\partial y} + fx = \frac{1}{\rho} \frac{\partial p_c}{\partial y} + \frac{\partial}{\partial x} \left(K_H \frac{\partial v}{\partial x} \right) + \frac{\partial}{\partial y} \left(K_H \frac{\partial v}{\partial y} \right) + \frac{C_D}{h} |V| v \quad (6)$$

where

u and v = wind velocities in the x- and y-directions, respectively

ρ = mean air density

p_c = atmospheric pressure

K_H = horizontal eddy viscosity coefficient

C_D = drag coefficient

h = depth of the planetary boundary layer

V = magnitude of wind velocity

The model includes parameterization of the momentum, heat, and moisture fluxes together with surface drag and roughness formulations.

An exponential pressure law is used to generate a circularly symmetric pressure field situated at the low-pressure center of the storm:

$$p_c(r) = p_0 + \Delta p e^{-(R/r)} \quad (8-7)$$

where

p_0 = pressure at center or eye of storm

Δp (equal to $p - p_0$) = pressure anomaly with p taken as an average background or far field pressure

R = scale radius, often assumed equivalent to radius to maximum wind

r = radial distance outward from eye of storm

Wind speeds generated with the model are converted to surface wind stresses using the following relationship proposed by Garratt (1977):

$$\frac{\tau_x}{\rho_0} = C_D \frac{\rho_{air}}{\rho_0} |V| u \quad (8-8)$$

and

$$\frac{\tau_y}{\rho_0} = C_D \frac{\rho_{air}}{\rho_0} |V| v \quad (9)$$

where

τ_x and τ_y = wind stresses in the x- and y-directions, respectively

$\rho_{air} / \rho_0 = 0.001293$ = ratio of air density to average density of seawater

C_D = frictional drag coefficient

The PBL hurricane wind model requires a series of "snapshots" for input consisting of a set of meteorological storm parameters defining the storm at various stages in its development or at particular times during its life. These parameters include latitude and longitude of the storm's eye, track direction and forward speed measured at the eye, radius to maximum winds, central and peripheral atmospheric pressures, and an estimate of the geostrophic wind speed and direction. Also, the direction and speed of steering currents can be provided for representing asymmetric hurricanes.

The spatial area over which a hurricane resides is defined in the model via a numerical grid or a lattice network of nodes. Wind velocities and atmospheric pressures are computed at each node in the grid. Whereas some models employ a fixed grid system to simulate a hurricane (i.e., stationary grid with a moving storm), the PBL model simulates the hurricane as a stationary storm with a moving grid. A hurricane's translational or forward motion is incorporated into model calculations by adding the forward and rotational velocity vector components.

The model uses a nested gridding technique, composed of five layers or subgrids, for computing the wind fields. Each subgrid measures 21 by 21 nodes in the x- and y-directions, respectively, and the centers of all subgrids, node (11,11), are defined at the eye of the hurricane. Whereas the number of nodes composing each subgrid is the same, the area of coverage and spatial resolution differs for each grid. For this study, the subgrid with the finest resolution had an incremental distance of 5 km between nodes. Incremental distances for the remaining subgrids were 10, 20, 40, and 80 km.

For each snapshot, the equations of motion are first solved using the grid covering the greatest area, which in this study is the grid having an incremental distance of 80 km between nodes. Computed wind velocities are then used as boundary conditions on the second-largest grid, and the equations of motion are solved again. This same procedure is followed for the remaining grids where wind fields are computed using sequentially smaller grids together with wind velocities computed with the next larger grid serving as boundary conditions. Thus, the nested gridding technique provides wind-field information over a wide spatial area, while sufficient grid resolution is provided to accurately compute winds within the eye of the hurricane.

After all snapshots have been processed, hourly wind and atmospheric pressure fields are interpolated using a nonlinear blending algorithm that produces a smooth transition from one snapshot to the next. Hourly wind and pressure fields are then interpolated from the PBL grid onto the hydrodynamic grid and subsequently stored for use by the hydrodynamic model.

Selection of Hurricanes

Designing a CDF to withstand waves induced by stronger hurricanes would probably be cost-prohibitive. For example, storm-surge levels induced by Hurricane Camille, storm-of-record for the study area, approached 7.62 m (25 ft) at Pascagoula. Assuming that waves break when their height approaches 0.78 of the water depth, wave crests could theoretically reach 10.36 m (34 ft). To design against overtopping by a storm of Camille's intensity would require a dike greater than 10.36 m (34 ft), adding surge and wave amplitude.

The first task in selecting hurricanes was to identify those storms that have impacted the study area. For this purpose, the Tropical Event Database-Surge (TEDS), developed through the Corps' DRP (Scheffner et al. 1994), was used. TEDS contains peak surge elevations for 134 historical tropical storms at 484 open-coast locations along the Atlantic and Gulf of Mexico shorelines of the United States. Peak surge elevations were computed using the ADCIRC model, and meteorological storm parameters were obtained from a NOAA National Hurricane Center (NHC) database, which summarizes all hurricanes and tropical storms that occurred in the North Atlantic Ocean over the 104-year period from 1886 through 1989.

TEDS contained 25 storms whose peak storm surge levels exceeded 0.30 m (1 ft) in the study area. With the storm-surge levels induced by these 25 storms, a cursory frequency-of-occurrence analysis was performed, using a standard-ranking method, for assigning return periods to the storm-surge levels. The frequency-of-occurrence relationship is presented in Figure 8-1. Of the 25 storms, 12 hurricanes were found to have produced surge levels having a return period greater than 25 years, and were omitted from further analyses.

In reviewing the remaining 12 hurricanes, each storm was characterized with respect to its direction as it approached shore (i.e., from the southeast, southwest, south). The intensity of each storm (e.g., central pressures and maximum wind speeds) was then evaluated for each direction, identifying a typical or average storm for each direction. A total of four hurricanes were selected in this evaluation; Hurricane Georges, a post 1990 storm, was added to this group because it was a strong storm that made a close approach to the study area. Table 8-1 summarizes the hurricanes chosen for this analysis.

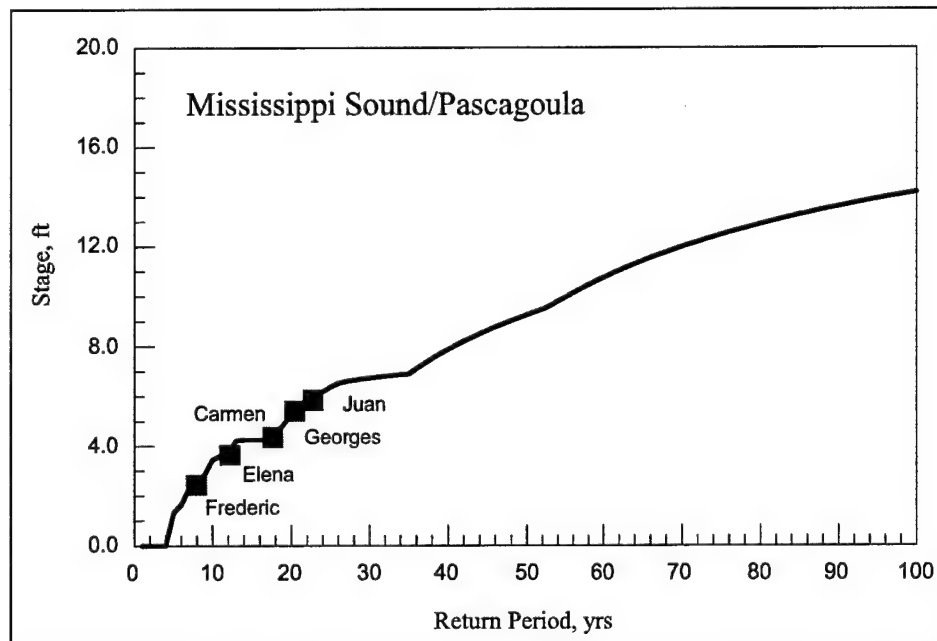


Figure 8-1. Frequency of occurrence for Pascagoula, MS

Table 8-1 Summary of Hurricanes				
Name	Date	Landfall	Maximum Wind Speed (mph)	Central Pressure (mb)
Carmen	29 Aug – 10 Sep, 1974	Landfall in west LA	130	928
Frederic	29 Aug – 15 Sep, 1979	Landfall on AL coast	115	943
Elena	28 Aug – 4 Sep, 1985	Landfall west of study area	110	953
Juan	26 Oct – 1 Nov, 1985	Landfall east of study area	75	971
Georges	15 Sep – 1 Oct, 1998	Landfall on western edge of study area	135	937

Implementation of PBL Model

Some meteorological storm parameters were obtained from the hurricane database developed by the NOAA NHC (Jarvinen, Neumann, and Davis 1988). This database summarizes all hurricanes and tropical storms that occurred in the North Atlantic Ocean over the 104-year period from 1886 through 1989. Information contained in this database is provided at 0000, 0600, 1200, and 1800 hours Greenwich Mean Time (GMT) and includes latitude and longitude of the storm, central pressure, and maximum wind speed.

Radius to maximum winds was approximated using a function that incorporates the maximum wind speed and atmospheric pressure anomaly published in Jelesnianski and Taylor (1973). Track directions and forward speeds required by the PBL model were approximated hourly, using a cubic spline interpolation technique, from the storm's 6 hr latitudinal and longitudinal positions provided in the database. Peripheral atmospheric pressures were assumed equal to 1,013 mb, and geostrophic wind speeds were specified as 6 knots and having the same direction as the storm track.

Implementation of Storm-Surge Model

All five storms presented in Table 8-1 were simulated with the PBL and storm surge model. Each simulation began approximately 2 days before making its closest approach to the study area. For all hurricanes, a temporal "ramp" was used to slowly increase, over a 1-day period, wind stresses and pressure gradients from zero to their measured intensity. (Using this ramp eliminates spurious modes of oscillation caused by suddenly imposing full-force winds and atmospheric pressure gradients on the flow field.)

All storm-surge simulations were performed independently of tidal action, eliminating the task of extracting surge levels from a time-series of combined tide- and surge-induced water-surface elevations. Therefore, storm-surge elevations computed in this task can be considered as approximations of the historical events. Although frequencies associated with their maximum surge may be considered relatively accurate, the value of the peak surge may not correspond to historically observed surge elevations. The hydrographs should not be considered a hindcast of the historical events for the following two reasons. First, the storm events were simulated without tides; therefore, peak values do not reflect the tidal stage at the time of their occurrence. Second, the hurricane parameters estimated from the storm database are only approximate; all information necessary to numerically simulate each event is unknown and has not been calibrated. For example, values of central pressure, radius to maximum winds, and far field pressure are not known and were estimated from available data or observations. Because little data exist for the earlier storms, a consistent approach for selecting storm parameters was developed.

Time-step used in these simulations varied from 1 to 5 sec, depending on the intensity of the storm and its distance from the eye of the storm to the study area. The 1-sec time-step was used for Hurricane Georges, which was relatively strong and moved in close proximity to the study area. Weaker storms with paths far from the study site were simulated with the larger time-step. During a given simulation, time-series of water-surface elevations were recorded at 15-min intervals at one station in close proximity to the three disposal sites. Figures 8-2 through 8-5 present the time-series of storm surge for each hurricane.

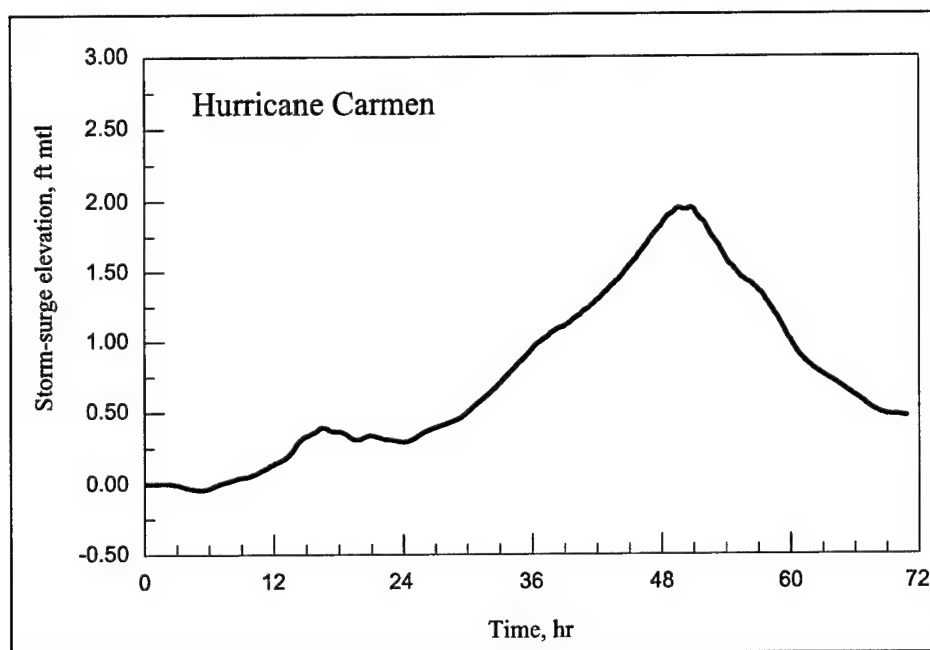


Figure 8-2. Storm surge hydrograph for station in close proximity to three disposal sites (30.3°N, 88.57°W) for Hurricane Carmen, September 1974

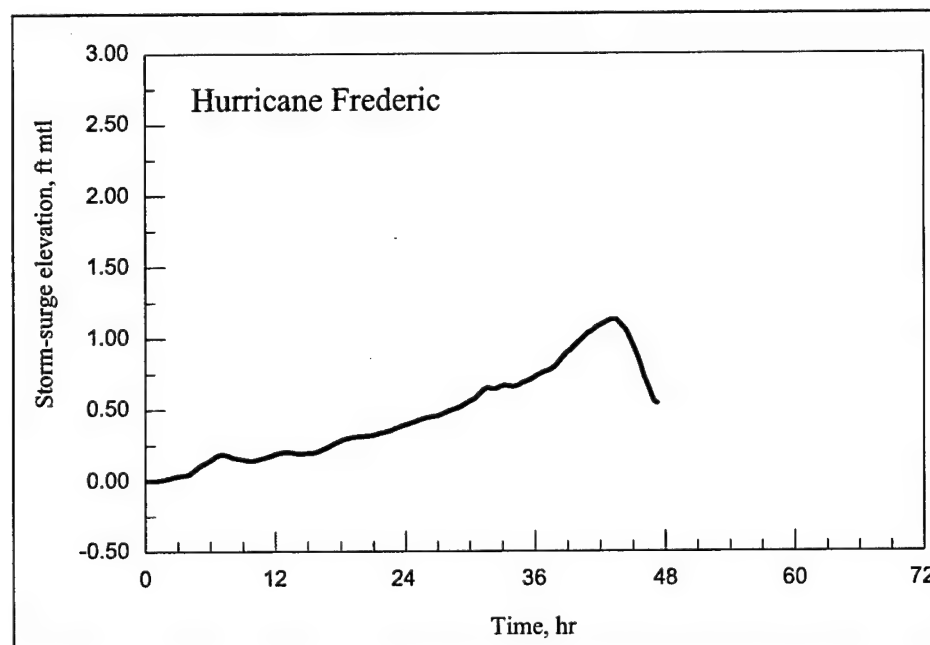


Figure 8-3. Storm surge hydrograph for station in close proximity to three disposal sites (30.3°N, 88.57°W) for Hurricane Frederic, September 1979

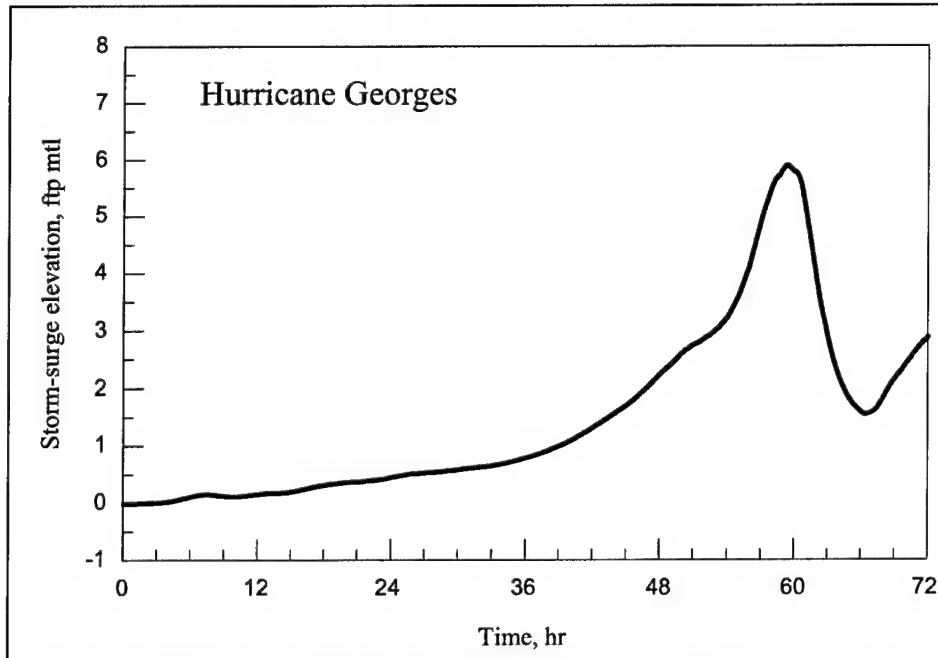


Figure 8-4. Storm surge hydrograph for station in close proximity to three disposal sites (30.3°N, 88.57°W) for Hurricane Georges, September 1998

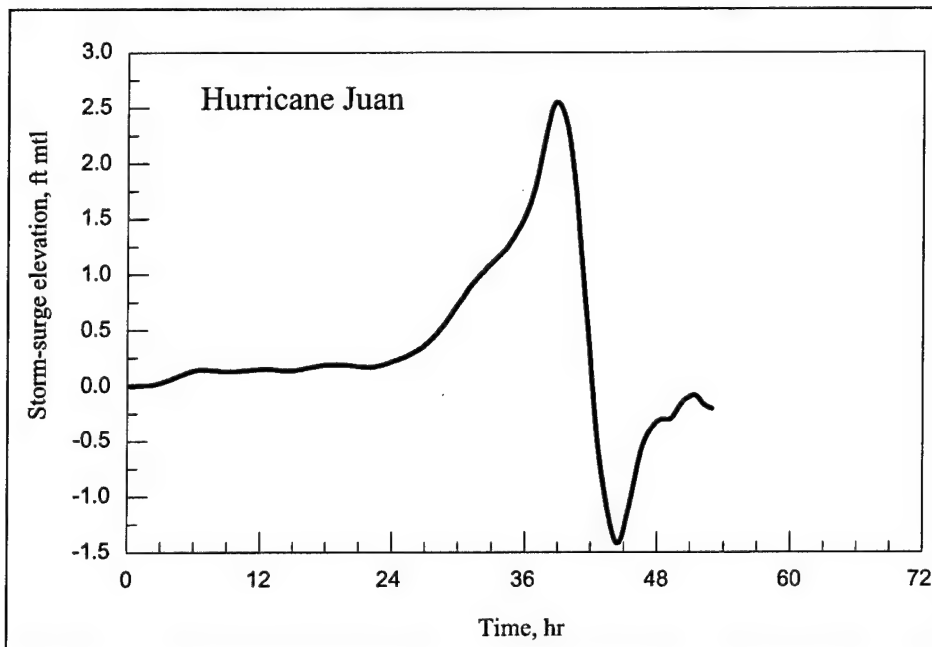


Figure 8-5. Storm surge hydrograph for station in close proximity to three disposal sites (30.3°N, 88.57°W) for Hurricane Juan, October 1985

Peak storm-surge levels varied from 1.0 ft for Hurricane Frederic to 6.0 ft for Hurricane Georges. Differences in storm-surge levels presented in this section and those used in the frequency-of-occurrence task are attributed to differences in locations where the surge levels were computed. In Scheffner et al. (1994), the station was located in the vicinity of Gulfport, about 30 miles to the west of the study site.

Implementation of Wave Model

Chapter 7, which presents the wave-modeling component of this study, includes a discussion of the 1990-1999 wave modeling hindcast for the Mississippi Sound. This hindcast was conducted using a nested grid approach where wave conditions were computed using five distinct grids, each having a different spatial resolution and coverage area. The coarser grid, referred to as Level 1, covers nearly the entire North Atlantic Ocean and has a nodal spacing or resolution of 1 deg in latitude and longitude. Figure 7-22 of Chapter 7 shows the nested grid system that was used in the 1990-1999 wave hindcast. For the hurricane component of this study, waves were computed using the Levels 2 through 5 grid system. (Level 1 was not used in the hurricane wave simulations because the selected hurricanes formed and resided within the Gulf of Mexico.) The finest grid covering the study area, Level 5, has a nodal spacing of 0.002 deg and encompasses the region of lat. 30.17 to 30.37°N and long. 88.48 to 88.63°W (see Figure 7-2 in Chapter 7 for region). Shallow-water effects, such as wave attenuation induced by bottom friction, can be modeled at this fine resolution.

For each hurricane, the model was first applied using the Level 2 grid, which encompassed the greatest area. Computed wave spectra are saved at locations coincident to the open-water boundary nodes of the next finer grid, the Level 3 grid. Using the saved spectra as boundary conditions, the model was applied using the Level 3 grid, again saving spectra at nodes coinciding to the open-water boundaries of the Level 4 grid. The same procedure was followed for estimating waves in the interior of the Level 5 grid. This nesting technique was especially important in hurricane applications because the compact rotational wind field associated with these storms can produce wind and waves from any possible direction. STWAVE was not used in the hurricane simulations because it currently uses only boundary information from the seaward boundary, but not open-water boundaries along the lateral sides of a grid, and is not sensitive to winds opposing the shoreward advance of waves; WISWAVE provides a more realistic hindcast of winds and waves because wave spectra can be specified at all open-water boundaries and offshore winds can be specified in the model.

Hourly wind fields were produced using the PBL hurricane wind model developed by Cardone at Oceanweather, Inc. (Cardone, Greenwood, and Greenwood 1992) described previously. Individual wind fields were computed for each of the four levels of wave hindcasting grids. The input snapshots and history files for the four simulated hurricanes previous to 1990 (Frederic 7908, Carmen 7408, Elena 8508, and Juan 8510) were developed by Oceanweather, Inc., and were used in the previous WIS hurricane hindcasting efforts described in Chapter 7. Oceanweather, Inc. used the NOAA NHC information as a starting point; and by incorporating all available meteorological information and applying expert analysis to the resulting wind fields, a more accurate snapshot and history

information were produced. Winds beyond the periphery of a hurricane were not blended with the hurricane wind fields; blending was not performed because only wave results at the height of the storm were of interest. Hurricane hindcasts began a few days before the hurricane came close to the study area. Figure 8-6 shows the hurricane tracks of the four storms in relation to the Level 5 hindcast grid. Hurricane Georges was included in the 1990-1999 wave hindcast and its wind fields were included within the wind product used in that hindcast.

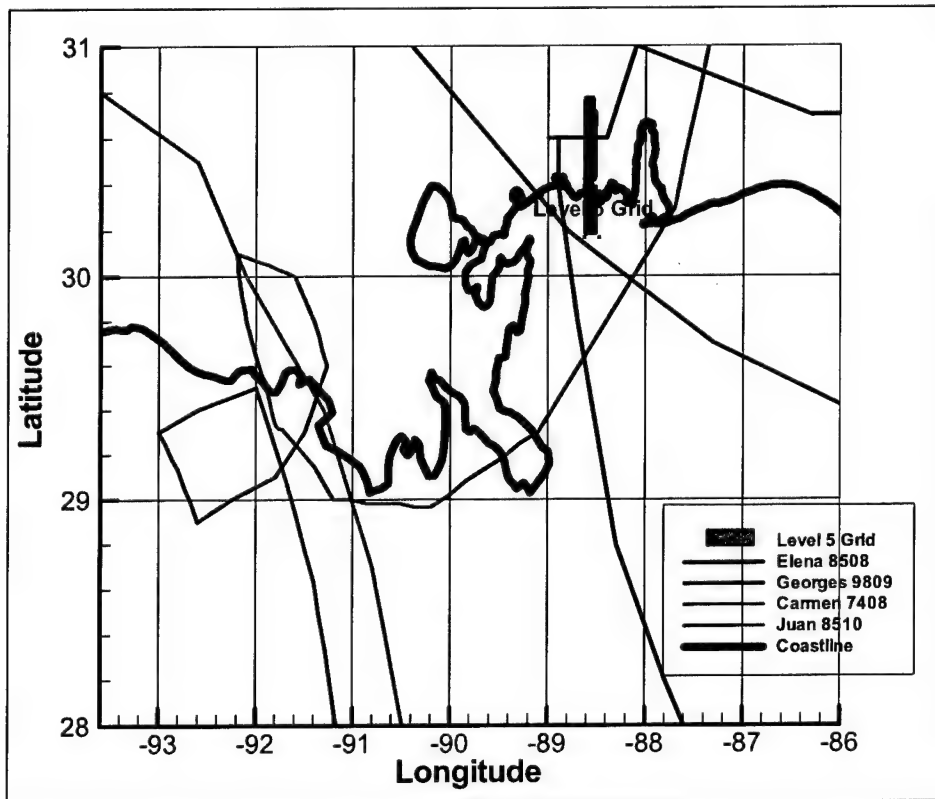


Figure 8-6. Tracks of the selected hindcast hurricanes in relation to Level 5 grid covering study area

WISWAVE permits fluctuating water levels to be incorporated into the hindcast, via updated grid depths at hourly intervals. Time-series of water-surface elevations generated in the ADCIRC storm-surge calculations at a site in close proximity to Singing River Island were used to adjust the depths specified in the Level 5 grid. Figure 8-7 shows plots of the hourly water level information used in the finest grid of the WISWAVE hindcasting system for the four pre-1990 tropical events. Inclusion of hurricane-induced storm-surge levels is especially important because increased water levels permit greater wave heights in the shallow areas of the study area during a hurricane. Water levels were not added to the Hurricane Georges hindcast that was part of the 1990-1999 hindcast.

Hurricane Model Results

Figures 8-8 through 8-12 present calculated wave height, period, and direction, together with wind speed, using the Level 5 grid, for a station located at lat. 30.3°N, long. 88.57°W, which resides near Singing River Island. Water depth at this station is 3 m (9.84 ft). As shown in these figures, the model produces a maximum wave height at this location of about 1.8 m (5.91 ft) for each storm. Hurricane Carmen, Figure 8-8, produced wave periods in excess of 16 sec, but the height for these longer period waves was well under 1 m (3.28 ft).

At the time of peak significant wave height, peak periods were 8 to 9 sec. Carmen's path was well to the west of the study area. For Hurricane Frederic, which made landfall to the east of the study area, the model-predicted maximum wave height and period are 1.8 m (5.91 ft) and 14 sec, respectively, with waves propagating from the south (Figure 8-9). The peak wave condition was coincident with 35-m/sec (114.82 ft/sec) wind speeds over the study area. Elena's, Figure 8-10, maximum condition shows a 1.5-m (4.92-ft) wave height associated with 12- to 13-sec wave periods and 35 m/sec (114.82 ft/sec) wind speeds. The wave direction shows some offshore directions near the peak of the storm. Juan, Figure 8-11, shows sustained 1.8-m (5.91-ft) to 1.9-m (6.23-ft) wave conditions for the storm's duration and a peak period of up to 14 sec. Wind conditions at the site during this time remained above 15 m/sec. Juan's wave direction was consistently from the south. Hurricane Georges (Figure 8-12) shows a maximum wave height of 1.6 m (5.25 ft) and a peak period of 12 to 14 sec. These waves show a southerly direction of approach. These results indicate that the CDF structure should be able to withstand wave action of up to 1.8 to 1.9 m (5.91 to 6.23 ft) in significant height at peak periods of 14 sec in order to withstand hurricanes with return periods of less than 25 years. Note that these wave conditions reflect the super-elevation in water level induced by the storm surge. Astronomical tide was not considered, but this is not a significant factor in terms of increased wave height that can exist at the site. Designing for a significant wave height of 2.0 m (39.37 ft), for return periods of less than 25 years is reasonable.

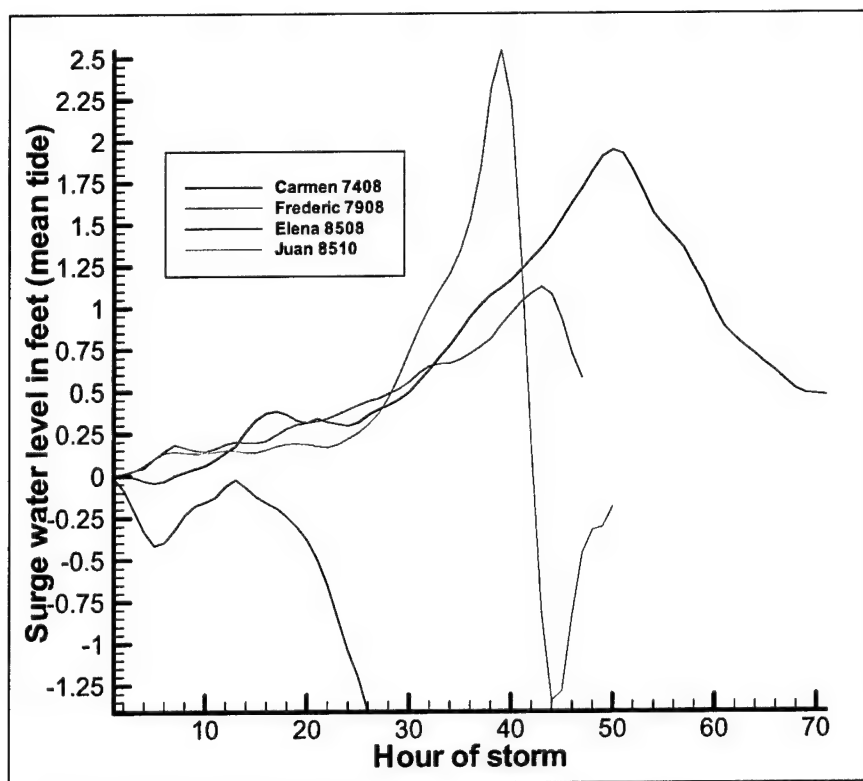


Figure 8-7. Interpolated hourly water level information from a site in close proximity to Singing River Island (30.3°N, 88.57°W) for each of the selected hindcast hurricanes

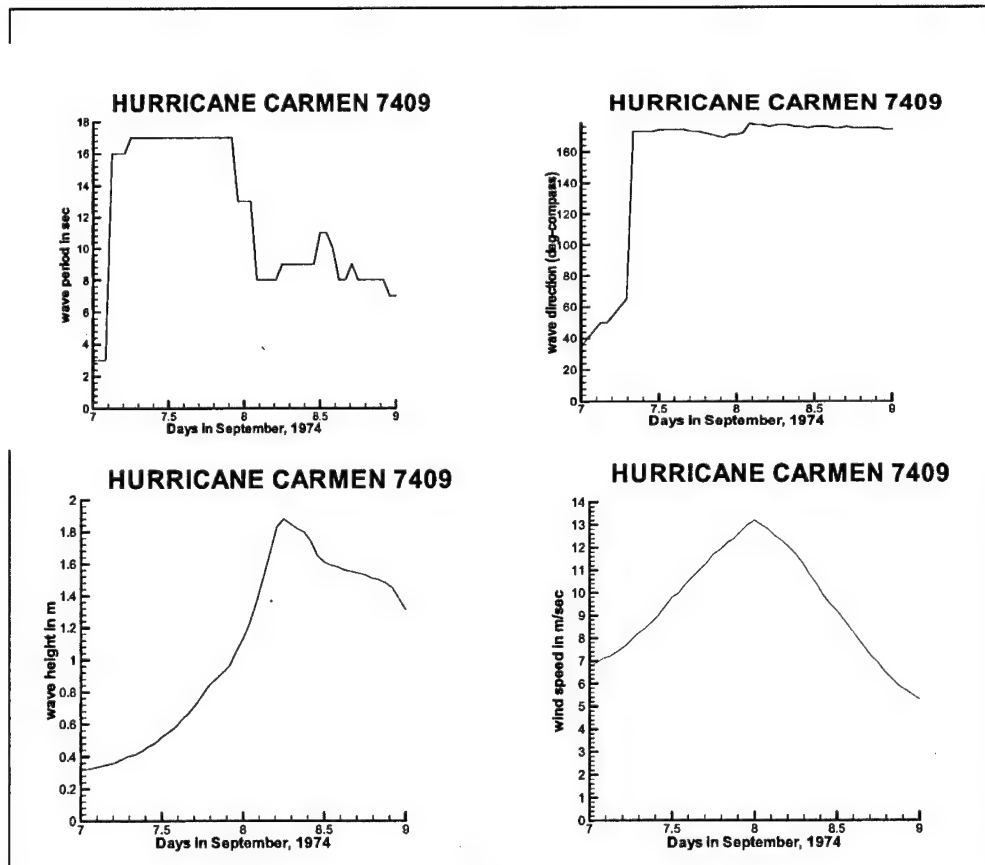


Figure 8-8. Wave height, period and direction and wind speed results for Hurricane Carmen at a location near Singing River (30.3°N, 88.57°W)

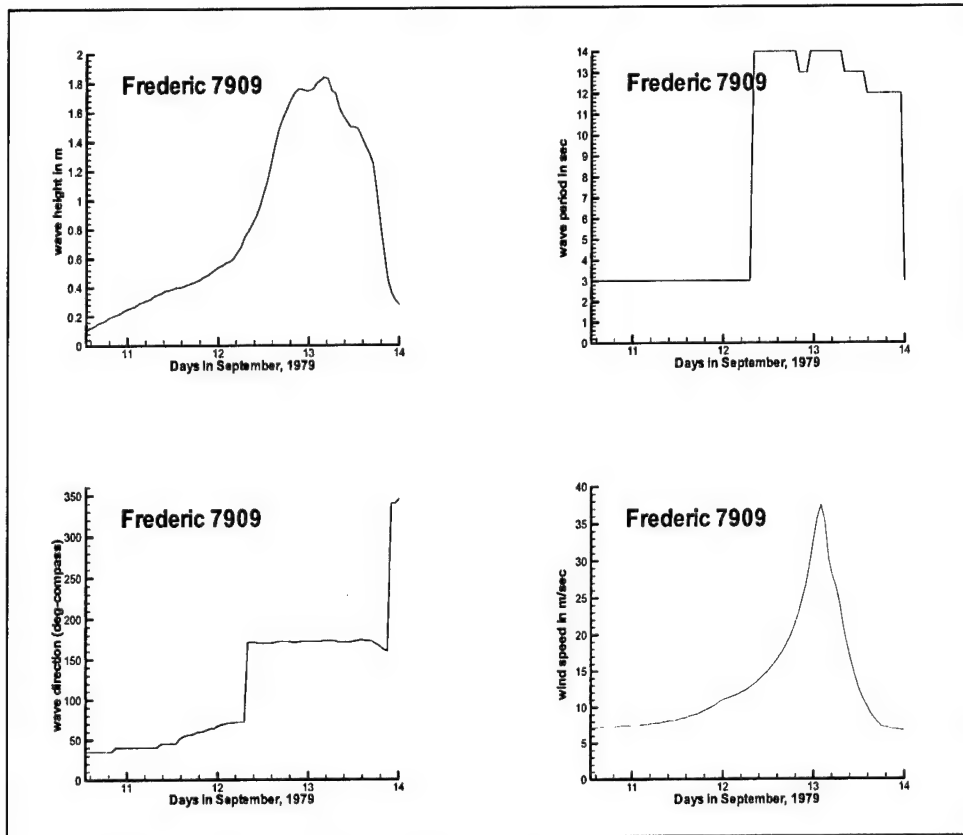


Figure 8-9. Wave height, period and direction and wind speed for Hurricane Frederic at a location near Singing River (30.3°N, 88.57°W)

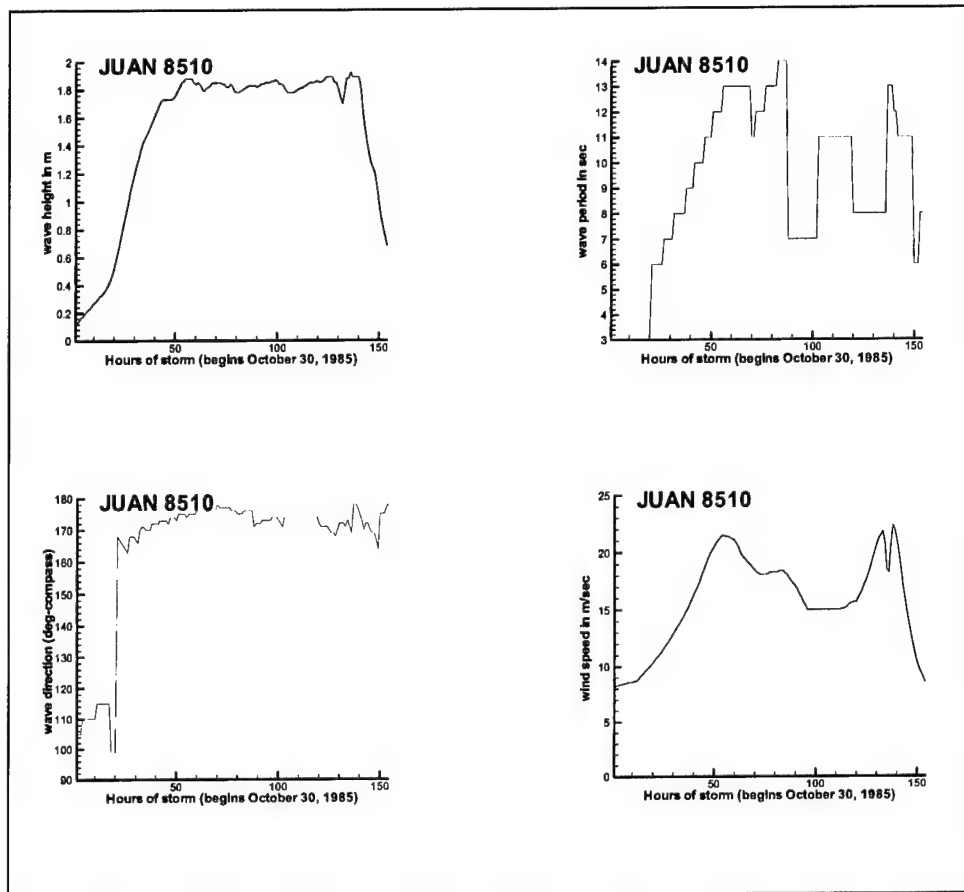


Figure 8-11. Wave height, period and direction and wind speed for Juan at a location near Singing River (30.3°N, 88.57°W)

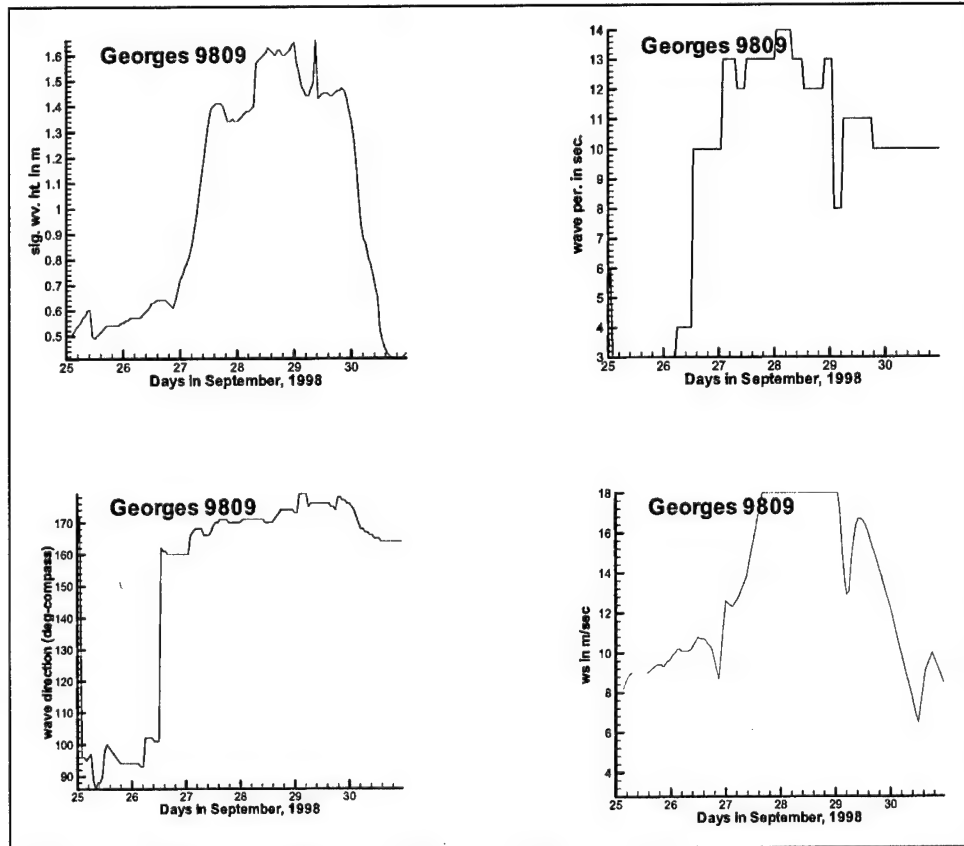


Figure 8-12. Wave height, period and direction and wind speed for Hurricane Georges at a location near Singing River (30.3°N, 88.57°W)

Data are not available to validate the results of the hurricane hindcast within the immediate study area. However, Figure 8-13 shows a comparison of the significant wave height and peak period at NDBC 42007, located lat. 30.09°N, long. 88.77°W, and a comparison output location from the Level 3 hindcast for Hurricane Georges in 1998. Results compare well in terms of magnitude of peak significant wave height and peak period.

For Hurricane Carmen, whose track is displayed in Figures 8-14, model results are presented in Figures 8-15 and 8-16 for the Level 3 and Level 5 simulations, respectively. Figure 8-15 displays wave height and period at a station near the path of the hurricane (shown as sta 1 in Figure 8-14), whereas Figure 8-16 presents these parameters at a station in the gulf near Petit Bois Island (shown as sta 2 and located at the point of the nearshore wave gage site MS01). Although Carmen's path was about 225.31 km (140 miles) west of the study area, the storm still produced significant hurricane wave energy at Horn Island Pass, which propagates towards the study area.

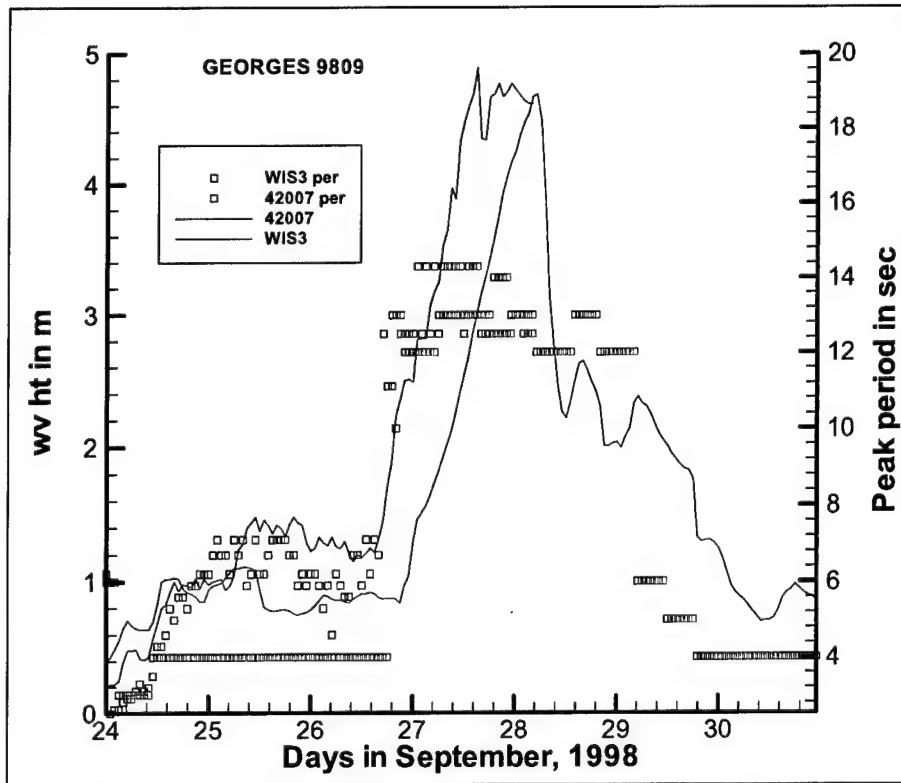


Figure 8-13. Comparison of measured and computed wave height and peak period; NDBC 42007 and WIS Level 3 model

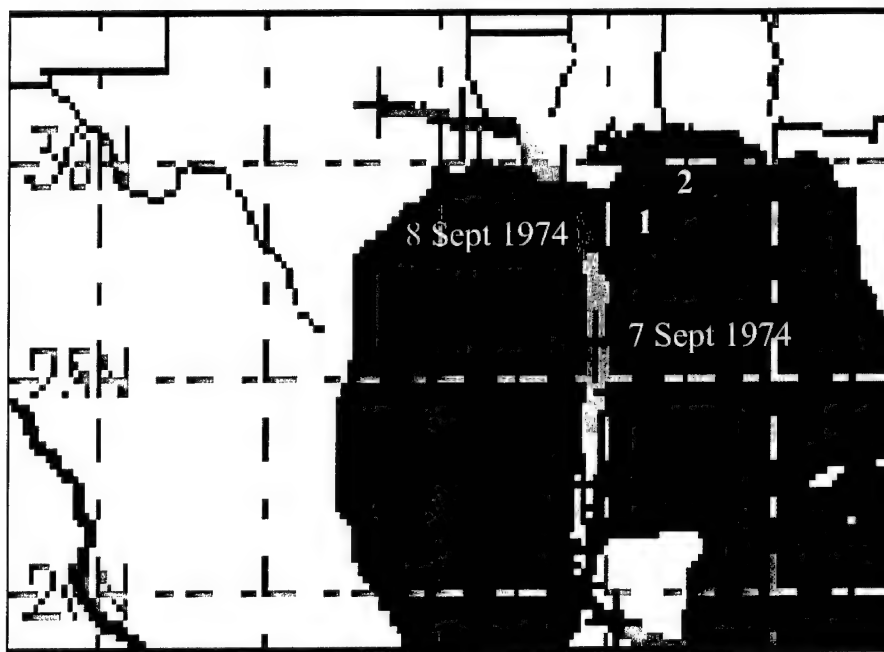


Figure 8-14. Track of Hurricane Carmen, September 1974 (after UnisysCorp¹).

¹ <http://weather.unisys.com/hurricane/atlantic/1974/index.html>

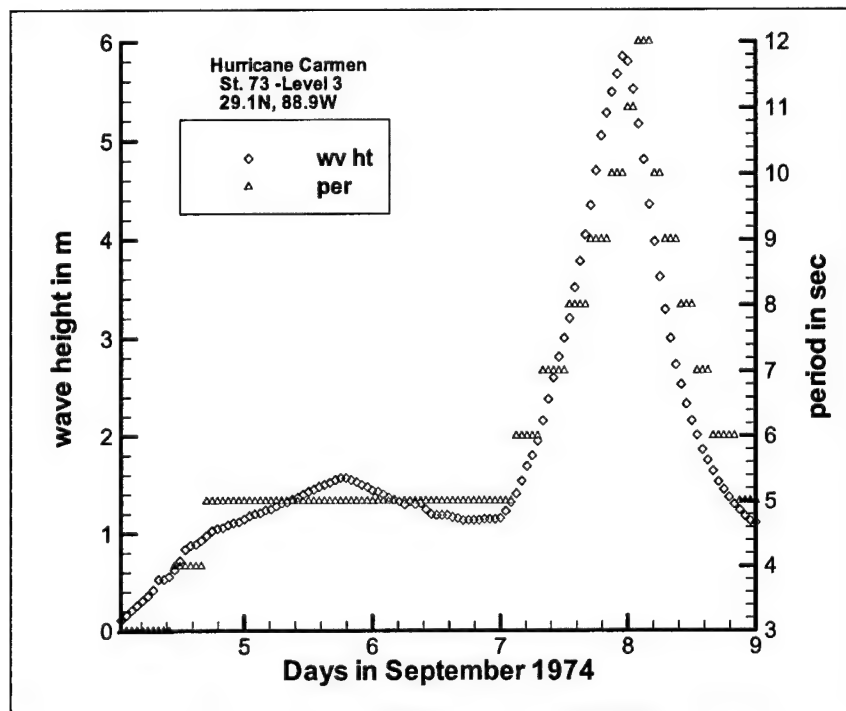


Figure 8-15. Wave height and period model results for Hurricane Carmen at a Level 3 grid point near its path (29.1°N, 88.9°W)

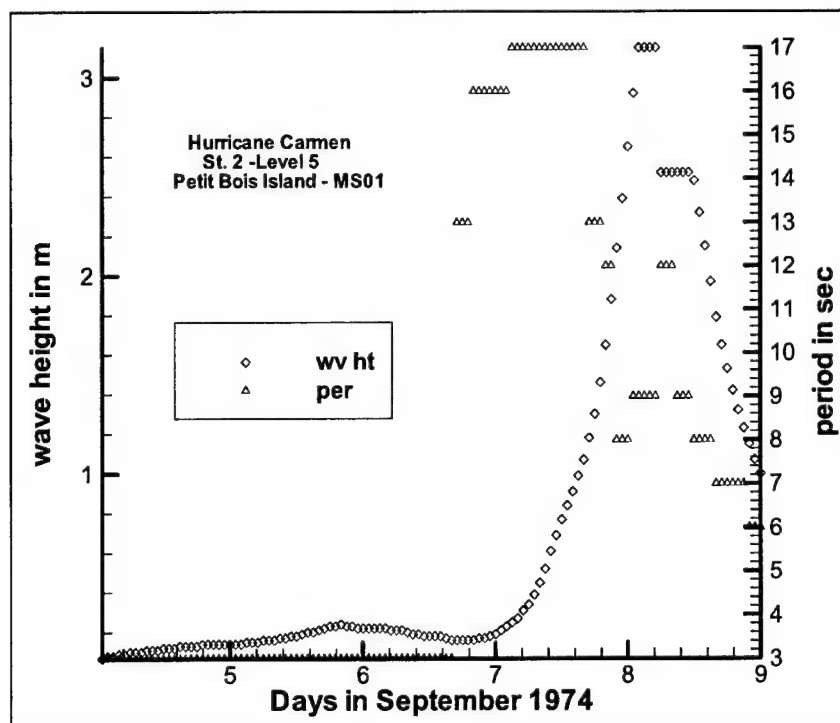


Figure 8-16. Wave height and period model results for Hurricane Carmen at a Level 5 grid point near Petit Bois Island

Summary

Hurricane-induced wave climates and water levels were analyzed to aid in designing the confining dike of the CDF so that it can withstand local wave forces. This analysis is limited to weaker hurricanes with return periods of less than 25 years, the approximate design life of the CDF. Wave height in the study area is limited by shallow water; hurricane-induced storm surge increases the water-surface level permitting greater wave heights. In the immediate study area, weaker hurricanes can induce a 0.61-m (2-ft) increase in water level due to storm surge with wave height and period of 2 m (6.56 ft) and 14 sec, respectively, propagating from the open gulf. More severe storms will create higher surge and wave conditions, although designing a CDF to withstand the effects of more severe storms was deemed unlikely.

References

- Cardone, V. J., Greenwood, C. V., and Greenwood, J. A. (1992). "Unified program for the specification of hurricane boundary layer winds over surfaces of specified roughness," Contract Report CERC-92-1, U.S. Army Engineer Waterways Experiment Station, Vicksburg, MS.
- Garratt, J. R. (1977). "Review of drag coefficients over oceans and continents," *Monthly Weather Review* 105, 915-929.
- Jarvinen, B. R., Neumann, C. J., and Davis, M. A. (1988). "A tropical cyclone data tape for the North Atlantic Basin, 1886-1983: Contents, limitations, and uses," NOAA Technical Memorandum NWS NHC 22, National Hurricane Center, Miami, FL.
- Jelesnianski, C. P., and Taylor, A. D. (1973). "A preliminary view of storm surges before and after storm modifications," NOAA Technical Memorandum ERL WMPO-3, Weather Modification Program Office, Boulder, CO.
- Scheffner, N. W., Mark, D. J., Blain, C. A., Westerink, J. J., and Luetich, R. A., Jr. (1994). "ADCIRC: An advanced three-dimensional circulation model for shelves, coasts, and estuaries; Report 5: A tropical storm database for the east and Gulf of Mexico coasts of the United States," Technical Report DRP-92-6, U.S. Army Engineer Waterways Experiment Station, Vicksburg, MS.

9 Summary and Conclusions

An island CDF is one of several alternatives being considered for placement of sediment dredged from the Federal navigation project that services the Pascagoula River and Bayou Casotte Harbors. Dredging quantities to be placed in the CDF are estimated to range from 2.37 to 3.06 million cu m (3.1 to 4.0 million cu yd) every 3 years, for the next 40 years. Three potential sites for an island CDF were considered in the study; each is located near the section of the project with the highest maintenance requirements, which is between mile markers 2 and 5 of the main Pascagoula Channel leading to the Pascagoula River Harbor and the U.S. naval facilities.

The three possible sites and configurations are (Figure 9-1): an expansion of Singing River Island on its south and southwest sides (Alternative 1), an island just to the northeast of Round Island and southeast of Singing River Island, between Round Island and the navigation channel (Alternative 2), and north of the point where the navigation channel bifurcates, between the bifurcation point and the mainland (Alternative 3). The approximate size of each CDF considered was 4,046,825 sq m (1,000 acres).

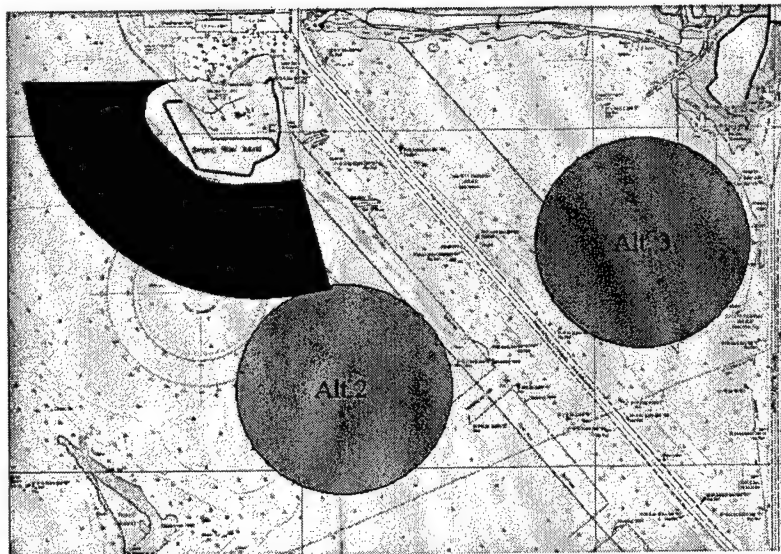


Figure 9-1. Locations of three alternative CDFs investigated in the engineering studies

CDF Capacity and Dike Elevation

A key design parameter for the CDF is the height of a dike required to contain the dredged material. Sediments will consolidate with time, and consolidation is an important process in determining required dike height. A number of studies were performed to examine the sediment consolidation process and to assess the site capacity of the CDF. Active management of sediments placed in the CDF (primarily dewatering) can reduce the required dike elevation. A series of sensitivity tests were conducted to examine reductions that are possible with increasing levels of site management. Construction of a perimeter dike using sediment is the primary method considered for containment. However, such a dike reduces the interior capacity of the CDF by reducing the surface area available for disposal. The benefits associated with constructing a dike using steel sheetpiling were also examined. For a given volume, use of a steel sheet-pile perimeter containment structure could reduce the CDF area from 4,046,825 sq m (1,000 acres) to 3,642,143 sq m (900 acres).

The following conclusions were derived from this series of studies. The proposed dredging quantities and dredging scenarios will require dike elevations in the range of 15.24-21.34 m (50-70 ft) for the original scenario (3.06 million cu m (4.0 million cu yd)) annually, 50 percent efficiency in terms of site management). This range considers variability in the consolidation characteristics of the four sediments that were tested. These results also assume an 8-month disposal period, once every 3 years, for 40 years. If a reduced dike volume configuration (steel pilings) is used, then the required dike elevations would decrease to the 7.01-12.19-m (23-40-ft) range. Sensitivity simulations comparing dike elevations for varying levels of drainage efficiency indicate the following: if the site management efficiency is increased from 50 to 75 percent, the required dike height decreased by an average of 3.96 m (13 ft); if the efficiency decreased to 25 percent, then the height required would increase by 2.74 m (9 ft). Site management includes dewatering measures during the 8 months of active filling and over 2 years of drying between placements. Other aspects of site management, with the aim of increasing consolidation and drying efficiency, include removal of surface water through lowering of weir crests and construction of surface trenches to promote improved drainage. Trenches placed adjacent to and parallel to the perimeter dike, and in the site interior facilitate removal of water off the site. As dredged material settles and dries, trenches can be progressively deepened.

Influence of a CDF on Water Circulation and Quality

Consideration of an island CDF has raised questions regarding the potential negative impacts of an island on water circulation and water quality. The influences of changes to circulation patterns on navigation and sediment transport processes are also of concern. Numerical modeling of circulation and water quality was performed to examine these potential impacts of an island. A 2-D hydrodynamic modeling approach was adopted to simulate circulation in the northern Gulf of Mexico and the entire Mississippi Sound. This model provided

boundary conditions to more detailed 3-D modeling of circulation and water quality in the vicinity of the proposed CDF sites.

Results from 2-D hydrodynamic modeling

A 2-D depth-averaged numerical model (ADCIRC) for simulating tidal circulation in the Mississippi Sound was developed and calibrated via comparisons to constituent-synthesized and measured water-surface elevations and currents. Model performance was evaluated for both astronomical tide and wind-generated flow conditions. For pure astronomical tide conditions, the model reproduced the constituent-synthesized water-surface levels to within 0.03 m (0.1 ft) in amplitude and 2 min in phase at peak spring tide, whereas differences between modeled and constituent-generated currents were generally within 0.03 m/sec (0.1 ft/sec) and 2 min. For conditions including effects of wind, examination of model accuracy was done for a period of time between 1 February 2001 and 15 March 2001, using data acquired on site as part of these investigations. The model generally matched measured water-surface elevations at the Pascagoula PI gage within 0.06 m (0.2 ft). Model-generated currents agreed well with those measured at the intersection of the GIWW with the Pascagoula Channel. However, model accuracy diminished when winds rapidly shifted direction, and was attributed to using wind fields having a temporal resolution of only 6 hr (the only available wind fields). This resolution was too coarse to depict rapidly changing wind directions that can occur sometimes at the site.

The following is a summary of changes to the current field that can result from construction of each proposed CDF alternative. These results are based on applications of the ADCIRC model.

Alternative 1. This alternative is constructed by expanding Singing River Island along its southern and western shore. Aligned with the northern shore, the expansion extends 1,310.64 m (4,300 ft) towards the west, and aligned with the eastern shore, the expansion extends about 1,188.72 m (3,900 ft) to the south. The southern shoreline of the expansion roughly parallels the existing arc-shaped southern shoreline of the island, and is displaced about 1,188.72 m (3,900 ft) from the present shoreline. The westward expansion blocks a greater portion of the inflow emanating from the West Pascagoula River and diverts it into the naval turning basin, located between Singing River Island and the mainland. Under solely astronomical forcing, model simulations show currents increasing by about 29 percent, whereas under winter storm conditions, model simulations show currents increased in the range of 19 to 43 percent. For more typical or average conditions, currents at the naval basin will increase from 18 to 33 percent. This expansion also increases currents flowing between Singing River and Round Islands, possibly leading to increased erosion pressure on Round Island.

Alternative 2. This alternative is circular in shape, having a diameter of about 2,286 m (7,500 ft), and a surface area of 4,046,825 sq m (1,000 acres). Its northern boundary is approximately 1,051.56 m (3,450 ft) south of Singing River Island, whereas its southwestern edge is located about 1,188.72 m (3,900 ft) from Round Island. Pascagoula Channel resides about 813.82 m (2,670 ft) (at its closest approach) to the east-northeast from this alternative. Under solely

astronomical forcing, the model predicts that ebb-current direction north of this CDF is directed towards Pascagoula Channel. However, model tests conducted with wind forcing show no significant change in current direction between the existing-condition and Alternative 2 configurations; it is possible that, under a westerly wind and ebb tide condition, Alternative 2 could induce greater crosscurrents at the channel. Also, a reduction in currents immediately west of Alternative 2 suggests that a greater percentage of West Pascagoula River discharge will be transported south of Round Island than presently occurs. For Alternative 2, results from tidal simulations show a small local increase in peak tide velocities along the northeastern part of Round Island. Increases in velocity could increase erosion pressure on Round Island at this location. Also, strong currents of 0.30 m/sec (1 ft/sec) and greater were calculated along the southwest portion of Alternative 2 for spring ebb tide conditions. Currents of this magnitude are capable of transporting fine sand, and this may be an important consideration in designing the perimeter dike.

Alternative 3. As with Alternative 2, this alternative is circular in shape with a diameter of 2,286 m (7,500 ft). Its southern extent resides about 2,682.24 m (8,800 ft) north from the intersection of the Pascagoula and Bayou Casotte Channels, and the minimum distance between this island and the mainland is about 609.6 m (2,000 ft). Furthermore, it is positioned so that its southwestern boundary is 259.08 m (850 ft) from the Pascagoula Channel (north of the intersection), and its eastern boundary is 259.08 m (850 ft) from the Bayou Casotte Channel. This alternative does not appear to modify currents between this CDF and the mainland. This alternative does impact, however, the speed and direction of currents along the Pascagoula Channel. Increases in speed are small, about 0.12 m/sec (0.4 ft/sec), and currents have a northerly, as opposed to a northwesterly, heading in the vicinity of Singing River Island and the channel.

Results from 3-D hydrodynamic modeling

The 2-D hydrodynamic model, ADCIRC, was also used to provide boundary conditions for 3-D model simulations of the base condition and three island alternatives using the CH3D model. The primary motivation for the 3-D circulation modeling was to provide hydrodynamics for the 3-D water quality model, CE-QUAL-ICM.

CH3D was calibrated to a reconstructed tide produced from astronomical tidal constituents developed from a limited dataset of water surface and current (Outlaw 1983)¹. The model reproduced currents with a comparable degree of accuracy as Outlaw's constituents. CH3D hydrodynamics were further validated by comparison of prototype data collected in February/March 2001, the same period considered in the 2-D model validation. The modeled water surface and currents compared well with measurements for larger-scale weather events, but limitations in the temporal and spatial scales of the wind fields and the model's representation of wind fields limited the representation of small-scale weather phenomenon.

¹ Outlaw. (1983). op cit. p. 5-35.

Hydrodynamic model results from the 3-D modeling were consistent with the results from the 2-D model.

Alternative 1. The expansion of Singing River Island constricts the area between Singing River Island and Round Island, which results in increased velocities between the two islands during both ebb and flood currents. Another change in circulation is located northwest of the expanded Singing River Island, where currents are decreased during flood tide.

Alternative 2. The island southeast of Singing River Island also constricts the flow between Singing River Island and Round Island, and noticeably more than Alternative 1. The constriction tends to increase velocities between the islands during both ebb and flood flows. In addition, stronger flood flows are estimated in the near-bottom currents through the turning basin north of Singing River Island, but weaker currents are observed between the western tips of Singing River and Round Islands. The changes in currents for this alternative are modest (approximately 0.05 m/sec (.16 ft/sec)) from the perspective of tidal circulation.

Alternative 3. An island in the triangle does not appear to have great influence on tidal circulation. Differences in circulation patterns between Singing River Island and Round Island and near the Pascagoula River mouth are hardly noticeable. A slight increase in bottom currents between the West Pascagoula River mouth and the turning basin north of Singing River Island is one of the few noticeable differences. However, for the flood tide, a zone of weaker currents develops in the lee of the proposed island. This calm zone does not persist for long and was seen to last for only a few hours during a portion of the flood cycle.

While differences in the tidal circulation were observed for each of the alternatives, the changes in velocities in the low-energy tidal environment were not remarkable from a tidal circulation perspective.

Results from water quality modeling

Validation of the CH3D modeling of temperature and salinity was performed to available data from April-September 1997 that were acquired from the Mississippi Department of Environmental Quality, the U.S. Geological Survey, and other data sources. Comparisons of model simulations to measured data indicated that the model accurately represents temperature and salinity within the study area. The water quality model, CE-QUAL-ICM was independently calibrated for the same period using these same measured data, hydrodynamics from the CH3D model, and appropriate kinetic rates determined in the ICM model calibration process. Both model simulations showed similar calculations of temperature and salinity, as expected.

The water quality modeling approach for this study was referred to as level 2 treatment, with level 1 being a full eutrophication calibration. This approach is similar to full calibration except that all oxygen demand is specified as a BOD. SOD is specified as a constant rate and together with BOD are the only sinks for DO. Final calibration results compared favorably to observed data given the limited amount of comparison and boundary data available to evaluate and drive the model, respectively.

Changes in bottom DO were an indicator of changes to water quality. Results for each option as compared to base condition (without-project) results are presented in the following paragraphs. Results were compared for a series of six model output locations (seen in Figure 6-14):

Alternative 1. Comparison of Alternative 1 results to base results showed minimal difference in water quality at all stations. The model output location just north of Singing River Island showed the greatest differences in bottom DO concentrations, but that was to be expected since it was the closest station to the expanded Singing River Island. Calculated total averaged flows for this alternative, for a transect entering the channel behind Singing River Island, decreased for all layers modeled in comparison to base total averaged flows; thus indicating that circulation had changed (especially in the lower layers) causing decreased DO concentrations.

Alternative 2. Comparison of Alternative 2 results to base results showed decreases in bottom DO concentrations ranging from approximately 0.7 g/m^3 to a maximum of 2.3 g/m^3 at most stations. The model output stations west of the West Pascagoula mouth (sta 1) and west of the Alternative 2 island (sta 3) showed the greatest differences. There does not appear to be much vertical advection in the system; consequently, concentrations are being affected through horizontal advection, diffusion, or increased residence time in an area. Once residence time is increased, bottom DO concentrations are adversely affected and lower DO concentration water is moved to different areas through horizontal advection.

Alternative 3. Comparison of Alternative 3 results to base results showed minimal differences at all stations. Similar to the other two options, the model output station just south of the mainland, between the mainland and the proposed island CDF showed the greatest differences with the maximum difference being around 0.6 g/m^3 . Total average flow calculated for the transect entering the channel behind the Singing River Island had increased for the bottom three layers modeled; this indicated a change in circulation. In addition, higher concentrations of bottom DO at the model output station just south of the West Pascagoula River mouth also indicate circulation changes with water being advected from southeast of Round Island and not from behind Singing River Island.

Overall, comparison of results from Alternatives 1 and 3 to base results showed changes in circulation but caused minor effects to surface or bottom DO concentrations in the area of the expanded/created islands. Creation of the island for Alternative 2, the CDF located between Singing River and Round Islands seemed to create the greatest effects to bottom DO concentrations; however, surface DO was only minimally affected. The island has partially blocked and redirected circulation of the water in the study area since all model output stations show some degree of effect to bottom DO.

Influence of a CDF on Local Wind Wave Conditions

Construction of an island CDF will also influence the nearshore wind wave climate at the site, particularly in the sheltered lee of an island. Numerical wave

modeling, using WISWAVE and STWAVE, was performed both to assess the impact of an island on wave conditions along adjacent shorelines and in the navigation channels, and to characterize the local wave climate for use in design of any shore protection measures that would be incorporated into construction of the dike perimeter.

A 1990-1999 wave hindcast provided information to characterize the local wind and wave climate at the sites of the island CDFs. Successful validation of the hindcast with deepwater buoy and nearshore gage measurements acquired as part of these investigations gives credence to the hindcast results. Most significant wave energy at the three CDF sites appears to originate in the Gulf of Mexico, and propagates into the sound through the gap between Horn and Petit Bois Islands. The maximum significant wave height simulated during the 10-year hindcast period, at a location near the proposed CDF locations, was about 1.8 m (5.91 ft). For 60 percent of the time, significant wave heights are less than 0.5 m (1.64 ft). The wave climate information is useful in designing any peripheral protection integrated into construction of a CDF.

The wave climate data were used to identify a set of most prevalent and storm wave conditions, which were then used to examine the impact of the three alternative CDFs on wave conditions along adjacent shorelines and channels. Patterns of wave height change induced by the CDFs were similar because of the dominance of southerly incident wave directions. The results of the STWAVE application, using prevalent and storm waves with the existing and three alternative conditions, aided evaluation of the impact of the proposed CDFs.

Alternative 1. The expansion to Singing River Island would provide protection to the existing Singing River Island and could also serve to protect wetlands west of Singing River Island from incident wave energy. Alternative 1 would have little or no impact on wave conditions in existing navigation channels.

Alternative 2. A CDF near Round and Singing River Islands has the least impact on the adjacent mainland shoreline. This alternative provides a reduction in wave energy within the navigation channel behind it.

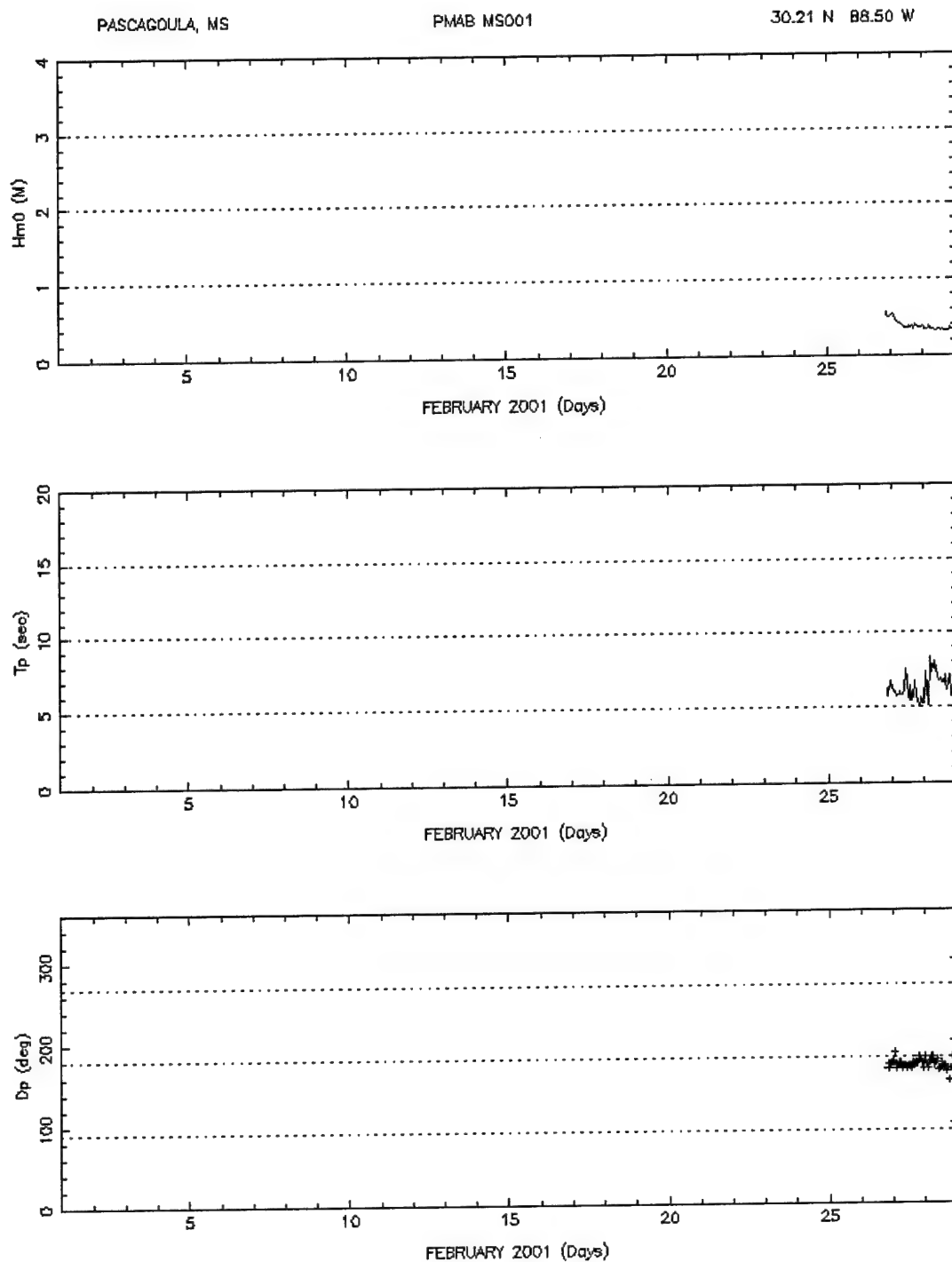
Alternative 3. A CDF in the triangle, just offshore of the mainland, had the most dramatic effect on waves in its lee, due to its proximity to shore. The sheltering of wave energy would normally produce local sediment accumulation behind the island for a sandy beach; and of the three alternatives, this alternative would have the greatest impact on the adjacent shoreline. However, this section of shoreline is depleted of sediment; no natural sandy beach exists. The island would greatly reduce waves in its lee, a benefit to the integrity and maintenance of coastal structures and docks behind it.

The studies documented here primarily examine the effects of an island CDF from a certain set of engineering perspectives, influence on waves and water circulation, and water quality. Alternatives were evaluated for each of the perspectives. It is difficult to rank the sites, without considering the full slate of factors that enter into this decision; and therefore, a ranking was not attempted. The same CDF location may be more favorable from one of these engineering perspectives and not from another. Other engineering considerations, such as impact of a CDF on channel sedimentation, were not directly investigated. Also, other perspectives will likely be factored into the decision-making process, such

as aesthetics, local preferences, cost, etc. A ranking process will have to consider a much larger slate of factors, as well as and the weighting assigned to different factors in the ranking process.

Appendix A

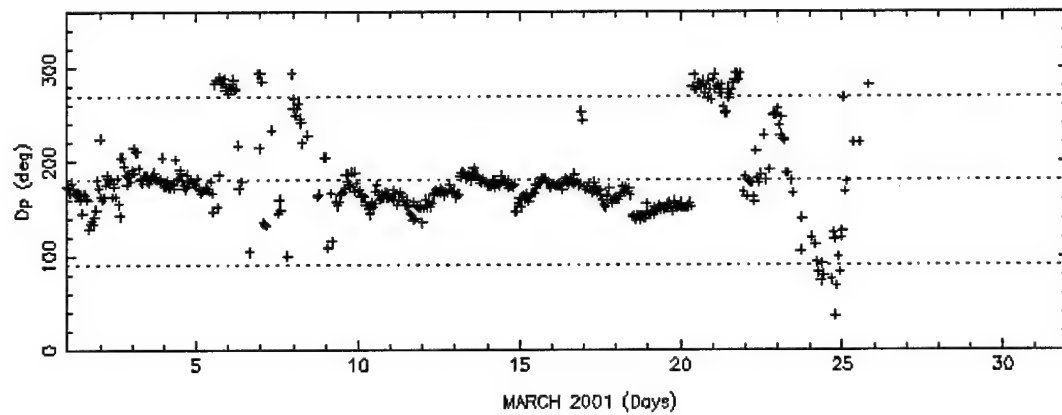
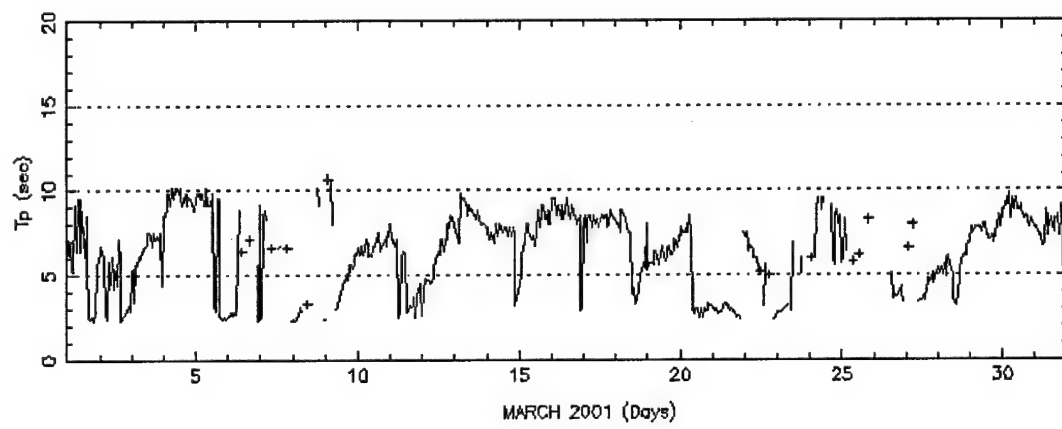
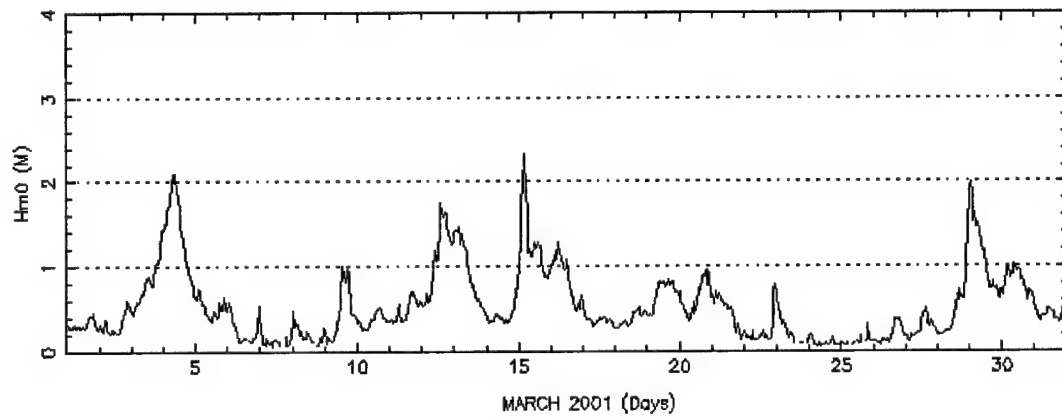
Gulf of Mexico Wave Gage Sta MS001 Data Plots

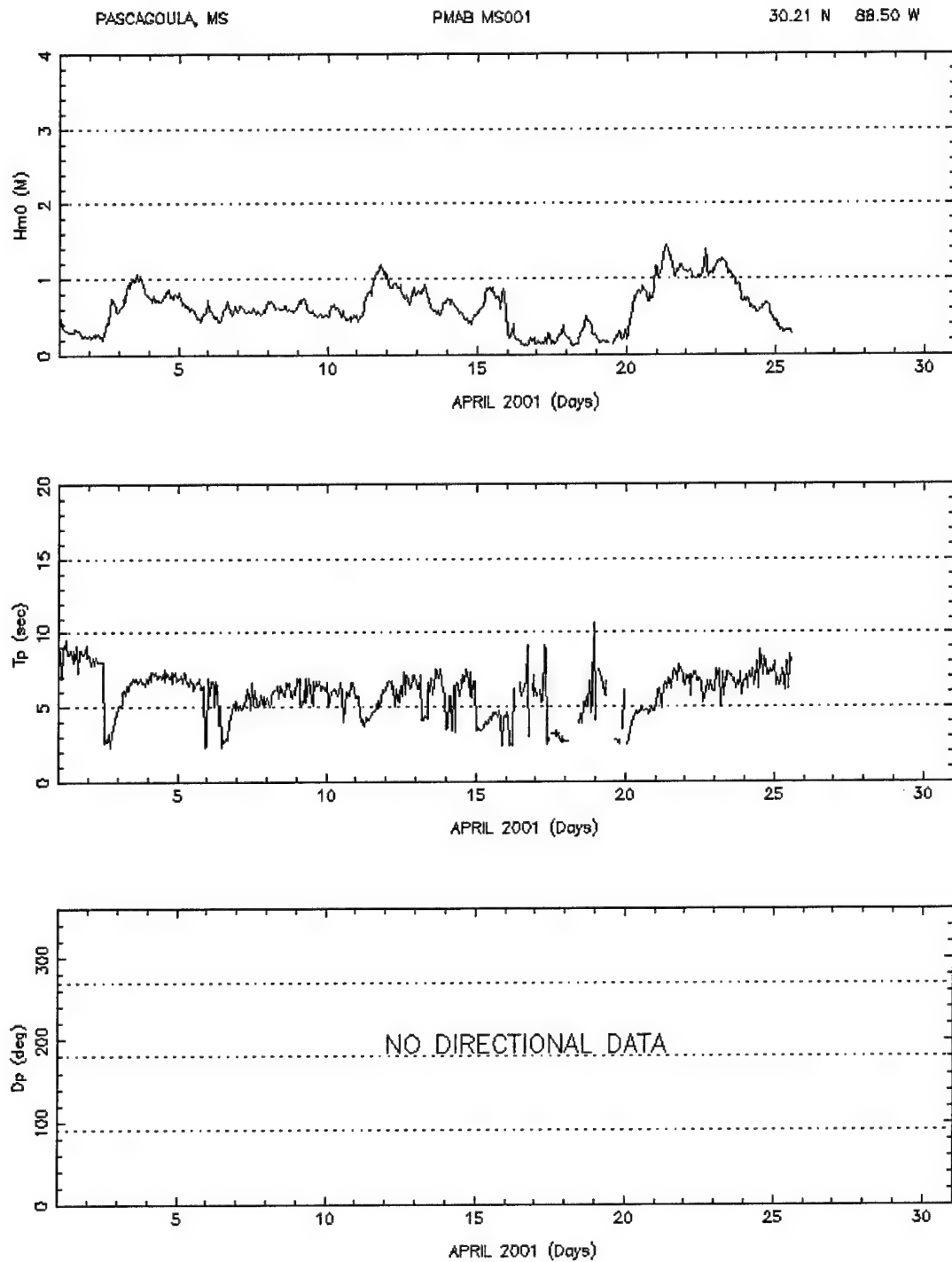


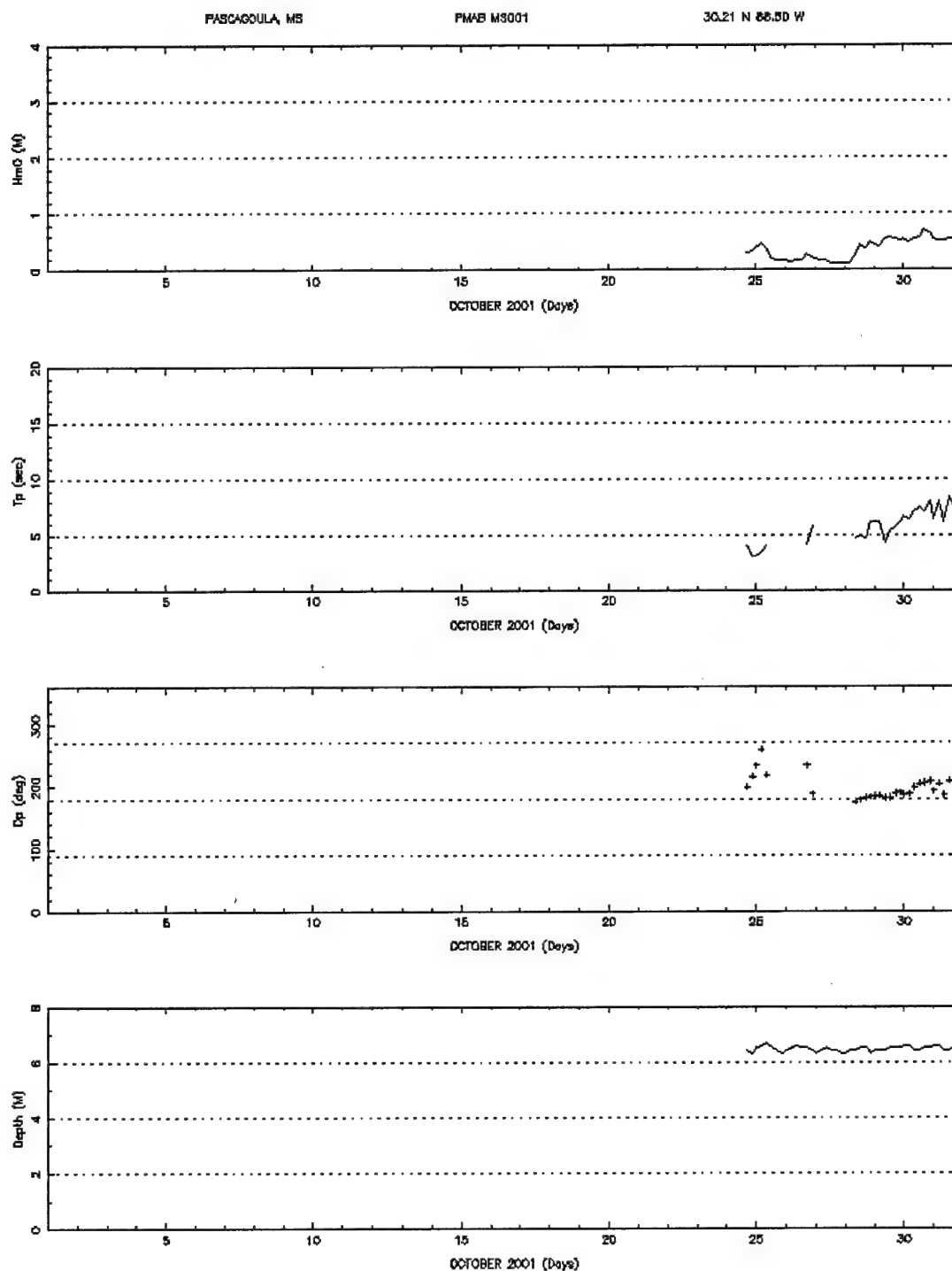
PASCAGOULA, MS

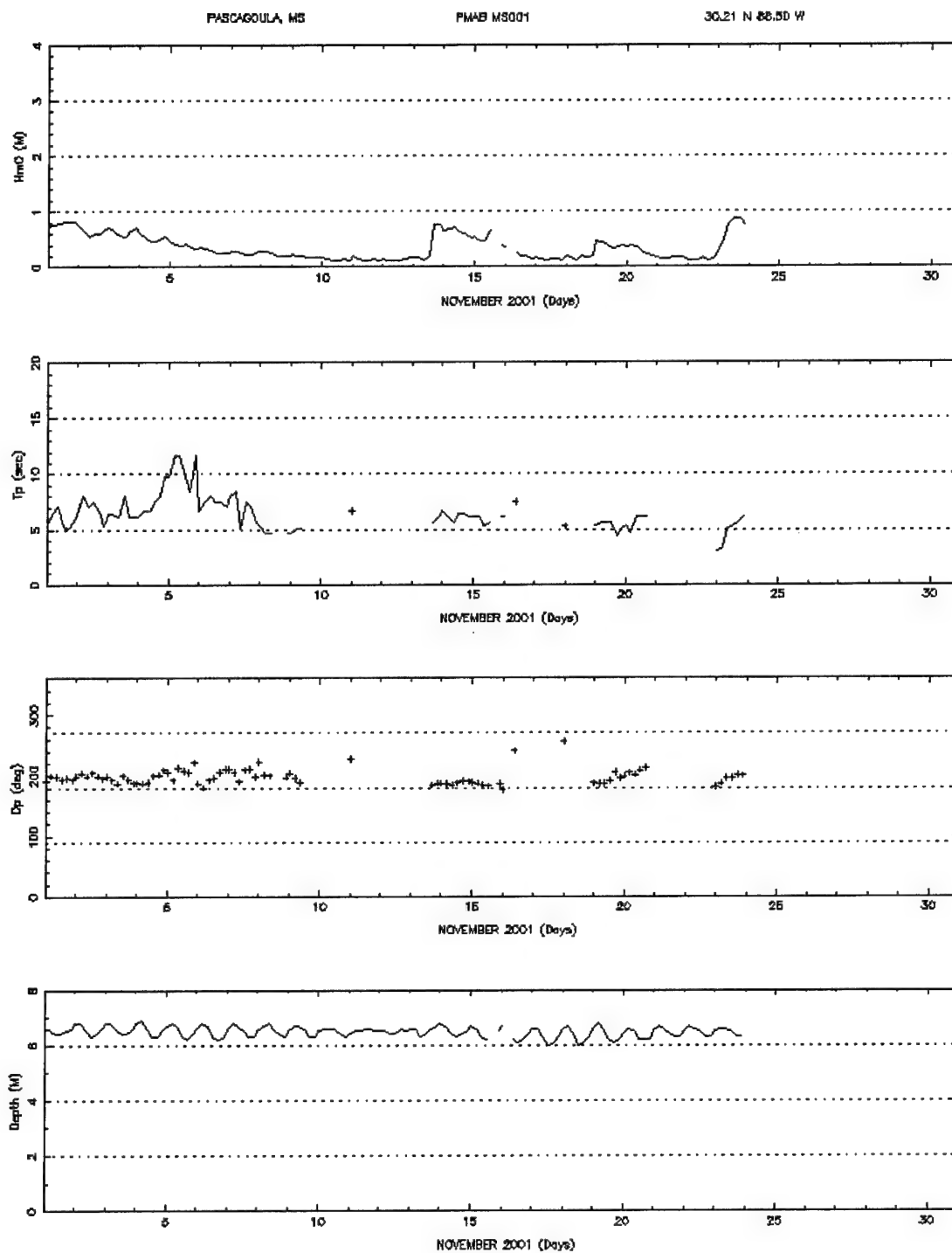
PMAB MS001

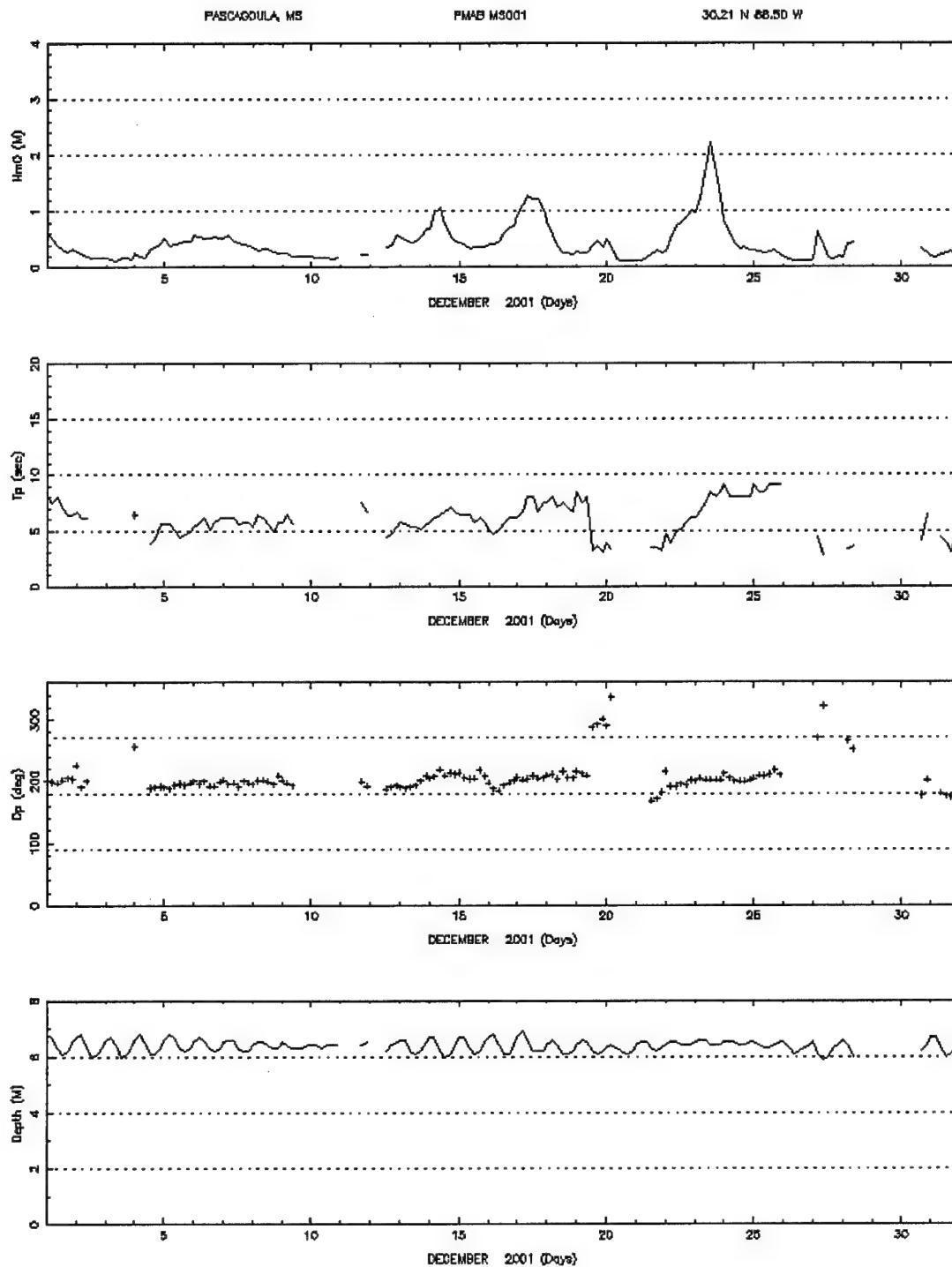
30.21 N 88.50 W

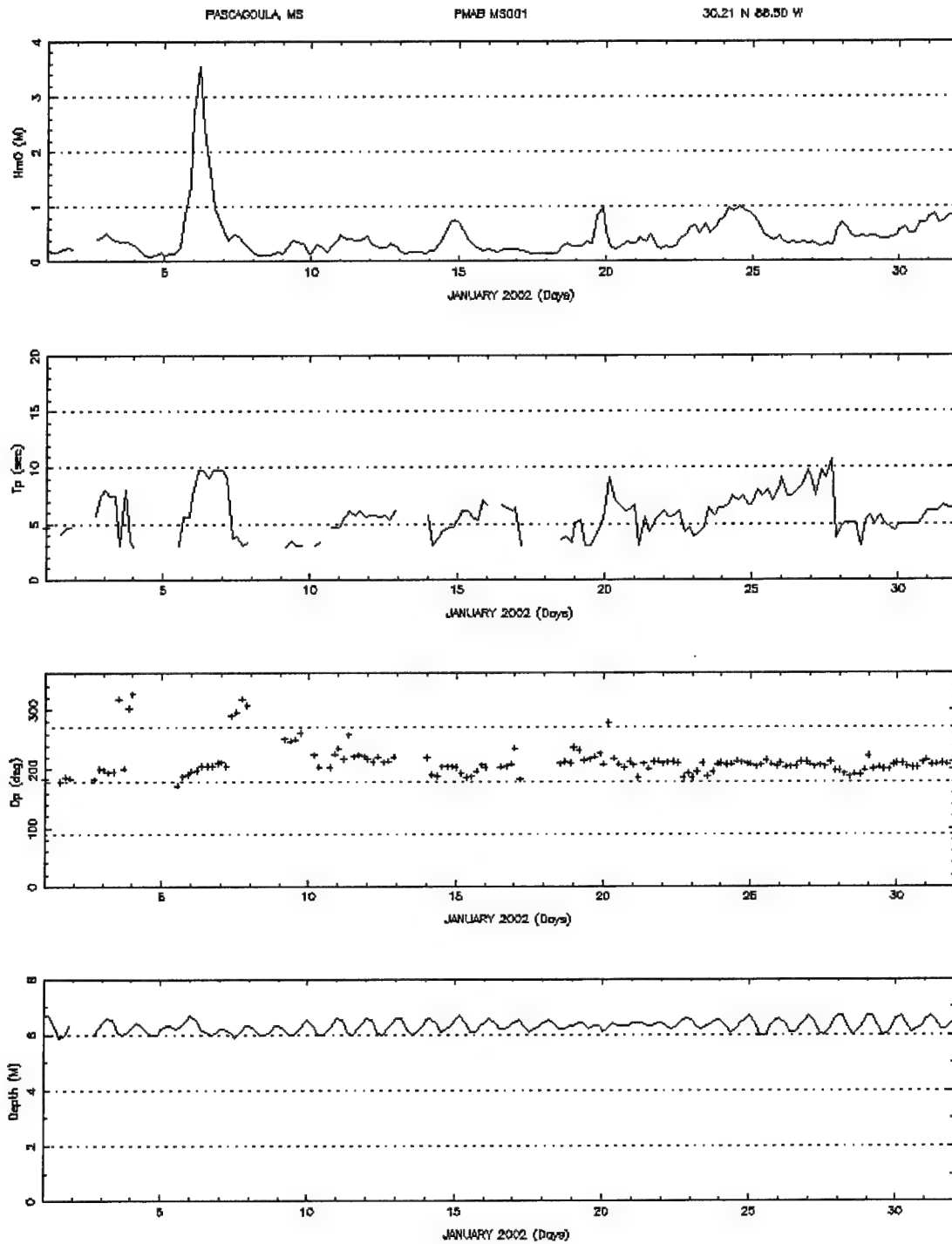


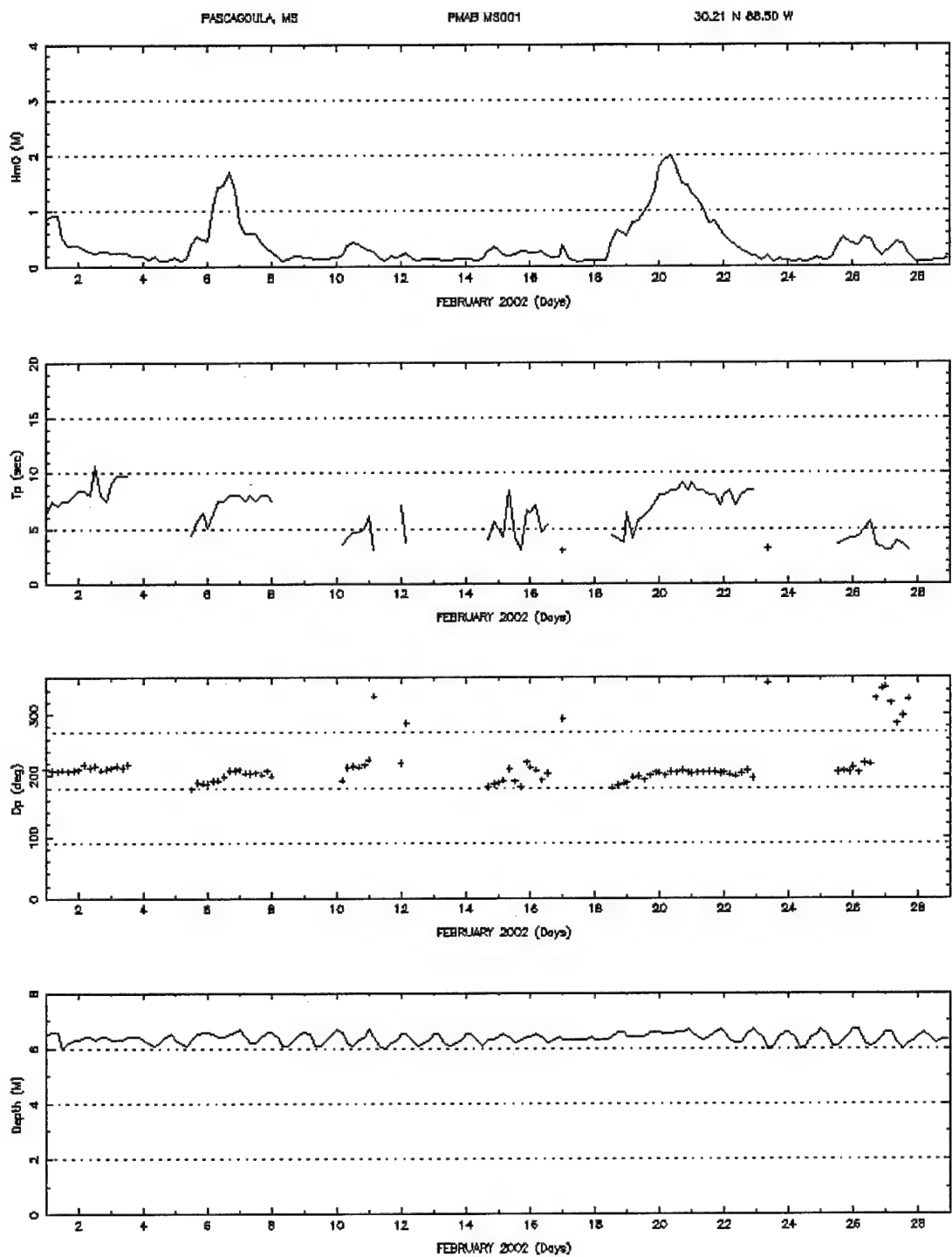


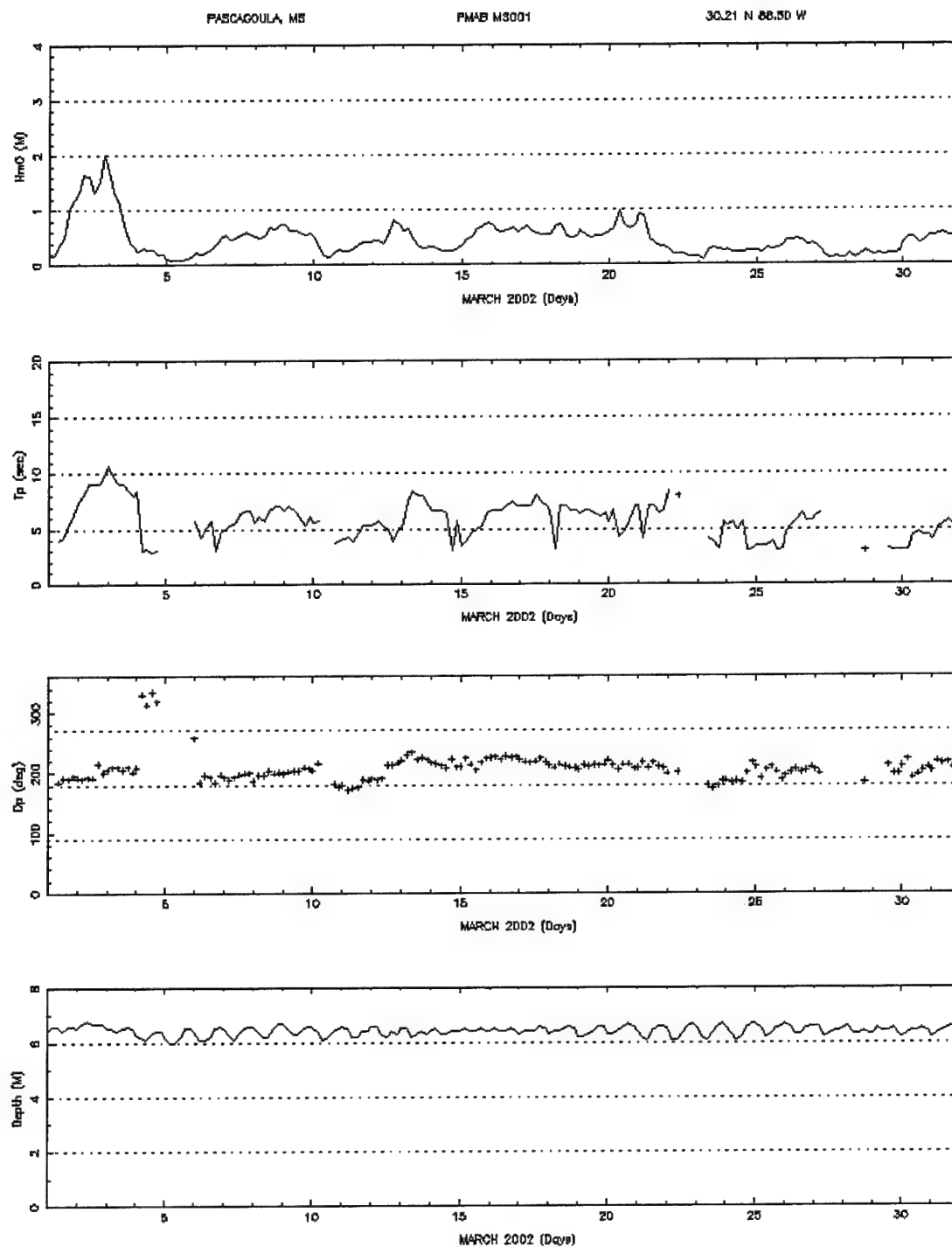


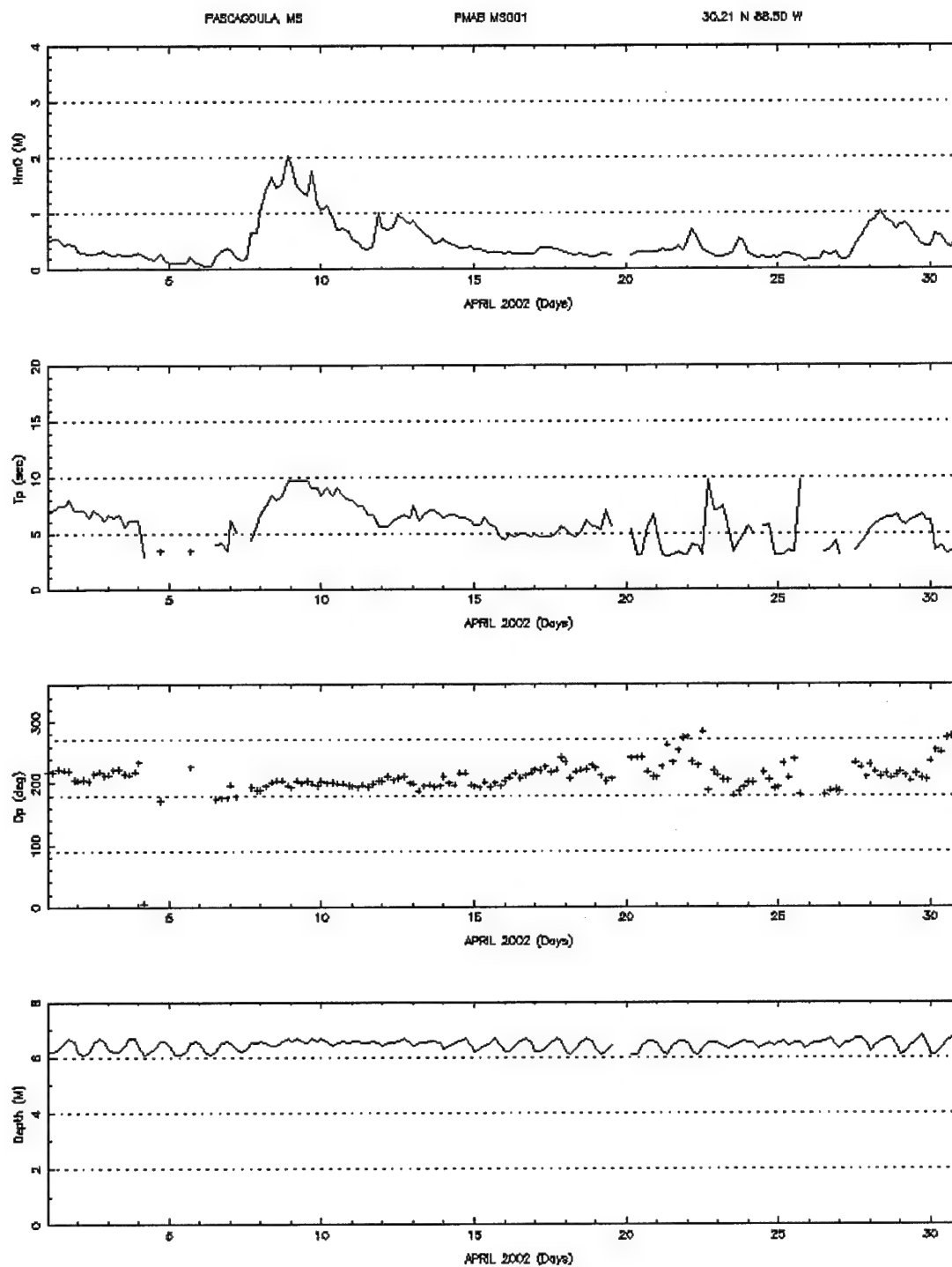


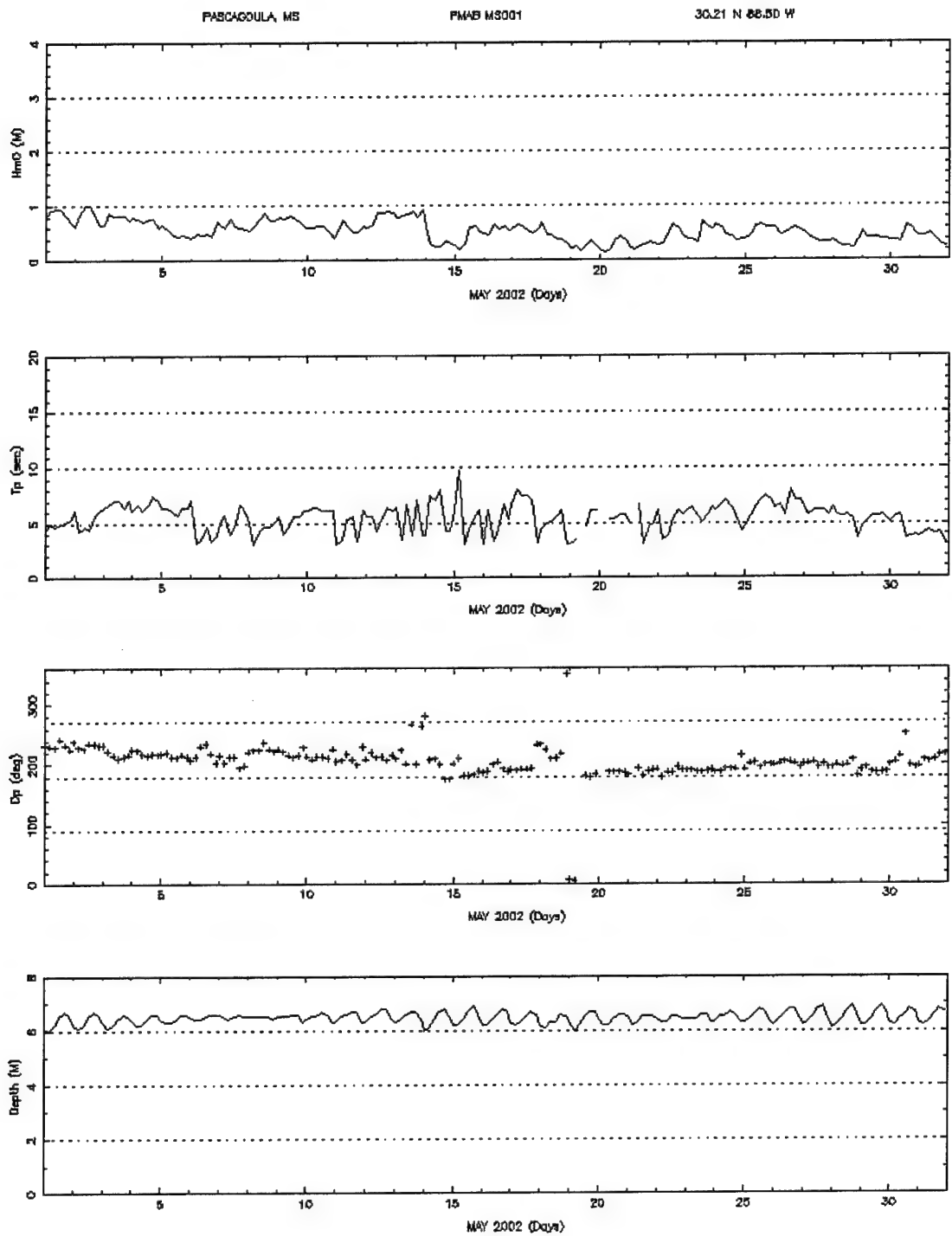


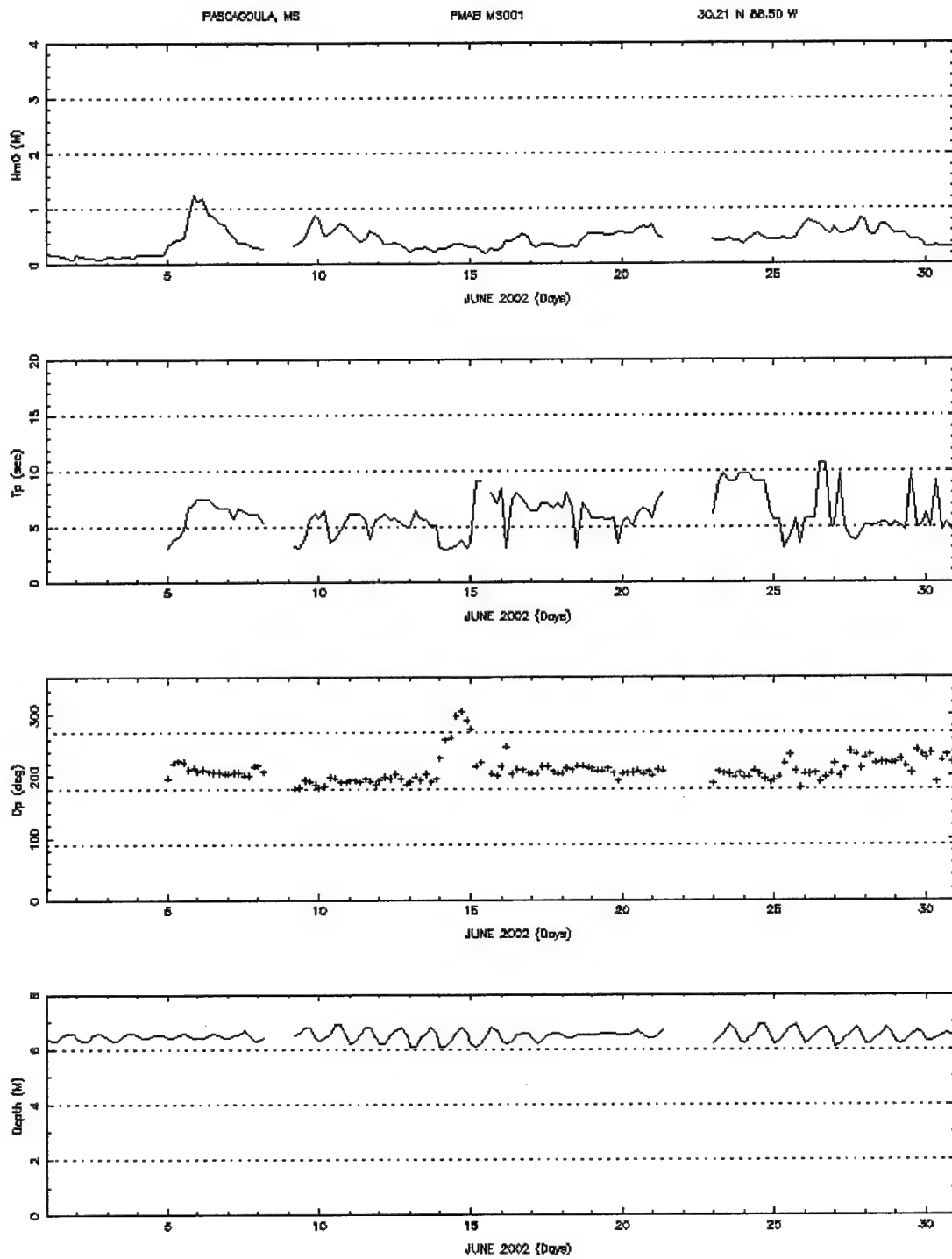


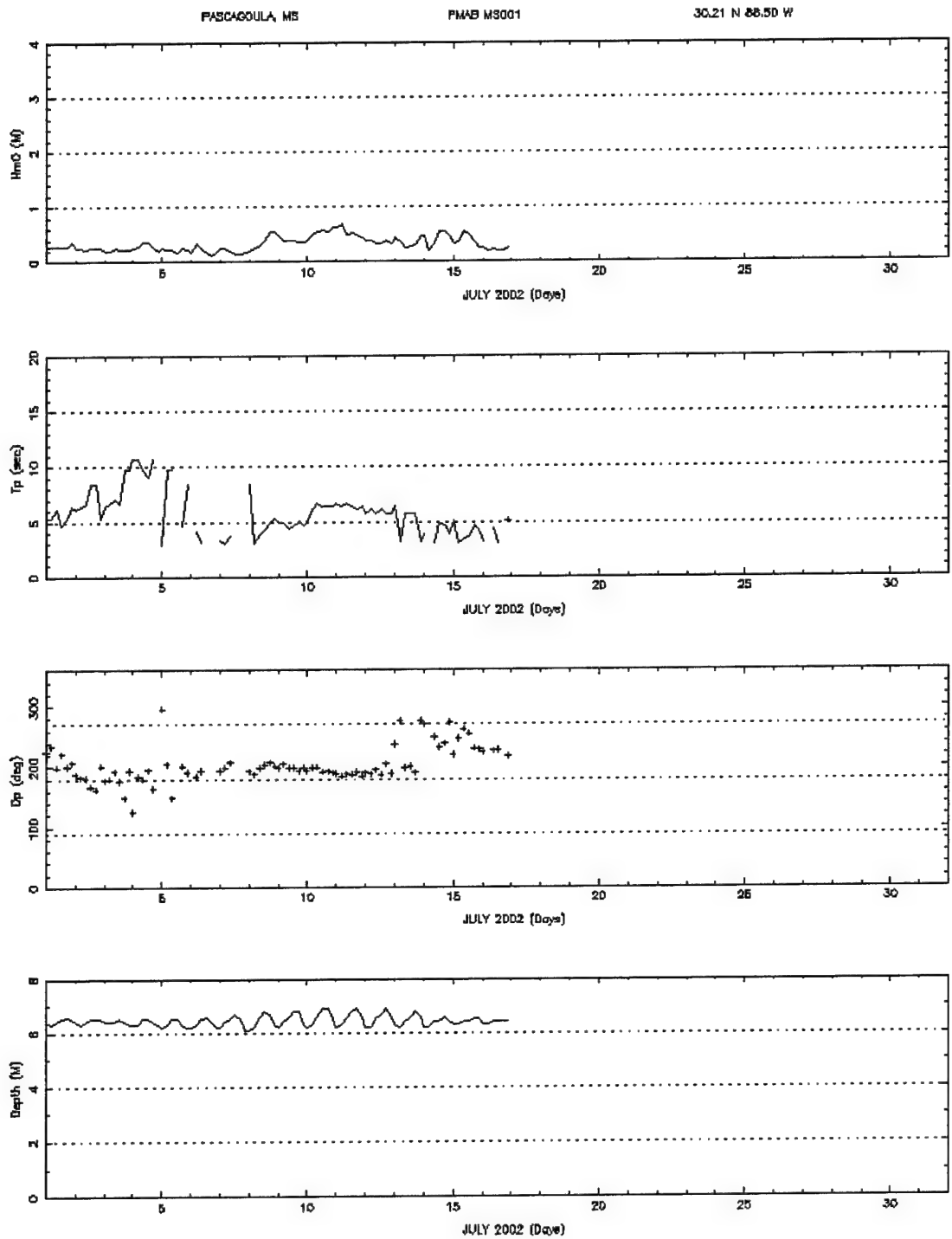








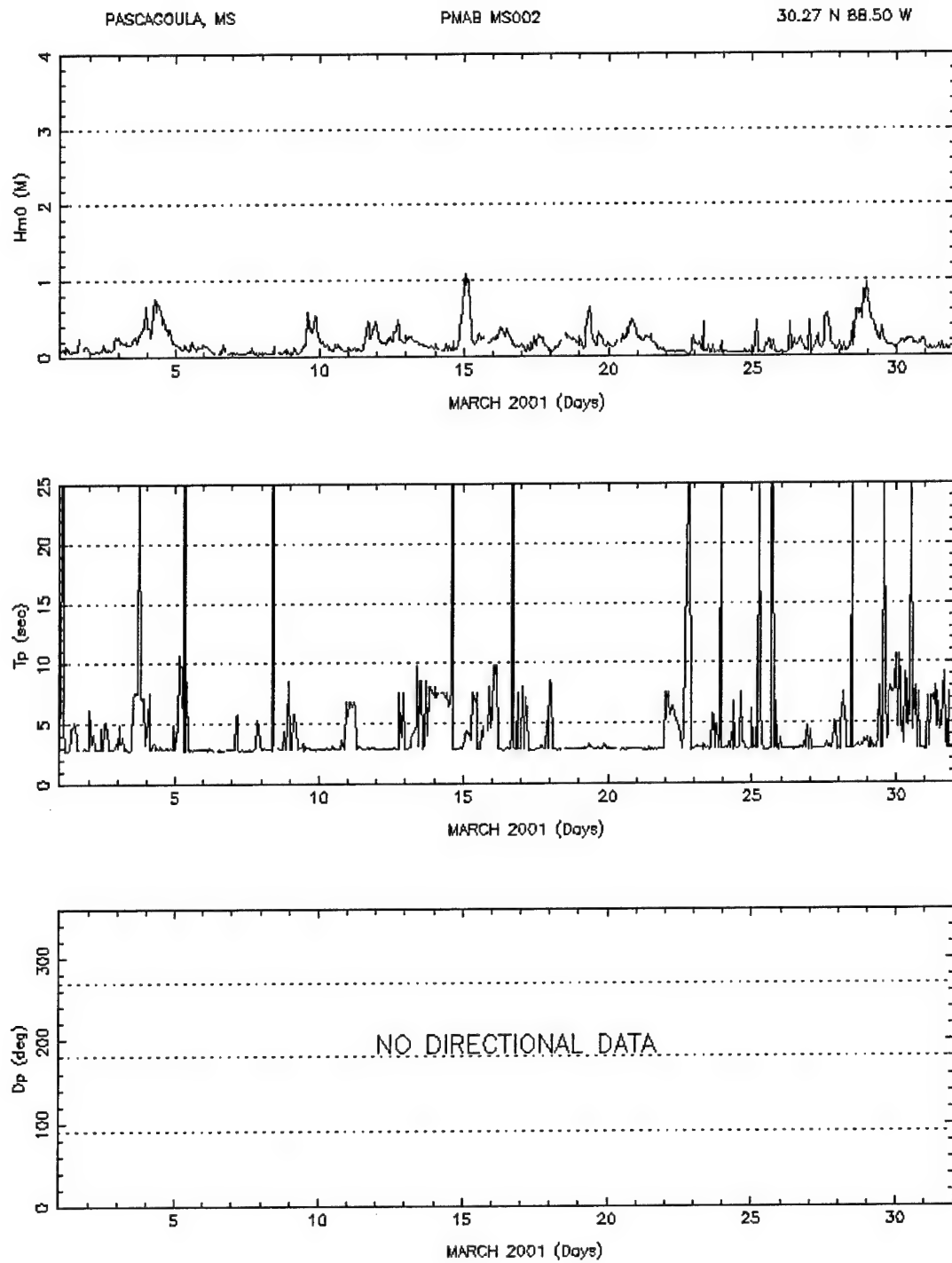


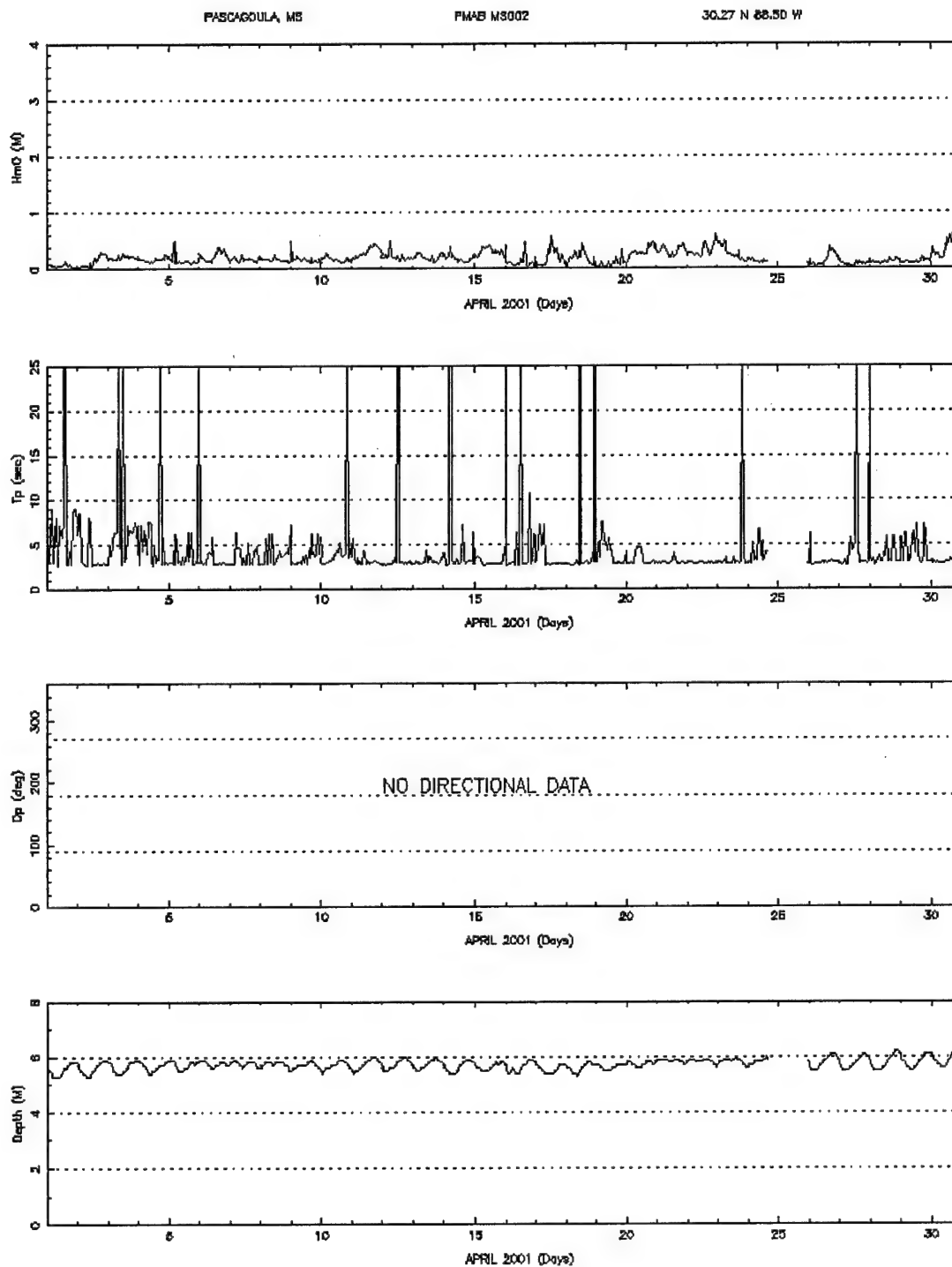


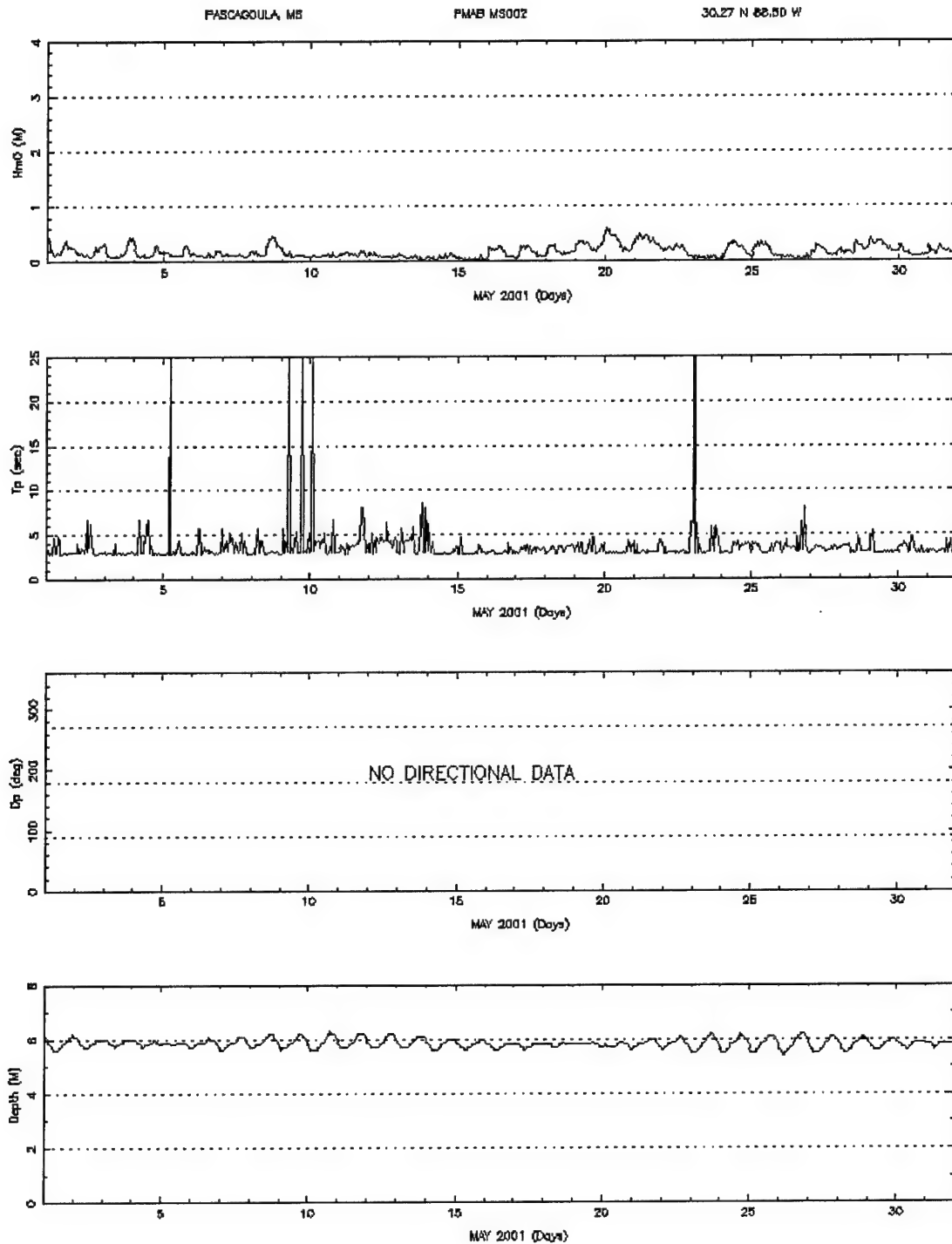
Appendix B

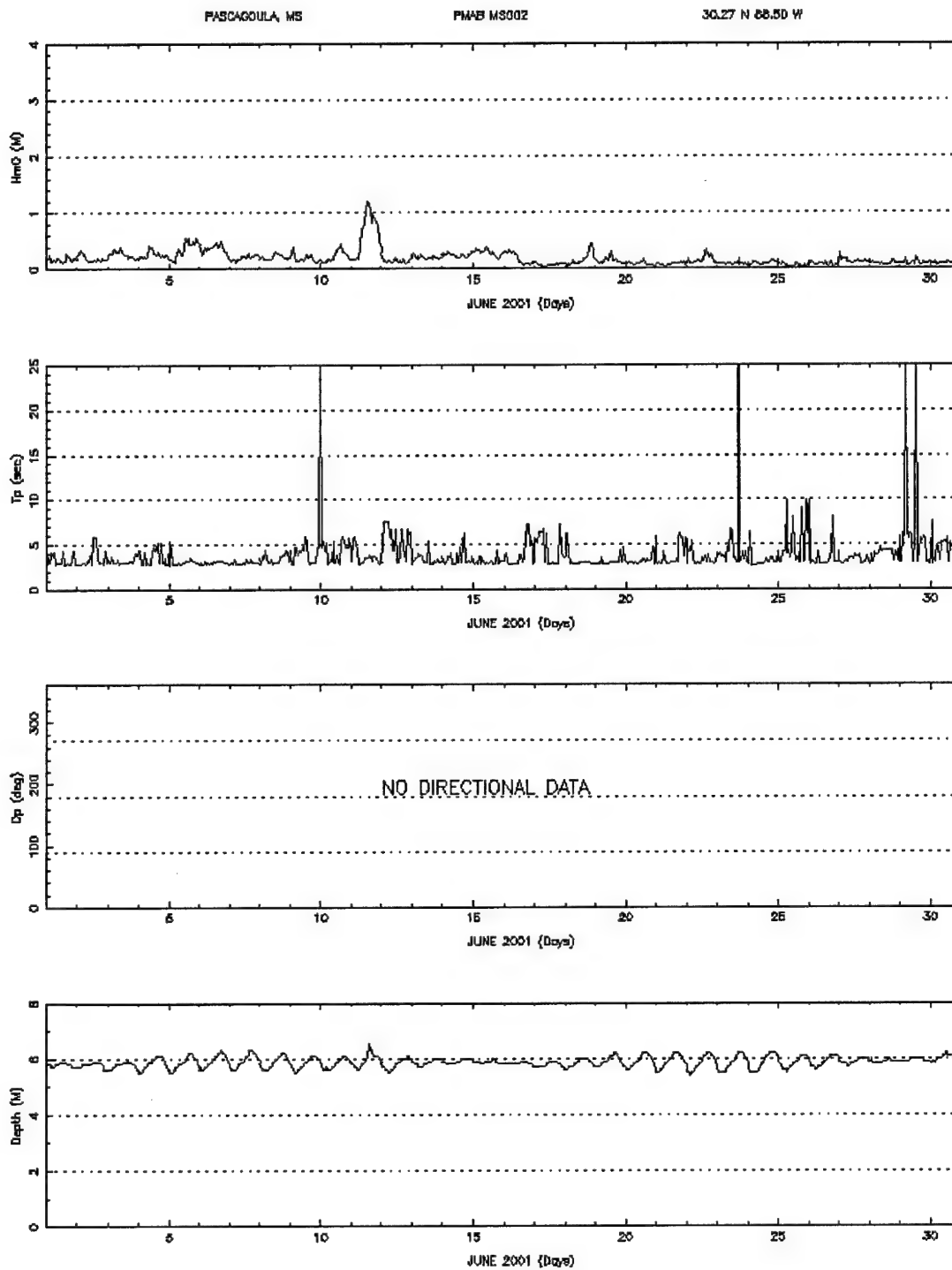
Mississippi Sound Wave Gage

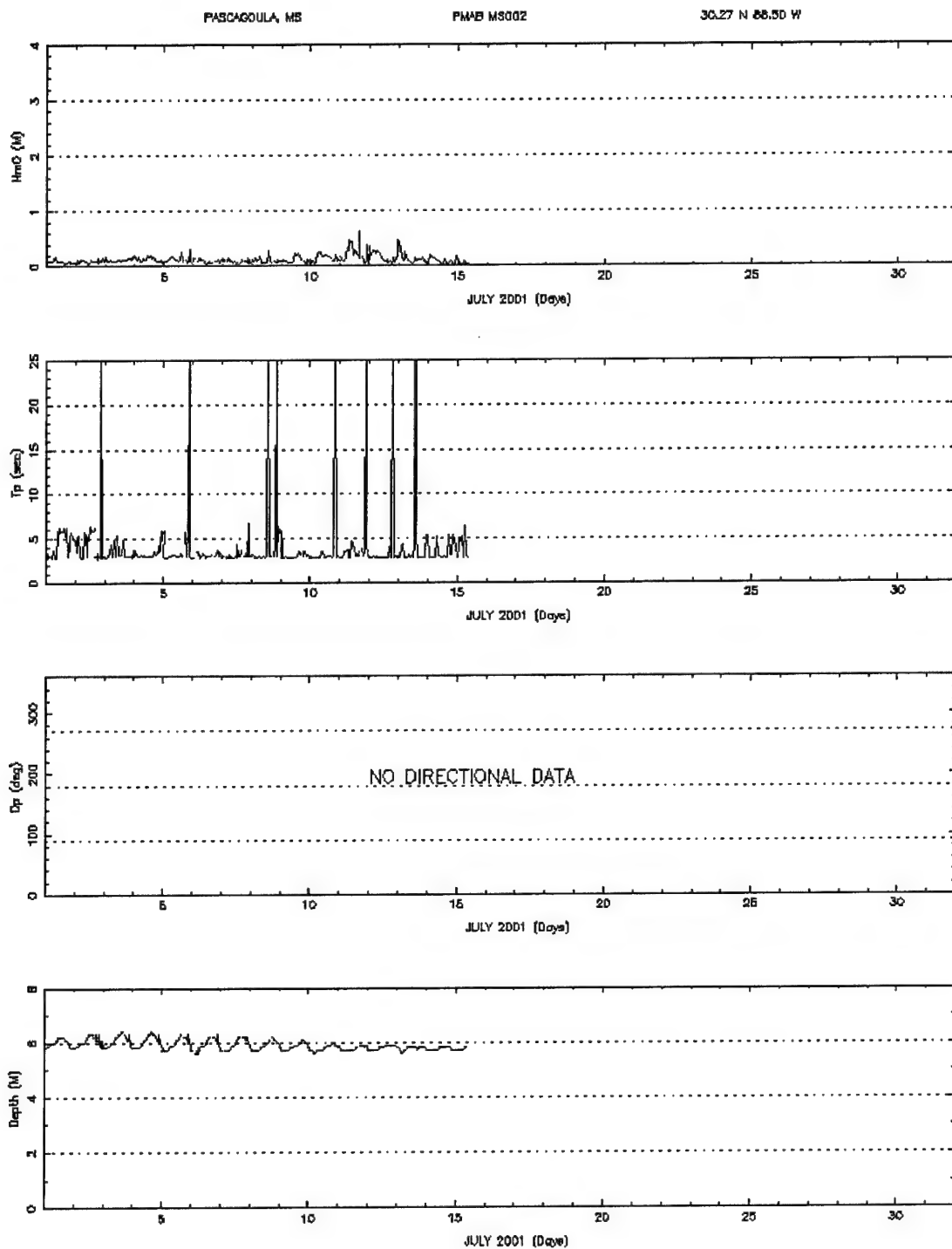
Sta MS00N Data Plots







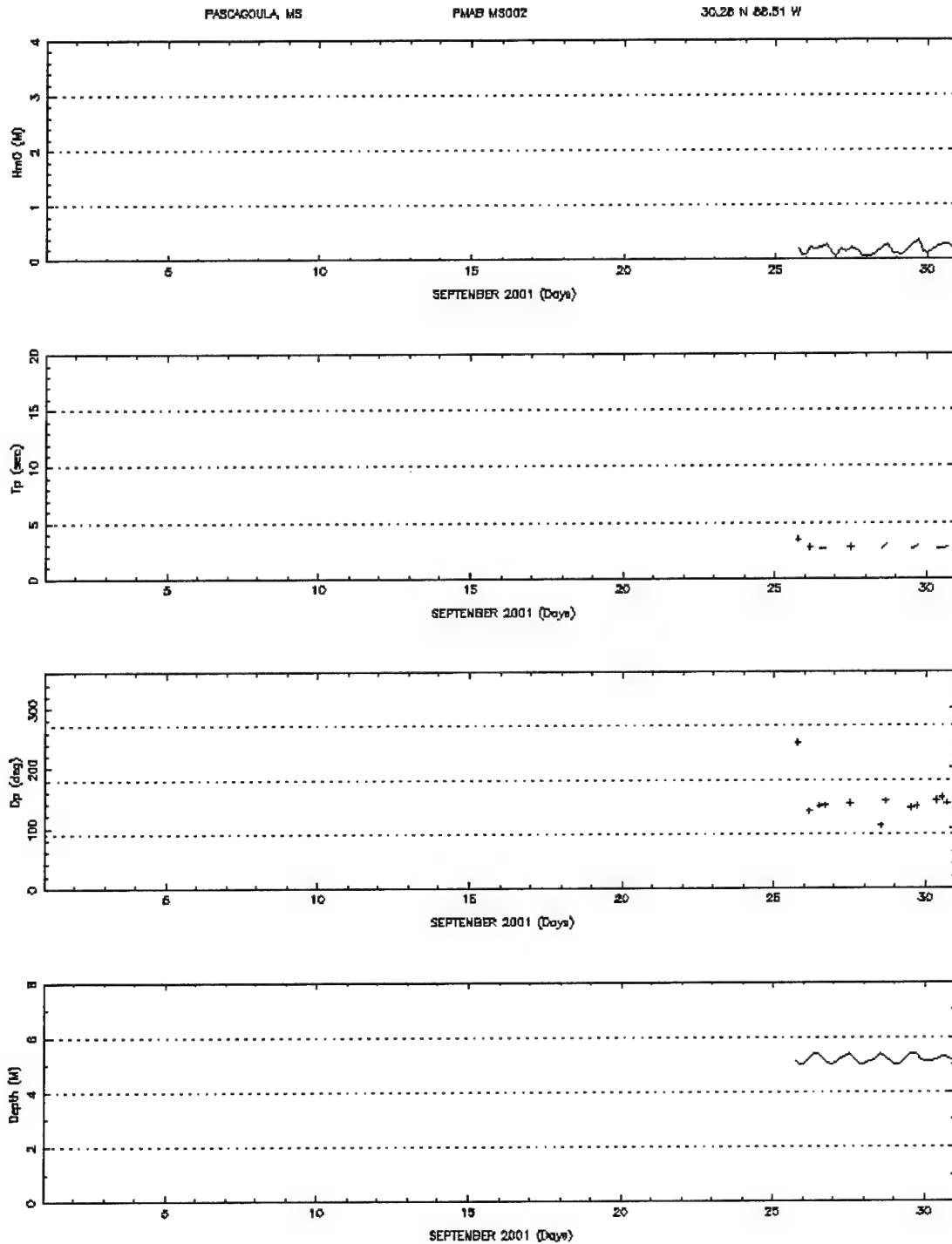


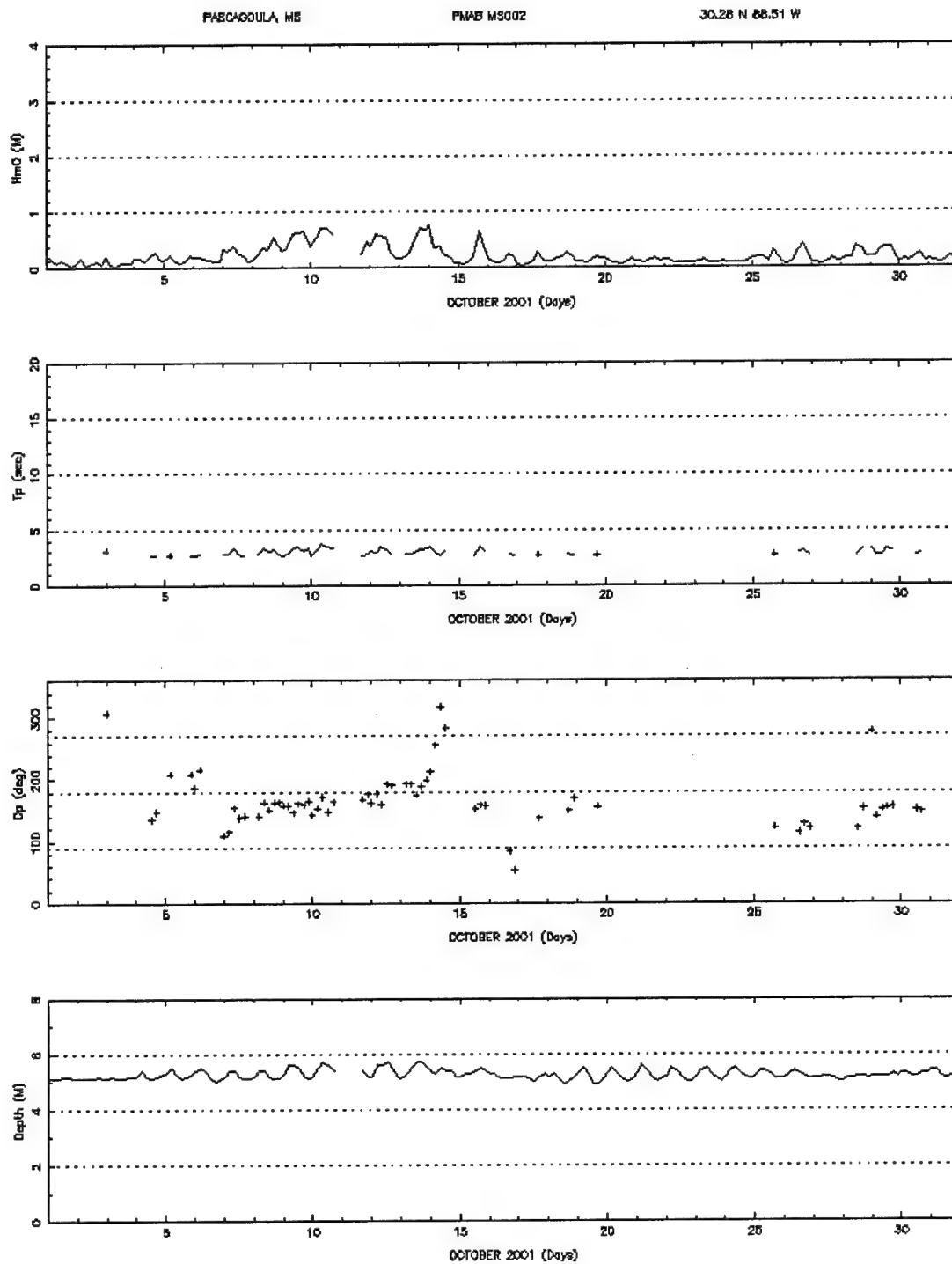


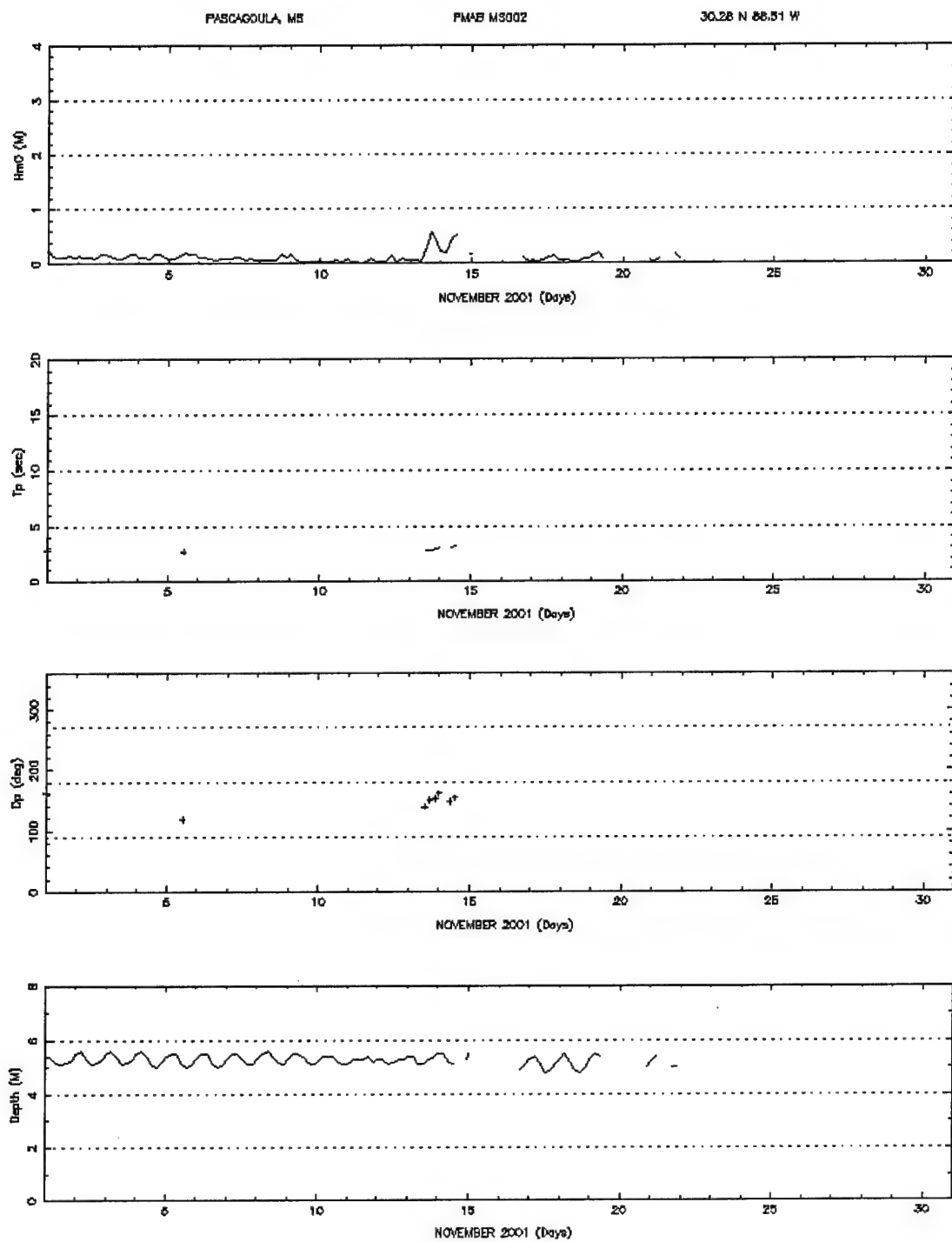
Appendix C

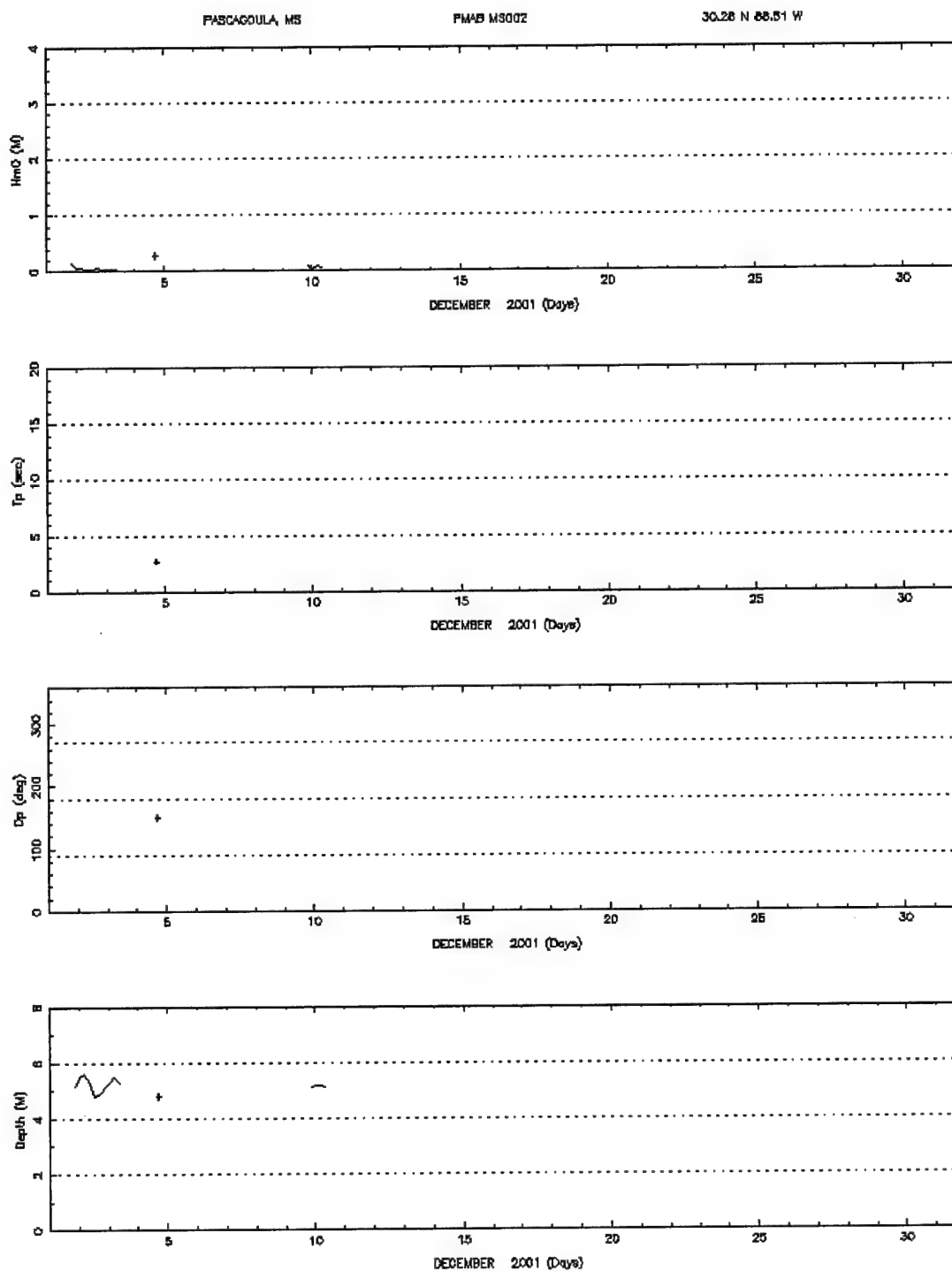
Mississippi Sound Wave Gage

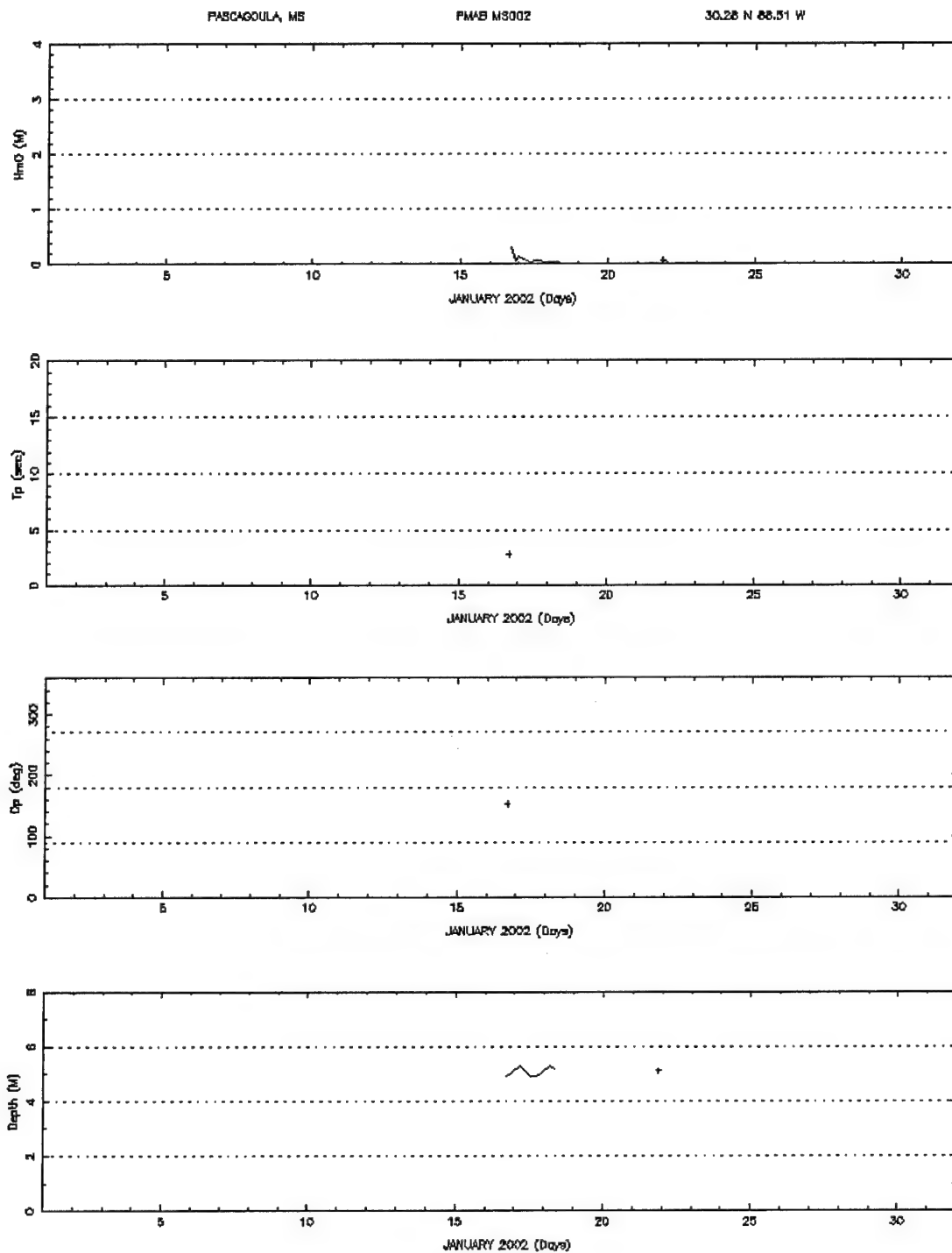
Sta MS002 Data Plots











Appendix D

Current Data Plots

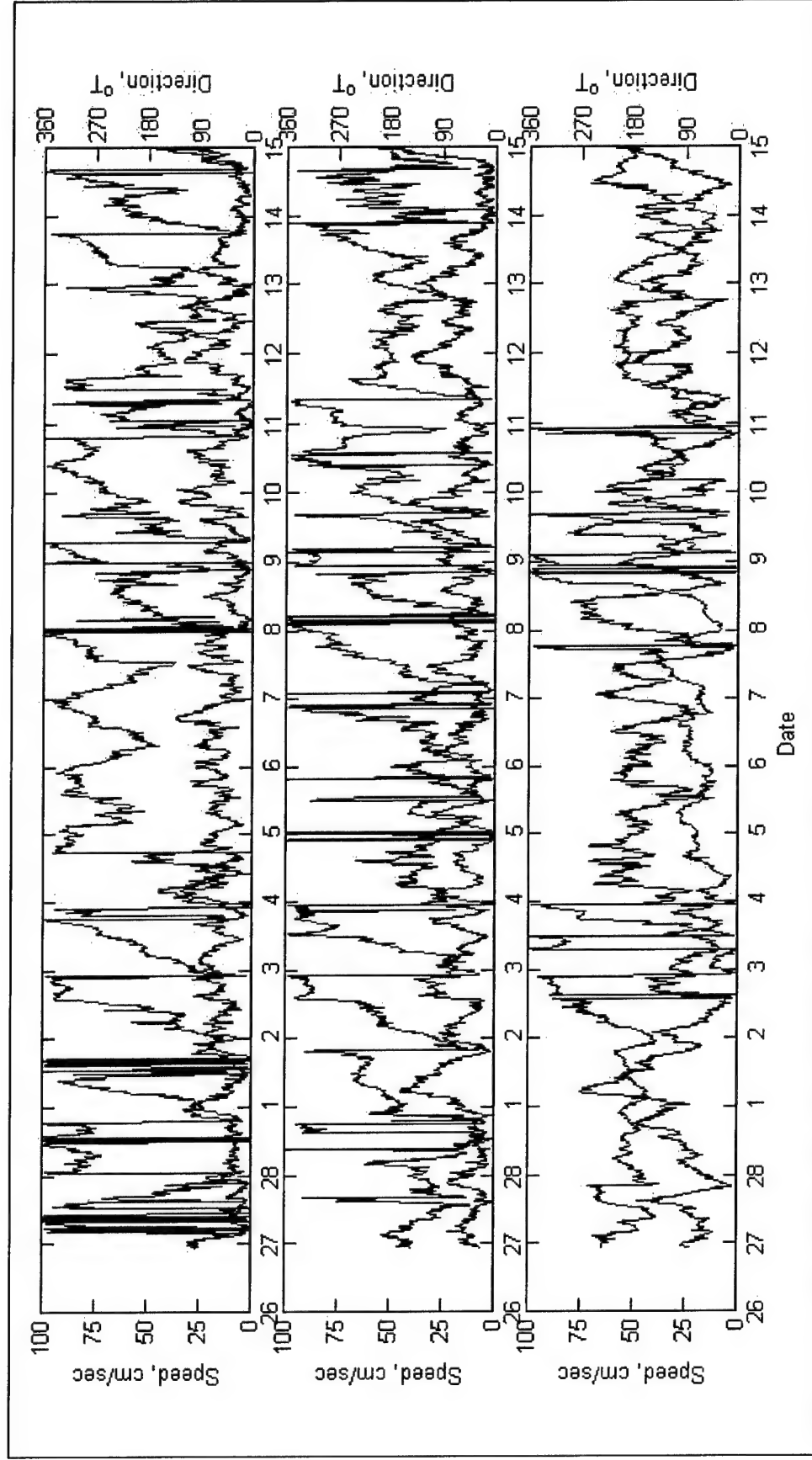


Figure D1. Current speed (black) and direction (red) at 2.0 m (top) and 3.5 m (middle) above seafloor, and near-surface (bottom) from 26 February to 15 March 2001 at sta MS_CM01

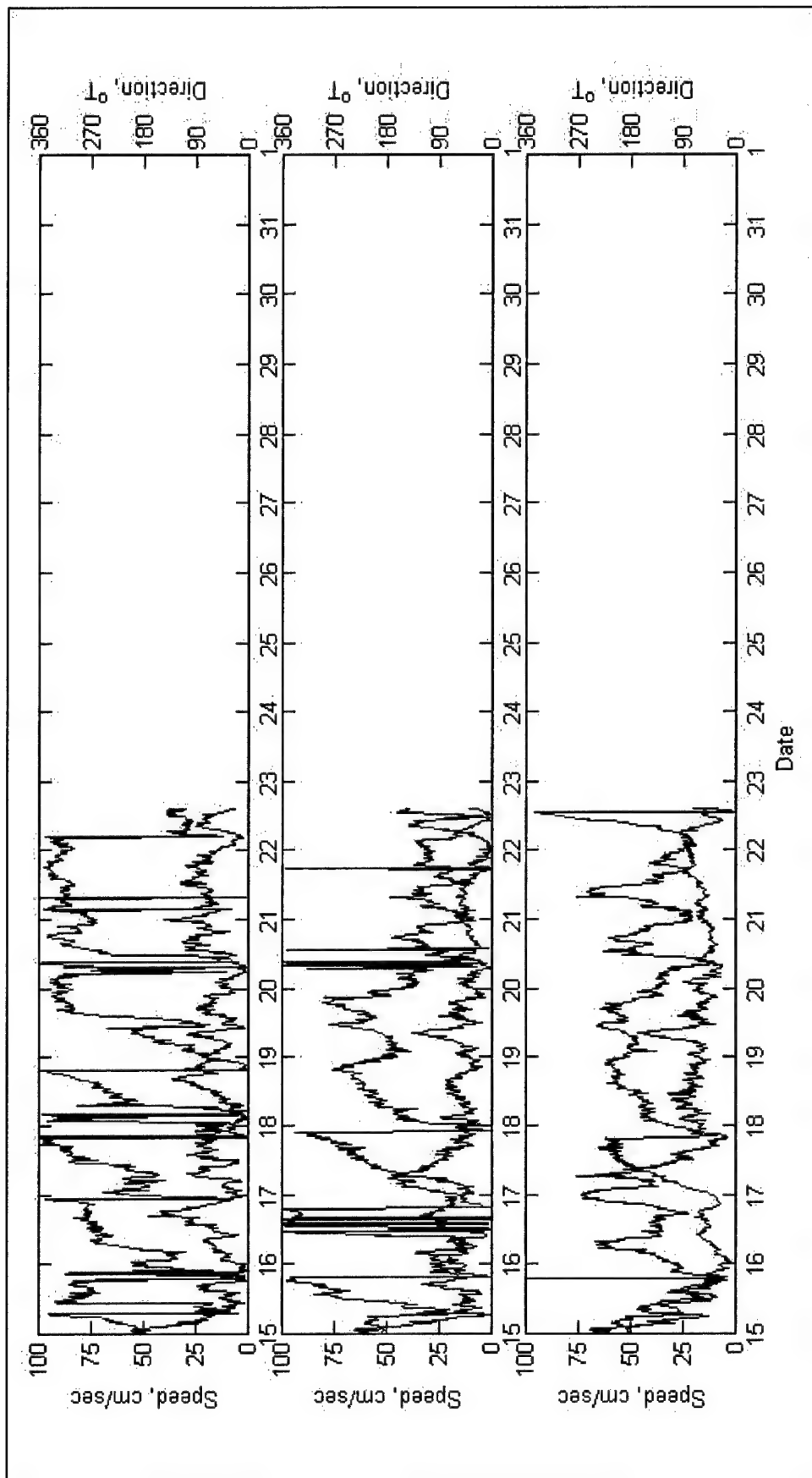


Figure D2. Current speed (black) and direction (red) at 2.0 m (top) and 3.5 m (middle) above seafloor, and near-surface (bottom) from 15 to 22 March 2001 at sta MS_CM01

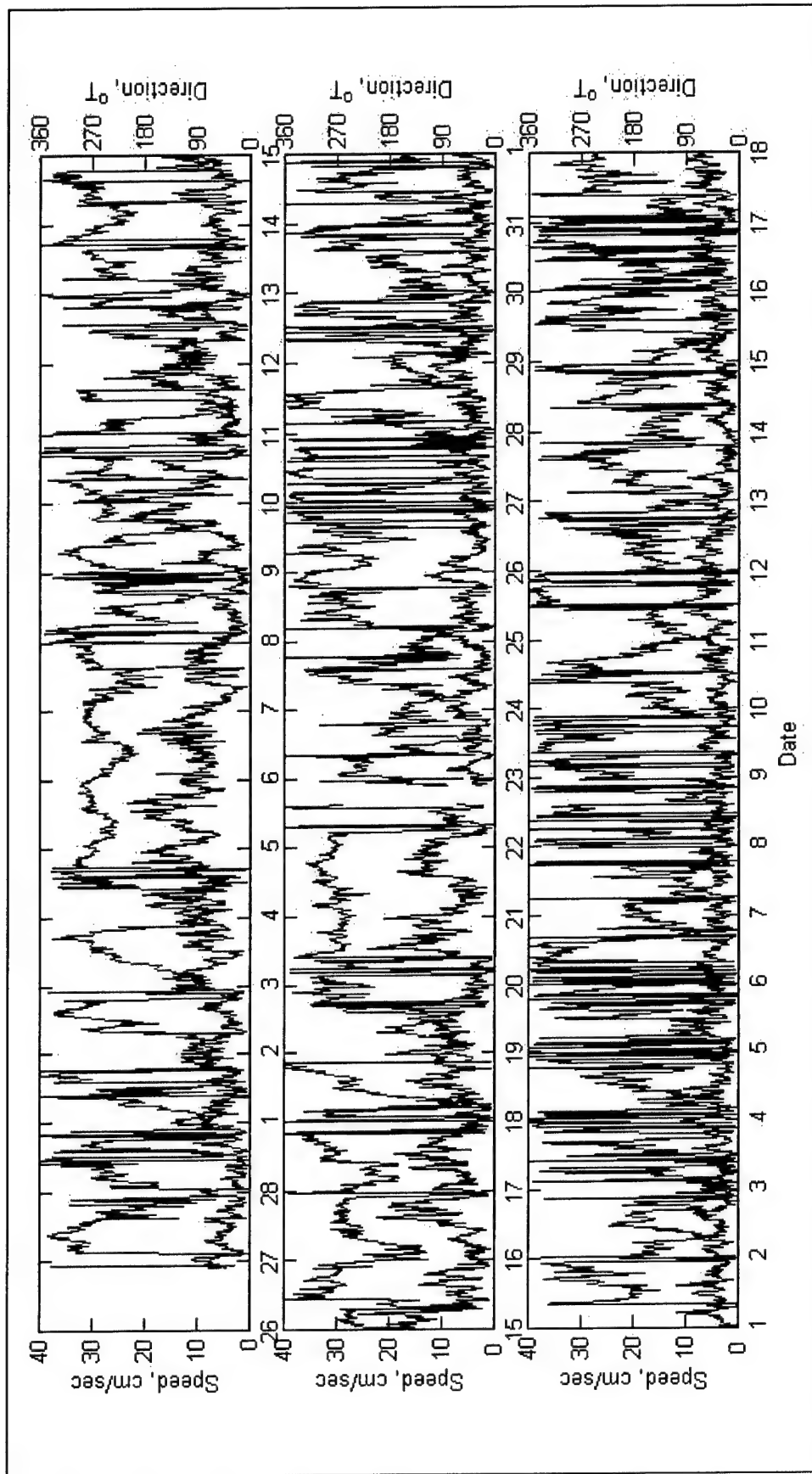


Figure D3. Current speed (black) and direction (red) approximately 0.5 m above seafloor from 26 February to 18 April 2001 at sta MS_CM01

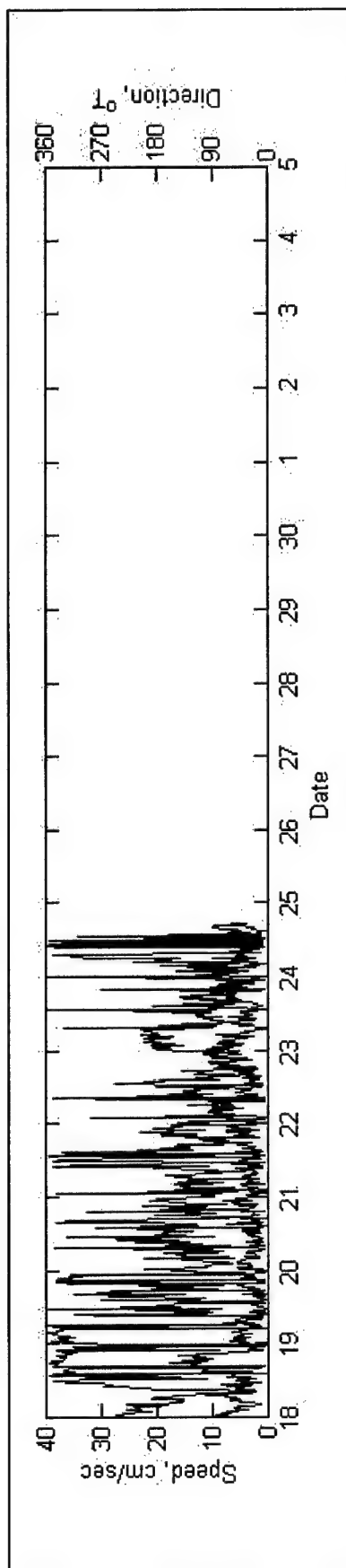


Figure D4. Current speed (black) and direction (red) approximately 0.5 m above seafloor from 18-24 April 2001 at sta MS_CM01

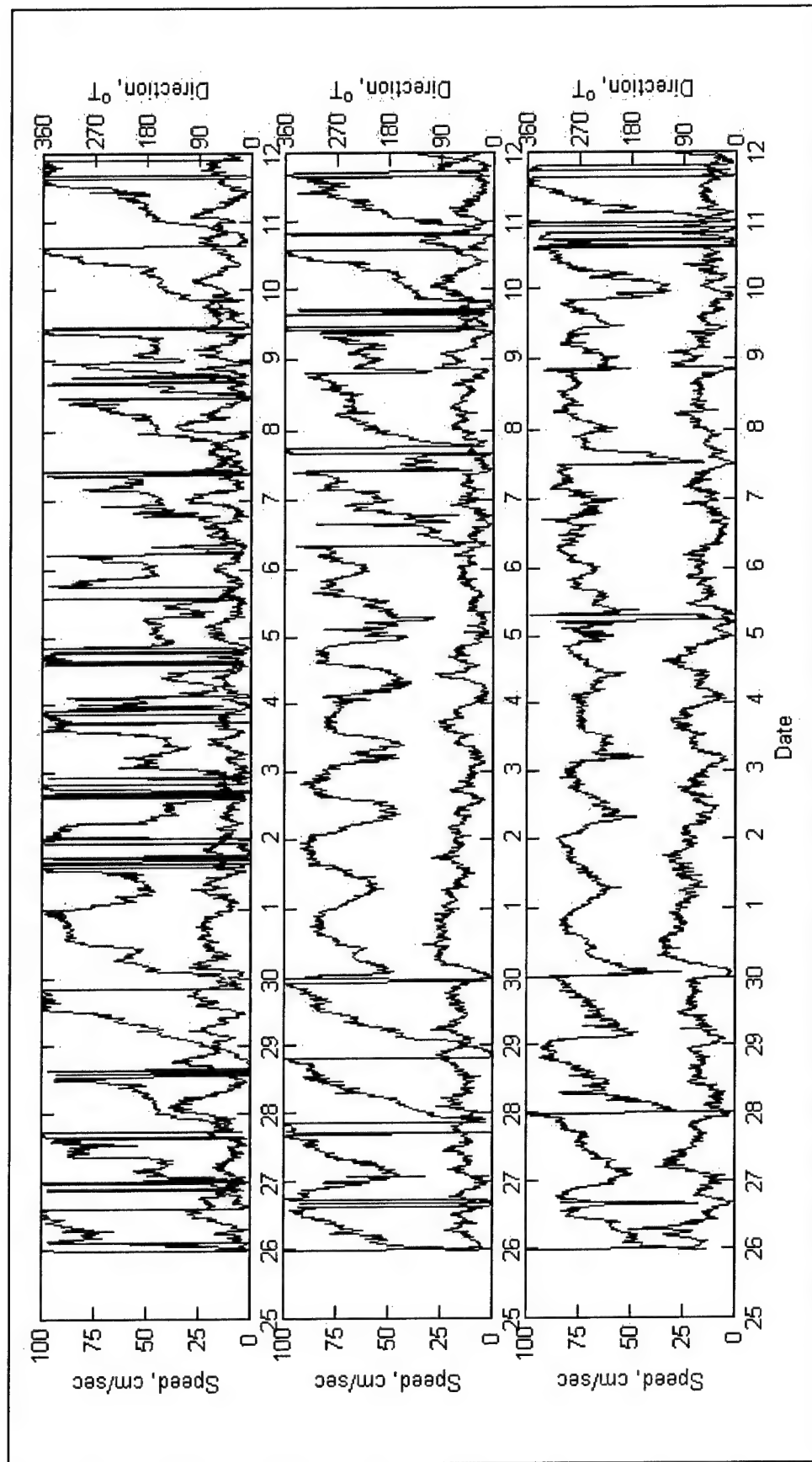


Figure D5. Current speed (black) and direction (red) at 2.0 m (top) and 3.5 m (middle) above seafloor, and near-surface (bottom) from 25 April to 12 May 2001 at sta MS_CM01

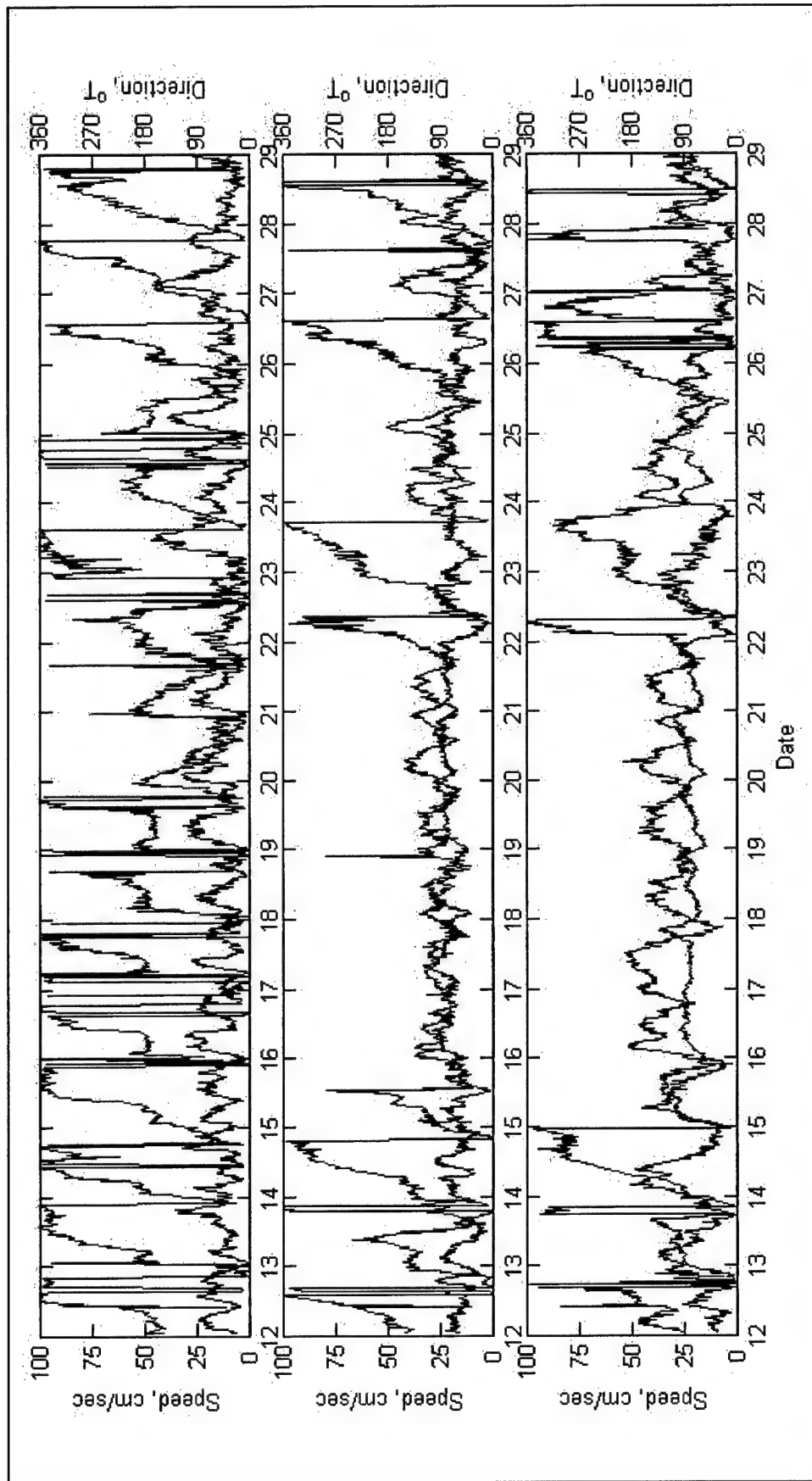


Figure D6. Current speed (black) and direction (red) at 2.0 m (top) and 3.5 m (middle) above seafloor, and near-surface (bottom) from 12 May to 29 May 2001 at sta MS_CM01

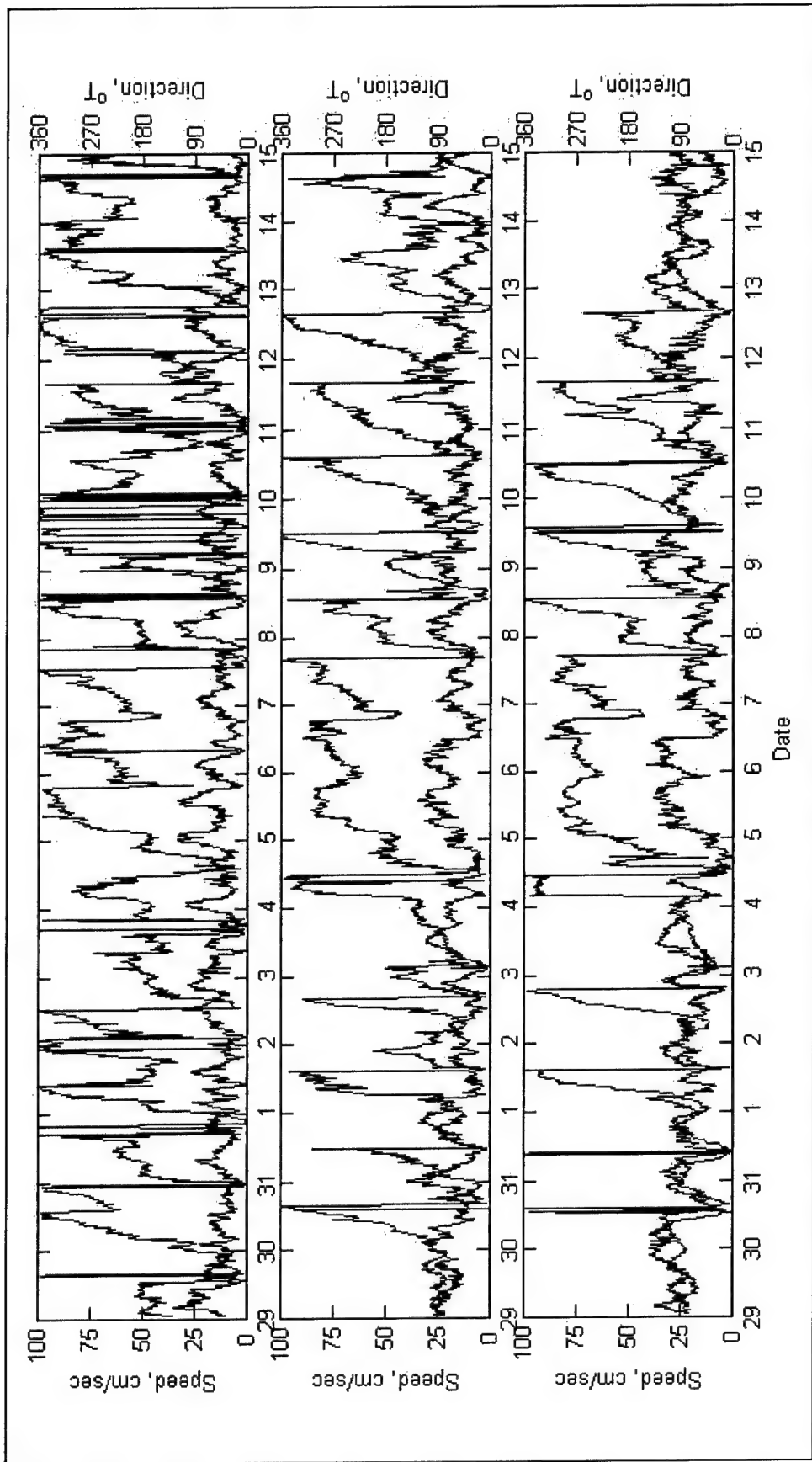


Figure D7. Current speed (black) and direction (red) at 2.0 m (top) and 3.5 m (middle) above seafloor, and near-surface (bottom) from 29 May to 15 June 2001 at sta MS_CM01

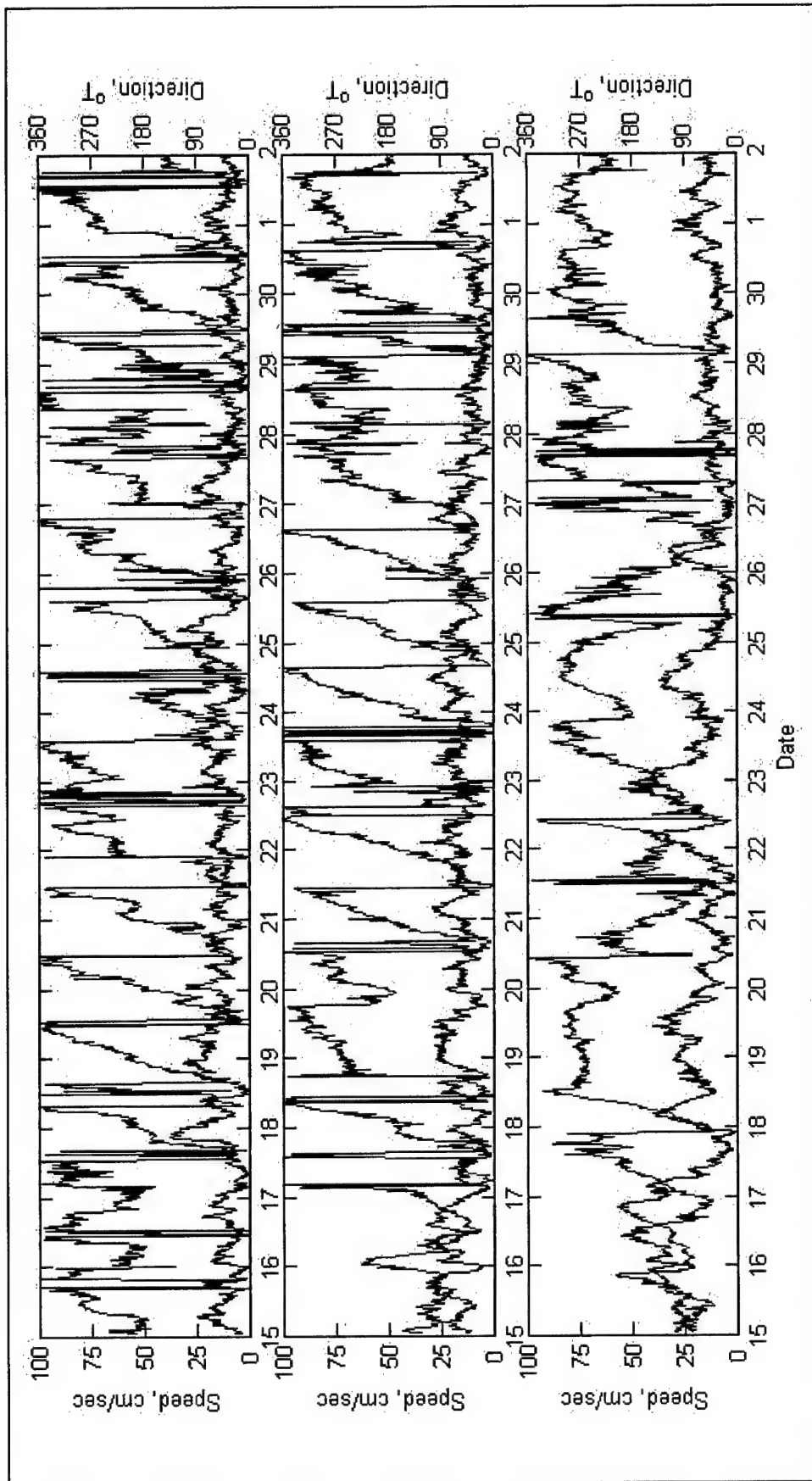


Figure D8. Current speed (black) and direction (red) at 2.0 m (top) and 3.5 m (middle) above seafloor, and near-surface (bottom) from 15 June to 2 July 2001 at sta MS_CM01

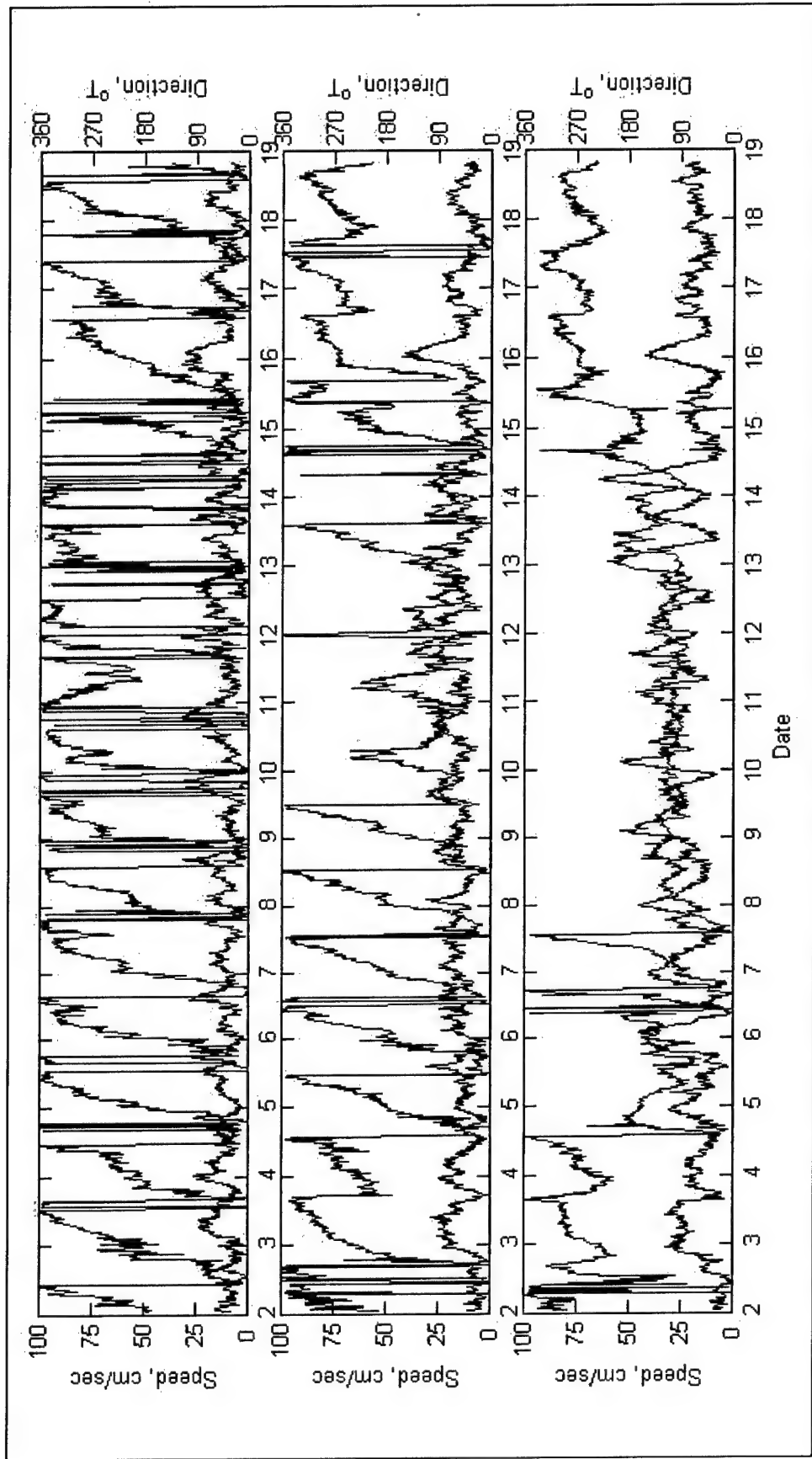


Figure D9. Current speed (black) and direction (red) at 2.0 m (top) and 3.5 m (middle) above seafloor, and near-surface (bottom) from 2 to 18 July 2001 at sta MS_CM01

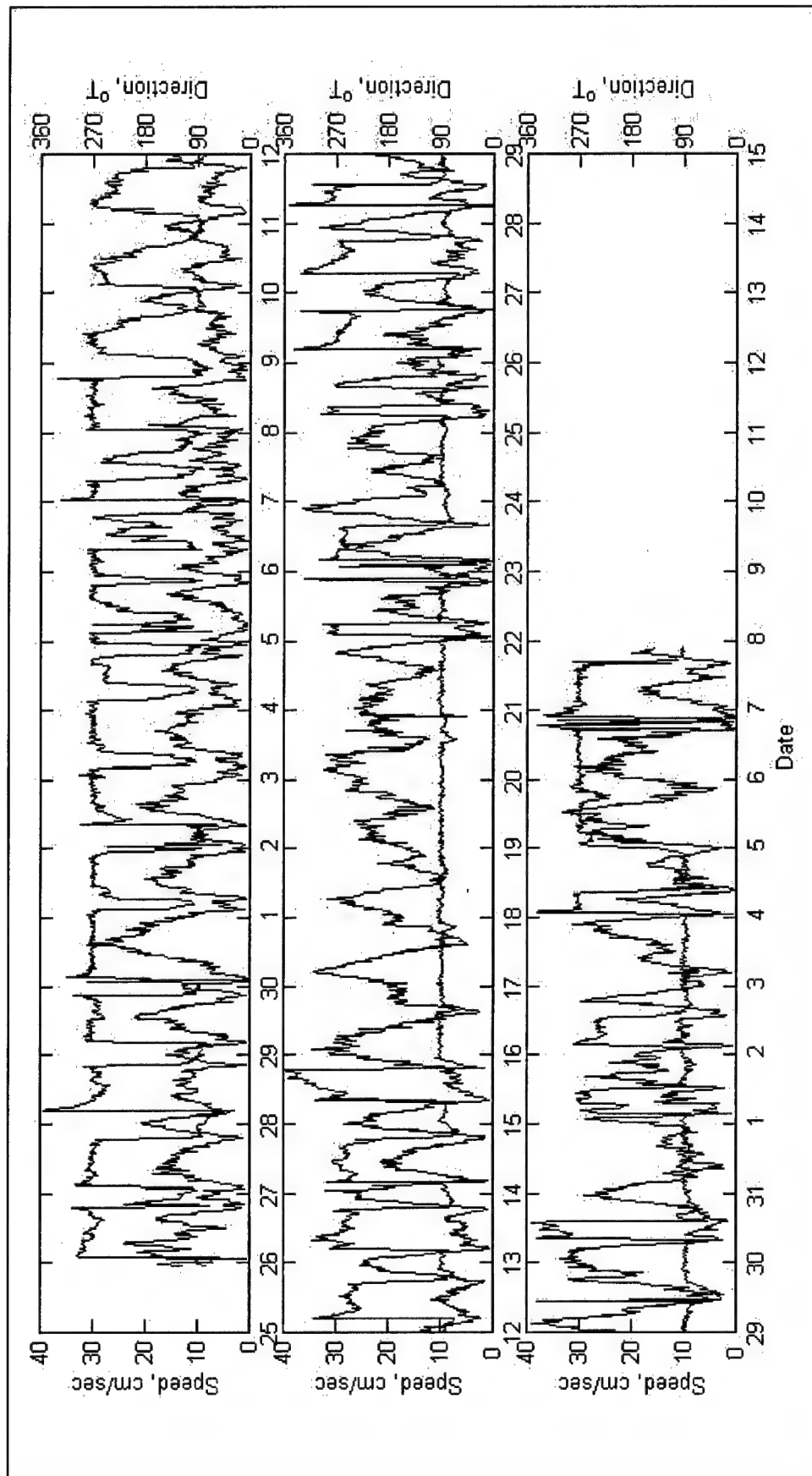


Figure D10. Current speed (black) and direction (red) approximately 0.8 m above seafloor from 25 April to 7 June 2001 at sta MS_CM02

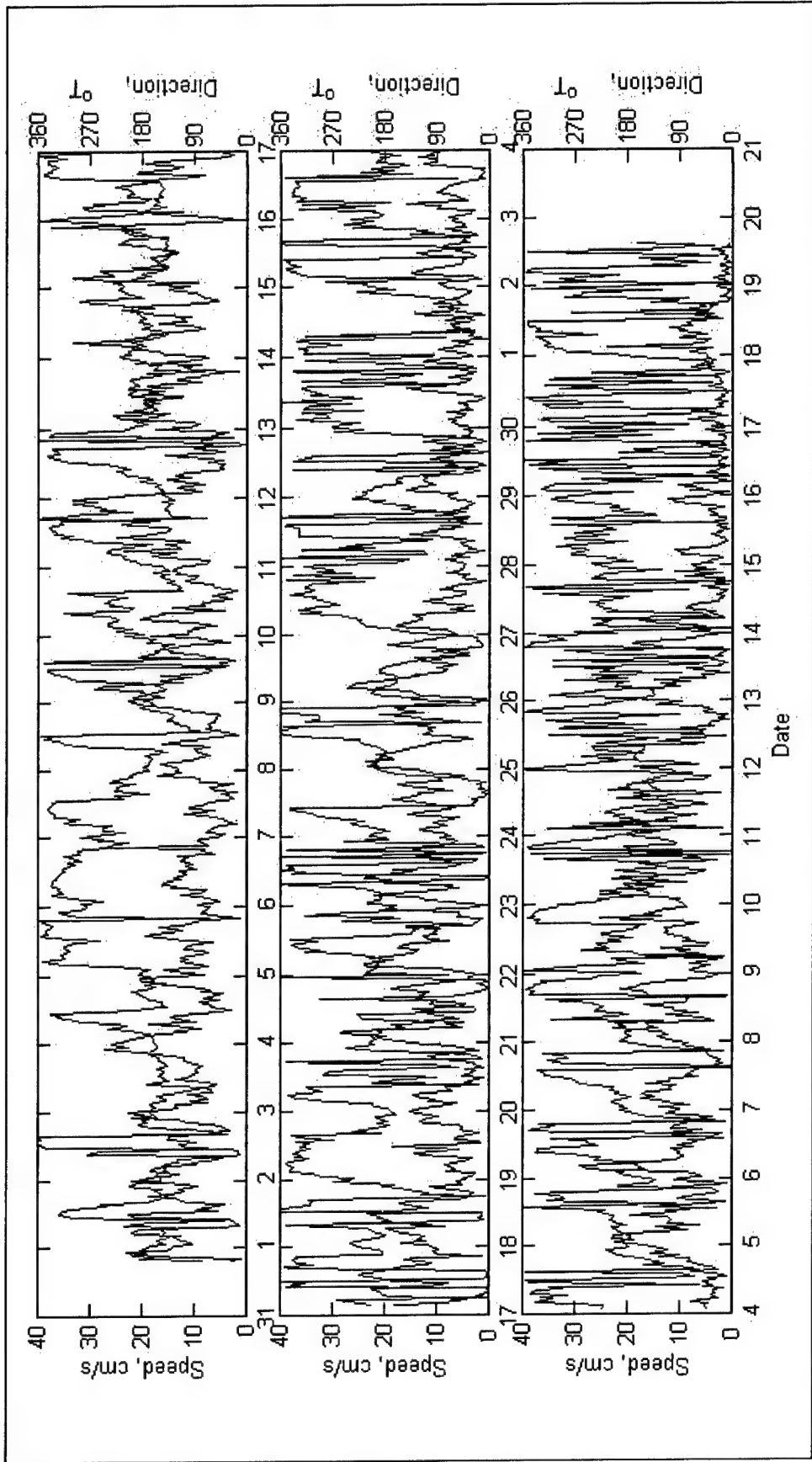


Figure D11. Current speed (black) and direction (red) 0.8 m above seafloor from 31 May to 19 July 2001 at sta MS_CM03

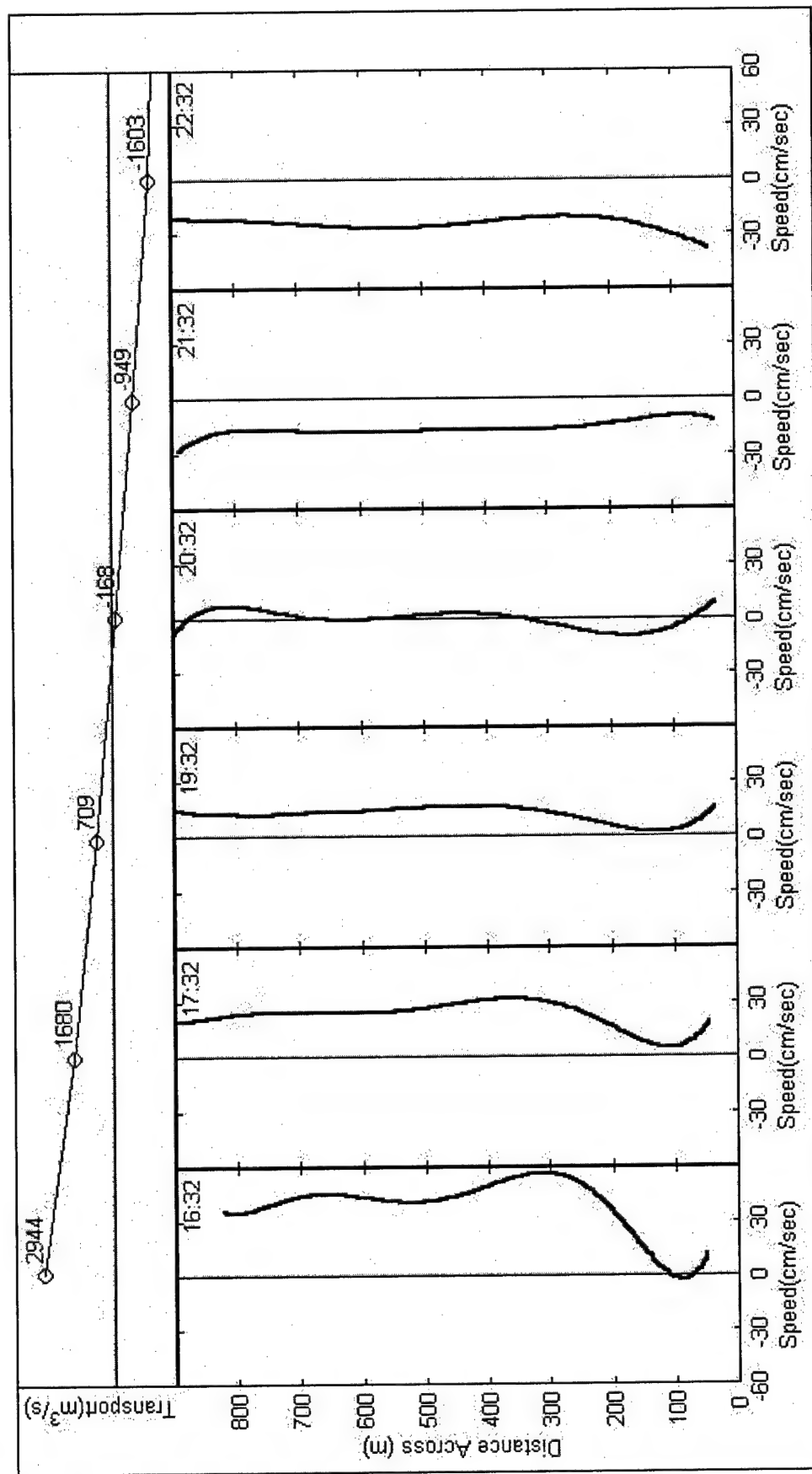


Figure D12. Horizontally-filtered, depth-averaged current profiles across Horn Island Pass on 27 February from 16:32 to 22:32. Representative time (GMT) is shown for each profile. At top is total transport through pass during each transect. Negative values are ebb, positive values are flood

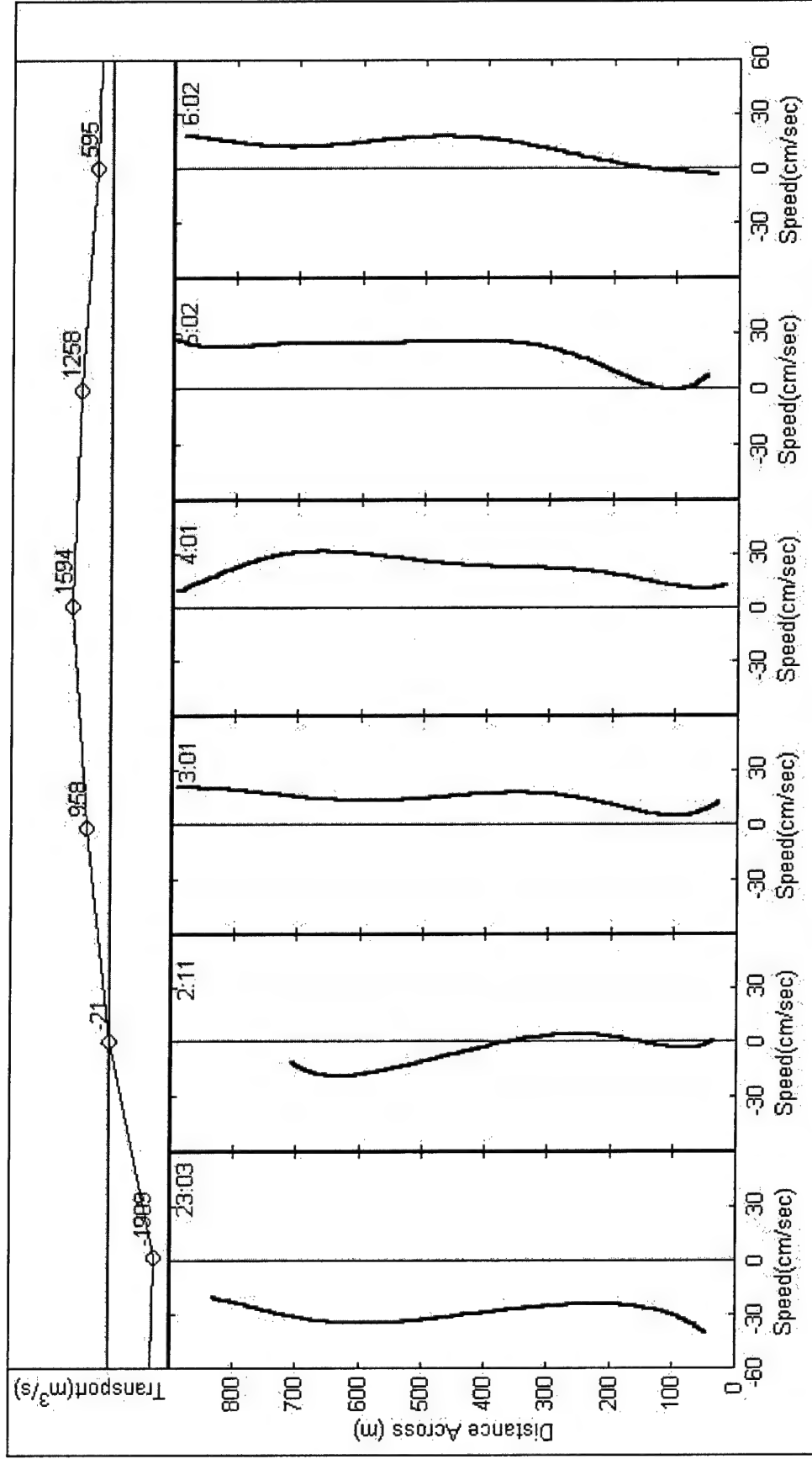


Figure D13. Horizontally-filtered, depth-averaged current speed profiles across Horn Island Pass on 27 and 28 February from 23:03 to 06:02. Representative time (GMT) is shown for each profile. At top is total transport through pass during each transect. Negative values are ebb, positive values are flood

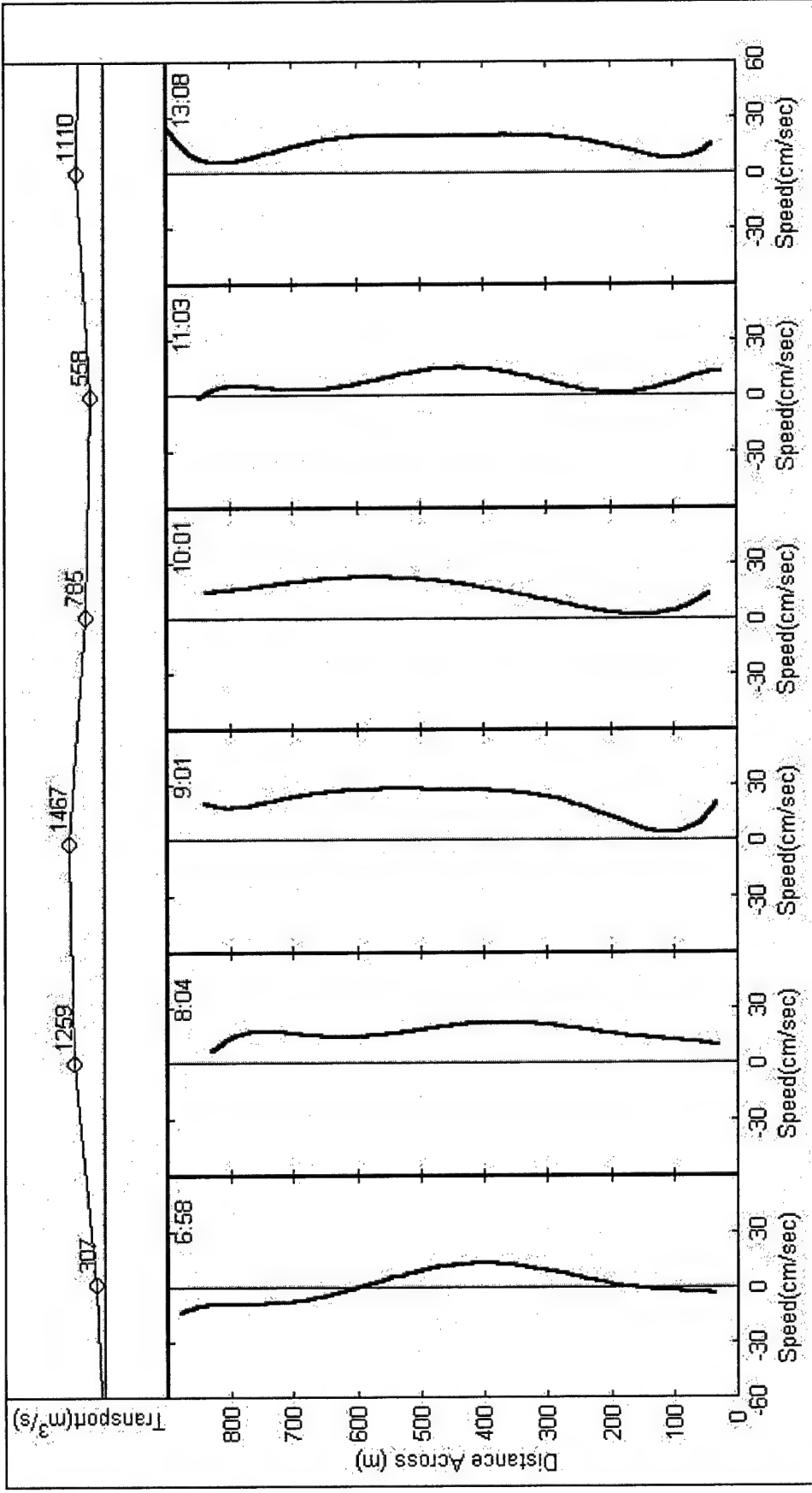


Figure D14. Horizontally-filtered, depth-averaged current speed profiles across Horn Island Pass on 28 February from 06:58 to 13:08. Representative time (GMT) is shown for each profile. At top is total transport through pass during each transect. Negative values are ebb, positive values are flood

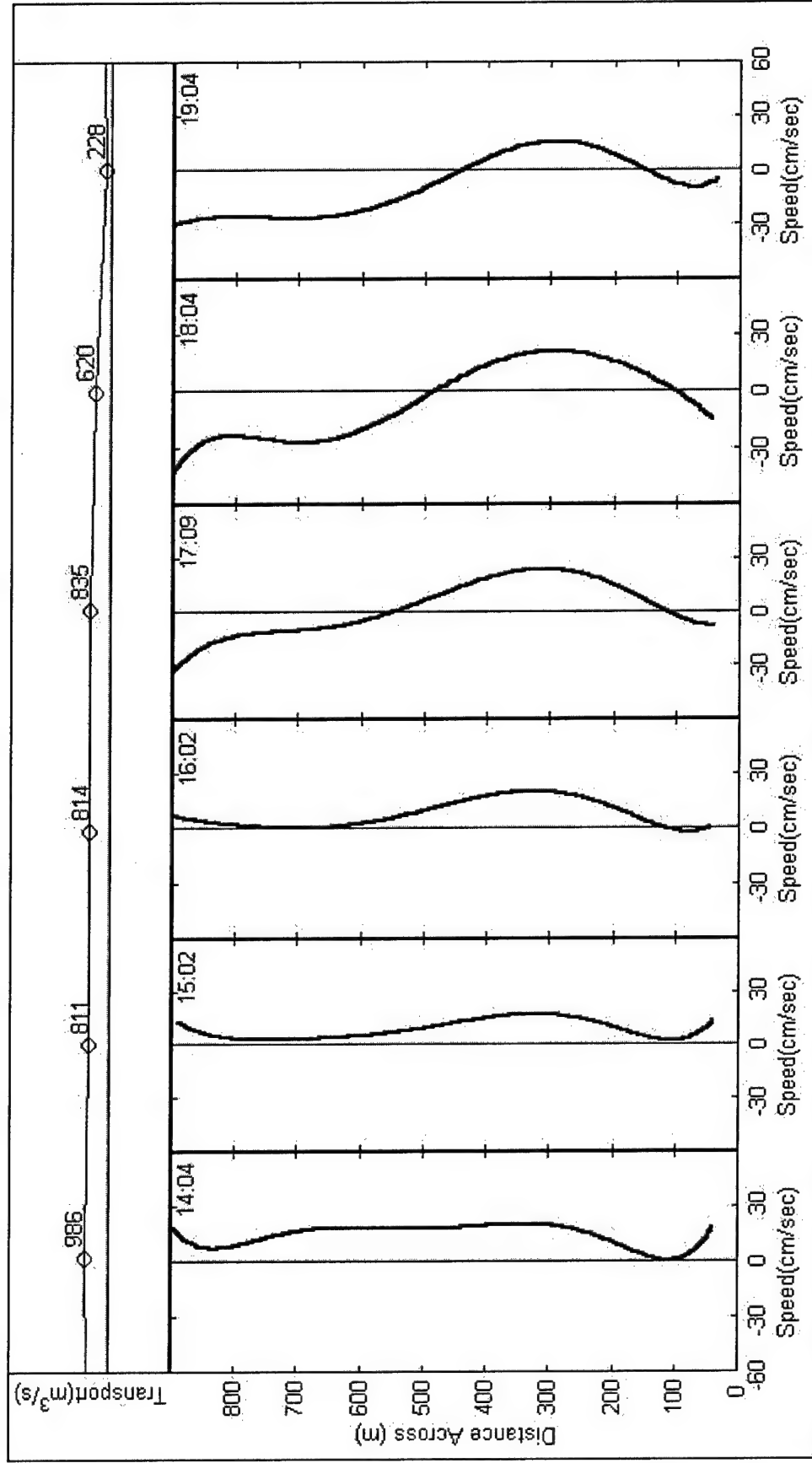


Figure D15. Horizontally-filtered, depth-averaged current speed profiles across Horn Island Pass on 28 February from 14:04 to 19:04. Representative time (GMT) is shown for each profile. At top is total transport through pass during each transect. Negative values are ebb, positive values are flood

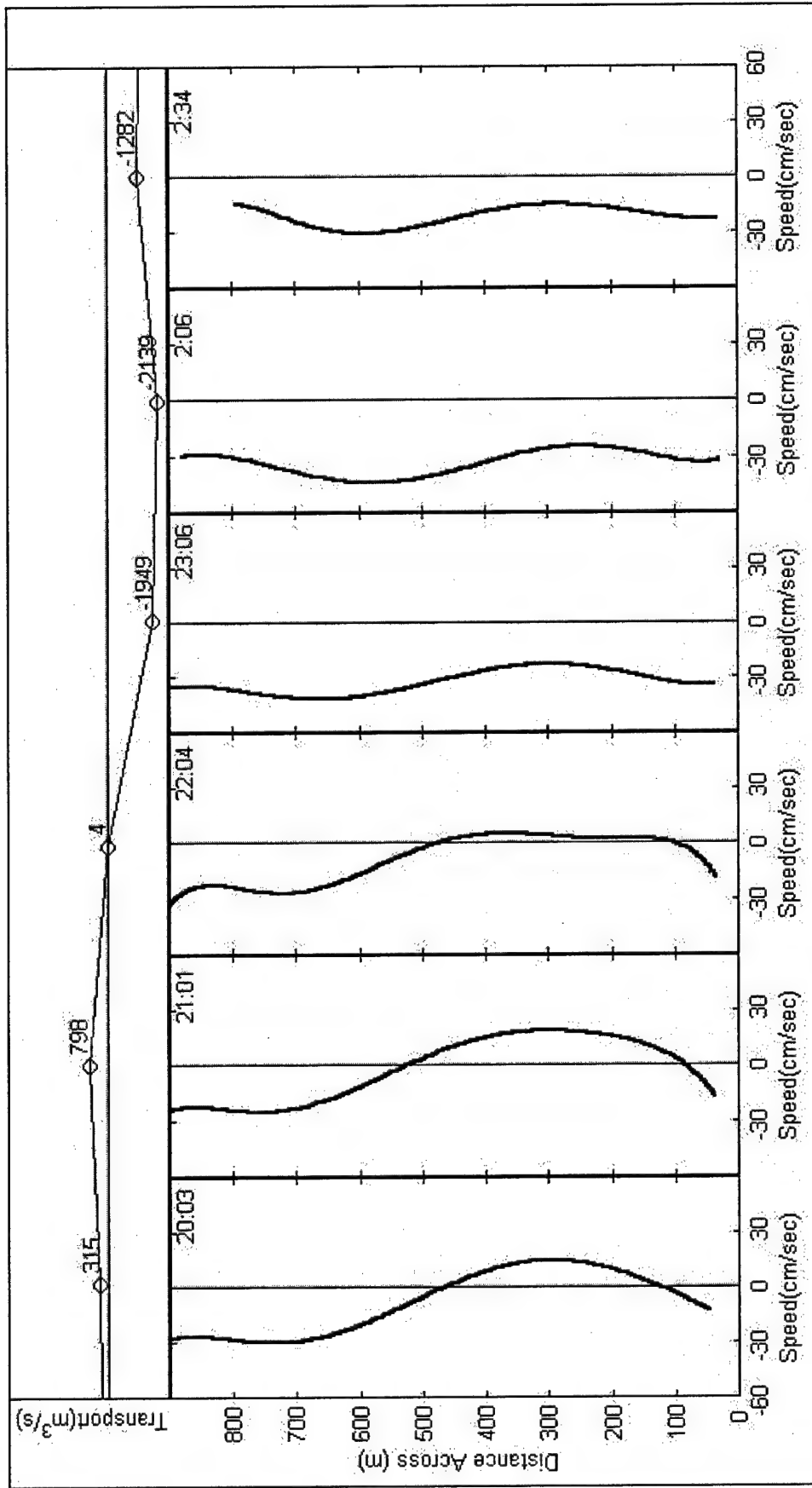


Figure D16. Horizontally-filtered, depth-averaged current speed profiles across Horn Island Pass on 28 February to 1 March from 20:03 to 02:34. Representative time (GMT) is shown for each profile. At top is total transport through pass during each transect. Negative values are ebb, positive values are flood

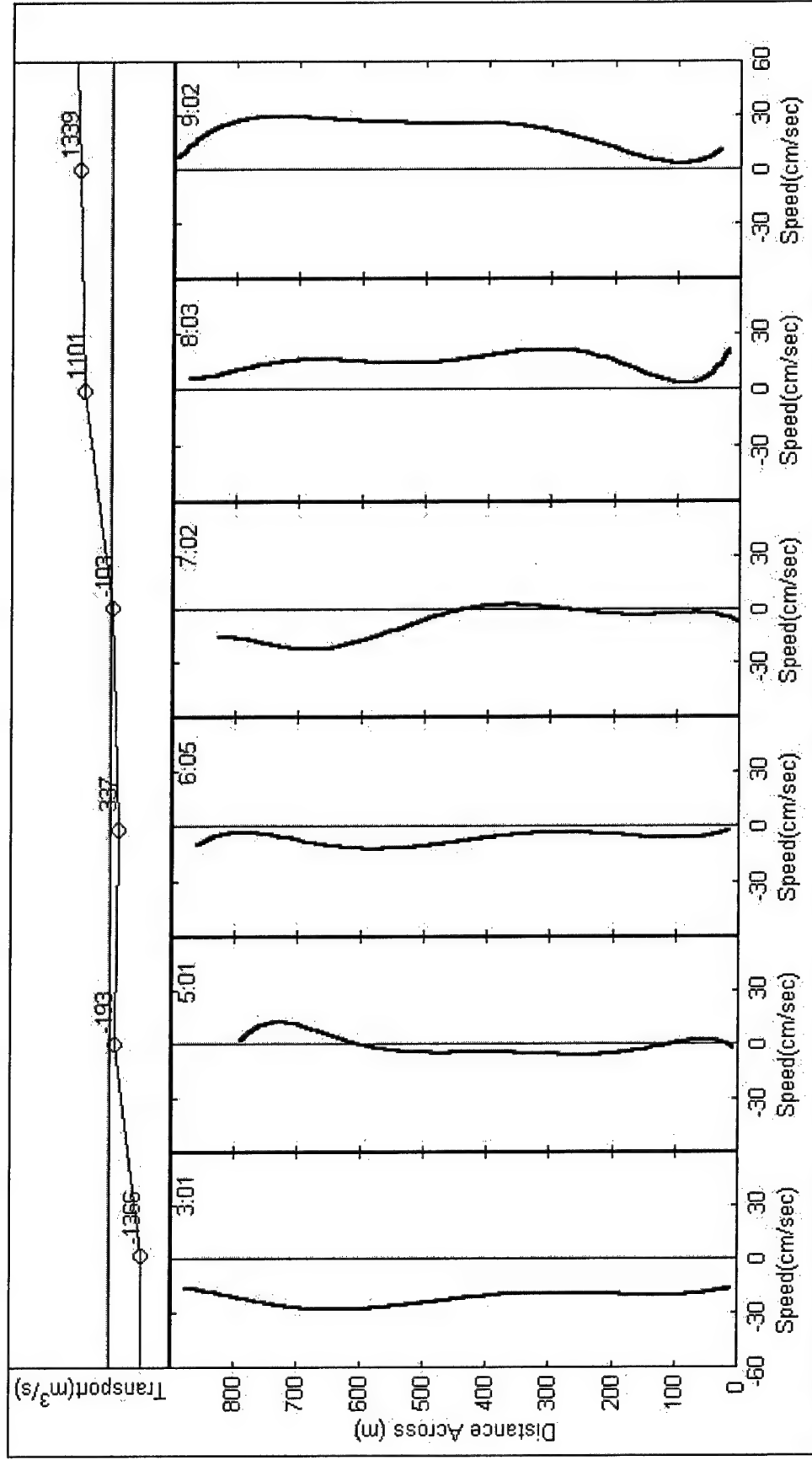


Figure D17. Horizontally-filtered, depth-averaged current speed profiles across Horn Island Pass on 1 March from 03:01 to 09:02. Representative time (GMT) is shown for each profile. At top is total transport through pass during each transect. Negative values are ebb, positive values are flood

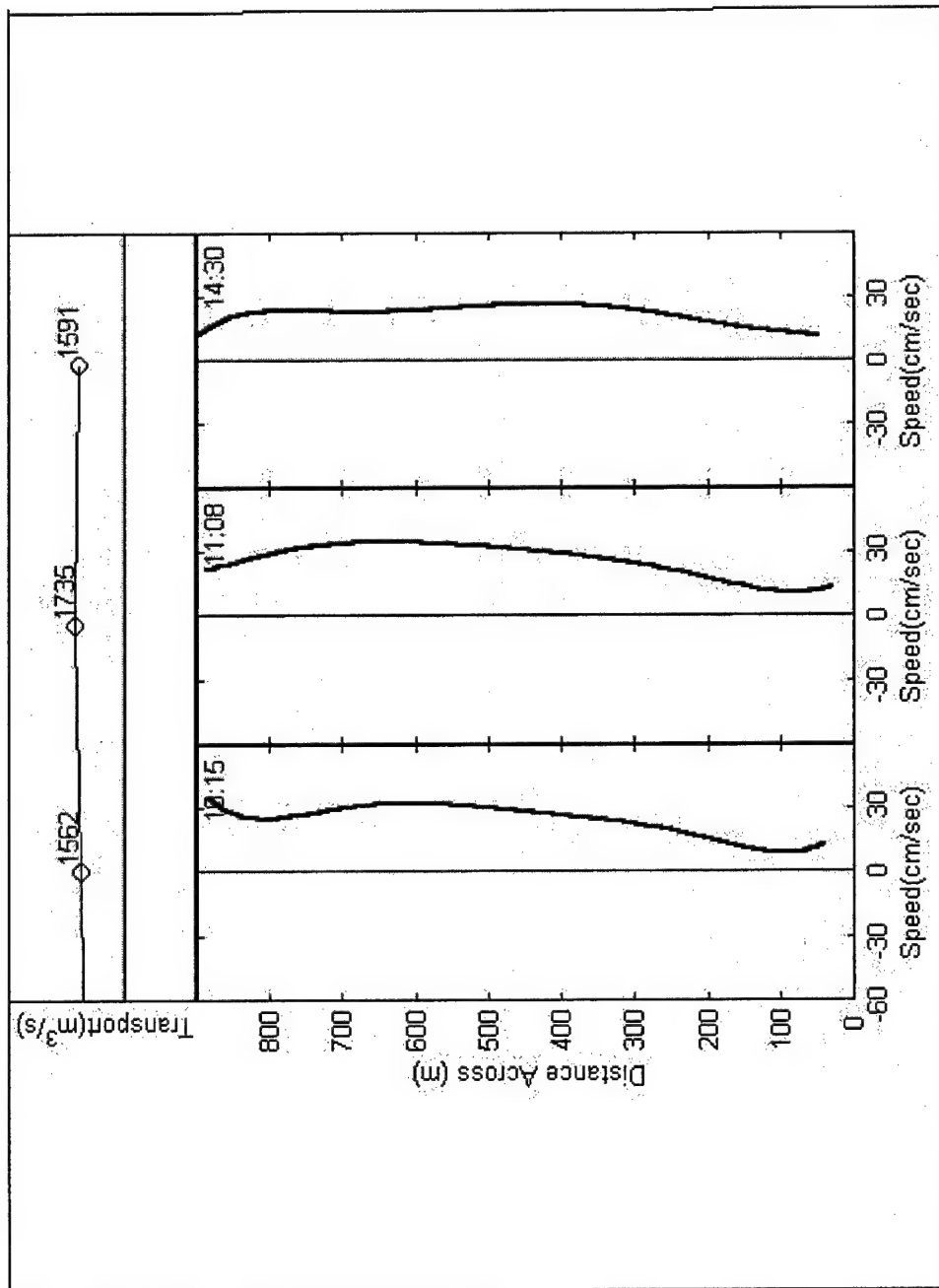


Figure D18. Horizontally-filtered, depth-averaged current speed profiles across Horn Island Pass on 1 March from 10:15 to 14:30. Representative time (GMT) is shown for each profile. At top is total transport through pass during each transect. Negative values are ebb, positive values are flood

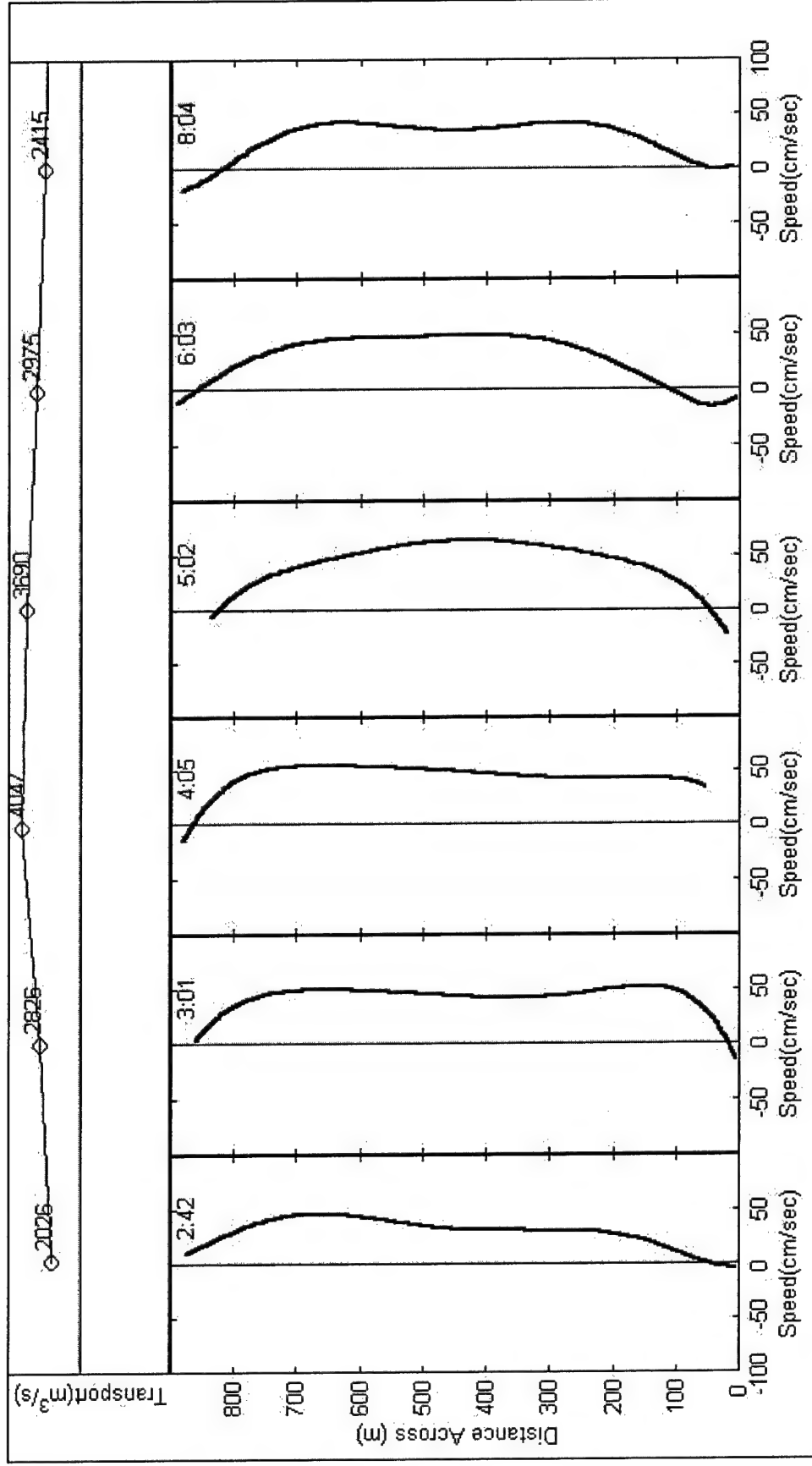


Figure D19. Horizontally-filtered, depth-averaged current profiles across Horn Island Pass on 20 June from 02:42 to 08:04. Representative time (GMT) is shown for each profile. At top is total transport through each transect. Negative values are ebb, positive values are flood

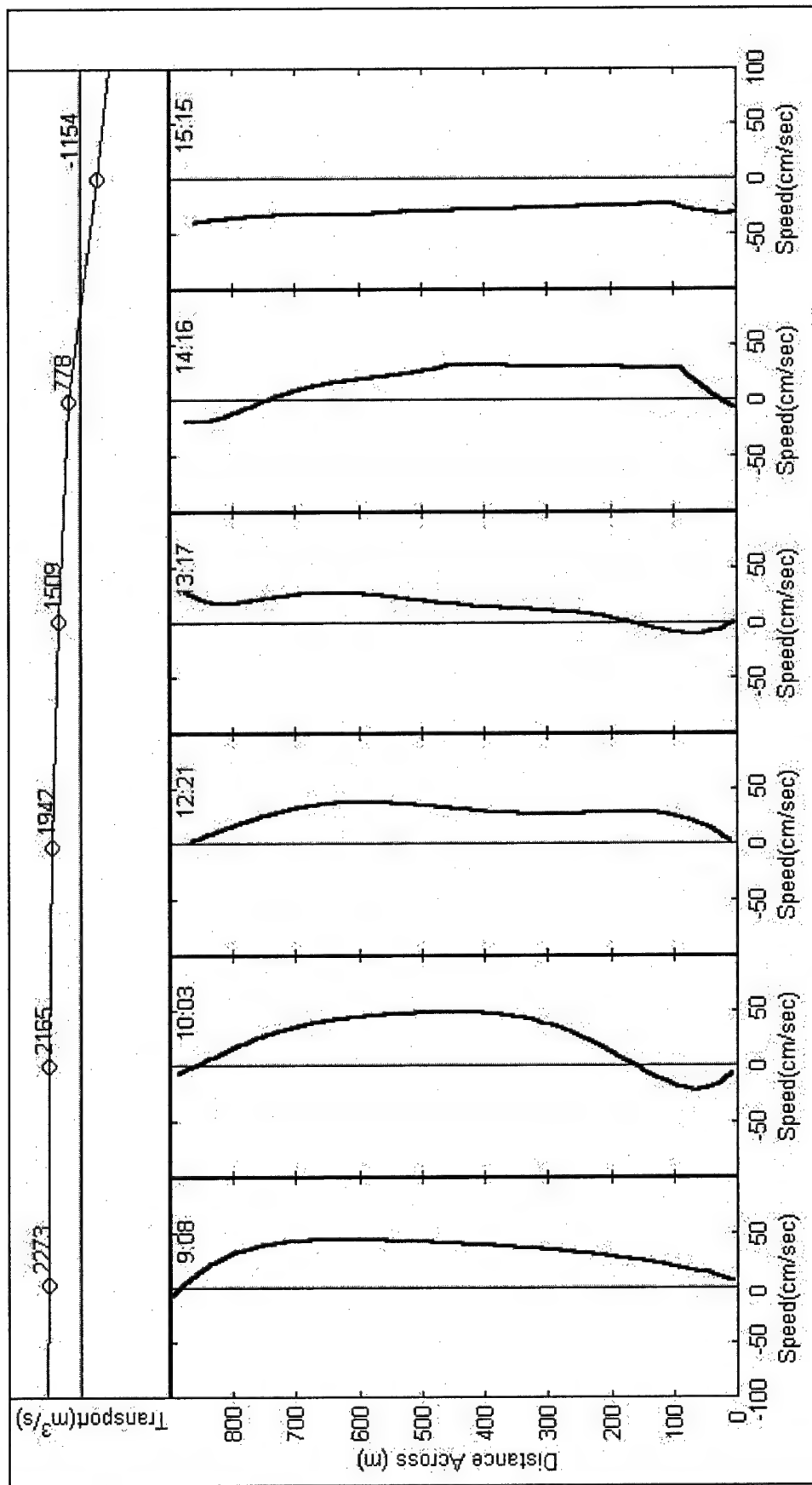


Figure D20. Horizontally-filtered, depth-averaged current profiles across Horn Island Pass on 20 June from 09:08 to 15:15. Representative time (GMT) is shown for each profile. At top is total transport through pass during each transect. Negative values are ebb, positive values are flood

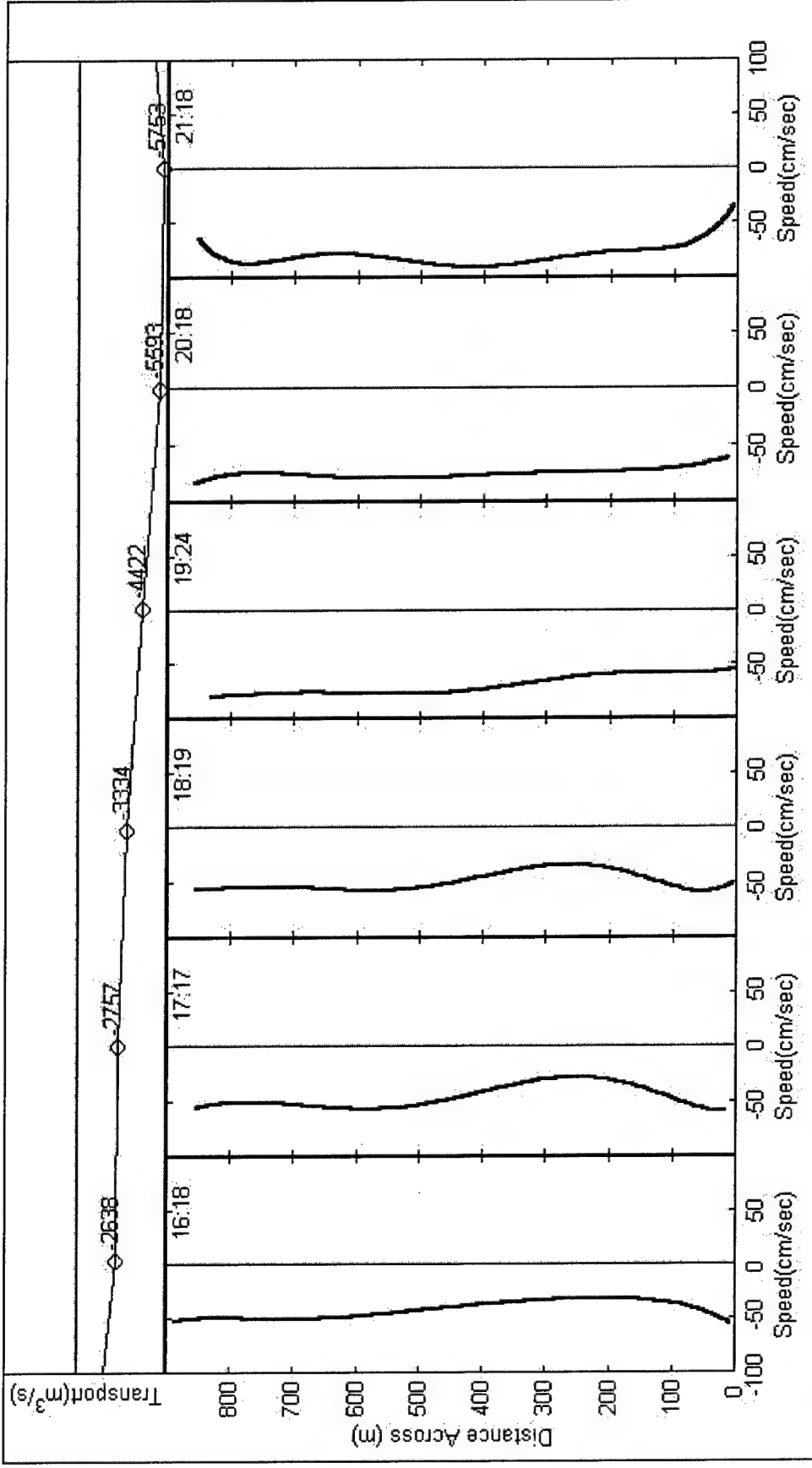


Figure D21. Horizontally-filtered, depth-averaged current profiles across Horn Island Pass on 20 June from 16:18 to 21:18. Representative time (GMT) is shown for each profile. At top is total transport through pass during each transect. Negative values are ebb, positive values are flood

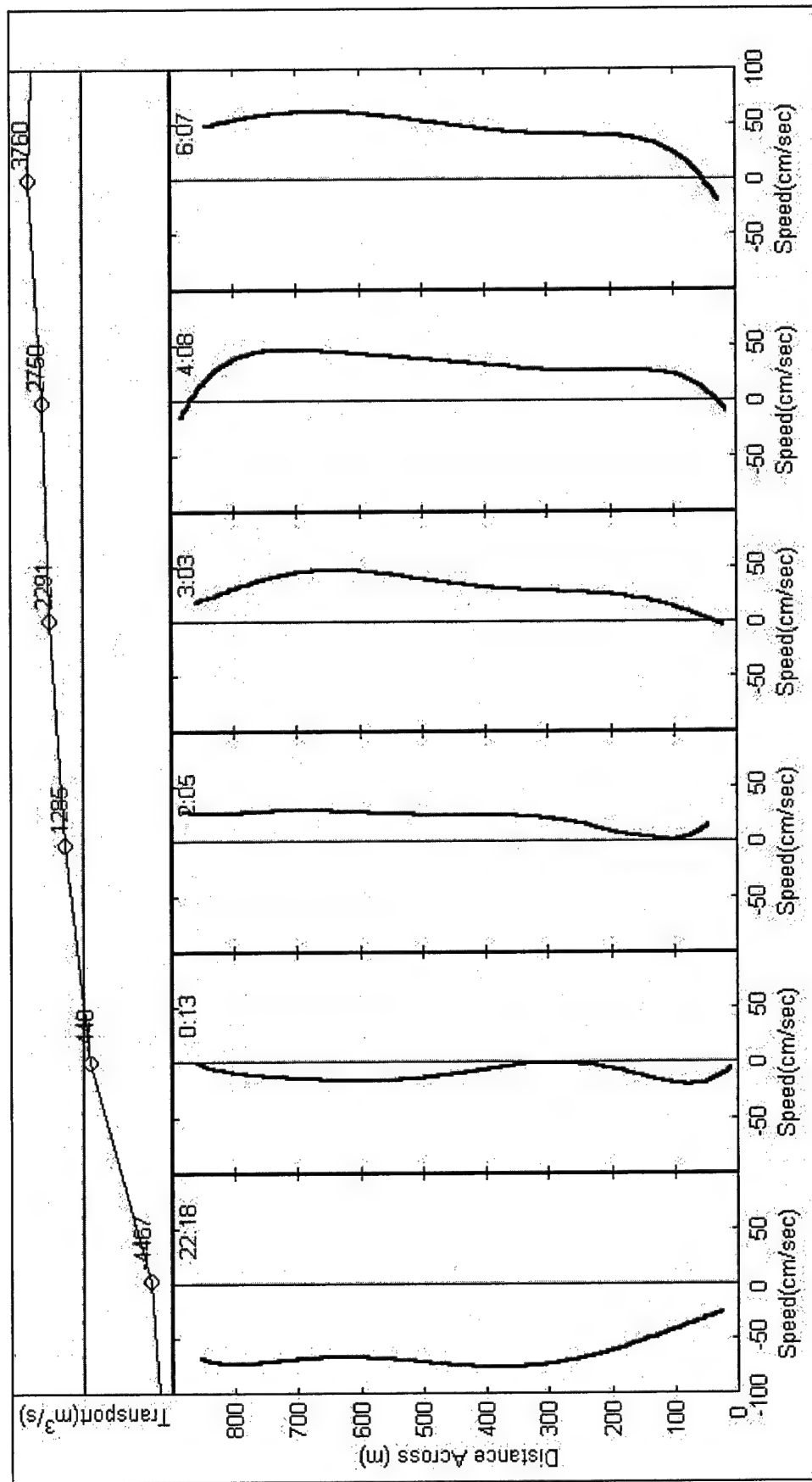


Figure D22. Horizontally-filtered, depth-averaged current profiles across Horn Island Pass on 20 and 21 June from 22:18 to 06:07. Representative time (GMT) is shown for each profile. At top is total transport through pass during each transect. Negative values are ebb, positive values are flood

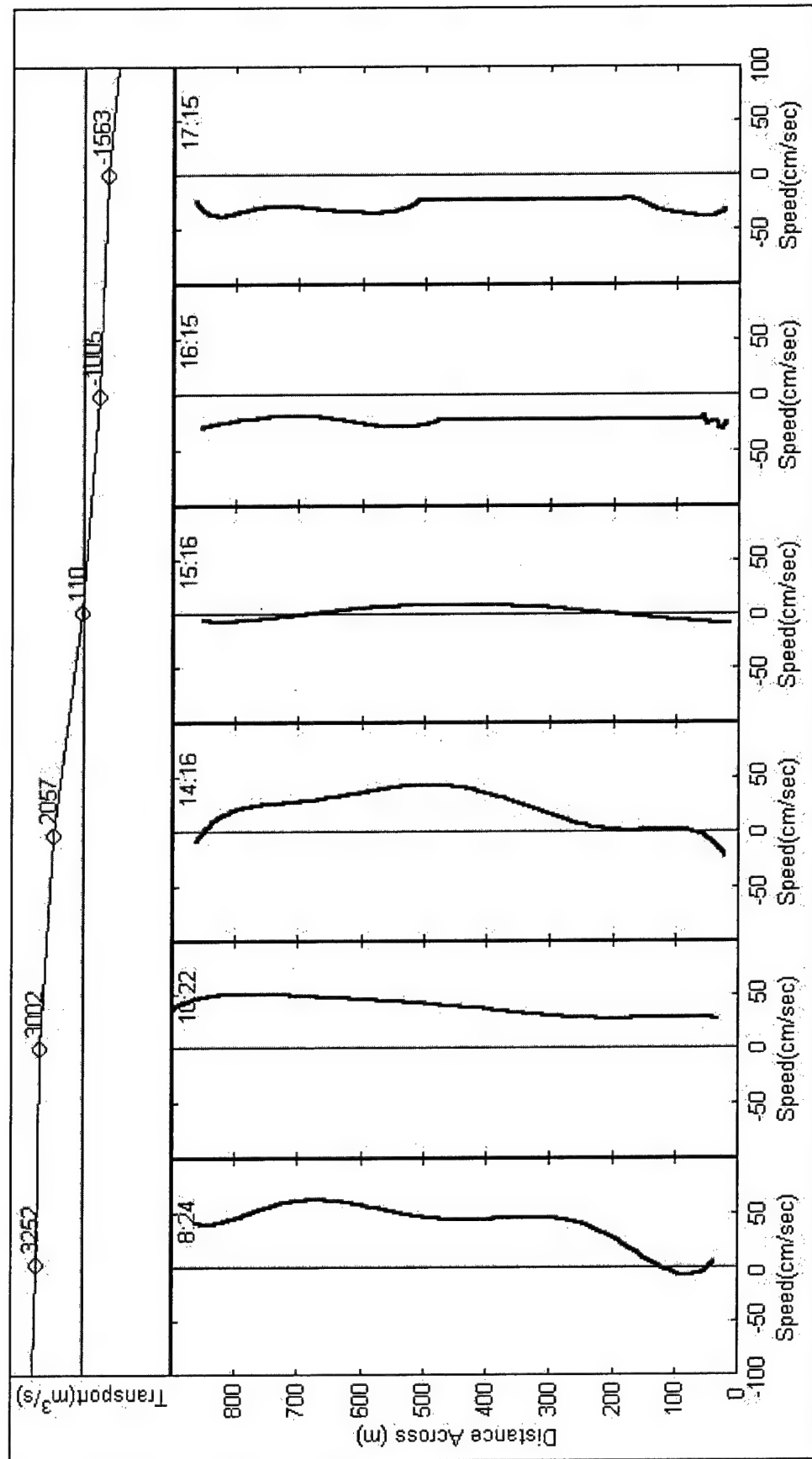


Figure D23. Horizontally-filtered, depth-averaged current profiles across Horn Island Pass on 21 June from 08:24 to 17:15. The representative time (GMT) is shown for each profile. At top is total transport through pass during each transect. Negative values are ebb, positive values are flood

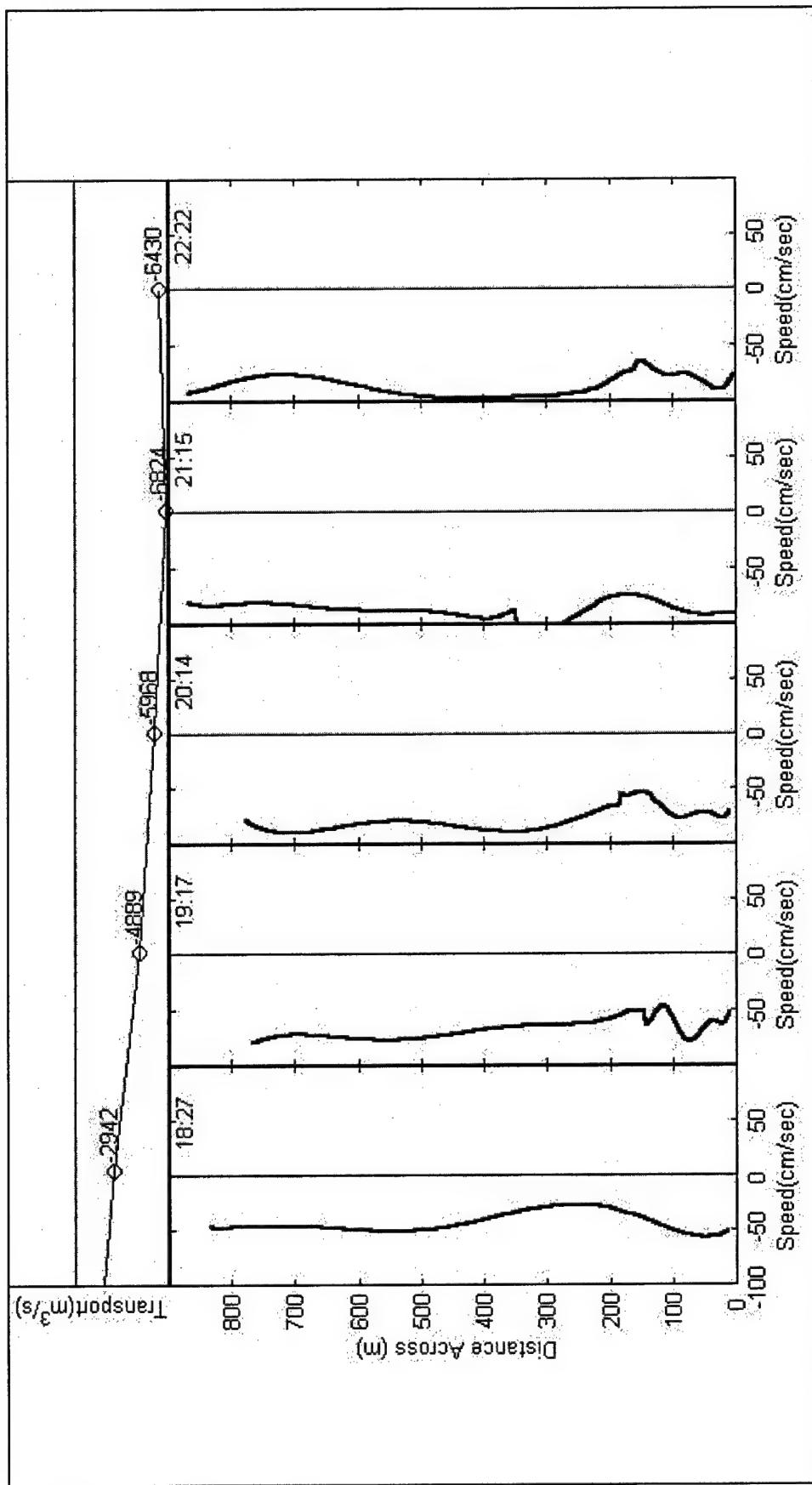


Figure D24. Horizontally-filtered, depth-averaged current profiles across Horn Island Pass on 21 June from 18:27 to 22:22. Representative time (GMT) is shown for each profile. At top is total transport through pass during each transect. Negative values are ebb, positive values are flood

Appendix E

Consolidation Characteristics of Foundation Material and Dredged Material

Table E1 Consolidation Characteristics of Foundation Material and Dredged Material PH-2					
Foundation Material			Dredged Material (PH-2) (Continued)		
Void Ratio	Effective Stress (lb/ft²)	Coefficient of Permeability (ft/day)	Void Ratio	Effective Stress (lb/ft²)	Coefficient of Permeability (ft/day)
2.50	0	2.00E-03	5.4	5.91	1.81E-03
2.45	1	1.89E-03	5.2	8.78	1.45E-03
2.42	2	1.75E-03	5.0	13.08	1.16E-03
2.25	16	1.21E-03	4.8	19.52	9.22E-04
2.15	32	9.49E-04	4.6	29.13	7.33E-04
2.05	64	7.33E-04	4.4	43.42	5.81E-04
1.76	256	2.60E-04	4.2	64.50	4.59E-04
1.58	512	1.20E-04	4.0	95.36	3.62E-04
1.39	1020	3.76E-05	3.8	140.06	2.85E-04
1.14	3000	8.00E-06	3.6	204.05	2.24E-04
			3.4	294.38	1.75E-04
Dredged Material (PH-2)			3.2	419.87	1.37E-04
8.0	0.10	2.65E-02	3.0	591.07	1.07E-04
7.8	0.12	2.19E-02	2.8	819.88	8.29E-05
7.6	0.15	1.80E-02	2.6	1118.79	6.43E-05
7.4	0.20	1.48E-02	2.4	1499.36	4.98E-05
7.2	0.26	1.21E-02	2.2	1970.21	3.84E-05
7.0	0.34	9.91E-03	2.0	2534.24	2.96E-05
6.8	0.47	8.08E-03	1.8	3185.65	2.27E-05
6.6	0.65	6.58E-03	1.6	3907.01	1.74E-05
6.4	0.91	5.34E-03	1.4	4667.36	1.33E-05
6.2	1.30	4.32E-03	1.2	5422.03	1.02E-05
6.0	1.87	3.49E-03	1.0	6115.04	7.70E-06
5.8	2.73	2.81E-03	0.8	6684.47	5.90E-06
5.6	4.00	2.26E-03	0.6	7070.48	4.40E-06
* A table of factors for converting non-SI to SI units of measurement is presented on page xvii.					

Table E2
Consolidation Characteristics of Foundation Material and Dredged
Material PH-4

Foundation Material			Dredged Material (PH-4) (Continued)		
Void Ratio	Effective Stress (lb/ft ²)	Coefficient of Permeability (ft/day)	Void Ratio	Effective Stress (lb/ft ²)	Coefficient of Permeability (ft/day)
2.50	0	2.00E-03	5.4	1.49	1.42E-03
2.45	1	1.89E-03	5.2	1.88	1.23E-03
2.42	2	1.75E-03	5.0	2.40	1.06E-03
2.25	16	1.21E-03	4.8	3.09	9.08E-04
2.15	32	9.49E-04	4.6	4.01	7.76E-04
2.05	64	7.33E-04	4.4	5.25	6.62E-04
1.76	256	2.60E-04	4.2	6.94	5.62E-04
1.58	512	1.20E-04	4.0	9.23	4.76E-04
1.39	1020	3.76E-05	3.8	12.38	4.02E-04
1.14	3000	8.00E-06	3.6	16.74	3.38E-04
			3.4	22.79	2.84E-04
Dredged Material (PH-4)			3.2	31.24	2.37E-04
8.0	0.18	7.15E-03	3.0	43.13	1.98E-04
7.8	0.19	6.44E-03	2.8	59.94	1.64E-04
7.6	0.22	5.78E-03	2.6	83.85	1.36E-04
7.4	0.24	5.17E-03	2.4	118.02	1.12E-04
7.2	0.28	4.61E-03	2.2	167.12	9.23E-05
7.0	0.32	4.10E-03	2.0	238.02	7.57E-05
6.8	0.38	3.63E-03	1.8	340.91	6.19E-05
6.6	0.44	3.21E-03	1.6	490.91	5.04E-05
6.4	0.53	2.82E-03	1.4	710.55	4.10E-05
6.2	0.64	2.48E-03	1.2	1033.57	3.32E-05
6.0	0.78	2.17E-03	1.0	1510.56	2.67E-05
5.8	0.96	1.89E-03	0.8	2217.65	2.15E-05
5.6	1.19	1.64E-03	0.6	3269.75	1.72E-05

Table E3
Consolidation Characteristics of Foundation Material and Dredged
Material PH-5

Foundation Material			Dredged Material (PH-5) (Continued)		
Void Ratio	Effective Stress (lb/ft ²)	Coefficient of Permeability (ft/day)	Void Ratio	Effective Stress (lb/ft ²)	Coefficient of Permeability (ft/day)
2.50	0	2.00E-03	5.4	5.91	1.81E-03
2.45	1	1.89E-03	5.2	8.78	1.45E-03
2.42	2	1.75E-03	5.0	13.08	1.16E-03
2.25	16	1.21E-03	4.8	19.52	9.22E-04
2.15	32	9.49E-04	4.6	29.13	7.33E-04
2.05	64	7.33E-04	4.4	43.42	5.81E-04
1.76	256	2.60E-04	4.2	64.50	4.59E-04
1.58	512	1.20E-04	4.0	95.36	3.62E-04
1.39	1020	3.76E-05	3.8	140.06	2.85E-04
1.14	3000	8.00E-06	3.6	204.05	2.24E-04
			3.4	294.38	1.75E-04
Dredged Material (PH-5)			3.2	419.87	1.37E-04
8.0	0.10	2.65E-02	3.0	591.07	1.07E-04
7.8	0.12	2.19E-02	2.8	819.88	8.29E-05
7.6	0.15	1.80E-02	2.6	1118.79	6.43E-05
7.4	0.20	1.48E-02	2.4	1499.36	4.98E-05
7.2	0.26	1.21E-02	2.2	1970.21	3.84E-05
7.0	0.34	9.91E-03	2.0	2534.24	2.96E-05
6.8	0.47	8.08E-03	1.8	3185.65	2.27E-05
6.6	0.65	6.58E-03	1.6	3907.01	1.74E-05
6.4	0.91	5.34E-03	1.4	4667.36	1.33E-05
6.2	1.30	4.32E-03	1.2	5422.03	1.02E-05
6.0	1.87	3.49E-03	1.0	6115.04	7.70E-06
5.8	2.73	2.81E-03	0.8	6684.47	5.90E-06
5.6	4.00	2.26E-03	0.6	7070.48	4.40E-06

Table E4
Consolidation Characteristics of Foundation Material and Dredged
Material PH-6

Foundation Material			Dredged Material (PH-6) (Continued)		
Void Ratio	Effective Stress (lb/ft ²)	Coefficient of Permeability (ft/day)	Void Ratio	Effective Stress (lb/ft ²)	Coefficient of Permeability (ft/day)
2.50	0	2.00E-03	5.4	0.82	1.18E-03
2.45	1	1.89E-03	5.2	1.04	1.08E-03
2.42	2	1.75E-03	5.0	1.34	9.82E-04
2.25	16	1.21E-03	4.8	1.74	8.85E-04
2.15	32	9.49E-04	4.6	2.28	7.92E-04
2.05	64	7.33E-04	4.4	3.01	7.04E-04
1.76	256	2.60E-04	4.2	4.02	6.21E-04
1.58	512	1.20E-04	4.0	5.40	5.44E-04
1.39	1020	3.76E-05	3.8	7.32	4.73E-04
1.14	3000	8.00E-06	3.6	9.99	4.08E-04
			3.4	13.73	3.50E-04
Dredged Material (PH-6)			3.2	19.00	2.98E-04
8.0	0.10	2.03E-03	3.0	26.44	2.51E-04
7.8	0.11	1.97E-03	2.8	37.01	2.11E-04
7.6	0.12	1.96E-03	2.6	52.10	1.76E-04
7.4	0.14	1.94E-03	2.4	73.69	1.45E-04
7.2	0.15	1.91E-03	2.2	104.72	1.19E-04
7.0	0.18	1.86E-03	2.0	149.46	9.70E-05
6.8	0.20	1.81E-03	1.8	214.14	7.84E-05
6.6	0.24	1.74E-03	1.6	307.88	6.30E-05
6.4	0.29	1.66E-03	1.4	444.05	5.02E-05
6.2	0.35	1.57E-03	1.2	642.19	3.97E-05
6.0	0.42	1.48E-03	1.0	930.95	3.12E-05
5.8	0.52	1.38E-03	0.8	1352.24	2.44E-05
5.6	0.65	1.28E-03	0.6	1967.33	1.89E-05

Table E5
Consolidation Characteristics of Foundation Material and Dredged
Material PH-10

Foundation Material			Dredged Material (PH-10) (Continued)		
Vold Ratio	Effective Stress (lb/ft ²)	Coefficient of Permeability (ft/day)	Vold Ratio	Effective Stress (lb/ft ²)	Coefficient of Permeability (ft/day)
2.50	0	2.00E-03	5.4	10.76	1.44E-03
2.45	1	1.89E-03	5.2	13.30	1.39E-03
2.42	2	1.75E-03	5.0	16.58	1.36E-03
2.25	16	1.21E-03	4.8	20.84	1.32E-03
2.15	32	9.49E-04	4.6	26.42	1.25E-03
2.05	64	7.33E-04	4.4	33.78	1.15E-03
1.76	256	2.60E-04	4.2	43.59	1.03E-03
1.58	512	1.20E-04	4.0	56.76	9.00E-04
1.39	1020	3.76E-05	3.8	74.59	7.63E-04
1.14	3000	8.00E-06	3.6	98.96	6.30E-04
			3.4	132.56	5.07E-04
Dredged Material (PH-10)			3.2	179.32	3.96E-04
8.0	1.33	2.14E-03	3.0	245.00	3.01E-04
7.8	1.50	2.09E-03	2.8	338.15	2.23E-04
7.6	1.70	2.03E-03	2.6	471.57	1.61E-04
7.4	1.95	1.98E-03	2.4	664.59	1.13E-04
7.2	2.24	1.93E-03	2.2	946.67	7.70E-05
7.0	2.59	1.87E-03	2.0	1363.22	5.12E-05
6.8	3.02	1.82E-03	1.8	1984.87	3.31E-05
6.6	3.54	1.77E-03	1.6	2922.63	2.08E-05
6.4	4.19	1.71E-03	1.4	4352.78	1.27E-05
6.2	4.98	1.66E-03	1.2	6558.26	7.60E-06
6.0	5.97	1.61E-03	1.0	9998.10	4.40E-06
5.8	7.21	1.55E-03	0.8	15425.17	2.50E-06
5.6	8.77	1.50E-03	0.6	24088.18	1.40E-06

Appendix F

Report of Field and Laboratory Data Subsurface Dredge Material Investigation



**REPORT
OF
FIELD AND LABORATORY DATA
SUBSURFACE DREDGE MATERIAL
INVESTIGATION**

**Pascagoula Harbor Channel Area
Pascagoula, Mississippi**

Prepared for:

U.S. Army Corps of Engineers – Mobile District

Contract No. DACW21-98-D-0025

Prepared by:

**Law Engineering & Environmental Services, Inc.
Kennesaw, Georgia**

October 2001

LAW Project No. 50160-8-0025-M10

October 16, 2001



U.S. Army Corps of Engineers, Mobile District
Operations Division
Attn: CESAM OP TN/ Mr. Stanley F. Clark
109 St. Joseph Street
P.O. Box 2288
Mobile, Alabama 36628-000

Subject: **Report of Field and Laboratory Data
Subsurface Dredge Material Investigation
Pascagoula Channel Area
Pascagoula, Mississippi
Contract No. DACW21-98-D-0025
LAW Project No. 50160-8-0025-M10**

Dear Mr. Clark:

Law Engineering and Environmental Services, Inc. (LAW) has completed the field and laboratory activities for the Subsurface Dredge Material Investigation for the Pascagoula Channel Area near Pascagoula, Mississippi. As outlined in the Scope of Work dated April 25, 2001, this data report summarizes the geotechnical testing performed and provides generic recommendations on use of the material in wetland creation. This report also includes field sampling information and the laboratory testing results as well as a brief description of the field and laboratory procedures.

Authorization for our notice to proceed on these services was provided on April 27, 2001. Laboratory testing assistance was provided by E2CR, Inc. (E2RC) located in Baltimore, Maryland and Law & Company Consulting and Analytical Chemists (Law & Company) located in Chamblee, Georgia. Gahagan & Byrant Associates, Inc (GBA) located in Houston, Texas assisted in preparation of the Part 4 of this report.

We appreciate the opportunity to serve the Corps of Engineers on this project. Please contact us if you have any questions.

Sincerely,

LAW ENGINEERING AND ENVIRONMENTAL SERVICES, INC.

X. Ching Wu, P.E.
Senior Engineer
Project Coordinator

Randy A. Knott, P.E. *By AB with permission*
Chief Engineer
Program Manager

Distribution: Addressee (10), Richard Brown, LAW Pensacola (1)
Wendell Mears, GBA (1), File (1)

TABLE OF CONTENTS

	<u>Page</u>
1.0 INTRODUCTION	1
2.0 FIELD ACTIVITIES	2
2.1 SEDIMENT SAMPLE COLLECTION.....	2
2.2 WATER SAMPLE COLLECTION.....	2
3.0 LABORATORY TESTING.....	3
3.1 CLASSIFICATION TESTS	3
3.2 CONSOLIDATION TESTS	3
4.0 EVALUATION FOR POTENTIAL BENEFICIAL USES OF DREDGED MATERIAL FOR MARSH AUGMENTATION, STABILIZATION OR RESTORATION.....	4
5.0 PROCEDURES.....	6
5.1 FIELD ACTIVITIES	6
5.1.1 Initial Sediment and Water Sample Collection.....	6
5.1.2 Additional Water Sample Collection	6
5.2 LABORATORY TESTING.....	6
5.2.1 Sample Preparation	6
5.2.2 Moisture Content	7
5.2.3 Atterberg Limits (Plasticity)	7
5.2.4 Grain Size Distribution	7
5.2.5 Specific Gravity	7
5.2.6 Unit Weight 8	
5.2.7 Salinity8	
5.2.8 Consolidation Tests.....	8
5.2.8.1 Long Tube Consolidation Test.....	9
5.2.8.2 Self-Weight Consolidation Test.....	9
5.2.8.3 Oedometer Consolidation Test.....	9
6.0 REFERENCES	11

LIST OF TABLES

- Table 1: Summary of Additional Water Sampling
- Table 2: Summary of Laboratory Classification and Index Property Testing Results
- Table 3: Summary of Laboratory Consolidation Testing Results

LIST OF FIGURES

- Figure 1: Project Area and Site Vicinity Map
- Figure 2: Field Sampling Location Plan

APPENDICES

APPENDIX A: WORK PLAN

Water Sample Collection Work Plan

APPENDIX B: LABORATORY DATA

Particle Size Distribution and other Classification and Index Properties
Salinity
Long Tube Consolidation
Self-weight Consolidation
Oedometer Consolidation

APPENDIX C: LABORATORY TESTING PROCEDURES

Salinity
Long Tube Consolidation
Self-weight Consolidation

1.0 INTRODUCTION

Law Engineering and Environmental Services, Inc. (LAW) was retained by the U.S. Army Corps of Engineers (COE) Mobile District to perform an investigation of the subsurface materials at the Pascagoula Harbor area near Pascagoula, Mississippi. The area is located as shown on the Project Area and Site Vicinity Map in Figure 1. The investigation includes field sampling, laboratory testing, and reporting. The results will be used for the basis of a design for constructing marsh habitats from materials to be dredged in the Pascagoula Channel within the Pascagoula River and Pascagoula Harbor.

A data report is to be prepared upon completion of the field and laboratory activities. This data report is to summarize the geotechnical investigation and sampling performed and include a description of the types and locations of materials and sampling completed, methods employed, a plan depicting relative sample locations, and our descriptions of the materials encountered. The report includes the results of the laboratory testing on the samples retrieved as well as a brief description of the field and laboratory procedures. Generic recommendations on use of the material in the wetland creation are provided in this report.

2.0 FIELD ACTIVITIES

2.1 SEDIMENT SAMPLE COLLECTION

Four potential dredge material (sediment) samples (designated 02—PH00, 04-NSP00, 06-PH00, and 10-PH00) that we understand were collected by the COE during the Fall of 2000 from the Pascagoula Channel. These samples were then shipped by the COE to GBA in Houston, Texas. GBA in turn shipped the samples to Baltimore, Maryland where they were stored at E2CR's laboratory. These samples were provided to LAW for laboratory testing. The reported sampling locations are shown in Figure 2.

2.2 WATER SAMPLE COLLECTION

We understand that water samples were collected simultaneously with each of the four sediment samples. These samples were also shipped and eventually stored at E2CR's laboratory. The approximate sampling locations are shown in Figure 2.

On May 1, 2001, two additional water samples (designed PS and PN) were collected in general accordance with the approved Work Plan (See Appendix A) by LAW using a boat equipped with a Global Positioning System. The approximate sampling locations are indicated on Figure 2.

Table 1 summarizes the samples collected. The additional water samples were shipped to the E2CR laboratory in Baltimore, Maryland.

3.0 LABORATORY TESTING

The laboratory testing of the materials include classification tests and consolidation tests as listed below.

3.1 CLASSIFICATION TESTS

- Moisture Content
- Atterberg Limits (Plasticity)
- Grain Size Distribution
- Unit Weight
- Specific Gravity of Solids
- Salinity

3.2 CONSOLIDATION TESTS

- Long Tube Consolidation
- Self-Weight Consolidation
- Oedometer Consolidation

E2CR's laboratory in Baltimore, Maryland performed moisture content, grain size distribution, plasticity, unit weight, specific gravity of solids, and long tube consolidation tests on the samples as well as preparing the samples for consolidation testing by removing the sand (See Section 5.2.1, below) from the samples. Salinity tests were performed by the Law & Company Laboratory (not affiliated with LAW) located in Chamblee, Georgia. The self-weight and oedometer consolidation tests were performed by LAW's laboratory in Atlanta, Georgia using samples prepared and forwarded by E2CR. The results of the laboratory testing are summarized in Tables 2 and 3 and presented in Appendix B.

4.0 EVALUATION FOR POTENTIAL BENEFICIAL USES OF DREDGED MATERIAL FOR MARSH AUGMENTATION, STABILIZATION OR RESTORATION

The materials tested are typical in gradation and geotechnical properties to that excavated during a maintenance-dredging event along the greater Gulf Coast. The relatively low sand, high silt and clay content are typical of an alluvial deposit or wind driven estuarine deposit within the navigation channels along the mid to western Gulf coast. The materials tested have material properties similar to those used in large volume beneficial uses along the Texas and Louisiana coastlines for marsh habitat creation, augmentation, stabilization, and restoration.

For continued evaluation, potential beneficial use sites should be identified and evaluated for wind and wave energy conditions, foundation characteristics, containment and stabilization alternatives, tidal influences, and bottom topography. Each site should be evaluated for equipment access and volume of dredged material utilized versus cost.

Additional settlement and consolidation modeling of the material characteristics is recommended using knowledgeable dredging experience and the COE programs SETTLE and Primary Consolidation Secondary Compression and Desiccation of Dredged Fill (PSDDF). The required containment height is evaluated based on procedures discussed in COE Manual EM 1110-2-5027, Confined Dredged Material Disposal. The program SETTLE is used to develop the relationship between fill concentration and time as described in Technical Note EEDP-06-18, Documentation of the SETTLE Module for ADDAMS, dated December 1992. PSDDF is used to evaluate the marsh fill settlement, providing parameters and ranges to evaluate the capacity of dredged material placed and containment methods at the alternative sites.

The types of materials tested can be utilized in relatively small amounts to augment or stabilize existing marshes using thin layer placement techniques along accessible fringes. If the existing marsh is exposed to increased erosion, or increased water depths due to subsidence or rise in sea level, the exposed fringe elevation can be raised intermittently to preserve the existing marsh.

These materials are also similar to relatively large amounts (> 100 acre) marsh stabilization and restoration projects that were designed as part of the projects Dredged Material Management Plan

(DMMP). With careful planning, single or multiple fill event sites have and continue to provide critical marsh and waterfowl habitat. Discharge points within the sites can be planned to create mounding for bird habitat. Planned dredged material discharge corridors and decant locations are critical to the sites intended usage. These locations will dictate inter-tidal features on large sites, minimizing mechanical manipulation of the site for the intended habitat.

Suggested marsh locations in the upper Pascagoula Harbor reach could include shoreline fringe marshes along the north, west and south sides of Singing River Island. These marshes would provide stabilization of the exposed shorelines, negating potential shore protection in the future and reduce storm surges on the island during storm events. A second and third alternative would be west of the Singing River Island parkway and the marshes along the western edge of Pascagoula Bay.

5.0 PROCEDURES

5.1 FIELD ACTIVITIES

5.1.1 Initial Sediment and Water Sample Collection

Details of the COE's procedures employed in sampling of sediment and water are not available.

5.1.2 Additional Water Sample Collection

Using a hand-held GPS (Magellan Model 315) unit and existing channel markers as guidance, the sampling team was transported to the designated sample locations by boat. Sampling locations were within the 40-foot degree of accuracy of the GPS unit. The depth of the water was measured to within 0.1 foot using a measuring pole. An approximately 2-inch diameter rubber hose was placed into the water to a depth approximately 2-feet above the channel bottom. The hose was connected to a five-horsepower pump on the boat. The pump was activated and the water sample was collected through the hose. The water samples were placed in painted metal 5-gallon buckets, sealed with plastic lids and labeled.

5.2 LABORATORY TESTING

5.2.1 Sample Preparation

Four samples collected by the COE and delivered to the E2CR laboratory in the fall of 2000. Samples are designated 02-PH00, 04-NSP00, 06-PH00, and 10-PH00. A water sample was initially collected at the same location as each sediment sample and given the same designation. Additional water samples collected by LAW were used to supplement the water requirements for washing the samples and conducting long tube and self-weight tests. The additional water samples, designated PN and PS were collected at the approximate locations where sediment samples 04-NSP00 and 10-PH00 were taken, respectively.

Classification and index property tests (Grain Size Distribution, Atterberg Limits, Moisture Content, Specific Gravity, Unit Weight) were conducted on the sediment samples and salinity tests were conducted on the water samples. To prepare samples for long-tube, self-weight, and oedometer consolidation testing, the sand (material larger than a US Standard #200 Sieve) was removed from the samples by washing samples through a US Standard #200 Sieve using the water from the same location. The washing substantially increased the moisture content of the washed samples.

5.2.2 Moisture Content

The moisture content of soil is defined as the weight of water in a given volume of soil divided by the weight of dry soil solids in the same mass. Moisture contents are determined in general accordance with ASTM D-2216.

5.2.3 Atterberg Limits (Plasticity)

The soil's plasticity index (PI) is determined by evaluating the soil's liquid limit (LL) and plastic limit (PL). The LL is the moisture content at which the soil will flow as a heavy viscous fluid. The PL is the moisture content at which the soil begins to lose its ability to deform plastically and becomes brittle. These determinations are made in general accordance with ASTM D-4318.

5.2.4 Grain Size Distribution

The grain size distribution of soils coarser than 0.75 mm in diameter is determined by passing the sample through a set of nested sieves. Material less than 0.075 mm in diameter is suspended in water and the grain size distribution measured by the rate of settlement using a hydrometer. These tests were performed in general accordance with ASTM D-1140 and D-422. The results are presented in the form of a curve showing the distribution of particle sizes or diameters.

5.2.5 Specific Gravity

The specific gravity of solids within a soil is defined as the density of the solid particles divided by the density of water (62.4 pcf). It is calculated by placing a known weight of dry sample in a known volume of

de-aired water and weighing the resulting mixture. Specific gravity tests are conducted in general accordance with ASTM D-854.

5.2.6 Unit Weight

The unit weight of the soil is defined as the weight of a unit volume of soil and is usually reported in pounds per cubic foot (pcf). The test procedure is described in ASTM D-2937. Dry unit weight on saturated samples can be calculated based on the specific gravity and moisture content. For partially saturated samples, the unit weight of a given volume is also required. Saturated samples are samples where all voids in the soil are filled with water. The void ratio (e), which is defined as the volume of voids (either water or air filled) divided by the volume of solids, is an important soil index property related to compressibility and can be calculated given the specific gravity of solids and moisture content on saturated samples or the unit density, moisture content, and specific gravity of solids on partially saturated soils.

5.2.7 Salinity

The water samples taken near the bottom of the channel were tested for salinity based on titration (AOAC 32.025-32.030, 13th edition) to measure chlorides using wet chemistry techniques. A description of the titrimetric method is included in Appendix C.

5.2.8 Consolidation Tests

Consolidation behavior of the very high void ratio dredge spoils is complex and varies with decreasing void ratio. For this reason, three separate tests are conducted at decreasing void ratios to assess overall consolidation behavior. These tests are the long tube test on very high void ratio slurry (initial $e > 15$), the self-weight test for intermediate void ratio slurries (initial e about 12), and the consolidation test using an oedometer for semi-solid materials (initial e about 3 to 5).

5.2.8.1 Long Tube Consolidation Test

The long tube consolidation test is used for very dilute slurries with void ratios in the range of 15 or greater. The slurry is agitated in a vertical tube of about 8-inch diameter and about 6 to 7 feet high. It is then allowed to settle and measurements of settlement with time and moisture content of the slurry with depth are collected. No external loads are applied to the sample. The test is in general accordance with the test method described in the Corps of Engineers EM-1110-2-5027. A copy of the test procedure is included in Appendix C.

The mode of settlement is determined, whether flocculent or dispersed. A curve of void ratio with time is developed for the sample. Flocculation, or the formation of very small silt and clay particles into flocs that are larger and settle more rapidly, is a critical concern for the overall sediment behavior of dredge material. Flocculation is greatly impacted by salinity.

5.2.8.2 Self-Weight Consolidation Test

The self weight test is similar to the long tube test except that it is conducted on slurries with initial void ratios of about 12 in a series of ½ inch high rings totaling about 8 inches high. The test progresses by allowing primary (hydrodynamic) settlement to occur and then measuring the moisture content calculating the void ratio profile through the sample after primary consolidation is complete. No external loads are applied to the sample. The test is conducted in general accordance with the Corps of Engineers GL-86-13. A copy of the test procedure is included in Appendix C.

5.2.8.3 Oedometer Consolidation Test

Consolidation tests were performed in general accordance with ASTM D-2435. These tests determine the one-dimensional consolidation (or compression) properties of the soil under loads in the range of about 100 to 1600 psf. The tests provide both stress-strain behavior and time-rate behavior. Test results are shown in the form of strain (expressed as change in void ratio) versus stress (compressive pressure) curves on the Consolidation Test Sheets in Appendix B. The test can typically only be conducted on soils that exhibit semi-solid behavior, generally with void ratios less than about 3 to 6, depending on the soil structure.

The sample is trimmed into a disc about 2.4 inches in diameter and 1-inch thick. The disc is confined in a stainless steel ring and sandwiched between porous plates that allow soil porewater to escape. The sample is prevented from desiccation, however. It is then subjected to incrementally increasing vertical loads and the resulting deformations are measured with a micrometer dial gauge over time.

6.0 REFERENCES

U.S. Army Corps of Engineers, "Program Documentation and User's Guide: PSDDF", Instruction Report EL-96-XX, November 1996.

U.S. Army Corps of Engineers, EM 1110-2-5027 "Confined Disposal of Dredged Material, September 1987 available at www.wes.army.mil/el/dots/guidance.html
<<http://www.wes.army.mil/el/dots/guidance.html>>

U.S. Army Corps of Engineers, "ADDAMS Program" available at
www.wes.army.mil/el/dots/models.html <<http://www.wes.army.mil/el/dots/models.html>>

U.S. Army Corps of Engineers, EM 1110-2-5025, "Dredging and Dredged Material Disposal"

October 16, 2001

**Table 1: Summary of Additional Water Sampling
 Subsurface Dredge Material Investigation - Pascagoula**

Sample Number	Sample Date	Sample Location	Sample Type/Volume/ Description	Depth of Channel (feet below water surface)	Sample Collection Depth (feet below water surface)
PS (approx. 10-PH00)	May 1, 2001	Pascagoula Channel Lat N 30 19' 08" Long W 88 32' 51"	WATER / 10 gal. / slightly turbid	40.0	38.0
PN (approx. 04- NSP00)	May 1, 2001	Pascagoula Channel Lat N 30 20' 39" Long W 88 34' 02"	WATER / 10 gal. / slightly turbid	40.0	38.0

Prepared by RJB 5-25-01

Checked by XCW, 10/15/01

Table -1

Table 2: Summary of Laboratory Classification and Index Property Testing Results
Subsurface Dredge Material Investigation - Pascagoula

Site	Sample No.	Moisture Content (%)	Atterberg Limits			Unit Dry Weight (pfc)	Gs	Salinity Titration	Sieve Analysis		USCS
			LL	PL	PI				% Fine	% Clay	
02-PH00	02	111	77	24	53	27.8	2.67	2.86	80	34	CH
04-NSP00	04	79	105	34	71	33.3	2.66	2.76	89	49	CH
06-PH00	06	95	67	23	44	37.8	2.69	2.98	98	39	CH
10-PH00	10	58	38	16	22	33.8	2.67	3.01	48	24	SC

Prepared by XCW 10/11/01

Checked by P44, 06/15/01

**Table 3: Summary of Consolidation Testing Results
 Subsurface Dredge Material Investigation - Pascagoula**

SITE	SAMPLE NO.	Gs	Long Tube Test		Self-Weight Test		Oedometer Test	
			e ₀	e _F	e ₀	e _F	e ₀	e _F
02-PH00	02	2.67	29.27	4.20	12.50	4.92	5.01	2.73
04-NSP00	04	2.66	21.05	5.91	13.00	4.40	3.99	1.54
06-PH00	06	2.69	25.50	5.94	10.00	3.92	3.38	1.16
10-PH00	10	2.67	17.67	7.51	12.70	6.80	3.98	2.30

Notes:

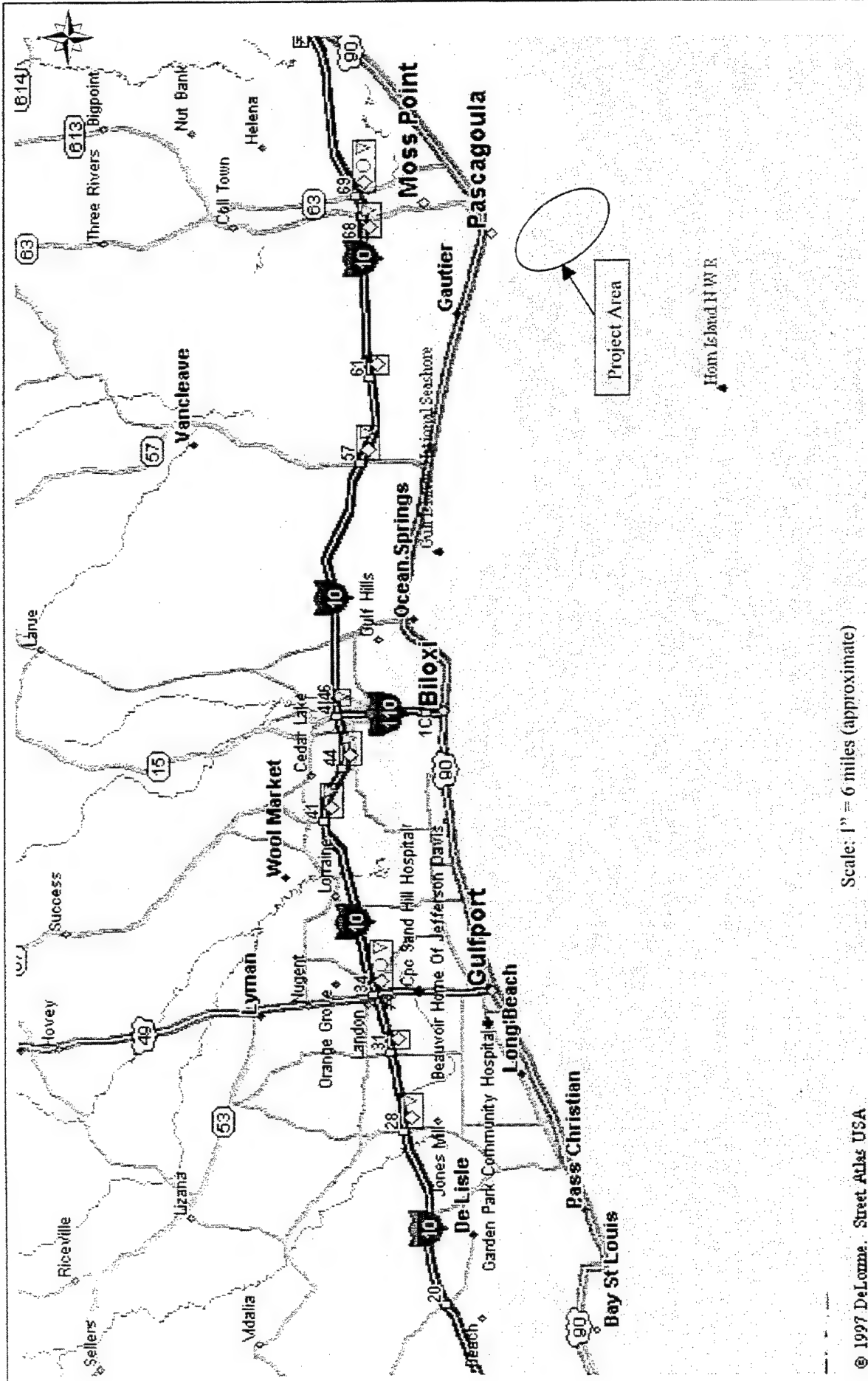
e₀ - Initial Void Ratio

e_F - Void Ratio at Finish of Test

Gs - Specific Gravity of Solids

Prepared by XCW 10/11/01

Checked by RAK, 10/15/01




Scale: 1" = 6 miles (approximate)

© 1997 DeLorme. Street Atlas USA

PROJECT AREA AND SITE VICINITY MAP

Job 50160-8-0025M10 Date: Oct 2001 Figure 1



LAW

LAWGIBB Group Member

Subsurface Dredge Material Investigation
Pascagoula, Mississippi

WORK PLAN

WATER SAMPLE COLLECTION TASK PASCAGOULA CHANNEL

SUBSURFACE DREDGE MATERIAL INVESTIGATION AND REPORT

April 27, 2001

The objective of this Work Plan is to outline procedures to be followed by LAW field personnel to properly perform the Water Sample Collection Task in Pascagoula Harbor Channel

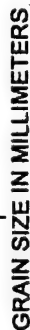
The objective of the Water Sample Collection Task is to collect water samples at the two locations from which sediment samples were previously collected in October 2000.

Equipment needed: Boat, pump capable of pumping at least 15-feet of head, four 5-gallon buckets that will not leak water when shipped.

Sample Locations: Two locations in Pascagoula Harbor Channel as indicated on the sample location map provided by Gahagan & Bryant and Associates on April 30, 2001.

1. Secure a boat with GPS equipment to access sampling locations.
2. At sample locations collect ten gallons of water from two feet above the channel bottom (channel bottom anticipated to be 15 feet below water surface).
3. Each sample is to be placed in two 5-gallon buckets (two samples – total 20 gallons of water collected).
4. Mark sample collection locations by lat/long With GPS equipment.
5. Samples to be labeled Sample PN (Pascagoula North) and Sample PS (Pascagoula South).
6. Properly seal sample containers and ship via Fed Ex to E2CR Laboratory located in Baltimore, MD.

U.S. SIEVE OPENING IN INCHES



Test performed by E2CR, Inc.

Project No.	5016080025.M10	02-PH00
-------------	----------------	---------

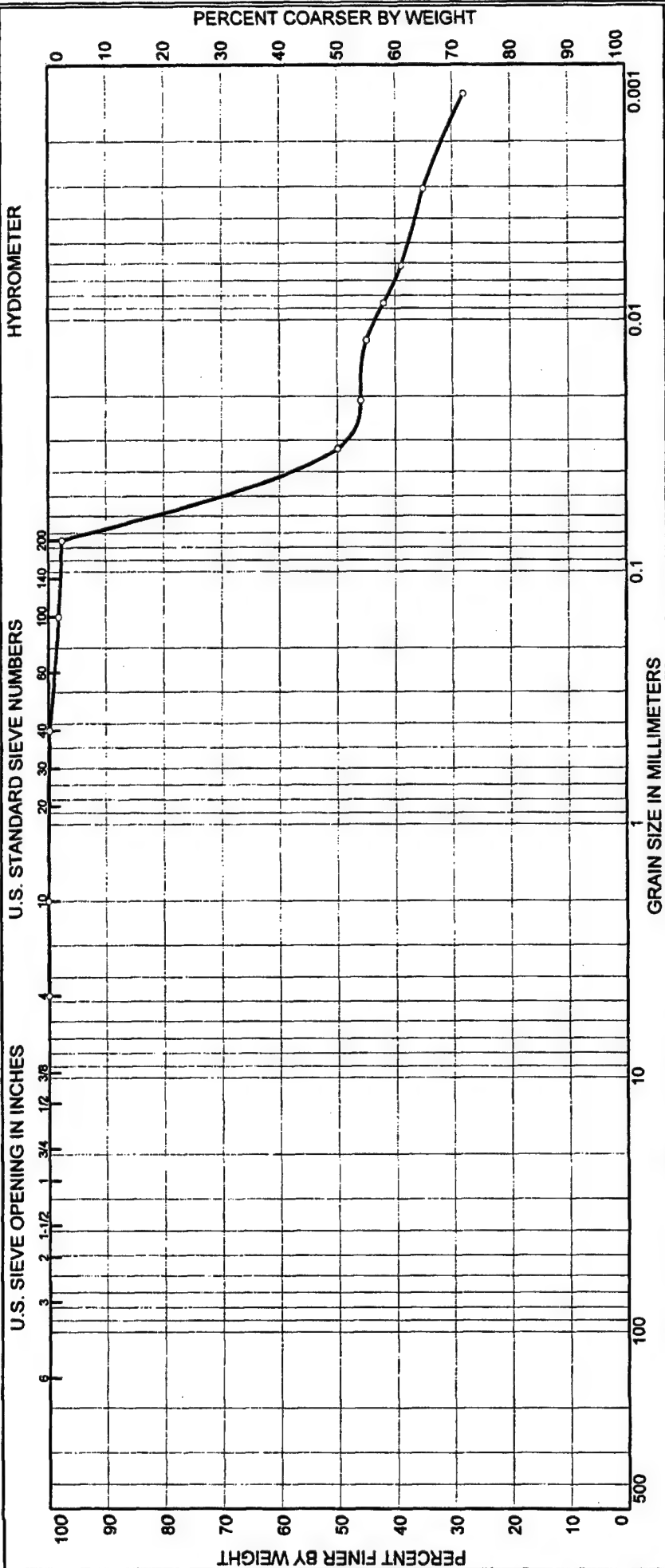
HYDROMETER



○ Test performed by E2CR, Inc.

Project No	5016080025 M10	04-NSP00
------------	----------------	----------

Particle Size Distribution Report ASTM D422/D1140



SOURCE	SAMPLE #	DEPTH/ELEV.	DATE SAMPLED	USCS	MATERIAL DESCRIPTION	NM %	LL	PL
PH00	06	--	Fall 2000	CH	Dark Greenish Brown Fat clay	--	67	23
					Specific Gravity 2.69			
					Moisture Content = 95.2%			

Client Corps of Engineers, Mobile District

Project Subsurface Dredge Material Investigation-Pascagoula

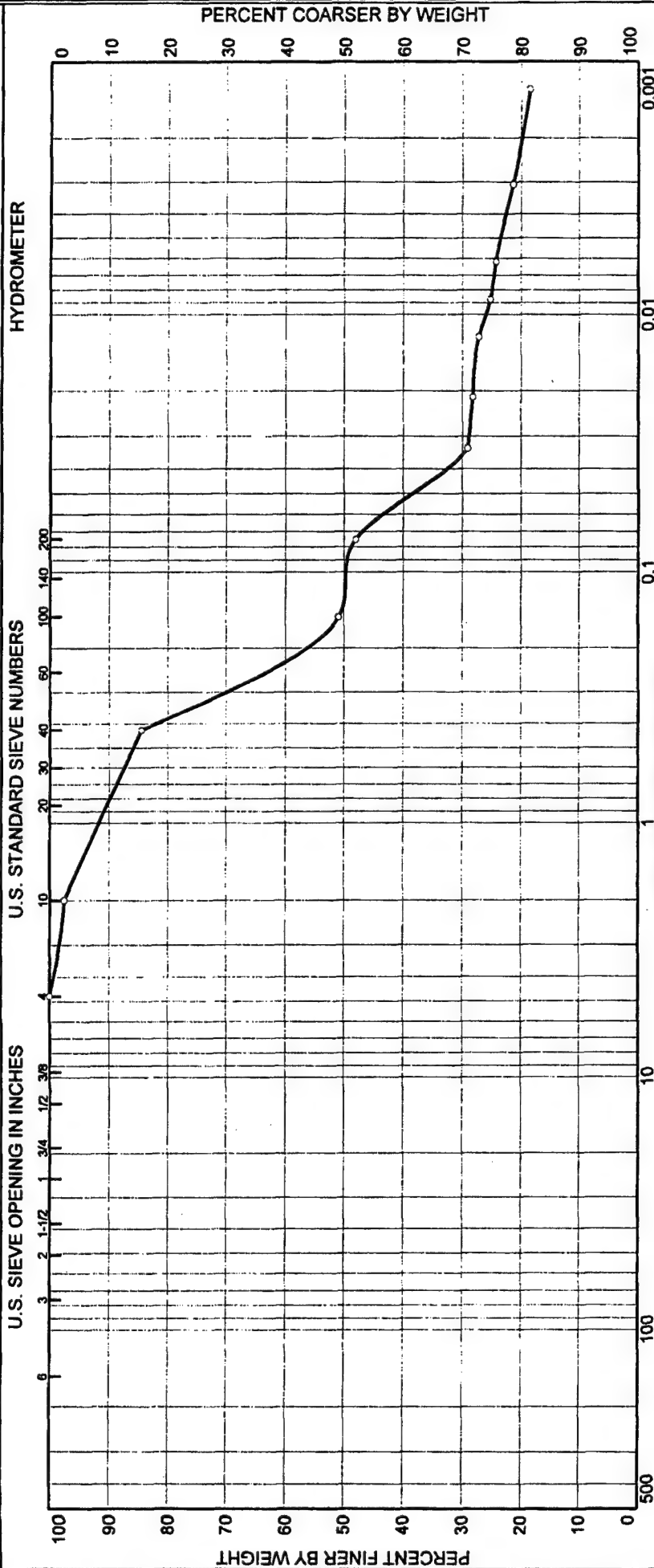
Project No. 5016080025.M10

LAW ENGINEERING AND ENVIRONMENTAL SERVICES, INC.

06-PH00

☐ Test performed by E2CR, Inc.

Particle Size Distribution Report ASTM D422/D1140



% COBBLES		% GRAVEL		% SAND			% FINES	
	COARSE	FINE	COARSE	MEDIUM	FINE		SILT	CLAY
0.0	0.0	0.0	2.4	13.1	36.5		24.4	23.6
SOURCE	SAMPLE #	DEPTH/ELEV.	DATE SAMPLED	USCS	MATERIAL DESCRIPTION			
PH00	10	--	Fall 2000	SC	Greenish Gray Clayey sand			
					Specific Gravity 2.67			
					Moisture Content = 58.4%			

Client Corps of Engineers, Mobile District		LAW ENGINEERING AND ENVIRONMENTAL SERVICES, INC.		<input type="radio"/> Test performed by E2CR, Inc.	
Project Subsurface Dredge Material Investigation-Pascagoula					
Project No.	5016080025.M10	10-PH00			

LAW & COMPANY
Consulting and Analytical Chemists

3770 GREEN INDUSTRIAL WAY
CHAMBLEE, GA. 30341

PHONE: 770-218-2044
FAX: 770-218-2045

Chemical Report

06/20/01

Laboratory Number: 825330-333

Received: 06/13/01

Law Gibb Group (Law Engineering)

Attn: Wenfeng Li

396 Plasters Ave., NE

Atlanta, GA 30324

Description: 4 water samples "Star Clorh", Pascagoula River, MS, 09/22/00

Lab ID	825330	825331	825332	82533
Sample ID	PH00-02	NSP00-04	PH00-06	PH00-10
Salinity				
Chlorides calculated as NaCl (g/100ml)	2.86	2.76	2.98	3.01

Respectfully Submitted,
LAW & COMPANY

By: Thomas E. Lantz

dh

Samples are retained for a period of thirty to sixty days after completion of testing. After that time, samples are disposed of in an environmentally sound manner unless other arrangements are made by the client.

**Long Tube Testing Results
PH002**

S.G. = 2.67
Average Moisture = 1097
Initial Void Ratio = 29.27

Starting at	Elapsed T Void Ratio		Min.	(e)	Elapsed T Void Ratio		Min.	(e)	Elapsed T Void Ratio		Min.	(e)
	Min.	(e)										
8/30/2001	0	29.27	3277	9.24	16140	5.57						
11:30 AM	15	28.98	3334	9.20	17100	5.44						
	30	28.67	6990	7.44	18510	5.32						
	45	28.38	7051	7.43	18900	5.28						
	60	28.11	7115	7.40	19043	5.26						
	90	27.60	7176	7.39	20100	5.17						
	120	27.14	7234	7.37	20430	5.14						
	180	26.10	7294	7.34	20565	5.13						
	240	25.06	7383	7.32	21450	5.06						
	300	24.07	7457	7.29	21750	5.04						
	360	23.17	7500	7.27	22005	5.01						
	420	22.30	7560	7.26	25830	4.79						
	480	21.41	7620	7.24	26310	4.76						
	1360	11.84	7680	7.21	27300	4.72						
	1420	11.68	7740	7.20	28740	4.65						
	1480	11.53	8480	6.97	29100	4.64						
	1590	11.27	8600	6.94	30060	4.59						
	1695	11.07	8660	6.93	31980	4.52						
	1740	10.98	8720	6.91	33150	4.48						
	1772	10.92	8869	6.87	33420	4.47						
	1832	10.83	8929	6.86	35910	4.40						
	1890	10.74	8990	6.84	36390	4.39						
	2670	9.72	9956	6.63	37230	4.36						
	2760	9.69	10190	6.55	40140	4.30						
	2790	9.66	10446	6.48	41580	4.26						
	2853	9.60	11280	6.31	42210	4.26						
	2913	9.55	11875	6.21	45885	4.20						
	2978	9.49	12720	6.05								
	3034	9.44	13177	5.98								
	3092	9.38	14340	5.70								
	3152	9.34	15750	5.62								
	3212	9.28	16035	5.58								

Subsurface Dredge Material Investigation
Biloxi - Lateral Channel
US Army Corps of Engineers
Mobile District
Contract No. DACW 21-98-D-0025

LAW

LAWGIBB Group Member 

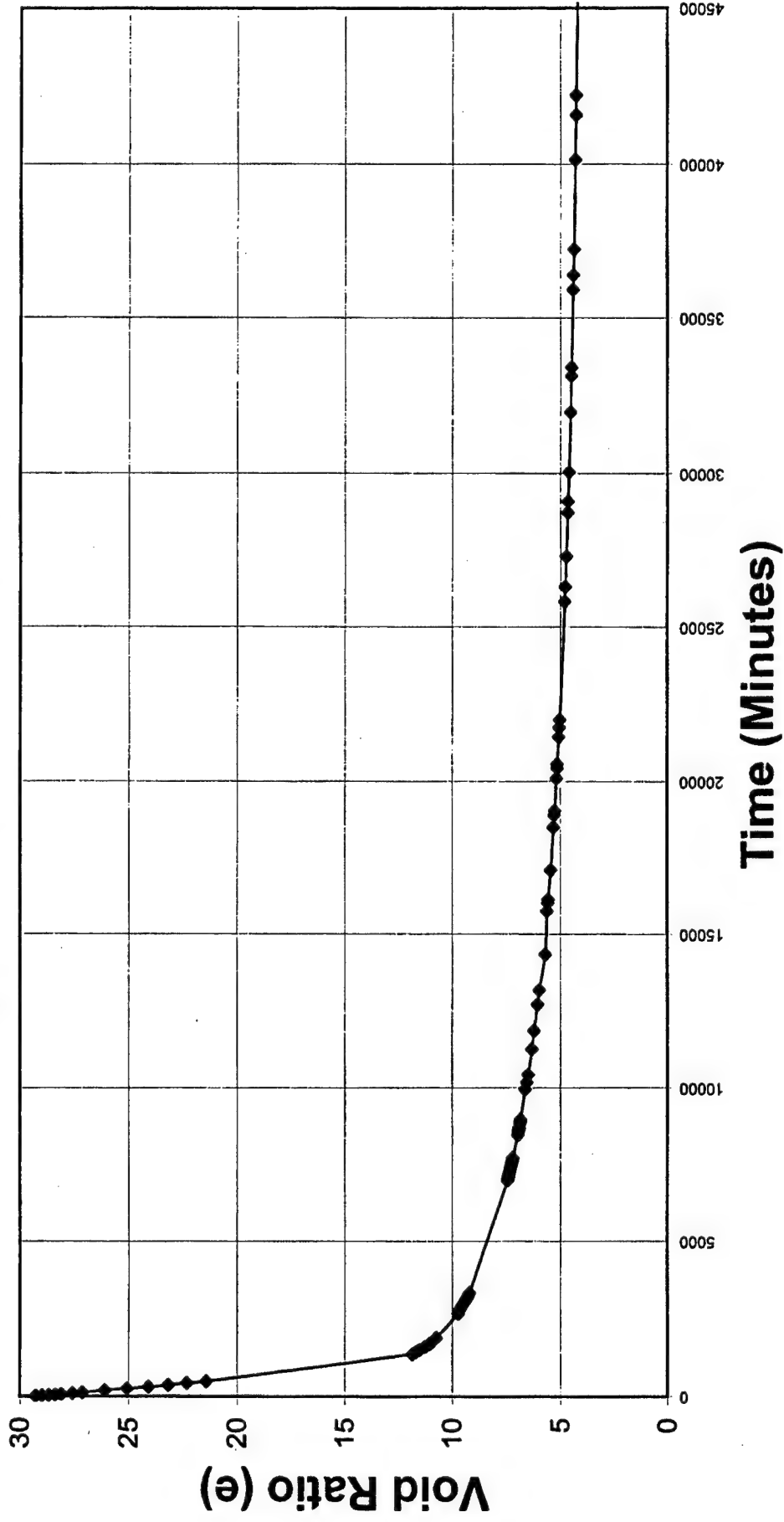
Atlanta, Georgia

Long Tube Testing Results
02-PH00

Project 50130-8-0025 M10

Date: 8/10/01 Figure 02-PH00

Long Tube Test - 02-PH00

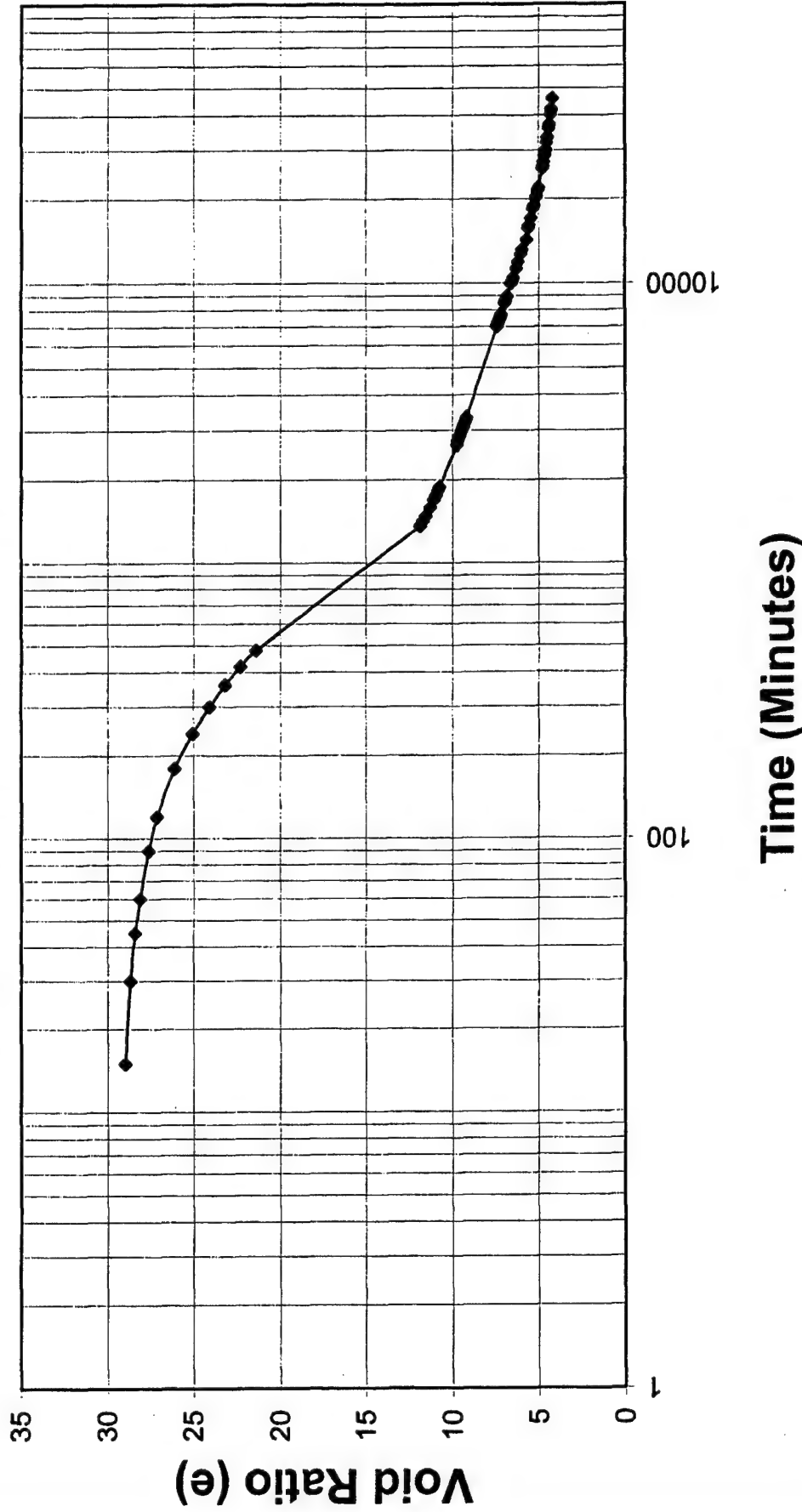


Subsurface Dredge Material Investigation
Pascagoula
US Army Corps of Engineers
Mobile District
Contract No. DACW 21-98-D-0025


LAW
LAWGIBB Group Member
Atlanta, Georgia

Long Tube Testing Results
02-PH00
DATE: October 2001
Project 50130-8-0025-M10Figure: 02-PH00-1

Long Tube Test - 02-PH00

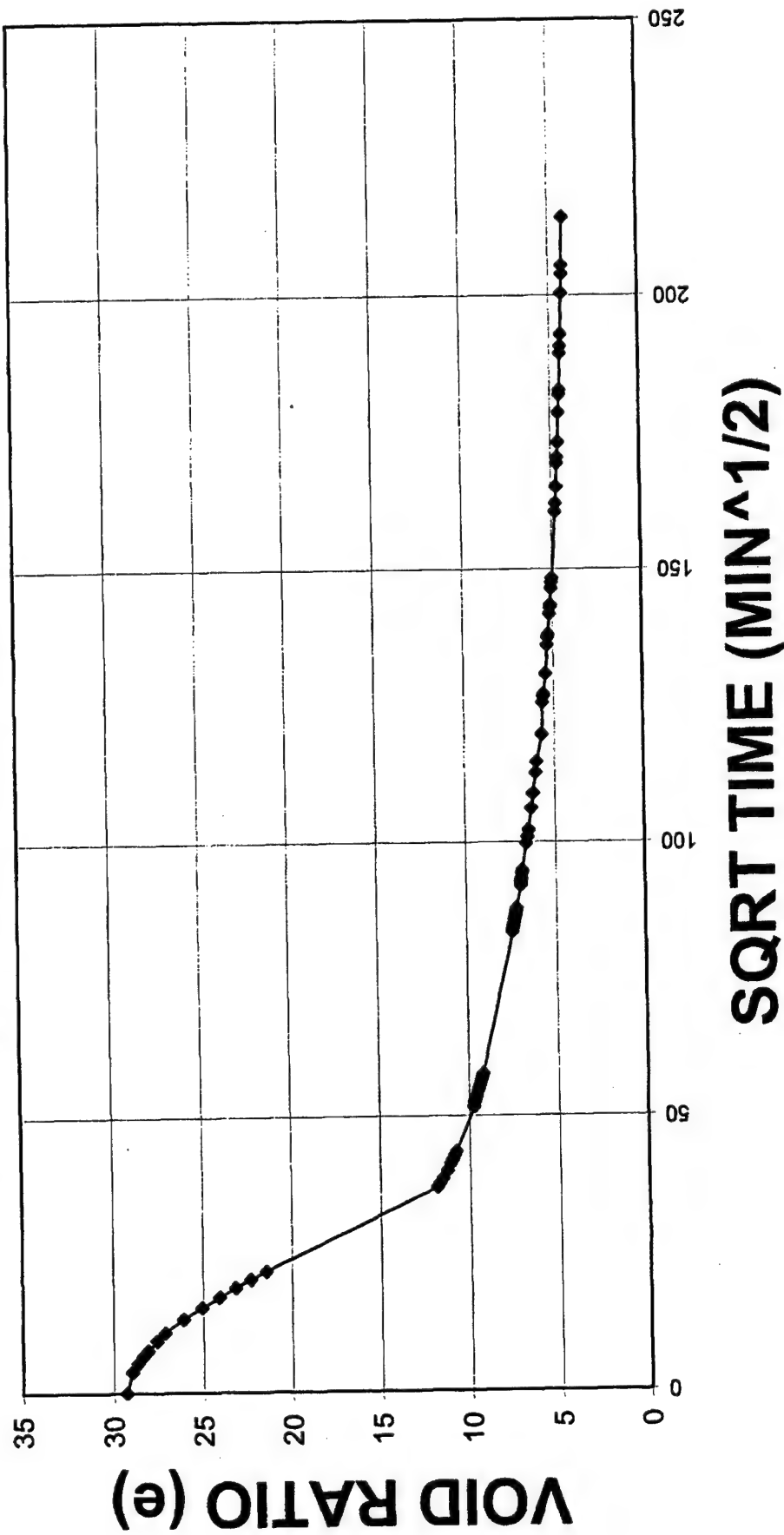


Subsurface Dredge Material Investigation
 Pascagoula
 US Army Corps of Engineers
 Mobile District
 Contract No. DACW 21-98-D-0025

LAW
 LAWGIBB Group Member 
 Atlanta, Georgia

Long Tube Testing Results
 02-PH00
 DATE: October 2001
 Project 50130-8-0025-M10 Figure: 02-PH00-2

Long Tube Test - 02-PH00



Subsurface Dredge Material Investigation
Pascagoula
US Army Corps of Engineers
Mobile District
Contract No. DACW 21-98-D-0025

LAW
LAWGIBB Group Member
Atlanta, Georgia

Long Tube Testing Results
02-PH00

DATE: October 2001


Project 50130-8-0025-M10 Figure: 02-PH00-3

**Long Tube Testing Results
04-SNP00**

S.G. = 2.66
Average Moisture = 792
Initial Void Ratio = 21.05

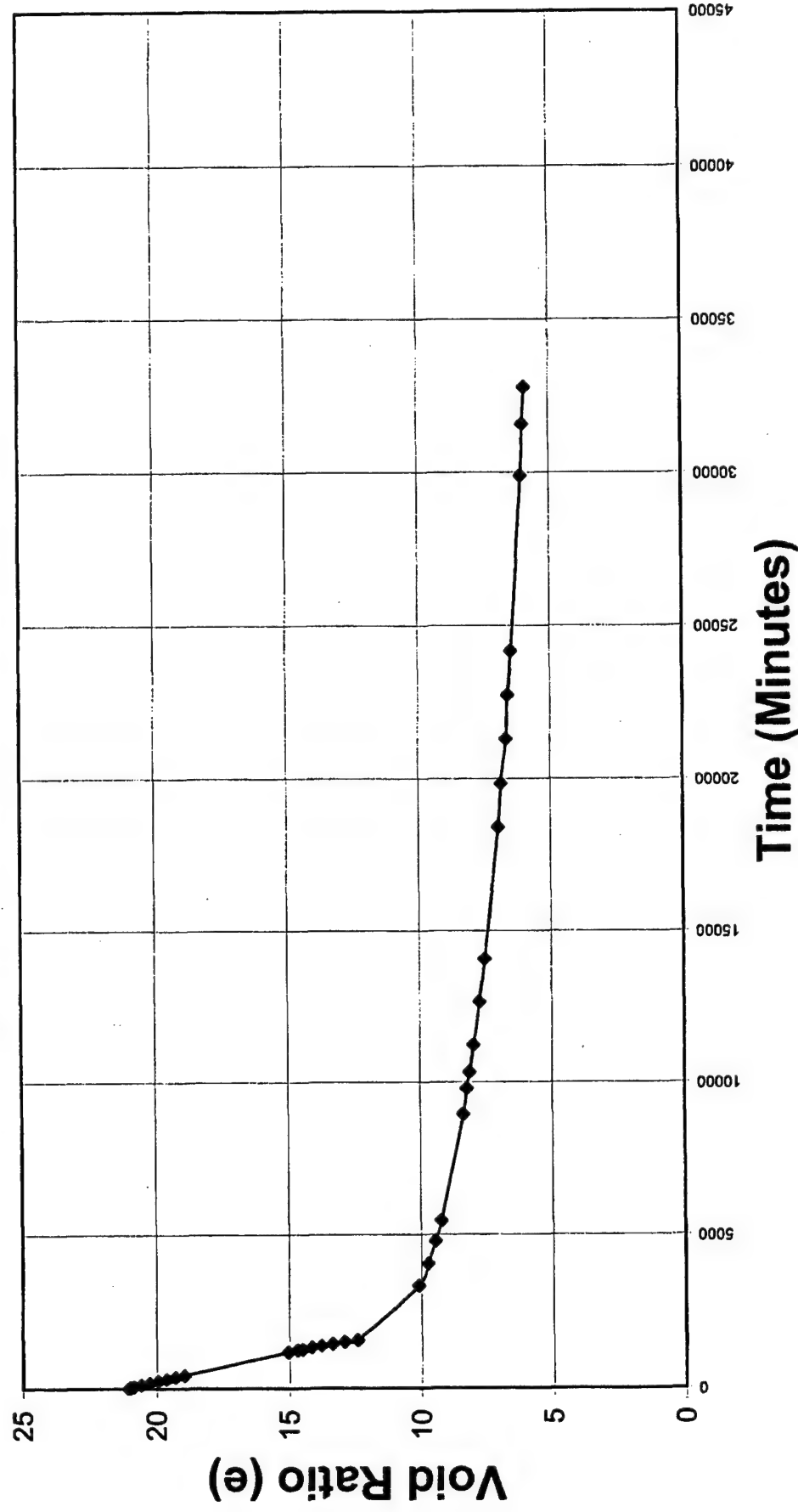
Starting at	Elapsed T Void Ratio		Elapsed T	Void Ratio	
	Min.	(e)	Min.	(e)	
7/31/01	0	21.05	18425	6.97	
1:45 PM	15	21.02	19845	6.87	
	30	20.99	21315	6.66	
	60	20.86	22730	6.59	
	120	20.59	24175	6.46	
	180	20.27	29895	6.07	
	240	19.94	31590	5.98	
	300	19.63	32785	5.91	
	360	19.30			
	420	18.97			
	1170	15.04			
	1230	14.69			
	1260	14.50			
	1320	14.15			
	1380	13.79			
	1440	13.36			
	1500	12.91			
	1560	12.42			
	3330	10.10			
	4050	9.74			
	4800	9.46			
	5460	9.23			
	8955	8.37			
	9800	8.22			
	10335	8.12			
	11235	7.96			
	12645	7.73			
	14070	7.51			

Subsurface Dredge Material Investigation
Pascagoula
US Army Corps of Engineers
Mobile District
Contract No. DACW 21-98-D-0025

LAW
LAWGIBB Group Member 
Atlanta, Georgia

Long Tube Testing Results
04-SNP00
Project 50130-8-0025 M10
Date: 10/15/01 Figure 04-SNP00

Long Tube Test - 04-NSP00



Subsurface Dredge Material Investigation

Pascagoula

US Army Corps of Engineers

Mobile District

Contract No. DACW 21-98-D-0025

LAW

LAWGIBB Group Member

Atlanta, Georgia

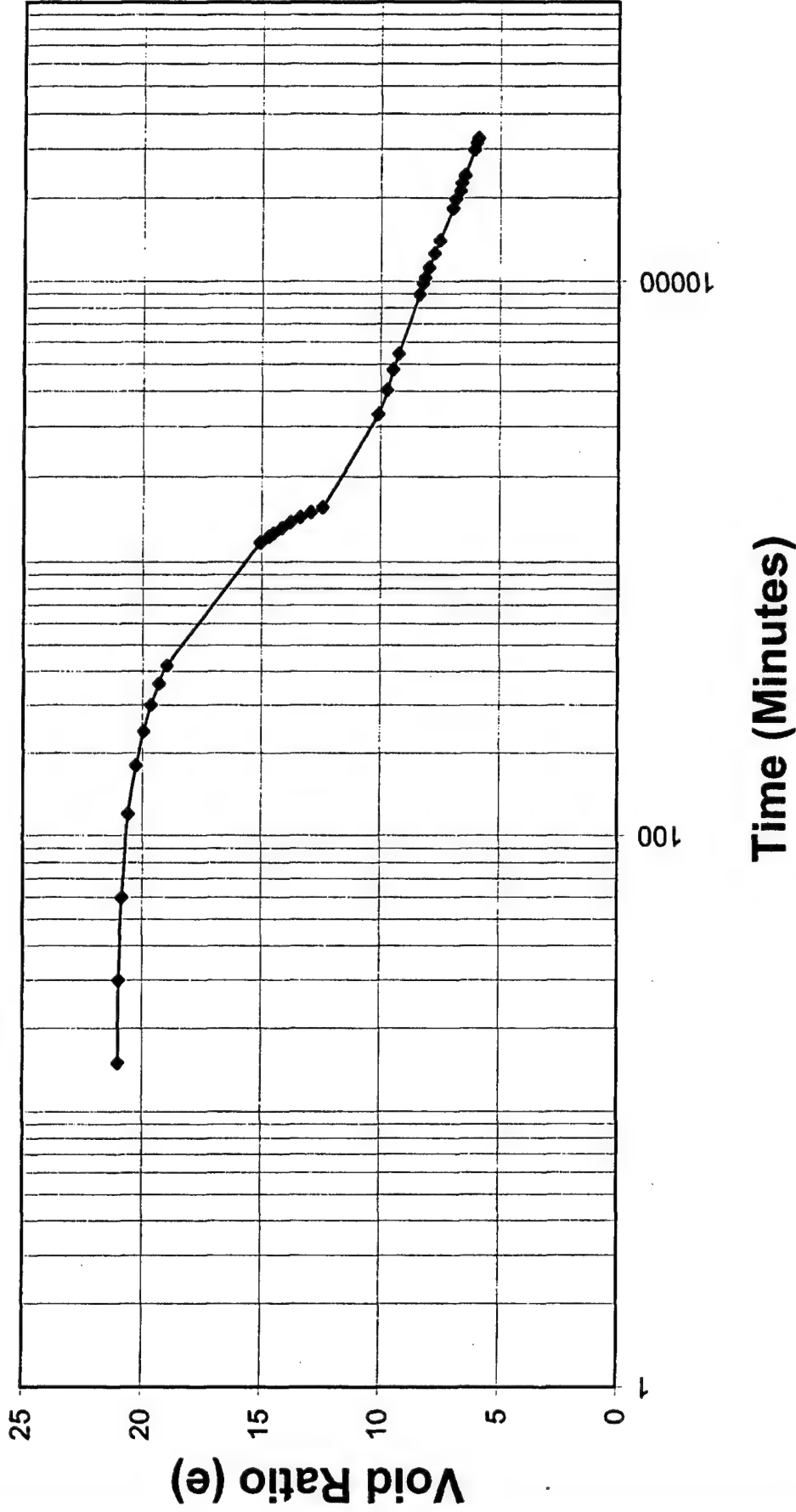
Long Tube Testing Results

04-NSP00

DATE: October 2001

Project 50130-8-0025-Mffigure: 04-NSP00-1

Long Tube Test - 04-NSP00



Subsurface Dredge Material Investigation
 Pascagoula
 US Army Corps of Engineers
 Mobile District
 Contract No. DACW 21-98-D-0025

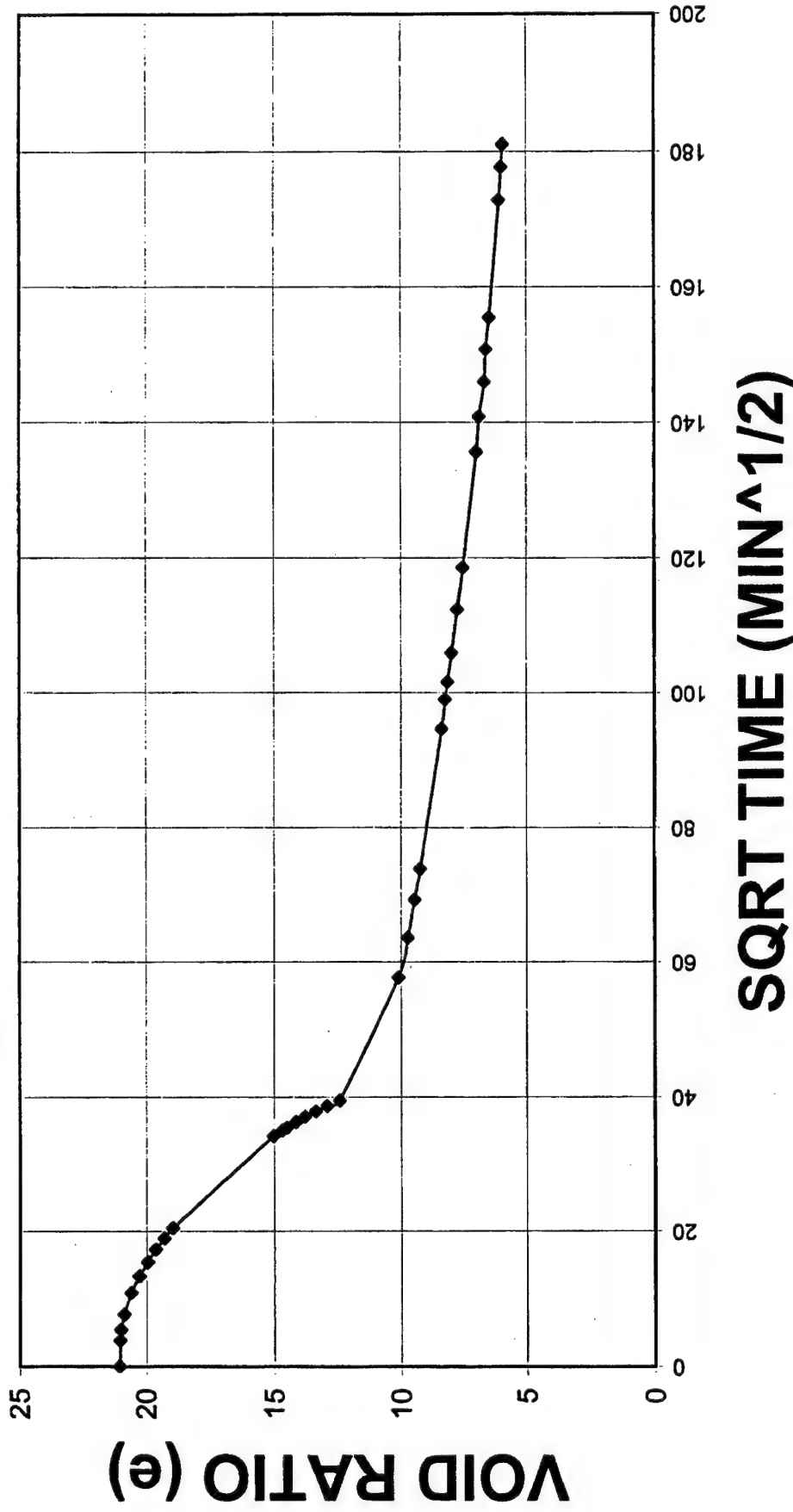
LAW
 LAWGIBB Group Member
 Atlanta, Georgia

Long Tube Testing Results
 04-NSP00

DATE: October 2001

Project 50130-8-0025-M Figure: 04-NSP00-2

Long Tube Test - 04-NSP00



Subsurface Dredge Material Investigation
Pascagoula
US Army Corps of Engineers
Mobile District
Contract No. DACW 21-98-D-0025

LAW
LAWGIBB Group Member
Atlanta, Georgia

Long Tube Testing Results
04-NSP00


DATE: October 2001
Project 50130-8-0025-M Figure: 04-NSP00-3

**Long Tube Testing Results
06-PH00**

S.G. = 2.69
Average Moisture = 948
Initial Void Ratio = 25.50

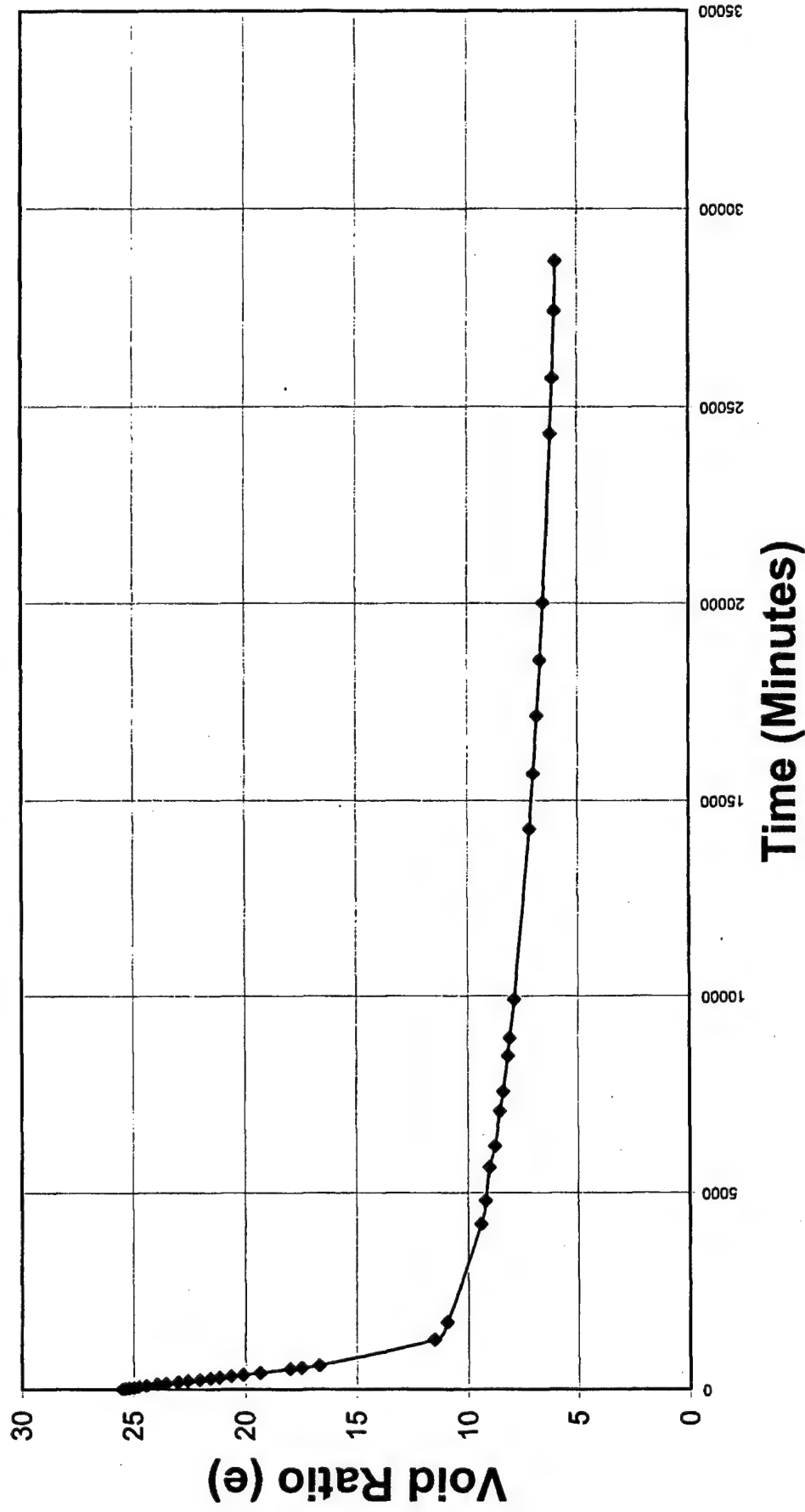
Starting at	Elapsed T Void Ratio		Elapsed T	Void Ratio	
	Min.	(e)	Min.	(e)	
7/31/01	0	25.50	8941	8.06	
1:45 PM	15	25.39	9915	7.86	
	30	25.21	14270	7.14	
	45	24.99	15690	6.97	
	60	24.77	17160	6.80	
	90	24.42	18570	6.65	
	125	23.94	20020	6.52	
	150	23.54	24315	6.18	
	180	23.01	25740	6.09	
	210	22.57	27435	5.99	
	240	22.04	28690	5.94	
	270	21.58			
	300	21.16			
	333	20.65			
	369	20.11			
	420	19.35			
	515	17.99			
	548	17.48			
	605	16.67			
	1260	11.53			
	1705	10.96			
	4200	9.42			
	4800	9.19			
	5645	9.02			
	6180	8.76			
	7080	8.52			
	7582	8.38			
	8490	8.16			

Subsurface Dredge Material Investigation
Pascagoula
US Army Corps of Engineers
Mobile District
Contract No. DACW 21-98-D-0025

LAW
LAWGIBB Group Member 
Atlanta, Georgia

Long Tube Testing Results
06-PH00
Project 50130-8-0025 M10
Date: 10/15/01 Figure 06-PH00

Long Tube Test - 06-PH00

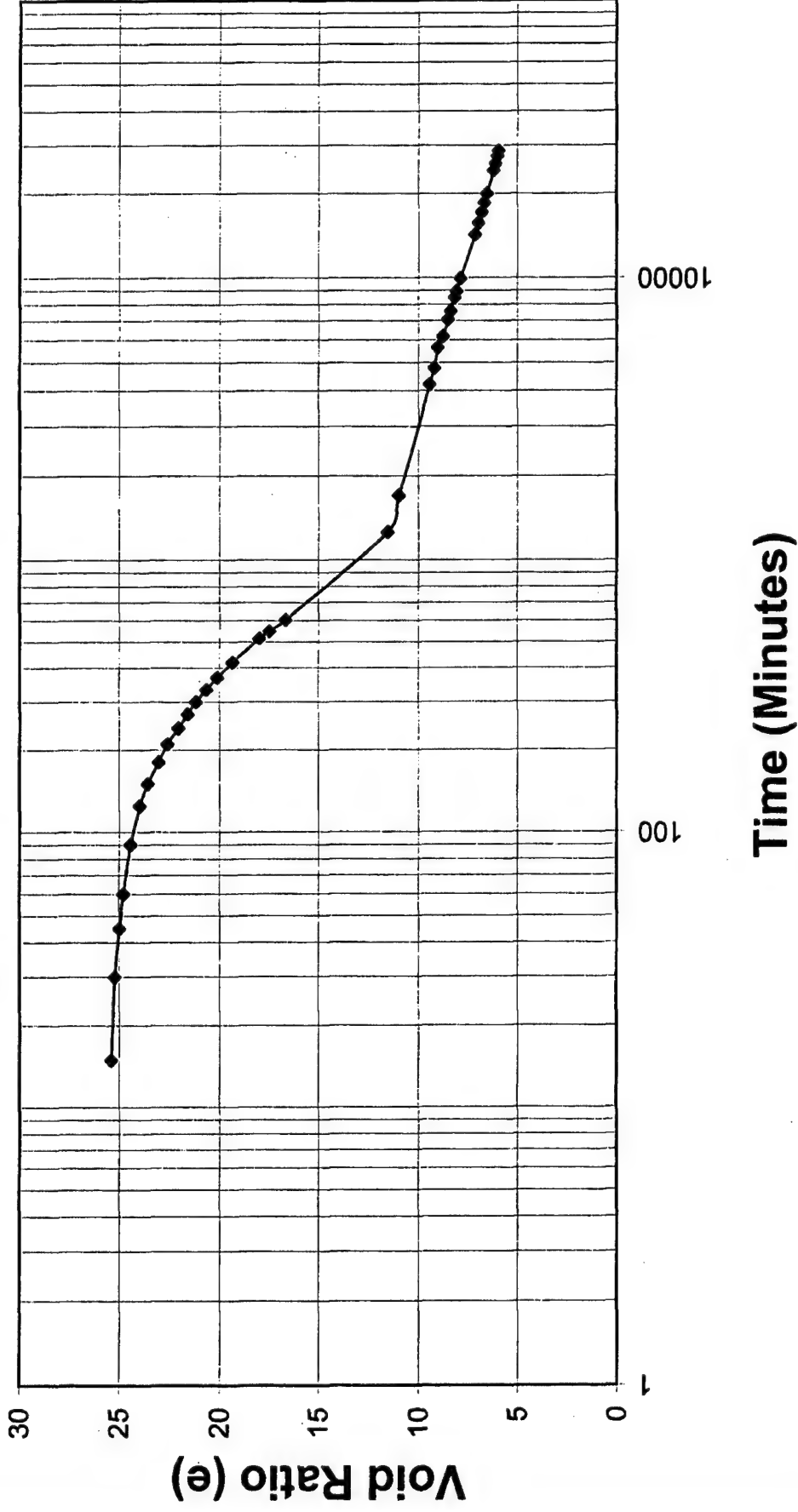


Subsurface Dredge Material Investigation
 Pascagoula
 US Army Corps of Engineers
 Mobile District
 Contract No. DACW 21-98-D-0025

LAW
 LAWGIBB Group Member
 Atlanta, Georgia

Long Tube Testing Results
 06-PH00
 DATE: October 2001
 Project 50130-8-0025-M10Figure: 06-PH00-1

Long Tube Test - 06-PH00



Subsurface Dredge Material Investigation
Pascagoula
US Army Corps of Engineers
Mobile District
Contract No. DACW 21-98-D-0025

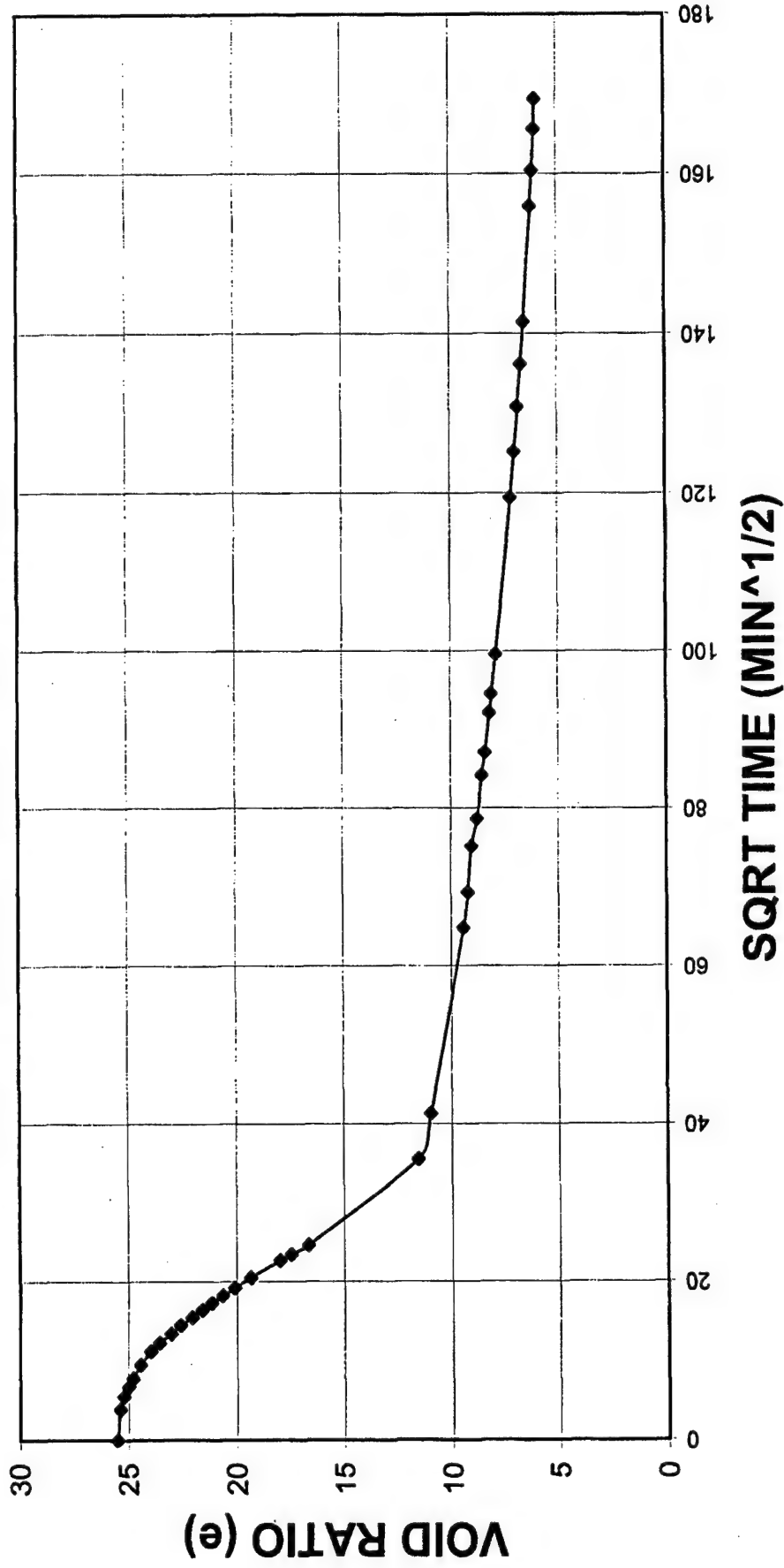
LAW
LAWGIBB Group Member
Atlanta, Georgia

Long Tube Testing Results
06-PH00

DATE: October 2001

Project 50130-8-0025-M10Figure: 06-PH00-2

Long Tube Test - 06-PH00



Subsurface Dredge Material Investigation
Pascagoula
US Army Corps of Engineers
Mobile District
Contract No. DACW 21-98-D-0025

LAW
LAWGIBB Group Member
Atlanta, Georgia

Long Tube Testing Results
06-PH00


DATE: October 2001
Project 50130-8-0025-M10 Figure: 06-PH00-3

**Long Tube Testing Results
10-PH00**

S.G. = 2.67
Average Moisture = 662
Initial Void Ratio = 17.67

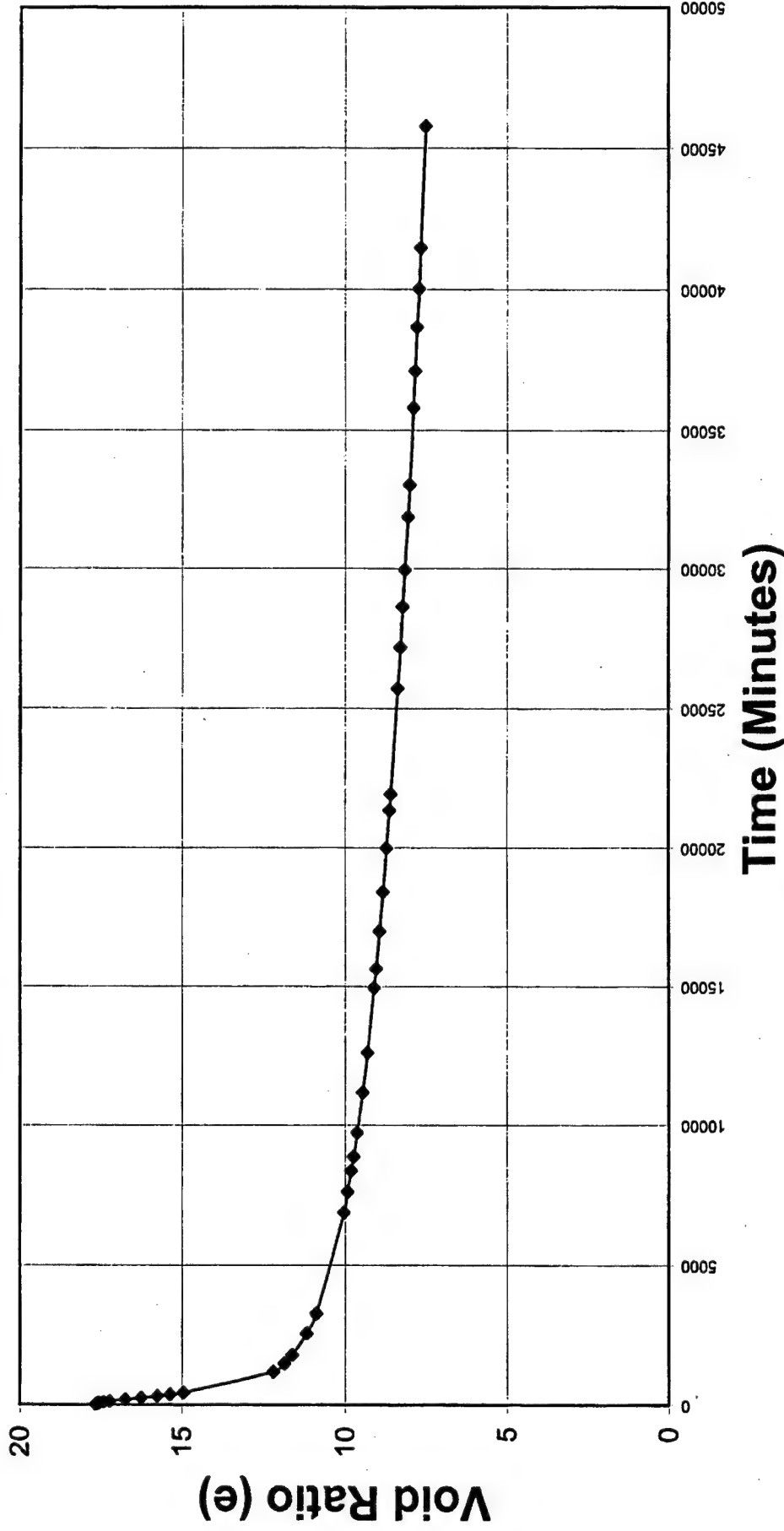
Starting at	Elapsed T Void Ratio		Elapsed T	Void Ratio	
	Min.	(e)	Min.	(e)	
7/31/01	0	17.67	19995	8.70	
1:45 PM	15	17.65	21345	8.61	
	30	17.62	21930	8.57	
	45	17.61	25725	8.36	
	60	17.57	27195	8.28	
	90	17.44	28635	8.21	
	120	17.25	29955	8.15	
	180	16.76	31875	8.05	
	240	16.26	33045	8.00	
	300	15.76	35805	7.88	
	360	15.36	37125	7.83	
	420	14.95	38685	7.77	
	1185	12.19	40035	7.71	
	1485	11.85	41475	7.66	
	1785	11.61	45780	7.51	
	2565	11.17			
	3285	10.88			
	6885	10.03			
	7635	9.92			
	8375	9.81			
	8885	9.73			
	9731	9.62			
	11175	9.45			
	12616	9.29			
	14955	9.08			
	15645	9.02			
	16995	8.92			
	18405	8.81			

Subsurface Dredge Material Investigation
Pascagoula
US Army Corps of Engineers
Mobile District
Contract No. DACW 21-98-D-0025

LAW
LAWGIBB Group Member 
Atlanta, Georgia

Long Tube Testing Results
10-PH00
Project 50130-8-0025 M10
Date: 10/15/01 Figure 10-PH00

Long Tube Test - 10-PH00



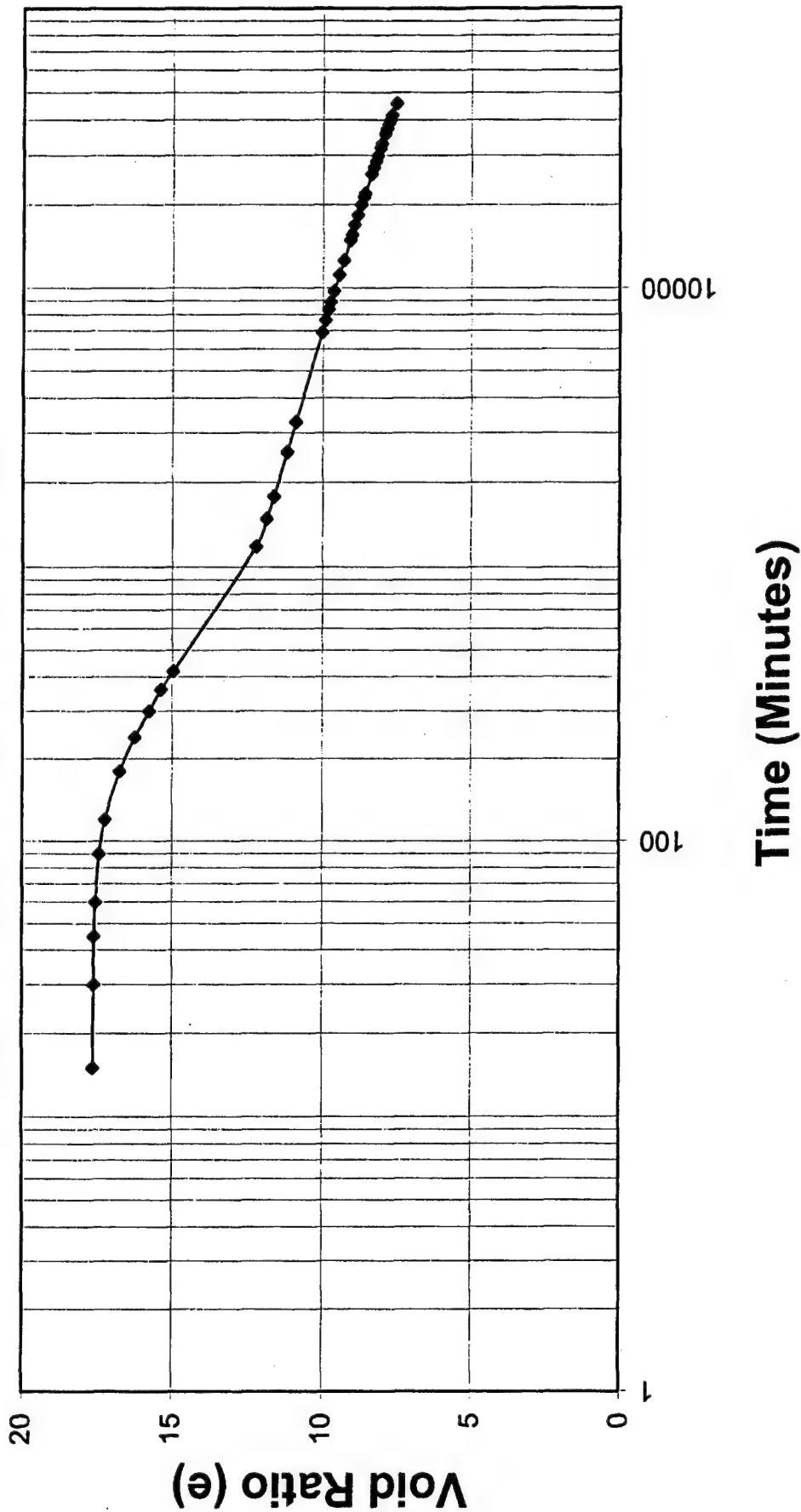
Subsurface Dredge Material Investigation
Pascagoula
US Army Corps of Engineers
Mobile District
Contract No. DACW 21-98-D-0025

LAW
LAWGIBB Group Member
Atlanta, Georgia

Long Tube Testing Results
10-PH00

DATE: October 2001
Project 50130-8-0025-M10Figure: 10-PH00-1

Long Tube Test - 10-PH00



Subsurface Dredge Material Investigation
Pascagoula
US Army Corps of Engineers
Mobile District
Contract No. DACW 21-98-D-0025

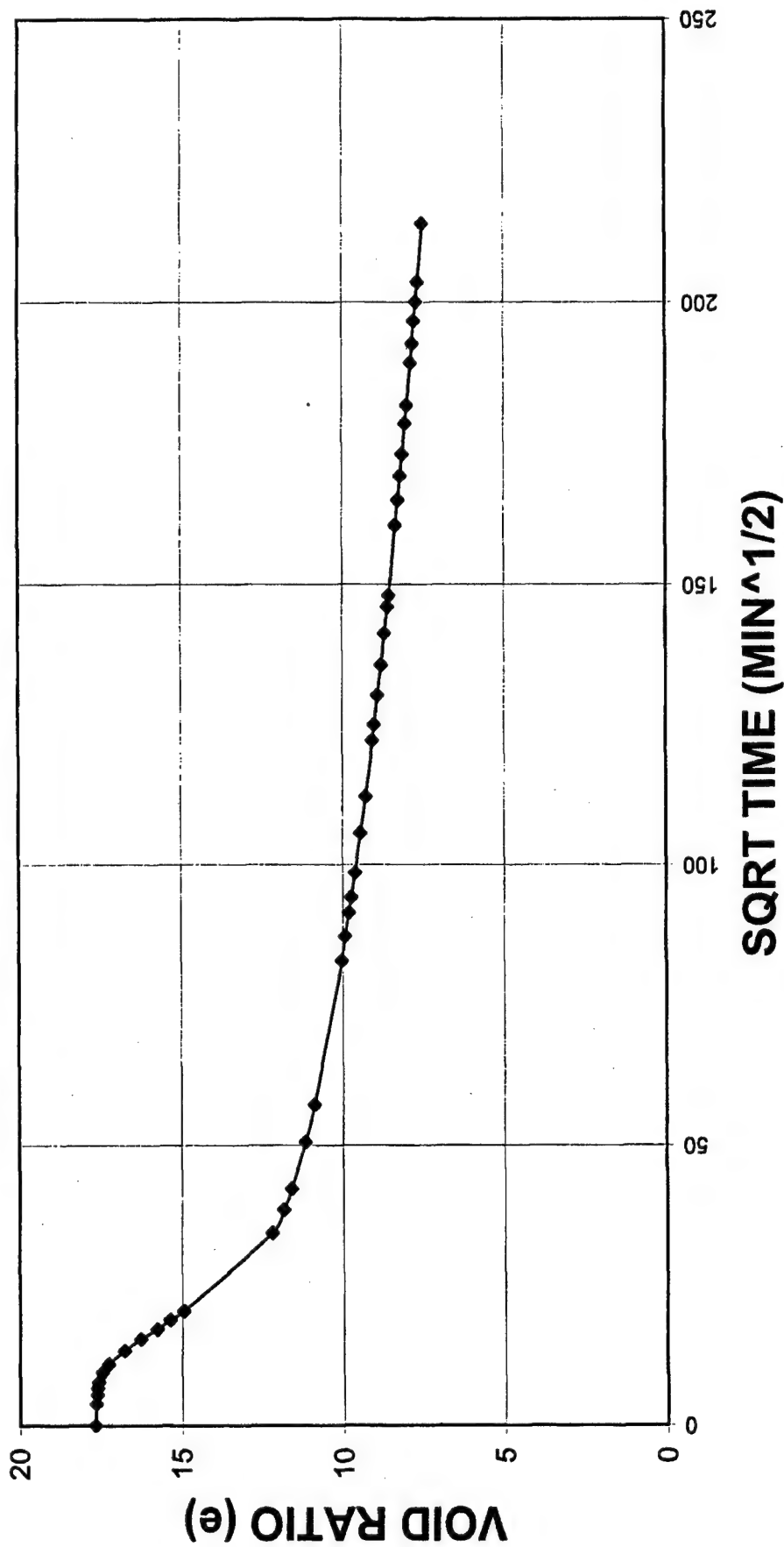
LAW
LAWGIBB Group Member
Atlanta, Georgia

Long Tube Testing Results
10-PH00

DATE: October 2001

Project 50130-8-0025-M10 Figure: 10-PH00-2

Long Tube Test - 10-PH00



Subsurface Dredge Material Investigation
Pascagoula
US Army Corps of Engineers
Mobile District
Contract No. DACW 21-98-D-0025

LAW
LAWGIBB Group Member
Atlanta, Georgia


Long Tube Testing Results
10-PH00
DATE: October 2001
Project 50130-8-0025-M10Figure: 10-PH00-3

**Self-weight Consolidation Results
02-PH00**

S.G. = 2.67
Initial Void Ratio = 12.50
Volume Solids (gal) = 0.053

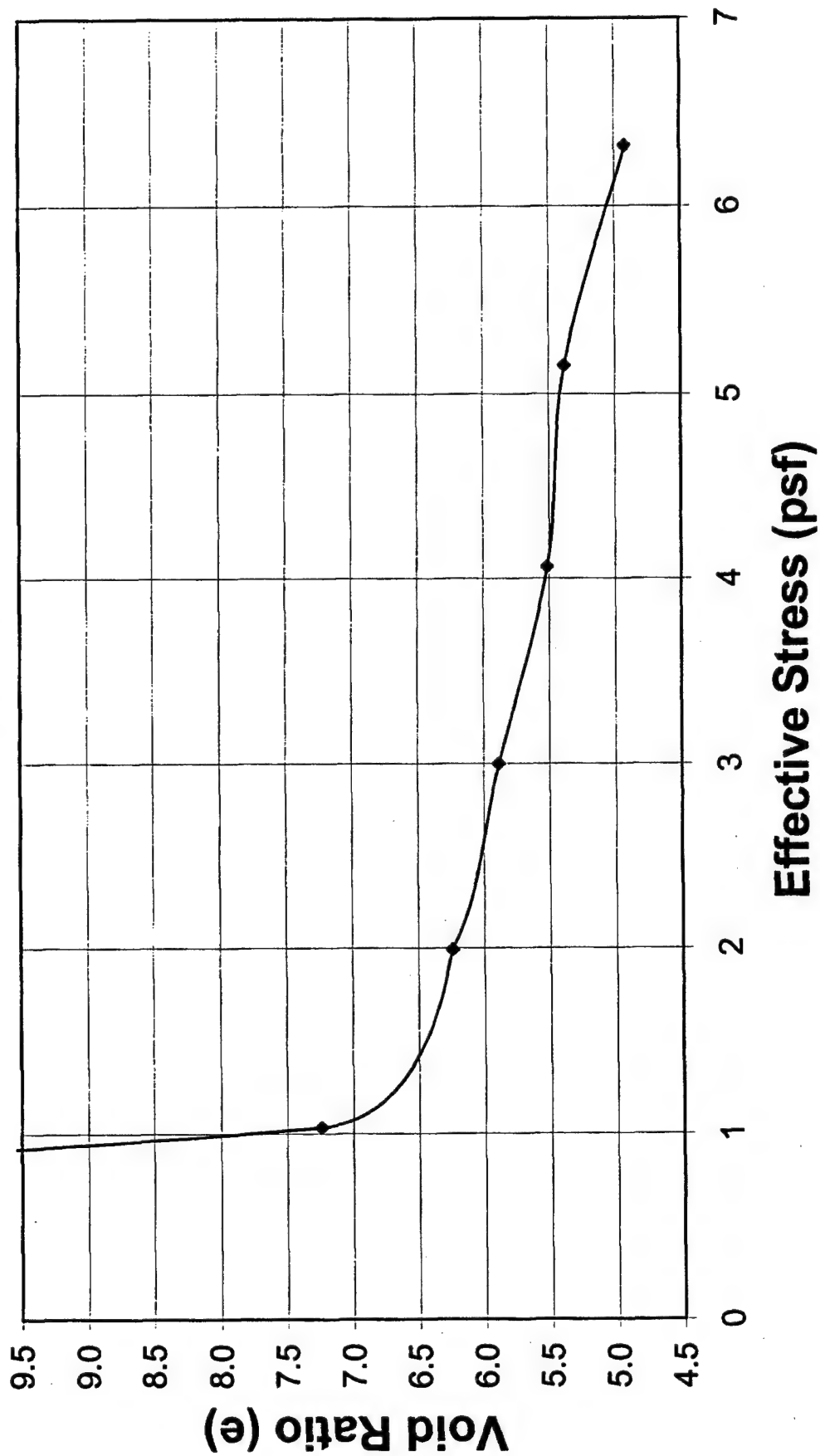
Starting	Elapse Min.	Sludge V Gal	Void Ratio (e)
	0	0.72	12.50
	1	0.72	12.50
	490	0.66	11.36
	1450	0.57	9.66
	1930	0.53	8.98
	2880	0.50	8.27
	7200	0.41	6.67
	10100	0.39	6.28
	12980	0.37	5.86

Subsurface Dredge Material Investigation
Pascagoula
US Army Corps of Engineers
Mobile District
Contract No. DACW 21-98-D-0025

LAW
LAWGIBB Group Member 
Atlanta, Georgia

Self-weight Consolidation Results
02SW
Project 50130-8-0025 M10
Date: Oct 2001 Figure 02SW

Self Weight - 02-PH00



Subsurface Dredge Material Investigation
Pascagoula

US Army Corps of Engineers
Mobile District

Contract No. DACW 21-98-D-0025

LAW
LAWGIBB Group Member

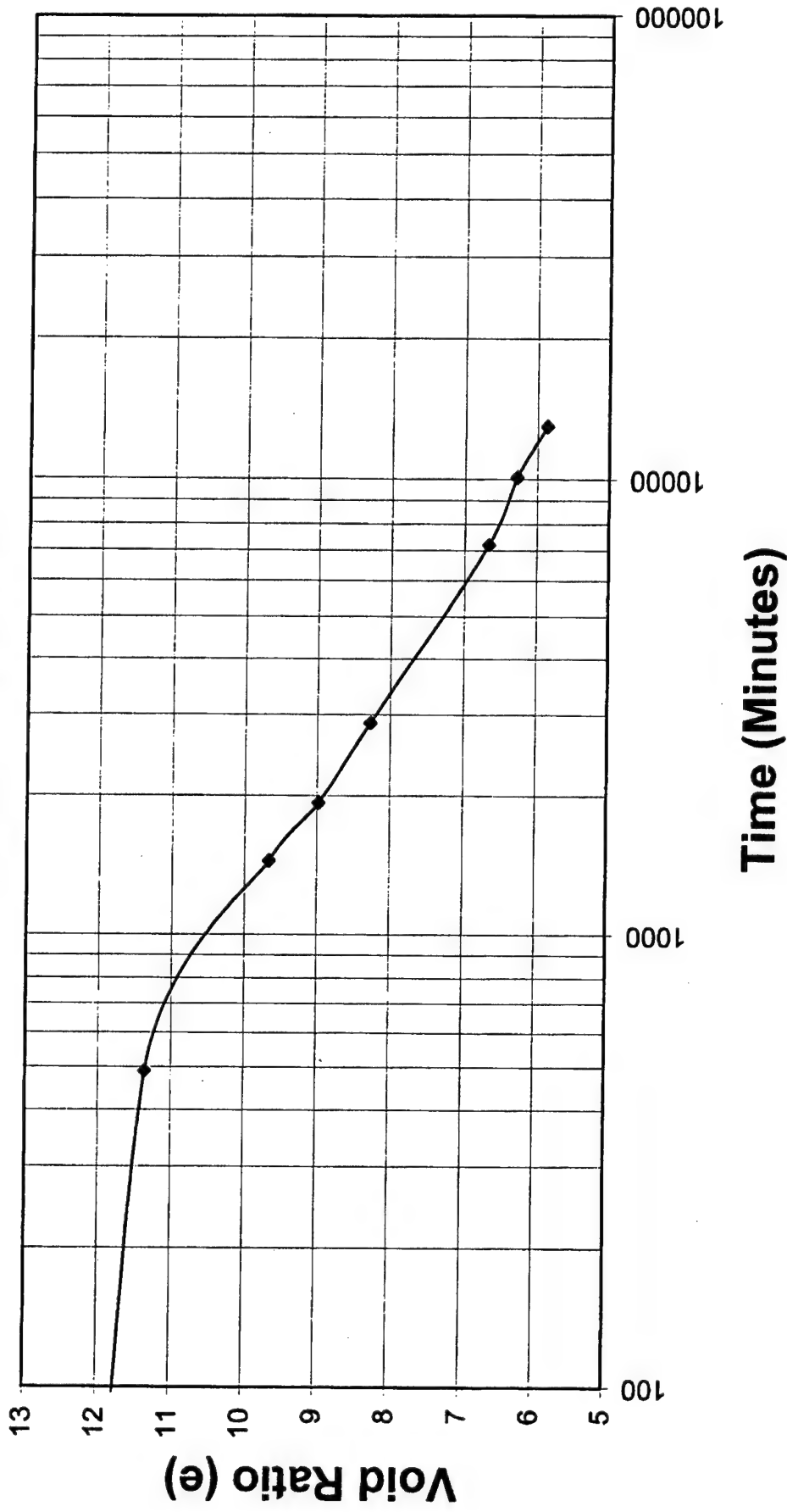
Atlanta, Georgia

Self-weight Consolidation Results
02SW1


DATE: October 2001

Project 50130-8-0025-M10 Figure: 02SW-1

Self Weight - 02-PH00



Subsurface Dredge Material Investigation
Pascagoula
US Army Corps of Engineers
Mobile District
Contract No. DACW 21-98-D-0025

LAW
LAWGIBB Group Member 
Atlanta, Georgia

Self-weight Consolidation Results
02SW2


DATE: October 2001
Project 50130-8-0025-M10 Figure: 02SW-2

**Self-weight Consolidation Results
04-PH00**

S.G. = 2.66
Initial Void Ratio = 13.00
Volume Solids (gal) = 0.053

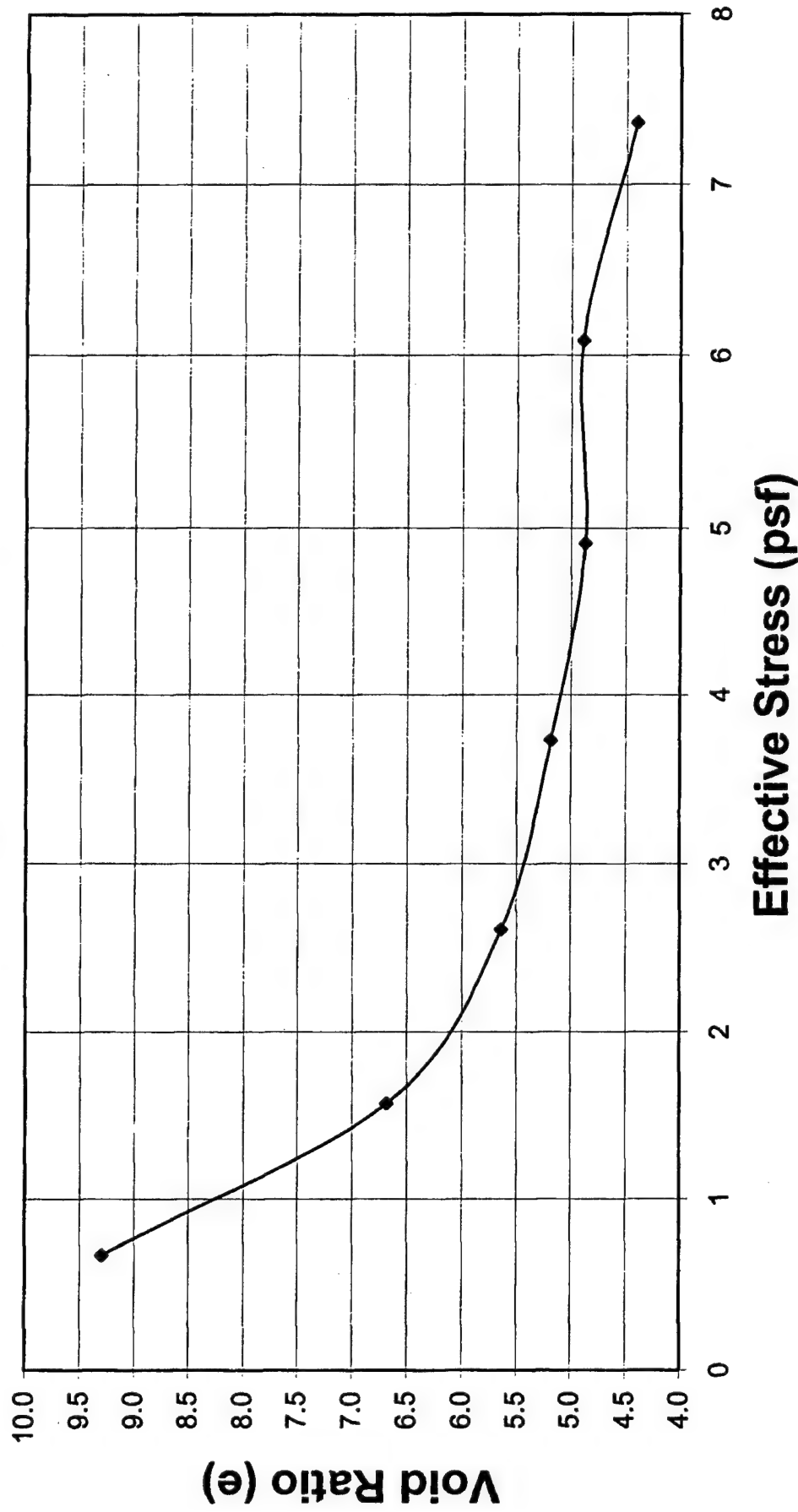
	Elapse Min.	Sludge V Gal	Void Ratio (e)
Starting	0	0.75	13.00
	1	0.75	13.00
	480	0.70	12.08
	1380	0.62	10.66
	1860	0.59	10.07
	5760	0.47	7.73
	8640	0.43	7.04
	11556	0.41	6.74
	17280	0.40	6.40
	31644	0.37	5.87

Subsurface Dredge Material Investigation
Pascagoula
US Army Corps of Engineers
Mobile District
Contract No. DACW 21-98-D-0025

LAW
LAWGIBB Group Member 
Atlanta, Georgia

Self-weight Consolidation Results
04SW
Project 50130-8-0025 M10
Date: Oct 2001 Figure 04SW

Self Weight - 04 NSP00

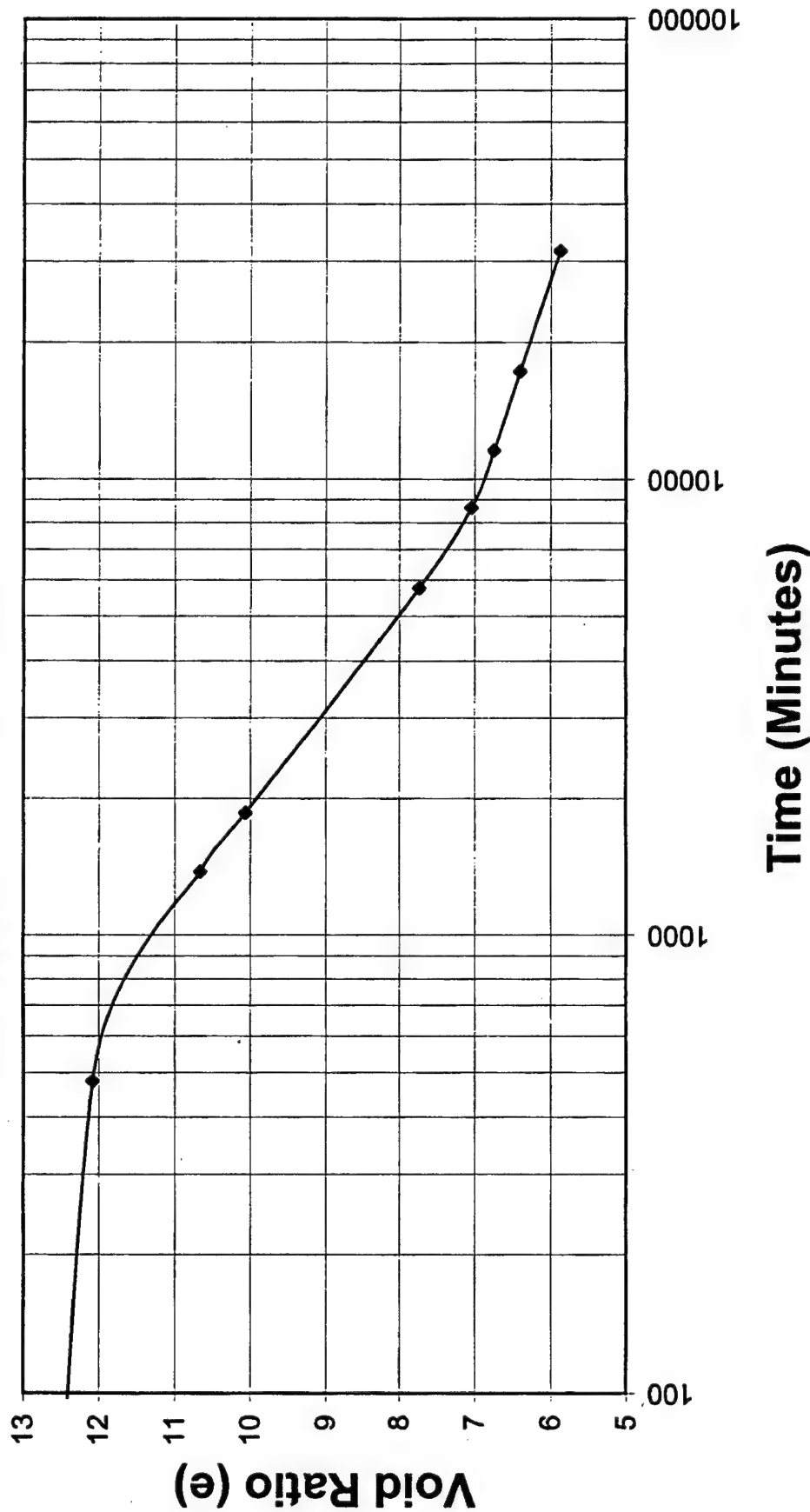


Subsurface Dredge Material Investigation
Pascagoula
US Army Corps of Engineers
Mobile District
Contract No. DACW 21-98-D-0025

LAW
LAWGIBB Group Member
Atlanta, Georgia

Self-weight Consolidation Results
04SW1
DATE: October 2001
Project 50130-8-0025-M10 Figure: 04SW-1

Self Weight - 04 NSP00



Subsurface Dredge Material Investigation
 Pascagoula
 US Army Corps of Engineers
 Mobile District
 Contract No. DACW 21-98-D-0025

LAW
 LAWGIBB Group Member
 Atlanta, Georgia


Self-weight Consolidation Results
 04SW2
 DATE: October 2001
 Project 50130-8-0025-M10 Figure: 04SW-2

**Self-weight Consolidation Results
06-PH00**

S.G. = 2.69
Initial Void Ratio = 10.00
Volume Solids (gal) = 0.065

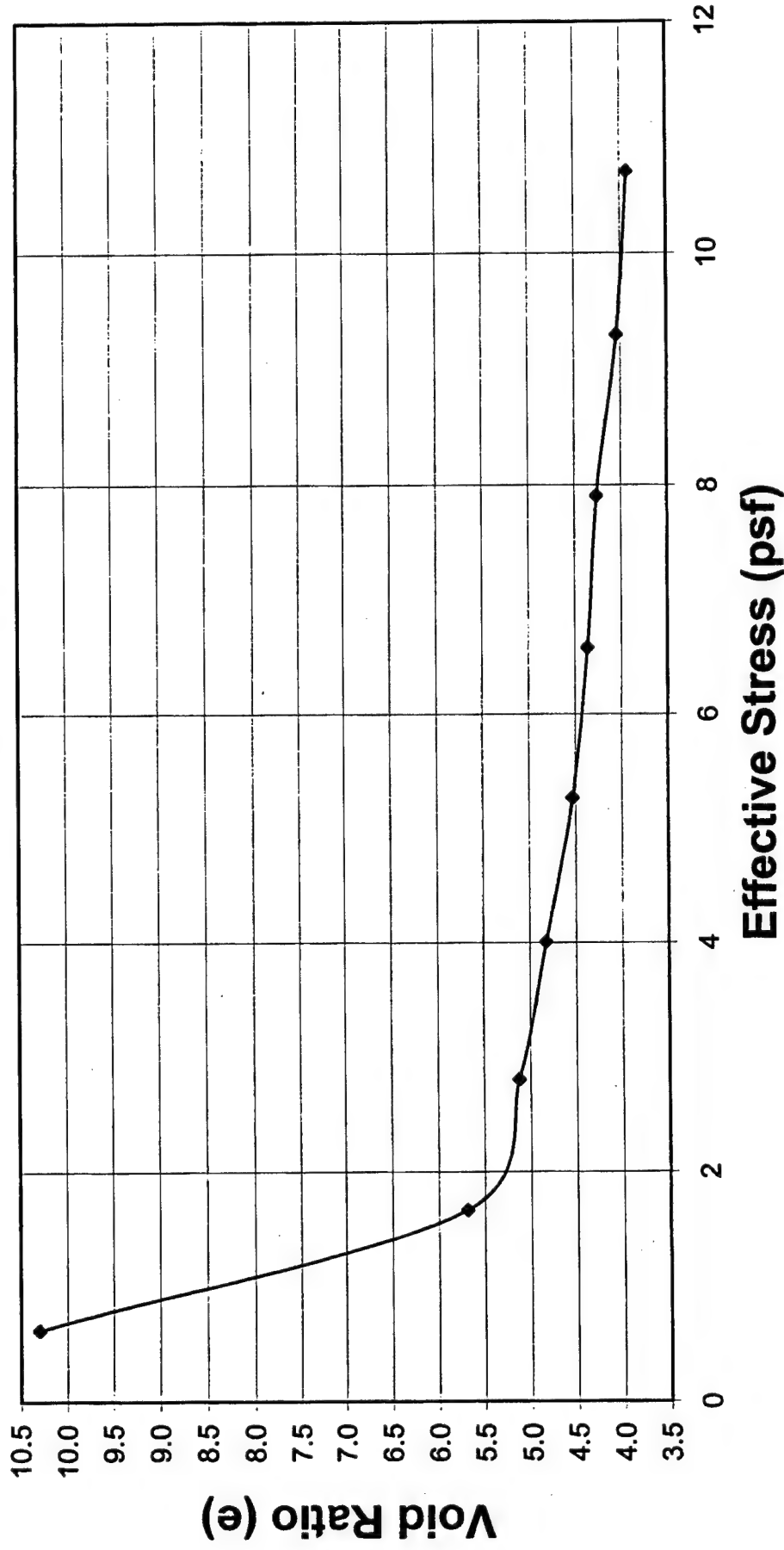
	Elapse Min.	Sludge V Gal	Void Ratio (e)
Starting	0	0.71	10.00
	1	0.71	10.00
	480	0.71	9.91
	1380	0.66	9.15
	1860	0.65	9.00
	5760	0.53	7.11
	8640	0.48	6.45
	11562	0.48	6.38
	17280	0.46	6.09
	31644	0.43	5.60

Subsurface Dredge Material Investigation
Pascagoula
US Army Corps of Engineers
Mobile District
Contract No. DACW 21-98-D-0025


LAW
LAWGIBB Group Member 
Atlanta, Georgia

Self-weight Consolidation Results
06SW
Project 50130-8-0025 M10
Date: Oct 2001 Figure 06SW

Self Weight - 06 PH00

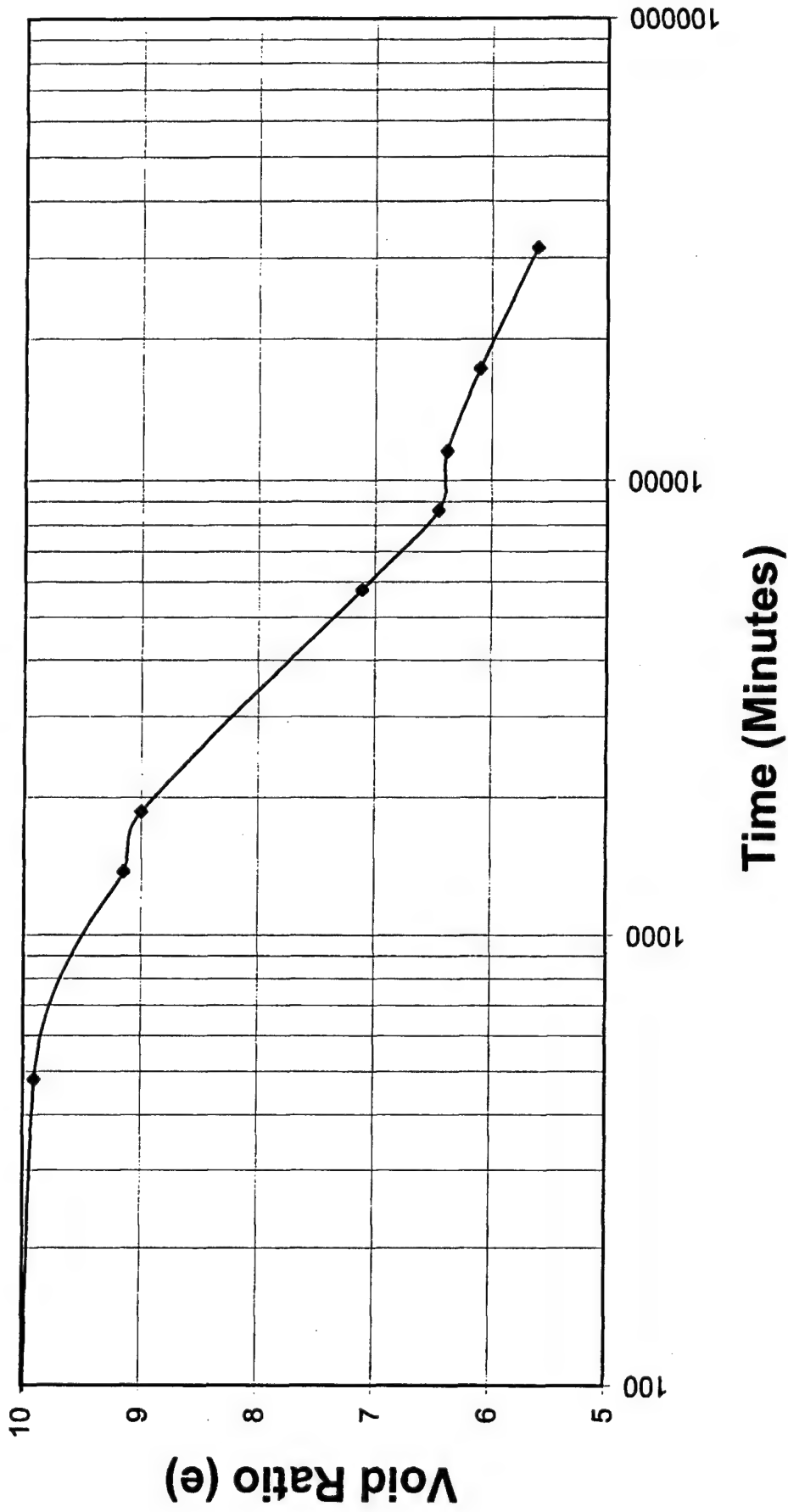


Subsurface Dredge Material Investigation
 Pascagoula
 US Army Corps of Engineers
 Mobile District
 Contract No. DACW 21-98-D-0025

LAW
 LAWGIBB Group Member 
 Atlanta, Georgia

Self-weight Consolidation Results
06SW1
 DATE: October 2001
 Project 50130-8-0025-M10 Figure: 06SW-1

Self Weight - 06 PH00



Subsurface Dredge Material Investigation
 Pascagoula
 US Army Corps of Engineers
 Mobile District
 Contract No. DACW 21-98-D-0025

LAW
 LAWGIBB Group Member
 Atlanta, Georgia

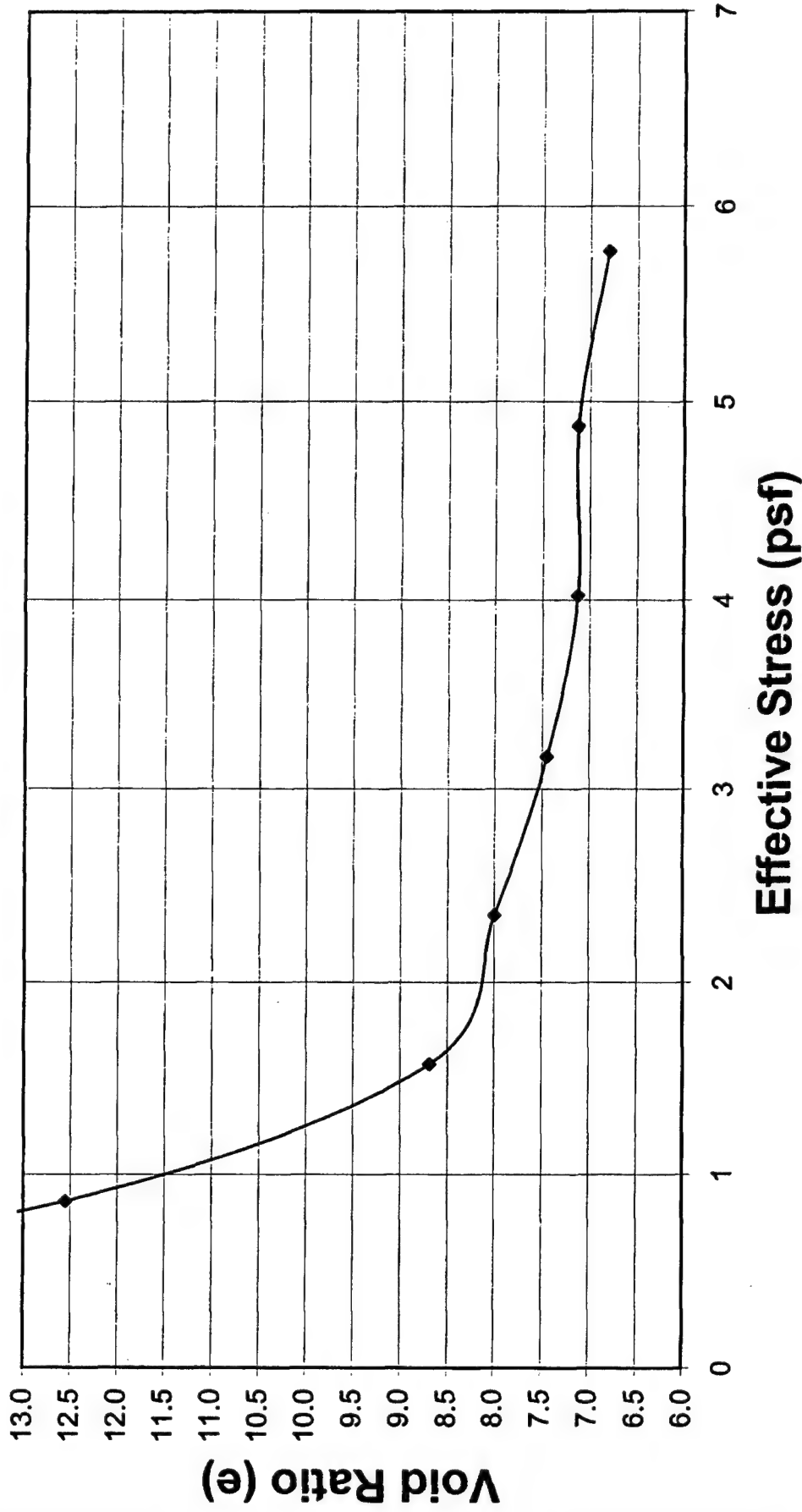
Self-weight Consolidation Results
06SW2
 DATE: October 2001
 Project 50130-8-0025-M10 Figure: 06SW-2

**Self-weight Consolidation Results
10-PH00**

S.G. = 2.67
Initial Void Ratio = 12.70
Volume Solids (gal) = 0.050

Starting	Elapse	Sludge V	Void Ratio
	Min.	Gal	(e)
	0	0.69	12.70
	1	0.69	12.70
	490	0.65	11.97
	1450	0.61	11.07
	1930	0.59	10.68
	2880	0.57	10.38
	7200	0.50	8.92
	10100	0.45	8.00
	12980	0.43	7.58
	17300	0.43	7.53

Self Weight - 10-PH00



Subsurface Dredge Material Investigation
Pascagoula

US Army Corps of Engineers
Mobile District

Contract No. DACW 21-98-D-0025

LAW

LAWGIBB Group Member

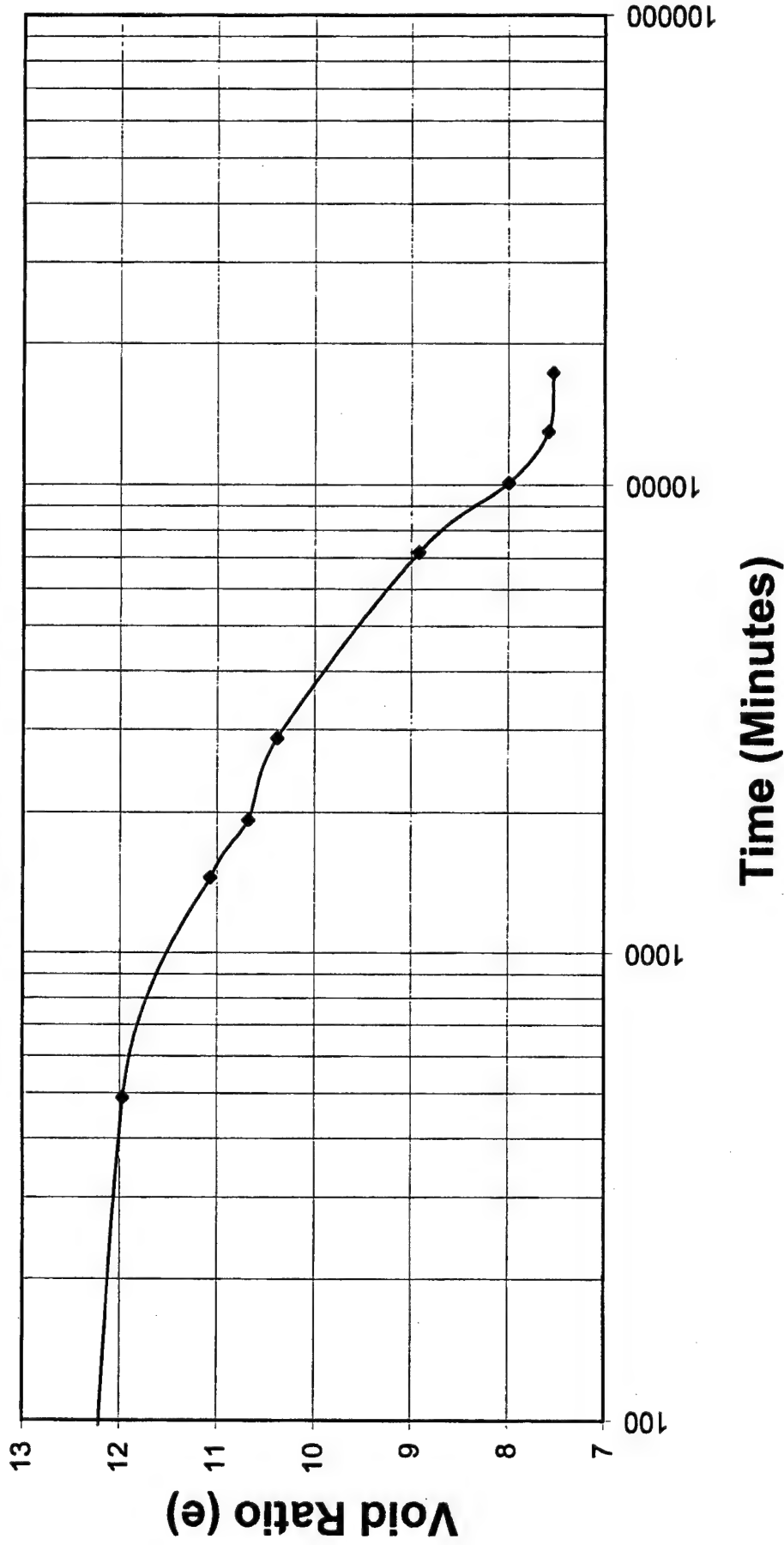
Atlanta, Georgia

Self-weight Consolidation Results
10SW1

DATE: October 2001

Project 50130-8-0025-M10 Figure: 10SW-1

Self Weight - 10-PH00



Subsurface Dredge Material Investigation

Pascagoula

US Army Corps of Engineers

Mobile District

Contract No. DACW 21-98-D-0025

LAW

LAWGIBB Group Member



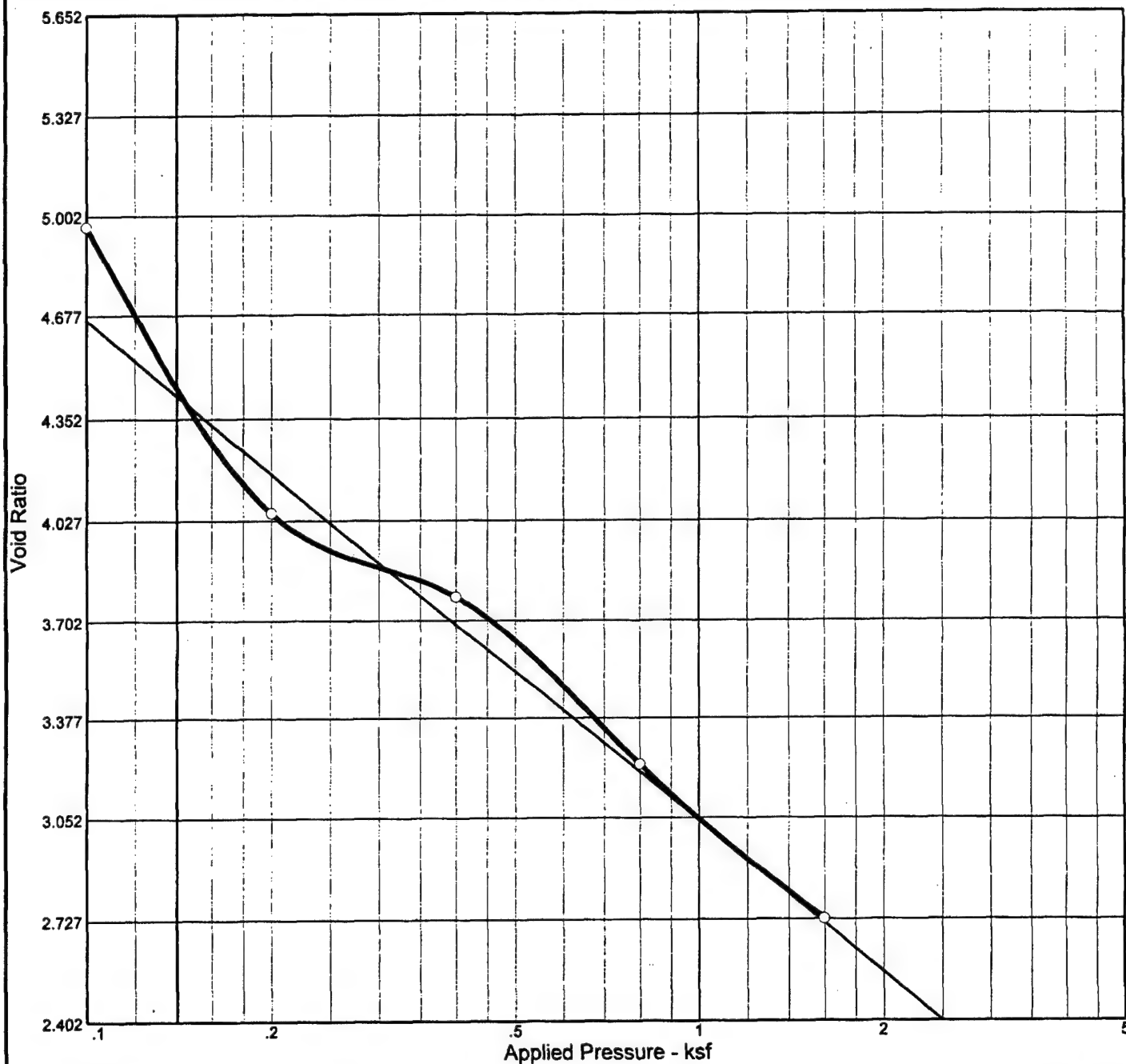
Atlanta, Georgia

Self-weight Consolidation Results
10SW2

DATE: October 2001

Project 50130-8-0025-M10 Figure: 10SW-2

CONSOLIDATION TEST REPORT ASTM D2435-96 Test Method B



Natural		Dry Dens. (pcf)	LL	PI	Sp. Gr.	Overburden (ksf)	P _c (ksf)	C _c	C _r	Initial Void Ratio
Saturation	Moisture									
106.4 %	199.5 %	27.8	77	53	2.67		0.00	1.62		5.006

MATERIAL DESCRIPTION								USCS	AASHTO
Dark Grayish Brown Fat clay with sand (Before Washing)								CH	

Project No. 5016080025.M10 Client: Corps of Engineers Mobile District

Project: Subsurface Dredge Material Investigation-Pascagoula

Source: Boring 02-PH00

Sample No.: 02-PH00

CONSOLIDATION TEST REPORT ASTM D2435-96 Test Method B

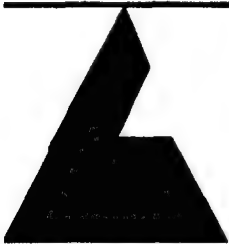
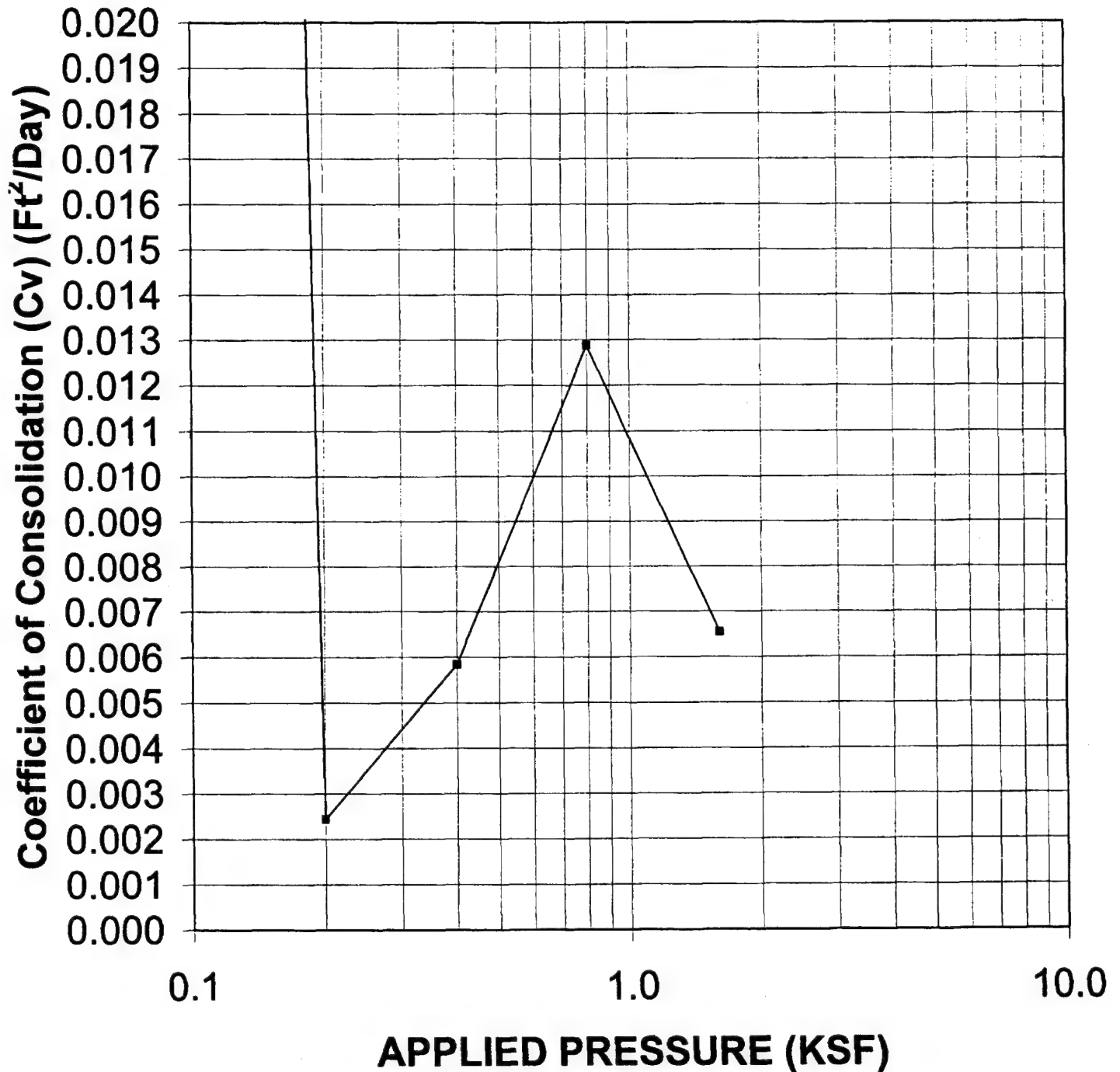
LAW ENGINEERING & ENVIRONMENTAL SERVICES, INC.

Remarks:

Tested by: JTM
Reviewed by: HJ

02-PH00

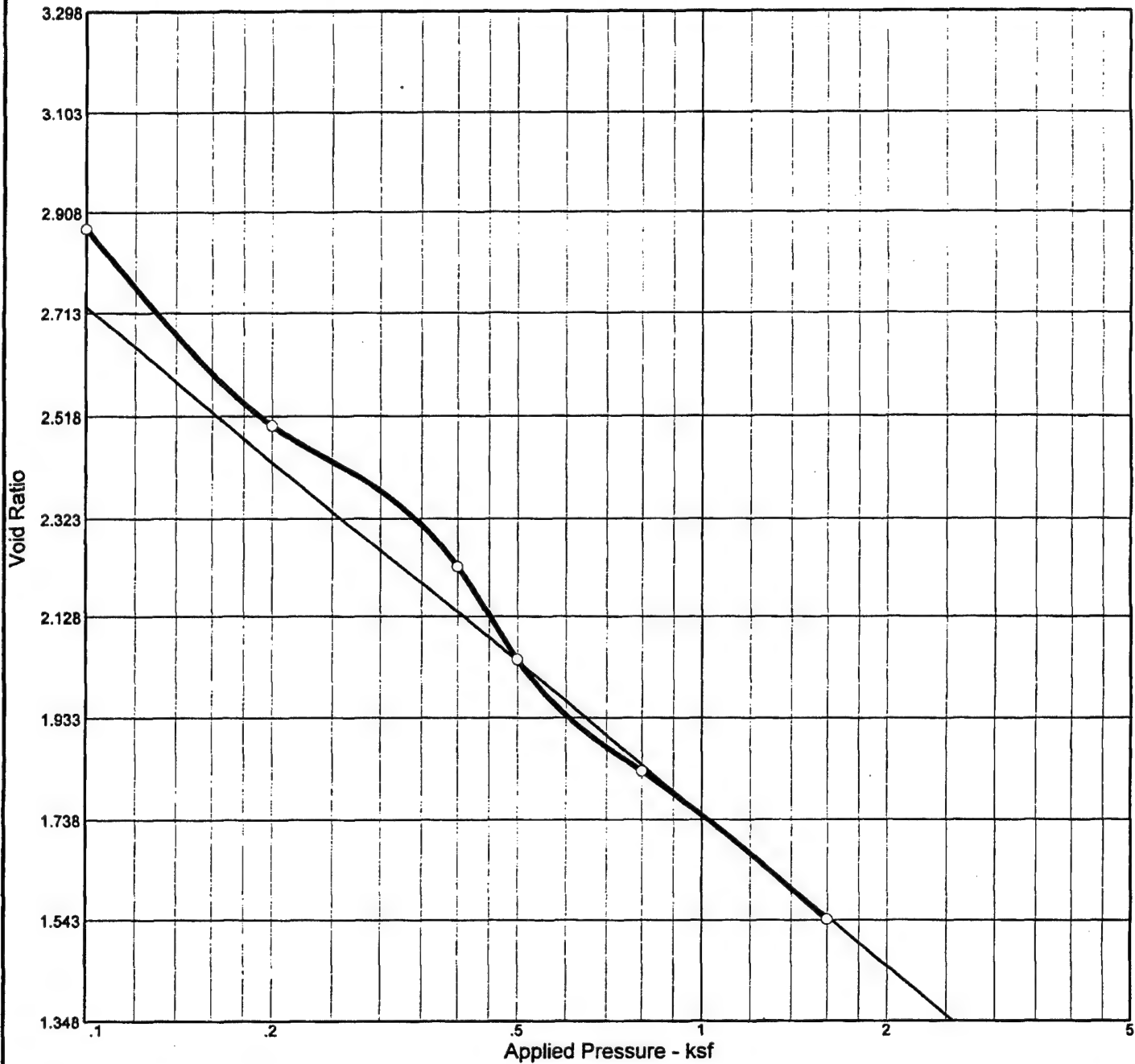
CONSOLIDATION TEST REPORT ASTM D2435-96 Test Method B



LAW
ENGINEERING AND ENVIRONMENTAL SERVICES

PROJECT: Subsurface Dredge Material
Investigation-Pascagoula
PROJ. NO: 50160-8-0025
SAMPLE: 02-PH00

CONSOLIDATION TEST REPORT ASTM D2435-96 Test Method B



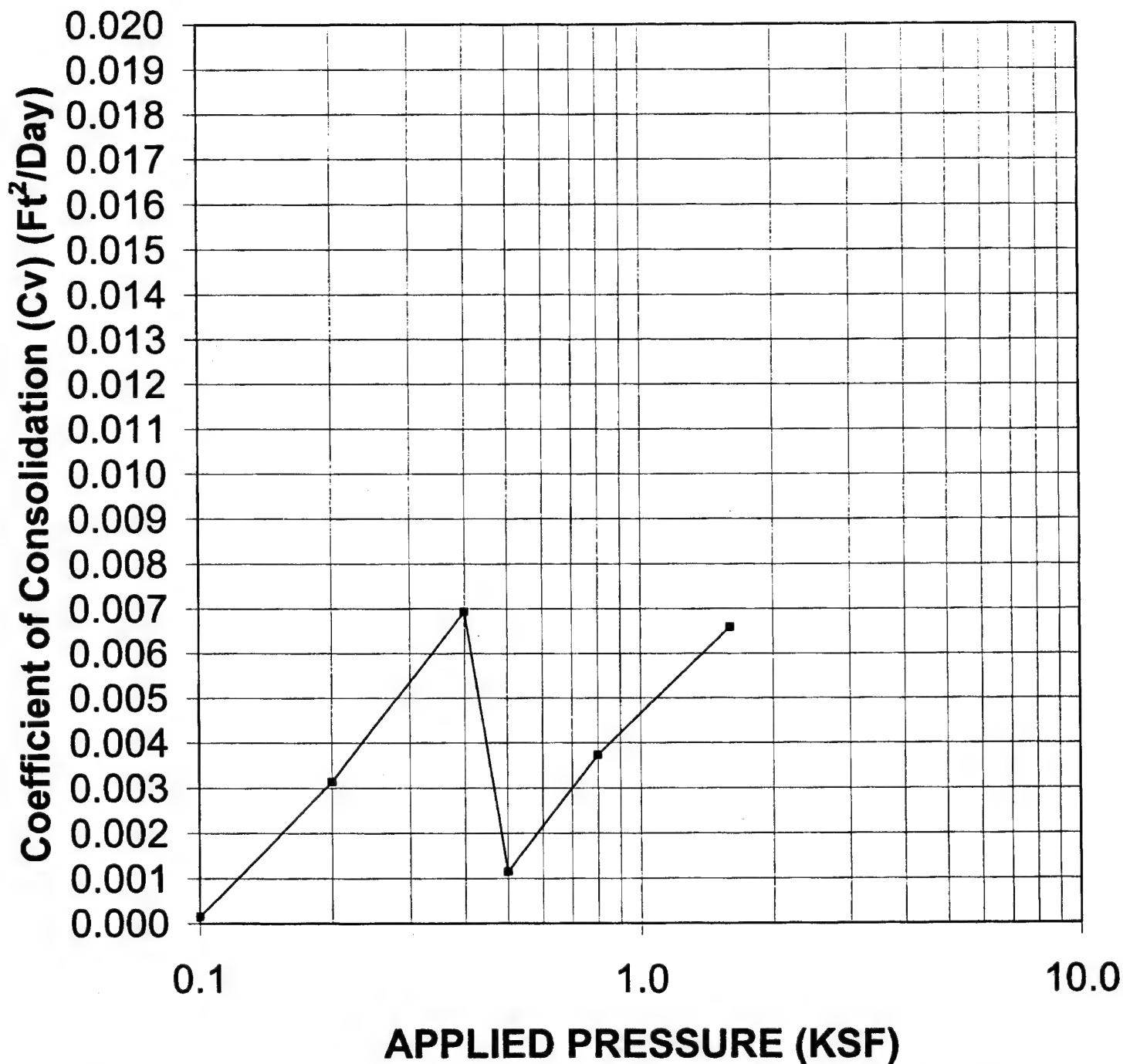
Natural		Dry Dens. (pcf)	LL	PI	Sp. Gr.	Overburden (ksf)	P_c (ksf)	C_c	C_r	Initial Void Ratio
Saturation	Moisture									
104.5 %	156.9 %	33.3	105	71	2.66		0.02	0.98		3.992

MATERIAL DESCRIPTION								USCS	AASHTO
Bluish Gray and Brown Fat clay (Before Washing)								CH	

Project No. 5016080025.M10 **Client:** Corps of Engineers Mobile District
Project: Subsurface Dredge Material Investigation-Pascagoula
Source: Boring 04-NSP00 **Sample No.:** 04-NSP00
 CONSOLIDATION TEST REPORT ASTM D2435-96 Test Method B
LAW ENGINEERING & ENVIRONMENTAL SERVICES, INC.

Remarks:
 Tested by: JTM
 Reviewed by: HJ
 04-NSP00

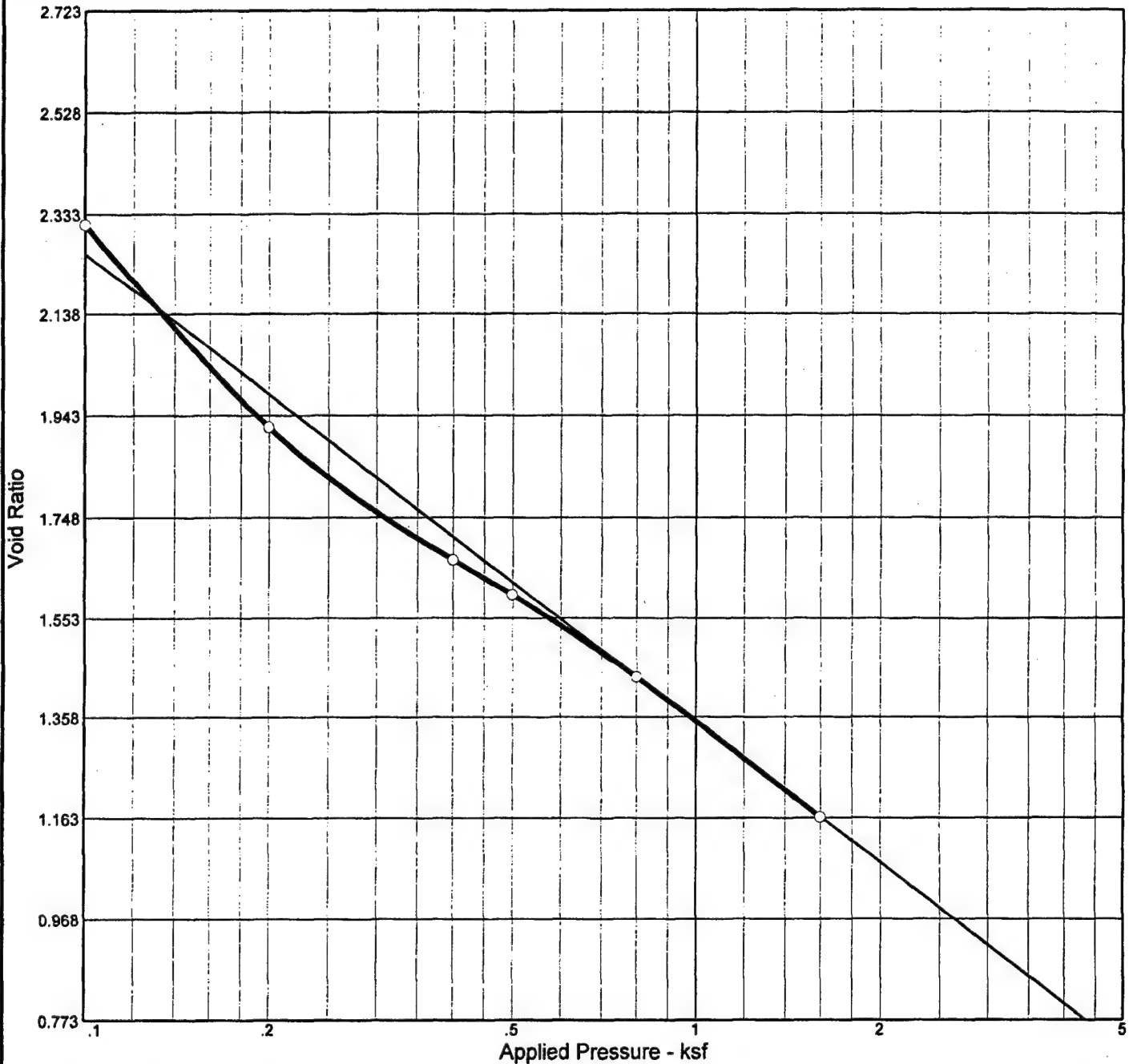
CONSOLIDATION TEST REPORT ASTM D2435-96 Test Method B



LAW
ENGINEERING AND ENVIRONMENTAL SERVICES

PROJECT: Subsurface Dredge Material
Investigation-Pascagoula
PROJ. NO: 50160-8-0025
SAMPLE: 04-NSP00

CONSOLIDATION TEST REPORT ASTM D2435-96 Test Method B



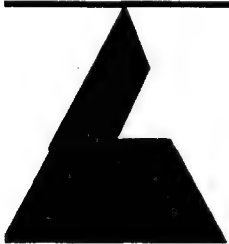
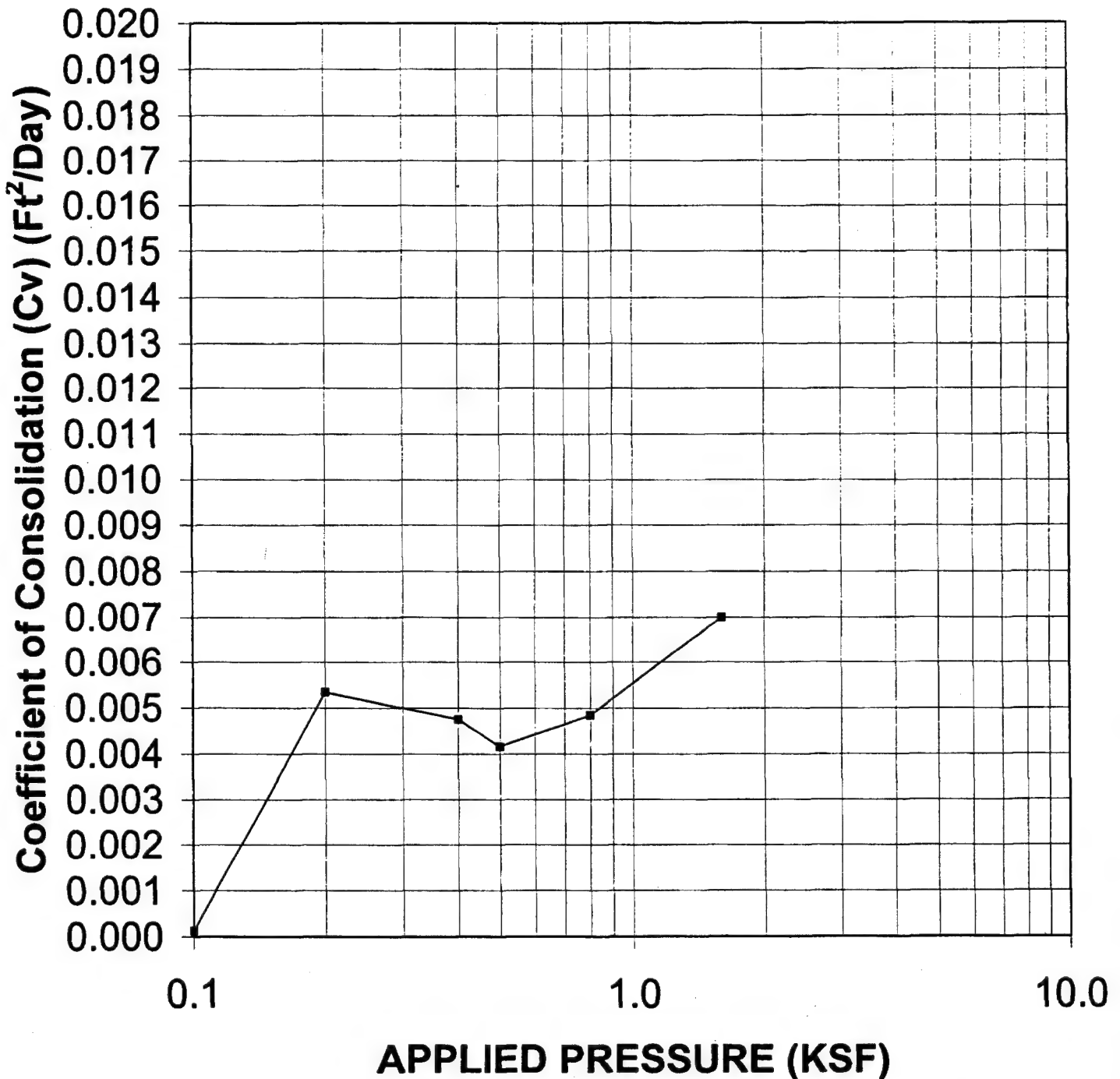
Natural		Dry Dens. (pcf)	LL	PI	Sp. Gr.	Overburden (ksf)	P _c (ksf)	C _c	C _r	Initial Void Ratio
Saturation	Moisture									
103.3 %	131.8 %	37.8	67	44	2.65		0.05	0.91		3.381

MATERIAL DESCRIPTION								USCS	AASHTO
Dark Greenish Brown Fat Clay (Before Washing)									

Project No. 5016080025.M10 **Client:** Corps of Engineers Mobile District
Project: Subsurface Dredge Material Investigation-Pascagoula
Source: Boring 06-PH00 **Sample No.:** 06-PH00
 CONSOLIDATION TEST REPORT ASTM D2435-96 Test Method B
LAW ENGINEERING & ENVIRONMENTAL SERVICES, INC.

Remarks:
 Tested by: JTM
 Reviewed by: HJ
 06-PH00

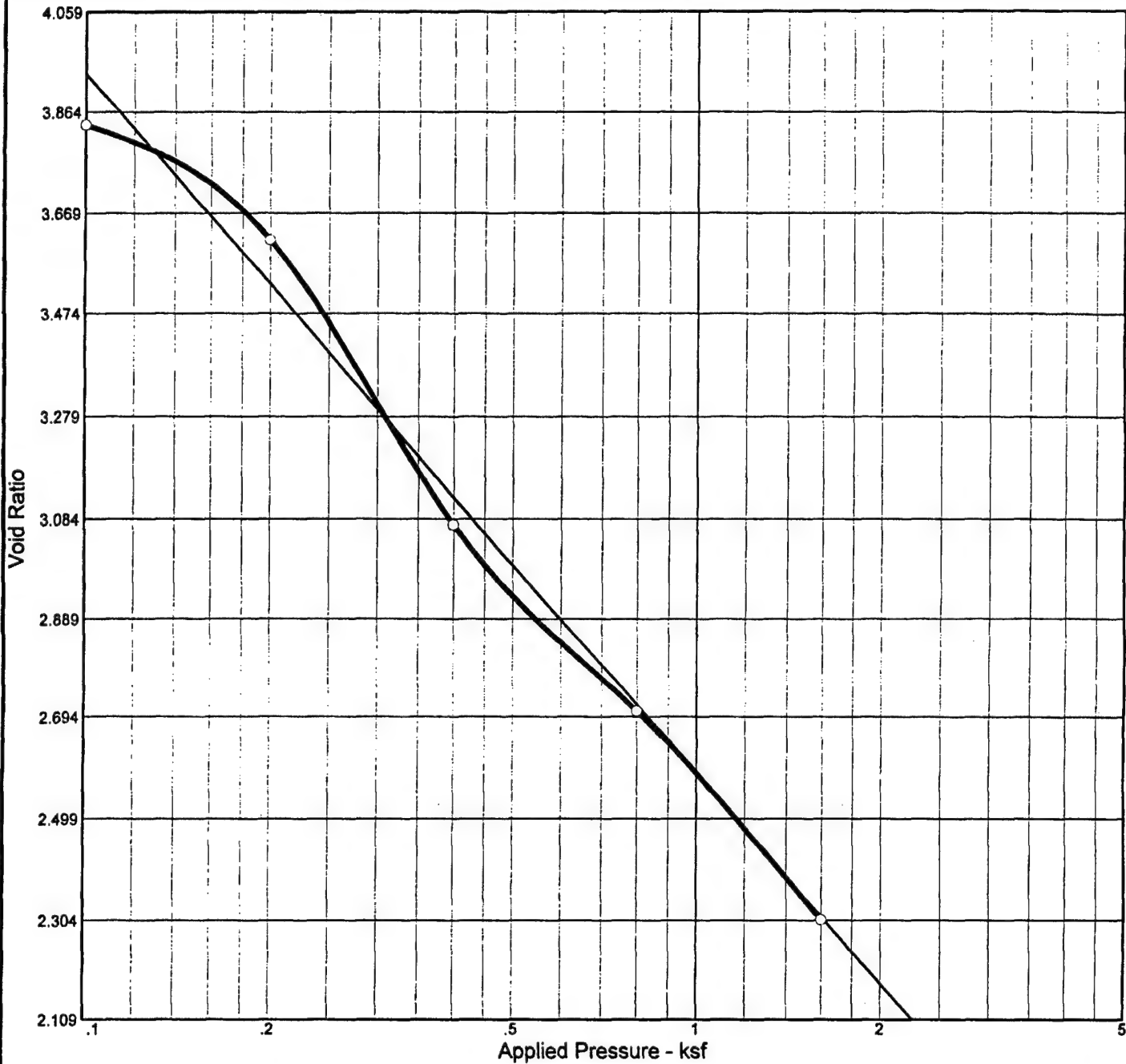
CONSOLIDATION TEST REPORT ASTM D2435-96 Test Method B



LAW
ENGINEERING AND ENVIRONMENTAL SERVICES

PROJECT: Subsurface Dredge Material
Investigation-Pascagoula
PROJ. NO: 50160-8-0025
SAMPLE: 06-PH00

CONSOLIDATION TEST REPORT ASTM D2435-96 Test Method B



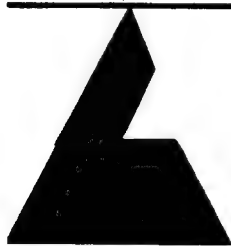
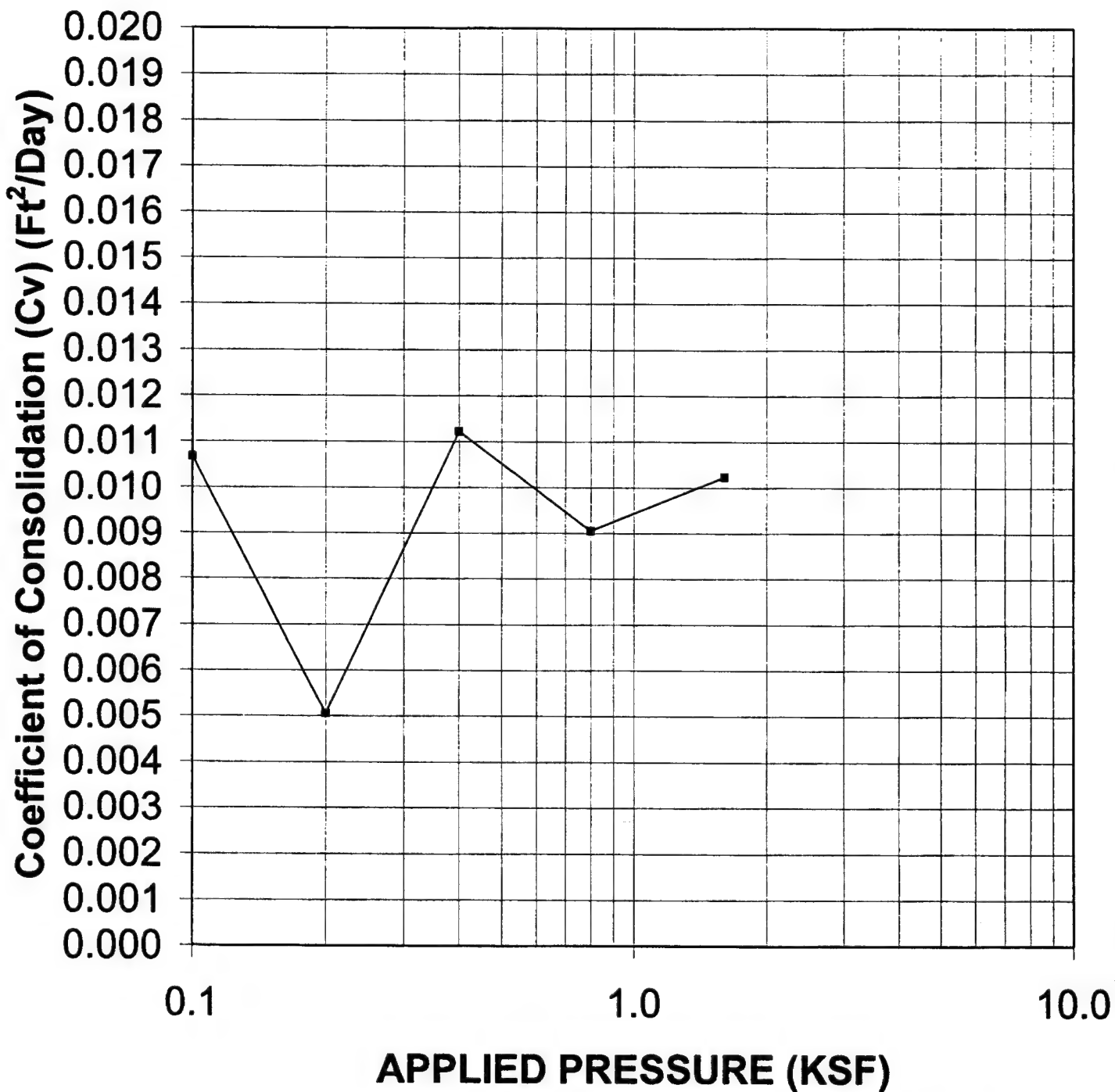
Natural		Dry Dens. (pcf)	LL	PI	Sp. Gr.	Overburden (ksf)	P _c (ksf)	C _c	C _r	Initial Void Ratio
Saturation	Moisture									
114.2 %	168.3 %	33.8	38	22	2.7		0.12	1.35		3.980

MATERIAL DESCRIPTION								USCS	AASHTO
Gray Clayey Sand (Before Washing)								SC	

Project No. 5016080025.M10 **Client:** Corps of Engineers Mobile District
Project: Subsurface Dredge Material Investigation-Pascagoula
Source: Boring 10-PH00 **Sample No.:** 10-PH00
 CONSOLIDATION TEST REPORT ASTM D2435-96 Test Method B
LAW ENGINEERING & ENVIRONMENTAL SERVICES, INC.

Remarks:
 Tested by: JTM
 Reviewed by: HJ
 10-PH00

CONSOLIDATION TEST REPORT ASTM D2435-96 Test Method B



LAW
ENGINEERING AND ENVIRONMENTAL SERVICES

PROJECT: Subsurface Dredge Material
Investigation-Pascagoula
PROJ. NO: 50160-8-0025
SAMPLE: 10-PH00

Tetrimetric Method

Accurately weigh approximate sample weight stated (if % NaCl \geq 5% weigh <5g sample rather than dilute to 100 ml, if more convenient). Use ca 0.1*N* AgNO₃ solution, accurately standardize as in 32.02B, without adjusting to specific normality, and titrate as in 32.02B.

$$\% \text{ NaCl} = \text{mL AgNO}_3 \times N \text{ AgNO}_3 \times 0.05844 \times 100/\text{g sample.}$$

If sample is overtitrated, add NaCl standard solution, and complete titration. Correct for volume of standard solution added.

LAW Engineering and Environmental Services, Inc.
Corps of Engineers EM-1110-2-5027
30 September 1987

Title: *Confined Disposal of Dredged Material - Long Tube Settling*

Material: *Dredged Material < 10% Retained on a # 200 sieve*

Scope: This test method covers the long tube-settling test of dredged material. The test method is dependent on the type of settling which is observed whether zone, flocculent or compression settling.

Result reported: Results are reported graphically and tabular format as one or more of the following:

- Void ratio change (unit less) over time (hrs)
- Solids concentration change (%) over time (hrs)
- Interface height change (cm) over time (hrs)

Test equipment: 8" diameter x 6'-8" clear tube with 13 x 1/4" extraction valves, porous stone filter at the bottom which overlays a 1/4" valve for air supply hook up. (Refer to Figures 1 & 2)

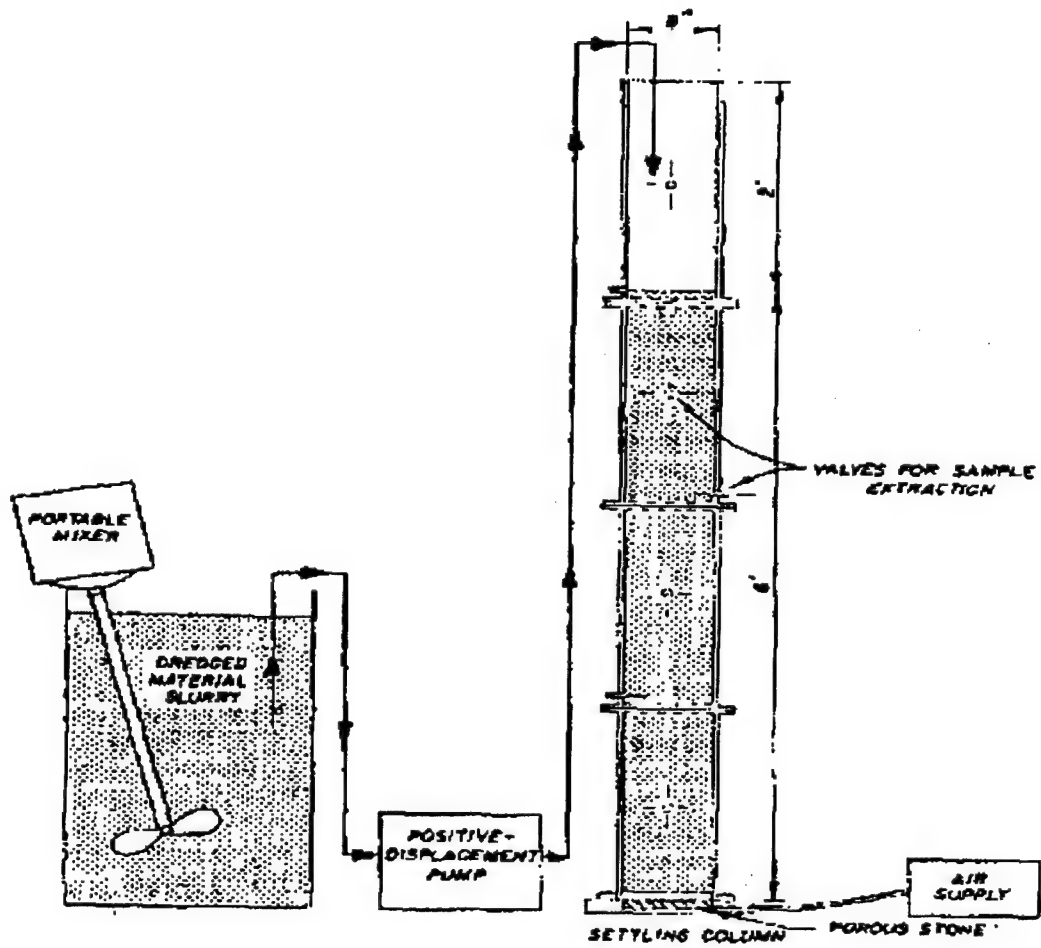
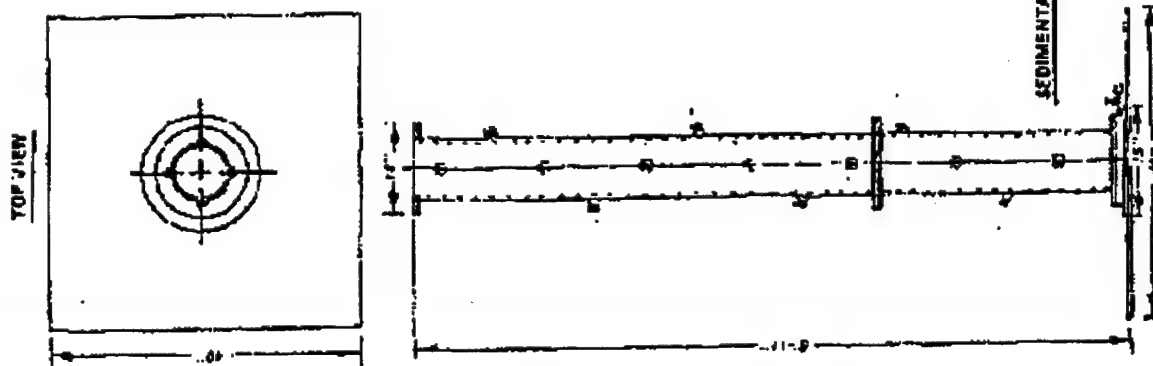


Fig. 1 schematic of apparatus for settling test



BILL OF MATERIAL		
QTY	MATERIAL	SIZE
1	AIR CHAMBER	12" I.D.
1	BALL VALVE (STAINLESS STEEL)	1/2" I.D.
1	BALL VALVE (STAINLESS STEEL)	3/4" I.D.
12	3040 LBS VALVE ASSEMBLY (STAINLESS STEEL)	3/8" I.D.
2	PIPE (STAINLESS STEEL)	1" O.D. 1/2" LONG
1	ENTERED STEEL FILTER DISK	1/4" THICK
1	3040 MICHIGAN PORT SHOWER	REPLACEMENT
1	MATERIAL FOR AT LEAST 7-12" DIAMETER C-THICK	1/2" FOR 12" LONG
1	ENTERED STEEL PLYWOOD	6" x 8" 1/2"
1	WATER TIGHT PLYWOOD PLATE FOR COLUMN BASE	16" DIAMETER
1	6" x 8" HEAD BOLT (1/2" DIA. 1/2" LONG)	1/2" x 1/2" x 1/2"
1	CAPRIQUE HEAD BOLT (1/2" DIA. 1/2" LONG)	1/2" x 1/2" x 1/2"
1	REINFORCEMENT FOR COLUMN HEADS	3" x 3" x 1/2"
2	REINFORCEMENT FOR COLUMN HEADS	1/2" THICK 12" x 12"
7	PANGLASS PLANCE FOR TOP COLUMN	1/2" THICK 14" x 14"
1	PANGLASS PLATE FOR COLUMN BODY	1/2" THICK 16" x 16"
1	PANGLASS CYLINDER	3" LONG 1/2" THICK
1	PANGLASS CYLINDER	6" LONG 1/2" THICK

	SUPPLIES
MATERIAL	COMPANY
10-10M	MOTT METALLURGICAL COMPANY, INC.
2-10M	FARMINGTON INDUSTRIAL PARK
	FARMINGTON, CT 06033
0-10M	ROBERTSON RUBBER AND SPECIALTY COMPANY
	819 SOUTH CONGRESS
	JACKSON, MS 39201
1-10M	CADILLAC PLASTIC COMPANY, ITALY, S.P.A., S.P.A.
	454 E. HOLLAND AVE
	P.O. BOX 1026
	TEMPA, FL 33603

Specifications for settling column and plan for sedimentation column

Definitions:

1. Salinity – Measure of dissolved salt content in a water sample. If salinity content >1 g/l, the water is considered to be saline, if <1 g/l, the water is considered to be fresh water. Salinity can be measured directly using a salinity conductivity meter or estimated by measuring dissolved solids.
2. Pilot Test – A "quick and dirty" settling test using a 4-liter graduated cylinder (hydrometer cylinder) and a slurry with solids concentration of approximately 150 g/l for the purpose of determining if the settling process is flocculent or zone type.
3. Flocculent Settling – Process whereby particles agglomerate during the settling period with a change in physical properties and settling rate. No discrete interface is observed. Typically, if salinity is less than 1 g/l (fresh water), initial settling is defined by flocculent settling.
4. Zone Settling – Process whereby the flocculent suspension forms a lattice structure and settles as a mass, and a distinct interface between the slurry and the supernatant water is exhibited.
5. Compression settling – Process whereby the settling occurs by compression of the lattice structure.

A. Samples:

1. 15-16 gallons of fine-grained (less than 10% $>$ No. 200 sieve) dredge material and water (representing a 6-ft. slurry column, 8" diameter)

Note: If coarse-grained material is $>10\%$ by dry wt., material should be wet washed and separated over a #200 sieve to remove coarse-grained material
2. Composite of several sediment samples can be used to be more representative of the dredged materials. Composite samples should be thoroughly mixed.
3. Additional water to mix the slurry should come from the dredge site.

B. Pilot Test:

1. Use a 4 liter graduated cylinder (Hydrometer cylinder).
2. Use the specified mix ratio. If not specified, use 150 g/l solids concentration
3. Place the required slurry wt. (W_{sw}) into the graduated cylinder.
4. Add site water into the cylinder, if necessary, in order to achieve a total volume of 4 liters.

5. Mix as per the standard hydrometer test, ASTM D422.
6. Let cylinder stay uncovered while making hourly observations and/or measurements as described below.
7. If an interface forms within a few hours, the slurry mass is exhibiting zone settling. If so:
 - a. Record the fall of the interface at 1 hr., 2 hrs, 4 hrs, 6 hrs, 12 hrs, 24 hrs, 48 hrs, etc.

Plot the data as shown in Figure 3.

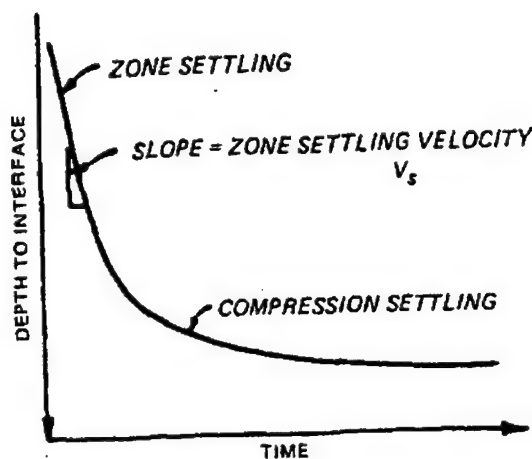


Fig. 3 Conceptual plot of interface height versus time

- b. The break in the curve will define the concentration at which compression settling occurs.
 - c. Use only lower concentrations for the zone-settling test in the large scale long tube test.
 - d. If no break is evident, the material is undergoing compression settling. Repeat pilot study at a lower slurry concentration.
8. If no interface is observed in the pilot test, flocculent settling is occurring. Then:
 - a. Continue test until an interface is observed between the turbid water above and solids below.

C. If Pilot Study Indicates Flocculent Settling:

1. Mix the appropriate wt. of as received slurry and water as specified.
2. Mix the slurry/water mixture with a mechanical mixer until all solids are in suspension.
3. Pump the mixture into the long tube to the 6' high elevation.
4. Connect the bottom valve to an air compressor in order to mix and agitate the solution in the tube.
5. When completely mixed, stop agitation. Immediately collect 50-ml specimens from all ports.
6. Determine moisture content of all specimens in accordance with ASTM D2216.
7. Determine initial solids contraction and void ratios of each as follows:

$$C_{ss} = \frac{W_{ss} * 1000}{\frac{W_{ss}}{G_s} + W_w}$$

Where:

C_{ss} = In-situ Suspended Solids concentration (g/l)

W_{ss} = Wt. of Suspended solids (g)

$$= W_{SD} - \left(W_w * \frac{sal.}{100} \right)$$

W_{SD} = Dry wt. of solids (g)

Sal. = Salinity concentration (g/l)

W_w = Wt. of water = wet wt. slurry - dry wt. of solids

G_s = specific gravity

$$e = \frac{(MC)G_s}{100}$$

Where:

e = In-situ void ratio

MC = moisture content (%)

G_s = specific gravity

8. Determine average initial solids concentration (C_i) and void ratio (e_i).
9. Withdraw additional 50 ml specimens from each port at 1 hr, 2 hrs, 4 hrs, 6 hr, 12 hrs, 24 hrs, 48 hrs, 96 hrs, etc until the end of the test, defined as the point when an interface can be seen near the bottom of the column and the solids concentration of the fluid is <1 g/l.

10. Take moisture content of each specimen (in accordance with ASTM D2216) and calculate void ratios and suspended solids, as described in Paragraph 7 above.
11. Tabulate results and as indicated in Figure 4 and Figure 5.

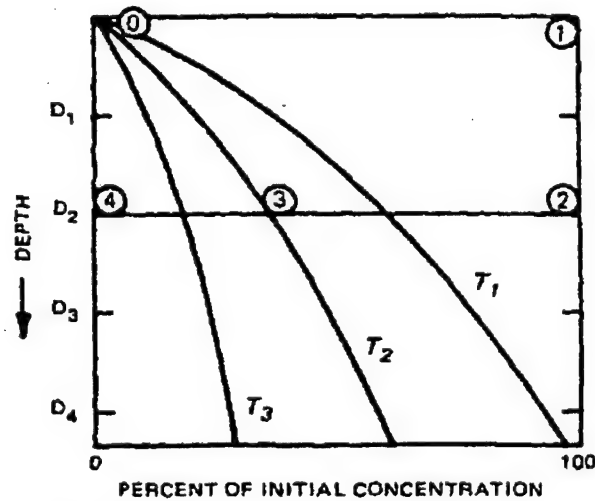


Fig. 4 Conceptual Concentration Profile Diagram

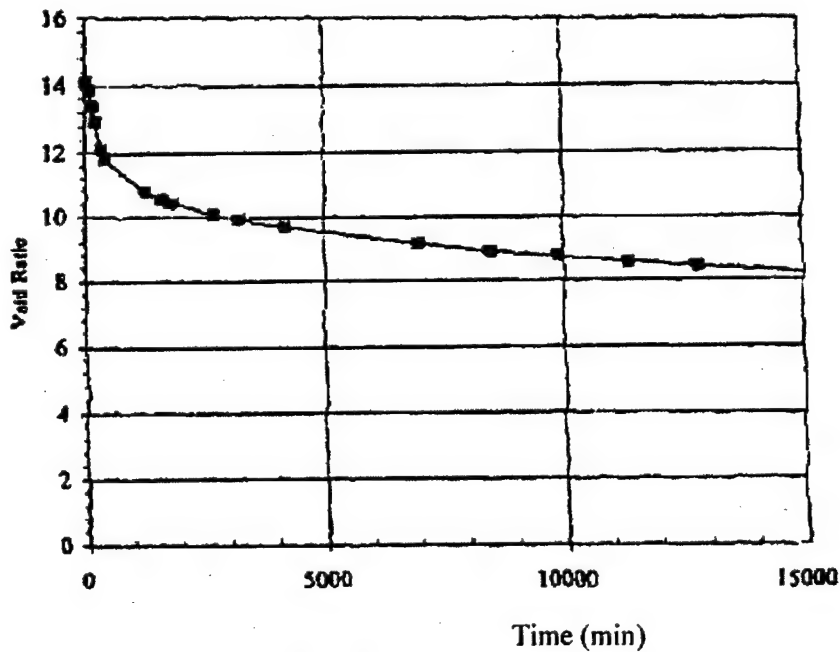


Fig. 5 Void Ratio vs. Time

12. If an interface has formed on the first day, zone settling is occurring in the slurry below the interface, and flocculent settling above. Then:

- a. Collect first sample immediately after interface has fallen below the uppermost port (usually within a few hours).
- b. Record the time of sample extraction.
- c. Collect 50-ml specimens from all ports that are above the interface at 1, 2, 4, 6, 12, 24, 48, and 96 hour intervals.
- d. Perform moisture content test of each specimen per ASTM D2216.
- e. Calculate suspended solids concentration and void ratios per Paragraph 7 above.
- f. Continue collecting specimens until the suspended solids concentration shows no increase and <1 g/l.
- g. Plot the data as shown in Figure 2 and Figure 3.

D. If Pilot Study Indicates Zone Settling:

1. Mix the appropriate wt. of as received slurry.
2. Follow the procedures described in Paragraph D-1 through 8.
3. Record the interface depth vs. time at 1, 2, 4, 6, 12, 24, 48, 96, etc hour intervals or as required to clearly define this curve.

Note: If compression settling data is desired, continue taking readings for 15 days.

4. Plot the results as shown in Figure 3.
5. Continue the readings until sufficient data are available to define the maximum point of curvature.
6. Calculate the settling velocity as the slope of the straight-line portion of the curve, from Figure 3. Report the result in cm/hr.
7. Calculate the concentrations for various interface heights, H_t for the 15-day period as follows:

$$C = \frac{C_o H_i}{H_t}$$

Where:

C = Solids concentration at time t (g/l)
 C_o = Initial solids concentration at time t .
 H_i = Initial interface height at time t
 H_t = Interface height at time t .

Note: Neglect solids in the water above the interface to simplify the calculations.

8. Plot concentrations vs. time on log-log paper as shown in figure 6.

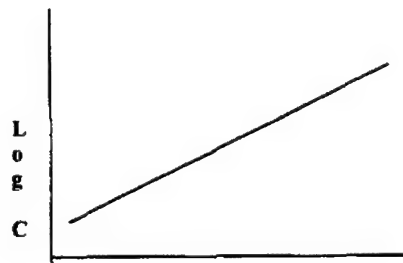


Fig. 6 Concentration vs Time

LAW Engineering and Environmental Services, Inc.
Corps of Engineers GL-86-13
July 1986

Title: *Confined Disposal of Dredged Material – Self Weight Consolidation Test*

Material: *Dredged Material < 10% Retained on a # 200 sieve*

Scope: This test method covers the self weight consolidation test of dredged material.

Result reported: Results are reported graphically and tabular format as one or more of the following:

- Void ratio change (unit less) over time (hrs)
- Solids concentration change (%) over time (hrs)
- Interface height change (cm) over time (hrs)

And as:

- Void ratio change with respect to effective vertical stress
- Void ratio change with respect to depth within the sample

Test equipment: 7" inside diameter x 12" clear tube with 16 6 ¼" diameter by ½" by ½" wall thickness rings, piston at the bottom. (Refer to Figures 1 & 2)

Samples:

1. 1-2 gallons of fine-grained (less than 10% > No. 200 sieve) dredge material and water.

Note: If coarse-grained material is >10% by dry wt., material should be wet washed and separated over a #200 sieve to remove coarse-grained material. Wash water should be sampled along with the sediment from the same location (ideally) or a mix of tap water and salt of similar salinity to the sampled water.

2. Composite of several sediment samples can be used to be more representative of the dredged materials. Composite samples should be thoroughly mixed.

3. Additional water to wash the sediment and mix the sediment to achieve the desired moisture contents should come from the dredge site.

Procedures:

1. Assemble the apparatus by pushing the piston to the bottom of the 7" tube and constructing a uniform stack of the 6 1/4" rings thoroughly greased so as to be water tight (grease between and around rings) placed within the 7" tube. There will be a 1/8" annulus.
2. Fill the annulus with clear water from the site sample to maintain pressures and reduce the potential of leaks from the central ring.
3. Mix sediment with water sample to achieve the specified initial void ratio. The initial void ratio is typically within the range of 8 to 12. Mix should be uniform.
4. Place the sediment sample within the ring stack. Completely fill stack level with uppermost ring top.
5. Sediment should form an interface of clear water over the top of the sediment. Measure the depth of this interface below the top of the ring stack at intervals. Suggested intervals are 1/4, 1/2, 1, 2, 4, 6, 8, 24, 32, 48, 72, 96, etc. hours, but these may need to be modified depending on the speed of the interface fall.
6. Calculate the void ratio of the sediment below the interface and plot with respect to the log of elapsed time. The inflection point of the resulting curve should indicate the completion of primary consolidation.
7. Shortly after primary consolidation is complete, remove the sample one ring at a time by moving piston up in 1/2 inch increments and slicing the sample between rings using a piece of sheet metal. The uppermost rings may contain only water. Prior to removing each ring, collect a sample for a moisture content determination. Use care to avoid disturbing the contents of underlying rings during collect.
8. Report column height with time and moisture content of each ring.

LAW

LAWGIBB Group Member 

FACSIMILE TRANSMITTAL SHEET

LAW ENGINEERING & ENVIRONMENTAL SERVICES, INC.

396 Plasters Ave.

Atlanta, Georgia 30324

(404) 873-4761 Fax (404) 881-6635

To: MR. TIM WOLF From: PIET OFFICE *Piete Dupree*
Company: WES COE Date transmitted: 1-9-01
Fax Number: 601 634 3151 Telephone 404-817-0264 *817-0264*
Subject: PASCAGOULA Fax Number 404-881-6635
No. Pages Transmitted (incl. cover) 13 Hard Copy to Follow: Yes ☐ No ☒
CC: CHING WU

Urgent ☐ For Review ☐ Please Comment ☐ Please Reply ☐

COMMENTS: HERE IS RAW GEOMETRIC DATA, PER YOUR

REQUEST.

THANKS,

PIET

CONFIDENTIALITY NOTICE: This message is intended only for the use of the individual or entity to which it is addressed, and may contain information that is privileged, confidential, and exempt from disclosure under applicable law. If the reader of this message is not the intended recipient, or the employee or agent responsible for delivering the message to the intended recipient, you are hereby notified that any dissemination, distribution, or copying of this communication is strictly prohibited. If you have received this communication in error, please notify us immediately by telephone and return the original message to us at the above address via the U.S. Postal Service. Thank you.

If transmission is not received in good order, please call _____

CONSOLIDATION TEST DATA

Client: Corps of Engineers Mobile District
Project: Subsurface Dredge Material Investigation-Pascagoula
Project Number: 5016080025.M10

Sample Data

Source: Boring 04-NSP00
Sample No.: 04-NSP00
Elev. or Depth: Sample Length (in./cm.):
Location:
Description: Gray Fat Clay with Sand (Before Washing)
Liquid Limit: 105 Plasticity Index: 71
USCS: CH AASHTO: Figure No.:
Testing Remarks: Tested by: JTM
Reviewed by: HJ

Test Specimen Data

TOTAL SAMPLE	BEFORE TEST	AFTER TEST
Wet w+t = 2100.20 g.	Consolidometer # = 5	Wet w+t = 2065.00 g.
Dry w+t = 2032.96 g.		Dry w+t = 2032.96 g.
Tare Wt. = 1990.10 g.	Spec. Gravity = 2.66	Tare Wt. = 1990.10 g.
Height = 1.00 in.	Height = 1.00 in.	
Diameter = 2.50 in.	Diameter = 2.50 in.	
Weight = 110.10 g.	Defl. Table = n/a	
Moisture = 156.9 %	Ht. Solids = 0.2003 in.	Moisture = 74.8 %
Wet Den. = 85.4 pcf	Dry Wt. = 42.86 g.	Dry Wt. = 42.86 g.*
Dry Den. = 33.3 pcf	Void Ratio = 3.992	Void Ratio = 1.544
	Saturation = 104.5 %	

* Final dry weight used in calculations

End-of-Load Summary

Pressure (ksf)	Final Dial (in.)	Machine Defl. (in.)	C_v (ft. ² /day)	C_α	Void Ratio	% Compression /Swell
start	0.01250				3.992	
0.10	0.19850	0.00000	0.00		2.876*	22.4 Compr.*
0.20	0.31670	0.00000	0.00		2.500*	29.9 Compr.*
0.40	0.37840	0.00000	0.01		2.226*	35.4 Compr.*
0.50	0.40620	0.00000	0.00		2.045*	39.0 Compr.*
0.80	0.44970	0.00000	0.00		1.832*	43.3 Compr.*
1.60	0.50820	0.00000	0.01		1.544*	49.1 Compr.*

*CALCULATED USING D_{100} INSTEAD OF FINAL READING

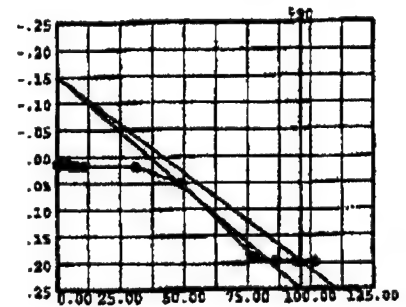
$C_c = 0.98$ $P_c = 0.50$ ksf

Pressure: 0.10 ksf

TEST READINGS

Load No. 1

No.	Elapsed Time	Dial Reading	No.	Elapsed Time	Dial Reading
1	0.00	0.01250	11	60.00	0.01860
2	0.10	0.01260	12	120.00	0.01890
3	0.25	0.01265	13	970.00	0.01990
4	0.50	0.01270	14	2410.00	0.04970
5	1.00	0.01275	15	6020.00	0.19050
6	2.00	0.01280	16	7460.00	0.19580
7	4.00	0.01285	17	8900.00	0.19710
8	8.00	0.01340	18	10340.00	0.19850
9	15.00	0.01420			
10	30.00	0.01620			



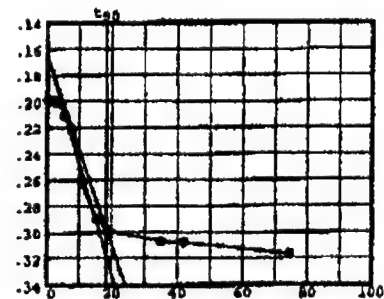
Void Ratio = 2.876 Compression = 22.4 % >>> CALCULATED USING D_{100}
 $D_0 = -0.15088$ $D_{90} = 0.19742$ $D_{100} = 0.23612$
 C_v at 9222.1 min. = 0.00 ft.²/day

Pressure: 0.20 ksf

TEST READINGS

Load No. 2

No.	Elapsed Time	Dial Reading	No.	Elapsed Time	Dial Reading
1	0.00	0.19850	11	60.00	0.22160
2	0.10	0.19870	12	120.00	0.26220
3	0.25	0.19890	13	240.00	0.28990
4	0.50	0.19900	14	360.00	0.29830
5	1.00	0.19920	15	1220.00	0.30700
6	2.00	0.19940	16	1770.00	0.30800
7	4.00	0.19960	17	5540.00	0.31670
8	8.00	0.20000			
9	15.00	0.20060			
10	30.00	0.21090			



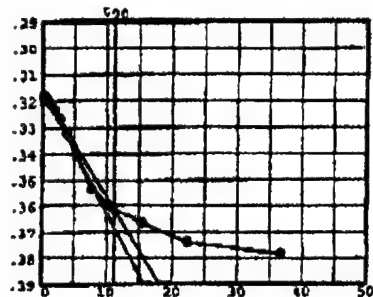
Void Ratio = 2.500 Compression = 29.9 % >>> CALCULATED USING D_{100}
 $D_0 = 0.16328$ $D_{90} = 0.29658$ $D_{100} = 0.31139$
 C_v at 333.3 min. = 0.00 ft.²/day

Pressure: 0.40 ksf

TEST READINGS

Load No. 3

No.	Elapsed Time	Dial Reading	No.	Elapsed Time	Dial Reading
1	0.00	0.31670	11	60.00	0.35360
2	0.10	0.31810	12	120.00	0.36090
3	0.25	0.31860	13	240.00	0.36660
4	0.50	0.31910	14	500.00	0.37390
5	1.00	0.32000	15	1340.00	0.37840
6	2.00	0.32120			
7	4.00	0.32320			
8	8.00	0.32650			
9	15.00	0.33210			
10	30.00	0.34080			



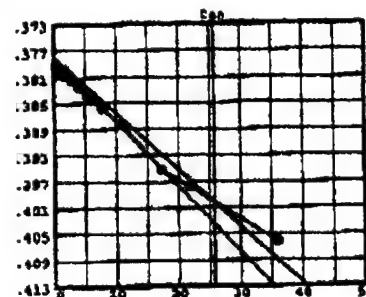
Void Ratio = 2.226 Compression = 35.4 % >>> CALCULATED USING D_{100}
 $D_0 = 0.31504$ $D_{90} = 0.36117$ $D_{100} = 0.36630$
 C_v at 124.8 min. = 0.01 ft.²/day

Pressure: 0.50 ksf

TEST READINGS

Load No. 4

No.	Elapsed Time	Dial Reading	No.	Elapsed Time	Dial Reading
1	0.00	0.37840	11	60.00	0.38580
2	0.10	0.37910	12	120.00	0.38830
3	0.25	0.37970	13	300.00	0.39520
4	0.50	0.37980	14	470.00	0.39770
5	1.00	0.38000	15	1300.00	0.40620
6	2.00	0.38030			
7	4.00	0.38080			
8	8.00	0.38140			
9	15.00	0.38240			
10	30.00	0.38390			



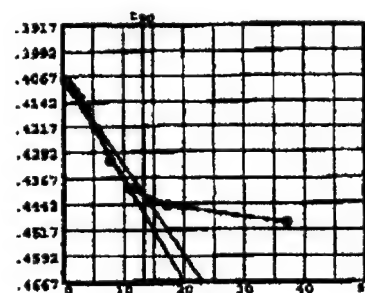
Void Ratio = 2.045 Compression = 39.0 % >>> CALCULATED USING D_{100}
 $D_0 = 0.37781$ $D_{90} = 0.40010$ $D_{100} = 0.40257$
 C_v at 662.2 min. = 0.00 ft.²/day

Pressure: 0.80 ksf

TEST READINGS

Load No. 5

No.	Elapsed Time	Dial Reading	No.	Elapsed Time	Dial Reading
1	0.00	0.40620	11	60.00	0.43150
2	0.10	0.40760	12	125.00	0.43970
3	0.25	0.40800	13	300.00	0.44480
4	0.50	0.40840	14	1380.00	0.44970
5	1.00	0.40900			
6	2.00	0.40990			
7	4.00	0.41110			
8	8.00	0.41300			
9	15.00	0.41600			
10	30.00	0.42230			



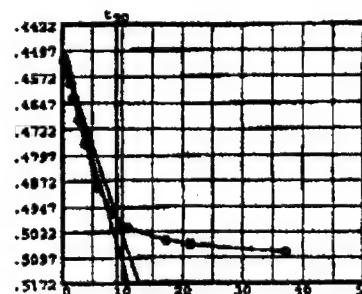
Void Ratio = 1.832 Compression = 43.3 % >>> CALCULATED USING D_{100}
 $D_0 = 0.40679$ $D_{90} = 0.44147$ $D_{100} = 0.44532$
 C_v at 177.1 min. = 0.00 ft.²/day

Pressure: 1.60 ksf

TEST READINGS

Load No. 6

No.	Elapsed Time	Dial Reading	No.	Elapsed Time	Dial Reading
1	0.00	0.44970	11	70.00	0.49660
2	0.10	0.45210	12	120.00	0.50090
3	0.25	0.45310	13	300.00	0.50460
4	0.50	0.45420	14	450.00	0.50570
5	1.00	0.45610	15	1380.00	0.50820
6	2.00	0.45900			
7	4.00	0.46330			
8	8.00	0.46950			
9	15.00	0.47630			
10	35.00	0.48900			



Void Ratio = 1.544 Compression = 49.1 % >>> CALCULATED USING D_{100}
 $D_0 = 0.44976$ $D_{90} = 0.49767$ $D_{100} = 0.50299$
 C_v at 81.2 min. = 0.01 ft.²/day

CONSOLIDATION TEST DATA

Client: Corps of Engineers Mobile District
Project: Subsurface Dredge Material Investigation-Pascagoula
Project Number: 5016080025.M10

Sample Data

Source: Boring 06-PH00
Sample No.: 06-PH00
Elev. or Depth: Sample Length (in./cm.):
Location:
Description: Gray Fat Clay with Sand (Before Washing)
Liquid Limit: 67 Plasticity Index: 44
USCS: AASHTO: Figure No.:
Testing Remarks: Tested by: JTM
Reviewed by: HJ

Test Specimen Data

TOTAL SAMPLE	BEFORE TEST	AFTER TEST
Wet w+t = 2111.70 g.	Consolidometer # = 6	Wet w+t = 2081.00 g.
Dry w+t = 2047.56 g.		Dry w+t = 2047.56 g.
Tare Wt. = 1998.90 g.	Spec. Gravity = 2.65	Tare Wt. = 1998.90 g.
Height = 1.00 in.	Height = 1.00 in.	
Diameter = 2.50 in.	Diameter = 2.50 in.	
Weight = 112.80 g.	Defl. Table = n/a	
Moisture = ^{127.6} 131.8 %	Ht. Solids = 0.2283 in.	Moisture = 68.7 %
Wet Den. = 87.5 pcf	Dry Wt. = 48.66 g.	Dry Wt. = 48.66 g.*
Dry Den. = 37.8 pcf	Void Ratio = 3.381	Void Ratio = 1.164
	Saturation = 103.3 %	

* Final dry weight used in calculations

End-of-Load Summary

Pressure (ksf)	Final Dial (in.)	Machine Defl. (in.)	C_v (ft. ² /day)	C_u	Void Ratio	% Compression /Swell
start	0.04220				3.381	
0.10	0.24420	0.00000	0.00		2.313*	24.4 Compr.*
0.20	0.33370	0.00000			1.921	33.3 Compr.
0.40	0.39170	0.00000			1.666	39.1 Compr.
0.50	0.40720	0.00000			1.599	40.7 Compr.
0.80	0.44450	0.00000			1.435	44.4 Compr.
1.60	0.50640	0.00000			1.164	50.6 Compr.

*CALCULATED USING D_{100} INSTEAD OF FINAL READING

$C_c = 0.91$ $P_c = 0.05$ ksf

Pressure: 0.50 ksf

TEST READINGS

Load No. 4

No.	Elapsed Time	Dial Reading	No.	Elapsed Time	Dial Reading
1	0.00	0.39170	11	60.00	0.39700
2	0.10	0.39210	12	120.00	0.40000
3	0.25	0.39230	13	300.00	0.40120
4	0.50	0.39250	14	460.00	0.40290
5	1.00	0.39270	15	1300.00	0.40670
6	2.00	0.39300	16	1450.00	0.40720
7	4.00	0.39350			
8	8.00	0.39420			
9	15.00	0.39490			
10	30.00	0.39580			

Void Ratio = 1.599 Compression = 40.7 %

Pressure: 0.80 ksf

TEST READINGS

Load No. 5

No.	Elapsed Time	Dial Reading	No.	Elapsed Time	Dial Reading
1	0.00	0.40720	11	60.00	0.42670
2	0.10	0.40790	12	120.00	0.43260
3	0.25	0.40820	13	300.00	0.43900
4	0.50	0.40850	14	1380.00	0.44450
5	1.00	0.40910			
6	2.00	0.41000			
7	4.00	0.41190			
8	8.00	0.41340			
9	15.00	0.41620			
10	30.00	0.42180			

Void Ratio = 1.435 Compression = 44.4 %

Pressure: 1.60 ksf

TEST READINGS

Load No. 6

No.	Elapsed Time	Dial Reading	No.	Elapsed Time	Dial Reading
1	0.00	0.44450	11	120.00	0.49740
2	0.10	0.44660	12	300.00	0.50240
3	0.25	0.44750	13	450.00	0.50360
4	0.50	0.44870	14	1380.00	0.50590
5	1.00	0.45050	15	1800.00	0.50640
6	4.00	0.45760			
7	8.00	0.46390			
8	15.00	0.47130			
9	30.00	0.48160			
10	60.00	0.49170			

Void Ratio = 1.164 Compression = 50.6 %

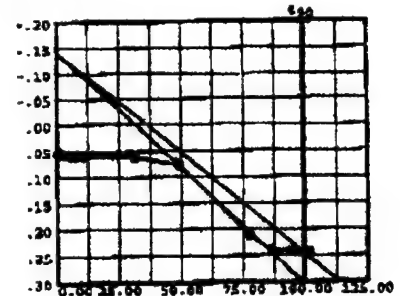
.0555

Pressure: 0.10 ksf

TEST READINGS

Load No. 1

No.	Elapsed Time	Dial Reading	No.	Elapsed Time	Dial Reading
1	0.00	0.04220	11	60.00	0.05920
2	0.10	0.05460	12	120.00	0.05930
3	0.25	0.05480	13	970.00	0.06210
4	0.50	0.05490	14	2410.00	0.07640
5	1.00	0.05520	15	6020.00	0.21200
6	2.00	0.05540	16	7460.00	0.24030
7	4.00	0.05580	17	8900.00	0.24160
8	8.00	0.05640	18	10340.00	0.24420
9	15.00	0.05730			
10	30.00	0.05820			



Void Ratio = 2.313 Compression = 24.4 % >>> CALCULATED USING D₁₀₀
D₀ = -0.14233 D₉₀ = 0.24319 D₁₀₀ = 0.28603
C_v at 9768.5 min. = 0.00 ft.²/day

Pressure: 0.20 ksf

TEST READINGS

Load No. 2

.102

No.	Elapsed Time	Dial Reading	No.	Elapsed Time	Dial Reading
1	0.00	0.24420	11	60.00	0.26990
2	0.10	0.24450	12	120.00	0.30820
3	0.25	0.24460	13	240.00	0.31840
4	0.50	0.24470	14	360.00	0.32160
5	1.00	0.24480	15	1220.00	0.32570
6	2.00	0.24500	16	1770.00	0.32630
7	4.00	0.24530	17	5540.00	0.33370
8	8.00	0.24580			
9	15.00	0.24660			
10	30.00	0.25840			

Void Ratio = 1.921 Compression = 33.3 %

Pressure: 0.40 ksf

TEST READINGS

Load No. 3

No.	Elapsed Time	Dial Reading	No.	Elapsed Time	Dial Reading
1	0.00	0.33370	11	60.00	0.36670
2	0.10	0.33530	12	120.00	0.37410
3	0.25	0.33570	13	240.00	0.38130
4	0.50	0.33630	14	500.00	0.38650
5	1.00	0.33720	15	1340.00	0.39130
6	2.00	0.33850	16	1464.00	0.39170
7	4.00	0.34070			
8	8.00	0.34400			
9	15.00	0.34860			
10	30.00	0.35590			

Void Ratio = 1.666 Compression = 39.1 %

CONSOLIDATION TEST DATA

Client: Corps of Engineers Mobile District
Project: Subsurface Dredge Material Investigation-Pascagoula
Project Number: 5016080025.M10

Sample Data

Source: Boring 10-PH00
Sample No.: 10-PH00
Elev. or Depth: Sample Length (in./cm.):
Location:
Description: Gray Clayey Sand (Before Washing)
Liquid Limit: 38 Plasticity Index: 22
USCS: SC AASHTO: Figure No.:
Testing Remarks: Tested by: JTM
Reviewed by: HJ

Test Specimen Data

TOTAL SAMPLE	BEFORE TEST	AFTER TEST
Wet w+t = 2115.90 g.	Consolidometer # = 6	Wet w+t = 2079.80 g.
Dry w+t = 2042.51 g.		Dry w+t = 2042.51 g.
Tare Wt. = 1998.90 g.	Spec. Gravity = 2.7	Tare Wt. = 1998.90 g.
Height = 1.00 in.	Height = 1.00 in.	
Diameter = 2.50 in.	Diameter = 2.50 in.	
Weight = 117.00 g.	Defl. Table = n/a	
Moisture = (147.4%) 168.3 %	Ht. Solids = 0.2008 in.	Moisture = 85.5 %
Wet Den. = 90.8 pcf	Dry Wt. = 43.61 g.	Dry Wt. = 43.61 g.*
Dry Den. = 33.8 pcf	Void Ratio = 3.980	Void Ratio = 2.305
	Saturation = 114.2 %	

* Final dry weight used in calculations

End-of-Load Summary

Pressure (ksf)	Final Dial (in.)	Machine Defl. (in.)	C _v (ft. ² /day)	C _α	Void Ratio	% Compression /Swell
start	0.02210				3.980	
0.10	0.05670	0.00000	0.01		3.839*	2.8 Compr.*
0.20	0.10120	0.00000			3.617	7.3 Compr.
0.40	0.21060	0.00000			3.072	18.2 Compr.
0.80	0.28440	0.00000			2.705	25.6 Compr.
1.60	0.36470	0.00000			2.305	33.6 Compr.

*CALCULATED USING D₁₀₀ INSTEAD OF FINAL READING

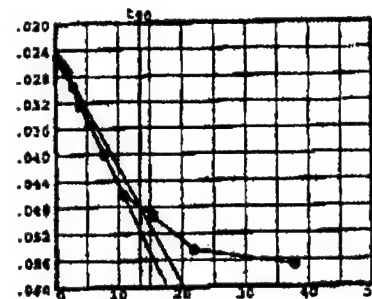
C_c = 1.35 P_c = 0.12 ksf

Pressure: 0.10 ksf

TEST READINGS

Load No. 1

No.	Elapsed Time	Dial Reading	No.	Elapsed Time	Dial Reading
1	0.00	0.02210	11	60.00	0.04000
2	0.10	0.02510	12	120.00	0.04620
3	0.25	0.02540	13	240.00	0.04930
4	0.50	0.02560	14	480.00	0.05450
5	1.00	0.02600	15	1430.00	0.05670
6	2.00	0.02650			
7	4.00	0.02750			
8	8.00	0.02960			
9	15.00	0.03260			
10	30.00	0.03560			



Void Ratio = 3.839 Compression = 2.8 % >>> CALCULATED USING D_{100}
 $D_0 = 0.02409$ $D_{90} = 0.04788$ $D_{100} = 0.05053$
 C_v at 180.0 min. = 0.01 ft.²/day

Pressure: 0.20 ksf

TEST READINGS

Load No. 2

No.	Elapsed Time	Dial Reading	No.	Elapsed Time	Dial Reading
1	0.00	0.05670	11	60.00	0.07470
2	0.10	0.05740	12	120.00	0.07880
3	0.25	0.05760	13	240.00	0.08900
4	0.50	0.05790	14	480.00	0.09210
5	1.00	0.05840	15	1410.00	0.09320
6	2.00	0.06010	16	5730.00	0.10120
7	4.00	0.06260			
8	8.00	0.06520			
9	15.00	0.06710			
10	30.00	0.06980			

Void Ratio = 3.617 Compression = 7.3 %

Pressure: 0.40 ksf

TEST READINGS

Load No. 3

No.	Elapsed Time	Dial Reading	No.	Elapsed Time	Dial Reading
1	0.00	0.10120	11	60.00	0.17100
2	0.10	0.10390	12	120.00	0.18820
3	0.25	0.10490	13	240.00	0.19800
4	0.50	0.10620	14	480.00	0.20520
5	1.00	0.10820	15	1360.00	0.21060
6	2.00	0.11140			
7	4.00	0.11630			
8	8.00	0.12340			
9	15.00	0.13540			
10	30.00	0.15060			

Void Ratio = 3.072 Compression = 18.2 %

Pressure: 0.80 ksf TEST READINGS Load No. 4

No.	Elapsed Time	Dial Reading	No.	Elapsed Time	Dial Reading
1	0.00	0.21060	11	60.00	0.25710
2	0.10	0.21310	12	120.00	0.26900
3	0.25	0.21400	13	240.00	0.27770
4	0.50	0.21520	14	390.00	0.28010
5	1.00	0.21670	15	1230.00	0.28440
6	2.00	0.21890			
7	4.00	0.22260			
8	8.00	0.22800			
9	15.00	0.23430			
10	30.00	0.24460			

Void Ratio = 2.705 Compression = 25.6 %

Pressure: 1.60 ksf TEST READINGS Load No. 5

No.	Elapsed Time	Dial Reading	No.	Elapsed Time	Dial Reading
1	0.00	0.28440	11	60.00	0.34500
2	0.10	0.28440	12	120.00	0.35410
3	0.25	0.28980	13	360.00	0.35860
4	0.50	0.29140	14	1200.00	0.36290
5	1.00	0.29370	15	1790.00	0.36370
6	2.00	0.29510	16	2630.00	0.36470
7	4.00	0.30180			
8	8.00	0.30850			
9	15.00	0.31710			
10	30.00	0.32900			

Void Ratio = 2.305 Compression = 33.6 %

CONSOLIDATION TEST DATA

Client: Corps of Engineers Mobile District
Project: Subsurface Dredge Material Investigation-Pascagoula
Project Number: 5016080025.M10

Sample Data

Source: Boring 02-PH00
Sample No.: 02-PH00
Elev. or Depth: Sample Length (in./cm.):
Location:
Description: Gray Sandy Fat Clay (Before Washing)
Liquid Limit: 77 Plasticity Index: 53
USCS: CH AASHTO: Figure No.:
Testing Remarks: Tested by: JTM
Reviewed by: HJ

Test Specimen Data

TOTAL SAMPLE	BEFORE TEST	AFTER TEST
Wet w+t = 2100.30 g.	Consolidometer # = 5	Wet w+t = 2053.30 g.
Dry w+t = 2028.96 g.		Dry w+t = 2028.96 g.
Tare Wt. = 1993.20 g.	Spec. Gravity = 2.67	Tare Wt. = 1993.20 g.
Height = 1.00 in.	Height = 1.00 in.	
Diameter = 2.50 in.	Diameter = 2.50 in.	
Weight = 107.10 g.	Defl. Table = n/a	
Moisture = 199.5 %	Ht. Solids = 0.1665 in.	Moisture = 68.1 %
Wet Den. = 83.1 pcf	Dry Wt. = 35.76 g.	Dry Wt. = 35.76 g.*
Dry Den. = 27.8 pcf	Void Ratio = 5.006	Void Ratio = 2.727
	Saturation = 106.4 %	

* Final dry weight used in calculations

End-of-Load Summary

Pressure (ksf)	Final Dial (in.)	Machine Defl. (in.)	C_v (ft. ² /day)	C_α	Void Ratio	% Compression /Swell
start	0.00340				5.006	
0.10	0.01850	0.00000	0.15		4.967*	0.7 Compr.*
0.20	0.19130	0.00000	0.00		4.051*	15.9 Compr.*
0.40	0.21910	0.00000	0.01		3.780*	20.4 Compr.*
0.80	0.31530	0.00000	0.01		3.225*	29.7 Compr.*
1.60	0.38600	0.00000	0.01		2.727*	37.9 Compr.*

*CALCULATED USING D₁₀₀ INSTEAD OF FINAL READING

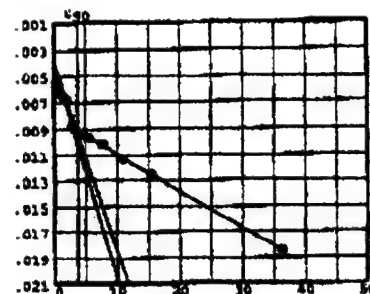
$C_c = 1.62$ $P_c = 0.29$ ksf

Pressure: 0.10 ksf

TEST READINGS

Load No. 1

No.	Elapsed Time	Dial Reading	No.	Elapsed Time	Dial Reading
1	0.00	0.00340	11	60.00	0.01020
2	0.10	0.00560	12	120.00	0.01130
3	0.25	0.00610	13	240.00	0.01260
4	0.50	0.00620	14	1320.00	0.01850
5	1.00	0.00630			
6	2.00	0.00650			
7	4.00	0.00680			
8	8.00	0.00880			
9	15.00	0.00940			
10	30.00	0.00960			



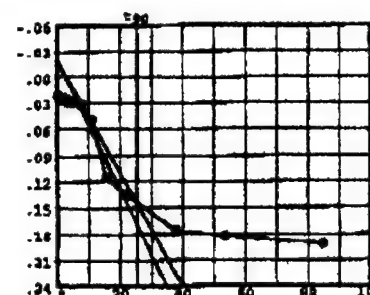
Void Ratio = 4.967 Compression = 0.7 % >>> CALCULATED USING D_{100}
 $D_0 = 0.00387$ $D_{90} = 0.00932$ $D_{100} = 0.00992$
 C_v at 13.9 min. = 0.15 ft.²/day

Pressure: 0.20 ksf

TEST READINGS

Load No. 2

No.	Elapsed Time	Dial Reading	No.	Elapsed Time	Dial Reading
1	0.00	0.01850	11	60.00	0.03140
2	0.10	0.02050	12	120.00	0.04980
3	0.25	0.02130	13	240.00	0.11500
4	0.50	0.02190	14	480.00	0.13550
5	1.00	0.02250	15	1430.00	0.17600
6	2.00	0.02310	16	2860.00	0.18130
7	4.00	0.02380	17	7180.00	0.19130
8	8.00	0.02410			
9	15.00	0.02790			
10	30.00	0.02950			



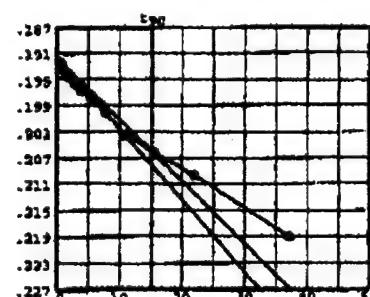
Void Ratio = 4.051 Compression = 15.9 % >>> CALCULATED USING D_{100}
 $D_0 = -0.02105$ $D_{90} = 0.14402$ $D_{100} = 0.16237$
 C_v at 637.9 min. = 0.00 ft.²/day

Pressure: 0.40 ksf

TEST READINGS

Load No. 3

No.	Elapsed Time	Dial Reading	No.	Elapsed Time	Dial Reading
1	0.00	0.19130	11	60.00	0.20000
2	0.10	0.19220	12	120.00	0.20340
3	0.25	0.19240	13	240.00	0.20620
4	0.50	0.19270	14	480.00	0.20960
5	1.00	0.19320	15	1380.00	0.21910
6	2.00	0.19390			
7	4.00	0.19460			
8	8.00	0.19550			
9	15.00	0.19660			
10	30.00	0.19800			



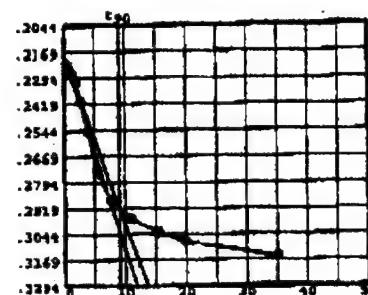
Void Ratio = 3.780 Compression = 20.4 % >>> CALCULATED USING D_{100}
 $D_0 = 0.19164$ $D_{90} = 0.20597$ $D_{100} = 0.20757$
 C_v at 228.8 min. = 0.01 ft.²/day

Pressure: 0.80 ksf

TEST READINGS

Load No. 4

No.	Elapsed Time	Dial Reading	No.	Elapsed Time	Dial Reading
1	0.00	0.21910	11	60.00	0.28790
2	0.10	0.22280	12	120.00	0.29670
3	0.25	0.22360	13	240.00	0.30370
4	0.50	0.22430	14	395.00	0.30770
5	1.00	0.22570	15	1235.00	0.31530
6	2.00	0.22790			
7	4.00	0.23160			
8	8.00	0.24090			
9	15.00	0.25520			
10	30.00	0.27390			

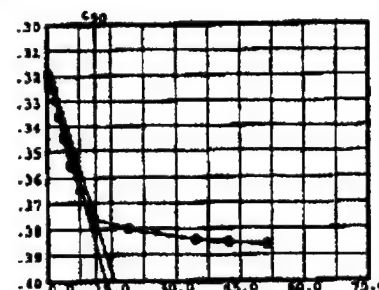
Void Ratio = 3.225 Compression = 29.7 % >>> CALCULATED USING D₁₀₀D₀ = 0.21696 D₉₀ = 0.29159 D₁₀₀ = 0.29988C_v at 82.6 min. = 0.01 ft.²/day

Pressure: 1.60 ksf

TEST READINGS

Load No. 5

No.	Elapsed Time	Dial Reading	No.	Elapsed Time	Dial Reading
1	0.00	0.31530	11	60.00	0.36500
2	0.10	0.31910	12	120.00	0.37600
3	0.25	0.32000	13	360.00	0.38010
4	0.50	0.32090	14	1200.00	0.38420
5	1.00	0.32260	15	1795.00	0.38520
6	2.00	0.32530	16	2635.00	0.38600
7	4.00	0.32960			
8	8.00	0.33620			
9	15.00	0.34470			
10	30.00	0.35550			

Void Ratio = 2.727 Compression = 37.9 % >>> CALCULATED USING D₁₀₀D₀ = 0.31586 D₉₀ = 0.37614 D₁₀₀ = 0.38283C_v at 125.9 min. = 0.01 ft.²/day

Appendix G

Properties of Placed Sediments – Sample PH-05

Background

One option for the storage of dredged material is through the use of a confined disposal facility (CDF). The conceptual design of the CDF requires an evaluation of the properties and settling behavior of the dredged material to be placed therein. This evaluation will provide information necessary to estimate storage requirements and to predict the concentration of suspended solids removed via supernatant discharge from the CDF.

This chapter presents the results of the laboratory tests performed to measure sedimentation properties of the dredged material from the Port of Pascagoula. Settling tests were run to determine the settling behavior of the Port of Pascagoula sediments when they are hydraulically dredged. This will aid the District in designing a proper CDF to meet their requirements. Also in support of the overall objective, data were collected on the turbidity and TSS concentrations in the water column during the settling column tests. This facilitated the development of a correlation curve for turbidity and total suspended solids (TSS) that a contractor and/or inspector can use to quickly estimate TSS by measuring turbidity. Turbidity is a much more easily and quickly measured parameter than TSS because turbidity is measured with a commercially available meter, while TSS has to be measured in a laboratory using ovens, analytical balances, filtration apparatus, etc.

Sediment Properties Tests

The physical characteristics of the dredged material are important in the design of a CDF and starting the column settling tests. A composite sediment sample was used to evaluate the physical characteristic of the Pascagoula sediment (Table G1). Descriptions of geotechnical and engineering testing are presented in the following paragraphs. Based on the Unified Soil Classification System the Pascagoula sediment was classified as a gray sandy clay (CH) (Figure G1).

Table G1
Sediment Physical Characteristics

Characteristic	Value
Specific Gravity	2.74
In Situ Solids Concentration	
Water Content	186.5%
Void Ratio	6.60
Solids Concentration (particulate)	315.0 g/L
Atterberg Limits	
Liquid Limit	136.0
Plastic Limit	37.0
Plasticity Index	99.0
Grain-Size Distribution	
Percent Gravel	0.0
Percent Sand	0.4
Percent Silt/Clay	99.6
Classification	Gray Sandy Clay (CH)

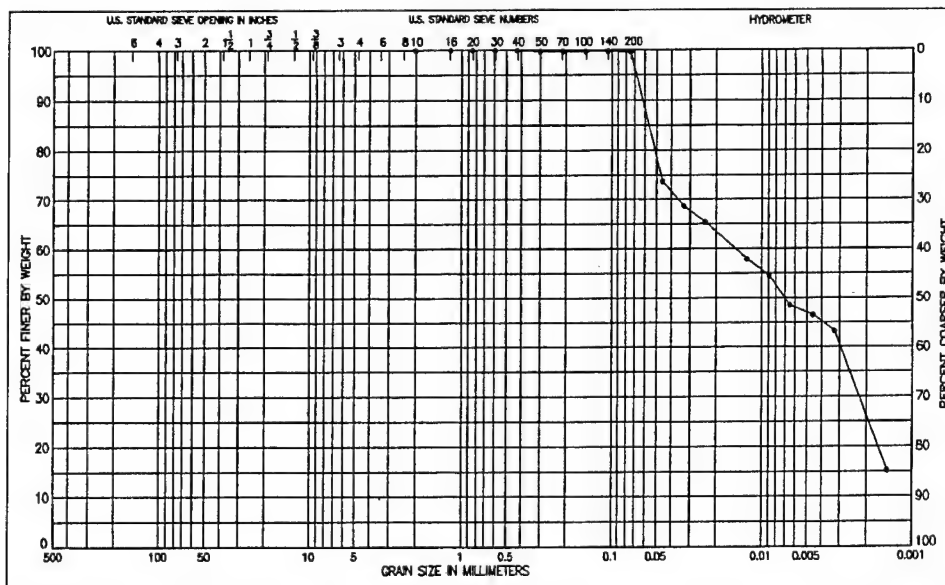


Figure G1. Grain-size distribution of Pascagoula sediment composite

Specific gravity. Specific gravity (SG) of the particulates in the sediment and tailing material were measured using the procedures given the Laboratory Soils Testing Engineering Manual (USACE 1970). The specific gravity of Pascagoula sediment was 2.74.

Water content. The in situ water content (W) of fine-grained sediment samples is also an important parameter evaluating settling behavior and the volumetric changes occurring following dredging and disposal. It should be noted that the water content in this appendix is identical to the geotechnical engineering water content. Since the water content is defined as the ratio of weight of water to weight of solids expressed as percent, it can exceed 100 percent. The procedures are given in the Laboratory Soils Testing Engineering Manual (USACE 1970). Using the specific gravity and water content, the void ratio (e) and solids concentration (S) can be expressed as follows:

$$e = \frac{W * SG}{100}$$

$$S = \frac{1000 * SG}{1 + e}$$

Grain-size Distribution. Grain-size distributions were determined on the samples using standard sieve and hydrometer analyses as outlined in the Laboratory Soils Testing Engineer Manual (USACE 1970).

Plasticity. Liquid limit (LL) and plastic limit (PL) were determined for composite sediment samples using standard soils testing procedures as outlined in the Laboratory Soils Testing Engineer Manual (USACE 1970). The plasticity index (PI) was then computed; $PI = LL - PL$.

Unified Soil Classification System (USCS) Classification. Visual classifications and classifications using results of the grain-size distribution and plasticity tests as described in the next section were determined using the USCS as outlined in the Laboratory Soils Testing Engineer Manual (USACE 1970).

Experimental Procedures

Sample collection

The Mobile District collected sediment and site-water samples from potential dredging areas. The sediment and site-water samples were delivered to ERDC's Environmental Research and Development Center, Environmental Laboratory (EL) in 5-gal containers. At that time, the samples were identified and labeled "Pascagoula." Samples were then stored in 4 °C coolers until tested. The EL personnel composited and homogenized several containers of the sediment to obtain a representative sample for testing. Total solids analyses were run on the

composite in triplicate to assure a homogenized sample. The composited samples were then replaced in a 4 °C cooler until tested.

Settling test procedures

The settling tests followed procedures found in Palermo, Montgomery, and Poindexter (1978), USACE (1987), and Palermo and Thackston (1988). The tests involved mixing sediment and site water to simulate the concentration of a dredged material slurry, placing the material in a settling column, and observing the different types of settling (i.e., zone, flocculent and compression) behavior. The general procedures are described in the following paragraphs.

Zone, compression, and flocculent settling data were collected by conducting a settling test for the composite samples. The three types of settling data were collected from a single settling test.

Slurry preparation

A target slurry concentration is used to simulate the solids concentration anticipated during production by a hydraulic dredge. Target slurry concentrations selected for settling tests are dependent on the grain-size distribution of the sample. The average solids content for the Pascagoula sediment sample prior to mixing was 315 gal/L, and the salinity of the site-water was 32.2 parts per thousand (salt water). To achieve a target concentration of 130 gal/L suspended solids, the slurry was prepared by mixing approximately 31 L of sediment with approximately 45 L of site water into a 130-L mixing chamber. The mixture of sediment and site water was then thoroughly blended using a Lightning mixer for 30 min.

After completely mixing the slurry, the mixing intensity was decreased to allow the majority of the coarse-grained material to settle in the mixing chamber while keeping the fine-grained material in suspension. While slowly mixing, the fine-grained slurry was transferred from the 130-L mixing chamber to an 8-in.¹ diam, 7-ft tall column with ports at 0.5-ft intervals starting at the 6.5-ft height (Figure G2). Immediately after loading the column with the slurry, samples were extracted from the sampling ports at 1.0-ft intervals throughout the column. The total solids concentrations for the slurry (representing the fine-grained fraction of the original slurry) that was transferred into the columns are given in Table G2. The average suspended solids concentration was determined to be 117 g/L. The difference between the target total solids concentration and the solids concentration of slurry as mixed is due to sedimentation of the coarse fraction provided in the 130-L mixing chamber.

¹ Units of measurement in this appendix are in non-SI units, a table of factors for converting non-SI to SI units of measurement is presented on page xvii.

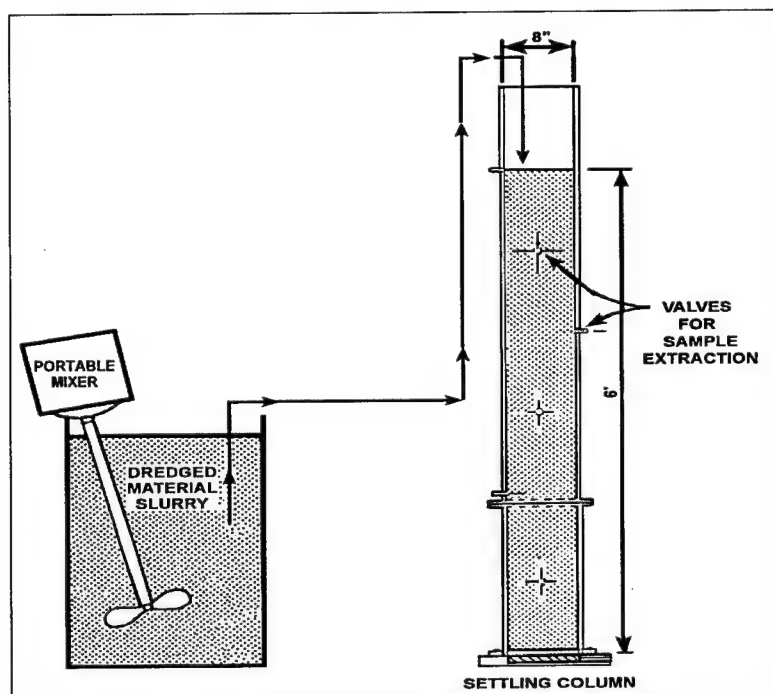


Figure G2. Schematic of settling column

Table G2 Total Solids Concentration of Column Slurry Sample	
Port Height (ft)	Total Suspended Solids Concentration (gal/L)
1.0	113.52
2.0	118.08
3.0	119.80
4.0	115.78
5.0	119.76
6.0	114.15
Average	116.85

Zone settling test

The zone settling test consisted of placing the slurry in a sedimentation column and reacing and recording the fall of the liquid-solids interface with time. These data are plotted as height of the interface versus time. The slope of the curve in the constant velocity settling zone is the zone settling velocity, which is a function of the initial slurry concentration. The zone settling velocity is used in the design process to determine the minimum ponded area required for a given flow rate. A photo of the settling test of the sediments from the Port of Pascagoula is shown in Figure G3.

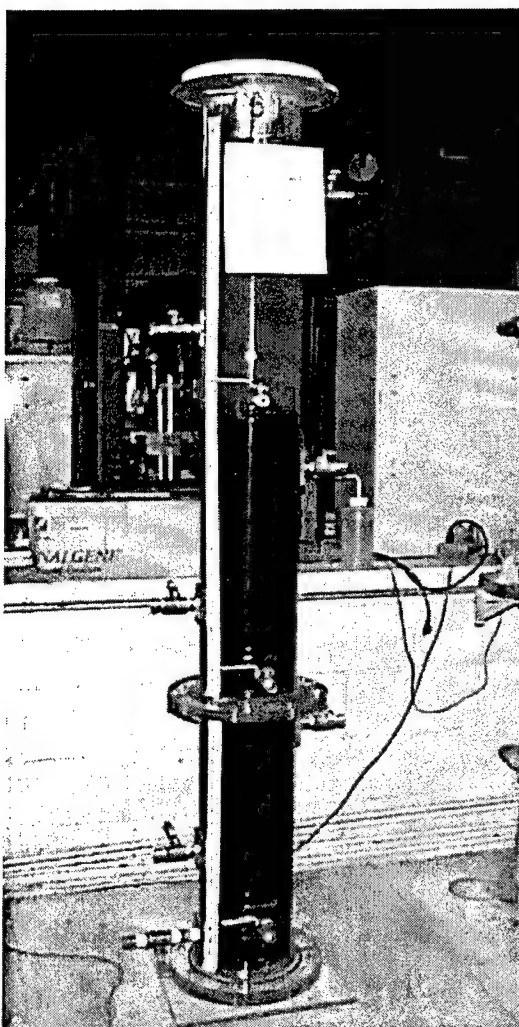


Figure G3. Pascagoula settling test

The zone settling test was performed concurrently with the compression settling test on the same slurry in the same column. Zone settling typically occurs during the first 12 hr of a dredged material settling test and compression settling occurs after the first 24 hr of the dredged material settling test. The height of the interface was read periodically during the first 12 hr with sufficient frequency to define the zone settling velocity. From the plot of the interface height (ft) versus time (hr), the zone settling velocity was determined.

Compression settling test

The compression settling test must be run to obtain data for estimating the volume required for initial storage of the dredged material. Following the zone-settling test (the first 12 hr immediately after the column was loaded with the slurry), the height of the interface was measured at approximately daily intervals for the next 15 days. The interface height, the initial height of the slurry, and the

initial solids concentration of the slurry in the column are used to estimate the concentration of settled solids below the interface as a function of time as required in the compression settling analysis.

Flocculent settling test

The flocculent settling test consisted of measuring the concentration of suspended solids at various depths and time intervals in a settling column. An interface formed near the top of the settling column during the first day of the test; therefore, sedimentation of the material below the interface is described by zone settling. The flocculent test procedure was continued only for that portion of the water column above the interface. Samples of the supernatant were extracted from each sampling port above the liquid-solid interface at different time intervals. The suspended solids concentrations of the extracted samples were determined. Substantial reductions of suspended solids are expected to occur during the early part of the test, but reductions should lessen at longer retention time (USACE 1987).

The flocculent settling test was performed concurrently with the zone and compression settling tests on the same slurry in the same column. Therefore, the initial slurry concentrations for the flocculent, zone, and compression settling tests were the same. Samples of the supernatant, if available, were extracted with a syringe at fixed ports located at heights of 6.0, 5.5, 5.0, 4.5, 4.0, and 3.5 ft above the bottom of the column. Supernatant samples were collected at 4, 6, 8, 12, 24, 48, 96, 168, 268, 312, and 360 hr after loading the slurry. Samples were taken at all ports above the supernatant-settled solids interface where supernatant was available. Suspended solids concentrations were then determined on the supernatant samples by Standard Method 2540D (APHA-AWWA-WPCF 1989). Turbidity of the supernatants were measured using a Hach Digital Model 2100 turbidimeter and determined by Standard Method 2130B (APHA-AWWA-WPCF 1989).

Data Analysis and Results

The behavior of CDF slurry inflow concentrations expected for Pascagoula sediment will be governed by zone settling processes. The sediments exhibited a clear interface between settled material and clarified supernatant.

The settling test data were analyzed using the Automated Dredging and Disposal Alternative Management Systems (ADDAMS) (Schroeder and Palermo 1995) which is a family of computer programs developed at ERDC to assist in planning designing, and operating dredging and dredged material disposal projects. The SETTLE module of ADDAMS was used for the settling test data (Hayes and Schroeder 1992).

Compression settling tests

For the compression tests, the initial slurry concentration and height, and height of the interface versus time were entered into SETTLE (Table G3). The SETTLE program uses the initial slurry concentrations of 117 gal/L and height of

6.29 ft to determine the solids concentration at a given time. A plot was generated showing the relationship between solids concentration (gal/L) and retention time (days) (Figure G4). SETTLE also generated a regression equation for the resulting power curve relating solids concentration to time. The composite sample regression equation may be used to determine the solid concentration at any given time. The regression equation used was:

$$C = 157 \times T^{0.144}$$

where

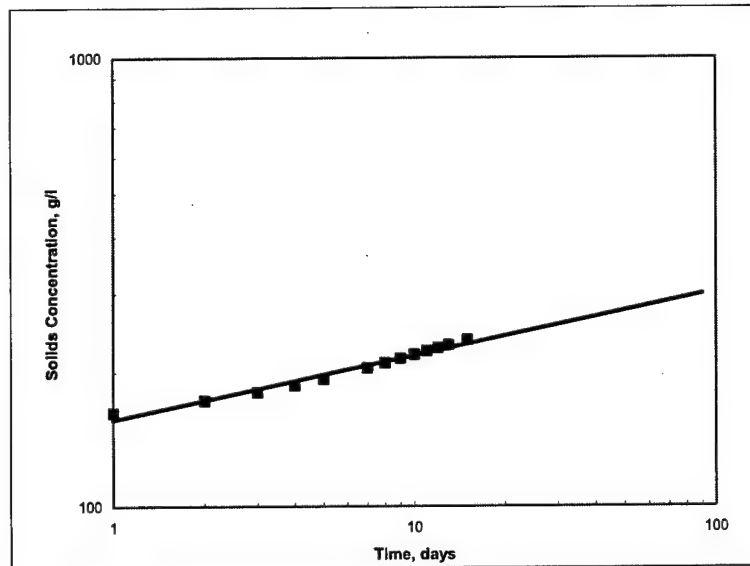
C = solids concentration, gal/L

T = time, days

Table G3 Compression Settling Test Data				
Date	Time	Time Interval (hr)	Time Interval (days)	Interface Height (ft)
20 April 2001	0833	0	1	4.52
21 April 2001	0833	24	2	4.25
22 April 2001	0833	48	3	4.07
23 April 2001	0833	96	4	3.93
24 April 2001	0833	120	5	3.80
25 April 2001	0833	144	6	3.69
26 April 2001	0833	168	7	3.59
27 April 2001	0833	192	8	3.50
28 April 2001	0833	216	9	3.42
29 April 2001	0833	240	10	3.35
30 April 2001	0833	264	11	3.29
01 May 2001	0833	288	12	3.24
02 May 2001	0833	312	13	3.19
03 May 2001	0833	336	14	3.15
04 May 2001	0833	360	15	3.11

Zone settling tests

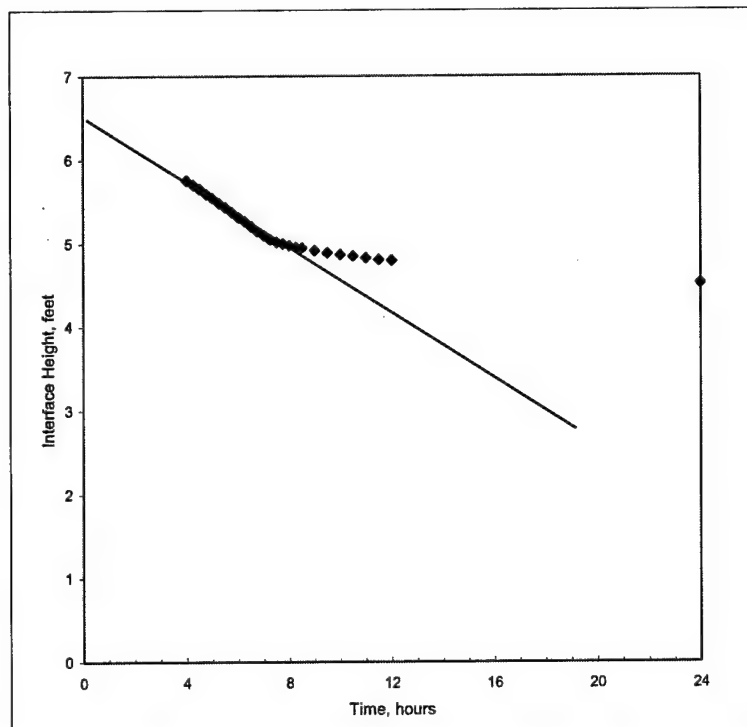
Zone settling velocity for the Port of Pascagoula sediment sample was determined to be 0.226 ft/hr for the zone settling test. The height of the interface and their corresponding elapsed time from the start of the test when the height was measured were entered (Table G4) and plotted in the SETTLE program to determine the zone settling velocity (Figure G5). When the zone settling curve departs from a linear relationship, compression settling begins. The transition from zone to compression settling occurred between 10 and 12 hr (Figure G5). The zone settling velocity is adjacent to the plot of the zone settling data.



$$\text{Conc} = 157 \times \text{Time}^{0.144}$$

$$R^2 = 0.978$$

Figure G4. Compression settling curve



$$\text{ZSV} = 0.226 \text{ ft/hr}$$

Figure G5. Pascagoula zone settling velocity curve

Table G4
Zone Settling Test Data

Time	Elapsed Time, hr	Interface Height, ft
0833 - 19 April 2001	0.00	6.29
0850	0.28	6.27
0903	0.50	6.25
0918	0.75	6.24
0933	1.00	6.23
0948	1.25	6.21
1003	1.50	6.19
1018	1.75	6.16
1033	2.00	6.13
1048	2.25	6.10
1103	2.50	6.05
1118	2.75	6.00
1133	3.00	5.96
1148	3.25	5.91
1203	3.50	5.86
1218	3.75	5.81
1233	4.00	5.76
1248	4.25	5.71
1303	4.50	5.66
1318	4.75	5.60
1333	5.00	5.55
1348	5.25	5.49
1403	5.50	5.44
1418	5.75	5.38
1433	6.00	5.32
1448	6.25	5.27
1503	6.50	5.21
1518	6.75	5.15
1533	7.00	5.10
1548	7.25	5.05
1503	7.50	5.02
1618	7.75	5.00
1633	8.00	4.98
1648	8.25	4.96
1703	8.50	4.95
1733	9.00	4.92
1803	9.50	4.89
1833	10.00	4.87
1903	10.50	4.85
1933	11.00	4.83
2003	11.50	4.81
2033	12.00	4.80
Notes: The initial interface depth was 6.29 ft. The slurry concentration was 117 gal/L. The salinity was 32.2 parts per thousand.		

Flocculent settling tests

An extension of the flocculent settling test is presented in USACE (1987). Palermo (1985) analyzed the effects of several possible assumptions regarding the magnitude of the value to be used as the initial concentration in the laboratory test and showed that all gave essentially the same final result. Therefore, it was recommended that, for simplicity, the concentration in the first sample taken at the highest sampling port be used as the initial concentration. SETTLE generates two curves based on the settle data in Table G5. The two plots generated by SETTLE are concentration profile curve (Figure G6) and supernatant suspended solids curve (Figure G7). The concentration profile curve, which plots the depth below the surface (ft) versus percent of initial concentration, shows that the suspended solids concentrations decrease with time and increase at deeper ponding depths (1, 2, and 3 ft) at the weir. The actual depth of withdrawal is a function of the flow rate and the weir length; the depth is shallower for lower flow rates and longer weir lengths. The supernatant suspended solids curves derived from the concentration profile curves compare the effects of retention time on the supernatant suspended solids concentration at 1-, 2-, and 3-ft ponding depths. Figure G6 shows that increasing the retention time beyond 24 hr for 1, 2, or 3 ft of ponding depth provides little additional improvement in supernatant suspended solids concentration. Actual field suspended solids will be somewhat greater because of resuspension by wind and wave action. Based on field experience, a resuspension factor is estimated to range from 1.5 to 2.5 depending on ponding depth and surface area (Shields, Schroeder, and Thackson 1987) (Table G6).

Table G5
Flocculent Settling Test Data

Time (hr)	Port Height (ft) ¹					
	6.00	5.50	5.00	4.50	4.00	3.50
4	105.00 ²	BI	BI	BI	BI	BI
6	30.00	55.20	BI	BI	BI	BI
8	41.50	29.20	BI	BI	BI	BI
12	44.30	51.70	49.10	BI	BI	BI
24	27.60	32.80	40.40	BI	BI	BI
48	30.00	28.00	22.00	78.00	BI	BI
96	BI	20.00	19.00	25.00	BI	BI
168	BI	20.00	25.00	22.00	35.00	BI
264	BI	9.00	12.00	11.00	61.00	78.00
312	BI	15.00	16.00	16.00	41.00	111.00
360	BI	9.00	32.00	5.00	27.00	37.00

¹ Initial slurry concentration was 117 gal/L.
² Concentration at highest port used as initial supernatant concentration (mg/L).
 BI = Port was below interface, and no sample was collected at this time interval.

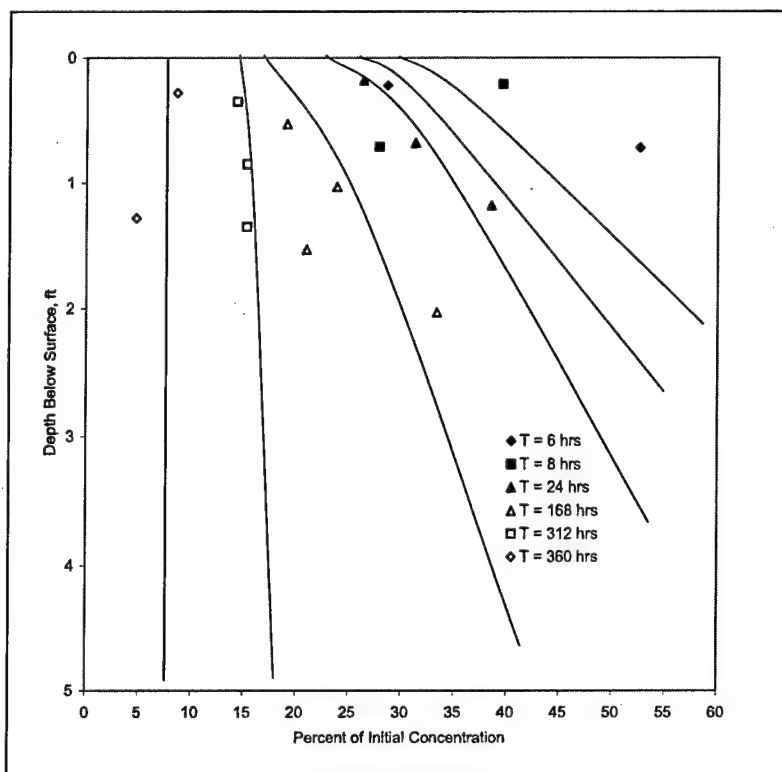


Figure G6. Flocculent settling test suspended solids relationship to time and depth below surface

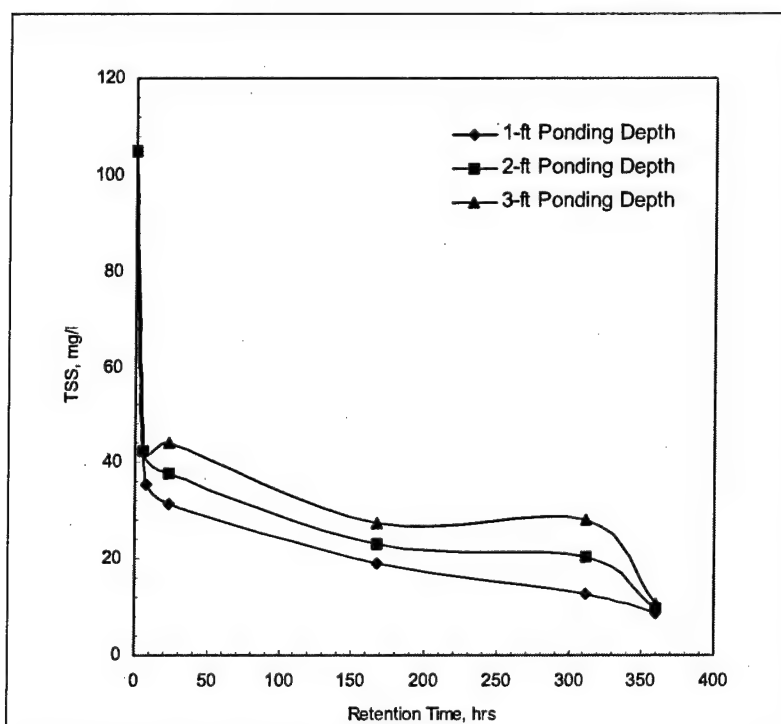


Figure G7. Supernatant suspended solids curve

Table G6
Recommended Resuspension Factors For Various Ponding
Areas and Depths

Anticipated Ponded Area	Anticipated Average Ponded Depth	
	Less than 2 ft	2 ft or Greater
Less than 100 acres	2.0	1.5
Greater than 100 acres	2.5	2.0

Turbidity

Samples of the supernatant from the flocculent settling test were split to measure turbidity of corresponding TSS concentration (Table G7). TSS is commonly used as an indicator of the overall performance of CDFs, both for solids retention and for most other contaminants, which are strongly associated with the solid particles by absorption or ion exchange. Turbidity, being much more easily measured than TSS, may be used instead of TSS during routine operational monitoring if approved by the regulatory agency.

Figure G8 shows the correlation curve between TSS and turbidity for the Pascagoula sediment. The field inspector and others can measure the turbidity of the effluent with a turbidity meter and estimate a TSS concentration from the curve. Samples for TSS measurement can be collected less frequently for compliance monitoring and to field verify the correlation for laboratory samples.

Consolidation tests

The consolidation test was conducted using the composite sample of the Pascagoula sediment. The test provides data for evaluation of filling and settlement rates for CDFs. The test results are applicable for evaluation of both intertidal and upland sites. The tests were conducted using standard oedometers and self-weight consolidation test procedures developed specially for soft sediments (Cargill 1983).

The results of the self-weight consolidation test are shown in Figure G9 where the consolidation of a 6-in. sample is plotted as a function of time. The self-weight consolidation test provides data for the initial period of consolidation including the period of compression settling. The time curves from the standard oedometer consolidation tests for nine loadings (0.01, 0.02, 0.04, 0.08, 0.16, 0.32, 0.64, 1.3, and 2.6 tons/sq ft) are plotted in Figure G10. The void ratio versus the effective stress relationship from the standard oedometer test is plotted in Figure G11. The standard oedometer test provides data for consolidation of thick layers or layers of dredged material with a desiccated crust. The combined relationship of void ratio versus the effective stress from the standard oedometer test and the self-weight test is plotted in Figure G12.

Table G7
TSS Concentrations and Turbidity Measurements

Time (hr)	Port No.	TSS (mg/L)	Turbidity (NTU)	Time (hr)	Port No.	TSS (mg/L)	Turbidity (NTU)
4	6.0	105	65.6	192	4.5	12	58.8
6	6.0	30	16.9	192	4.0	47	90.0
6	5.5	55	19.4	216	5.5	8	42.6
8	6.0	42	31.1	216	5.0	52	97.5
8	5.5	29	48.8	216	4.5	13	59.5
12	6.0	44	51.9	216	4.0	55	83.8
12	5.5	52	21.1	240	5.5	16	51.2
12	5.0	49	52.7	240	5.0	41	74.6
24	6.0	28	47.3	240	4.5	11	53.3
24	5.5	33	44.6	240	4.0	5	21.4
24	5.0	40	55.9	240	3.5	17	55.4
48	6.0	30	54.5	264	5.5	9	19.0
48	5.5	28	67.1	264	5.0	12	22.3
48	5.0	22	54.7	264	4.5	11	15.3
48	4.5	78	118	264	4.0	61	76.7
72	5.5	21	43.7	264	3.5	78	89.0
72	5.0	21	39.9	288	5.5	23	27.3
72	4.5	23	68.6	288	5.0	32	49.9
96	5.5	20	47.2	288	4.5	15	28.3
96	5.0	19	65.2	288	3.5	58	62.0
96	4.5	25	64.7	312	5.5	15	33.1
120	5.5	15	33.1	312	5.0	16	24.9
120	5.0	14	45.1	312	4.5	16	33.8
120	4.5	19	53.9	312	4.0	41	55.2
120	4.0	58	198	312	3.5	111	120.0
144	5.5	11	33.7	336	5.5	8	27.2
144	5.0	25	57.6	336	5.0	8	16.4
144	4.5	17	42.8	336	4.5	11	27.9
144	4.0	46	80.3	336	4.0	32	44.1
168	5.5	20	63.1	336	3.5	8	24.6
168	5.0	25	61.4	360	5.5	9	23.4
168	4.5	22	48.6	360	5.0	32	27.8
168	4.0	35	27.5	360	4.5	5	26.8
192	5.5	10	59.6	360	4.0	27	42.6
192	5.0	19	66.7	360	3.5	37	49.1

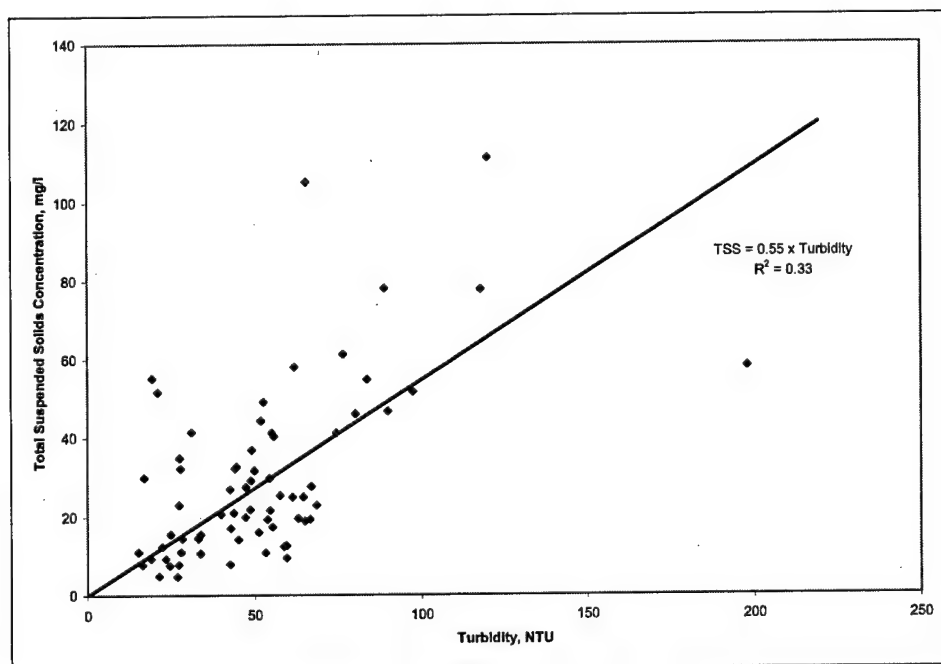


Figure G8. TSS versus turbidity curve

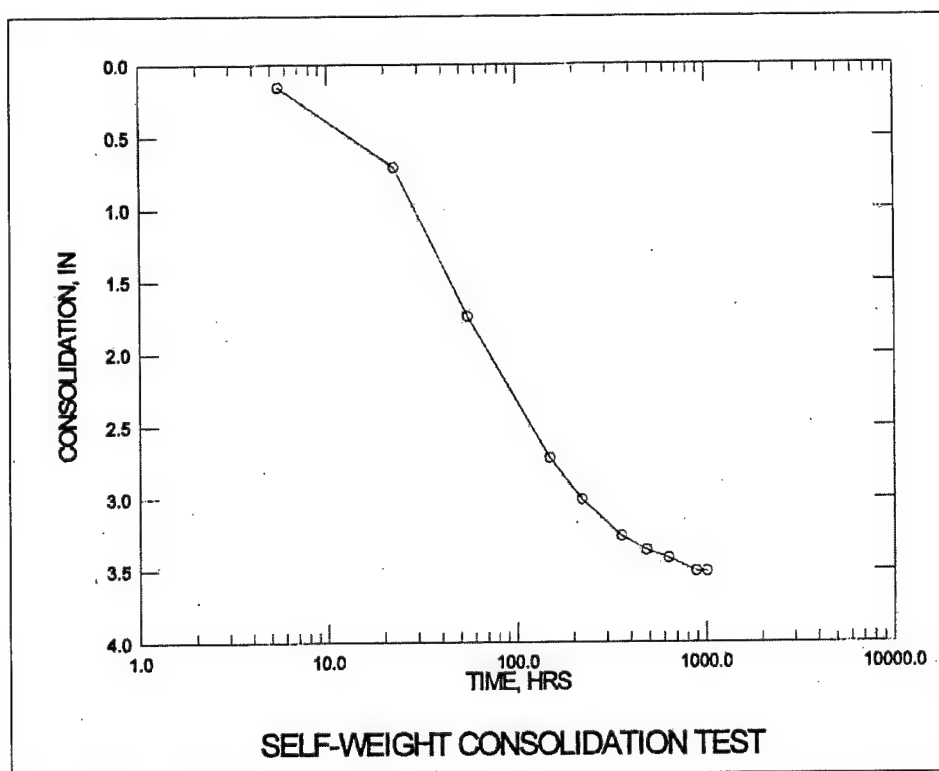


Figure G9. Self-weight consolidation test results for Pascagoula sediment

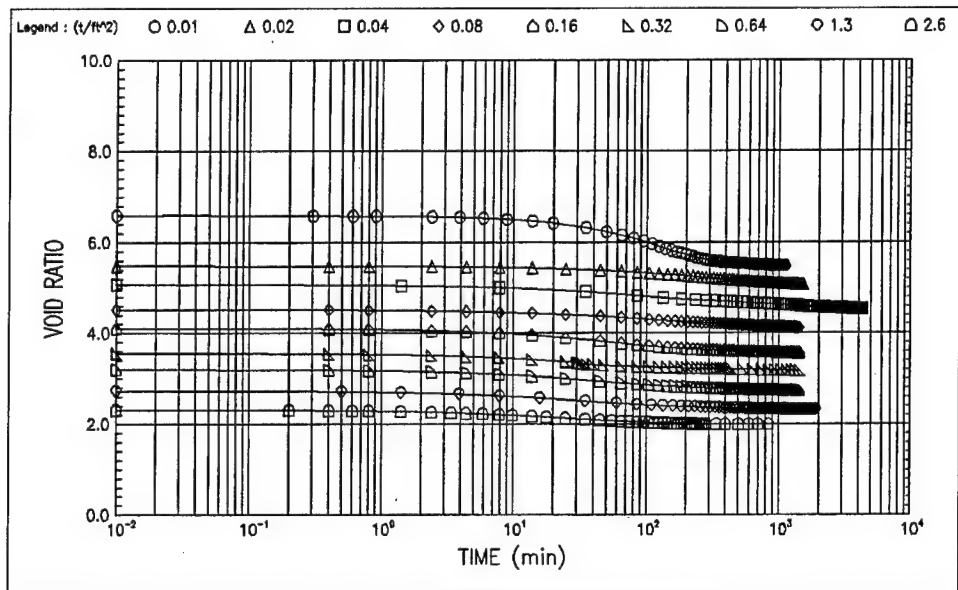


Figure G10. Time curves from standard oedometer consolidation test

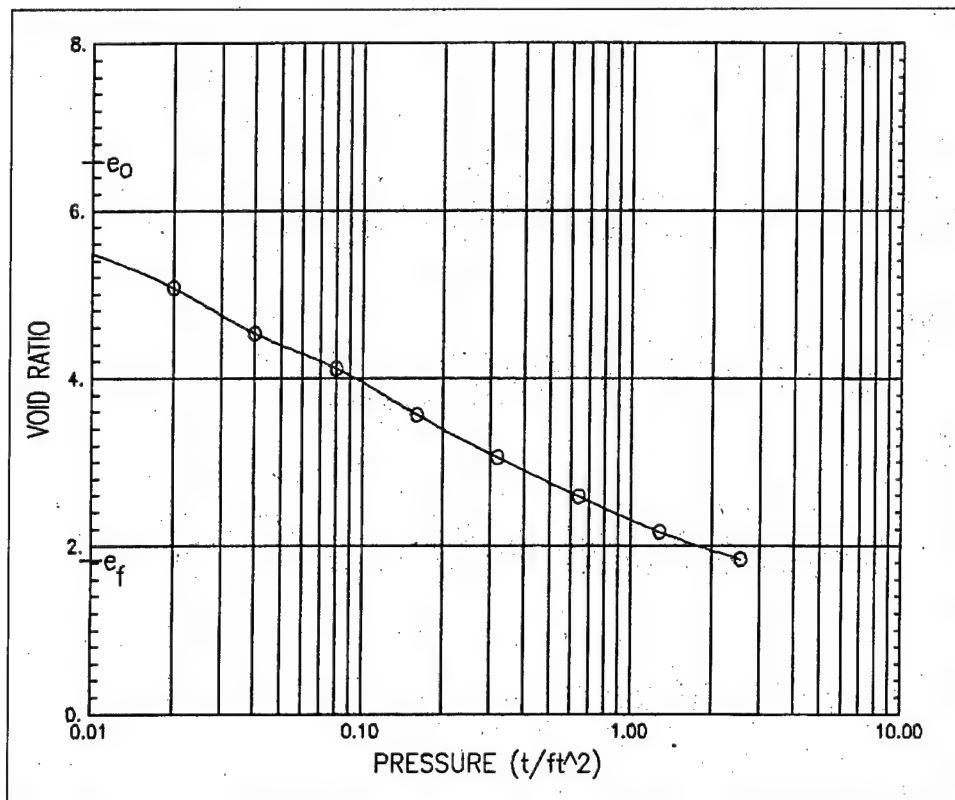


Figure G11. Void ratio-effective stress relationship from standard oedometer consolidation test

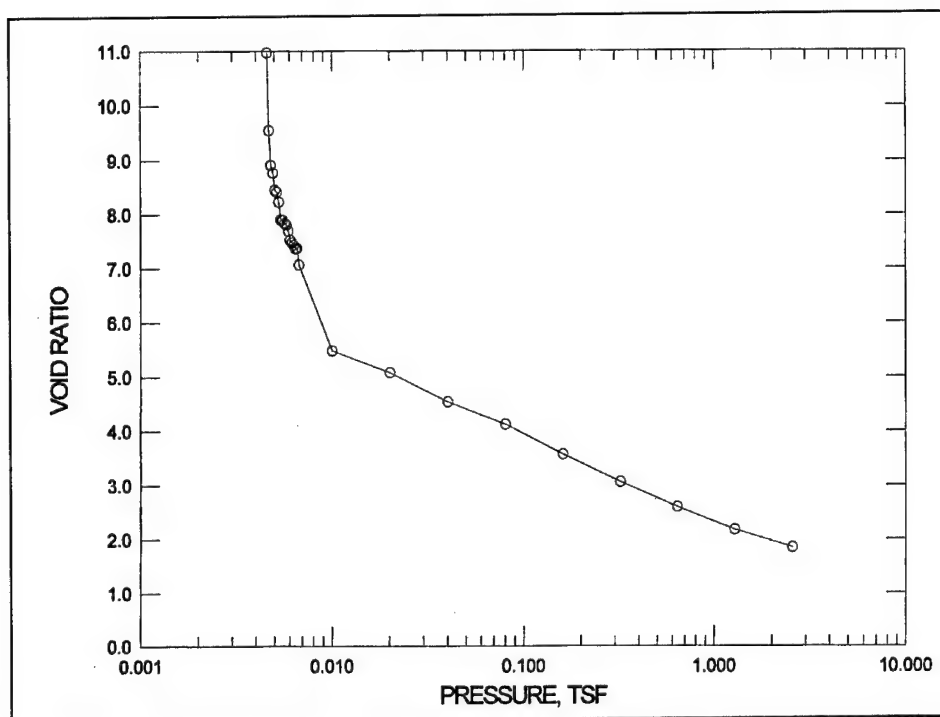


Figure G12. Combined void ratio-effective stress relationship

Conclusions

Based on the result of the settling tests, consolidation tests, and turbidity measurements, it is concluded that:

- a. Dredged material from the Pascagoula site is primarily fine-grained silt/clay with a trace of sand. The dredged material has high plasticity and is highly compressible.
- b. The Pascagoula sediment exhibited zone settling. The zone settling velocity was 0.226 ft/hr.
- c. The suspended solids concentration in the supernatant under quiescent settling conditions falls below 25 mg/L in 10 days and below 20 mg/L in 13 days.
- d. The curve developed for the correlation between TSS and turbidity has a correlation coefficient of 0.55. This allows a rapid estimation of TSS by simply multiplying the turbidity (NTU) by 0.55 to achieve TSS (mg/L). It should be noted that this is a rough approximation and should be used for no other reason than to estimate TSS.

References

- APHA-AWWA-WPCF. (1989). *Standard methods - for the examination of water and wastewater*. 17th ed., Washington, DC.
- Cargill, K. W. (1983). "Procedures for prediction of consolidation in soft fine-grained dredged material," Technical Report D-83-1, U.S. Army Engineer Waterways Experiment Station, Vicksburg, MS.
- Hayes, D. F., and Schroeder, P. R. (1992). "Documentation of the SETTLE Module for ADDAMS: Design of confined disposal facilities for solids retention and initial storage," Environmental Effects of Dredging Technical Notes EEDP-06-18, U.S. Army Engineer Waterways Experiment Station, Vicksburg, MS.
- Headquarters, U.S. Army Corps of Engineers. (1970). "Laboratory soils testing," Engineer Manual EM 1110-2-1906, Washington, DC.
- _____. (1987). "Confined disposal of dredged material," Engineer Manual 1110-2-5027, Washington, DC.
- Palermo, M. R., Montgomery, R. L., and Poindexter, M. E. (1978). "Guidelines for designing, operating, and managing dredged material containment areas," Technical Report DS-78-10, U.S. Army Engineer Waterways Experiment Station, Vicksburg, MS.
- Palermo, M. R., and Thackston, E. L. (1988). "Refinement of column settling test procedures for estimating the quality of effluent from confined dredged material disposal areas," Technical Report D-88-9, U.S. Army Engineer Waterways Experiment Station, Vicksburg, MS.
- Palermo, M. R. (1985). "Interim guidance for predicting quality of effluent discharged from confined dredged material disposal areas," Environmental Effects of Dredging Programs Technical Notes EEDP-0201 through 4, U.S. Army Engineer Waterways Experiment Station, Vicksburg, MS.
- Schroeder, P. R., and Palermo, M. R. (1995). "The Automated Dredging and Disposal Alternatives Management System (ADDAMS)," Environmental Effects of Dredging Programs Technical Note EEDP-06-12, U.S. Army Engineer Waterways Experiment Station, Vicksburg, MS.
- Shields, D. F., Schroeder, P. R., and Thackston, E. L. (1987). "Design and management of dredged material containment areas to improve hydraulic performance," Technical Report D-87-2, U.S. Army Engineer Waterways Experiment Station, Vicksburg, MS.

Appendix H

Additional Calibration and Verification Comparisons

This appendix presents additional calibration and verification comparisons that were not included in the main text of Chapter 5, "3-D Circulation Model Studies (CH3D)." Additional comparisons are given for the meteorological validation for February-March 2001 and for the validation of temperature and salinity for April-September 1997.

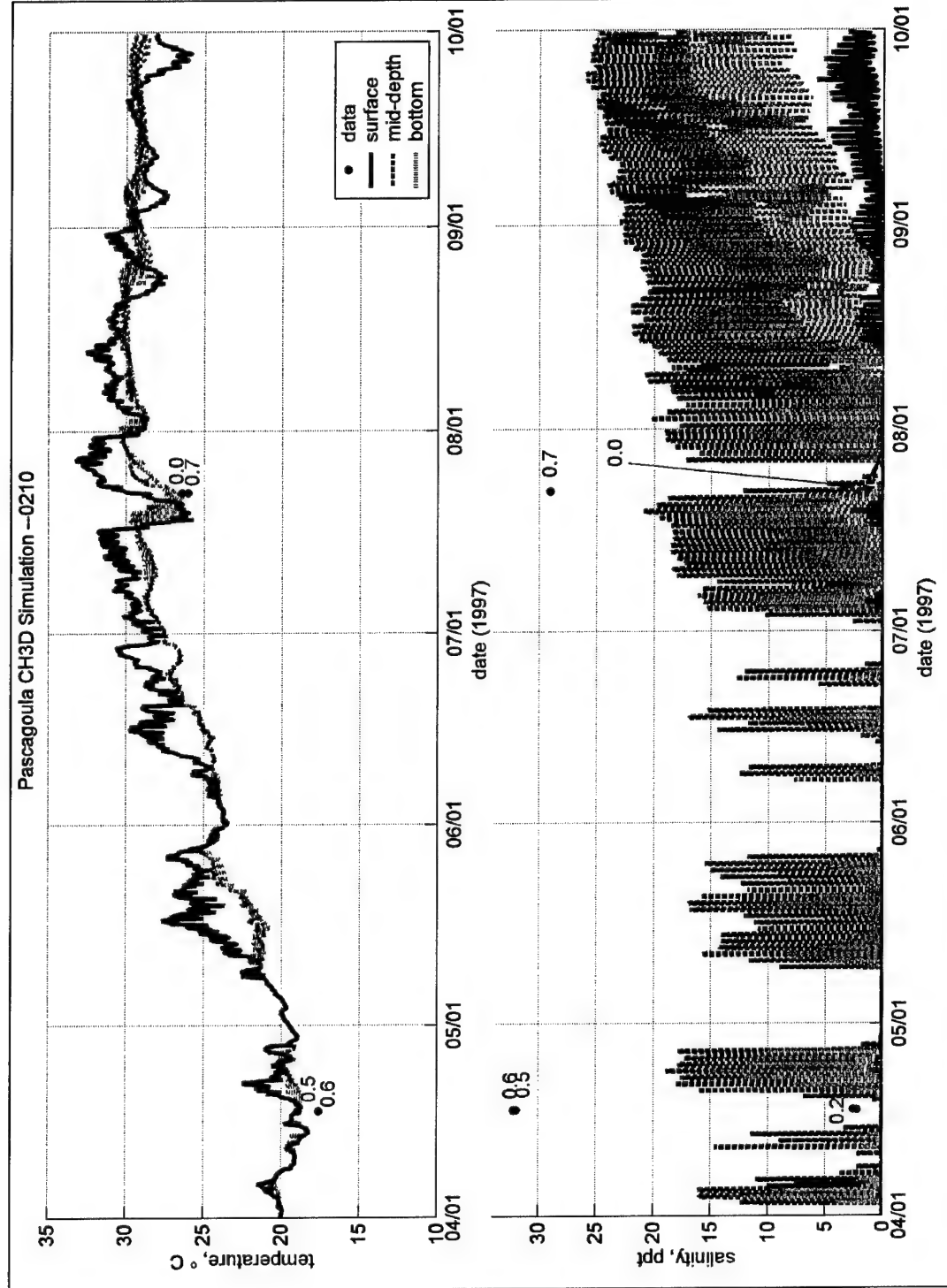


Figure H1. Comparison of measured and modeled temperature and salinity at sta 0210 (Figure 5-6). Points are measured data, solid line represents surface layer of CH3D, and green-dashed and red-dotted lines represent mid-depth and bottom layers of CH3D, respectively. Annotated values assigned to data points indicate normalized position in water column. 0= surface, 1= bottom

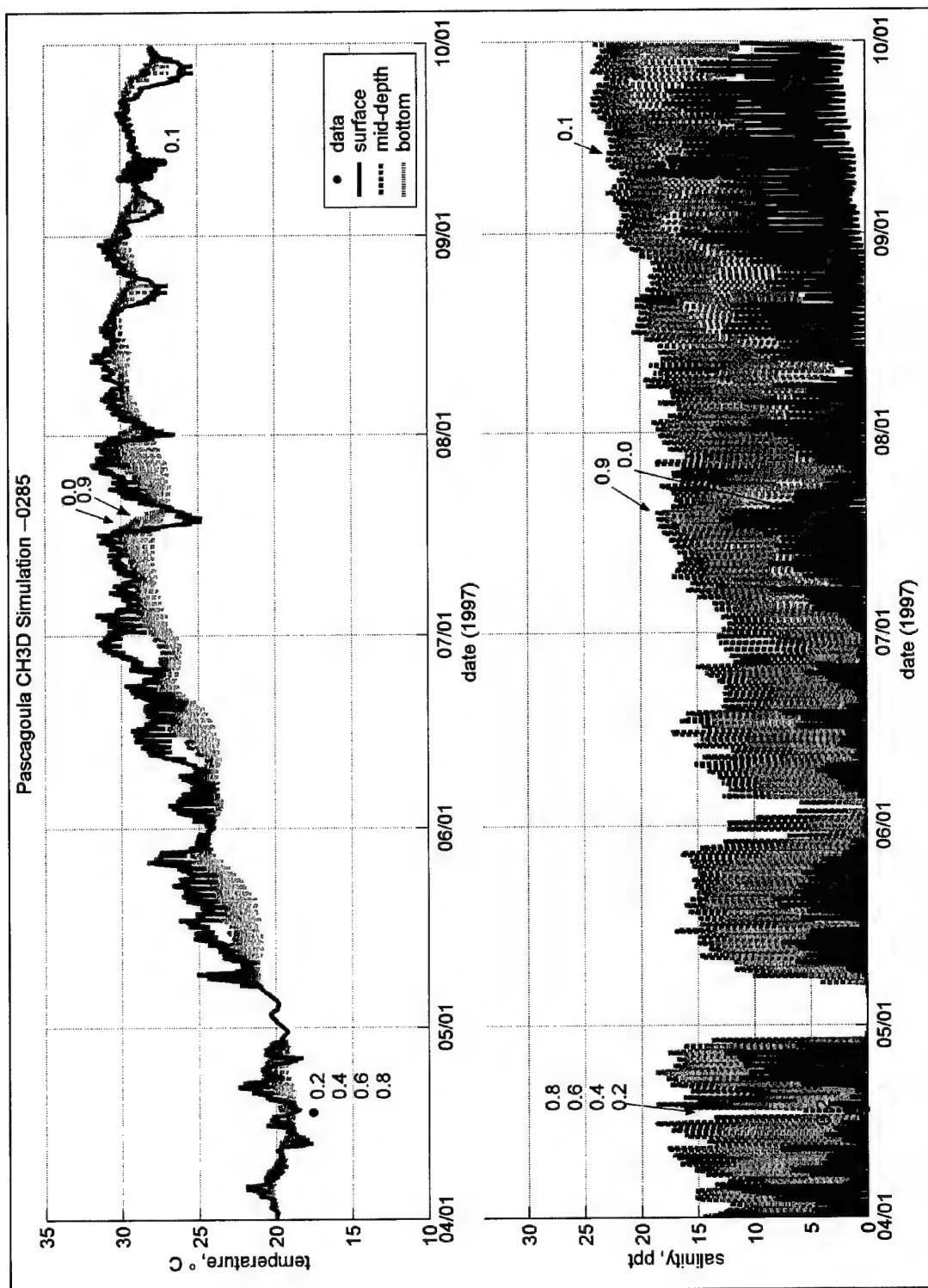


Figure H2. Comparison of measured and modeled temperature and salinity at sta 0285 (Figure 5-6). Points are measured data, solid line represents surface layer of CH3D, and green-dashed and red-dotted lines represent middepth and bottom layers of CH3D, respectively. Annotated values assigned to data points indicate normalized position in water column. 0= surface, 1= bottom

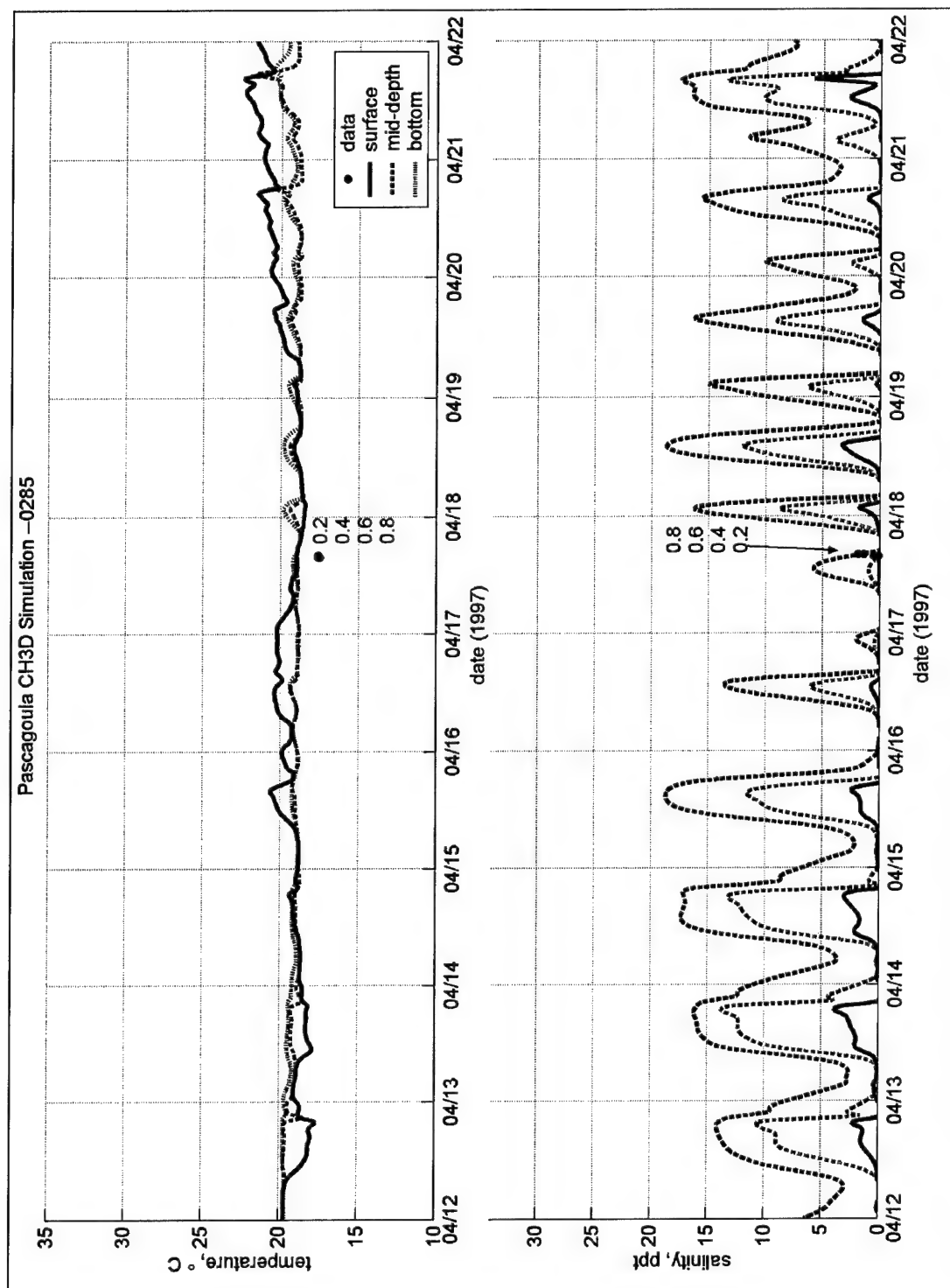


Figure H3. Comparison of measured and modeled temperature and salinity at sta 0285 (Figure 5-6) during April 1997. Points are measured data, solid line represents surface layer of CH3D, and green-dashed and red-dotted lines represent middepth and bottom layers of CH3D, respectively. Annotated values assigned to data points indicate normalized position in water column. 0= surface, 1= bottom

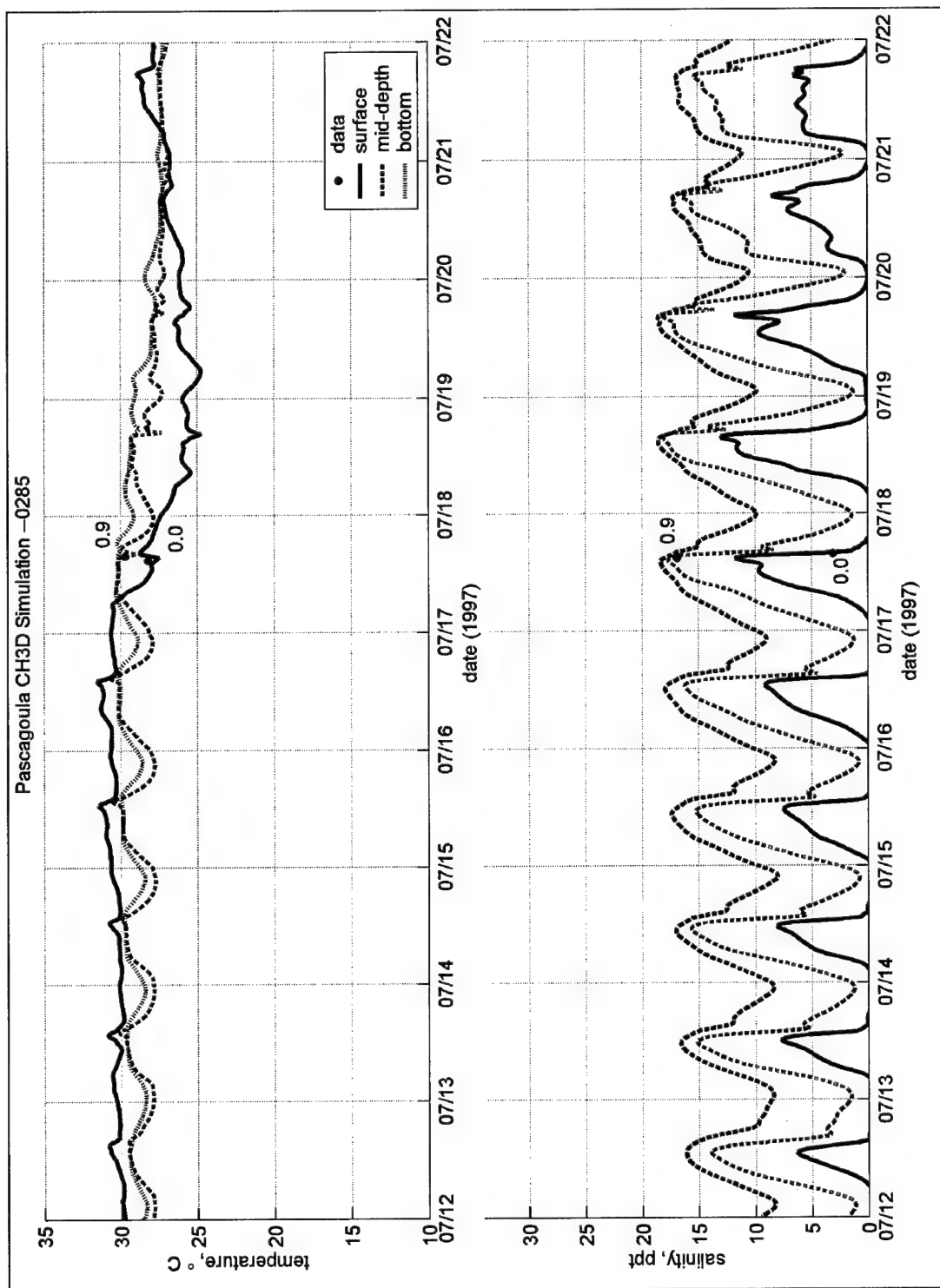


Figure H4. Comparison of measured and modeled temperature and salinity at sta 0285 (Figure 5-6) during July 1997. Points are measured data, solid line represents surface layer of CH3D, and green-dashed and red-dotted lines represent mid-depth and bottom layers of CH3D, respectively. Annotated values assigned to data points indicate normalized position in water column. 0 = surface, 1 = bottom

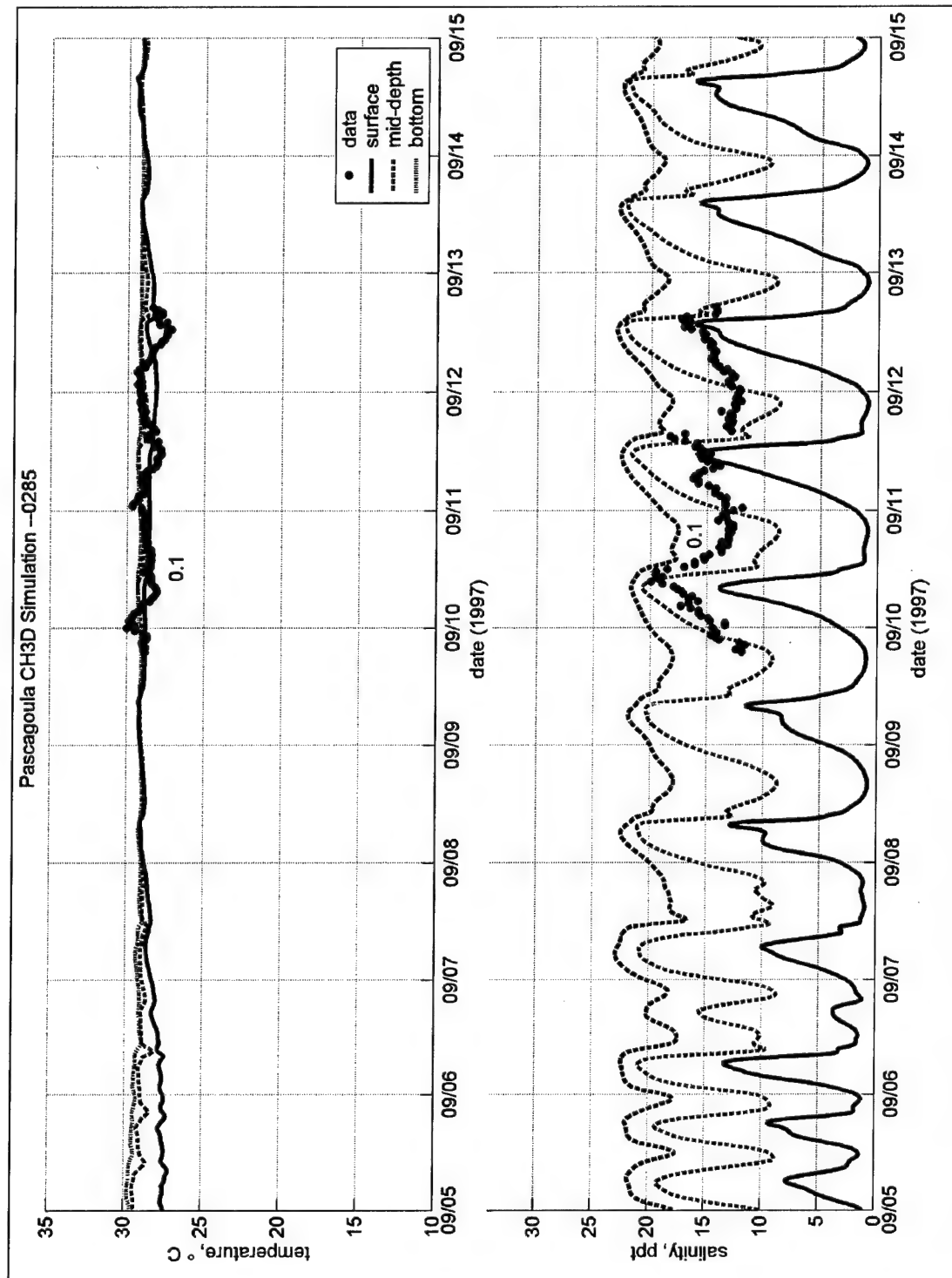


Figure H5. Comparison of measured and modeled temperature and salinity at sta 0285 (Figure 5-6) during September 1997. Points represent measured data, solid line represents surface layer of CH3D, and green-dashed and red-dotted lines represent middepth and bottom layers of CH3D, respectively. Annotated values assigned to data points indicate normalized position in water column. 0 = surface, 1 = bottom

Appendix I

CH3D Grid Representation of Island Alternatives

This appendix presents the CH3D grid representation of the three island alternatives simulated for this study. Each alternative consists of a single dredged material disposal island covering an area of approximately 1,000 acres.¹ The grids were boundary-fitted where practical to the margins of the proposed islands, and grid stepping was utilized where boundary-fitting was not possible. Alternative 01 is represented as a quarter-circular arc, expanding Singing River Island to the southwest. Alternative 02 is a circular island located south-southeast of Singing River Island. Alternative 03 is a circular island located in the triangle of the Bayou Casotte and Pascagoula River navigation channels.

¹ A table of factors for converting non-SI to SI units of measurement is presented on page xvii.

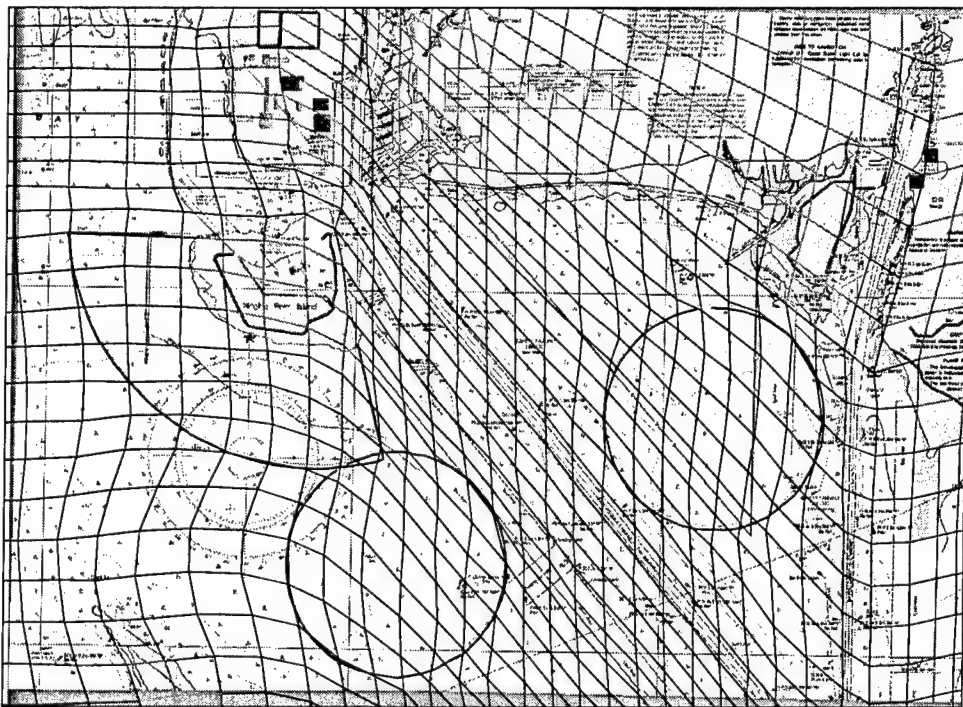


Figure 11 Alternative 00, present conditions with island boundaries outlined in red

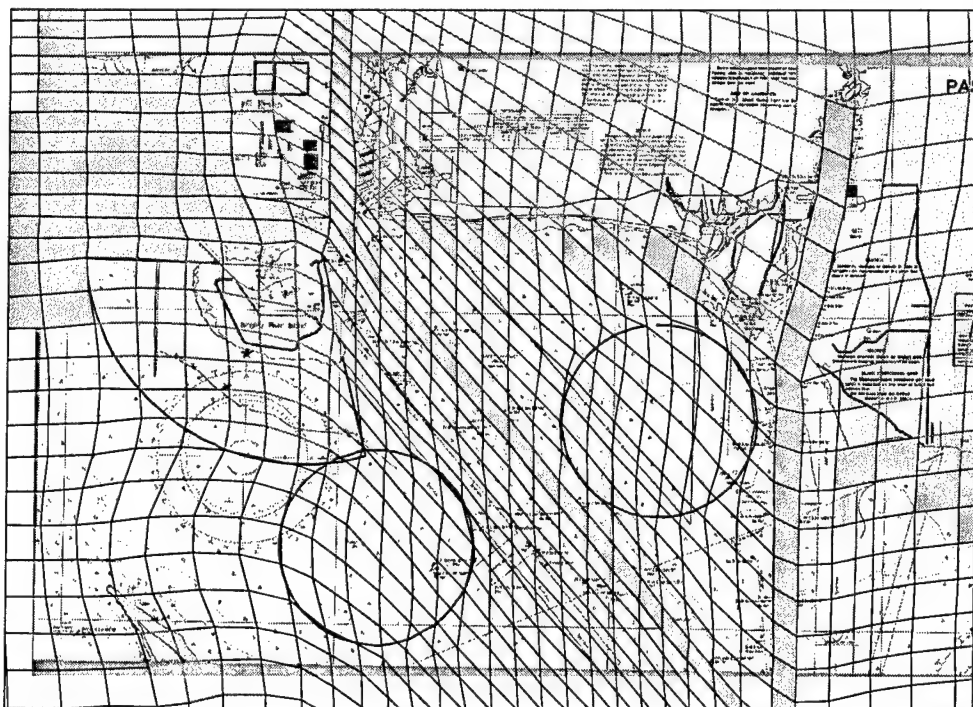


Figure 12. Alternative 01, Singing River extension

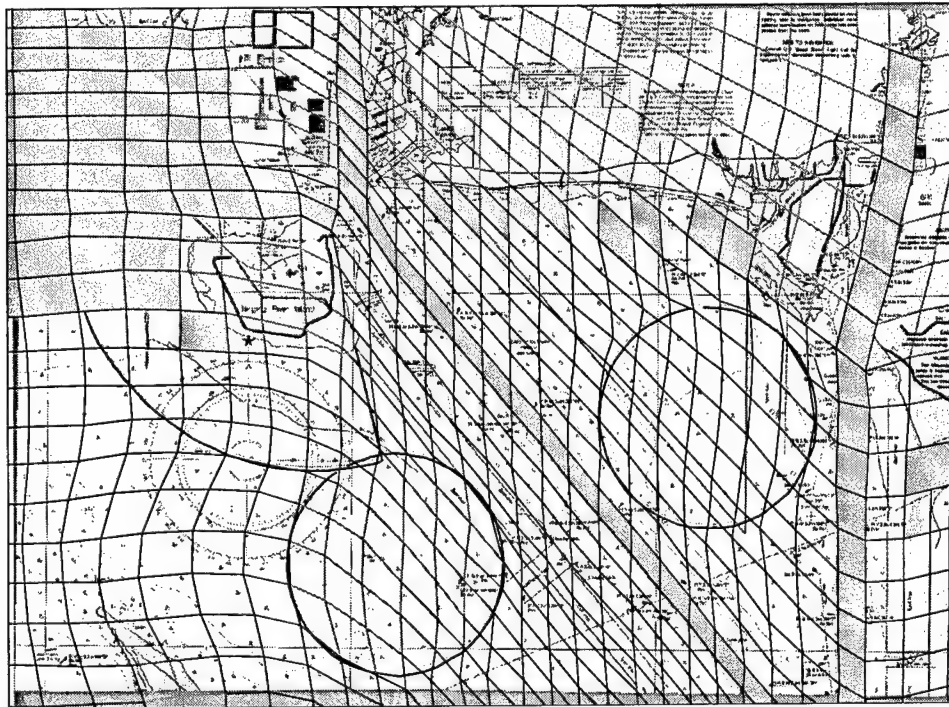


Figure I3. Alternative 02, Island south of Singing River

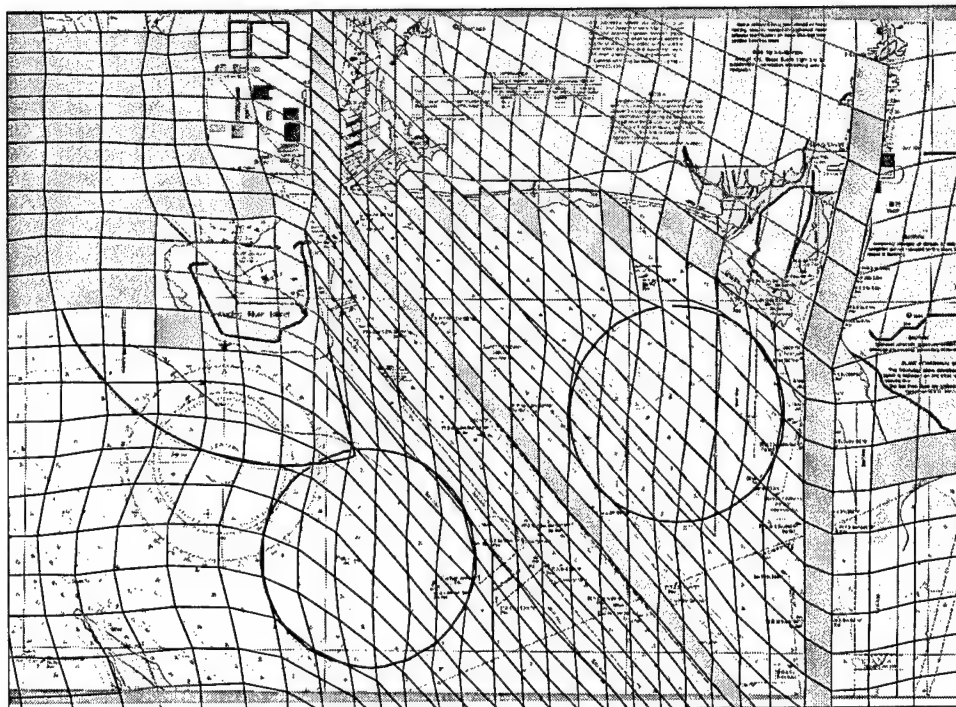


Figure I4. Alternative 03, Island in triangle between Pascagoula and Bayou Casotte navigation channels

Appendix J

Hindcast Wave Information Products at CDF Sites

WIS HINDCAST for PASCAGOULA 1990 - 1999
LAT: 30.30 N, LONG: 88.57 W, DEPTH: 3 M
SUMMARY OF WAVE INFORMATION BY MONTH

STATION: 10

OCCURRENCES OF WAVE HEIGHT BY MONTH FOR ALL YEARS

Hmo (m)	JAN	FEB	MAR	APR	MAY	JUN	JUL	AUG	SEP	OCT	NOV	DEC	TOTAL
0.00 - 0.49	3608	3495	3398	2798	4322	4755	6227	6642	5141	4514	4186	3950	53036
0.50 - 0.99	2919	2222	2623	3073	2544	2177	1007	685	1646	2359	2326	2817	26398
1.00 - 1.49	824	906	1262	1235	514	264	190	89	368	486	607	609	7354
1.50 - 1.99	88	145	157	94	60	4	16	24	45	81	81	64	859
2.00 - 2.49	0
2.50 - 2.99	0
3.00 - 3.49	0
3.50 - 3.99	0
4.00 - 4.49	0
4.50 - 4.99	0
5.00 - GREATER	0
TOTAL	7439	6768	7440	7200	7440	7200	7440	7440	7200	7440	7200	7440	87647

WIS HINDCAST for PASCAGOULA 1990 - 1999
LAT: 30.30 N, LONG: 88.57 W, DEPTH: 3 M
SUMMARY OF WAVE INFORMATION BY MONTH

STATION: 10

OCCURRENCES OF PEAK PERIOD BY MONTH FOR ALL YEARS

TP(sec)	JAN	FEB	MAR	APR	MAY	JUN	JUL	AUG	SEP	OCT	NOV	DEC	TOTAL
3.0 - 3.9	1275	1417	1260	921	996	724	776	1484	1684	2074	2130	1871	16612
4.0 - 4.9	383	433	577	362	903	1524	1580	1340	841	678	344	592	9557
5.0 - 5.9	683	874	933	1025	1675	1509	1844	1540	1147	632	707	785	13354
6.0 - 6.9	1394	1315	1242	1955	2062	2224	1466	1526	1700	969	937	1254	18044
7.0 - 7.9	1637	1033	1485	1887	1291	967	949	879	780	986	1195	1199	14288
8.0 - 8.9	881	908	1091	740	376	187	549	373	424	689	774	955	7947
9.0 - 9.9	638	513	538	261	108	22	207	188	234	537	503	510	4259
10.0 - 10.9	375	178	241	23	29	10	65	73	223	366	378	195	2156
11.0 - 13.9	173	97	73	26	.	33	4	37	160	495	229	70	1397
14.0 - LONGER	7	14	3	9	33
TOTAL	7439	6768	7440	7200	7440	7200	7440	7440	7200	7440	7200	7440	87647

WIS HINDCAST for PASCAGOULA 1990 - 1999
LAT: 30.30 N, LONG: 88.57 W, DEPTH: 3 M
SUMMARY OF WAVE INFORMATION BY MONTH

STATION: 10

OCCURRENCES OF MEAN DIRECTION BY MONTH FOR ALL YEARS

Dp(deg) DIRECTION BAND & CENTER	JAN	FEB	MAR	APR	MAY	JUN	JUL	AUG	SEP	OCT	NOV	DEC	TOTAL
348.75 - 11.24 (0.0)	291	281	225	135	124	193	165	319	296	390	470	425	3314
11.25 - 33.74 (22.5)	260	157	120	139	130	114	104	349	392	438	472	354	3029
33.75 - 56.24 (45.0)	303	240	232	156	214	187	135	418	614	640	526	342	4007
56.25 - 78.74 (67.5)	216	225	122	137	185	158	67	391	498	435	356	315	3105
78.75 - 101.24 (90.0)	623	635	541	318	472	382	155	775	977	1173	954	755	7760
101.25 - 123.74 (112.5)	450	385	401	324	361	232	211	258	396	410	414	446	4288
123.75 - 146.24 (135.0)	241	163	233	189	386	263	253	251	355	133	172	163	2802
146.25 - 168.74 (157.5)	1073	636	825	1033	1000	787	435	347	706	850	705	1054	9451
168.75 - 191.24 (180.0)	3266	3260	3770	4117	3329	2840	1988	1016	1798	2191	2577	2889	33041
191.25 - 213.74 (202.5)	88	49	62	112	158	297	232	225	111	78	48	114	1574
213.75 - 236.24 (225.0)	66	79	174	120	283	533	547	398	136	92	74	52	2554
236.25 - 258.74 (247.5)	88	111	136	65	179	413	630	458	181	79	55	37	2432
258.75 - 281.24 (270.0)	124	157	140	123	232	324	1035	753	219	114	46	56	3323
281.25 - 303.74 (292.5)	83	104	148	65	148	180	664	671	170	85	67	117	2502
303.75 - 326.24 (315.0)	122	121	165	95	144	147	568	521	180	129	106	142	2440
326.25 - 348.74 (337.5)	145	165	146	72	95	150	251	290	171	203	158	179	2025
TOTAL	7439	6768	7440	7200	7440	7200	7440	7440	7200	7440	7200	7440	87647

WIS HINDCAST for PASCAGOULA 1990 - 1999
LAT: 30.30 N, LONG: 88.57 W, DEPTH: 3 M
OCCURRENCES OF WAVE HEIGHT AND PEAK PERIOD FOR 22.5-DEG DIRECTION BANDS
STATION: 10
(348.75 - 11.24) 0.0 DEG

Hmo (m)	Tp (sec)										TOTAL
	3.0- 3.9	4.0- 4.9	5.0- 5.9	6.0- 6.9	7.0- 7.9	8.0- 8.9	9.0- 9.9	10.0- 10.9	11.0- 13.9	14.0- LONGER	
0.00 - 0.49	617	223	337	707	604	391	238	110	85	1	3313
0.50 - 0.99	1	1
1.00 - 1.49	0
1.50 - 1.99	0
2.00 - 2.49	0
2.50 - 2.99	0
3.00 - 3.49	0
3.50 - 3.99	0
4.00 - 4.49	0
4.50 - 4.99	0
5.00 - GREATER	0
TOTAL	618	223	337	707	604	391	238	110	85	1	3314

WIS HINDCAST for PASCAGOULA 1990 - 1999

LAT: 30.30 N, LONG: 88.57 W, DEPTH: 3 M

STATION: 10

(11.25 - 33.74) 22.5 DEG

Hmo (m)	Tp(sec)										TOTAL
	3.0-	4.0-	5.0-	6.0-	7.0-	8.0-	9.0-	10.0-	11.0-	14.0-	
	3.9	4.9	5.9	6.9	7.9	8.9	9.9	10.9	13.9	LONGER	
0.00 - 0.49	663	160	391	588	529	335	158	108	86	3	3021
0.50 - 0.99	8	8
1.00 - 1.49	0
1.50 - 1.99	0
2.00 - 2.49	0
2.50 - 2.99	0
3.00 - 3.49	0
3.50 - 3.99	0
4.00 - 4.49	0
4.50 - 4.99	0
5.00 - GREATER	0
TOTAL	671	160	391	588	529	335	158	108	86	3	3029

WIS HINDCAST for PASCAGOULA 1990 - 1999

LAT: 30.30 N, LONG: 88.57 W, DEPTH: 3 M

STATION: 10

(33.75 - 56.24) 45.0 DEG

Hmo (m)	Tp(sec)										TOTAL
	3.0-	4.0-	5.0-	6.0-	7.0-	8.0-	9.0-	10.0-	11.0-	14.0-	
	3.9	4.9	5.9	6.9	7.9	8.9	9.9	10.9	13.9	LONGER	
0.00 - 0.49	1386	211	463	552	514	411	169	99	105	.	3910
0.50 - 0.99	97	97
1.00 - 1.49	0
1.50 - 1.99	0
2.00 - 2.49	0
2.50 - 2.99	0
3.00 - 3.49	0
3.50 - 3.99	0
4.00 - 4.49	0
4.50 - 4.99	0
5.00 - GREATER	0
TOTAL	1483	211	463	552	514	411	169	99	105	0	4007

WIS HINDCAST for PASCAGOULA 1990 - 1999

LAT: 30.30 N, LONG: 88.57 W, DEPTH: 3 M

STATION: 10

(56.25 - 78.74) 67.5 DEG

HmO (m)	Tp(sec)										TOTAL
	3.0-	4.0-	5.0-	6.0-	7.0-	8.0-	9.0-	10.0-	11.0-	14.0-	
	3.9	4.9	5.9	6.9	7.9	8.9	9.9	10.9	13.9	LONGER	
0.00 - 0.49	1212	189	287	485	356	252	113	70	73	.	3037
0.50 - 0.99	68	68
1.00 - 1.49	0
1.50 - 1.99	0
2.00 - 2.49	0
2.50 - 2.99	0
3.00 - 3.49	0
3.50 - 3.99	0
4.00 - 4.49	0
4.50 - 4.99	0
5.00 - GREATER	0
TOTAL	1280	189	287	485	356	252	113	70	73	0	3105

WIS HINDCAST for PASCAGOULA 1990 - 1999

LAT: 30.30 N, LONG: 88.57 W, DEPTH: 3 M

STATION: 10

(78.75 - 101.24) 90.0 DEG

Hmo (m)	Tp(sec)										TOTAL
	3.0-	4.0-	5.0-	6.0-	7.0-	8.0-	9.0-	10.0-	11.0-	14.0-	
	3.9	4.9	5.9	6.9	7.9	8.9	9.9	10.9	13.9	LONGER	
0.00 - 0.49	2679	224	418	514	457	205	139	104	58		4798
0.50 - 0.99	2310	592	45	2947
1.00 - 1.49	.	.	12	3	15
1.50 - 1.99	0
2.00 - 2.49	0
2.50 - 2.99	0
3.00 - 3.49	0
3.50 - 3.99	0
4.00 - 4.49	0
4.50 - 4.99	0
5.00 - GREATER	0
TOTAL	4989	816	475	517	457	205	139	104	58	0	7760

WIS HINDCAST for PASCAGOULA 1990 - 1999

LAT: 30.30 N, LONG: 88.57 W, DEPTH: 3 M

STATION: 10

(101.25 - 123.74) 112.5 DEG

Hmo (m)	Tp(sec)										TOTAL
	3.0-	4.0-	5.0-	6.0-	7.0-	8.0-	9.0-	10.0-	11.0-	14.0-	
	3.9	4.9	5.9	6.9	7.9	8.9	9.9	10.9	13.9	LONGER	
0.00 - 0.49	1442	266	286	407	329	199	80	69	26	.	3104
0.50 - 0.99	1096	71	13	1180
1.00 - 1.49	.	.	.	4	4
1.50 - 1.99	0
2.00 - 2.49	0
2.50 - 2.99	0
3.00 - 3.49	0
3.50 - 3.99	0
4.00 - 4.49	0
4.50 - 4.99	0
5.00 - GREATER	0
TOTAL	2538	337	299	411	329	199	80	69	26	0	4288

WIS HINDCAST for PASCAGOULA 1990 - 1999

LAT: 30.30 N, LONG: 88.57 W, DEPTH: 3 M

STATION: 10

(123.75 - 146.24) 135.0 DEG

Hmo (m)	Tp(sec)										TOTAL
	3.0-	4.0-	5.0-	6.0-	7.0-	8.0-	9.0-	10.0-	11.0-	14.0-	
	3.9	4.9	5.9	6.9	7.9	8.9	9.9	10.9	13.9	LONGER	
0.00 - 0.49	775	383	400	437	278	185	105	68	23	.	2654
0.50 - 0.99	86	13	24	20	143
1.00 - 1.49	5	5
1.50 - 1.99	0
2.00 - 2.49	0
2.50 - 2.99	0
3.00 - 3.49	0
3.50 - 3.99	0
4.00 - 4.49	0
4.50 - 4.99	0
5.00 - GREATER	0
TOTAL	861	396	424	457	283	185	105	68	23	0	2802

WIS HINDCAST for PASCAGOULA 1990 - 1999

LAT: 30.30 N, LONG: 88.57 W, DEPTH: 3 M

STATION: 10

(146.25 - 168.74) 157.5 DEG

HmO (m)	Tp(sec)										TOTAL
	3.0-	4.0-	5.0-	6.0-	7.0-	8.0-	9.0-	10.0-	11.0-	14.0-	
	3.9	4.9	5.9	6.9	7.9	8.9	9.9	10.9	13.9	LONGER	
0.00 - 0.49	597	884	735	688	326	208	126	67	53	.	3684
0.50 - 0.99	23	209	1110	1558	1410	393	107	112	37	.	4959
1.00 - 1.49	.	.	.	40	266	279	147	47	10	.	789
1.50 - 1.99	1	11	7	.	.	19
2.00 - 2.49	0
2.50 - 2.99	0
3.00 - 3.49	0
3.50 - 3.99	0
4.00 - 4.49	0
4.50 - 4.99	0
5.00 - GREATER	0
TOTAL	620	1093	1845	2286	2002	881	391	233	100	0	9451

WIS HINDCAST for PASCAGOULA 1990 - 1999

LAT: 30.30 N, LONG: 88.57 W, DEPTH: 3 M

STATION: 10

(168.75 - 191.24) 180.0 DEG

Hmo (m)	Tp (sec)										TOTAL
	3.0-	4.0-	5.0-	6.0-	7.0-	8.0-	9.0-	10.0-	11.0-	14.0-	
	3.9	4.9	5.9	6.9	7.9	8.9	9.9	10.9	13.9	LONGER	
0.00 - 0.49	521	1857	1560	1631	1412	1037	429	189	118	10	8764
0.50 - 0.99	18	1144	4444	5153	3098	1473	876	452	235	3	16896
1.00 - 1.49	.	.	48	1376	2412	1370	703	319	306	7	6541
1.50 - 1.99	.	.	.	24	240	227	212	97	40	.	840
2.00 - 2.49	0
2.50 - 2.99	0
3.00 - 3.49	0
3.50 - 3.99	0
4.00 - 4.49	0
4.50 - 4.99	0
5.00 - GREATER	0
TOTAL	539	3001	6052	8184	7162	4107	2220	1057	699	20	33041

WIS HINDCAST for PASCAGOULA 1990 - 1999

LAT: 30.30 N, LONG: 88.57 W, DEPTH: 3 M

STATION: 10

(191.25 - 213.74) 202.5 DEG

Hmo (m)	Tp(sec)										TOTAL
	3.0-	4.0-	5.0-	6.0-	7.0-	8.0-	9.0-	10.0-	11.0-	14.0-	
	3.9	4.9	5.9	6.9	7.9	8.9	9.9	10.9	13.9	LONGER	
0.00 - 0.49	266	370	257	360	136	89	71	18	5	.	1572
0.50 - 0.99	.	.	2	2
1.00 - 1.49	0
1.50 - 1.99	0
2.00 - 2.49	0
2.50 - 2.99	0
3.00 - 3.49	0
3.50 - 3.99	0
4.00 - 4.49	0
4.50 - 4.99	0
5.00 - GREATER	0
TOTAL	266	370	259	360	136	89	71	18	5	0	1574

WIS HINDCAST for PASCAGOULA 1990 - 1999

LAT: 30.30 N, LONG: 88.57 W, DEPTH: 3 M

STATION: 10

(213.75 - 236.24) 225.0 DEG

Hmo (m)	Tp (sec)										TOTAL
	3.0-	4.0-	5.0-	6.0-	7.0-	8.0-	9.0-	10.0-	11.0-	14.0-	
	3.9	4.9	5.9	6.9	7.9	8.9	9.9	10.9	13.9	LONGER	
0.00 - 0.49	342	724	428	559	246	136	94	16	9	.	2554
0.50 - 0.99	0
1.00 - 1.49	0
1.50 - 1.99	0
2.00 - 2.49	0
2.50 - 2.99	0
3.00 - 3.49	0
3.50 - 3.99	0
4.00 - 4.49	0
4.50 - 4.99	0
5.00 - GREATER	0
TOTAL	342	724	428	559	246	136	94	16	9	0	2554

WIS HINDCAST for PASCAGOULA 1990 - 1999

LAT: 30.30 N, LONG: 88.57 W, DEPTH: 3 M

STATION: 10

(236.25 - 258.74) 247.5 DEG

Hmo (m)	Tp (sec)										TOTAL
	3.0-	4.0-	5.0-	6.0-	7.0-	8.0-	9.0-	10.0-	11.0-	14.0-	
	3.9	4.9	5.9	6.9	7.9	8.9	9.9	10.9	13.9	LONGER	
0.00 - 0.49	372	605	402	584	232	119	75	31	12	.	2432
0.50 - 0.99	0
1.00 - 1.49	0
1.50 - 1.99	0
2.00 - 2.49	0
2.50 - 2.99	0
3.00 - 3.49	0
3.50 - 3.99	0
4.00 - 4.49	0
4.50 - 4.99	0
5.00 - GREATER	0
TOTAL	372	605	402	584	232	119	75	31	12	0	2432

WIS HINDCAST for PASCAGOULA 1990 - 1999

LAT: 30.30 N, LONG: 88.57 W, DEPTH: 3 M

STATION: 10

(258.75 - 281.24) 270.0 DEG

Hmo (m)	Tp(sec)										TOTAL
	3.0-	4.0-	5.0-	6.0-	7.0-	8.0-	9.0-	10.0-	11.0-	14.0-	
	3.9	4.9	5.9	6.9	7.9	8.9	9.9	10.9	13.9	LONGER	
0.00 - 0.49	619	606	677	786	318	160	91	46	20	.	3323
0.50 - 0.99	0
1.00 - 1.49	0
1.50 - 1.99	0
2.00 - 2.49	0
2.50 - 2.99	0
3.00 - 3.49	0
3.50 - 3.99	0
4.00 - 4.49	0
4.50 - 4.99	0
5.00 - GREATER	0
TOTAL	619	606	677	786	318	160	91	46	20	0	3323

WIS HINDCAST for PASCAGOULA 1990 - 1999

LAT: 30.30 N, LONG: 88.57 W, DEPTH: 3 M

STATION: 10

(281.25 - 303.74) 292.5 DEG

Hmo (m)	Tp (sec)										TOTAL
	3.0-	4.0-	5.0-	6.0-	7.0-	8.0-	9.0-	10.0-	11.0-	14.0-	
	3.9	4.9	5.9	6.9	7.9	8.9	9.9	10.9	13.9	LONGER	
0.00 - 0.49	523	375	404	558	303	164	73	40	19	.	2459
0.50 - 0.99	24	19	43
1.00 - 1.49	0
1.50 - 1.99	0
2.00 - 2.49	0
2.50 - 2.99	0
3.00 - 3.49	0
3.50 - 3.99	0
4.00 - 4.49	0
4.50 - 4.99	0
5.00 - GREATER	0
TOTAL	547	394	404	558	303	164	73	40	19	0	2502

WIS HINDCAST for PASCAGOULA 1990 - 1999

LAT: 30.30 N, LONG: 88.57 W, DEPTH: 3 M

STATION: 10

(303.75 - 326.24) 315.0 DEG

Hmo (m)	Tp(sec)										TOTAL
	3.0-	4.0-	5.0-	6.0-	7.0-	8.0-	9.0-	10.0-	11.0-	14.0-	
	3.9	4.9	5.9	6.9	7.9	8.9	9.9	10.9	13.9	LONGER	
0.00 - 0.49	468	264	373	518	441	181	82	31	33	.	2391
0.50 - 0.99	49	49
1.00 - 1.49	0
1.50 - 1.99	0
2.00 - 2.49	0
2.50 - 2.99	0
3.00 - 3.49	0
3.50 - 3.99	0
4.00 - 4.49	0
4.50 - 4.99	0
5.00 - GREATER	0
TOTAL	517	264	373	518	441	181	82	31	33	0	2440

WIS HINDCAST for PASCAGOULA 1990 - 1999

LAT: 30.30 N, LONG: 88.57 W, DEPTH: 3 M

STATION: 10

(326.25 - 348.74) 337.5 DEG

Hmo (m)	Tp(sec)										TOTAL
	3.0-	4.0-	5.0-	6.0-	7.0-	8.0-	9.0-	10.0-	11.0-	14.0-	
	3.9	4.9	5.9	6.9	7.9	8.9	9.9	10.9	13.9	LONGER	
0.00 - 0.49	345	168	238	492	376	132	160	56	44	9	2020
0.50 - 0.99	5	5
1.00 - 1.49	0
1.50 - 1.99	0
2.00 - 2.49	0
2.50 - 2.99	0
3.00 - 3.49	0
3.50 - 3.99	0
4.00 - 4.49	0
4.50 - 4.99	0
5.00 - GREATER	0
TOTAL	350	168	238	492	376	132	160	56	44	9	2025

WIS HINDCAST for PASCAGOULA 1990 - 1999

LAT: 30.30 N, LONG: 88.57 W, DEPTH: 3 M

STATION: 10

ALL DIRECTIONS

Hmo (m)	Tp (sec)										TOTAL
	3.0-	4.0-	5.0-	6.0-	7.0-	8.0-	9.0-	10.0-	11.0-	14.0-	
	3.9	4.9	5.9	6.9	7.9	8.9	9.9	10.9	13.9	LONGER	
0.00 - 0.49	12827	7509	7656	9866	6857	4204	2203	1122	769	23	53036
0.50 - 0.99	3785	2048	5638	6731	4508	1866	983	564	272	3	26398
1.00 - 1.49	.	.	60	1423	2683	1649	850	366	316	7	7354
1.50 - 1.99	.	.	.	24	240	228	223	104	40	.	859
2.00 - 2.49	0
2.50 - 2.99	0
3.00 - 3.49	0
3.50 - 3.99	0
4.00 - 4.49	0
4.50 - 4.99	0
5.00 - GREATER	0
TOTAL	16612	9557	13354	18044	14288	7947	4259	2156	1397	33	87647

WIS HINDCAST for PASCAGOULA 1990 - 1999

LAT: 30.30 N, LONG: 88.57 W, DEPTH: 3 M

STATION: 10

OCCURRENCES OF WIND SPEED BY MONTH FOR ALL YEARS

WS(m/sec)	JAN	FEB	MAR	APR	MAY	JUN	JUL	AUG	SEP	OCT	NOV	DEC	TOTAL
0.00 - 1.99	82	89	137	97	160	163	83	228	116	86	116	122	1479
2.00 - 3.99	965	869	1152	968	1634	1930	2117	2775	1911	987	856	867	17031
4.00 - 5.99	1889	1824	1888	1946	2868	2992	3505	2873	2394	2015	1894	1968	28056
6.00 - 7.99	1867	1726	1968	2229	2036	1431	1425	1246	1414	1993	1996	2093	21424
8.00 - 9.99	1474	1226	1227	1486	547	560	203	209	933	1574	1401	1373	12213
10.00 - 11.99	778	681	713	438	162	124	55	63	316	457	680	693	5160
12.00 - 13.99	315	274	268	36	33	.	25	40	46	211	209	267	1724
14.00 - 15.99	64	70	57	.	.	.	7	6	17	101	48	51	421
16.00 - 17.99	5	9	10	.	.	.	16	.	17	7	.	6	70
18.00 - 19.99	.	.	20	.	.	.	4	.	36	9	.	.	69
20.00 - GREATER	0
TOTAL	7439	6768	7440	7200	7440	7200	7440	7440	7200	7440	7200	7440	87647

WIS HINDCAST for PASCAGOULA 1990 - 1999

LAT: 30.30 N, LONG: 88.57 W, DEPTH: 3 M

STATION: 10

OCCURRENCES OF WIND DIRECTION BY MONTH FOR ALL YEARS

WD(deg) DIRECTION BAND & CENTER	JAN	FEB	MAR	APR	MAY	JUN	JUL	AUG	SEP	OCT	NOV	DEC	TOTAL
348.75 - 11.24 (0.0)	676	706	541	462	271	210	180	350	418	682	913	889	6298
11.25 - 33.74 (22.5)	638	435	377	389	248	138	118	401	536	786	789	625	5480
33.75 - 56.24 (45.0)	663	534	483	391	345	231	149	449	822	1106	886	606	6665
56.25 - 78.74 (67.5)	452	437	323	308	307	249	86	508	914	1087	707	629	6007
78.75 - 101.24 (90.0)	749	670	575	481	623	532	260	776	1085	1007	744	745	8247
101.25 - 123.74 (112.5)	597	417	627	709	620	367	315	333	582	681	511	519	6278
123.75 - 146.24 (135.0)	741	407	855	1002	1085	542	441	363	558	400	598	627	7619
146.25 - 168.74 (157.5)	367	498	639	994	801	523	319	279	309	218	339	617	5903
168.75 - 191.24 (180.0)	399	496	620	663	794	731	612	288	300	234	331	430	5898
191.25 - 213.74 (202.5)	243	251	283	319	515	858	576	326	203	141	178	260	4153
213.75 - 236.24 (225.0)	182	269	380	299	567	1137	834	484	228	144	158	168	4850
236.25 - 258.74 (247.5)	182	259	265	154	298	642	762	516	223	116	102	105	3624
258.75 - 281.24 (270.0)	257	296	281	226	364	439	1129	787	291	171	134	158	4533
281.25 - 303.74 (292.5)	258	217	288	177	219	221	725	685	216	119	164	215	3504
303.75 - 326.24 (315.0)	539	417	487	349	218	200	648	574	278	217	230	398	4555
326.25 - 348.74 (337.5)	496	459	416	277	165	180	286	321	237	331	416	449	4033
TOTAL	7439	6768	7440	7200	7440	7200	7440	7440	7200	7440	7200	7440	87647

WIS HINDCAST for PASCAGOULA 1990 - 1999

LAT: 30.30 N, LONG: 88.57 W, DEPTH: 3 M

STATION: 10

SUMMARY OF MEAN Hmo (m) BY MONTH AND YEAR

YEAR	JAN	FEB	MAR	APR	MAY	JUN	JUL	AUG	SEP	OCT	NOV	DEC	MEAN
1990	0.46	0.69	0.55	0.50	0.59	0.36	0.31	0.23	0.25	0.36	0.46	0.64	0.45
1991	0.61	0.65	0.90	0.77	0.73	0.42	0.27	0.25	0.39	0.41	0.51	0.49	0.53
1992	0.49	0.49	0.50	0.54	0.31	0.38	0.43	0.35	0.41	0.39	0.67	0.54	0.46
1993	0.49	0.61	0.53	0.75	0.54	0.52	0.27	0.29	0.42	0.46	0.47	0.49	0.49
1994	0.62	0.51	0.55	0.52	0.35	0.55	0.39	0.35	0.44	0.55	0.54	0.44	0.48
1995	0.60	0.56	0.64	0.67	0.64	0.48	0.41	0.40	0.31	0.64	0.56	0.45	0.53
1996	0.64	0.56	0.70	0.65	0.46	0.34	0.42	0.34	0.41	0.62	0.60	0.66	0.53
1997	0.60	0.68	0.56	0.66	0.44	0.45	0.30	0.26	0.31	0.61	0.52	0.55	0.49
1998	0.58	0.74	0.74	0.84	0.48	0.53	0.25	0.28	0.97	0.45	0.50	0.52	0.57
1999	0.69	0.45	0.63	0.65	0.47	0.42	0.38	0.24	0.40	0.48	0.36	0.58	0.48
MEAN	0.58	0.59	0.63	0.66	0.50	0.44	0.34	0.30	0.43	0.50	0.52	0.54	

WIS HINDCAST for PASCAGOULA 1990 - 1999

LAT: 30.30 N, LONG: 88.57 W, DEPTH: 3 M

STATION: 10

MAX Hmo(m) WITH ASSOCIATED Tp(sec) AND Dm(deg to nearest 10) BELOW BY MONTH AND YEAR

YEAR	JAN	FEB	MAR	APR	MAY	JUN	JUL	AUG	SEP	OCT	NOV	DEC	MAY
1990	1.0 9	1.5 8	1.5 8	1.4 7	1.3 6	0.8 5	1.1 5	0.7 9	0.6 3	0.9 6	1.6 8	1.5 8	1.6 8
	180	180	180	180	180	170	180	180	50	180	180	180	180
1991	1.5 8	1.6 9	1.7 7	1.6 8	1.6 10	1.1 8	0.7 5	0.6 4	0.8 6	0.9 6	1.5 7	1.5 9	1.7 7
	180	180	180	180	170	170	180	180	180	160	180	170	180
1992	1.6 8	1.5 9	1.6 7	1.5 8	0.6 4	1.2 6	1.4 6	1.6 8	0.8 4	1.3 10	1.5 6	1.5 8	1.6 8
	180	180	180	180	100	180	180	180	90	180	180	180	180
1993	1.2 7	1.6 7	1.5 11	1.6 10	1.4 7	1.1 8	0.5 4	0.8 5	1.0 6	1.7 8	1.6 7	1.7 9	1.7 8
	170	180	180	180	180	170	180	180	180	180	180	180	180
1994	1.5 10	1.5 7	1.6 8	1.2 7	0.8 5	1.6 6	1.0 9	0.8 5	1.5 8	1.5 12	1.7 9	1.1 7	1.7 9
	180	180	180	180	180	180	170	180	180	180	180	180	180
1995	1.6 7	1.7 8	1.5 8	1.5 6	1.5 7	1.4 11	1.4 9	1.5 7	1.0 11	1.6 13	1.6 7	1.5 8	1.7 8
	180	180	180	180	180	180	180	180	180	180	180	180	180
1996	1.6 10	1.6 7	1.5 6	1.2 7	1.3 6	1.0 7	1.3 7	1.1 11	1.5 7	1.6 10	1.6 7	1.6 7	1.6 7
	180	180	180	180	180	170	180	180	180	170	180	180	180
1997	1.6 7	1.5 9	1.5 7	1.5 8	0.9 6	1.2 6	1.8 8	0.7 5	1.2 6	1.6 8	1.3 7	1.5 7	1.8 8
	180	180	180	180	180	180	180	180	180	180	180	180	180
1998	1.5 8	1.6 9	1.6 9	1.5 7	1.5 6	1.3 7	0.5 7	0.8 4	1.7 9	1.0 9	1.5 9	1.5 8	1.7 9
	180	180	180	180	180	180	180	100	180	180	180	180	180
1999	1.6 7	1.4 6	1.7 7	1.5 7	1.6 10	1.1 6	0.9 5	0.5 4	1.0 10	1.2 8	1.2 6	1.6 9	1.7 7
	180	180	180	180	180	180	180	180	170	170	180	180	180
MAX	1.6 8	1.7 8	1.7 7	1.6 10	1.6 10	1.6 6	1.8 8	1.6 8	1.7 9	1.7 8	1.7 9	1.7 9	
	180	180	180	180	180	180	180	180	180	180	180	180	

MAX Hmo(m): 1.8 MAX Tp(sec): 8. MAX Dp(deg): 176. DATE(gmt): 97071903

MAX WIND SPEED(m/sec): 18. MAX WIND DIRECTION(deg): 320. DATE(gmt): 93031313

MEAN Hmo(m): 0.5 MEAN Tp(sec): 6.

STANDARD DEVIATION Hmo(m): 0.3 STANDARD DEVIATION Tp(sec): 2.0

REPORT DOCUMENTATION PAGEForm Approved
OMB No. 0704-0188

Public reporting burden for this collection of information is estimated to average 1 hour per response, including the time for reviewing instructions, searching existing data sources, gathering and maintaining the data needed, and completing and reviewing this collection of information. Send comments regarding this burden estimate or any other aspect of this collection of information, including suggestions for reducing this burden to Department of Defense, Washington Headquarters Services, Directorate for Information Operations and Reports (0704-0188), 1215 Jefferson Davis Highway, Suite 1204, Arlington, VA 22202-4302. Respondents should be aware that notwithstanding any other provision of law, no person shall be subject to any penalty for failing to comply with a collection of information if it does not display a currently valid OMB control number. PLEASE DO NOT RETURN YOUR FORM TO THE ABOVE ADDRESS.

1. REPORT DATE (DD-MM-YYYY) September 2003		2. REPORT TYPE Final report		3. DATES COVERED (From - To)	
4. TITLE AND SUBTITLE Evaluation of Island and Nearshore Confined Disposal Facility Alternatives, Pascagoula River Harbor Dredged Material Management Plan				5a. CONTRACT NUMBER	
				5b. GRANT NUMBER	
				5c. PROGRAM ELEMENT NUMBER	
5. AUTHOR(S) Barry W. Bunch, Mike Channell, William D. Corson, Bruce A. Ebersole, Lihwa Lin, David J. Mark, James P. McKinney, Steve A. Pranger, Paul R. Schroeder, S. Jarrell Smith, Dorothy H. Tillman, Barbara A. Tracy, Michael W. Tubman, Timothy L. Welp				5d. PROJECT NUMBER	
				5e. TASK NUMBER	
				5f. WORK UNIT NUMBER	
7. PERFORMING ORGANIZATION NAME(S) AND ADDRESS(ES) U.S. Army Engineer Research and Development Center Coastal and Hydraulics Laboratory Environmental Laboratory 3909 Halls Ferry Road Vicksburg, MS 39180-6199				8. PERFORMING ORGANIZATION REPORT NUMBER ERDC TR-03-3	
9. SPONSORING / MONITORING AGENCY NAME(S) AND ADDRESS(ES) U.S. Army Engineer District, Seattle P.O. Box 3755, Seattle, WA 98124-3755				10. SPONSOR/MONITOR'S ACRONYM(S)	
				11. SPONSOR/MONITOR'S REPORT NUMBER(S)	
12. DISTRIBUTION / AVAILABILITY STATEMENT Approved for public release; distribution is unlimited.					
13. SUPPLEMENTARY NOTES					
14. ABSTRACT The U.S. Army Engineer Research and Development Center (ERDC) performed a number of engineering studies in support of U.S. Army Engineer District, Mobile (SAM) efforts to develop a Dredged Material Management Plan (DMMP) for the Federal navigation project at Pascagoula, MS. The studies focused on evaluating an option under consideration for the placement of dredged material in an island confined disposal facility (CDF). Numerical modeling of circulation, water quality, and wave climatology were performed to examine the potential impacts of an island CDF, and for engineering design considerations. Field measurements of currents and waves in the Mississippi Sound were made. A number of studies were performed to examine the sediment consolidation process in the CDF with the primary objective of assessing its dredged material volume capacity. Quantitative and qualitative studies results were produced for three alternative locations. The three locations are an island CDF just northeast of Round Island and southeast of the Singing River, between Round Island and the main navigation channel leading to Horn Island Pass and the Gulf of Mexico, and north of the point where the main navigation channel bifurcates to service the Pascagoula River and Bayou Casotte Harbors.					
15. SUBJECT TERMS Confined disposal facility Currents		Dredged material Dredged Material Placement Plan Mississippi Sound		Numerical modeling Pascagoula, MS Waves	
16. SECURITY CLASSIFICATION OF:			17. LIMITATION OF ABSTRACT	18. NUMBER OF PAGES 451	19a. NAME OF RESPONSIBLE PERSON
a. REPORT UNCLASSIFIED	b. ABSTRACT UNCLASSIFIED	c. THIS PAGE UNCLASSIFIED			19b. TELEPHONE NUMBER (include area code)